TESTING AND MODELING OF AN IMPROVED DAMPER CONFIGURATION FOR STIFF STRUCTURAL SYSTEMS

by

M.C. Constantinou, Professor
Department of Civil Engineering
State University of New York
Buffalo, NY 14260

P. Tsopelas, Research Scientist
Department of Civil Engineering
State University of New York
Buffalo, NY 14260

W. Hammel, Graduate Student
Department of Civil Engineering
State University of New York
Buffalo, NY 14260

Technical Report Submitted to the Center for Industrial Effectiveness and Taylor Devices, Inc.

TESTING AND MODELING OF AN IMPROVED DAMPER CONFIGURATION FOR STIFF STRUCTURAL SYSTEMS

by

M.C. Constantinou[1], P. Tsopelas[2] and W. Hammel[3]

State University of New York at Buffalo
Department of Civil Engineering
Buffalo, New York 14260

Technical Report Submitted to the Center
for Industrial Effectiveness and Taylor Devices, Inc.

August 31, 1997

---

[1] Professor, Department of Civil Engineering, State University of New York at Buffalo

[2] Research Scientist, Department of Civil Engineering, State University of New York at Buffalo

[3] Graduate Student, Department of Civil Engineering, State University of New York at Buffalo

ABSTRACT

It is generally recognized that stiff structural systems, such as reinforced concrete shear wall systems and steel-braced dual systems, are characterized by small drifts and small relative velocities such that the implementation of seismic energy dissipation devices is likely not feasible. This report presents a study on an improved configuration for fluid viscous dampers that is applicable to stiff structural systems. It utilizes a toggle-brace-damper system that magnifies the damper displacement and reduces the required damper force, while still producing the desired damping effect. The report presents the concept, a theoretical treatment, an experimental study with cyclic and shake table testing of a model structure, and procedures for response history and simplified analysis.

ACKNOWLEDGEMENTS

Financial support for this project has been provided by the Greater Regional Industrial Technology (GRIT) Program and Taylor Devices, Inc.

TABLE OF CONTENTS

TABLE OF CONTENTS (Cont'd)

LIST OF ILLUSTRATIONS

LIST OF ILLUSTRATIONS (Cont'd)

LIST OF ILLUSTRATIONS (Cont'd)

LIST OF TABLES

SECTION 1
INTRODUCTION

The concept of adding energy dissipation devices to improve seismic performance has been often demonstrated by researchers. In the past few years, many practicing engineers have selected this technology as a primary constituent of a structure's seismic protection system. In comparison, conventional seismic designs are based on the concept of the lateral force resisting system being able to dissipate seismic energy in a stable manner for a large number of cycles. Energy dissipation occurs in specially detailed plastic hinge regions of beams and column bases, which also form part of the gravity-load carrying system. That is, acceptable performance is achieved at the expense of damage to the gravity frame. Such damage may be irreparable.

Energy dissipation is a new and viable design strategy that has been already used for new designs and for the seismic rehabilitation of a number of building and bridge structures (Constantinou et al., 1997; Soong and Dargush, 1997). The function of the energy dissipation system, which typically is not part of the gravity-load-carrying frame, is to primarily dissipate seismic energy. The dissipation of seismic energy in the energy dissipation system results in significant reduction of drift. As an example, Table 1-1 presents the calculated response of a single-degree-of-freedom yielding structural system without and with a linear viscous energy dissipation system (Tsopelas et al., 1997). The structural system is characterized by the elastic period T_e (= 0.3, 0.5 and 1.0 sec.), ratio of yield strength to required elastic strength $F_y / (m\ S_a) = 0.3$ (S_a = spectral acceleration for 5-percent damping, m = mass) and post yielding stiffness to elastic stiffness ratio equal to 0.05. The seismic excitation consisted of 20 scaled components that represented, on the average, the 1994 NEHRP Recommended Provisions (Federal Emergency Management Agency, 1995) response spectrum with site coefficients $C_a = 0.4$, $C_v = 0.6$ and $T_o = 0.6$ sec. The results of Table 1-1 represent average values of the calculated responses in the 20 motions.

The strength of the analyzed system ($F_y / m\ S_a = 0.3$) represents its actual yield strength. If this were a code-compliant structural system, it would have a ratio of yield

strength to design strength of approximately 2 to 4 (Osteraas and Krawinkler, 1990). Accordingly, the R_w value (Uniform Building Code, 1994) for this system is approximately in the range of 6 to 12. Table 1-1 compares the response of this system to those of the same system when enhanced with linear viscous energy dissipating devices that provide, under elastic conditions, an added damping ratio, β_v, of either 15-percent or 25-percent of critical. Results on peak drift, drift divided by theoretical yield displacement (to obtain a measure of inelastic action in the structural system), peak relative velocity and shear force divided by weight are presented. Shear forces at three distinct instants are given:

(a) at the instant of peak drift,

(b) at the instant of peak relative velocity (this is the horizontal component of the force in the energy dissipating devices), and

(c) at the instant of peak acceleration (which occurs at a displacement less than peak drift).

The results of Table 1-1 demonstrate a pattern that is typical for energy dissipation systems. Specially:

(1) Drifts are reduced by factors of 1.6 and 2.0, on the average, for 15-percent and 25-percent added viscous damping ratio. Nevertheless, this code-compliant structural system with added damping undergoes inelastic action. Elimination of inelastic action (without designing with lower R_w value) is possible by providing higher damping.

(2) The shear force at peak displacement is only marginally reduced with addition of the energy dissipation system. This is a result of the very low post-yielding stiffness of the structural system. Had the system been elastoplastic, the shear force would have not changed. Conversely, the shear force would have significantly reduced in an elastic system.

(3) The shear force at peak acceleration (that is, the total shear force, including the viscous force component) is increased with the addition of the energy dissipation system. Again this is a result of the very low post yielding stiffness of the structural system. Since this force includes a viscous component, which occurs at a different instant than the peak drift, its main effect is an increase in column axial forces. That

is, this force is not the lateral force for the design of lateral force-resisting system (see Constantinou et al., 1997 and Federal Emergency Management Agency, 1996 for details).

(4) The peak damping force increases with reducing elastic period and it is nearly constant for periods within the constant acceleration region of the response spectrum. Following procedures presented in FEMA 274 (Federal Emergency Management Agency, 1996; Constantinou et al., 1997), it may be easily shown that the ratio of peak damping force (horizontal component) to weight is

$$\frac{F_D}{W} = 2\beta_{eff}\frac{S_a(T_{eff},\beta_{eff})}{g} = \frac{4\pi\beta_v}{gT_e}\sqrt{AD} \qquad (1\text{-}1)$$

where β_v = added damping ratio under elastic conditions, T_{eff} and β_{eff} are the effective period and effective damping, respectively, of the structural system inclusive of the energy dissipation devices, S_a=A= spectral acceleration for period T_{eff} and damping β_{eff}, and D=drift. It should be noted that (1-1) is approximate since it was derived by using pseudo-velocity as a measure for the peak relative velocity. If we concentrate on short period structures (with elastic period in the acceleration-controlled domain of the spectrum) and elastoplastic behavior with yield force F_y (so that A~ F_y/mass), then

$$\frac{F_D}{W} = 2\beta_v\sqrt{\frac{F_y}{W}\frac{S_{peak}}{g}}\ e \qquad (1\text{-}2)$$

where S_{peak} = peak spectral acceleration (for damping β_v) and e=square root of the ratio of the actual drift to the drift under elastic conditions (but with added damping). It should be noted that e may be approximated by the square root of the modification factor C_1 of the FEMA 273 (Federal Emergency Management Agency, 1996).

(5) Stiff structural systems are characterized by small drifts and small relative velocities. This is a generally recognized fact. For example, the Federal Emergency Management Agency, 1995 states that *"structural systems best suited for implementation of energy dissipation devices are the moment-resisting frame and the flexible dual system, in either structural steel or reinforced concrete. The interstory response of a stiff lateral load-resisting system, such as a reinforced concrete shear*

wall system or a steel-braced dual system, is generally characterized by both small relative velocities and small relative displacements. As such it may not be feasible to implement supplemental energy dissipation."

In reality, the application of energy dissipation to stiff structural systems is feasible, however when conventionally applied it may be costly for the following reasons:

(a) Drifts are very small. For example, a code-compliant stiff structure (say T_e = 0.3 sec.) with the energy system designed so that a performance level of immediate occupancy or nearly so (Federal Emergency Management Agency, 1996) is achieved, would undergo drifts of the order of 10 mm. Displacements in the energy dissipation device will be less if the devices are installed inclined. Fluid viscous energy dissipation devices require special detailing when operating at very small stroke. In general, this results in an increased volume of the device and, accordingly, cost.

(b) Required damping forces are large.

The work reported herein deals with an energy dissipation device configuration that is practical for installation in stiff structural systems. It utilizes a brace and damper configuration (termed "toggle brace") that results in a magnification of the damper displacement and a reduction in the damper force, while still delivering the required large damping force to the structural frame. That is, the configuration resolves the aforementioned problems with the application of energy dissipation systems to stiff structures. The report presents the concept, a theoretical treatment, simplified procedures for predicting the behavior of the damped system and an experimental study that includes cyclic and shake table testing.

TABLE 1-1 Response of Yielding System without ($\beta_v = 0$) and with Added Viscous Energy Dissipation System ($\beta_v = 0.15$ and 0.25 under elastic conditions)

	Without EDS ($\beta_v = 0$)			With EDS ($\beta_v = 0.15$)			With EDS ($\beta_v = 0.25$)		
T_e (sec)	0.3	0.5	1.0	0.3	0.5	1.0	0.3	0.5	1.0
Drift (mm)	34.1	62.1	135.5	20.4	38.2	89.4	16.3	30.7	73.4
Drift/Yield Displacement	5.1	3.3	3.0	3.0	2.1	2.0	2.4	1.7	1.6
Peak Velocity (mm/s)	285.0	436.9	551.7	194.6	323.8	448.8	166.3	277.8	405.3
Shear/Weight (at peak displ.)	0.36	0.33	0.20	0.33	0.32	0.19	0.32	0.31	0.19
Damping Force /Weight	0	0	0	0.12	0.12	0.09	0.18	0.18	0.13
Shear/Weight (at peak accel.)	0.37	0.34	0.21	0.42	0.41	0.26	0.44	0.42	0.28

SECTION 2
TOGGLE BRACE-DAMPER SYSTEM FOR STIFF STRUCTURES

2.1 Introduction

There is a variety of configurations that can magnify displacements, and, therefore, can be utilized in energy dissipation systems for stiff structures. All require the use of a mechanism that magnifies displacements. Given that conceiving such mechanisms out of thin air is likely impossible, one can draw upon experiences in other fields and, particularly, the field of mechanical engineering. The reader may find enlightening to review one of the many books with illustrations of concepts and devices in this field (e.g., Chironis, 1991).

Two such practical and tested systems are briefly described herein. The one is based on the lever principle and has been developed by Taisei Corporation in Japan. The other is based on the slider-crank mechanism (which is based on the simple toggle) and is the subject of this report.

Figure 2-1 illustrates the Japanese DREAMY system (Hibino et al., 1989). It is simple in concept and functional but cumbersome to construct due to its size, large sections (forces are carried by bending) and complicated requirements for pinning.

Figure 2-2 illustrates the toggle brace-damper system. The system consists of toggles ABC which are configured as a shallow truss. Dampers are placed perpendicular to member AB. Most effective is placement at location 2. Movement of point C with respect to A (interstory drift u) causes member AB to rotate. The resulting changes of distance between points B and D and B and E are the damper displacements u_D and u_{D2}, respectively. These displacements are related to the drift u through simple equations, which will be derived in the sequel.

Damper forces in the toggle brace-damper system are small, however, they are magnified in the shallow truss configuration of the system and delivered to the frame by compression or tension in the braces. The absence of bending in the system allows the use of small sections and standard connections details. Moreover, the entire system may be placed within a square with side equal to the column height.

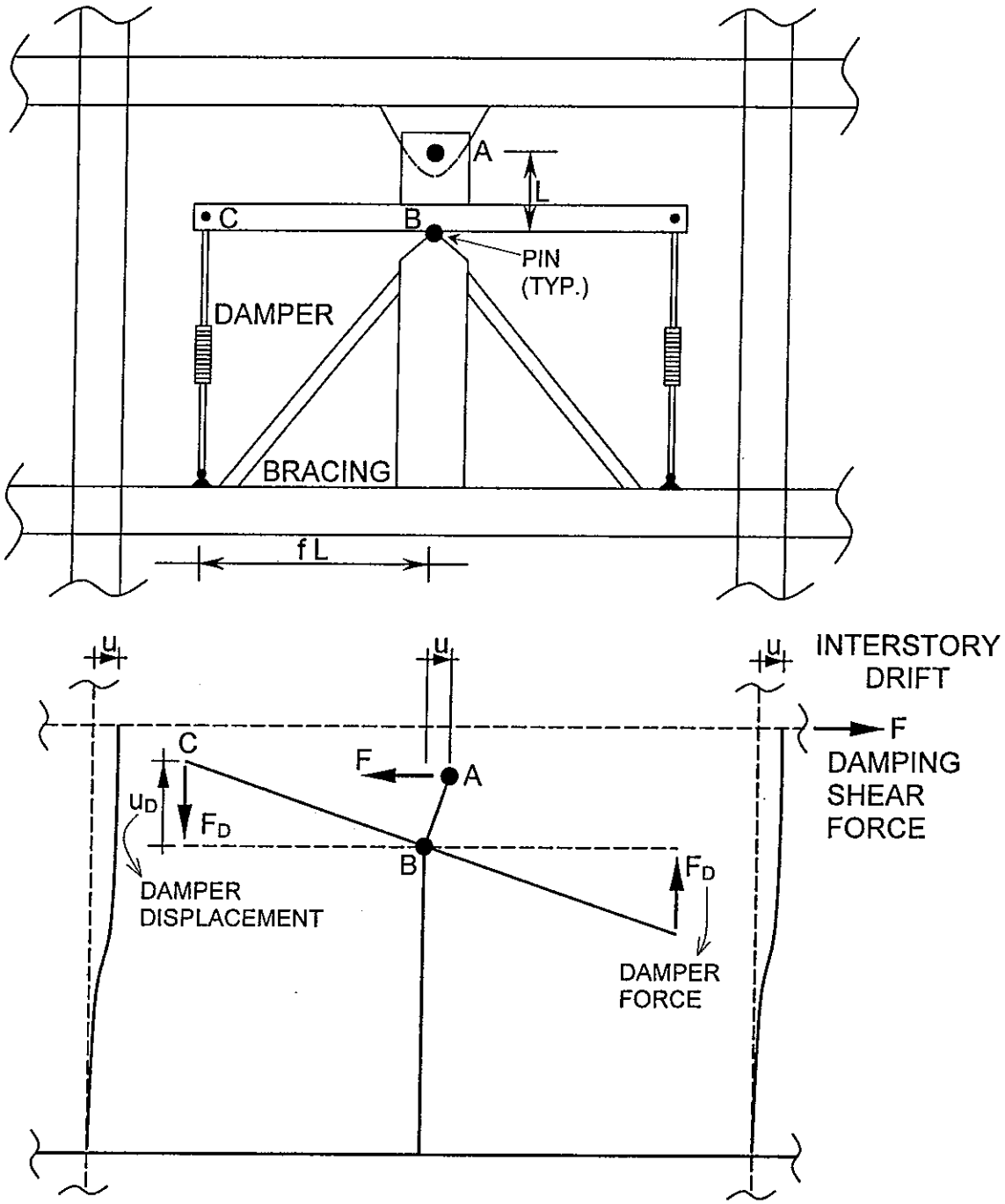

$$u_D = f\,u$$

$$F = 2f\,F_D$$

FIGURE 2-1 Illustration of DREAMY System of Taisei Corporation

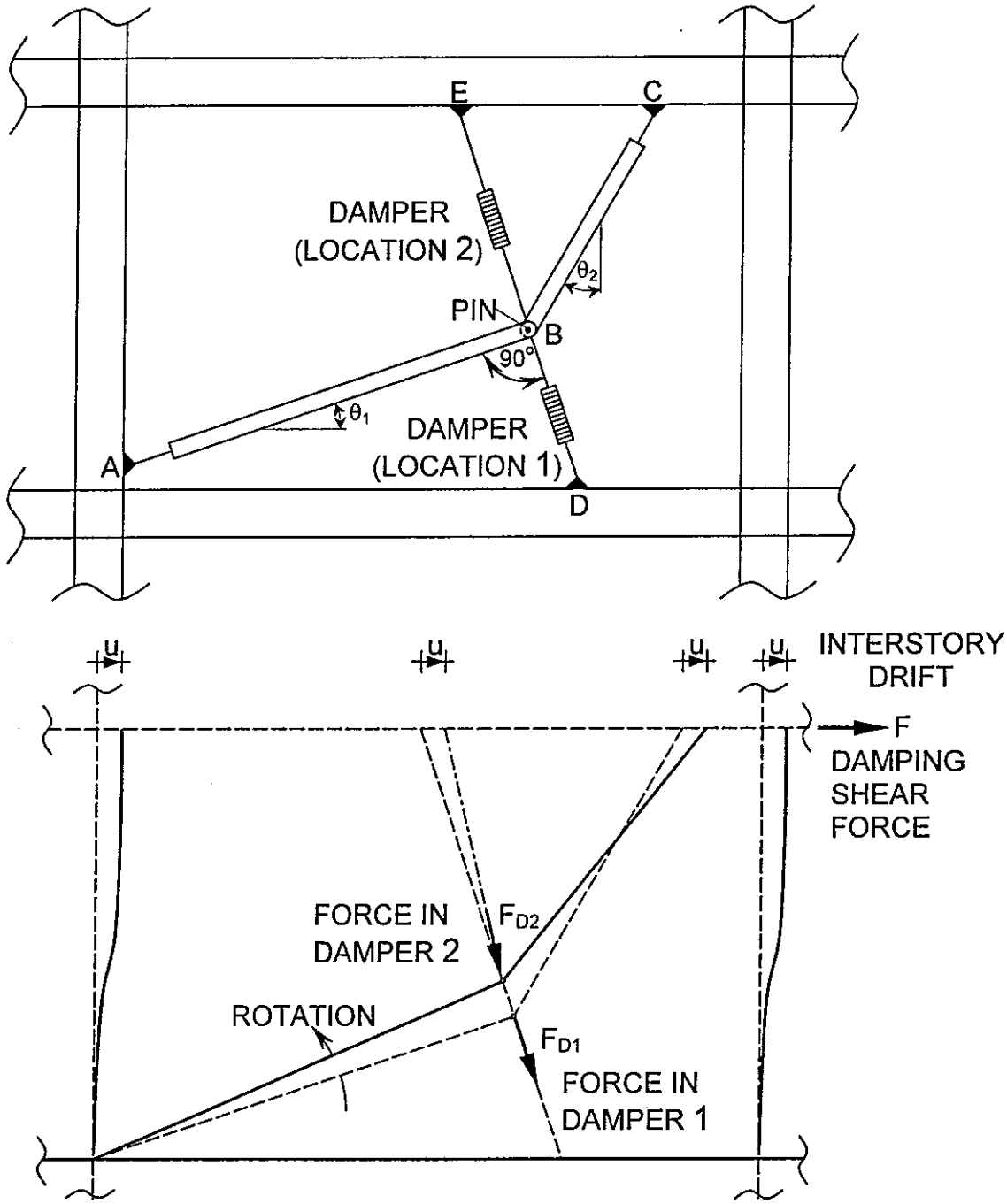

Location 1: $u_{D_1} = f_1 u$, $f_1 = \dfrac{\sin\theta_2}{\cos(\theta_1 + \theta_2)}$

Location 2: $u_{D_1} = f_2 u$, $f_2 = \dfrac{\sin\theta_2}{\cos(\theta_1 + \theta_2)} + \sin\theta_1$

$$F = f_1 F_{D_1} + f_2 F_{D_2}$$

FIGURE 2-2 Illustration of Toggle Brace-Damper System

2.2 Toggle Brace Theory

Consider the toggle brace configuration of Figure 2-3. For drift towards the right (positive u), point B moves upwards (positive angle ϕ). Assuming inextensible members the condition for preservation of length is

$$\ell_2^2 = h^2 + \ell_1^2 + (\ell + u)^2 - 2h\ell_1 \sin(\theta_1 \pm \phi) - 2(\ell + u)\ell_1 \cos(\theta_1 \pm \phi) \qquad (2\text{-}1)$$

The displacement of the lower damper (movement of point B with respect to point of attachment) is

$$u_D = \pm \ell_1 \left[\left(1 + \frac{1}{\cos^2 \theta_1} - \frac{2\cos(\theta_1 \pm \phi)}{\cos \theta_1} \right)^{1/2} - \tan \theta_1 \right] \qquad (2\text{-}2)$$

The displacement of the upper damper (movement of point B with respect to point of attachment at the beam above) is.

$$u_D = \pm \left\{ \frac{h}{\cos \theta_1} - \ell_1 \tan \theta_1 - \left[\left(h \tan \theta_1 - u - \frac{\ell_1}{\cos \theta_1} + \ell_1 \cos(\theta_1 \pm \phi) \right)^2 + (h - \ell_1 \sin(\theta_1 \pm \phi))^2 \right]^{1/2} \right\} \qquad (2\text{-}3)$$

It should be noted that in (2-1) to (2-3) the plus sign holds for positive rotation ϕ (which corresponds to positive displacement u as illustrated in Fig. 2-3) and the negative sign holds for negative rotation. Moreover, displacement u in (2-1) to (2-3) is with its correct sign, that is, not the absolute value.

Equations (2-1) to (2-3) reveal a complex nonlinear relation between damper displacement (u_D) and lateral frame displacement (u). Given a displacement u, (2-1) can be exactly solved for the rotation ϕ. This solution is presented in the next subsection, although it is of little practical use.

Equations (2-1) to (2-3) can be significantly simplified when recognizing that angle ϕ is very small and that displacement u is small by comparison to the dimensions. Retaining only linear terms in ϕ and u, we obtain

$$\phi = f \frac{u}{\ell_1} \qquad (2\text{-}4)$$

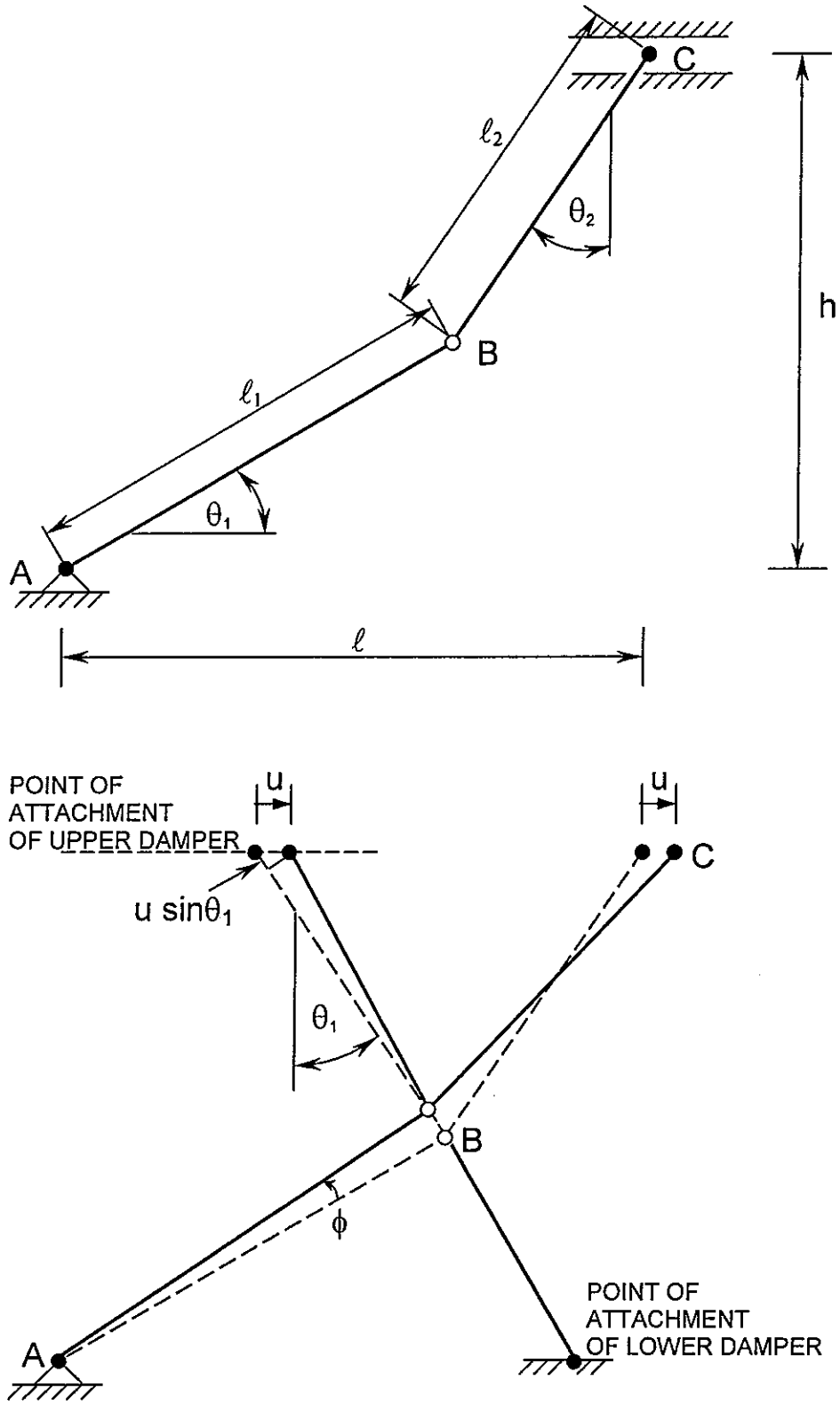

FIGURE 2-3 Analysis of Toggle Brace Movement (drawing not to scale)

Moreover, for the lower damper

$$u_D = f\,u \tag{2-5}$$

and for the upper damper

$$u_D = (f + \sin\theta_1)u = f_u\,u \tag{2-6}$$

where

$$f = \frac{\sin\theta_2}{\cos(\theta_1 + \theta_2)} \tag{2-7}$$

It may be noted that quantity u $\sin\theta_1$ in (2-6) is the component of displacement u along the axis of the upper damper, as illustrated in Figure 2-3.

Quantities f and f_u, the displacement magnification factors, depend only on the inclination of the toggles and not their dimensions. Figures 2-4 and 2-5 present graphs of the magnification factors for a range of angles θ_1 and θ_2. It may be noted that very high magnification factors can be achieved, although they are very sensitive to small changes in the angles. However, magnification factors in the range of 2 to 3 are insensitive to small variations in the inclination of the toggles.

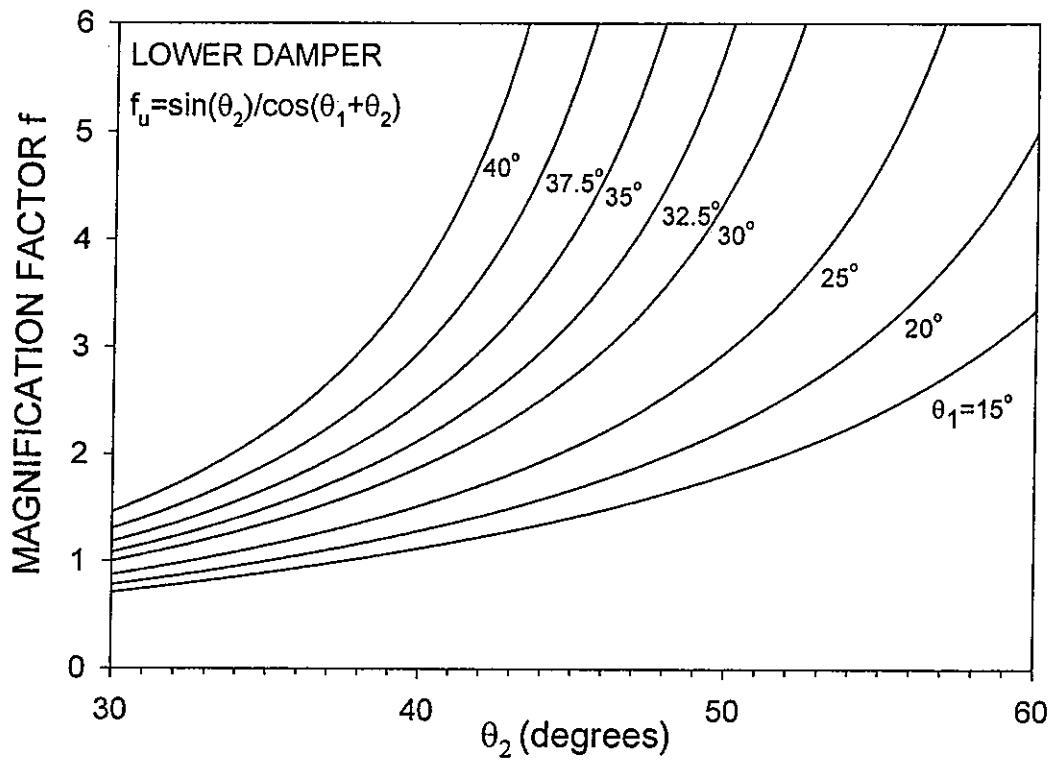

FIGURE 2-4 Magnification Factor f for Lower Damper Position

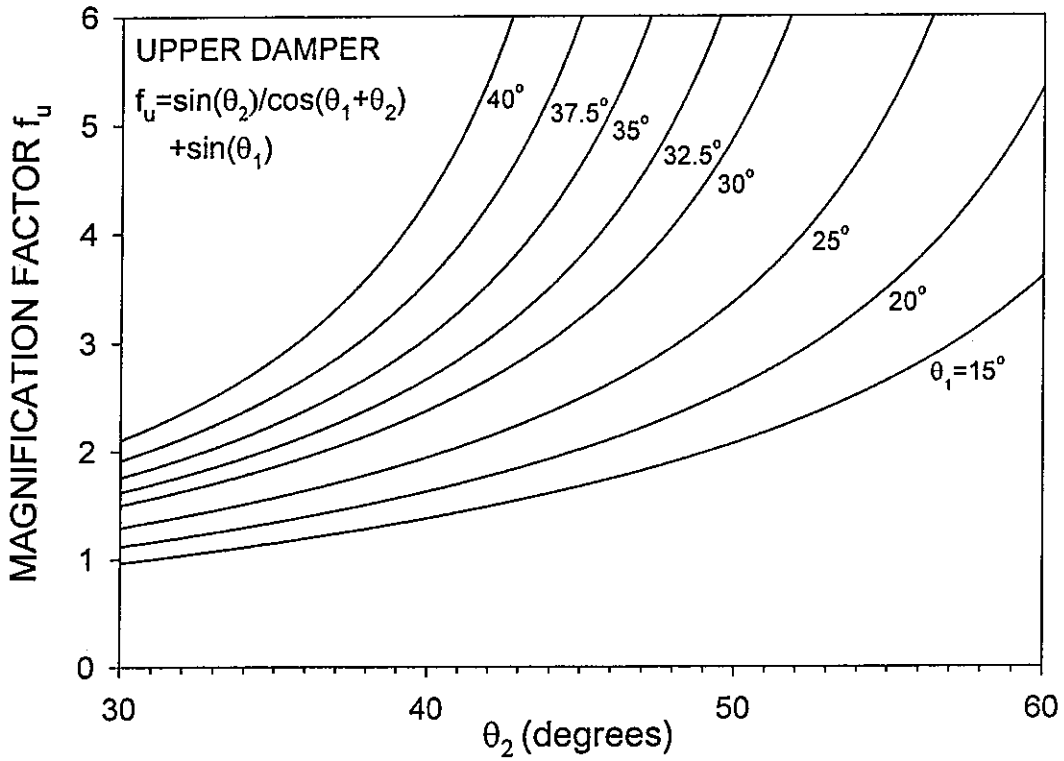

FIGURE 2-5 Magnification Factor f_u for Upper Damper Position

2.3 Analysis of Motion for Large Rotations

The analysis of motion of the toggle brace for large rotations requires solution of (2-1) for the rotation ϕ and then substitution into (2-2) and (2-3) to obtain the damper displacement. An exact solution is possible in the following form:

$$\sin x = \frac{b - \left(b^2 - 4c\right)^{1/2}}{2} \tag{2-8}$$

in which

$$b = \frac{h \ell_1 D}{h^2 \ell_1^2 + (\ell + u)^2 \ell_1^2} \tag{2-9}$$

$$c = \frac{D^2 - 4(\ell + u)^2 \ell_1^2}{4h^2 \ell_1^2 + 4(\ell + u)^2 \ell_1^2} \tag{2-10}$$

$$D = h^2 + \ell_1^2 - \ell_2^2 + (\ell + u)^2 \tag{2-11}$$

and

$$x = \theta_1 \pm \phi \tag{2-12}$$

where the plus sign holds for u being positive (towards the right in Fig.2-3) and the minus sign holds for u being negative. That is, ϕ is calculated in absolute value. To obtain the damper displacement, ϕ in absolute value is substituted into (2-2) and (2-3).

Figure 2-6 presents the relation between the lower damper and frame displacements for a configuration that is representative of the tested frame at prototype (full) scale. The geometry (shown on the figure) is representative of what might be used in actual applications. Equations (2-8) to (2-12) were used in calculating the exact (large rotation) relation, whereas (2-5) was used for calculating the relation based on the assumption of small rotations. It is observed that the small rotation theory underpredicts the damper displacement for positive (towards the right) lateral displacement and it overpredicts the damper displacement for negative lateral displacement. This explained by the changes in the geometry of the toggle brace: the angle between the two toggles increases for movement towards the right, whereas it decreases for movement towards the left. That is, for movement towards the right, angles θ_1 and θ_2 (eq. 2-7, see Fig. 2-3) increase so that the instantaneous magnification factor (eq. 2-7) increases. The opposite is true for movement towards the left.

Figure 2-7 compares experimental and analytical results on the displacement of the lower damper for large toggle rotations. The experimental results were obtained with the reduced-scale frame shown in Fig 2-8. Further details on the tested frame are presented in Section 3. The frame was subjected to lateral displacement u with amplitude of 13 mm and frequency of 0.05 Hz. The lower damper displacement was measured as the change of distance AB (see Fig. 2-8), with positive damper displacement corresponding to an extension of the damper.

The top graph in Figure 2-7 presents the experimental results. It may be observed that the graph, which is for three fully-reserved cycles of movement, displays "hysteresis", that is, there is a difference between the ascending and the descending branches of the loop. This is caused by deformations in the toggle brace due to development of force in the damper (testing was under nearly static conditions, so that this force is just friction in the seals of the damper).

The middle graph presents the analytical results based on the large rotation theory of this subsection. Finally, the bottom graph presents analytical results obtained with the

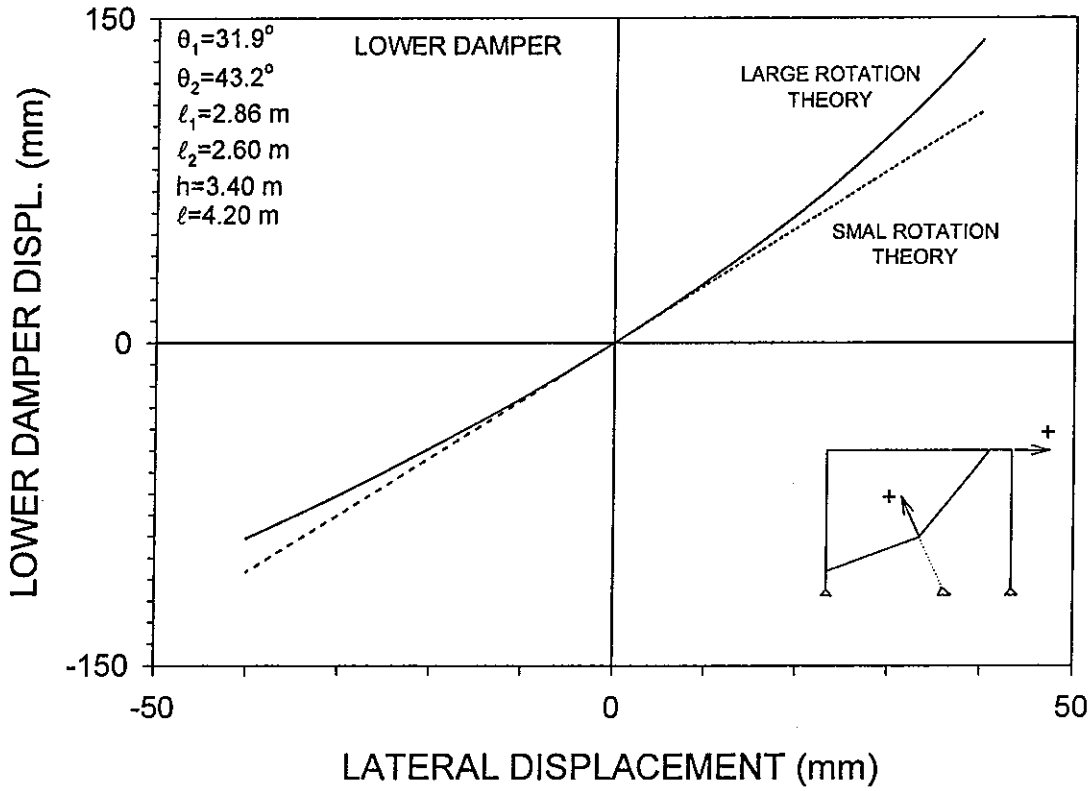

FIGURE 2-6 **Relation between Lower Damper Displacement and Lateral Displacement**

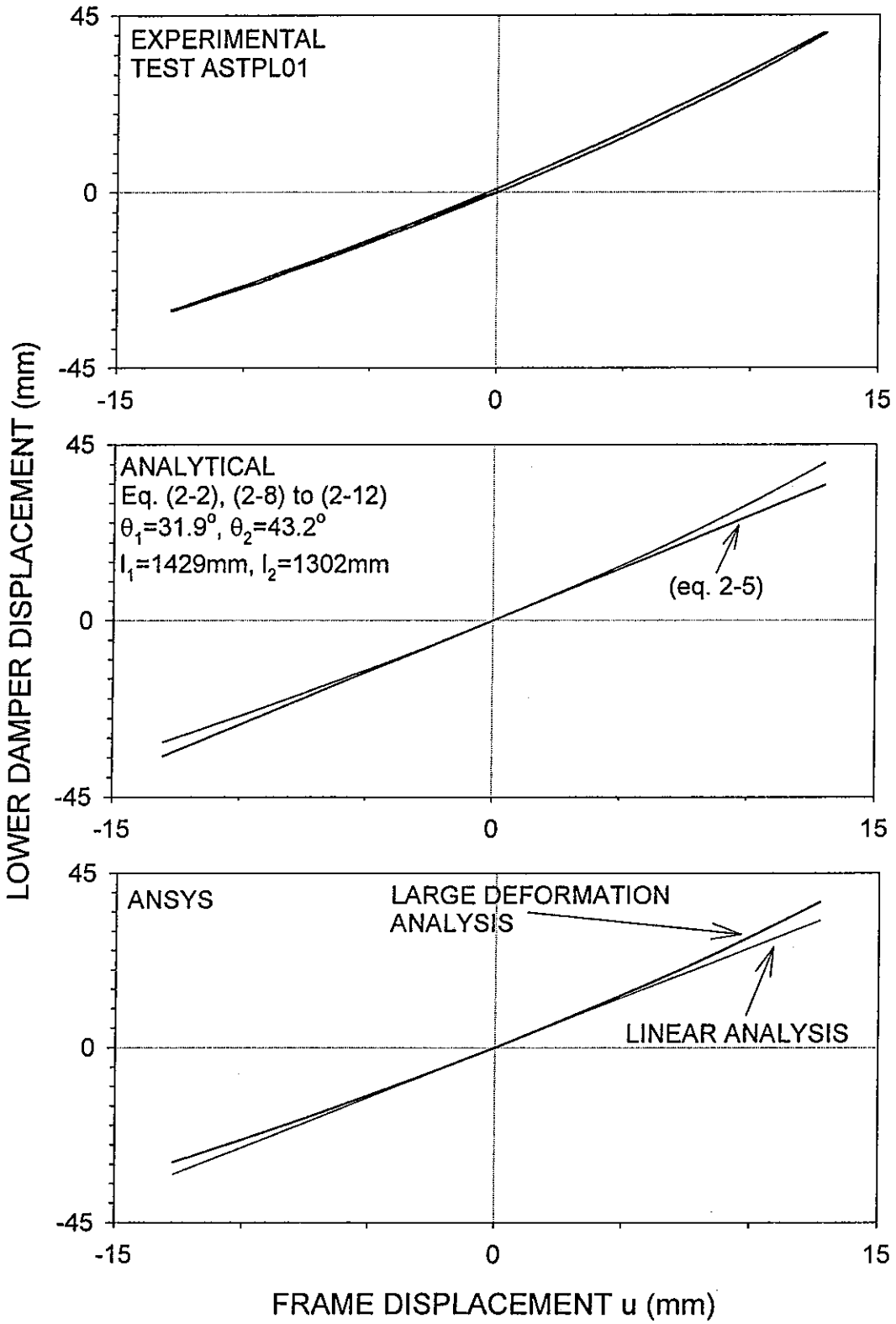

FIGURE 2-7 **Comparison of Experimental and Analytical Results on Lower Damper Displacement for Large Rotations**

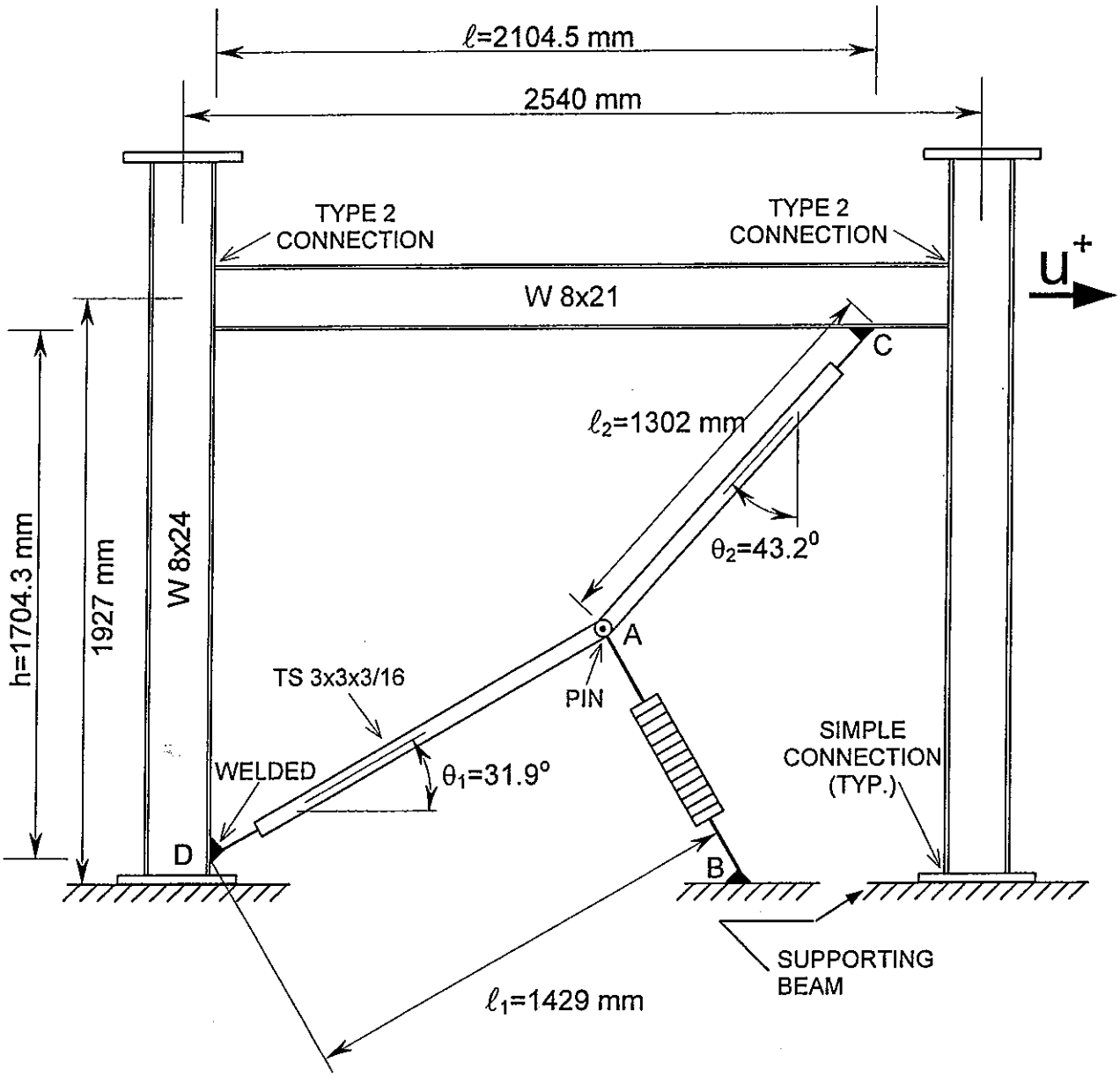

FIGURE 2-8 Tested Frame with Toggle Brace-Damper System

structural analysis program ANSYS (Swanson Analysis Systems IP, 1996). In this analysis, a detailed model of the entire frame was analyzed (details of the modeling are presented later in this report). Evidently, the analytical prediction is nearly exact.

2.4 Damping Force and Damping Ratio

Stiff structures with energy dissipation systems will undergo small seismic interstory drifts (e.g., see Table 1-1). Moreover, small drifts are expected for stiff and for flexible structures under wind loading. Under these conditions, the application of the small rotation theory produces results of acceptable accuracy.

The small rotation theory produces a number of simple and very useful results for analysis and design. The first is the relation between the damper force and the damping component of the shear force that acts on a frame. Consider a frame with a toggle brace-damper system like the one shown in Figure 2-8. Considering first the case of the lower damper, the damper force, F_D, is related to the damper velocity, $\dot{u}_D$, which by virtue of (2-5) is

$$\dot{u}_D = f\,\dot{u} \tag{2-13}$$

where $\dot{u}$ is the frame horizontal velocity. For a linear damper with coefficient C_o,

$$F_D = C_o\,\dot{u}_D = C_o\,f\,\dot{u} \tag{2-14}$$

Considering equilibrium of the toggle brace in the original, undeformed configuration (see Figure 2-9), the force in the two toggle braces are

$$T_1 = F_D \tan(\theta_1 + \theta_2) \tag{2-15}$$

$$T_2 = \frac{F_D}{\cos(\theta_1 + \theta_2)} \tag{2-16}$$

Forces T_1 and T_2 can be substantially larger than the damper force because of the shallow truss configuration of the toggle brace. Figure 2-10 presents graphs of these forces for a range of feasible toggle geometries.

The horizontal component of force T_2 is equal to the damping component of the horizontal force acting on the frame. That is, for the lower damper

$$F = T_2 \sin\theta_2 = \frac{\sin\theta_2}{\cos(\theta_1 + \theta_2)} F_D = f\,F_D \tag{2-17}$$

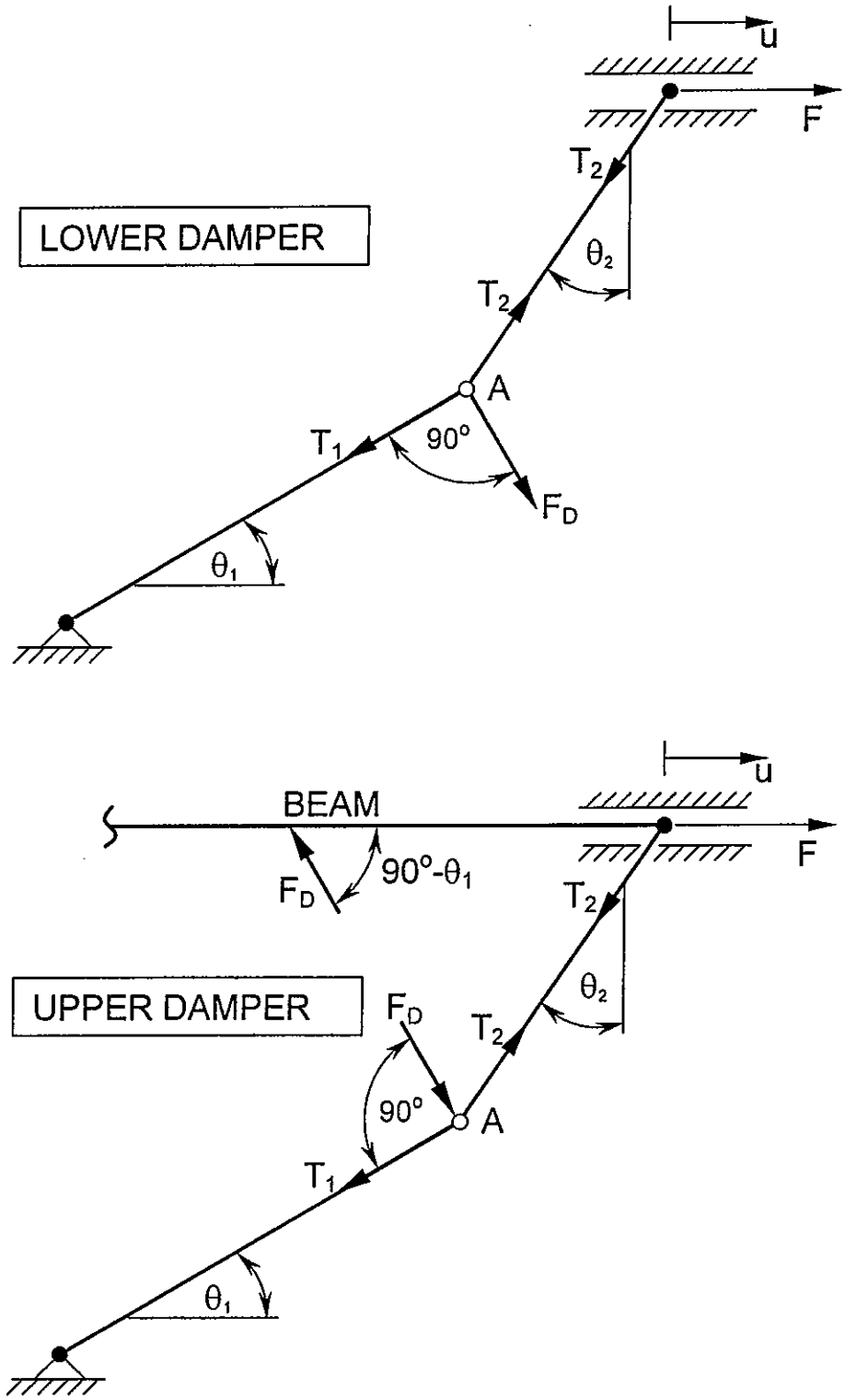

FIGURE 2-9 Forces Acting on Toggle Brace and Frame

In the case of the upper damper, force F is (see Figure 2-9)

$$F = \left(\frac{\sin\theta_2}{\cos(\theta_1 + \theta_2)} + \sin\theta_1 \right) F_D = f_u F_D \tag{2-18}$$

Equations (2-17) and (2-18) demonstrate that the damper force is magnified by the same factor as the frame lateral displacement (see eqs. 2-5 and 2-6).

The relation between the frame damping force, F, and frame lateral velocity, $\dot{u}$, is derived from (2-14), (2-17) and (2-18):

$$F = C_o f^2 \dot{u} \tag{2-19}$$

for the lower case and

$$F = C_o f_u^2 \dot{u} \tag{2-20}$$

for the upper case. That is, the effective damping coefficient for the frame is $C_o f^2$ or $C_o f_u^2$, which is substantially larger than the damping coefficient of the damper. It follows that the damping ratio of a frame with effective weight W and period T is

$$\beta = \frac{C_o f^2 g T}{4\pi W} \text{ or } \frac{C_o f_u^2 g T}{4\pi W} \tag{2-21}$$

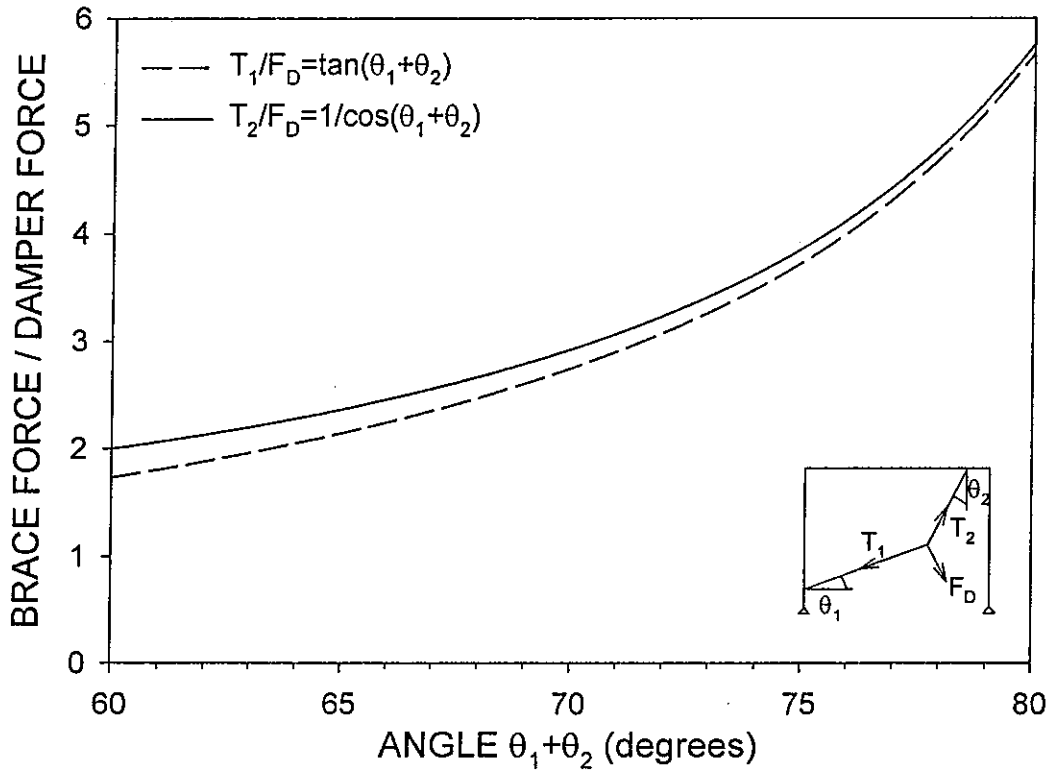

FIGURE 2-10 **Ratio of Toggle Brace Axial Force to Damper Force for Various Feasible Geometries**

Figure 2-11 provides a comparison of various configurations of dampers within a frame. It may be noted that the equations relating damper displacement to frame drift and frame damping force to interstory velocity, and the equation for the damping ratio have identical forms in the four illustrated configurations. What distinguishes the four configurations is the displacement magnification factor: being cos θ for the inclined dampers, unity for the chevron brace, and f or f_u for the toggle brace configurations.

Figure 2-11 also presents a comparison of the four configurations in two cases:

(a) Case 1 in which a frame (geometry and weight are representative of the tested frame) is equipped with a single linear viscous damper. The provided damping ratio is, of course, significantly higher in the toggle brace than in the other two configurations.

(b) Case 2 in which the damper requirements in terms of displacement, force and damping coefficient are compared for the same result, that is, resulting damping ratio and peak frame drift. It should be noted that the energy dissipated per cycle of drift is the same in the four configurations (the reader may verify that the product $F_D * u_D$ is the same for the four configurations).

2.5 Other Useful Results

The toggle brace-damper configuration may be used for frame displacements that are less than the limit for which the two toggles assume a straight line position (that is, in the deformed position $\theta_1+\theta_2 = 90^\circ$). It may be shown that the limit on the frame displacement u_ℓ is

$$u_\ell = \left[(\ell_1 + \ell_2)^2 - h^2\right]^{1/2} - \ell \qquad (2\text{-}22)$$

For example, (2-22) gives u_ℓ = 29.5 mm for the tested frame of Figure 2-8. The maximum displacement during testing of the frame did not exceed 13 mm.

Equations (2-19) and (2-20) are valid for the case of linear viscous damper. Nonlinear viscous dampers may have the constitutive relation

$$F_D = C_o \left|\dot{u}_D\right|^\alpha \operatorname{sign}(\dot{u}_D) \qquad (2\text{-}23)$$

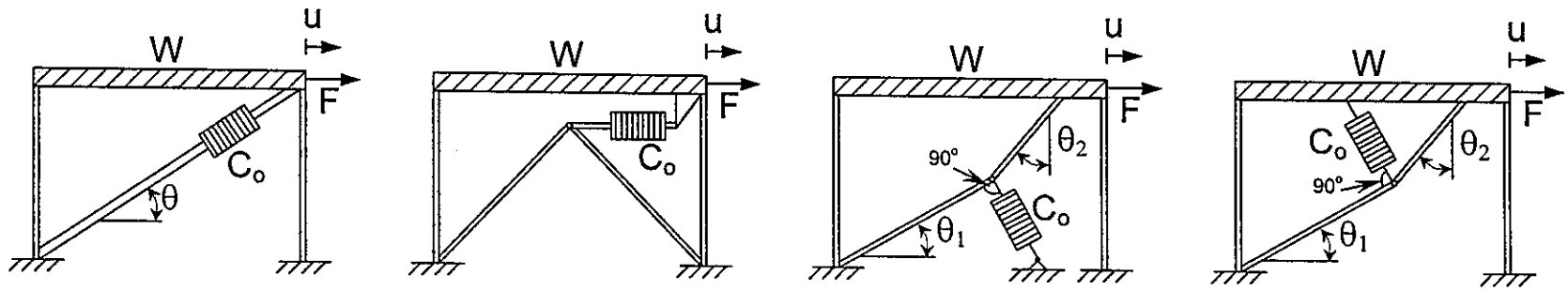

$u_D = u\cos\theta$	$u_D = u$	$u_D = f\,u$	$u_D = f_u\,u$
$F = C_o \cos^2\theta\,\dot{u}$	$F = C_o\,\dot{u}$	$F = C_o f^2\,\dot{u}$	$F = C_o f_u^2\,\dot{u}$
$\beta = \frac{C_o \cos^2\theta\, g\, T}{4\pi W}$	$\beta = \frac{C_o\, g\, T}{4\pi W}$	$\beta = \frac{C_o f^2\, g\, T}{4\pi W}$	$\beta = \frac{C_o f_u^2\, g\, T}{4\pi W}$

CASE 1: (damping ratio for frame with T=0.3 sec, C_o=16 Ns/mm, W=137 kN, θ=37°, θ_1=31.9°, θ_2=43.2°)

$\beta = 0.017$	$\beta = 0.027$	$\beta = 0.194$	$\beta = 0.279$

CASE 2: (required C_o for β=0.25, other properties as in case 1; resulting damper displacement and damper force for u=10mm)

$C_o = 229.3\,\text{Ns/mm}$	$C_o = 146.2\,\text{Ns/mm}$	$C_o = 20.6\,\text{Ns/mm}$	$C_o = 14.4\,\text{Ns/mm}$
$u_D = 8\,\text{mm}$	$u_D = 10\,\text{mm}$	$u_D = 26.6\,\text{mm}$	$u_D = 31.9\,\text{mm}$
$\frac{F_D}{W} = 0.280$	$\frac{F_D}{W} = 0.224$	$\frac{F_D}{W} = 0.084$	$\frac{F_D}{W} = 0.070$

FIGURE 2-11 Comparison of Effectiveness of Various Configurations of Dampers

in which α is a parameter with values less than unity (Constantinou et al., 1997). In this case, the frame damping force-frame lateral velocity relation (the equivalent to eq. 2-19) becomes

$$F = C_o f^{1+\alpha} |\dot{u}|^{\alpha} \text{sign}(\dot{u}) \tag{2-24}$$

2.6 Connection Details For Toggle Brace-Damper System

Ideally, all connections of the toggle brace-damper system should be true pins. In this subsection we present a number of connections details, which were used in the tested frame. In two of these details, an attempt was made to avoid the use of true pins at the point of connection of the two toggles. A third detail utilized a pin.

The connections of the toggle braces to the column and beam (points C and D in the frame of Fig. 2-8) were combined welded-bolted connections that allowed for adjustment of position so that the specified toggle geometry could be achieved. Figure 2-12 illustrates the connection detail of the toggle brace to the column. A similar connection was used at the beam. Note that use of slotted holes and/or the insertion of another plate between the column and the ½''x 6''x 9'' plate allows for adjustment of the geometry of the toggle brace system. Figure 2-13 shows a view of the connection in which a plate was utilized to achieve the desired geometry. The shown connection has been designed for an axial brace force of 35.6 kN (8 kips) and brace rotation of 0.035 rad (2^o). The connection underwent over 200 large rotation cycles in the floor and shake table testing without any evidence of distress.

Three different details were developed for the connection of the two toggle braces (point A in the frame of Fig. 2-8). The first was a typical true pin connection as illustrated in Figure 2-14. Figure 2-15 presents a view of the connection. The damper is connected directly to the pin by a standard (off-the-shelf) rod end. This connection detail performed to expectation and was utilized in the shake table testing.

The other two connection details utilized steel plates between the two toggle braces. The one utilized an arrangement with a very high strength steel plate (automobile spring leaf) as shown in Figures 2-16 and 2-17. Rotational capability was achieved by bending of the spring leaf, which developed bending stresses in excess of 830 MPa (120 ksi). The connection performed well, however, it exhibited notable deformations in the

spring leaf, which reduced the effectiveness of the system in magnifying displacement.

The other connection detail utilized a bent steel plate as illustrated in Figures 2-18 and 2-19. In this case, hinging action developed with the formation of plastic hinges in the bent plate. The connection was subjected to a large number of tests within the frame of Figure 2-8. A total of 30 fully-reversed cycles at a frame lateral displacement of 6.35 mm and 40 fully-reversed cycles at a frame lateral displacement of 12.5 mm were conducted. While the bent plate showed some distortion (see Fig. 2-19), the arrangement perform very well through the entire testing sequence.

Figure 2-20 presents a comparison of recorded lower damper displacements versus frame displacements graphs in three cases of connection detail. In the tests at frequency of 0.05 Hz the damper force is very small so that the toggle brace has negligible deformations. In the tests at frequency of 2 Hz, the damper force is large (approximately 6 kN or 1.35 kips) and causes some notable deformation of the toggle brace system. This is reflected in the hysteresis seen in the damper displacement-frame displacement graphs. An examination of these graphs reveals displacement magnification factors of about 2.6 for the pin and bent plate connections and about 2.2 for the spring leaf connection. The theoretical value is 2.66 (eq. 2-7). That is, the pin and bent plate connections performed as expected, whereas the spring leaf connection reduced the effectiveness of the toggle brace system. However, when the issue of out of plane buckling is considered in large scale applications, the cost of a properly detailed pin may be very high. Thus, the bent plate connection detail may become the preferred option.

2.7 Effect of Toggle Brace Stiffness

The results presented in the preceding subsection demonstrate that the stiffness of the toggle brace may have an important role. It should be noted that the theory of sections 2.2 to 2.4 is based on the assumption of infinite stiffness.

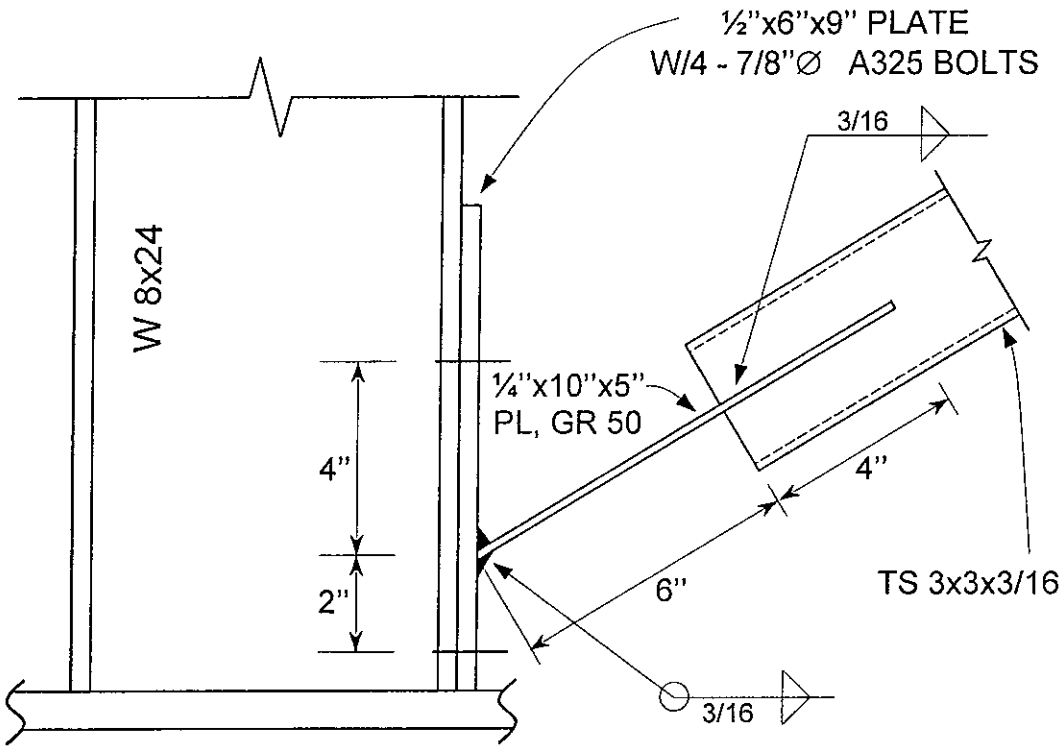

FIGURE 2-12 **Detail of Connection of Toggle Brace to Column (Sections per AISC, 1 in=25.4mm)**

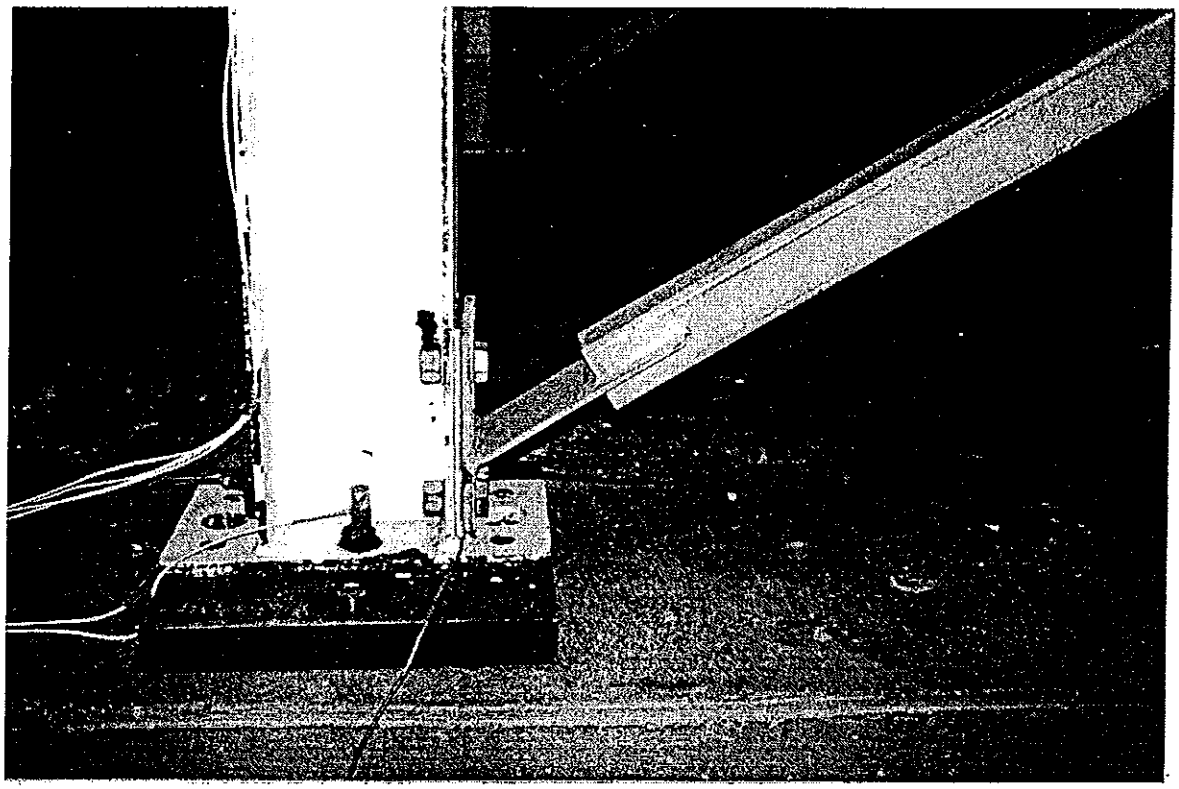

FIGURE 2-13 View of Toggle Brace to Column Connection

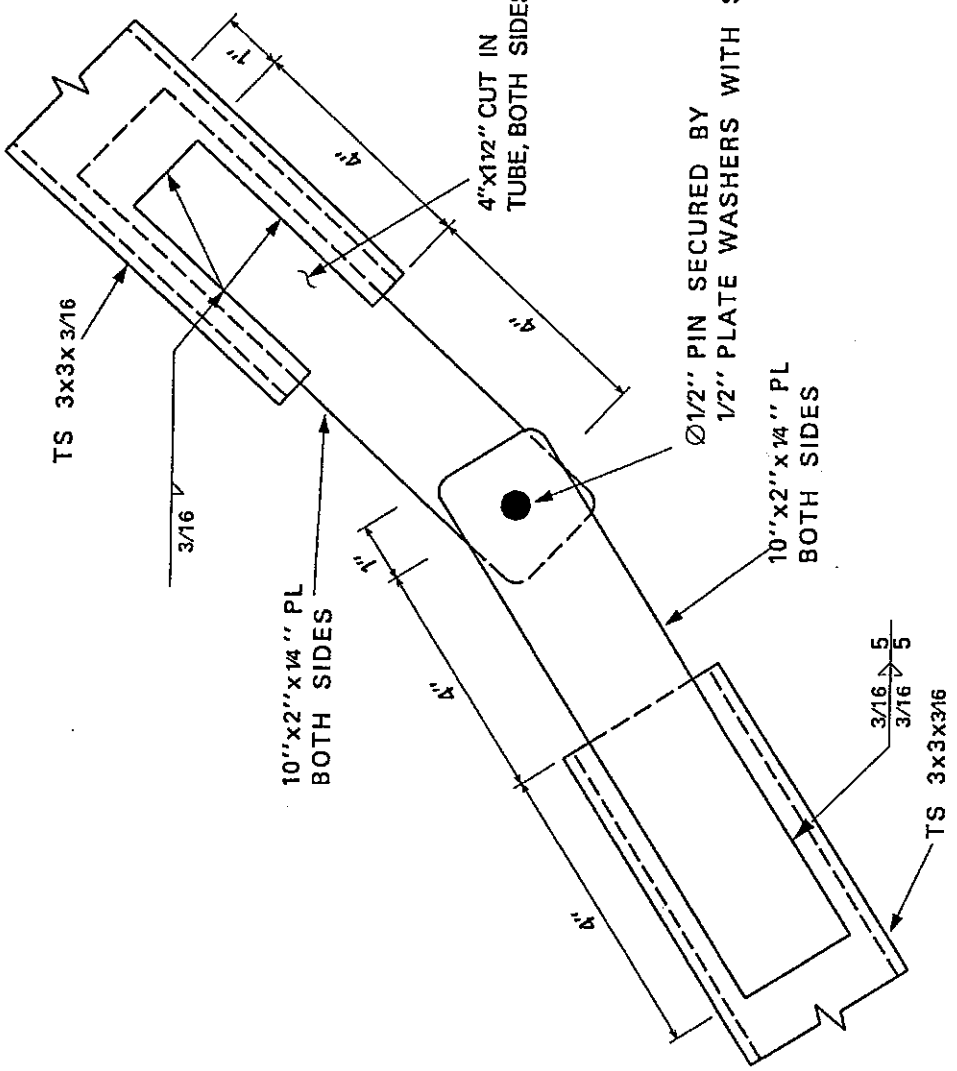

FIGURE 2-14 Detail of True Pin Connection of Toggle Braces (1 in. = 25.4 mm)

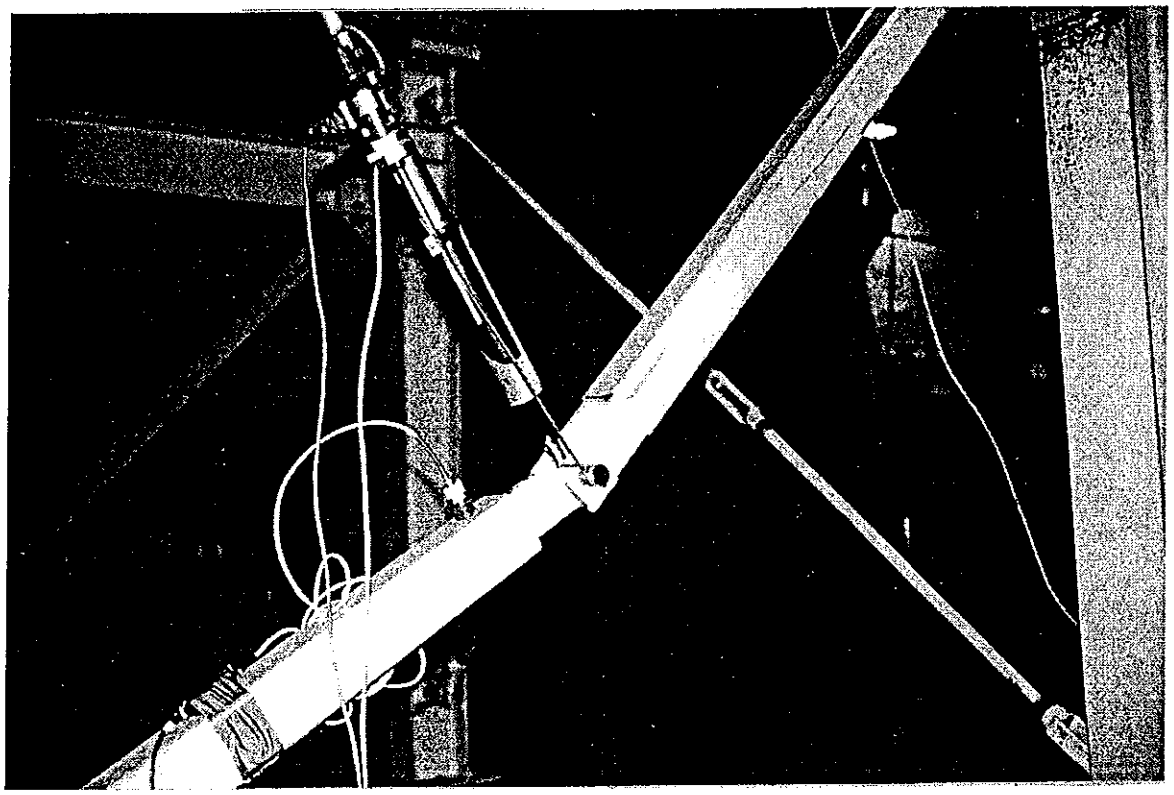

FIGURE 2-15 View of True Pin Toggle to Damper Connection

The effect of the toggle brace flexibility is to reduce the damper displacement from f u to f u–F_D/K_b, where F_D is the damper force and K_b is the stiffness of the toggle brace-frame assembly. This stiffness is determined by applying a force along the damper axis (direction AB in Figure 2-8) while maintaining the frame lateral displacement at a prescribed amount, and calculating the displacement of point A (Fig. 2-8) along the damper axis.

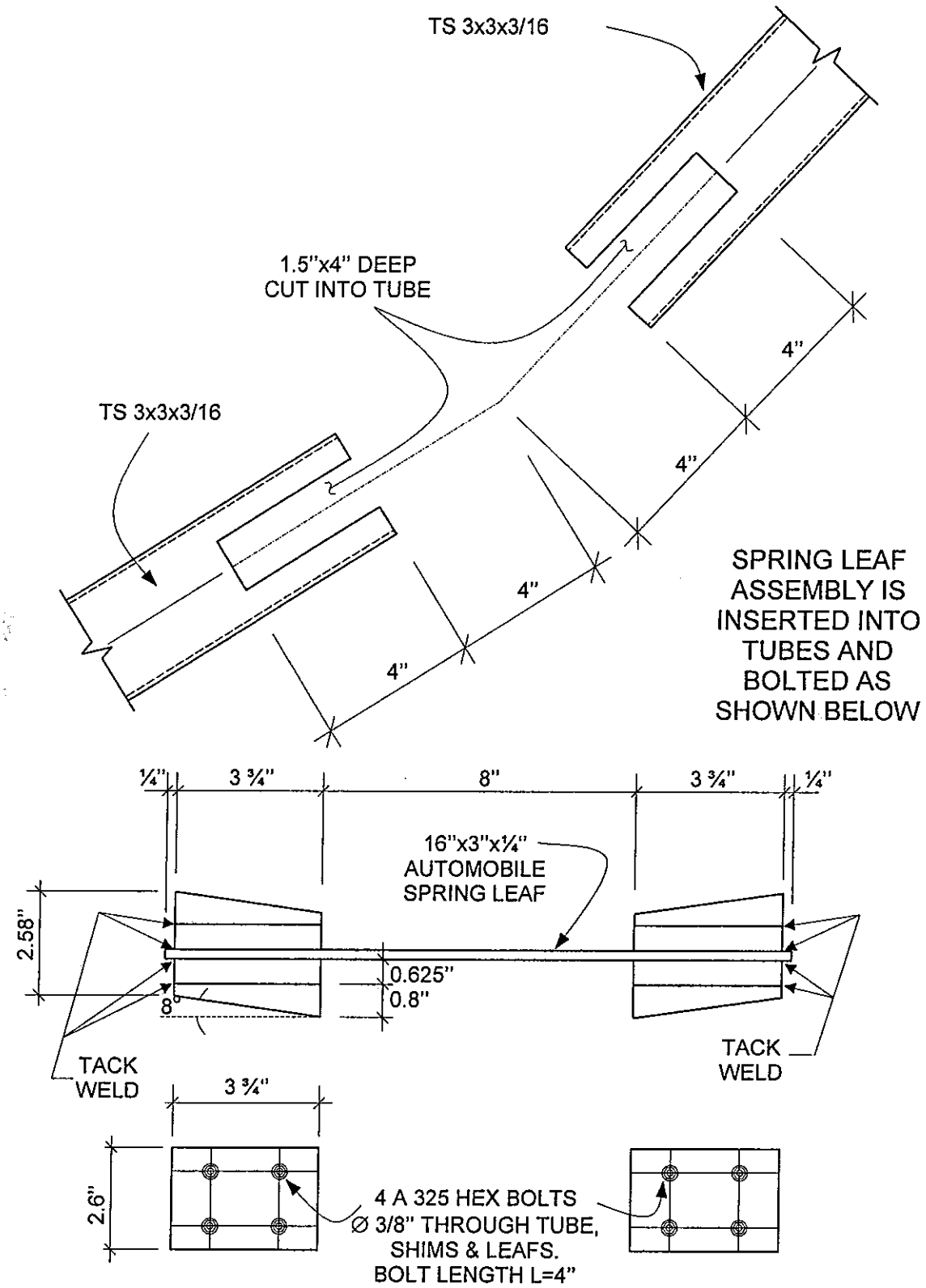

FIGURE 2-16 Spring Leaf Detail for Connection of Toggle Braces (1 in.=25.4 mm)

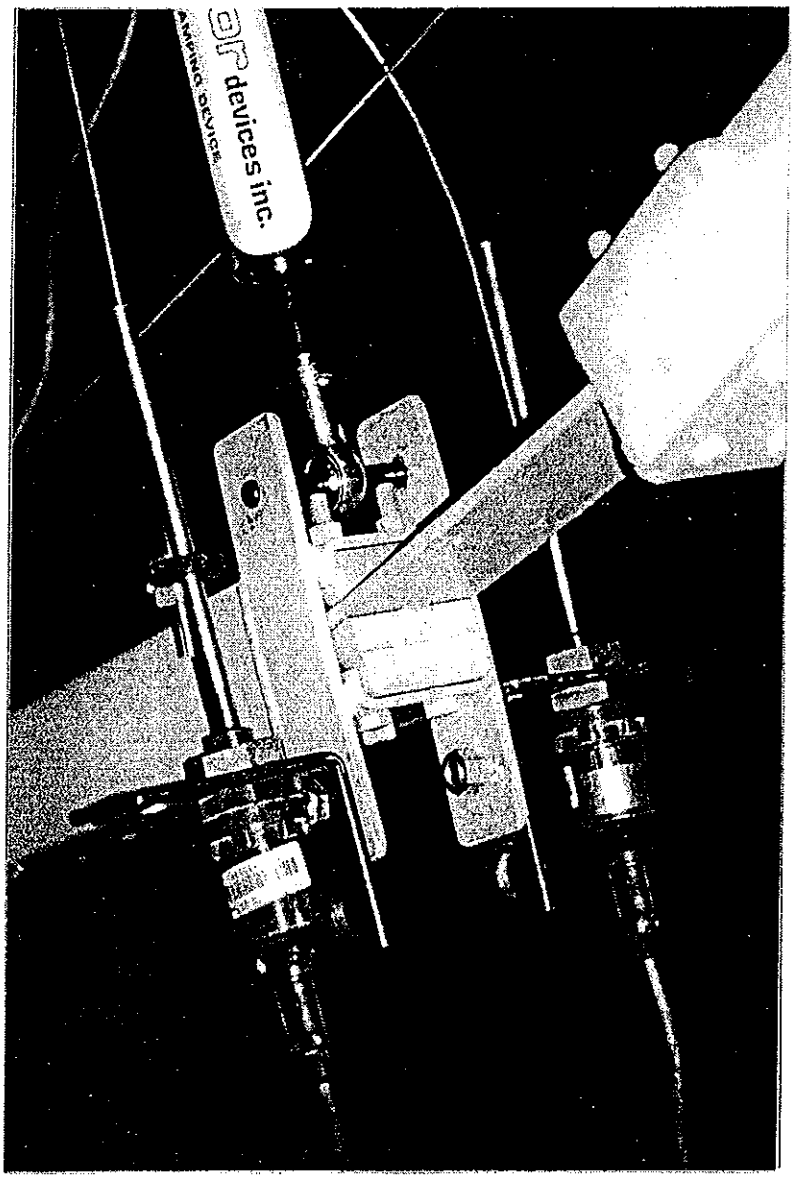

FIGURE 2-17 View of Spring Leaf Connection Detail

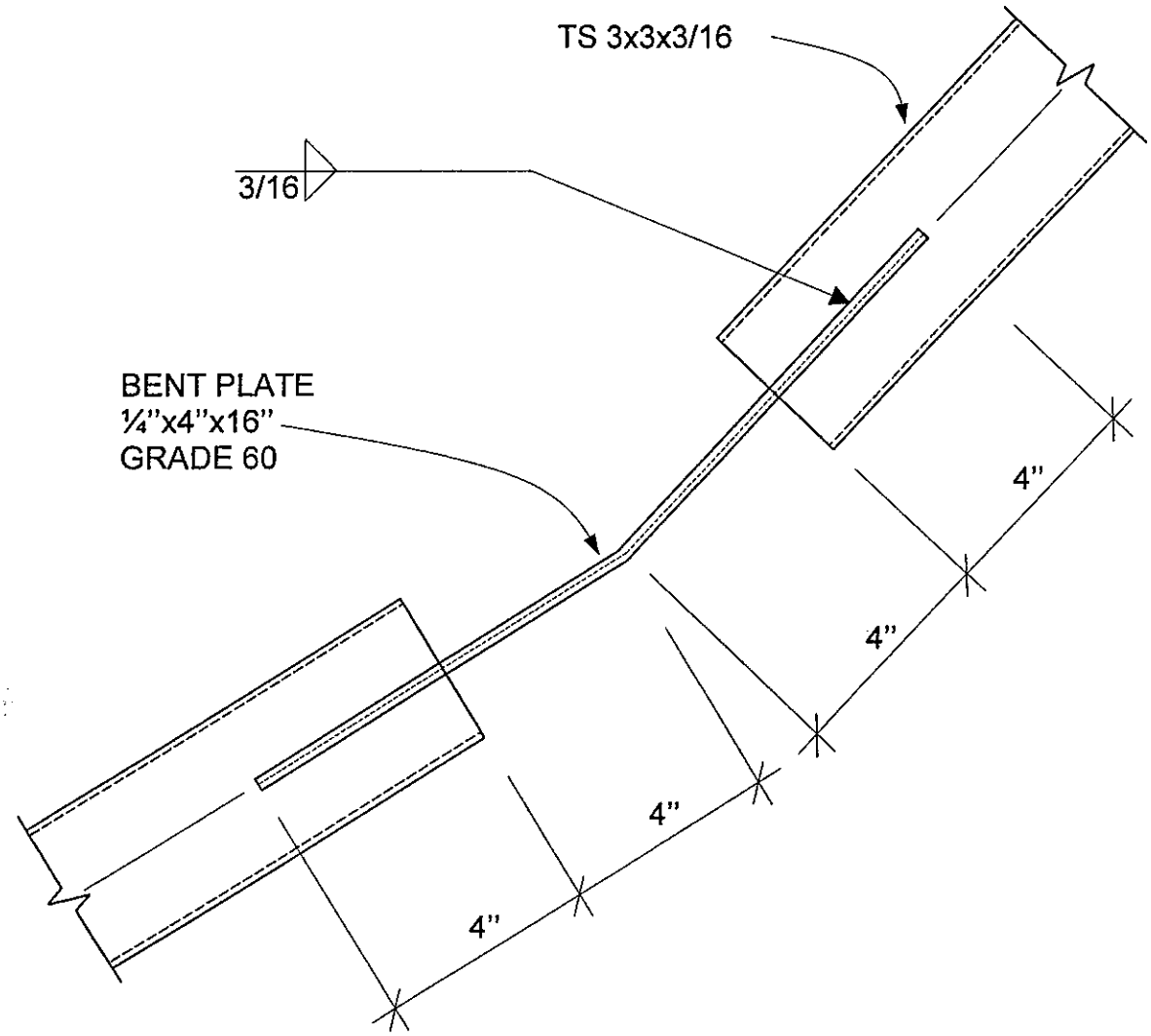

FIGURE 2-18 Bent Plate Detail for Connection of Toggle Braces (1in. = 25.4 mm)

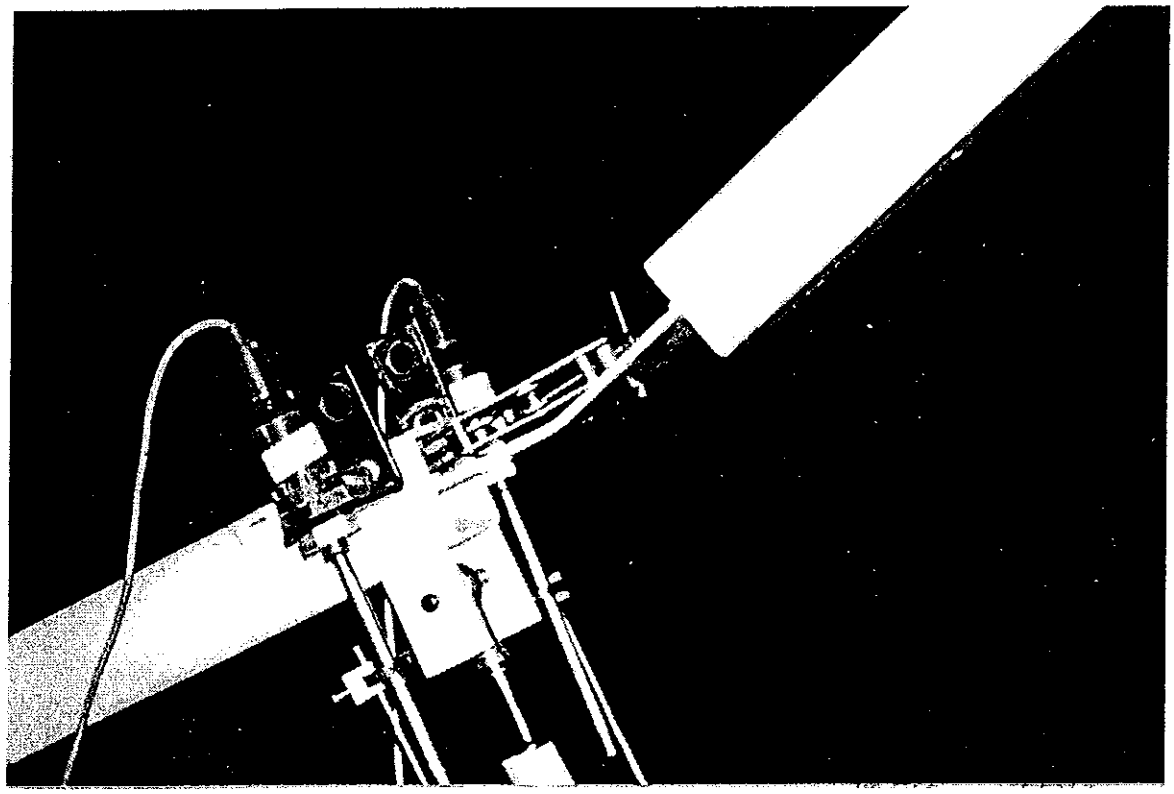

FIGURE 2-19 View of Bent Plate Connection Detail

The stiffness of the assembly is affected by geometric nonlinearities due to the shallow truss configuration of the toggle brace system. For the tested configuration, the angle between the toggle and line DC (Fig. 2-8) is about 7°. On lateral movement of the frame, the angle varies between about 6° and 8°. That is, the configuration is not very shallow and geometric nonlinearities are not significant. Calculations of stiffness at various angles of the toggle braces, utilizing large displacement formulation and for a damper force of 4.45 kN (1kip) resulted in values of stiffness K_b in the range of 4.2 to 4.7 kN/mm, whereas the linear stiffness was found to be 4.4 kN/mm (25 kip/in). These values are valid for the pinned toggle brace configuration.

The effects of the toggle brace flexibility are:

(1) Reduction of damper displacement so that

$$u_D = f u - \frac{F_D}{K_b} \tag{2-25}$$

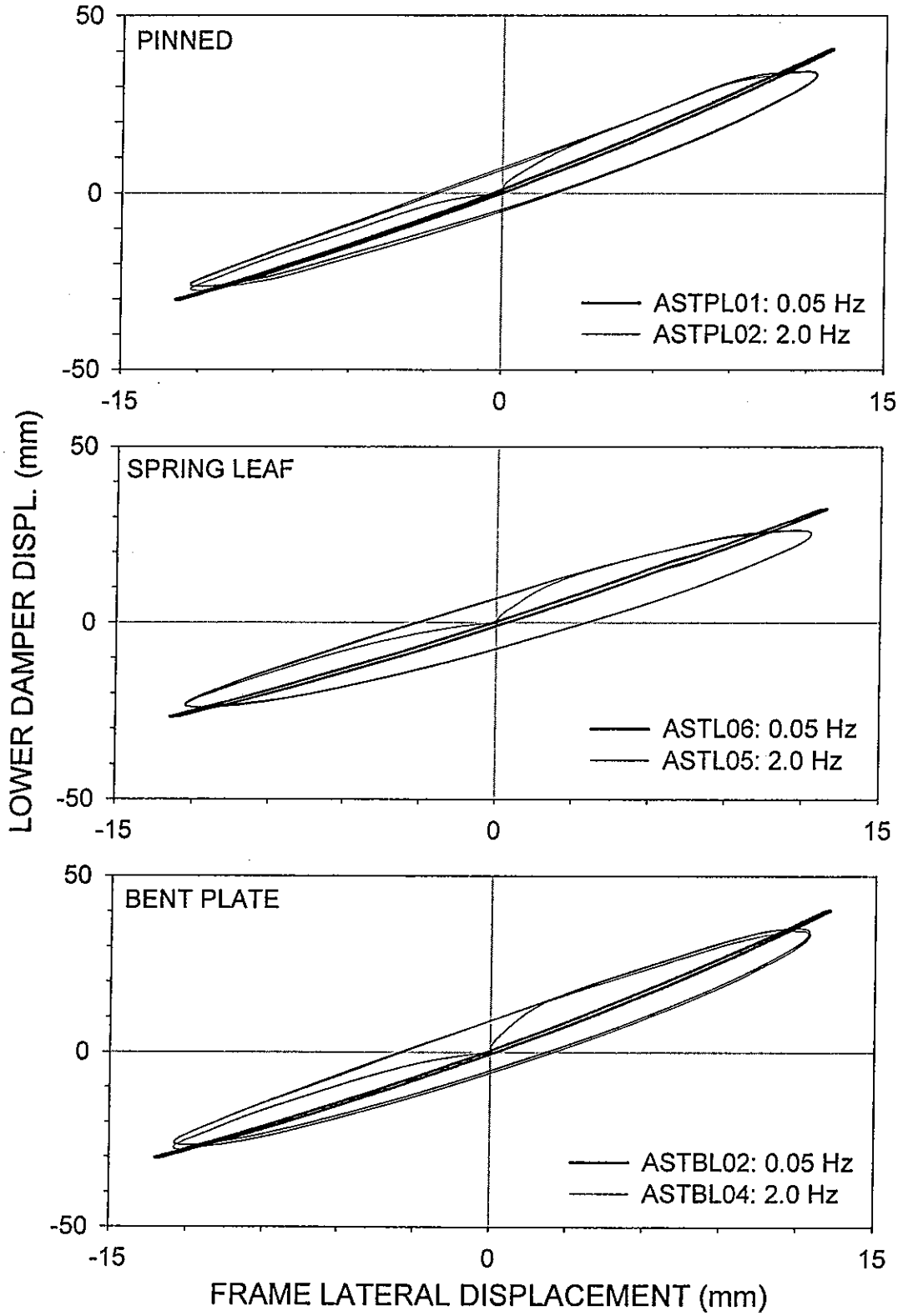

FIGURE 2-20 **Comparison of Performance of Three Toggle Brace Connection Details**

(2) Modification of frame damping force-frame lateral displacement relation. This relation is given by (2-19) for the case of infinite brace stiffness. The modified relation is obtained by use of equations (2-14), (2-25) and (2-17) to be

$$F + \frac{C_o}{K_b}\dot{F} = C_o f^2 \dot{u} \tag{2-26}$$

That is, the relation is changed from a purely viscous fluid one (eq. 2-19) to a viscoelastic fluid relation. Quantity $C_o/K_b = \tau$ is known as the relaxation time. The implications of this change in relation are (Constantinou et al., 1997):

(a) Introduction of additional lateral stiffness to the frame

$$K' = \frac{C_o f^2 \tau \omega^2}{1 + \omega^2 \tau^2} \tag{2-27}$$

where ω is the frequency of the motion.

(b) Modification of the damping coefficient of the frame to

$$C' = \frac{f^2 C_o}{1 + \omega^2 \tau^2} \tag{2-28}$$

Note that for infinite brace stiffness $C' = f^2 C_o$ (eq. 2-19).

(c) Change of the phase angle between the frame damping force, F, and the lateral frame displacement, u, from 90° to Φ, where

$$\tan\Phi = \frac{1}{\omega\tau} \tag{2-29}$$

Based on the values of C_o = 15.7 N-s/mm (from testing of the damper) and K_b = 4.4 kN/mm (from analysis of the system), we calculate for frequency of 2 Hz (test data at this frequency will be presented next) and lower damper placement: K' = 0.06 kN/mm (by comparison, the frame had stiffness of 3.8 kN/mm), C=0.998 $f^2 C_o$ and Φ = 87.4°. That is, the viscoelastic effects are insignificant and the toggle brace system behaves as if it were rigid.

The frame of Figure 2-8 was modified by converting the connection of the beam to the left column to rigid. This was accomplished by bolting stiffened angles to the flanges of the beam and column. In this configuration the frame had a lateral stiffness of about 3.8 kN/mm. Considerable contribution to the stiffness was provided by the simple

connections of the beam to the other column and of the columns to the supporting beam. The moment-rotation relations of these connections depended on the axial load in the bolts and surface condition of the connected steel elements (both varied during the testing program due to frequent disassembly and modifications of the frame), and level of deformation in the frame.

The frame was furnished with a lower damper in the pinned toggle configuration (as shown in Fig. 2-8), and subjected to a lateral frame sinusoidal movement of 2 Hz frequency and amplitude of 6.35 mm (0.25 in.). The recorded response is presented in Figure 2-21. For comparison, Figure 2-22 presents the recorded response at frequency of 0.05 Hz. It may be concluded that energy dissipation in the frame is almost entirely provided by the damper.

There is a number of interesting observations to be made in the results presented in Figure 2-21:

(1) The peak damper displacement is less than what is predicted by theory (u_D = fu = 2.66 x 6.35 = 16.9 mm; the experimental is 13.9 mm). The origin of this phenomenon may be traced in the damper displacement-lateral displacement graph which flattens as the lateral displacement approaches its peak value. This behavior, which is more pronounced for positive lateral displacement (that is, movement causing extension of the lower damper), has been observed in all tests regardless of the type of connection (e.g., see Fig. 2-20). Analysis of the frame, however complex, could not reproduce this behavior. Observing, however, that the difference of 3 mm in the theoretical and experimental values of the damper displacement corresponds to mere 1.1 mm lateral frame displacement, the observed behavior may be explained by a very small slippage in the joints of the frame.

(2) The peak damper force is nearly identical to the theoretically predicted value (eq. 2-14). This is true despite the lower peak value of the damper displacement. Again, this may be explainable by a very small joint slippage.

(3) From the plot of damper displacement versus lateral displacement we observe that at zero lateral displacement, the damper displacement is between 2.5 and 3.5 mm depending on the direction of movement. This displacement occurs at nearly the

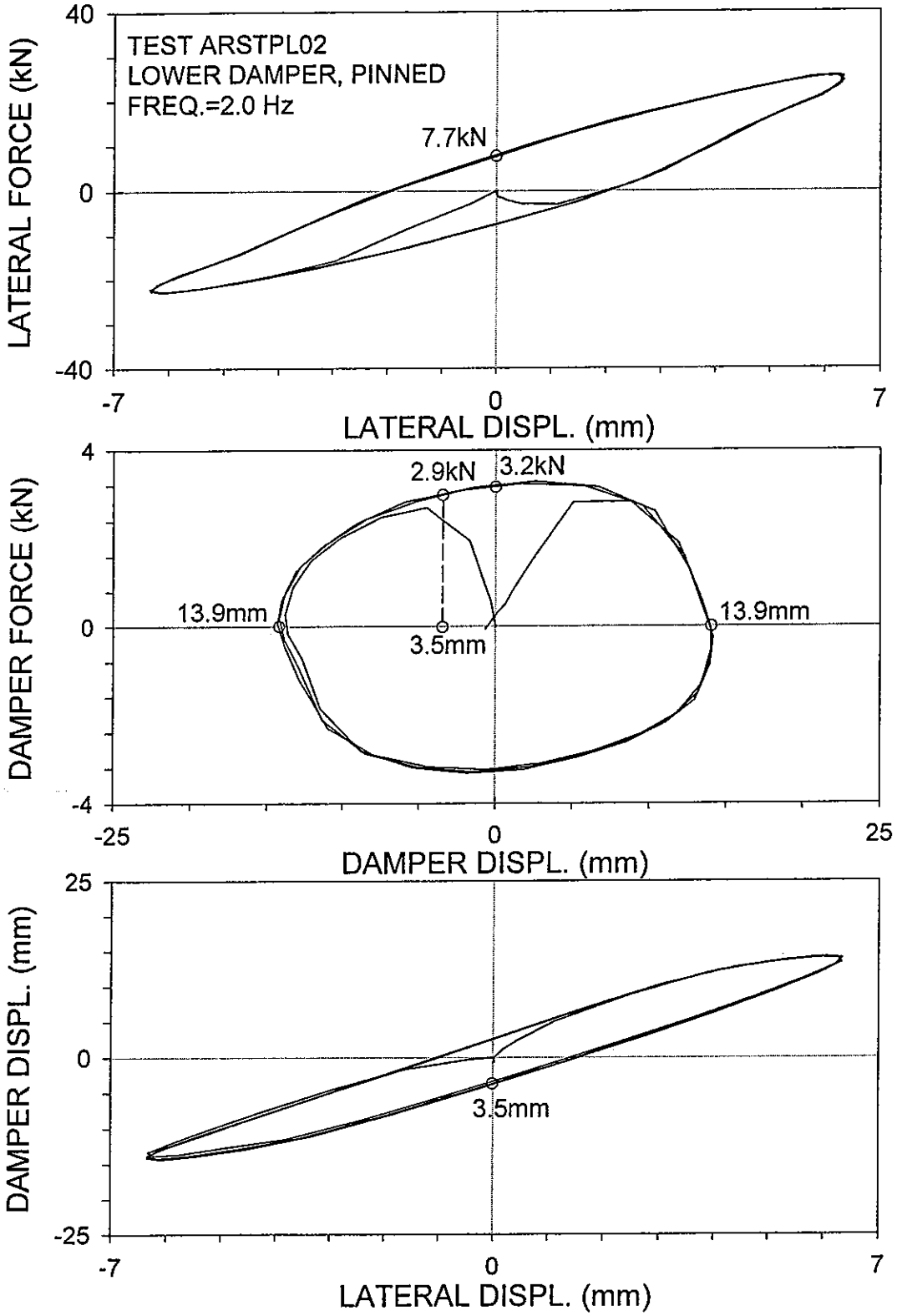

FIGURE 2-21 Recorded Response of Frame for High Frequency Lateral Motion

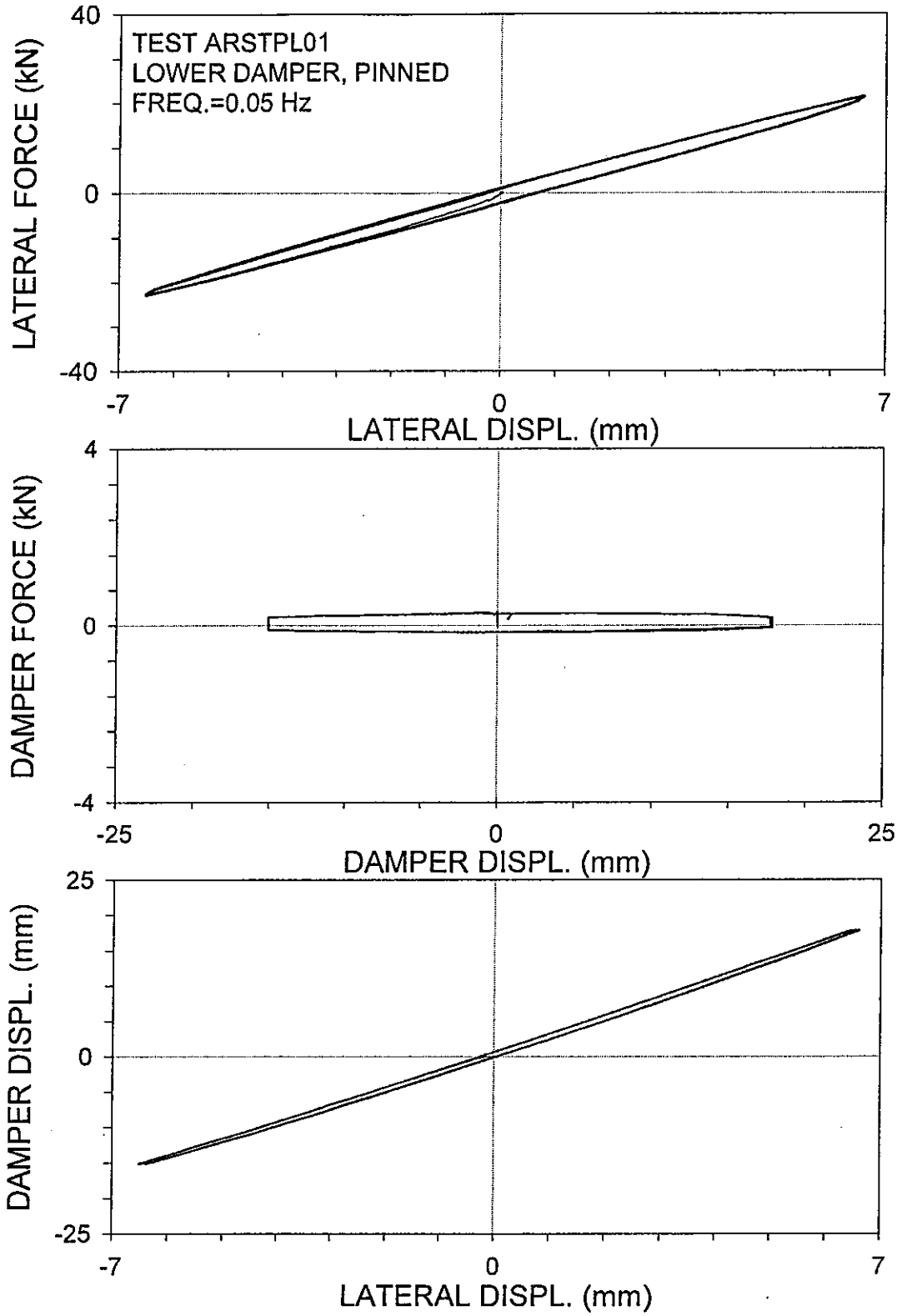

FIGURE 2-22 Recorded Response of Frame for Nearly Static Lateral Motion

instant of maximum damper force, which is equal to 3.2 kN. If this were the result of deformation in the toggle brace system, it would have been equal to $F_D/K_b = 3.2/4.4 =$ 0.73 mm. The difference between this value and the 3.5 mm experimental value is rigid body motion that corresponds to about 1 mm lateral frame movement, which is explainable by the joint slippage assumption.

(4) The peak value of the damping component of the lateral frame force (force at zero lateral displacement) can be predicted by eq. (2-17). This peak value occurs at an instant at which the damper force is slightly less than its peak value (2.9 kN at damper displacement of 3.5 mm due to delays caused by rigid body movement and elastic deformation in the toggle braces). Indeed, (2-17) predicts $F = f F_D = 2.66 \times 2.9 = 7.7$kN, which is the experimental value.

That is, the recorded response of the frame is almost entirely predictable by the small rotation theory and on the assumption of very small rigid body motion in the frame system. The implications of this rigid body motion are:

(a) A small reduction in the ability of the toggle brace-damper system to dissipate energy. This is primarily manifested as thinning of the lateral force-lateral displacement loops in the neighborhood of the peak displacement (see Fig. 2-21).

(b) A reduction and equaling of the positive and negative values of the peak damper displacement. This is a beneficial effect since it is first safer for the damper and second it allows use of the simple small rotation theory for the analytical prediction.

An analytical simulation of the response of the tested frame (test ARSTPL02, Fig.2-21) was performed using the computer code ANSYS (Swanson Analysis Systems IP, 1996). Both linear and large deformation analyses were performed. The results are presented in Figure 2-23. Of interest is to observe the differences in the predicted response by the two methods of analysis. The large displacement predicts more damper displacement for positive lateral movement and lesser for negative lateral displacement. As a result of this behavior, the lateral force displacement loops appears slightly distorted. Both methods of analysis predict a small delay between damper and lateral displacement, which is consistent with the low flexibility of the toggle braces. The actual measured delay could not be predicted given that it was likely caused by very small

slippage in the joints. Nevertheless, the linear theory provides a prediction of the lateral force-lateral displacement relation that is of acceptable accuracy.

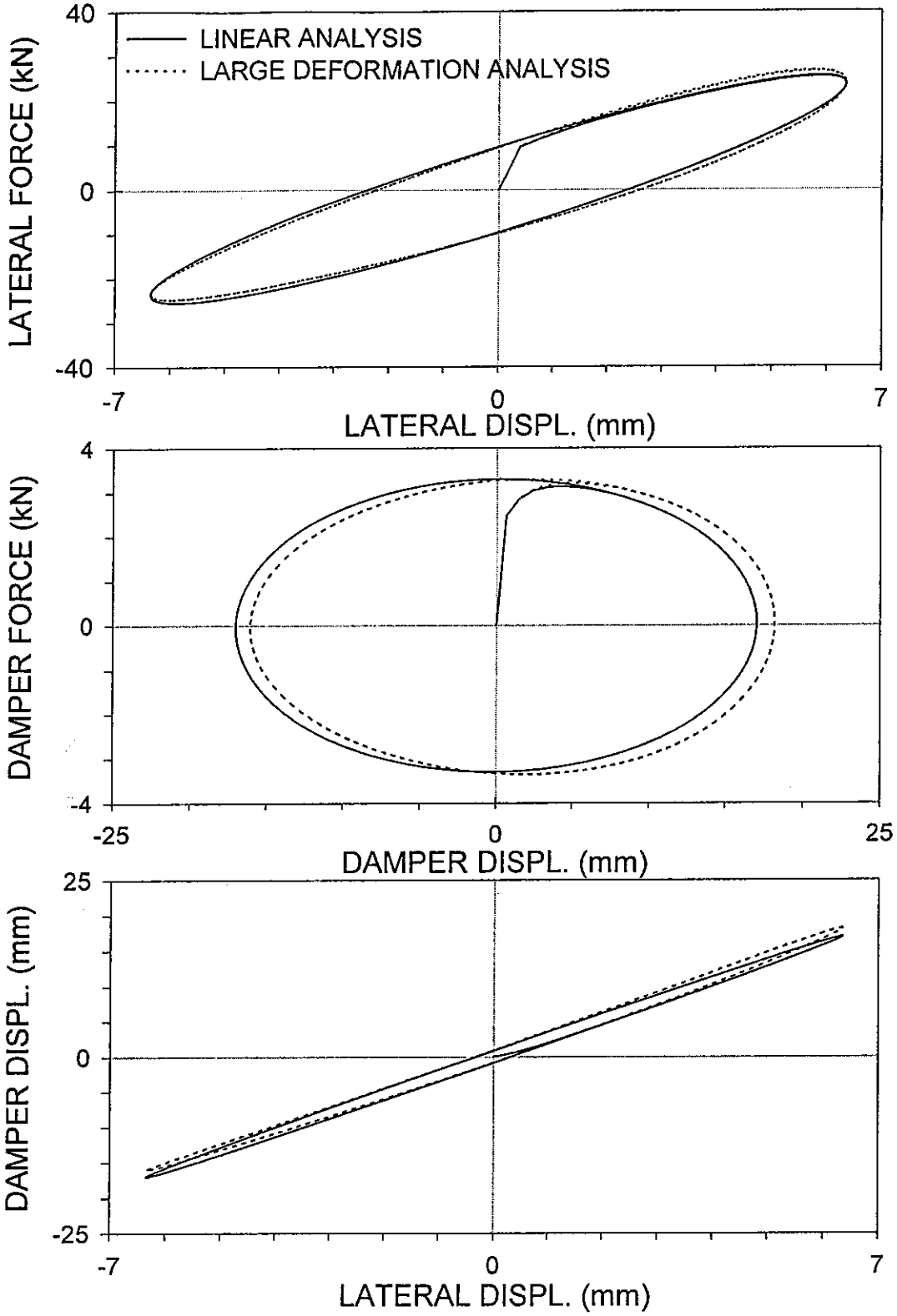

FIGURE 2-23 **Analytical Simulation (in ANSYS) of Frame Response in Test ARSTPL02 (compare to Fig. 2-21)**

SECTION 3
TESTED STRUCTURE AND TESTING PROGRAM

3.1 Description of Tested Structure

The tested structure was designed as a half length scale steel frame. It consisted of two identical plane frames that could be tested individually on the floor and together, with a mass attached on their tops, on the shake table. Appendix A provides detailed drawings of the tested structure.

The frame featured simple connections with the option of converting selected or all of its connections to rigid. For the beam to column connections, this could be achieved by bolting stiffened angles as shown in the drawings of Appendix A. The column base plates were designed for rigid connections. The base plates were bolted, using either two or six bolts, to heavy plates, which were bolted onto the shake table. In the floor testing, the column base plates were directly bolted to the top flange of a W21x50 beam. The two-bolt configuration provided limited rotation capability at the base, whereas the six bolt configuration was effectively rigid.

Figures 3-1 and 3-2 show views of the frame during floor testing. A range of frame connection details, the three different toggle brace connection details described in Section 2, and upper and lower damper positions were tested. The floor testing was conducted in order

(a) to study the behavior of various toggle brace connection details, and

(b) to confirm the predictions of theory. Accordingly, the testing was conducted only under imposed sinusoidal motion of various frequencies and amplitudes.

Figure 3-3 shows a view of the tested frame on the shake table. Two concrete blocks, weighing 143 kN (32 kips), were mounted on top of two identical frames. The connections of the concrete blocks to the tops of the frame were detailed to transfer minimum moment. The majority of tests were conducted with one beam to column connection being rigid and the other being simple. This configuration resulted in the desired frequency characteristics of the model structure. The fundamental frequency of the model structure was equal to 3.2 Hz, which, for length scale $S_L = 2$ and time scale S_T

$= \sqrt{2}$, nearly corresponded to the desired frequency in the prototype scale of 2.5 Hz (period of 0.4 sec.).

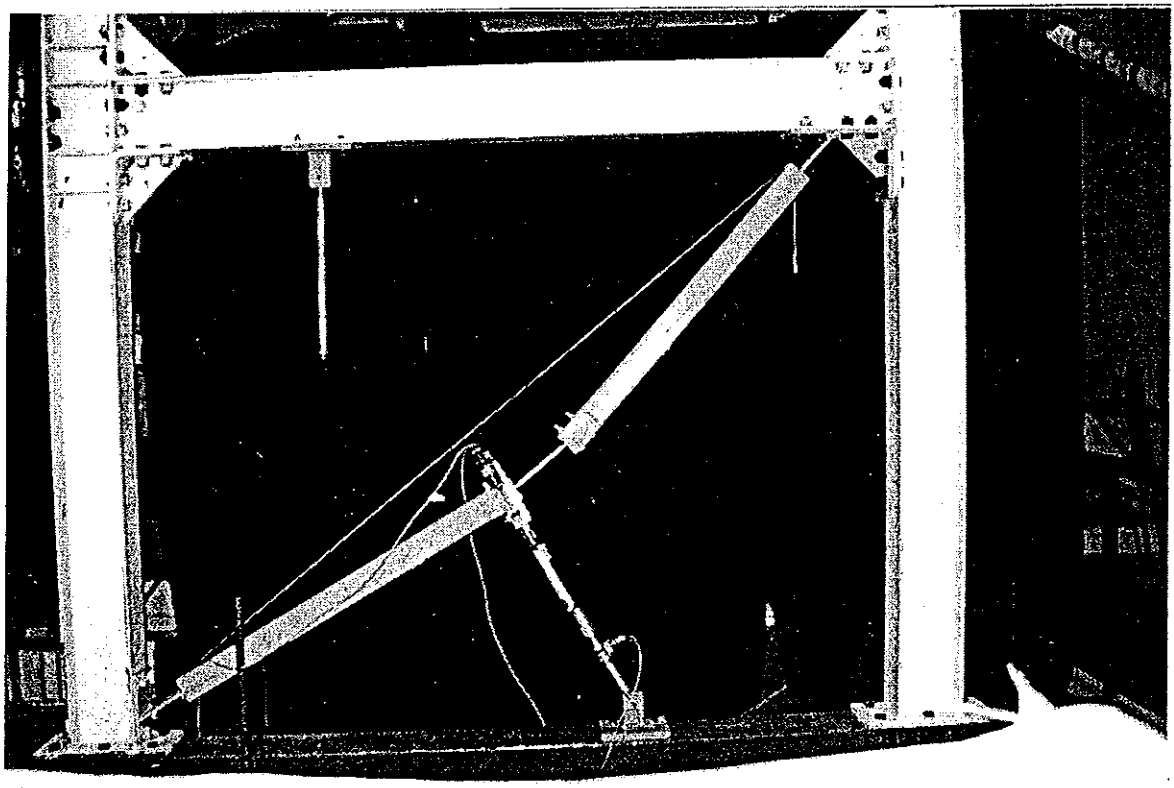

FIGURE 3-1 Front View of Frame with Lower Damper during Floor Testing (Rigid-Rigid Connections)

3.2 Floor Testing Program

The floor testing was conducted with an actuator attached to the tested frame as shown in the drawings of Appendix A and to a reaction frame, which may be seen in Figure 3-2. The actuator was used to impose prescribed motion of the frame at the beam to column joint. This motion was sinusoidal of frequency in the range of 0.05 Hz (quasi static conditions) to 4 Hz and amplitude in the range of 6.35 to 12.7 mm (0.25 to 0.5 in.). Measurements of the frame displacements, the damper (relative end to end) displacement, damper force and the force needed to impose the motion were made. The latter included the resisting force of the frame and the inertia force. The inertia force was estimated to

be insignificant (peak value in the tests at frequency of 4 Hz was less than 1.5-percent of the resisting force) and, thus, no correction has been made.

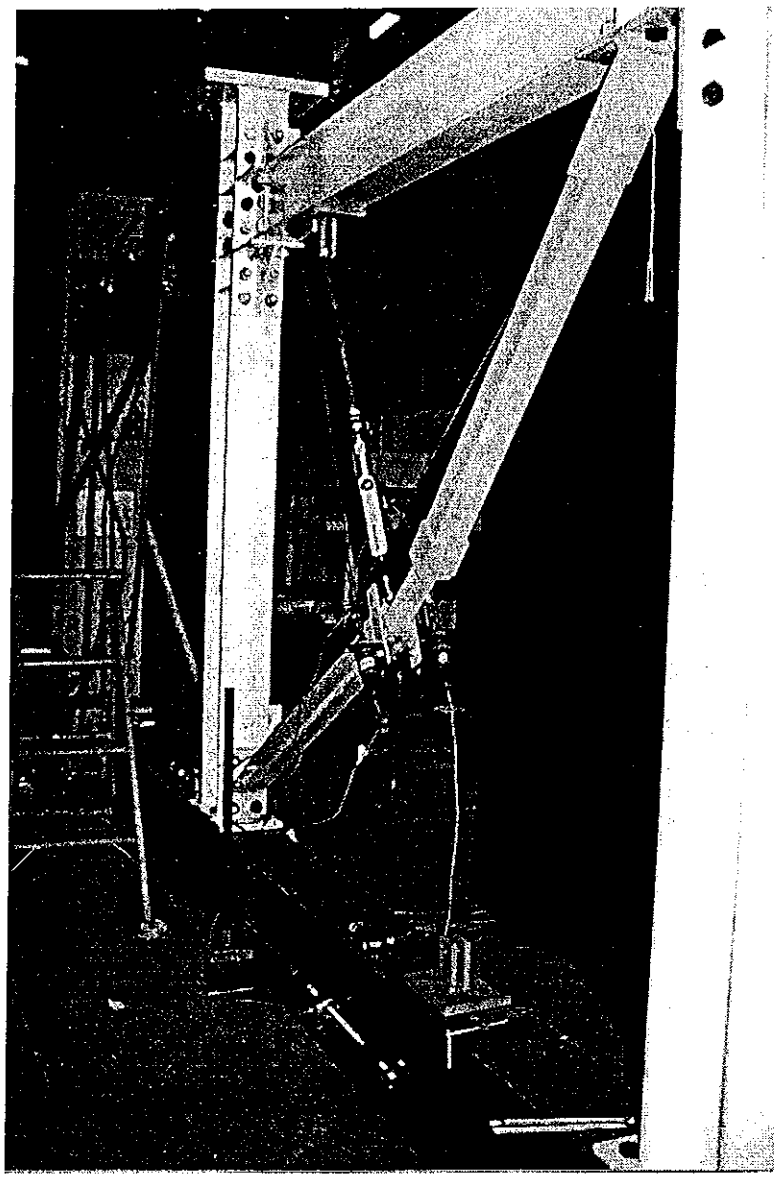

FIGURE 3-2 Front View at an Angle of Frame with Upper Damper during Floor Testing

3.3 Instrumentation of Model Structure for Shake Table Testing

Figures 3-4 and 3-5 present instrumentation diagrams of the tested structure. A complete list of monitored channels is presented in Table 3-1. A total of 32 channels

were monitored, of which only a small number resulted in useful measurements. The rest were used either for controlling the motion of the shake table, or for measuring other response quantities that could be useful in the case of unanticipated response. All measured signals were filtered using a low pass filter with a cutoff frequency of 25 Hz in the D/A and A/D input.

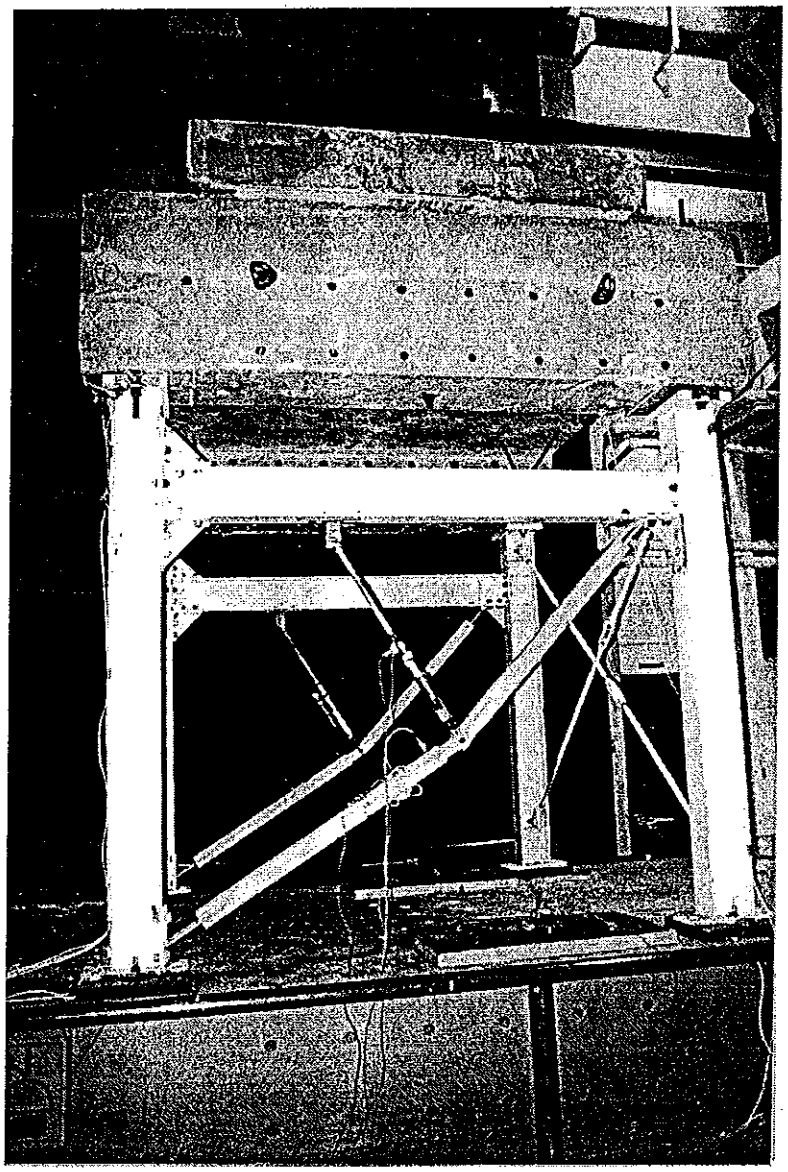

FIGURE 3-3 View of Frame on Shake Table

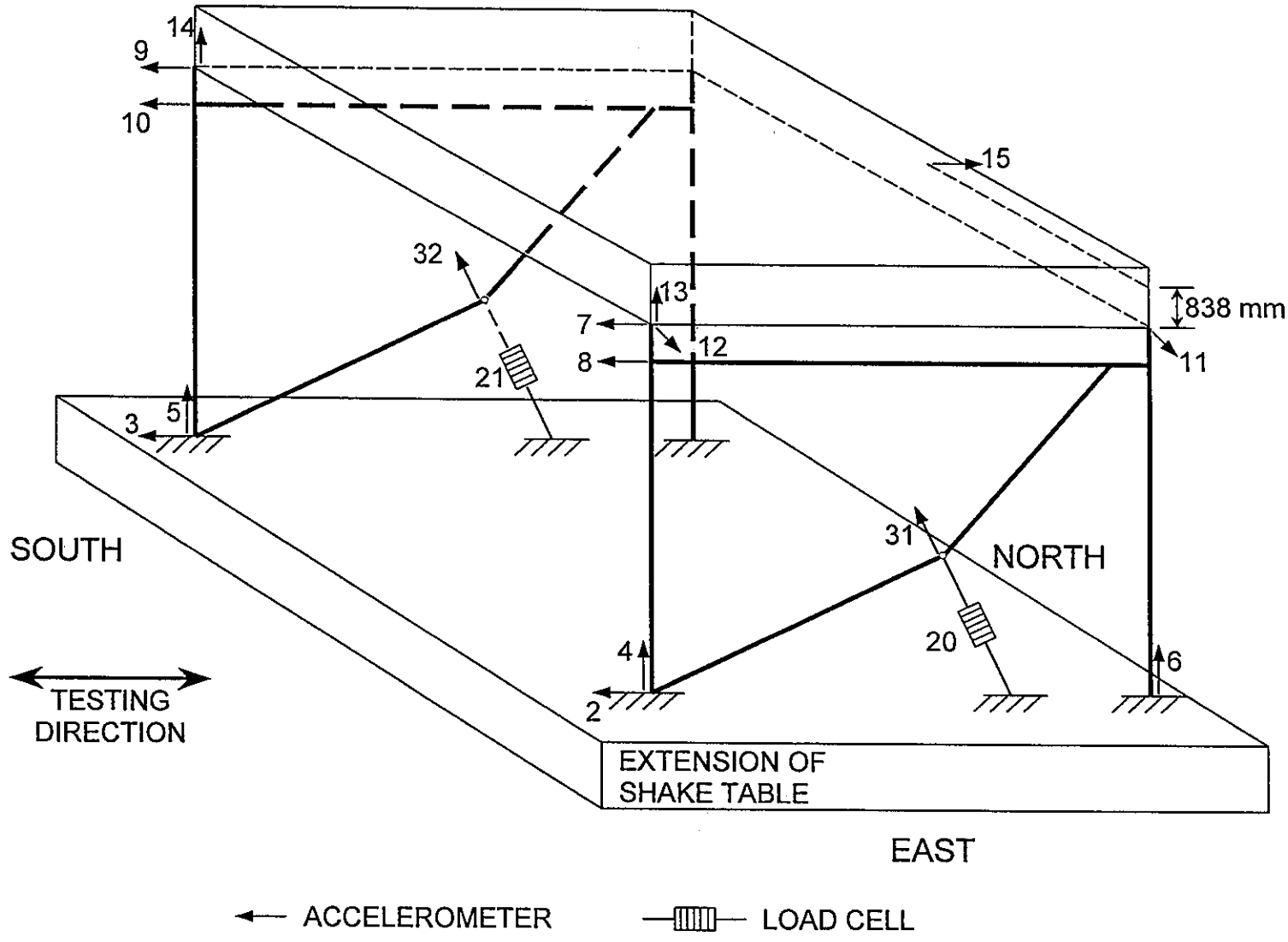

FIGURE 3-4 Accelerometer and Load Cell Instrumentation Diagram of Tested Structure

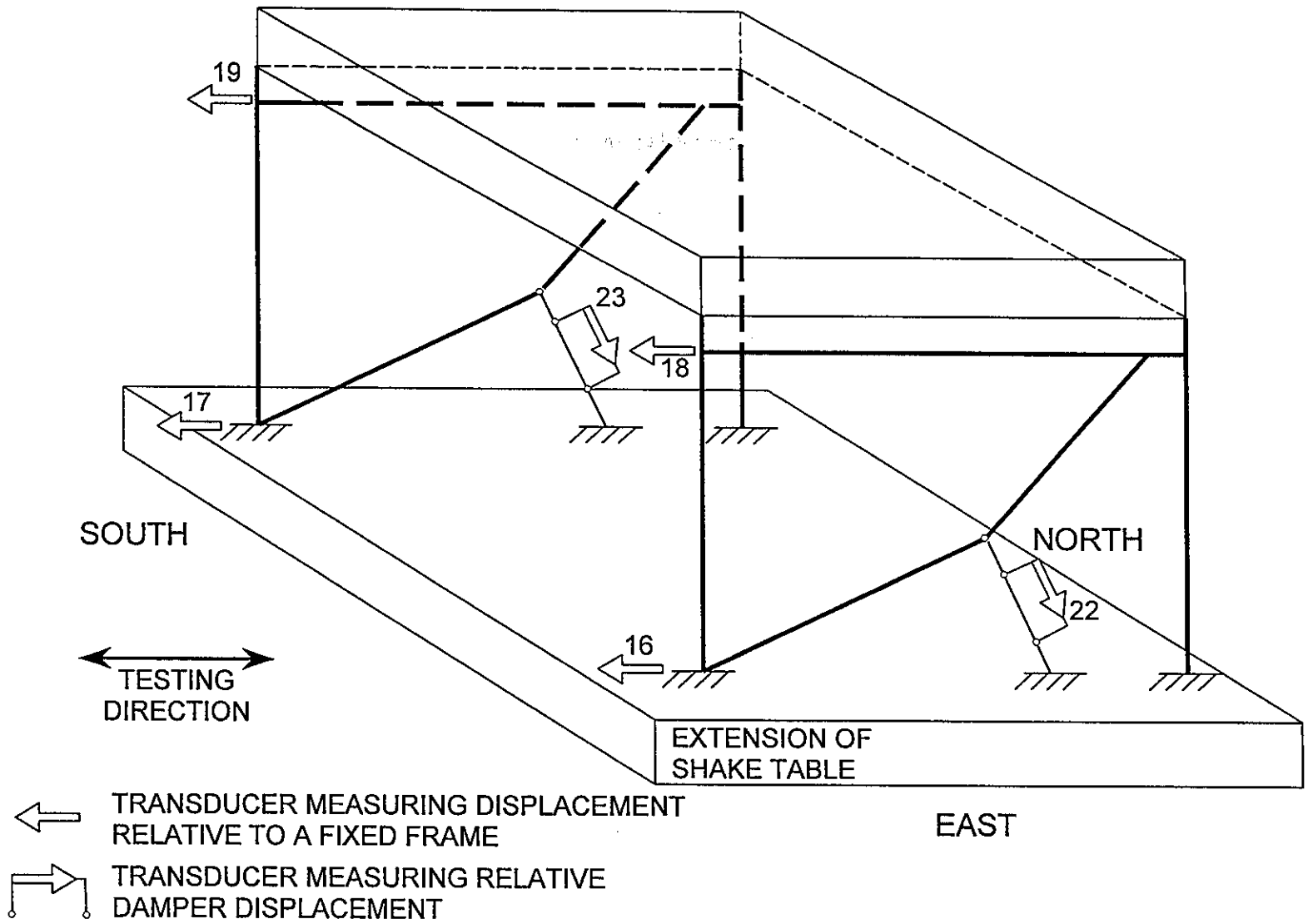

FIGURE 3-5 Displacement Transducer Instrumentation Diagram of Tested Structure

TABLE 3-1 List of Channels Utilized in Shake Table Testing (refer to Figs. 3-3 and 3-4 for location)

CHANNEL	INSTRUMENT	NOTATION	RESPONSE MEASURED	UNITS
1	/	TIME	Time	sec
2	Accelerometer	ABEH	Base Horizontal Accel.-E	g
3	Accelerometer	ABWH	Base Horizontal Accel.-W	g
4	Accelerometer	ABSEV	Base Vertical Accel.-SE	g
5	Accelerometer	ABSWV	Base Vertical Accel.-SE	g
6	Accelerometer	ABNEV	Base Vertical Accel.-NE	g
7	Accelerometer	ACTE	Column Top Horiz. Accel.-E	g
8	Accelerometer	ACJE	Column Joint Horiz. Accel.-E	g
9	Accelerometer	ACTW	Column Top Horiz. Accel.-W	g
10	Accelerometer	ACJW	Column Joint Horiz. Accel.-W	g
11	Accelerometer	ACTTN	Column Top Transverse Accel.-N	g
12	Accelerometer	ACTTS	Column Top Transverse Accel.-S	g
13	Accelerometer	ACTVE	Column Top Vertical Accel.-E	g
14	Accelerometer	ACTVW	Column Top Vertical Accel.-W	g
15	Accelerometer	ATBH	Top Block Horizontal Accel.	g
16	Displ. Transducer	DBE	Base Horiz. Displ.-East	in.
17	Displ. Transducer	DBW	Base Horiz. Displ.-West	in.
18	Displ. Transducer	DTE	Top Horiz. Displ.-East	in.
19	Displ. Transducer	DTW	Top Horiz. Displ.-West	in.
20	Load Cell	Dp_Frc_E	Damper Force-East	kips
21	Load Cell	Dp_Frc_W	Damper Force-West	kips
22	Displ. Transducer	Dp_Dsp_E	East Damper Displacement	in.
23	Displ. Transducer	Dp_Dsp_W	West Damper Displacement	in.
24	Displ. Transducer	Di_Dsp_E	East Diagonal Displacement	in.
25	Displ. Transducer	Di_Dsp_W	West Diagonal Displacement	in.
26*	Accelerometer	ALAT	Table Horiz. Accel.	g
27*	Displ. Transducer	DLAT	Table Horiz. Displ.	in.
28*	Accelerometer	AVRT	Table Vertical Accel.	g
29*	Displ. Transducer	DVRT	Table Vertical Displ.	in.
30	Displ. Transducer	DRIFT	Column Drift-East (DTE-DBE)	in.
31	Accelerometer	ADBE	Brace Joint Accel.-E	g
32	Accelerometer	ADBW	Brace Joint Accel.-W	g

E = East, W = West, N = North, S = South, SE = South East, SW = South West, NE = North East, * Channels Used to Control Shake Table

3.4 Shake Table Testing Program

Testing was conducted with white noise excitation for the identification of the dynamic characteristics and with seismic excitation. Most tests were conducted with horizontal only excitation. Selected tests were repeated with the vertical component of the excitation included.

Table 3-2 lists the earthquake motions used in the shake table testing together with some of their characteristics in prototype scale. Each record was compressed in time by factor of $\sqrt{2}$ to satisfy the similitude requirements of the half length scale model. Moreover, each of these records was applied with various scale factors, the maxima of which are presented in Table 3-2 as percentage of the actual record. For example, the El Centro motion was applied in various scales up to one and half times (150%) the actual record, that is, with peak acceleration being 0.51g.

Figure 3-6 presents the 5-percent damped acceleration spectra of some of the shake table motions together with the spectra of the actual motions in order to demonstrate the fidelity of reproduction of the actual motion.

TABLE 3-2 Earthquake Motions Used in Shake Table Testing and Characteristics in Prototype Scale (all components are horizontal)

NOTATION	RECORD	PEAK ACCEL. (g)	PEAK VEL. (mm/s)	PEAK DISPL. (mm)	MAX SCALE FACTOR*
El Centro S00E	Imperial Valley, May 18, 1940, component S00E	0.34	334.5	108.7	150
Taft N21E	Kern County, July 21, 1952 component N21E	0.16	157.2	67.1	300
Pacoima S74W	San Fernando, February 9, 1971, component S74W	1.08	568.2	108.2	50
Pacoima S16E	San Fernando, February 9, 1971, component S16E	1.17	1132.3	365.3	50
Miyagiken-Oki	Tohuku University, Sendai, Japan, June 12, 1978, component EW	0.16	141.0	50.8	300
Hachinohe NS	Tokachi-Oki earthquake, Japan, May 16, 1968, component NS	0.23	357.1	118.9	150
Mexico N90W	Mexico City, September 19, 1985, SCT building, component N90W	0.17	605.0	212.0	125
Sylmar 90	Northridge, January 17, 1994, County Hosp.-Parking Lot component 90	0.60	76.9	15.2	100
Newhall 90	Northridge, January 17, 1994, LA County Fire Station, component 90	0.58	74.8	17.6	50
Newhall 360	Northridge, January 17, 1994, LA County Fire Station, component 360	0.59	94.7	30.5	50
Kobe EW	Hyogo-Ken Nanbu Earthquake, Japan, January 17, 1995, JMA-Kobe, component EW	0.63	74.2	19.1	50

* used in testing as percent of actual record

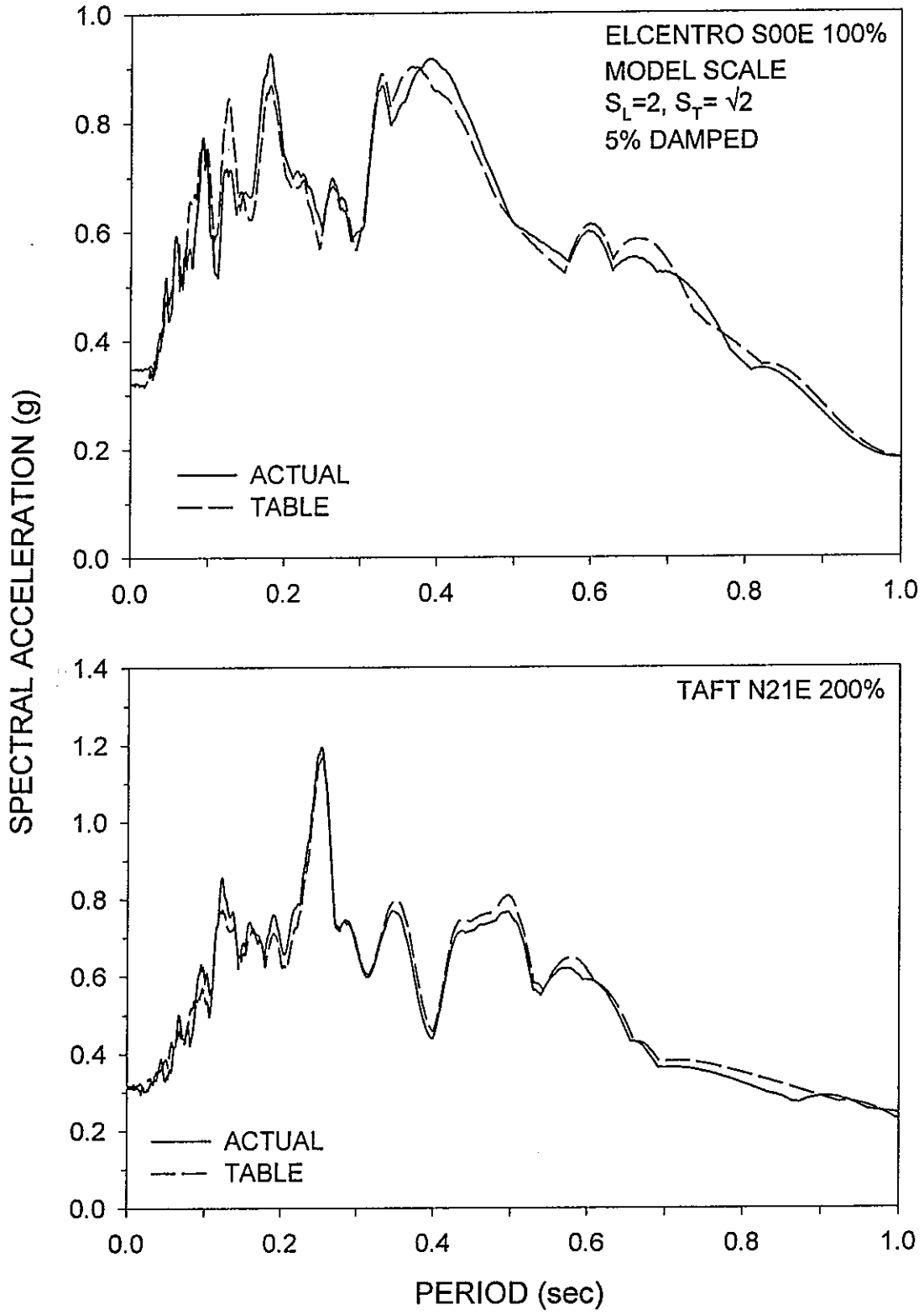

FIGURE 3-6 **Response Spectra in Model Scale of Actual Earthquake Motions and Motions Produced by Shake Table**

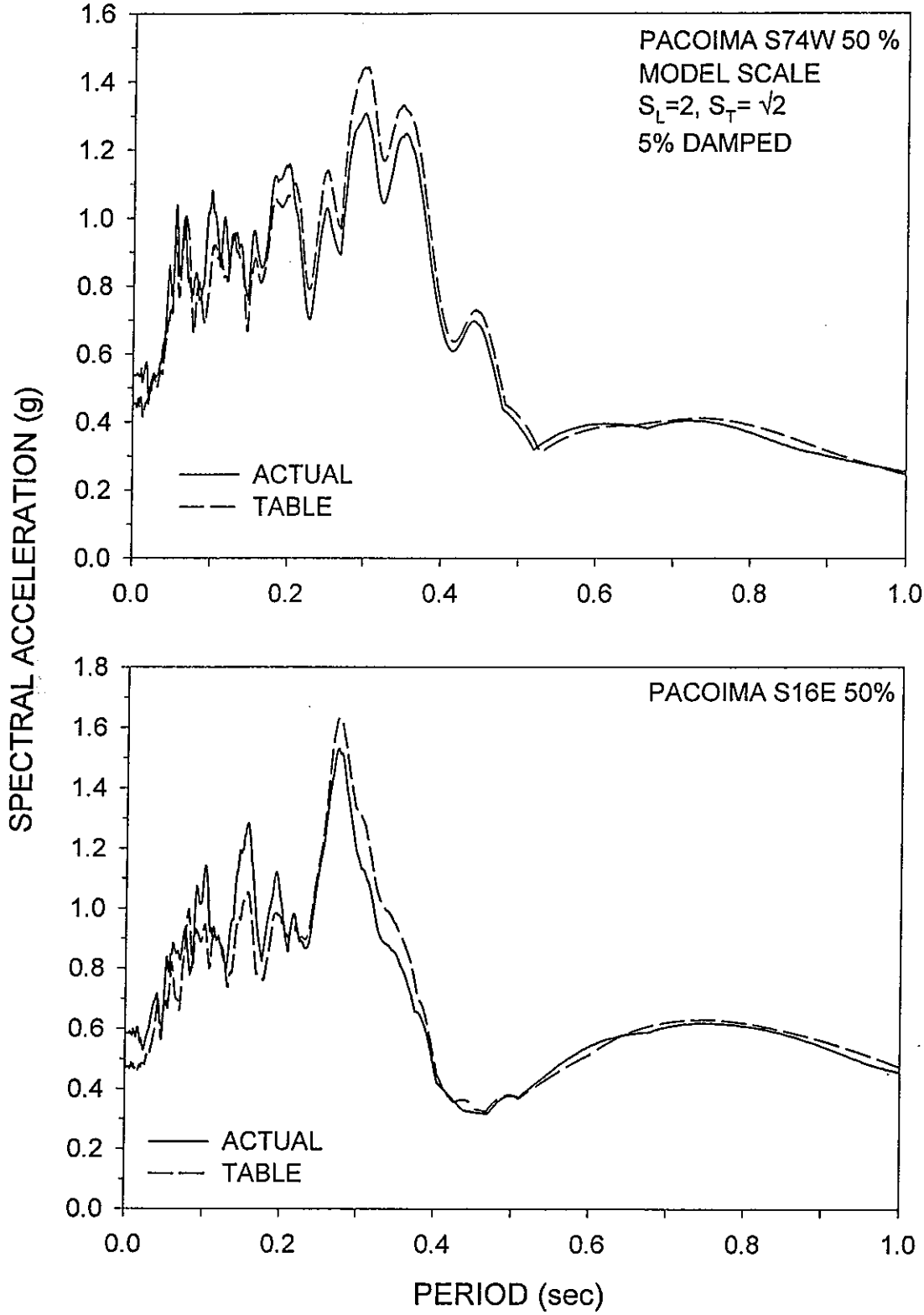

FIGURE 3- 6 continued

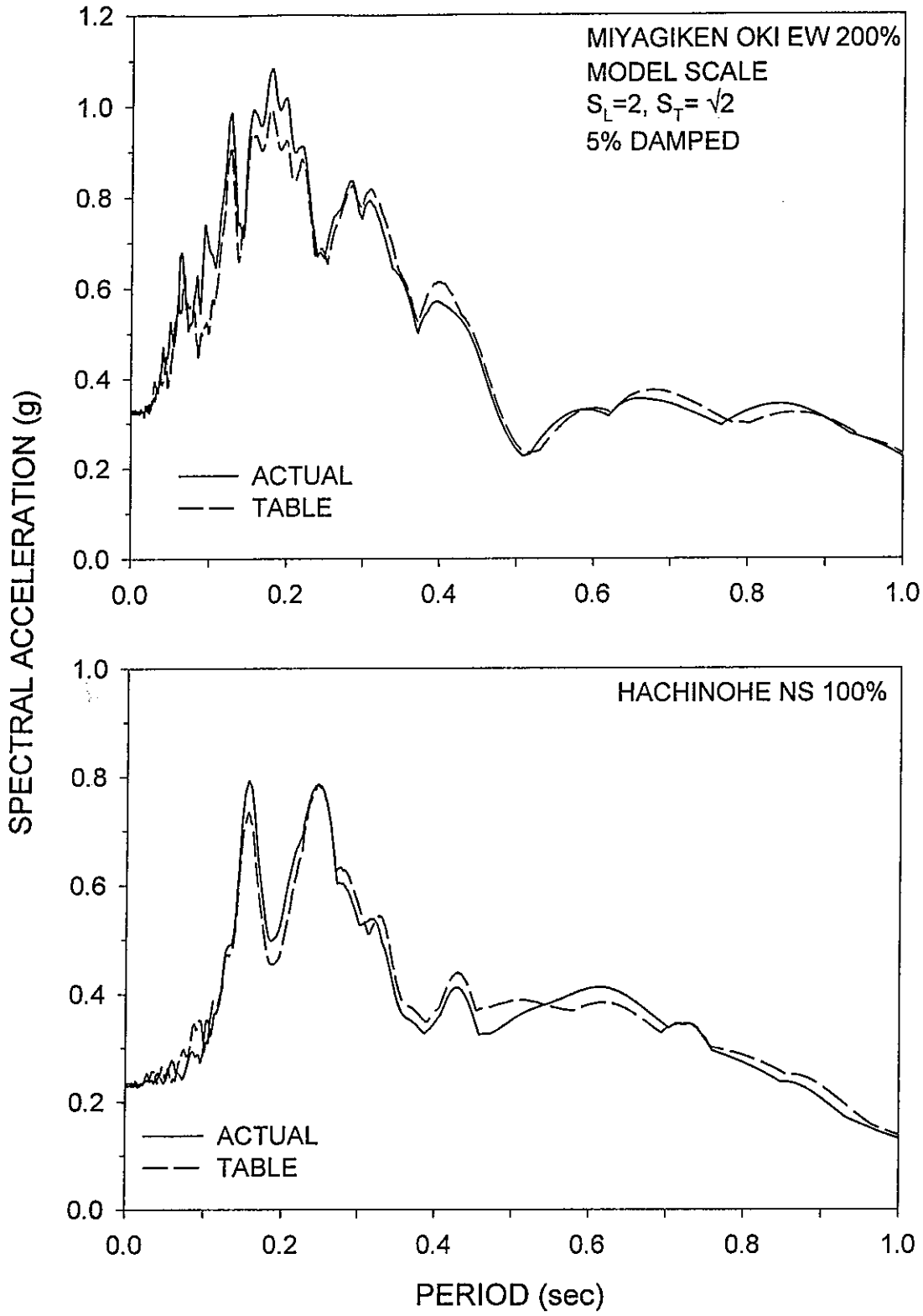

FIGURE 3-6 continued

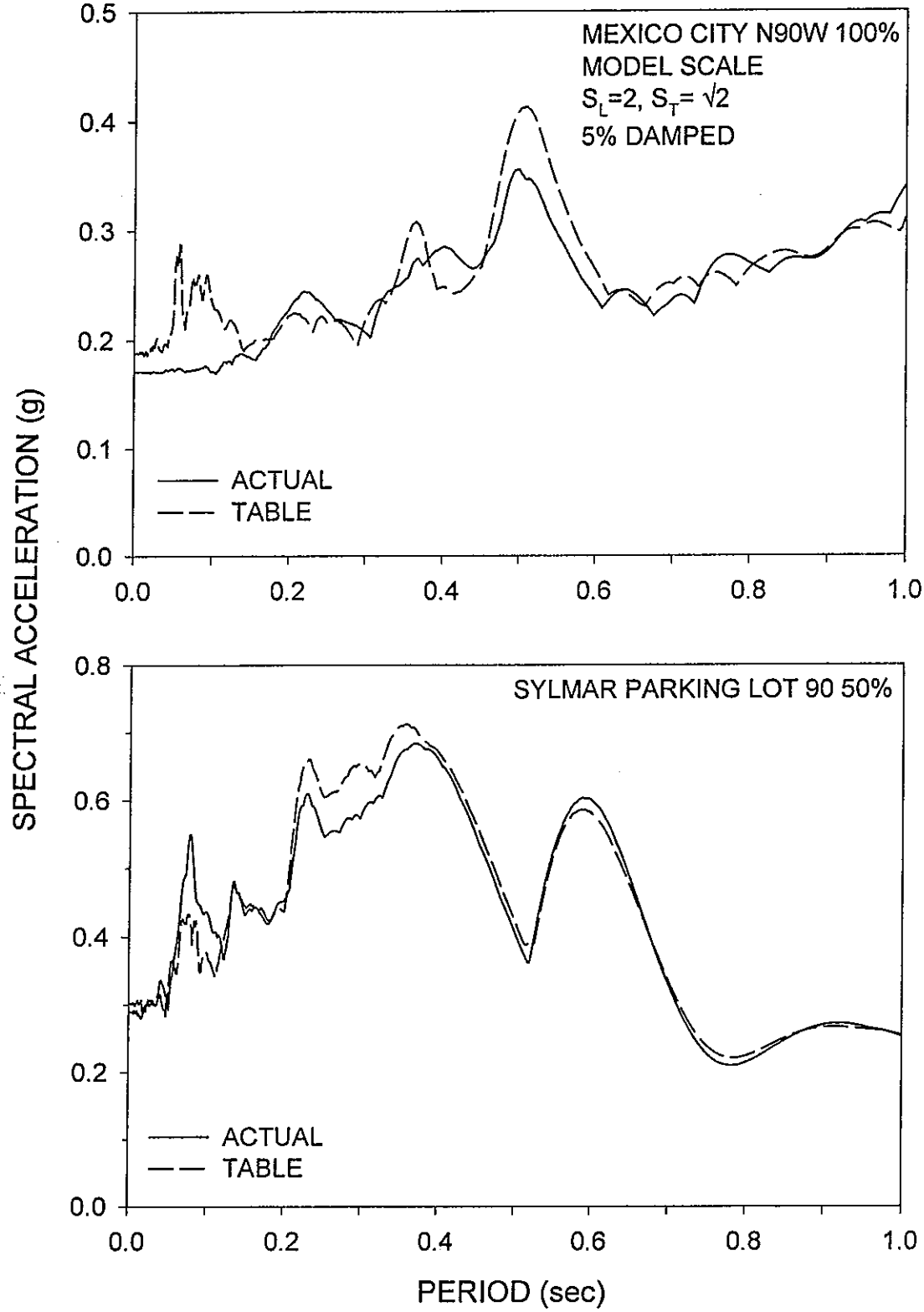

FIGURE 3-6 continued

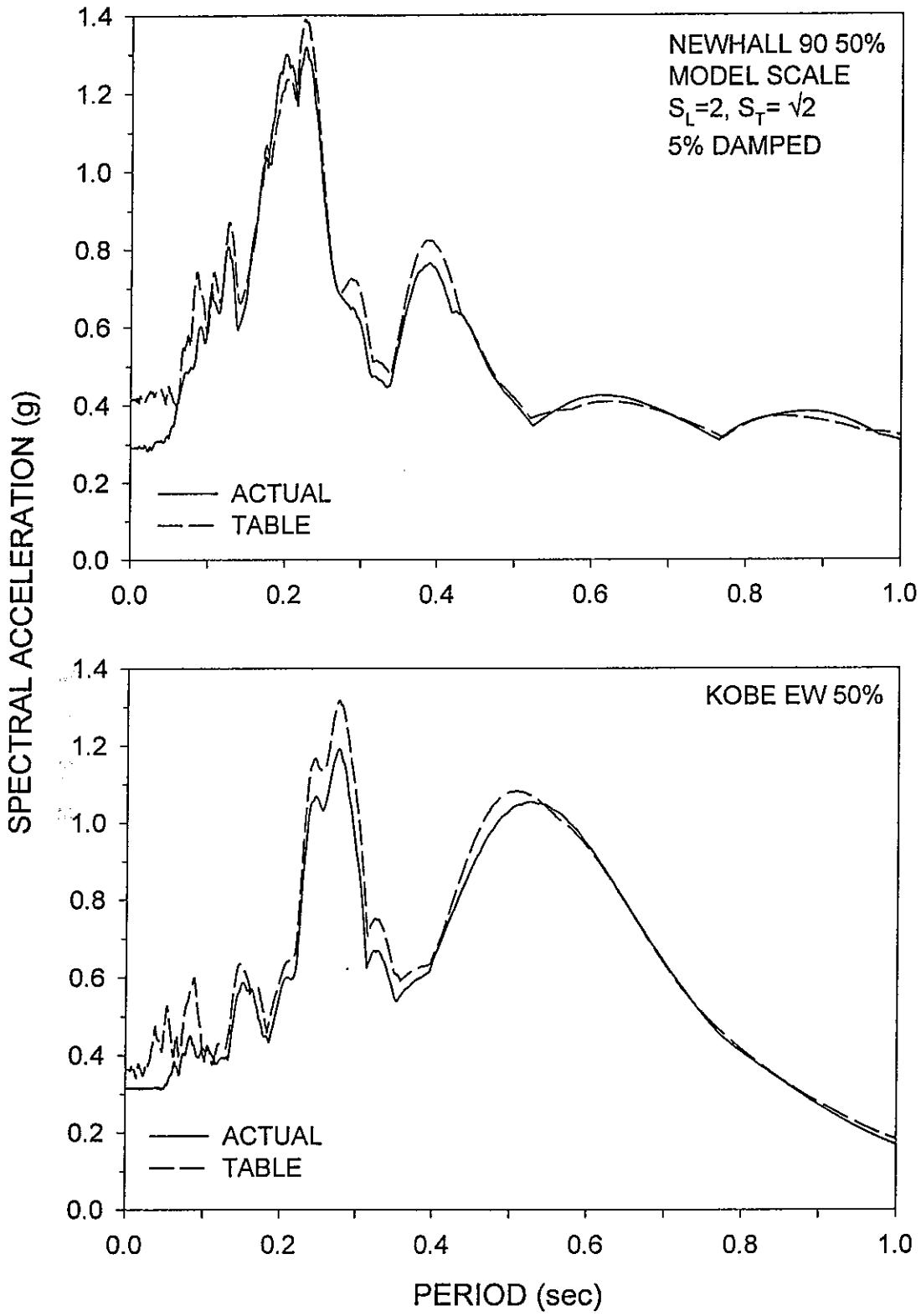

FIGURE 3-6 continued

3.5 Fluid Viscous Dampers

Two fluid viscous dampers with the geometry illustrated in Figure 3-7 were used. They were specified to be of through rod construction (without an accumulator) and 100 mm stroke (± 50 mm). The through-rod was selected for the following reasons:

(1) A through-rod design without accumulator has completely symmetrical operation in tension and compression, i.e., the same oil volume is swept by identical orifice areas in either direction. This damper design was the easiest to use given that only one damper per frame was utilized.

(2) Through-rod dampers without accumulators are considered capable of operation over a very wide frequency range without changing performance. This is due to the damper using no accumulator control valves or differential orifice control valves.

Testing the dampers was conducted by imposing sinusoidal motion to the piston rod of specified frequency and amplitude and by measuring the reaction force. Figure 3-8 presents recorded loops of force versus displacement of one of the dampers. The damper exhibits purely viscous behavior. From these loops, the peak force at peak velocity (instant of zero displacement) has been extracted and presented in Figure 3-9 as function of the peak velocity. The relation is substantially linear with slope, the damping coefficient, C_o = 15.7 N-s/mm.

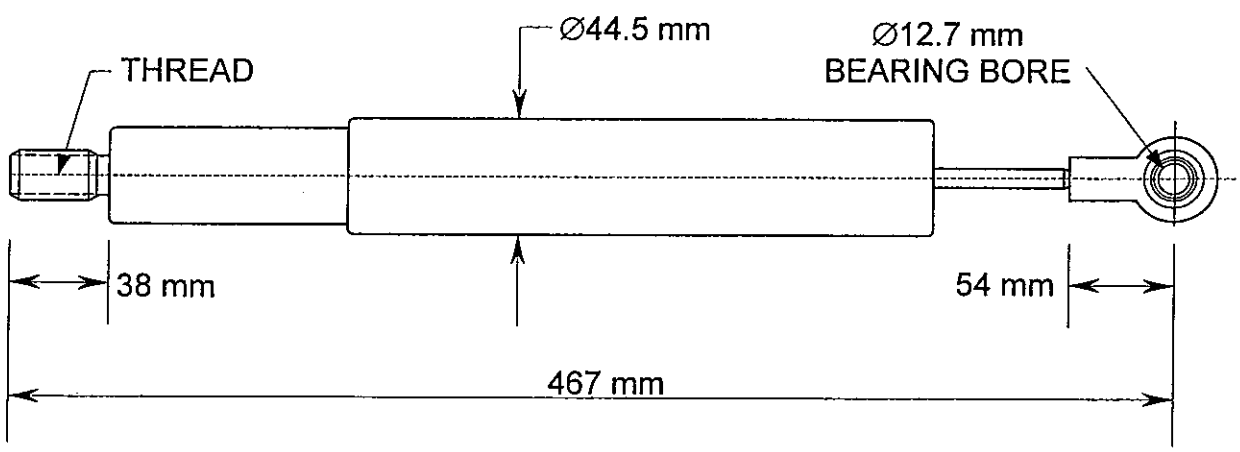

FIGURE 3-7 Geometry of Fluid Viscous Damper

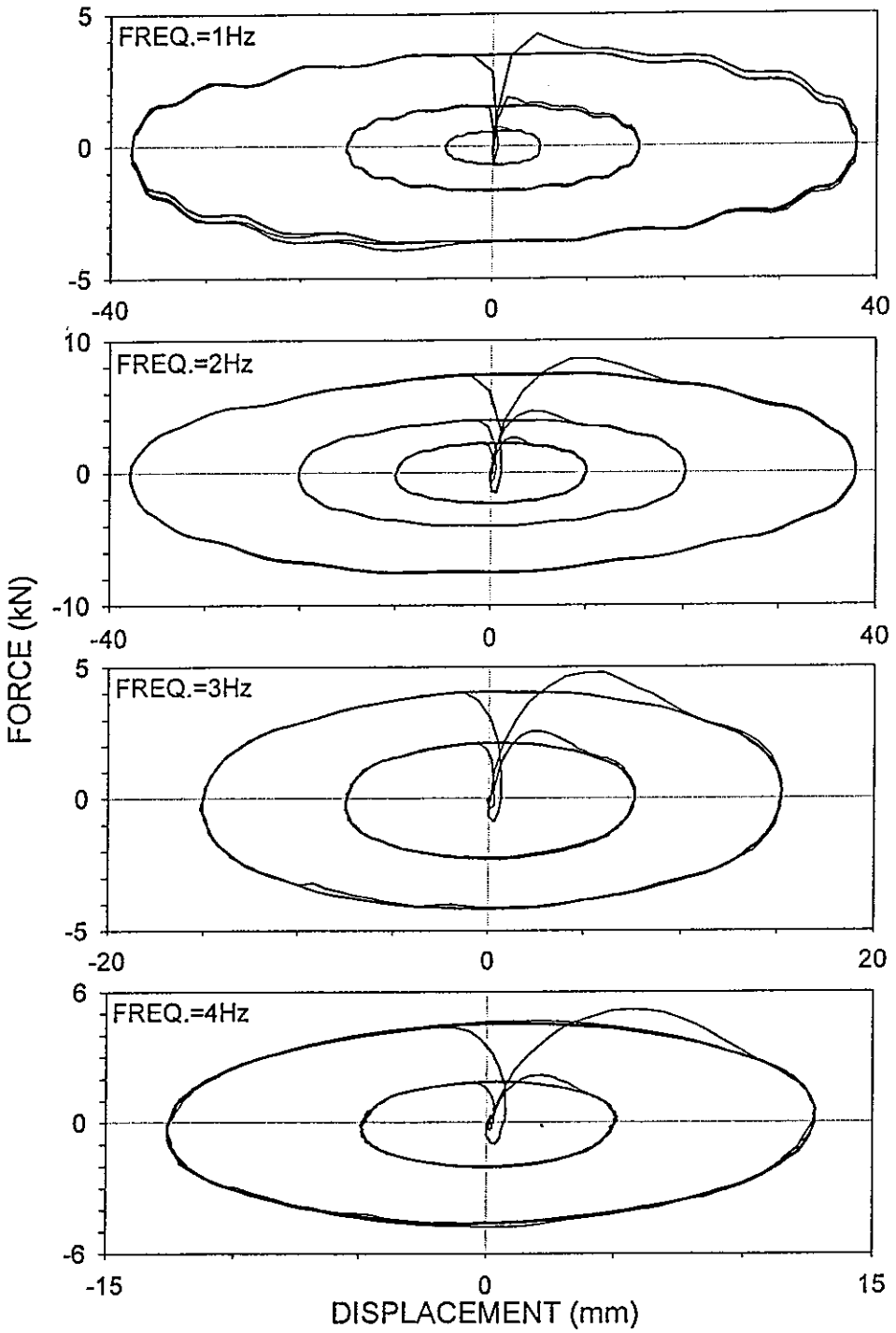

FIGURE 3-8 **Recorded Force-Displacement Loops of Fluid Viscous Damper (Damper A)**

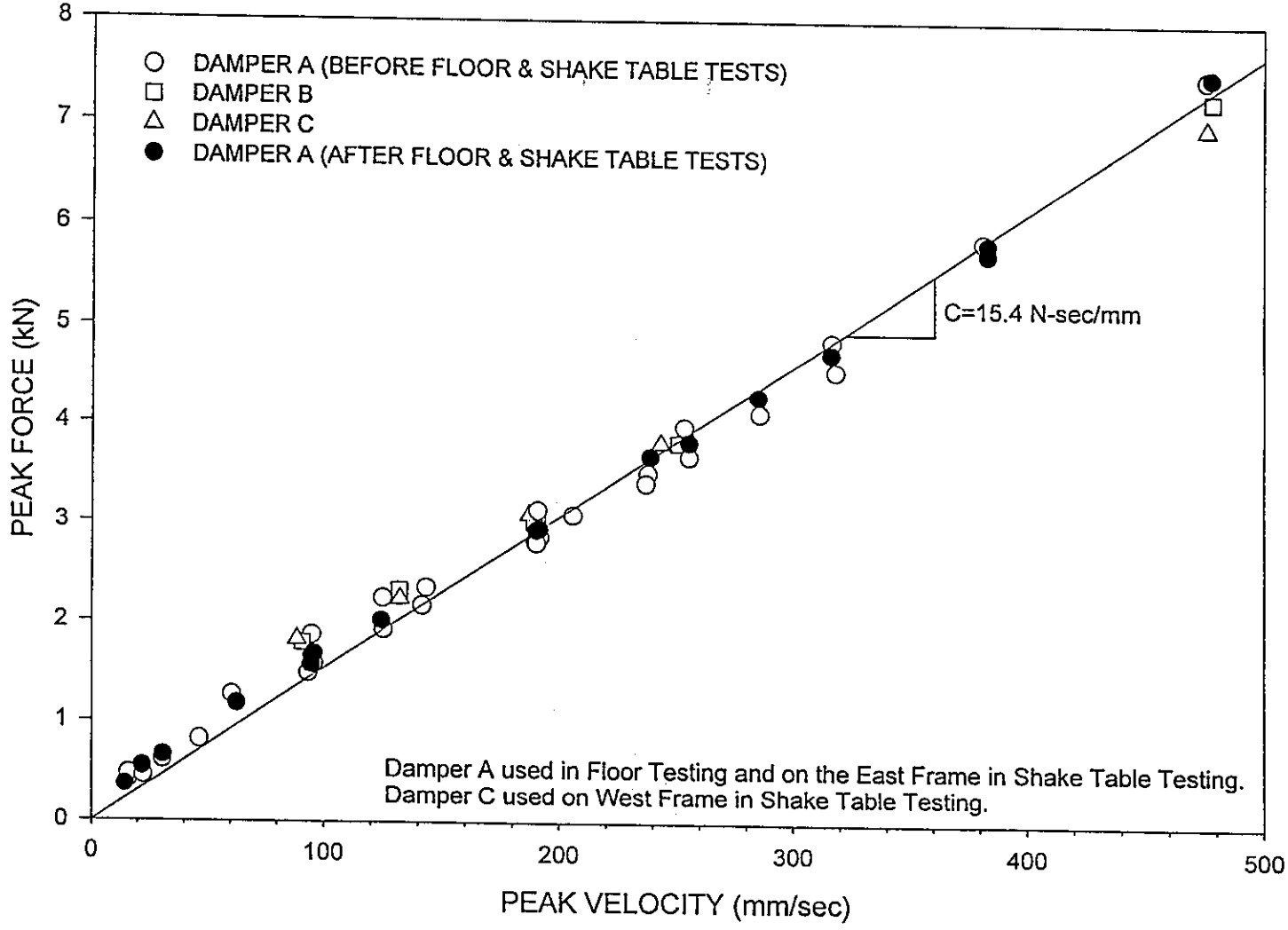

FIGURE 3-9 Recorded Peak Force-Peak Velocity Relation of Fluid Viscous Dampers

SECTION 4
TEST RESULTS

4.1 Test Results on Frame

Some test results on the behavior of a single frame with the toggle brace system have been presented in Section 2. A significant number of tests have been conducted on the frame using three different connection details of the toggle braces, various connection details of the frame, and two damper locations. Results of these tests are presented in Appendix B for the spring leaf connection detail, Appendix C for the bent plate connection detail, and Appendix D for the pinned connection detail (see Section 2.6 for details). These appendices contain one page per conducted test. The page includes the following:

(1) Test number, frame connection information, toggle brace connection information, damper location, conditions of test (frequency and amplitude of imposed motion), and date and time of test.

(2) Graph of the lateral frame displacement (see Figure 2-8)

(3) Graph of the damper force versus damper displacement (relative displacement of its two ends).

(4) Graph of damper displacement versus lateral displacement.

All tests were conducted with sinusoidal motion of three cycles and of prescribed frequency and amplitude. The connection details described in these appendices are:

(1) Toggle brace connections: spring leaf (see Figures 2-16 and 2-17), bent plate (see Figures 2-18 and 2-19), and pinned (see Figures 2-14 and 2-15).

(2) Frame connections. All columns to supporting beam connections were simple. The connections described in the appendices are for the beam to the columns. They are: (a) rigid connections, (b) simple connections, and (c) rigid-simple connections, that is, the connection at the actuator side is rigid and the connection at the other side is simple (see Figures 3-1 and 3-2).

A discussion and interpretation of the results obtained in the floor testing of the frame have been provided in Section 2. It is worthy, however, of elaborating on some of the comments made in Section 2:

(1) The spring leaf connection detail for the toggle braces was found unacceptably flexible. This connection became particularly problematic in the high frequency testing of the frame with rigid connections (e.g., see Appendix B, tests ARTL03, ARTL05 and ARTL06). We can observe in the results of these tests that the magnification of displacement is very small. Essentially, the damper displacement is equal to the frame lateral displacement, that is, $f \approx 1.0$. Moreover, there is a considerable delay between the lateral and damper displacements.

Most interesting is the behavior observed in test ARTL06 (case of lower damper) at frequency of 5Hz and amplitude of lateral displacement of 6.35 mm (0.25 in.). At zero lateral displacement, the damper displacement is equal to 5.6 mm (0.22 in.) and the damper force is about equal to 3.3 kN (0.75 kips). Given that the magnification factor f is approximately unity, the lateral force on the frame at zero lateral displacement should have been about equal to 3.3 kN (0.75 kips). Yet, the experiment shows zero force and complete lack of energy dissipation. These observations let to the discard of the spring leaf connection detail.

(2) The pinned connection detail for the toggle braces performed substantially better than the spring leaf connection. For example, observe the behavior in the case of rigid connection, frequency of 5 Hz, amplitude of 6.3 mm (0.25 in.) and lower damper installation in test ARTPL05 in Appendix D. The magnification of displacement is as predicted by theory, except for the aforementioned effect of rigid body movement (see Section 2.7). By comparison to test ARTPL06 (spring leaf, Appendix B), the lateral force-displacement exhibits substantially more energy dissipation, however, it is still somehow less than what the theory predicts. This behavior has been confirmed in the identification testing that was performed on the model structure on the shake table.

The authors could not find a satisfactory physical explanation for this behavior. However, this behavior was observed only when the connection adjacent to the toggle brace was rigid, and particularly when the shim plate (see Appendix A, detail BB) of

the toggle brace connection to the beam and column was present. Nevertheless, the effect was not significant for the pinned and bent plate connections.

(3) The bent plat connection detail performed very well despite the large number of inelastic cyclic movement it was subjected to.

4.2 Identification of Model Structure

The vibrational characteristics of the model structure (Figure 3-3) have been identified by exciting the structure with white noise excitation and constructing transfer functions. The structure was identified in the configurations of rigid-simple and rigid-rigid beam to column connections using a 0-50 Hz banded white noise excitation of the shake table. Transfer functions were obtained by dividing the Fourier transforms of the acceleration records obtained by channels ACJE (instrument No. 8 in Fig 3-4) and ABEH (instrument No. 2 in Fig. 3-4). That is, the identification relates to a model of the structure with the beam to column joint lateral displacement being the single degree of freedom of the structural system.

Amplitudes of the obtained transfer functions are presented in Figures 4-1 to 4-4. The structure behaves essentially as a single degree of freedom system. The location and magnitude of the primary peak provide information on the fundamental frequency and damping ratio of the structure. Table 4-1 lists the obtained frequencies and damping ratios. The results indicate an increase in frequency with the addition of dampers. This has been caused

TABLE 4-1 Vibrational Characteristics of Tested Structure as Determined from Transfer Functions

CONFIGURATION	DAMPERS	FUNDAMENTAL FREQUENCY (Hz)	DAMPING RATIO (% OF CRITICAL)
RIGID-SIMPLE CONNECTIONS	NO	3.0	4.5
	LOWER	3.0-3.2	21.5
	UPPER	3.4	25-27
RIGID-RIGID CONNECTIONS	NO	4.0	3.7
	LOWER	4.3	13.2
	UPPER	4.5	16.5

(a) by the flexibility of the toggle brace system (including the effect of joint slippage; see Section 2), and

(b) by difference in the moment-rotation relations of the joints, that is, the degree of fixity of the joints. Due to frequent changes made in the frame configuration and the dependency of this degree of fixity on the bolt tension, it is likely that the properties of the structure varied during testing.

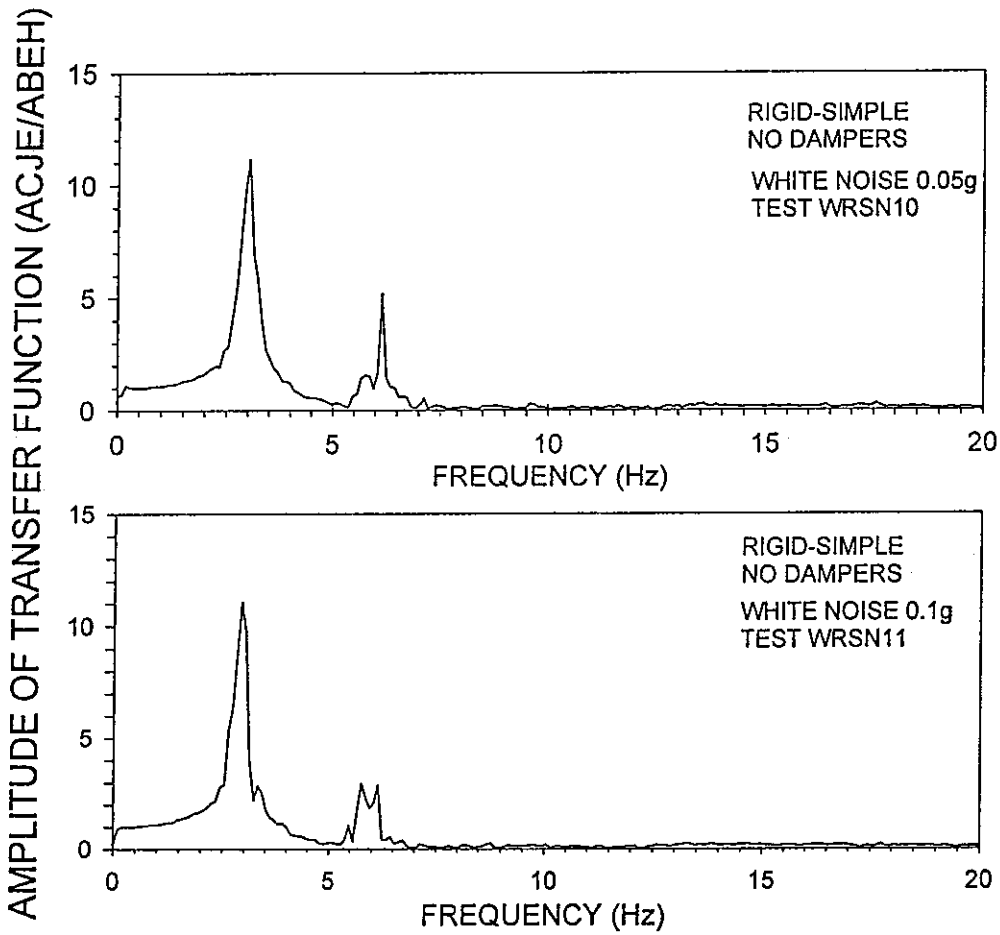

FIGURE 4-1 **Amplitude of Transfer Function of Rigid-Simple Structure Without Dampers**

Prediction of the damping ratio by analytical means can be made by the theory presented in Section 2.4, after modification for the effect of placing the mass at a location higher than the beam of the frame (this causes reduction of damping ratio). This

prediction is presented in Section 5. However, we obtain a quick confirmation of the theory as follows. Based on (2-21), the ratio of the damping ratio for the upper damper location, β_u, to the damping ratio for the lower damper location, β_ℓ, is

$$\frac{\beta_u}{\beta_\ell} = \left(\frac{f_u}{f}\right)^2 \frac{T_u}{T_\ell} \tag{4-1}$$

where T_u and T_ℓ are the periods in the two cases (inverse of frequencies in Table 4-1). To apply (4-1) we have to first subtract and later add the damping contributed by the frame

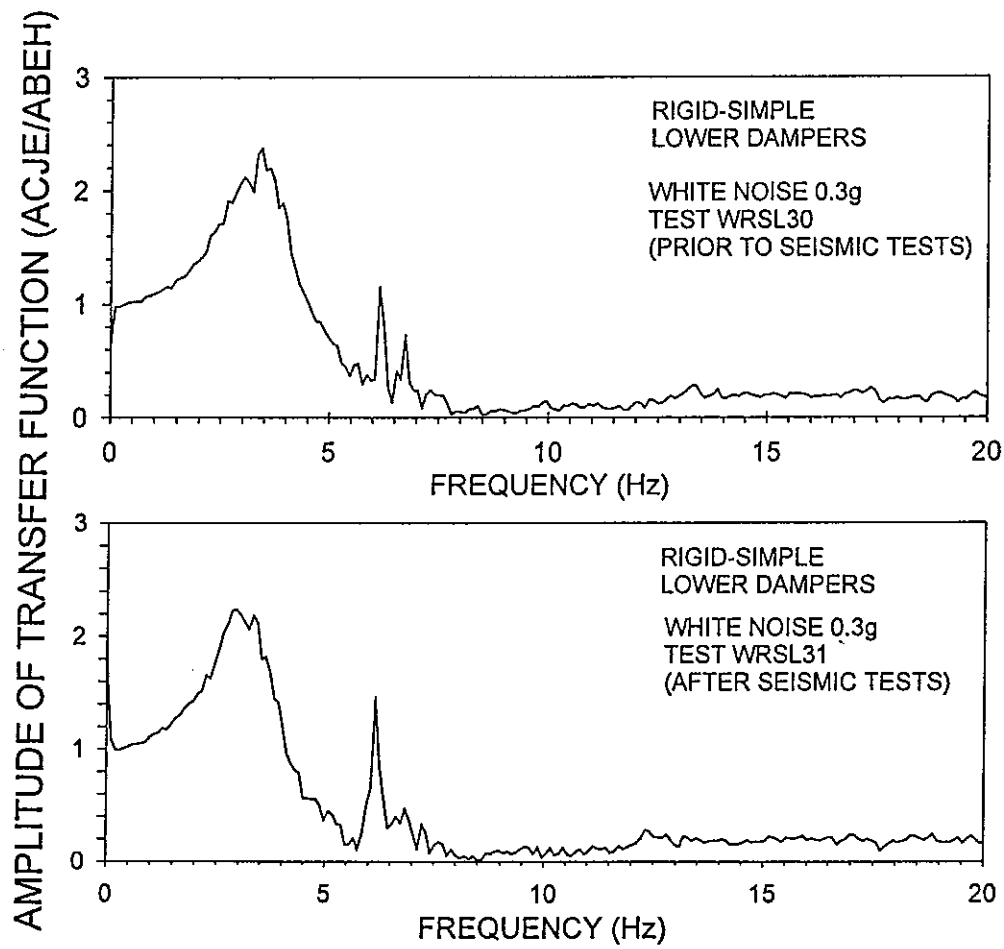

FIGURE 4-2 **Amplitude of Transfer Function of Rigid-Simple Structure with Lower Damper**

itself, which may be taken as the one obtained in the testing without dampers. Therefore, for the case of rigid-simple connections:

$$\beta_u = 4.5 + (21.5 - 4.5) \times \left(\frac{3.195}{2.666}\right)^2 \times \frac{(3.0 \text{ to } 3.2)}{3.4} = 26\% \text{ to } 27.5\%$$

The experimental values are 25% to 27%.

For the case of rigid-rigid connections:

$$\beta_u = 3.7 + (13.2 - 3.7) \times \left(\frac{3.195}{2.666}\right)^2 \times \frac{(4.3)}{4.5} = 16.7\%$$

The experimental value is 16.5%. That is, the predicted values for the upper damper configuration are in excellent agreement with the experiment.

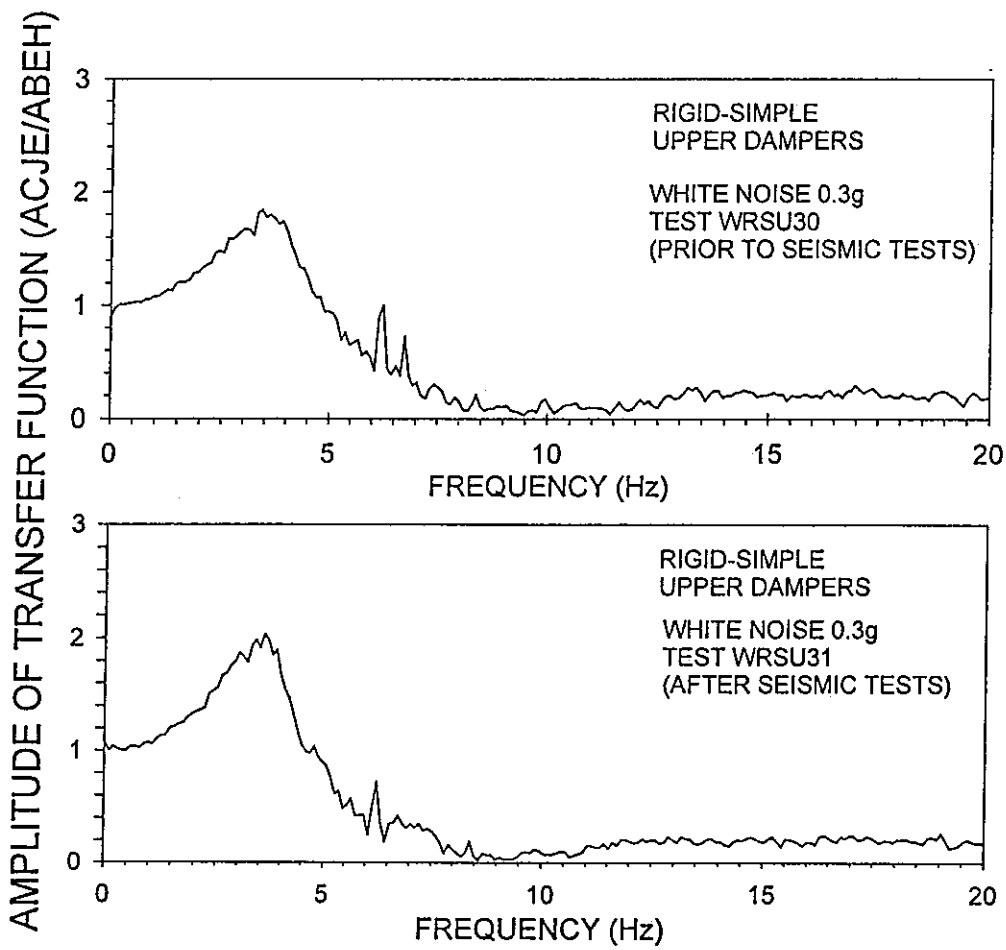

FIGURE 4-3 **Amplitude of Transfer Function of Rigid-Simple Structure with Upper Dampers**

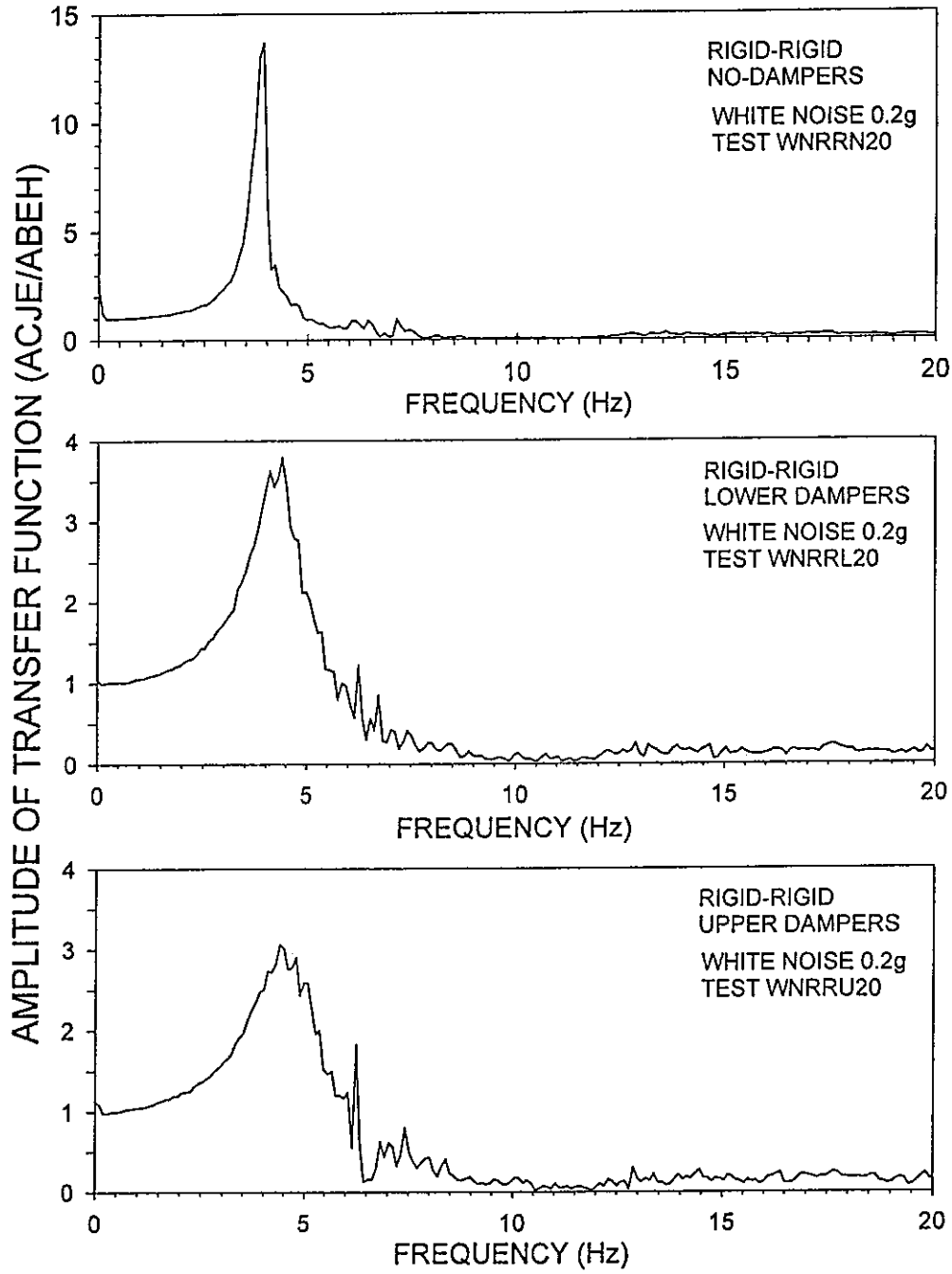

FIGURE 4-4 Amplitude of Transfer Function of Rigid-Rigid Structure

4.3 Shake Table Testing Results

Table 4-2 presents a summary of the shake table testing results. It should be noted that all these tests were conducted with the pinned toggle brace connection detail. The table contains the following:

(1) Test number.

(2) Description of seismic excitation. This includes the earthquake motion (e.g., El Centro), the component (e.g., S00E), and the scale factor (e.g., 150% implies that the motion's acceleration was multiplied by factor 1.5). Moreover, the notation H+V denotes simultaneous application of horizontal and vertical motion.

(3) The recorded peak table acceleration, velocity and displacement. The acceleration was recorded by accelerometer ABEH (No. 2 on east side in Figure 3-4) and the displacement was recorded by displacement transducer DBE (No. 16 on east side in Figure 3-5). The velocity was obtained by numerical differentiation of the displacement record.

(4) Drift (that is, displacement of the beam to column connection with respect to the column base), acceleration at the beam to column connection, and the damper force and damper relative displacement. The peak values of these response quantities are given for the east and west side frames in order to expose any torsional motion of the structure.

(5) Information on the structural configuration such as location of dampers (upper, lower or no dampers) and frame connection details (R-S for rigid-simple and R-R for rigid-rigid).

Testing was primarily conducted in the rigid-simple connection configuration since it gave the desired frequency characteristics. A large number of tests were also conducted on the stiffer rigid-rigid connection configuration. Moreover, nine more tests were conducted on a configuration with one frame having rigid-rigid connections and the other frame having rigid-simple connections. Since the two frames differed in stiffness by a factor of approximately 1.8, this configuration had an eccentricity between the center of mass and the center of resistance of about 14% of the width of the model structure.

TABLE 4-2 Summary of Shake Table Results

		PEAK TABLE MOTION			EAST FRAME PEAK VALUES				WEST FRAME PEAK VALUES				CONFIGURATION		
Test No	Excitation	Accel. (g)	Veloc. (mm/s)	Displ. (mm)	Drift (mm)	Damper Displ. (mm)	Damper Force (kN)	Accel. at Joint (g)	Drift (mm)	Damper Displ. (mm)	Damper Force (kN)	Accel. at Joint (g)	Frame East	Frame West	Damper
AELRSN01	EL CENTRO S00E 25%	0.084	57.8	10.4	5.6	-	-	0.204	6.4	-	-	0.242	R-S	R-S	NO DAMPERS
AELRSL01	EL CENTRO S00E 50%	0.15	110.4	20.7	4.3	9.8	3.25	0.196	3.9	10.1	3.59	0.178	R-S	R-S	LOWER
AELRSL02	EL CENTRO S00E 100%	0.32	222	41.6	10.8	23.9	6.79	0.394	9.8	23.7	7.82	0.361	R-S	R-S	LOWER
AELRSL03	EL CENTRO S00E 100%	0.292	222.7	41.6	11.4	25	7.38	0.413	10.6	24.7	7.75	0.371	R-S	R-S	LOWER
AELRSU02	EL CENTRO S00E 100%	0.297	226.6	41.4	8.6	25.3	7.63	0.365	8.1	24.7	7.63	0.338	R-S	R-S	UPPER
AELRRSU1	EL CENTRO S00E 100%	0.289	223.7	41.2	6.3	18.6	7.69	0.385	5.7	17	6.15	0.374	R-S	R-R	UPPER
AEVRRSU1	EL CENTRO S00E H+V 50%	0.155	109.2	20.5	3.2	8.9	3.60	0.221	2.8	7.3	2.81	0.213	R-S	R-R	UPPER
AEVRRSU2	EL CENTRO S00E H+V 100%	0.288	222.9	41.1	6.6	19.3	7.63	0.401	5.4	16.1	6.25	0.38	R-S	R-R	UPPER
AELRRN01	EL CENTRO S00E 50%	0.145	106.4	20.4	6.3	-	-	0.421	6.6	-	-	0.381	R-R	R-R	NO DAMPERS
AELRRU01	EL CENTRO S00E 100%	0.29	225.5	41.2	5.2	15.4	6.34	0.453	5.4	15.1	6.08	0.419	R-R	R-R	UPPER
AELRRU02	EL CENTRO S00E 150%	0.543	337.6	61.9	7.8	23.5	10.40	0.673	8.3	24.8	10.23	0.637	R-R	R-R	UPPER
AEVRRU01	EL CENTRO S00E H+V 100%	0.292	225.6	41.2	5.2	15.3	6.37	0.448	5.8	15.4	6.25	0.422	R-R	R-R	UPPER
AEVRRU02	EL CENTRO S00E H+V 150%	0.535	337.7	61.9	8	24.1	10.25	0.626	8.7	25.3	10.02	0.632	R-R	R-R	UPPER
ATARSN01	TAFT N21E 75%	0.115	98	16.4	7	-	-	0.246	8.1	-	-	0.31	R-S	R-S	NO DAMPERS
ATARSN02	TAFT N21E 100%	0.165	112.5	21.9	8.3	-	-	0.278	9.7	-	-	0.341	R-S	R-S	NO DAMPERS
ATARSL02	TAFT N21E 100%	0.155	102.5	21.8	4.4	10	3.02	0.183	4.3	10.2	3.04	0.2	R-S	R-S	LOWER
ATARSL03	TAFT N21E 200%	0.309	199.3	43.7	9.2	21.3	6.13	0.344	8.7	20.5	5.90	0.359	R-S	R-S	LOWER
ATARSL04	TAFT N21E 200%	0.317	197.6	43.7	9.4	21.3	6.25	0.343	8.9	21.1	5.99	0.361	R-S	R-S	LOWER
ATARSU02	TAFT N21E 200%	0.318	199.9	43.5	7.1	21.8	6.00	0.301	6.8	21.1	6.74	0.349	R-S	R-S	UPPER
ATARRSU1	TAFT N21E 200%	0.335	201	43.4	6.5	19.2	6.96	0.368	5.5	16.3	5.66	0.348	R-S	R-R	UPPER
ATVRRSU1	TAFT N21E H+V 100%	0.158	101	21.7	3.5	10	3.77	0.23	2.7	8.2	2.92	0.21	R-S	R-R	UPPER
ATVRRSU2	TAFT N21E H+V 200%	0.313	202.2	43.5	6.5	19.6	6.74	0.36	5.3	16.2	5.85	0.358	R-S	R-R	UPPER
ATFRRN01	TAFT N21E 75%	0.1	71.9	16.3	4.9	-	-	0.306	4.8	-	-	0.286	R-R	R-R	NO DAMPERS
ATFRRN02	TAFT N21E 100%	0.14	98.4	21.8	6.6	-	-	0.392	6.6	-	-	0.375	R-R	R-R	NO DAMPERS
ATARRU01	TAFT N21E 200%	0.364	203	43.4	5.9	16.2	6.31	0.425	5.7	16.2	5.90	0.397	R-R	R-R	UPPER
ATARRU02	TAFT N21E 300%	0.607	308.7	65.2	8.7	23.2	9.82	0.574	8.3	23.4	9.56	0.558	R-R	R-R	UPPER
ATVRRU01	TAFT N21E H+V 200%	0.367	203.9	43.3	6.1	16.8	6.13	0.436	5.6	16.7	5.97	0.43	R-R	R-R	UPPER

TABLE 4-2 continued

		PEAK TABLE MOTION			EAST FRAME PEAK VALUES				WEST FRAME PEAK VALUES				CONFIGURATION		
Test No	Excitation	Accel. (g)	Veloc. (mm/s)	Displ. (mm)	Drift (mm)	Damper Displ. (mm)	Damper Force (kN)	Accel. at Joint (g)	Drift (mm)	Damper Displ. (mm)	Damper Force (kN)	Accel. at Joint (g)	Frame East	Frame West	Damper
AHARSN01	HACHINOHE NS 25%	0.059	53.4	12.3	2.8	-	-	0.103	2.7	-	-	0.117	R-S	R-S	NO DAMPERS
AHARSN02	HACHINOHE NS 50%	0.107	104.3	24.7	5.7	-	-	0.199	5.6	-	-	0.251	R-S	R-S	NO DAMPERS
AHARSL02	HACHINOHE NS 50%	0.118	102.6	24.8	3.3	8.1	2.37	0.138	3.5	7.1	2.59	0.157	R-S	R-S	LOWER
AHARSL03	HACHINOHE NS 100%	0.234	207	49.5	6.5	15.5	4.89	0.256	6.5	14.2	4.55	0.313	R-S	R-S	LOWER
AHARSU01	HACHINOHE NS 100%	0.21	207.3	49.4	5.3	16.3	5.11	0.254	5.4	16	4.98	0.323	R-S	R-S	UPPER
AHARSU02	HACHINOHE NS 150%	0.325	313.8	74.1	7.5	22.4	7.27	0.365	7.6	22	7.55	0.436	R-S	R-S	UPPER
AHARRSU1	HACHINOHE NS 100%	0.27	208.7	49.3	5	15.2	4.70	0.268	4.4	12.9	3.94	0.315	R-S	R-R	UPPER
AHARRN01	HACHINOHE NS 75%	0.198	140.8	37.4	8.4	-	-	0.459	8.6	-	-	0.478	R-R	R-R	NO DAMPERS
AHARRU01	HACHINOHE NS 100%	0.243	215.2	49.4	4.2	11.4	4.38	0.322	4.3	12	4.15	0.335	R-R	R-R	UPPER
AHARRU02	HACHINOHE NS 200%	0.504	438	99	8.7	24.9	8.09	0.582	8.9	25.4	8.03	0.591	R-R	R-R	UPPER
AMYRSN01	MYAGIKEN EW 100%	0.165	89	17.4	9.5	-	-	0.344	9.6	-	-	0.367	R-S	R-S	NO DAMPERS
AMYRSL01	MYAGIKEN EW 100%	0.145	95.1	17.3	3.9	9.7	2.74	0.203	4.4	8.1	3.04	0.184	R-S	R-S	LOWER
AMYRSL02	MYAGIKEN EW 200%	0.323	192	34.6	7.1	19.3	5.49	0.365	8.1	17.9	5.50	0.317	R-S	R-S	LOWER
AMYRSU01	MYAGIKEN EW 200%	0.323	192.8	34.6	5.4	18	5.52	0.325	5.8	18.7	5.23	0.283	R-S	R-S	UPPER
AMYRSU02	MYAGIKEN EW 300%	0.492	294.5	52.1	7.5	26.4	8.13	0.453	8.4	27.8	7.72	0.393	R-S	R-S	UPPER
AMYRRN01	MYAGIKEN EW 100%	0.146	102.7	17.1	7.5	-	-	0.41	7.7	-	-	0.45	R-R	R-R	NO-DAMPERS
AMYRRU01	MYAGIKEN EW 200%	0.357	196.9	34.6	5.2	15	5.27	0.423	5.3	14.7	5.06	0.383	R-R	R-R	UPPER
AMYRRU02	MYAGIKEN EW 300%	0.536	299.2	52	7.7	23.5	7.63	0.61	8.1	23.7	7.22	0.559	R-R	R-R	UPPER
AMXRRU01	MEXICO CITY N90W 125%	0.225	518.8	124.6	2.8	10	1.72	0.243	3.3	9.6	1.70	0.244	R-R	R-R	UPPER
AMXRSL01	MEXICO CITY N90W 100%	0.188	415.2	100.3	4.6	12.4	1.74	0.205	4.9	12.2	2.06	0.194	R-S	R-S	LOWER
AMXRSU01	MEXICO CITY N90W 100%	0.125	253.4	67.8	2.5	9.3	0.90	0.137	2.8	8.7	0.94	0.154	R-S	R-S	UPPER
AMXRSU02	MEXICO CITY N90W 125%	0.234	518.4	124.9	5.1	18	2.20	0.255	5.7	17.8	2.24	0.239	R-S	R-S	UPPER
APERSN01	PACOIMA S16E 10%	0.099	60	14.8	4.1	-	-	0.149	4.3	-	-	0.178	R-S	R-S	NO DAMPERS
APERSL02	PACOIMA S16E 50%	0.541	303.6	74.1	9.1	21.8	7.87	0.411	8.9	20.9	7.83	0.409	R-S	R-S	LOWER
APARSU01	PACOIMA S16E 50%	0.474	306.6	73.9	7.1	23.1	8.11	0.417	7.3	22.8	7.47	0.37	R-S	R-S	UPPER
APERRN01	PACOIMA S16E 10%	0.099	61.1	14.8	6.1	-	-	0.366	6.2	-	-	0.361	R-R	R-R	NO DAMPERS
APERRU01	PACOIMA S16E 50%	0.472	303.4	73.9	7.2	20.9	7.42	0.556	7.3	21.9	6.73	0.517	R-R	R-R	UPPER
APWRSL01	PACOIMA S74W 25%	0.257	99	13.7	7.3	16.5	4.49	0.276	6.9	15.3	4.59	0.343	R-S	R-S	LOWER
APWRSU01	PACOIMA S74W 25%	0.229	102.1	13.6	5.4	15.9	4.18	0.263	5.2	14.3	4.27	0.315	R-S	R-S	UPPER
APWRRU01	PACOIMA S74W 50%	0.453	220.5	27.5	7	20.5	7.69	0.563	7.1	21.7	7.85	0.533	R-R	R-R	UPPER

TABLE 4-2 continued

Test No	Excitation	PEAK TABLE MOTION			EAST FRAME PEAK VALUES				WEST FRAME PEAK VALUES				CONFIGURATION		
		Accel. (g)	Veloc. (mm/s)	Displ. (mm)	Drift (mm)	Damper Displ. (mm)	Damper Force (kN)	Accel. at Joint (g)	Drift (mm)	Damper Displ. (mm)	Damper Force (kN)	Accel. at Joint (g)	Frame East	Frame West	Damper
ASYRSN01	SYLMAR 90 10%	0.054	47.8	10.1	3.7	-	-	0.131	4	-	-	0.184	R-S	R-S	NO DAMPERS
ASYRSL05	SYLMAR 90 25%	0.155	108	25.2	4.7	11.2	2.54	0.199	4.5	9.9	3.13	0.201	R-S	R-S	LOWER
ASYRSL06	SYLMAR 90 40%	0.233	167.4	40.3	7.8	18.3	4.37	0.284	7.7	16.5	4.70	0.286	R-S	R-S	LOWER
ASYRSU01	SYLMAR 90 50%	0.293	209	50.4	8.1	24.1	5.34	0.328	7.8	23.3	5.31	0.354	R-S	R-S	UPPER
ASYRRSUI	SYLMAR 90 50%	0.277	207.4	50.2	5.9	18	5.21	0.307	5.2	15.2	4.40	0.314	R-S	R-R	UPPER
ASYRRN01	SYLMAR 90 25%	0.148	108.9	24.9	4.9	-	-	0.293	4.8	-	-	0.28	R-R	R-R	NO DAMPERS
ASYRRU01	SYLMAR 90 50%	0.289	205.1	50.3	4.2	12.1	4.36	0.313	4.4	12.4	4.34	0.331	R-R	R-R	UPPER
ASYRRU02	SYLMAR 90 100%	0.528	417.2	100.8	9	26.2	9.93	0.605	9.6	26.9	10.15	0.618	R-R	R-R	UPPER
AN3RSL02	NEWHALL 360 40%	0.304	244	47.6	10.2	23.1	5.72	0.373	9.8	22.1	5.55	0.358	R-S	R-S	LOWER
AN3RSU01	NEWHALL 360 40%	0.307	241.3	47.6	8.1	24.4	5.52	0.339	7.7	23.5	5.64	0.342	R-S	R-S	UPPER
AN3RRN01	NEWHALL 360 25%	0.172	154.9	29.8	6	-	-	0.363	6.1	-	-	0.357	R-R	R-R	NO DAMPERS
AN3RRU01	NEWHALL 360 50%	0.346	295.8	59.8	6.2	17.2	6.09	0.437	6	17	6.06	0.45	R-R	R-R	UPPER
AN3RRU02	NEWHALL 360 75%	0.536	462.5	89.7	10.1	27.8	9.63	0.631	10	27.9	9.23	0.627	R-R	R-R	UPPER
AN9RSL01	NEWHALL 90 25%	0.163	104.1	17.8	4.7	11.1	2.79	0.182	4.7	10.4	2.80	0.228	R-S	R-S	LOWER
AN9RSL02	NEWHALL 90 40%	0.28	166.1	28.4	8.2	18.7	4.78	0.302	8	17.2	4.42	0.346	R-S	R-S	LOWER
AN9RSU01	NEWHALL 90 50%	0.381	205.2	35.4	8.7	24.7	6.31	0.336	8.6	26.3	7.01	0.421	R-S	R-S	UPPER
AN9RRN01	NEWHALL 90 25%	0.158	97	18	6	-	-	0.341	5.8	-	-	0.343	R-R	R-R	NO DAMPERS
AN9RRU01	NEWHALL 90 50%	0.415	215.5	35.4	7.4	21	7.28	0.552	7.5	21	6.83	0.529	R-R	R-R	UPPER
AKORSL01	KOBE EW 25%	0.146	142.8	17.6	4.9	12	3.22	0.206	4.7	9.5	3.29	0.208	R-S	R-S	LOWER
AKORSL02	KOBE EW 40%	0.229	231.1	28.3	8.6	19.9	5.17	0.32	8.2	19	5.03	0.314	R-S	R-S	LOWER
AKORSU01	KOBE EW 40%	0.251	231.6	28.3	7.4	22.1	5.16	0.308	7.1	22	5.32	0.322	R-S	R-S	UPPER
AKORRSUI	KOBE EW 50%	0.344	293	35.2	7.5	22.7	7.25	0.392	6	17.9	5.65	0.408	R-S	R-R	UPPER
AKORRU01	KOBE EW 50%	0.363	294.6	35.3	6.8	18.9	6.99	0.465	6.5	19.4	6.53	0.455	R-R	R-R	UPPER

Table 4-2 contains all of the conducted tests except two, which will be discussed later. Both were conducted in the rigid-rigid connection configuration with the El Centro earthquake.

Based on the results of Table 4-2, Figures 4-5 and 4-6 were developed. They present the recorded peak response quantities (maximum among the two sides) versus the peak table acceleration. As it was expected, the damping system is effective in reducing the peak response of the structure. Interesting, however, is the required peak damper force as portion of the tributary weight. By comparison to other tested damper configurations (e.g., Constantinou et al., 1992; Reinhorn et al., 1995; Seleemah et al., 1997), the required damper force in the toggle brace configuration is substantially smaller.

The results of Table 4-2 demonstrate minor effects of the vertical component of seismic excitation. Moreover, the results in the case of the structure with asymmetric configuration (one frame with rigid-rigid connections and the other frame with rigid-simple connections) demonstrate a torsional response (i.e., differences in the drifts of the columns of the two frames) that is of the same magnitude as that of the symmetric configurations.

Figure 4-7 presents the ratio of the peak corner column drift to the average column drift in the various tested configurations, without dampers and with upper dampers. For all tested configurations, whether symmetric or asymmetric, this ratio is in the range of 1.0 to about 1.1. Very interesting is that the tested damped, highly asymmetric structure does not exhibit any substantially larger torsional response. Actually, the three tests with the highest ratio of drifts in Figure 4-7 are tests with combined horizontal and vertical excitation. In these tests, in which control of the shake table is imperfect, the unwanted torsional motion of the shake table may have contributed to an increase in the torsional response of the structure.

Detailed results for each conducted test are presented in Appendix E in the form of time histories of response and damper force-displacement loops.

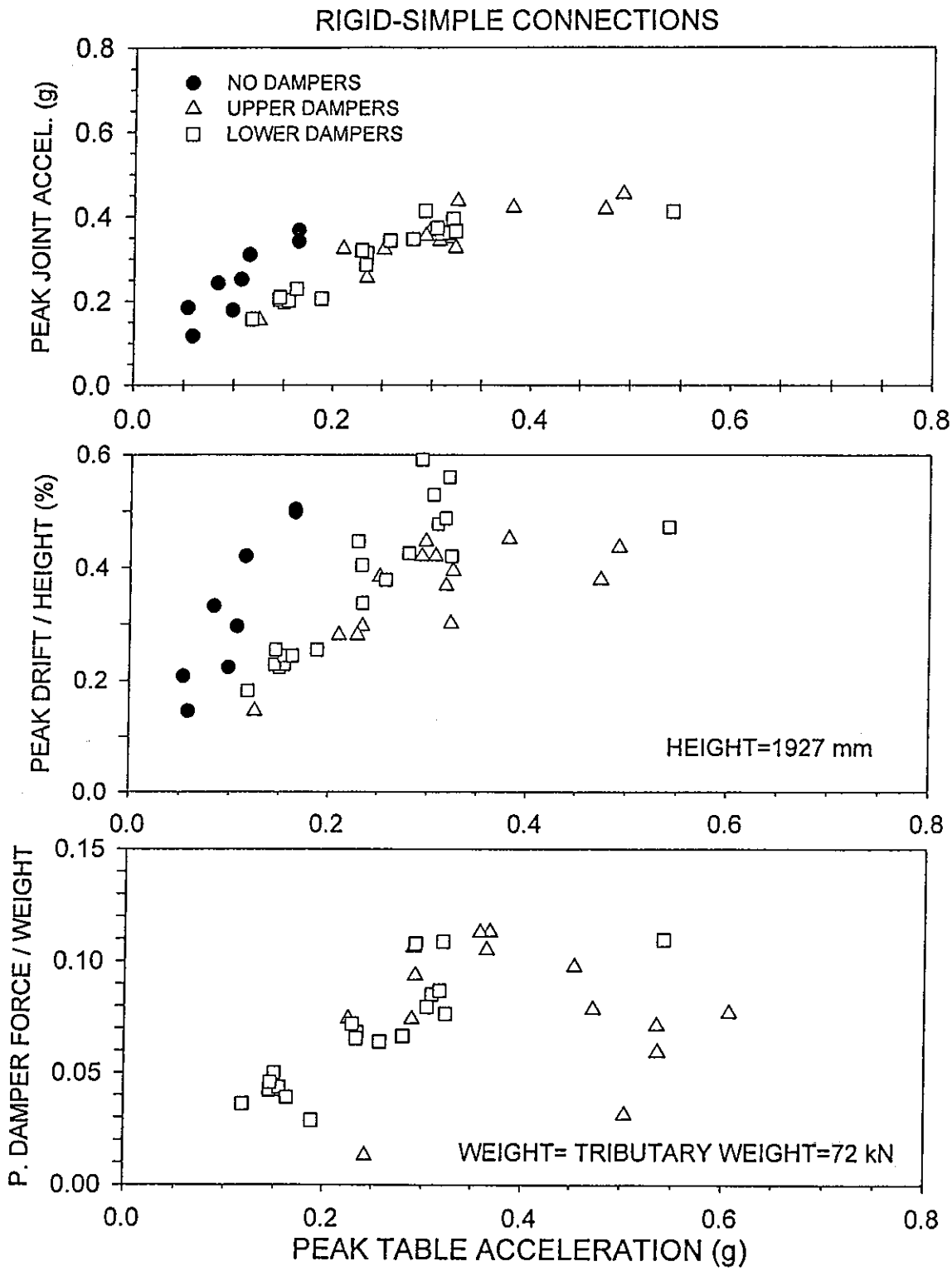

FIGURE 4-5 **Peak Response of Model Structure in the Rigid-Simple Connection Configuration as Function of Peak Table Acceleration**

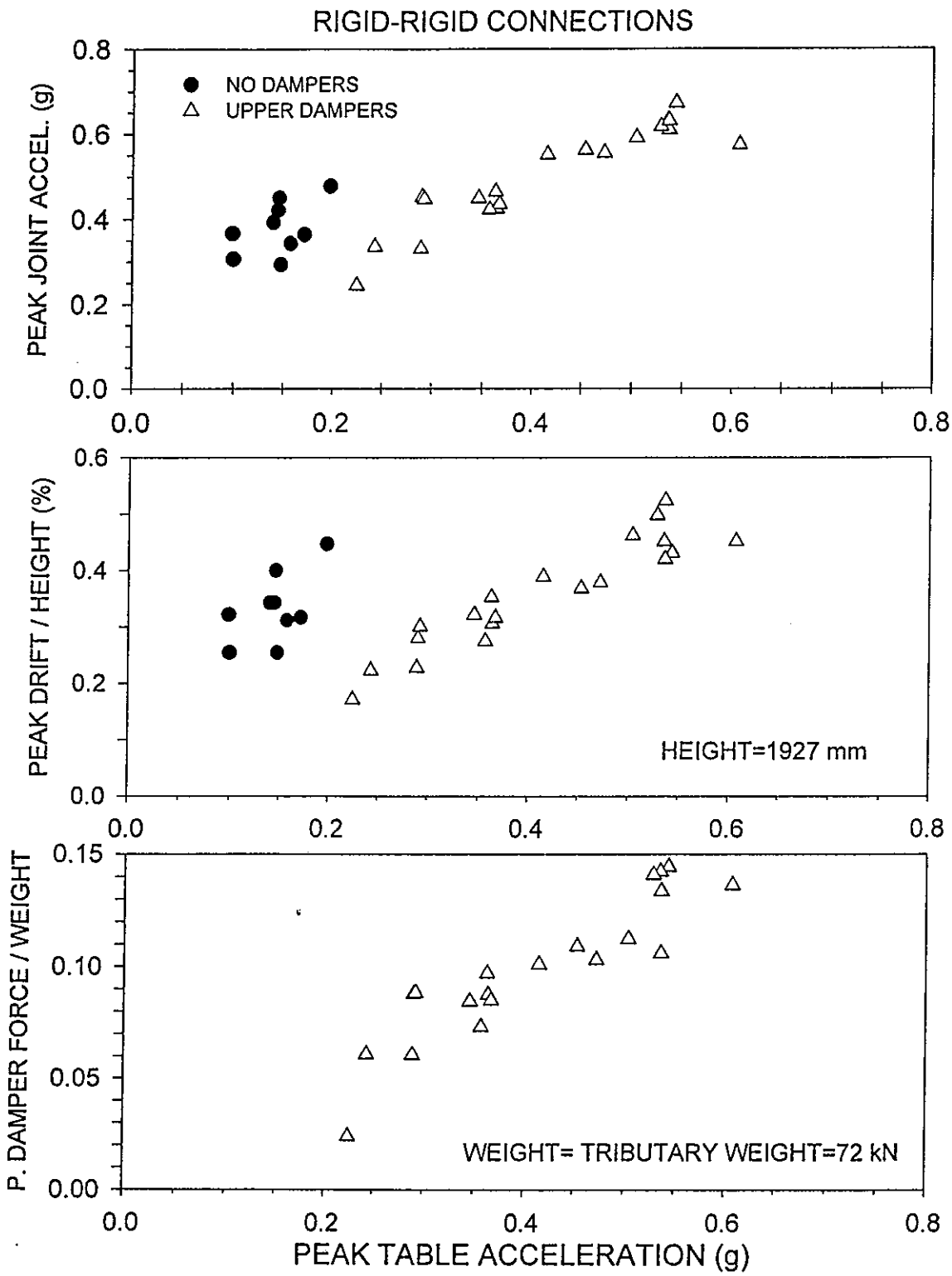

FIGURE 4-6 Peak Response of Model Structure in the Rigid-Rigid Connection Configuration as Function of Peak Table Acceleration

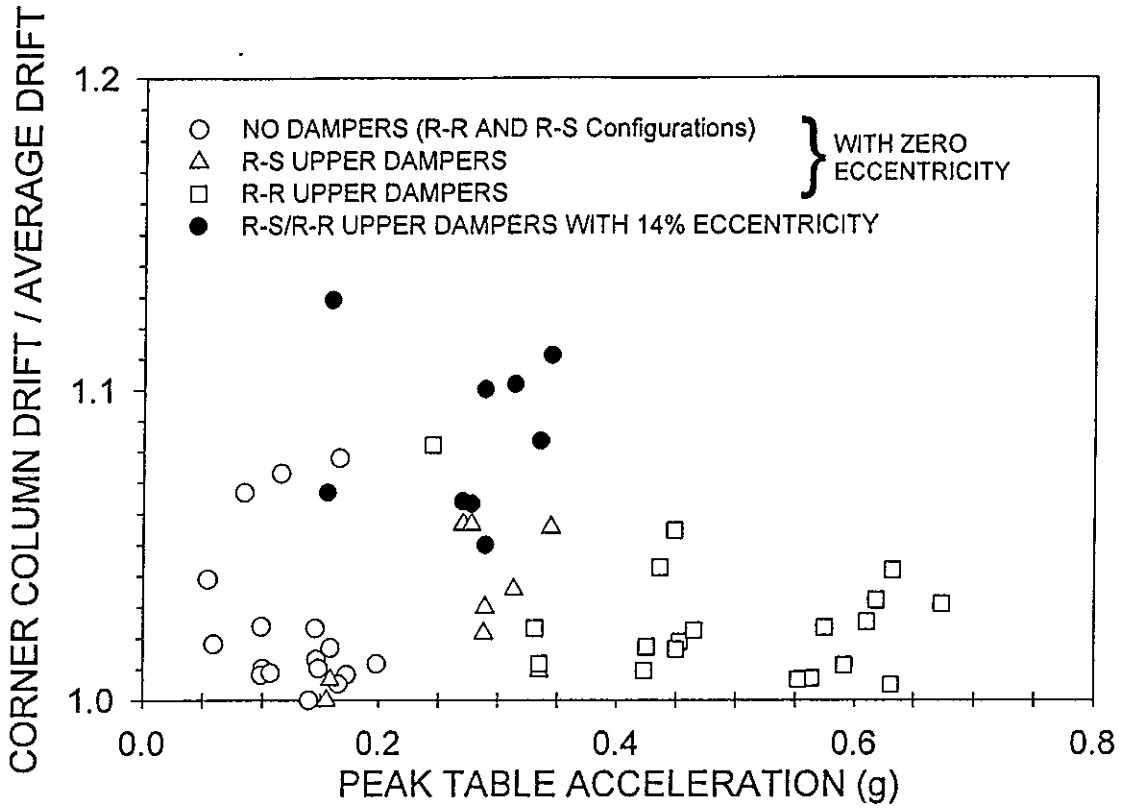

FIGURE 4-7 **Ratio of Corner Column Drift to Average Column Drift for Various Tested Configurations**

Finally, it is interesting to present in some detail the results of two tests in the rigid-rigid connection configuration with upper dampers. Both were conducted with the El Centro motion specified to be 200 % of the actual record. However, for an unknown reason the table motion reached a peak acceleration of 0.935 g. Figure 4-8 presents the recorded acceleration histories at the two instrumented column bases of the structure. Given the low period of the model structure (4.5 Hz frequency or 0.22 sec period in the model scale and 3.2 Hz or 0.31 sec in prototype scale), which lies in the acceleration controlled portion of the spectrum, the response of the structure was markedly affected by the very strong input.

Figure 4-9 presents the recorded column drifts in this test. The peak drift ratio reached 0.6-percent of the column height. It may have caused minor inelastic action in the structure. Of interest is to note in Figure 4-9 that following a peak in response at about 2.5 sec, the structure undergoes larger drift on the west side than on the east side.

Interestingly, the difference occurs only for negative column drift, that is, when the dampers are subjected to compression forces. It was observed during testing that the west side damper assembly had some "play" in the connection of the damper to the load cell. This was caused by insufficient tightening of the threaded part of the damper to the load cell.

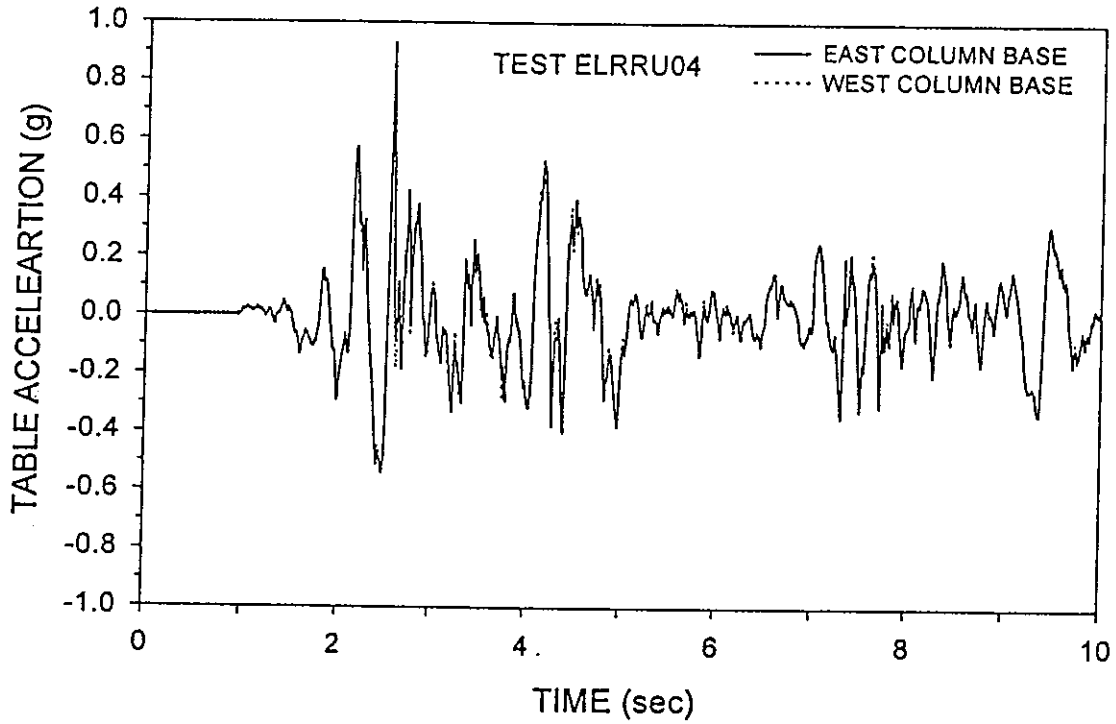

FIGURE 4-8 **Table Acceleration History in Test ELRRU04 (specified to be El Centro 200%)**

Recorded force displacement loops for the two dampers are presented in Figure 4-10. The west side damper shows abnormal behavior and reaches a peak force of about 22.5 kN. The quality of this measurement is questionable given the condition of the load cell. However, the east side damper shows proper performance with a peak force of about 16 kN. To confirm the accuracy of this measurement, the east side damper displacement record was differentiated to obtain the velocity record. A peak velocity of 863 mm/s was obtained, which confirms the quality of the measurement of the damper

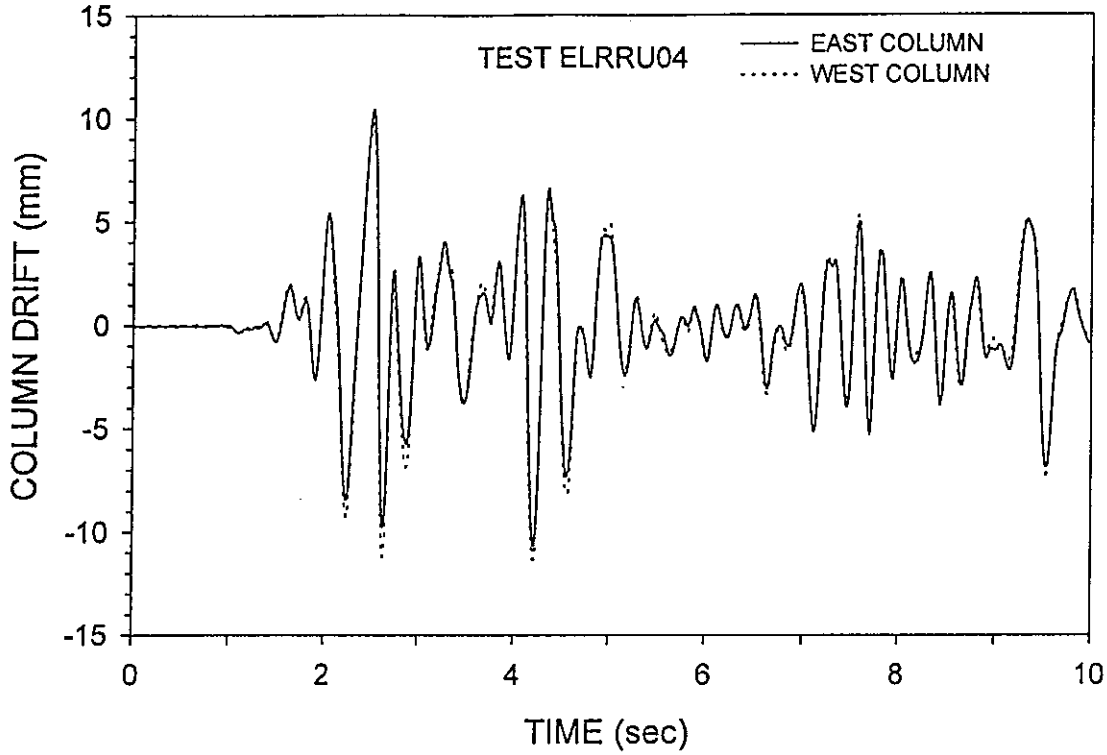

FIGURE 4-9 **Recorded Column Drifts in Test ELRRU04 with 0.935 g Peak Table Acceleration**

force. Note that the dampers were designed for a peak velocity of 585 mm/s and had a rated capacity of 9kN. Ultimate load should have been about 22 kN.

At the conclusion of test ELRRU04 none of these facts were known other than that the load cell connection exhibited some "play". Particularly, the very strong table input was not noticed. Accordingly, the load cell connection was tightened and the test was repeated. This was test ELRRU05. An identical to test ELRRU04 table acceleration history was obtained. At approximately the time of 2.5 sec from the start problems developed. The west side load cell, which was now closely observed, bent (it may have been already damaged from the previous test but not noticed) and resulted in eccentric load application on the damper. The damper failed at the point of connection of its rod to the spherical bushing. This point, which by design had a reduced area so that failure occurs there and not at an internal non-visible part, showed a failure pattern consistent with bending action.

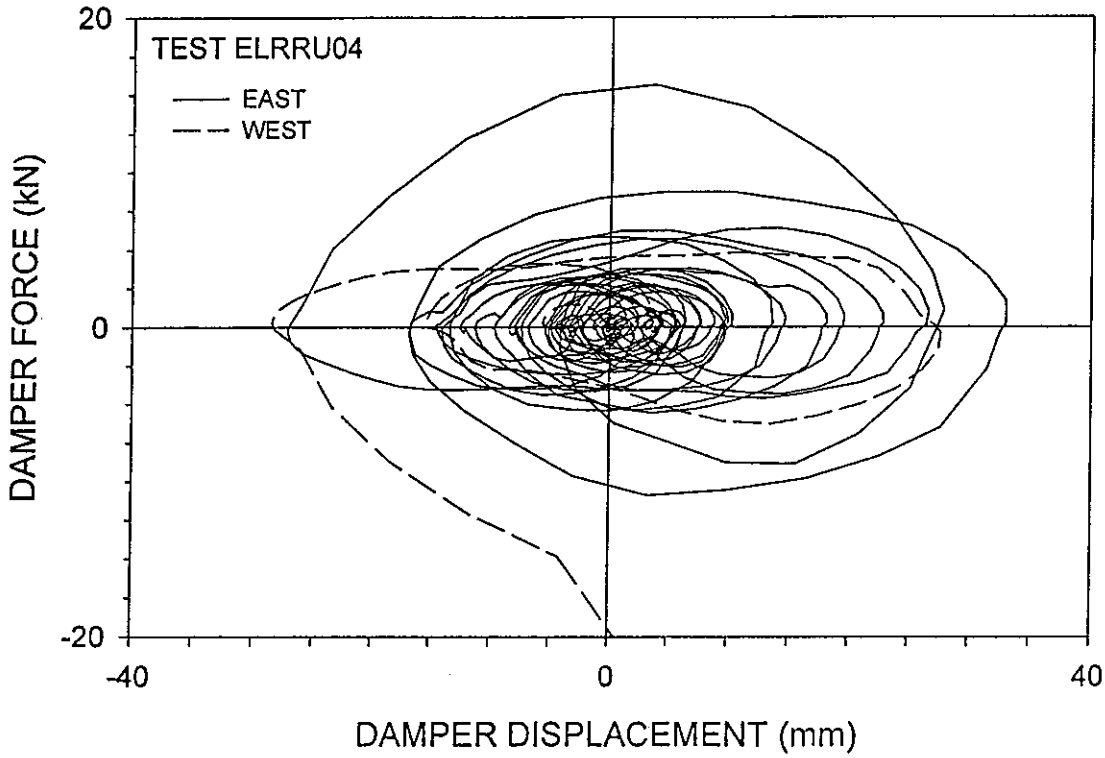

FIGURE 4-10 Recorded Damper Force-Displacement Loops in Test ELRRU04

Figure 4-11 shows the recorded column drifts in test ELRRU05. Note that the test was terminated at about 5 sec following its start. Of interest is to note that the peak drift on the east side reached about 17 mm or about 0.9-percent of the column height. On the east side it remained at approximately the same level as in the previous test.

Figure 4-12 presents the recorded damper force-displacement loops in test ELRRU05. The record for the west damper is, of course, corrupt given that the load cell bent permanently. The east side damper reaches a peak force of about 17 kN, that is, 90-percent above its rated capacity. Of interest is to note the level of inertia forces that developed on the structure during these two last tests. Records of acceleration on the concrete blocks (instrument No.15 in Fig 3-4) showed peak values of 1.04 g in test ELRRU04 and 1.03 g in test ELRRU05. At the joint of the beam to column the accelerations were at 0.82 g.

Without realizing the very high level of input acceleration in these last two tests and believing that the problem was caused by improper installation of the load cells, we

proceeded with installing a new load cell and damper B (the third spare damper) on the west side. The test was repeated and identical results with those of test ELRRU05 were obtained. The west side load cell bent permanently and the damper failed exactly as in the previous test. Still the damper on the east side performed very well despite the very high force that developed. It was removed and inspected and found to be in excellent condition.

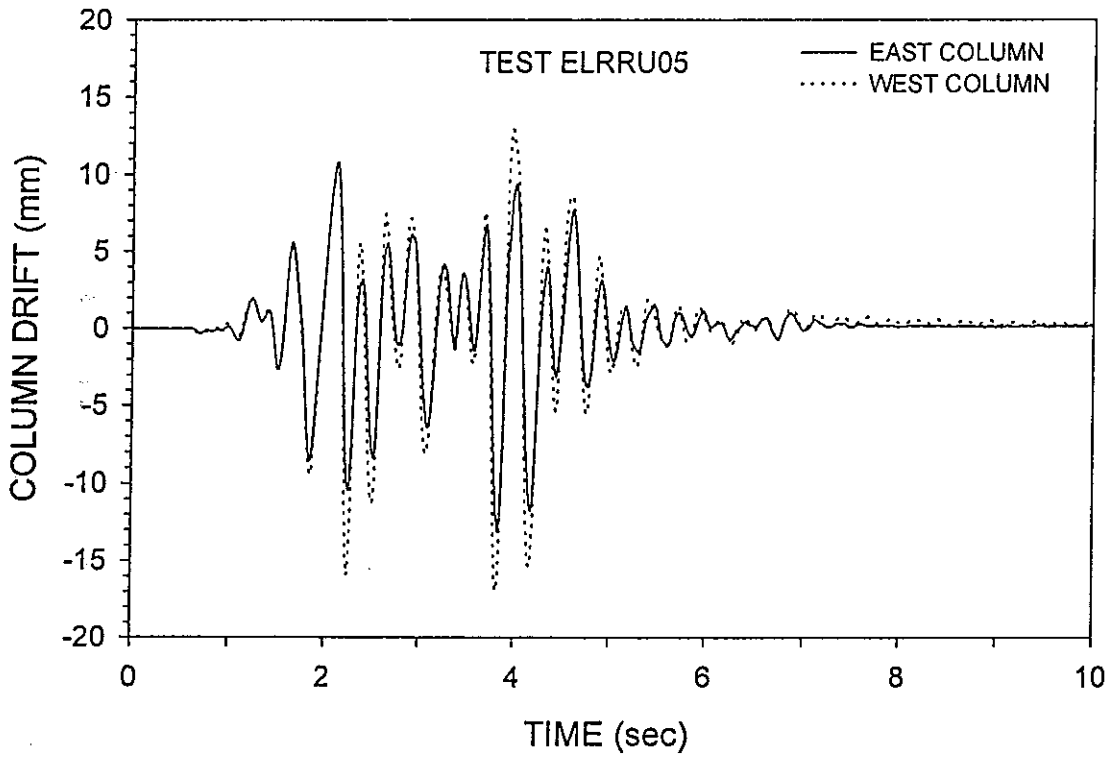

FIGURE 4-11 **Recorded Column Drifts in Test ELRRU05 (West Side Damper Failed)**

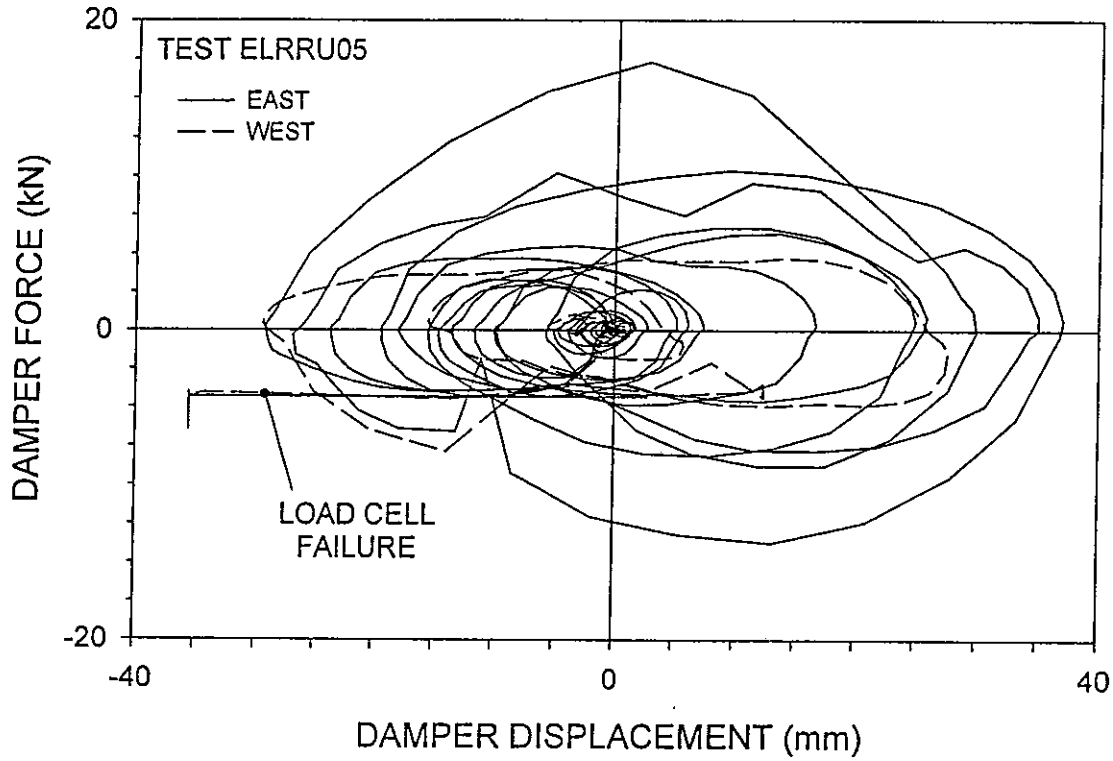

FIGURE 4-12 **Recorded Damper Force-Displacement Loops in Test ELRRU05 (West Side Damper Failed)**

SECTION 5
ANALYTICAL PREDICTION OF RESPONSE

5.1 Introduction

This section presents results of analysis of the tested structure, and comparisons of analytical and experimental results. Dynamic response history analysis of the tested structure has been performed with computer code ANSYS (Swanson Analysis Systems IP, 1996) utilizing a detailed model of the structure. This model allowed calculation of histories of displacements, accelerations and forces at locations where instruments were placed on the structure. Moreover, results of simplified analysis methods are presented. They are based on the theory of Section 2, after some modification to apply for the tested frame, and the use of response spectra.

5.2 Dynamic Response History Analysis

Dynamic analysis could be performed with a variety of commercially available computer programs. Computer code ANSYS (Swanson Analysis Systems IP, 1996) has been selected primary for its capability for large deformation analysis. This type of analysis was required in the simulation of the behavior of the frame in the floor testing with imposed large lateral movement. Results of this type of analysis have been presented in Section 2.

The ANSYS model used to simulate the behavior of the structure under support motion (shake table testing) is illustrated in Figures 5-1 and 5-2, whereas Tables 5-1 and 5-2 list the joint coordinates and the properties of the members, respectively. The schematic in Figure 5-1 illustrates the beam elements (beam, columns and braces) with a single line and the rigid elements with a triple line. Rigid elements (actually beam elements with large section properties) were used to model the behavior of the joints and of the concrete blocks (elements 4 to 7 represent the concrete blocks).

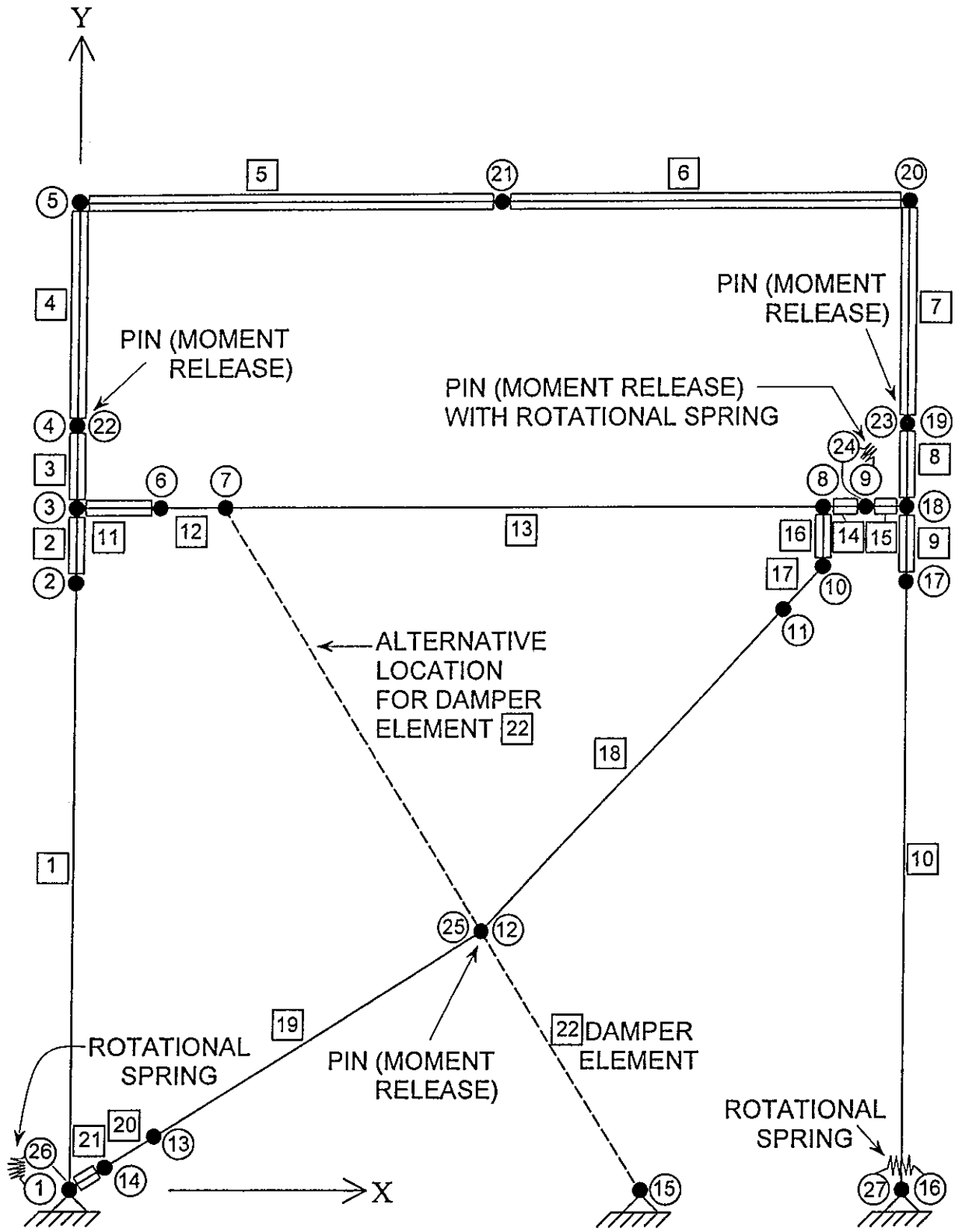

FIGURE 5-1 **Schematic Illustrating Joints and Elements in ANSYS Model of Frame with Rigid-Simple Connections (see Tables 5-1 and 5-2 for coordinates and member properties).**

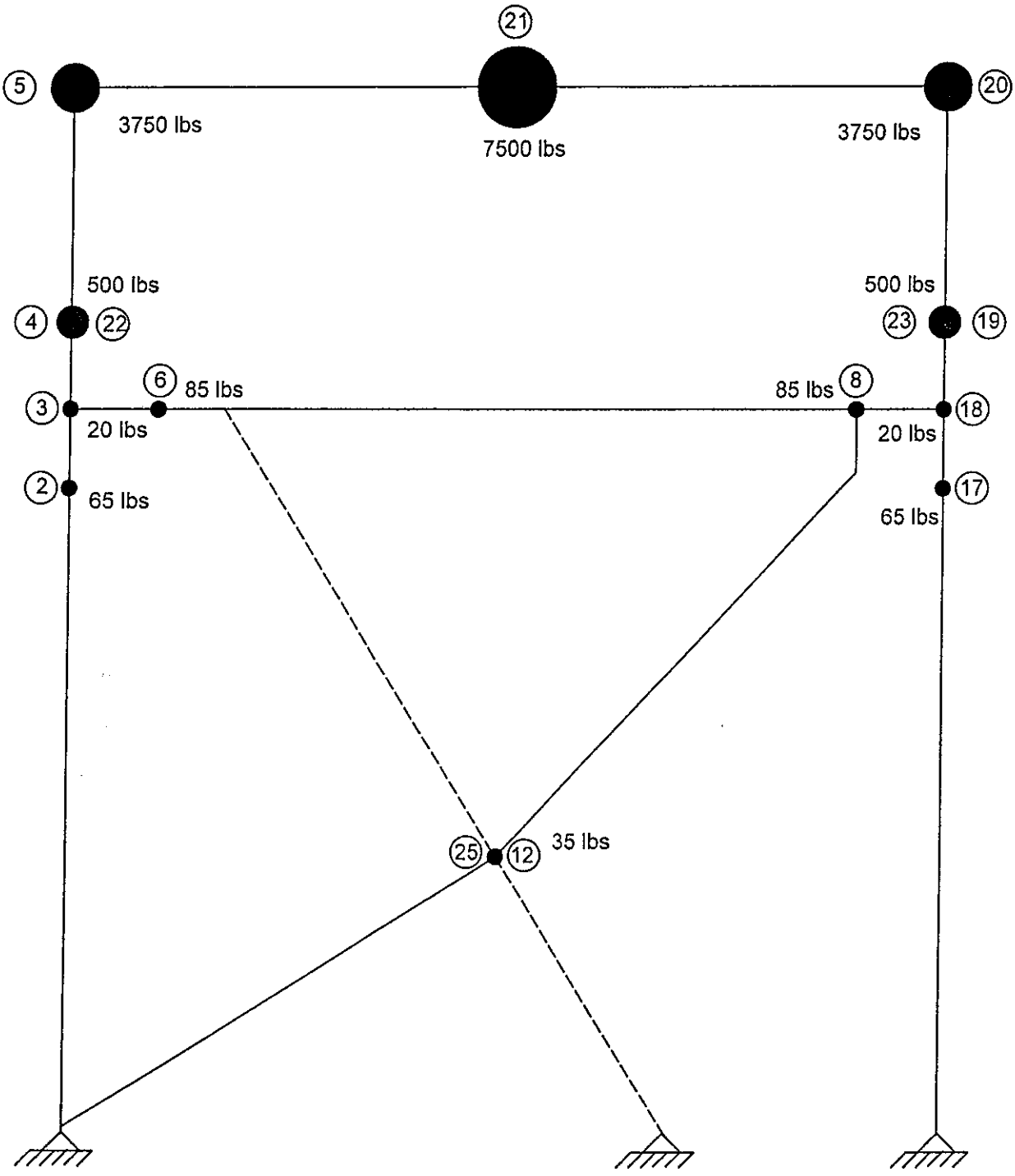

FIGURE 5-2 **Schematic Illustrating Location of Lumped Masses in ANSYS Model of Frame (values denote weight in pounds; 1 lb=4.45 N).**

TABLE 5-1 Joint Coordinates in ANSYS Model (1 in = 25.4 mm)

NODE	X (in)	Y (in)	NODE	X (in)	Y (in)	NODE	X (in)	Y (in)
1	0	0	10	87.45	69.85	19	99	92
2	0	62	11	83.34	65.48	20	99	117.8
3	0	74	12	52.61	32.74	21	49.5	117.8
4	0	92	13	8.49	5.28	22	0	92
5	0	117.8	14	3.4	2.11	23	99	92
6	12	74	15	71.08	0	24	95	74
7	26.13	74	16	99	0	25	52.61	32.74
8	87.45	74	17	99	62	26	0	0
9	95	74	18	99	74	27	99	0

The connections of the columns to their base plates were modeled as pins with rotational springs in order to simulate their actual semi-rigid behavior. A rotational spring was also used at the connection of the beam to the right column. The values of these rotational springs were selected so that the calculated fundamental frequency of the frame matched the one obtained in the testing. It should be noted that due to symmetry only one of the two frames was modeled. The ANSYS input files are presented in Appendix F.

For the analysis of the frame under imposed motion at the beam to column joint (floor testing), members 4 to 7 were de-activated, the masses at joints 4, 5, 21, 20 and 23 were removed and joint 3 was subjected to lateral movement.

Comparison of analytical and experimental response of the tested frame are presented in Figures 5-3 to 5-8 for the case of the structure with rigid-simple connections, and in Figures 5-9 and 5-10 for the structure with rigid-rigid connections. The compared responses are histories of drift (displacement of joint 3 with respect to joint 1) and of the total acceleration of joint 3, and loops of damper force-displacement. All analytical results were produced utilizing the small deformation theory, which was found to produce results of acceptable accuracy. As seen in these figures, the analytical prediction is good, although the displacements tend to be under-predicted. There are several reasons for this under-prediction:

TABLE 5-2 Element Properties in ANSYS Model (1 in = 25.4 mm, 1 kip = 4.45 kN)

ELEMENT	NODE I	NODE J	A_x (in^2)	A_y (in^2)	I_y (in^4)	MASS ($kips*sec^2/in$)
1	1	2	7.08	1.95	82.8	-
2	2	3	100	100	1000	-
3	3	4	100	100	1000	-
4	22	5	100	100	1000	-
5	5	21	100	100	1000	-
6	21	20	100	100	1000	-
7	20	19	100	100	1000	-
8	23	18	100	100	1000	-
9	18	17	100	100	1000	-
10	17	16	7.08	1.95	82.8	-
11	3	6	100	100	1000	-
12	6	7	6.16	2.07	75.3	-
13	7	8	6.16	2.07	75.3	-
14	8	9	100	100	1000	-
15	24	18	100	100	1000	-
16	8	10	100	100	1000	-
17	10	11	1	1	0.005	-
18	11	12	2.02	1.125	2.6	-
19	13	25	2.02	1.125	2.6	-
20	14	13	1	1	0.005	-
21	1	14	100	100	1000	-
22	15 (7)	25	$C_o = 0.0088$ kips*sec/in			
23	21	-	-	-	-	1.94E-2
24	5	-	-	-	-	9.71E-3
25	20	-	-	-	-	9.71E-3
26	19	-	-	-	-	1.295E-3
27	4	-	-	-	-	1.295E-3
28	18	-	-	-	-	5.178E-5
29	3	-	-	-	-	5.178E-5
30	6	-	-	-	-	2.2E-4
31	8	-	-	-	-	2.2E-4
32	17	-	-	-	-	1.683E-3
33	2	-	-	-	-	1.683E-3
34	12	-	-	-	-	9.062E-5
35	26	1	$K_{rot} = 10000$ kips*in/radian			
36	27	16	$K_{rot} = 10000$ kips*in/radian			
37	24	9	$K_{rot} = 15000$ kips*in/radian			

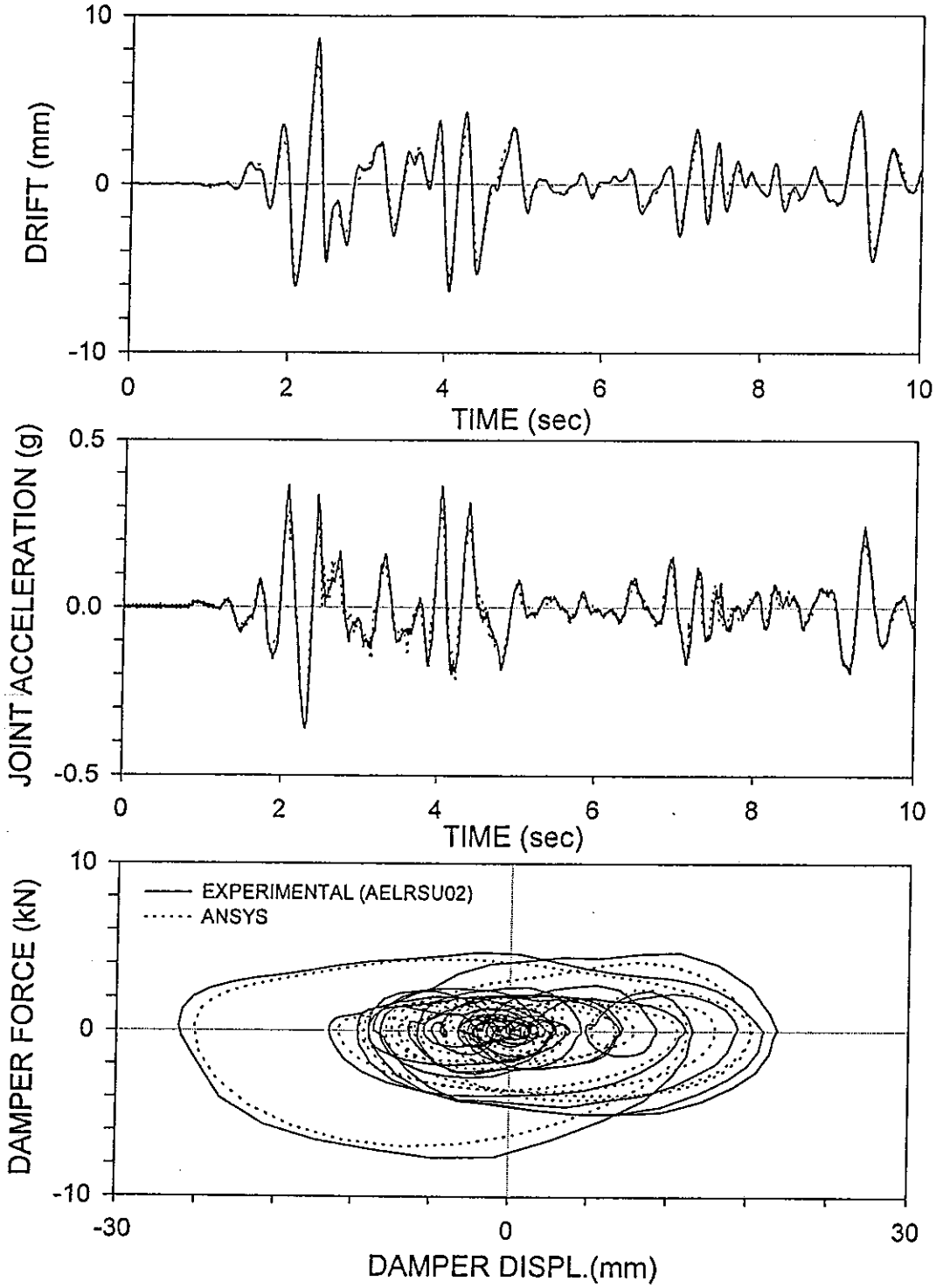

FIGURE 5-4 **Comparison of Analytical (ANSYS, small Deformation Analysis) and Experimental Response of Rigid-Simple Structure with Upper Dampers for El Centro 100% Input**

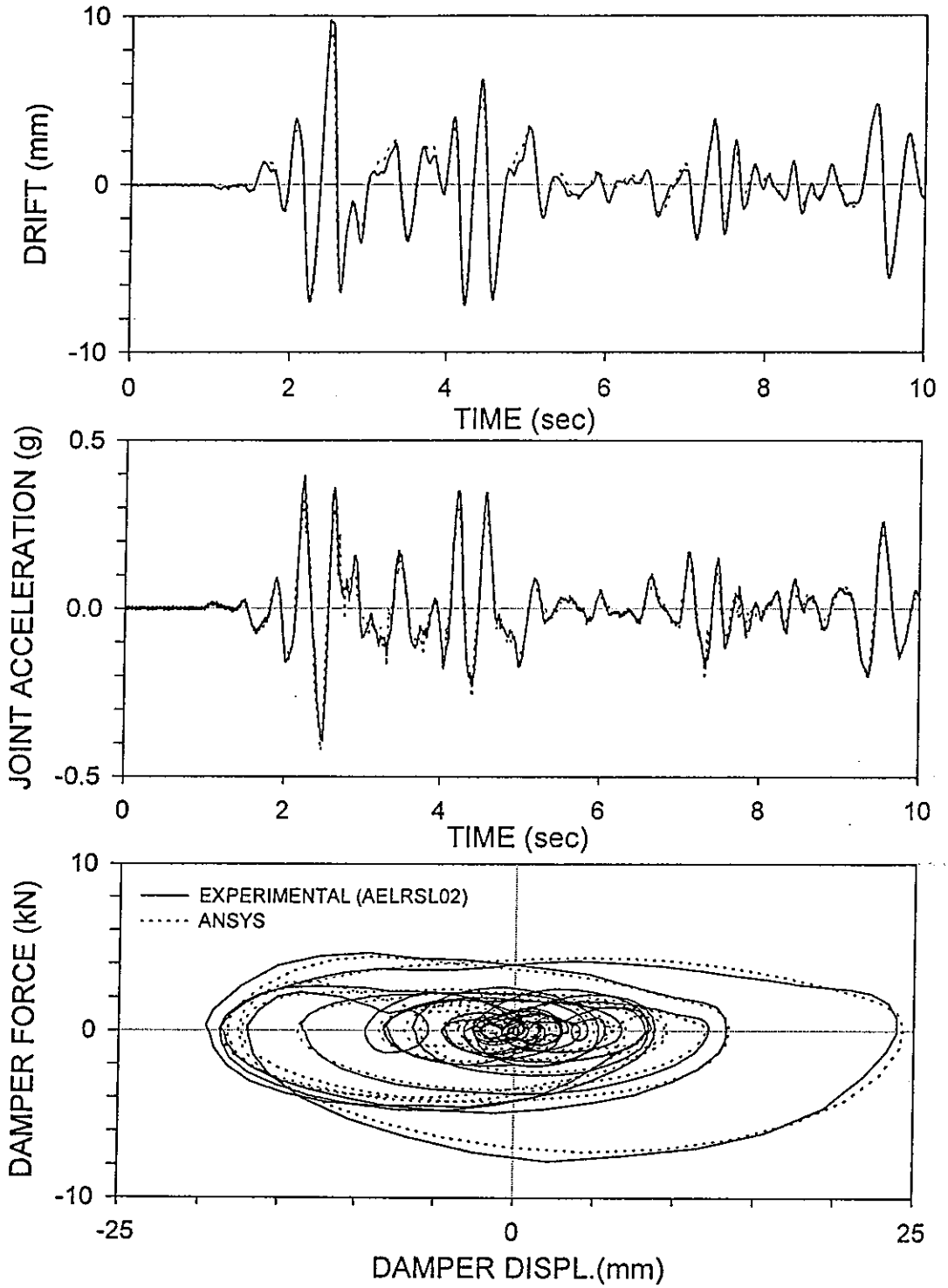

FIGURE 5-3 **Comparison of Analytical (ANSYS, small Deformation Analysis) and Experimental Response of Rigid-Simple Structure with Lower Dampers for El Centro 100% Input**

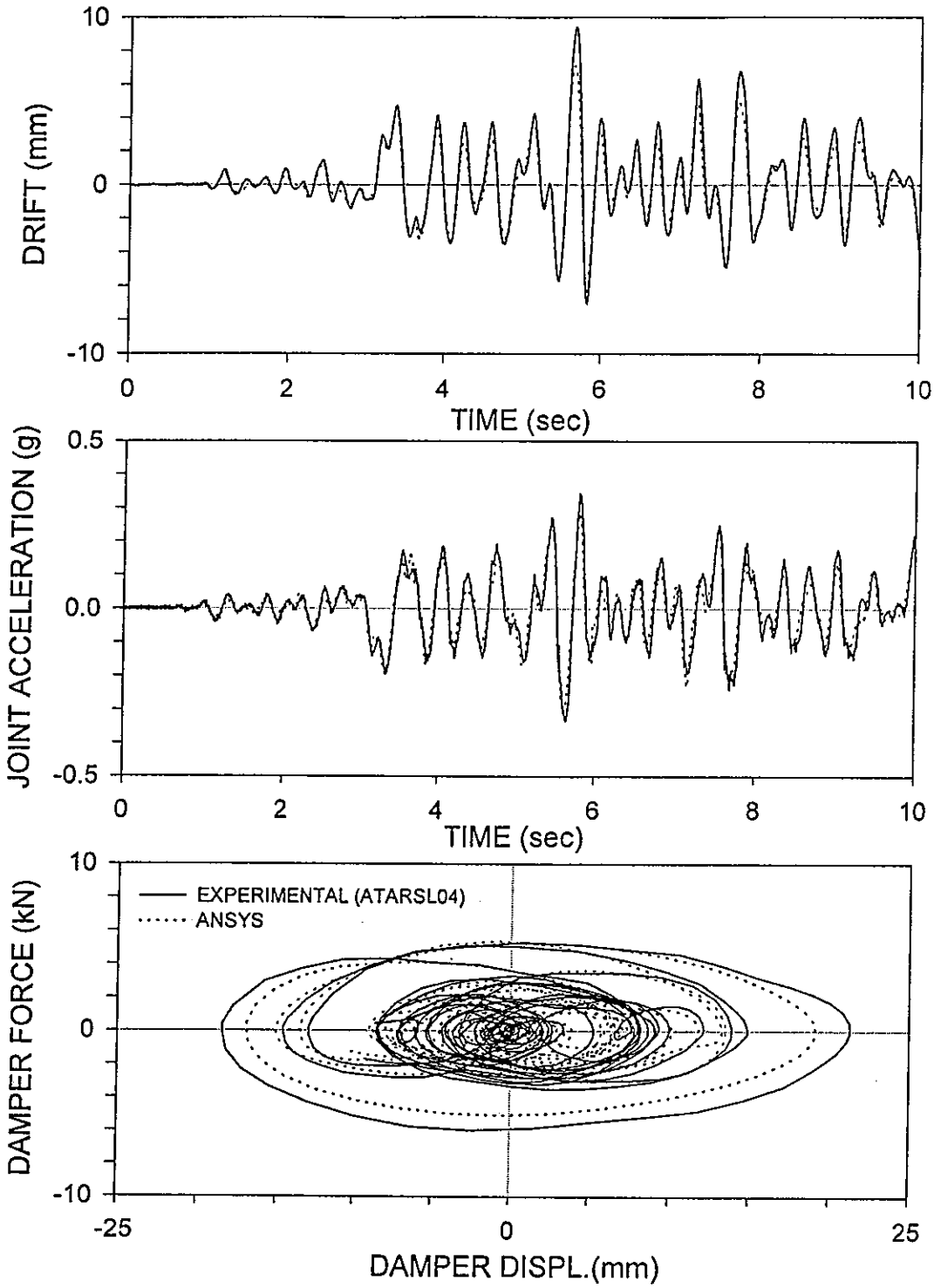

FIGURE 5-5 **Comparison of Analytical (ANSYS, small Deformation Analysis) and Experimental Response of Rigid-Simple Structure with Lower Dampers for Taft 200% Input**

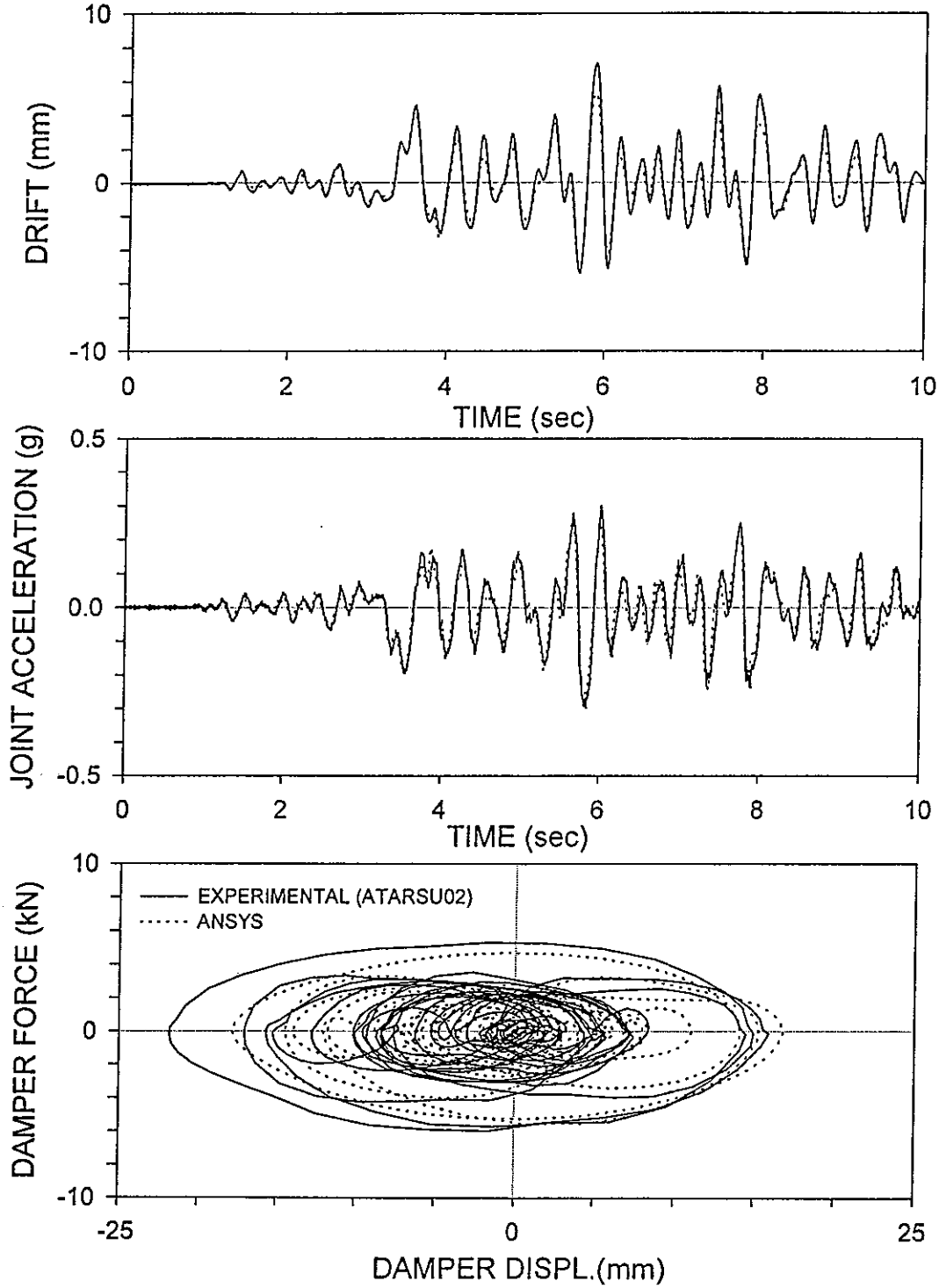

FIGURE 5-6 **Comparison of Analytical (ANSYS, small Deformation Analysis) and Experimental Response of Rigid-Simple Structure with Upper Dampers for Taft 200% Input**

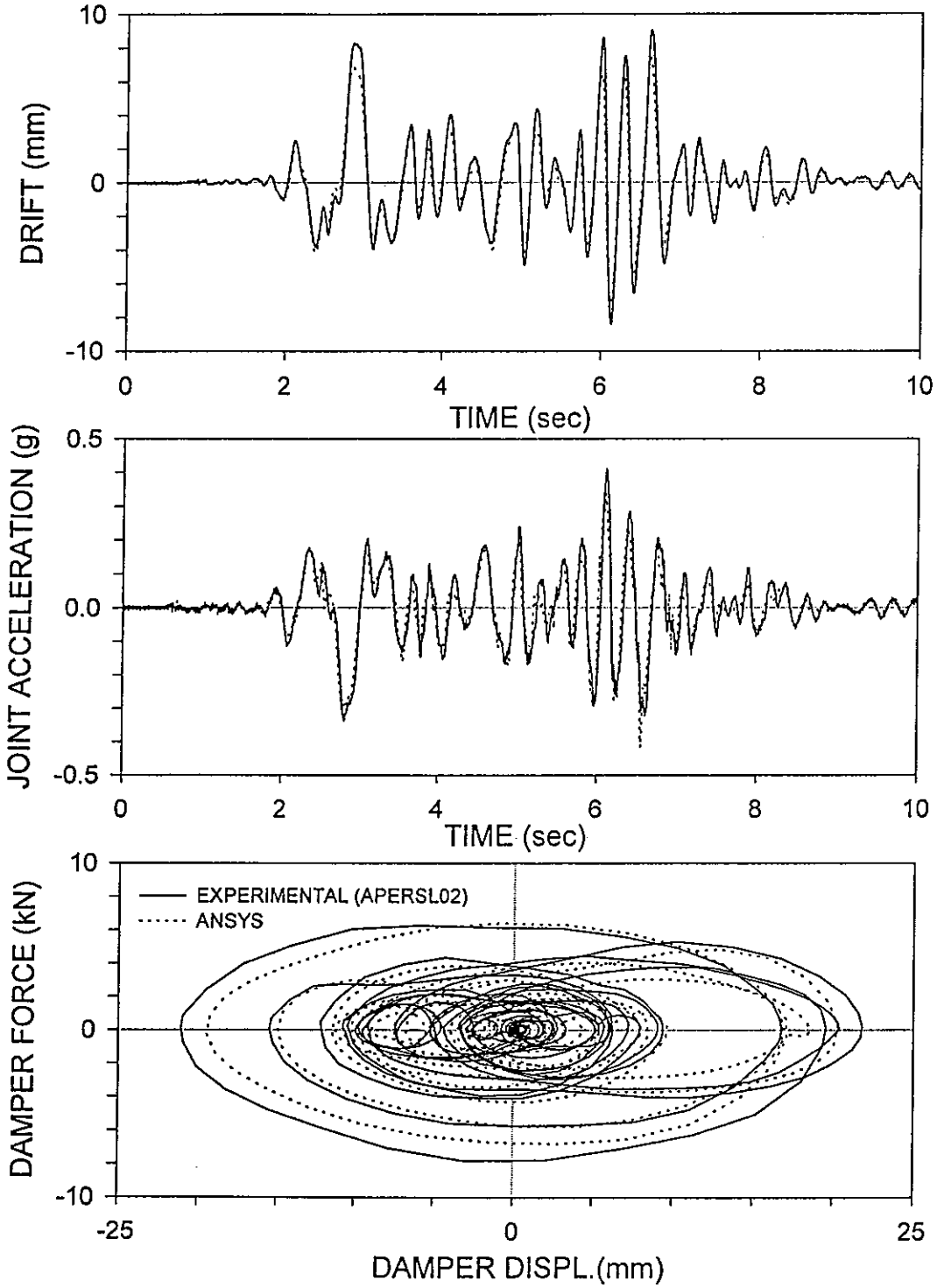

FIGURE 5-7 **Comparison of Analytical (ANSYS, small Deformation Analysis) and Experimental Response of Rigid-Simple Structure with Lower Dampers for Pacoima S16E 50% Input**

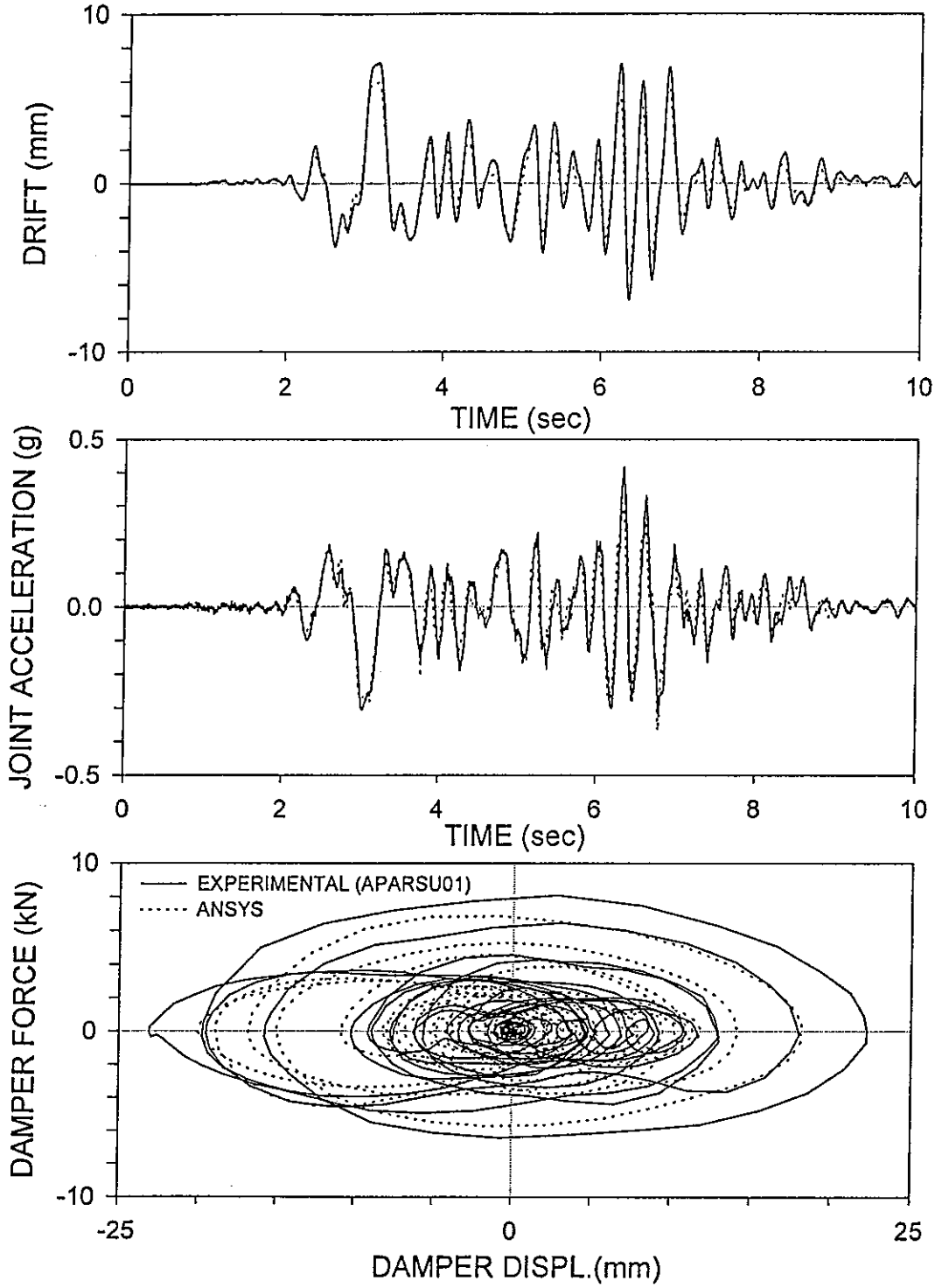

FIGURE 5-8 **Comparison of Analytical (ANSYS, small Deformation Analysis) and Experimental Response of Rigid-Simple Structure with Upper Dampers for Pacoima S16E 50% Input**

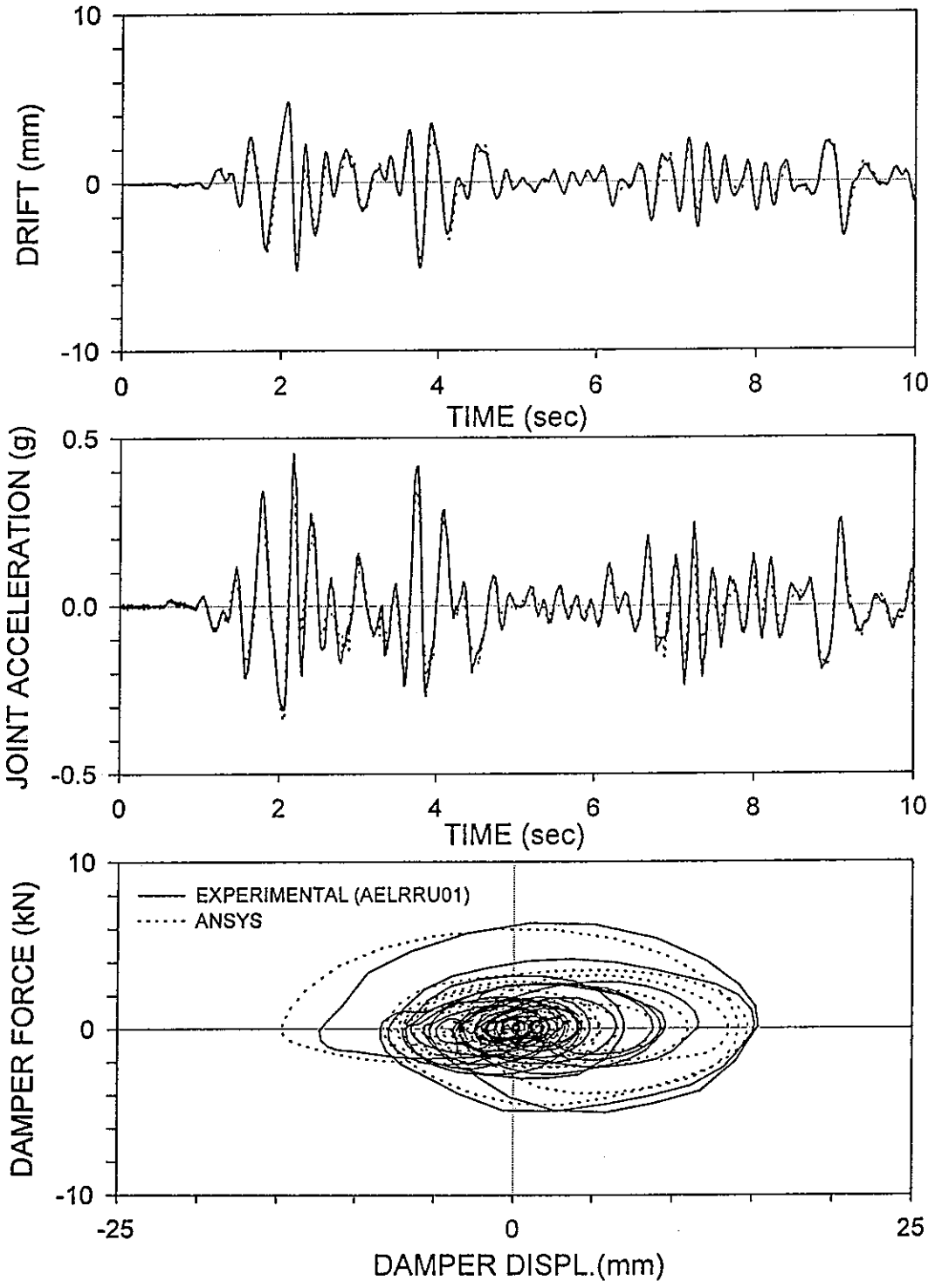

FIGURE 5-9 **Comparison of Analytical (ANSYS, small Deformation Analysis) and Experimental Response of Rigid-Rigid Structure with Upper Dampers for El Centro 100% Input**

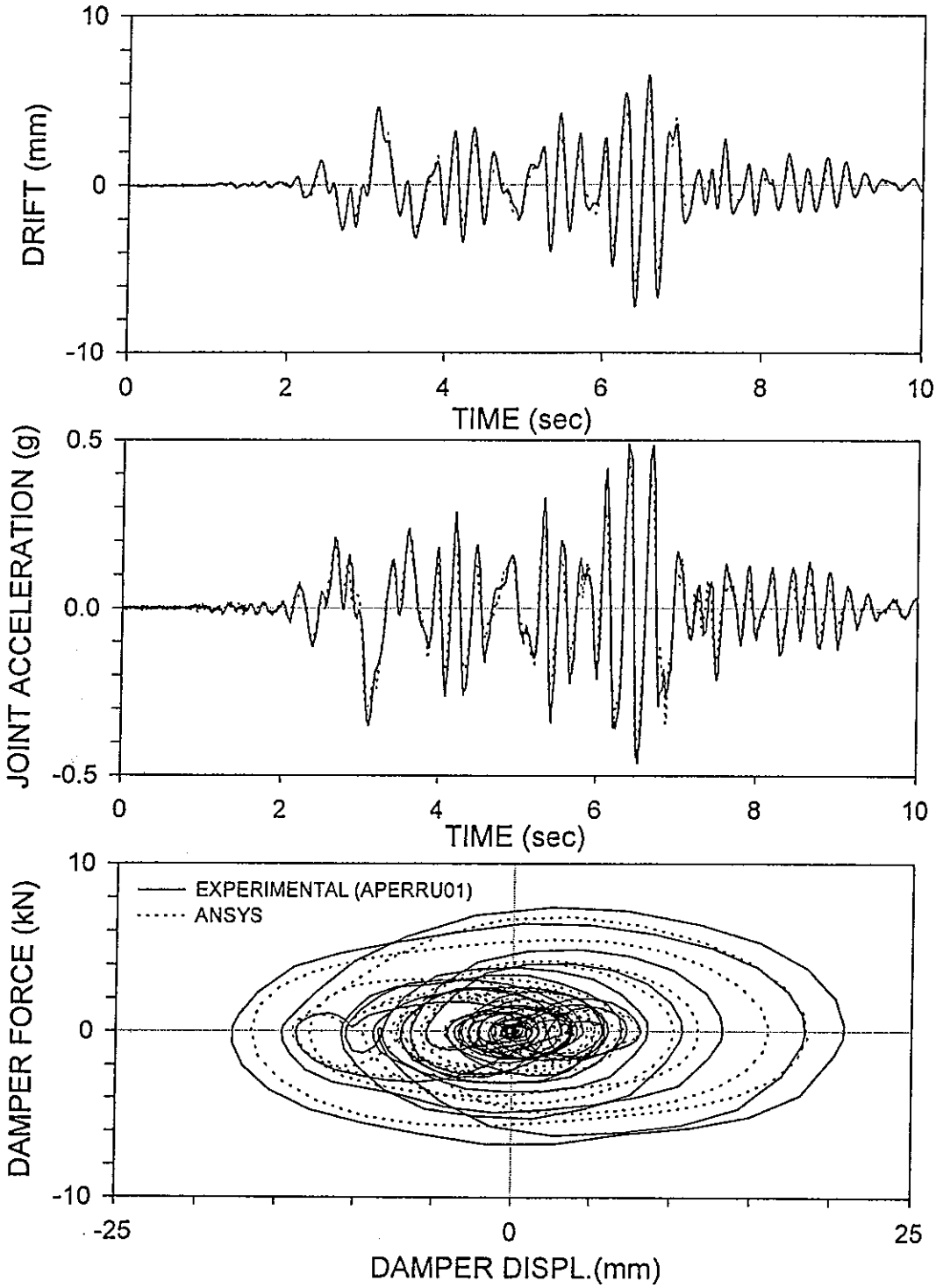

FIGURE 5-10 **Comparison of Analytical (ANSYS, small Deformation Analysis) and Experimental Response of Rigid-Rigid Structure with Upper Dampers for Pacoima S16E 50% Input**

(a) as discussed in Section 2, a very small slippage in the joints could result in small reduction in the energy dissipation of the capability toggle-damper system,

(b) the properties of the frame exhibited small changes during testing due to the frequent changes made in its configuration, and

(c) significant changes in the temperature of the dampers during continuous testing without idle time in-between tests have caused fluctuations in the properties of the dampers.

Finally, Figure 5-11 presents a comparison of analytical results produced by ANSYS when utilizing first the small deformation theory and then the large deformation theory. There is very small difference between the two sets of results. This should be expected given the evidence provided in Section 2.

5.3 Simplified Analysis

Simplified methods of analysis have been described in Federal Emergency Management Agency, 1996. In general, such methods utilize response spectra and require the determination of mode shapes, frequencies and damping ratios. For elastic structural systems with fluid viscous dampers (that is, without viscoelastic effects), the mode shapes and frequencies are those of the undamped structural system and, thus, can be easily determined. The damping ratios are then obtained on the basis of energy considerations (e.g., Constantinou and Symans, 1992). That is, based on the structural system depicted in Figure 5-12 the damping ratio of mode k is

$$\xi_k = \xi_{strk} + \frac{1}{2}\frac{\sum_j C_{0j} f_j^2 (\phi_j - \phi_{j-1})^2}{\omega_k \sum_i m_i \phi_i^2} \qquad (5\text{-}1)$$

where ξ_{strk} is the damping ratio due to damping inherent to the structure, ω_k is the frequency of mode k and ϕ_j is the component of the kth mode corresponding to floor j (i.e., the horizontal displacement of each floor represents a degree of freedom). Summation j extends over all dampers (ϕ_j-ϕ_{j-1} is the relative modal displacement of the two ends of the toggle braces) and summation i extends over all lumped masses. Moreover, f_j is the displacement magnification factor of damper system j.

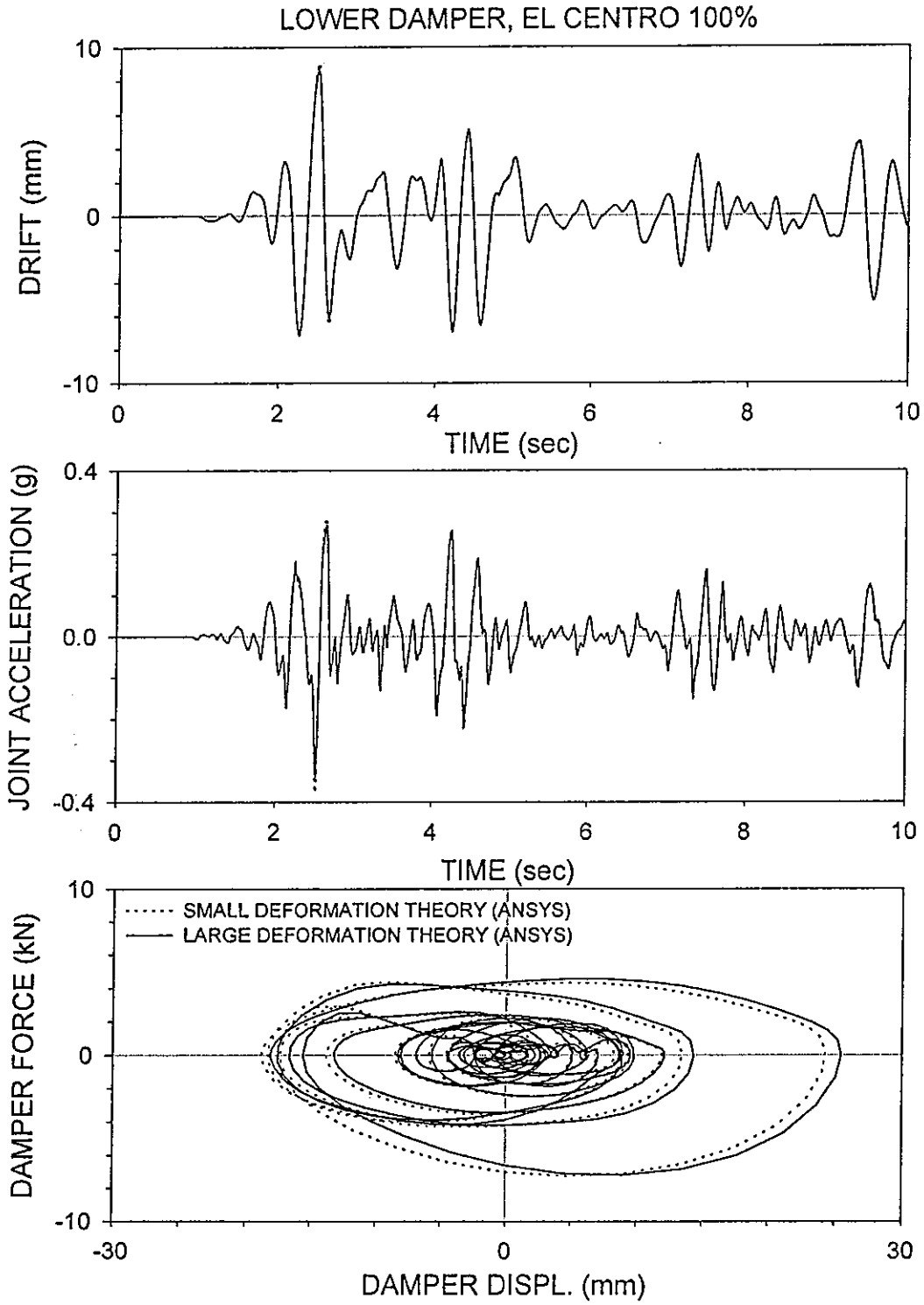

Figure 5-11 **Comparison of Analytical Results for Test AELRSL02 Utilizing Small and Large Deformation Theories**

The application of (5-1) to the tested structural system is simple given that the system is essentially a single degree of freedom system. Based on Figure 5-13, the modal displacement of the center mass of the concrete block, ϕ_2, is the same as the displacement of the points of connection of the blocks to the columns (pins). Moreover, the relative modal displacement of the toggle brace system is ϕ_1. That is,

$$\xi_1 = \xi_{str1} + \frac{C_o f^2 \phi_1^2}{2\omega_1 m \phi_2^2} \tag{5-2}$$

or

$$\xi_1 = \xi_{str1} + \frac{C_o f^2 g T}{4\pi W}\left(\frac{\phi_1}{\phi_2}\right)^2 \tag{5-3}$$

where T is the period and W is the weight of the blocks (half of the total weight since only one frame is considered).

The period and mode shape could be easily determined given that an analytical model of the structure has been developed for response history analysis. The ratio ϕ_1/ϕ_2 was determined to be 0.828. However, one could simply estimate this ratio by recognizing that ϕ_1/ϕ_2 is approximately equal to H_1/H_2, where H_1 is the height of the upper end of the toggle brace (joint 10 in Fig. 5-1) and H_2 is the height of the point of connection of the concrete block to the column (joint 19). That is (see Table 5-1), H_1/H_2 = 69.85/92 =0.759. Use of (5-3) with T = 0.29 to 0.32sec (freq. = 3.1 to 3.4 Hz, see Table 4-1), W = 72 kN, C_o = 15.4 N s/mm, and f= 2.66 (lower damper) and f_u = 3.19 (upper damper), we obtain for the case of the configuration with rigid-simple connections the following results:

(a) Case of lower damper: ξ_1 = 0.26, T = 0.32 sec,

(b) Case of upper damper: ξ_1 = 0.34, T = 0.29 sec.

The calculated values of damping ratio are higher than the values determined from transfer functions (see Table 4-1). The primary reason for this is the use of the theoretical values of the displacement magnification factors which are somewhat higher than the actual ones due to slippage in the joints (see Section 2). More realistic values would have been f = 2.5 and f_u = 3.0 rather than 2.66 and 3.19, respectively.

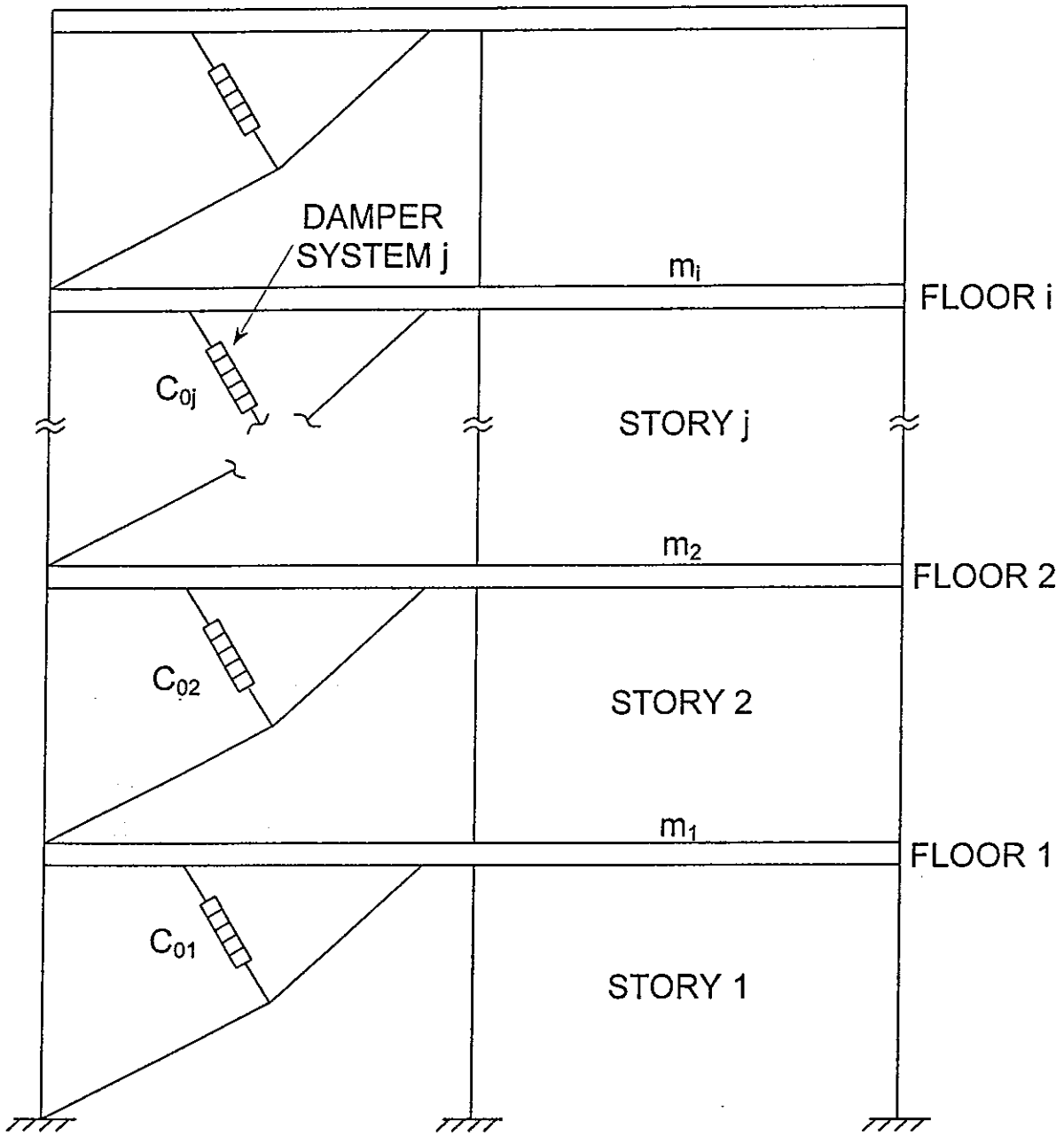

FIGURE 5-12 Plane Structural System with Linear Dampers

Determination of the peak dynamic response can be made by use of response spectra for high damping like those of Figure 5-14 for the El Centro motion. Note that acceleration spectrum is the maximum acceleration spectrum (not the pseudo-acceleration). Moreover, these spectra are for the time scale ($\sqrt{2}$) used in the testing so that they can be used to predict the peak experimental response. It should be noted that

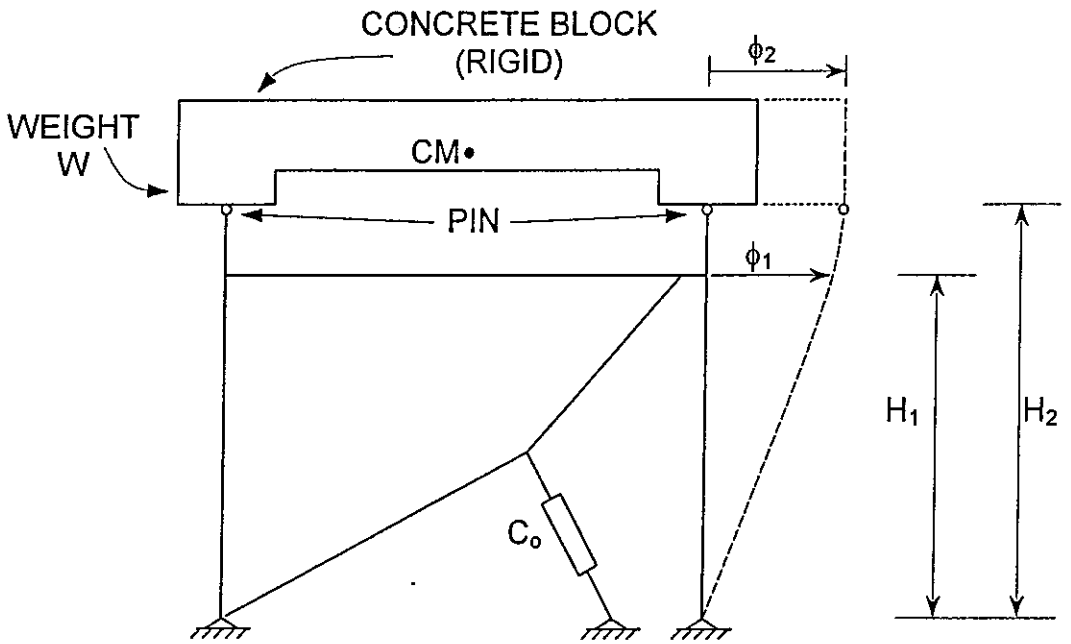

FIGURE 5-13 Schematic of Tested Structural System Showing Modal Displacements

the calculated peak response is the one of the center of mass of the concrete blocks. Therefore to calculate the peak response of the column to beam joint (the one reported in Table 4-2), one has to multiply by the factor $\phi_1/\phi_2 = 0.828$.

The peak response in tests AELRSL02 and AELRSU02 (with El Centro 100% input) has been calculated and is presented in Table 5-3 together with the experimental response. The peak damper displacement was calculated by equations (2-5) and (2-6), whereas the peak damper force was calculated by

$$F_D = C_o\left(\frac{2\pi}{T}\right)u_D \qquad (5\text{-}4)$$

where u_D is the peak damper displacement. It should be noted that the quantity $(2\pi/T)\ u_D$ is the damper pseudo-velocity which is used as a measure of the peak damper velocity. It may be observed in Table 5-3 that the analytical prediction is generally good although the structural drift is underpredicted. The reasons for this under-prediction are:

(a) The damping ratio has been overestimated, although this was insignificant as it is evident in the displacement spectrum of Figure 5-14.

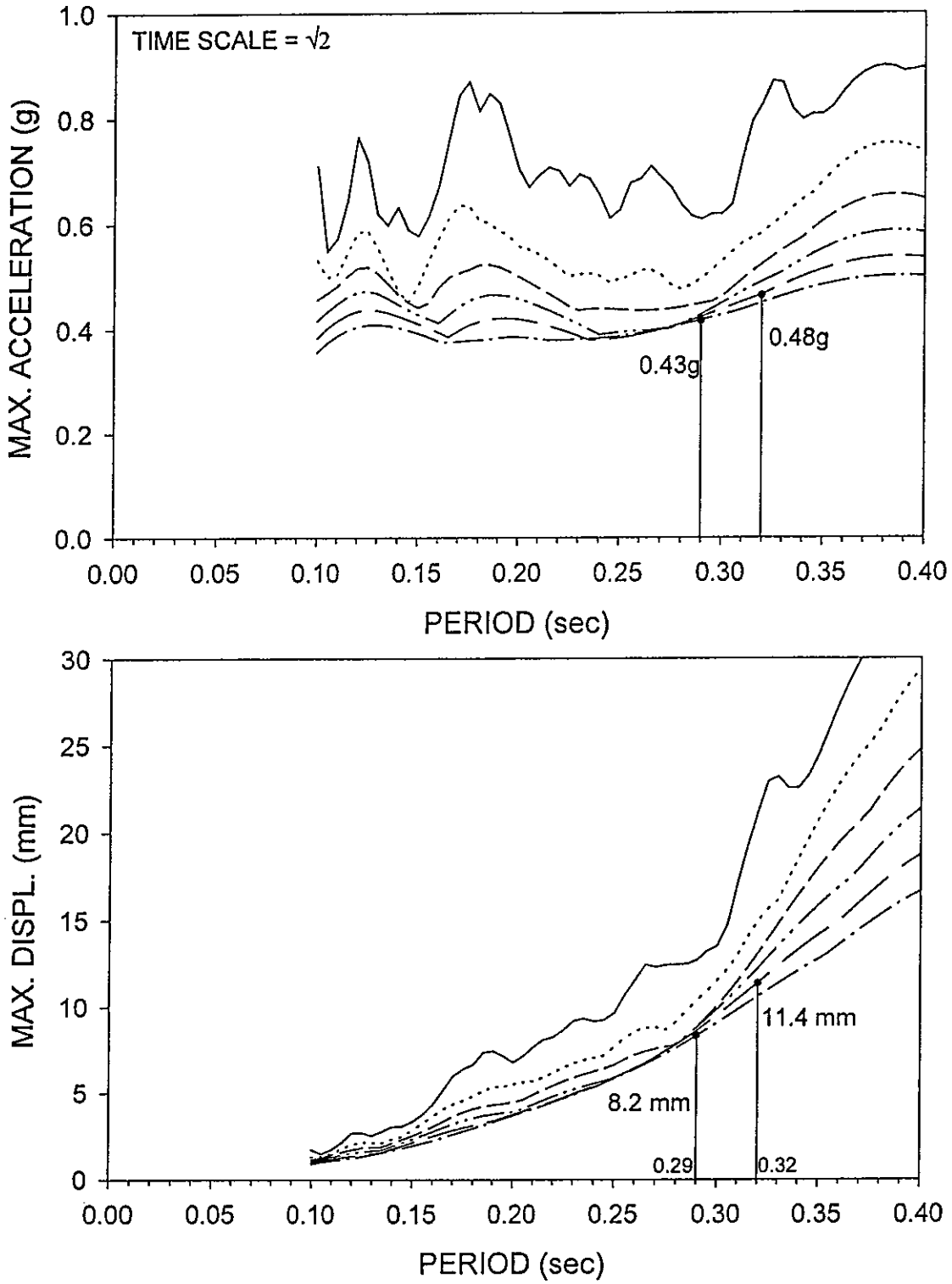

FIGURE 5-14 **Damped Response Spectra of El Centro S00E (100%) for Damping Ratios of 0.05, 0.10, 0.15, 0.20, 0.25 and 0.30.**

(b) The period of the system may have been different than assumed. As seen in Figure 5-14, the period has significant effect on the displacement response given that it lies in acceleration region of the spectrum (displacement proportional to period squared).

TABLE 5-3 Peak Response of Tested Structure with Rigid-Simple Connections as Calculated by Simplified Analysis and Comparison to Experimental Response (El Centro 100% input)

PEAK RESPONSE QUANTITY	ANALYTICAL		EXPERIMENTAL *	
	LOWER DAMPER	UPPER DAMPER	LOWER DAMPER [1]	UPPER DAMPER [2]
DRIFT (mm)	9.4	6.8	10.3	8.4
JOINT ACCELERATION (g)	0.40	0.36	0.38	0.35
PEAK DAMPER FORCE (kN)	7.6	7.3	7.3	7.6
PEAK DAMPER DISPLACEMENT (mm)	25.0	21.7	23.8	25.0

*: Experimental is average of two sides
1: Test AELRSL02
2: Test AELRSU02

SECTION 6
CONCLUSIONS

Stiff structural systems exhibit small drifts and small interstory velocities so that the conventional application of energy dissipation may not be feasible. The improved damper configuration investigated in this report utilizes a mechanism for magnifying displacements so that it is practical for application in stiff structural systems.

The studied damper configuration utilizes toggle braces that result in damper displacements that are significantly larger than the structural drift. While this configuration is compact by comparison to other proposed configurations, it undergoes large rotations that, on first sight, appear to require complex analysis. An exact analytical treatment of the kinematics of this configuration has been developed. The exact solution has then been reduced to the limit of small rotations, resulting in simple equations that can used in the simplified analysis of structures with this energy dissipation system.

An experimental study of a structural system equipped with the improved damper configuration has been conducted. The study included cyclic and shake table testing of the system. A variety of configurations and connection details have been investigated in the experimental study. Of these, two connection details, termed the pinned and the bent plate connections, were found to perform in accordance with the theoretical predictions. Another connection detail, termed the spring leaf connection, was found to be unacceptable.

The results of the shake table testing demonstrated the theoretically predicted ability of the tested structure to dissipate seismic energy and, thus, reduce drifts and lateral forces in comparison to the same structure but without the improved energy dissipation system. Analytical predictions of the dynamic response of the tested structure have been made using the computer code ANSYS by utilizing both large and small deformation theories. It has been demonstrated that the use of the small deformation theory produces results that are nearly identical to those of the large deformation theory, and that both produce results of acceptable accuracy. Moreover, simplified analysis procedures have been presented that can provide good estimates of the peak dynamic

response by utilizing information on the dynamic characteristics of the undamped structural system, the geometry of the toggle-brace-damper system and the properties of the dampers, and response spectra of the ground motion.

An important conclusion of this study is that the analysis of structures with the toggle-brace-damper system can be performed by establishing procedures (e.g., those described in the FEMA 273 and 274 reports) with one simple modification: instead of using the quantity $\cos\theta$ (where θ is the angle of inclination of the damper in a conventional installation), the displacement magnification factor f (see equations 2-5 to 2-7) is used. This factor is simply related to the geometry of the toggle-brace system.

SECTION 7
REFERENCES

1. Chironis, N.P. (1991), *Mechanisms and Mechanical Devices Sourcebook*, Mc Graw-Hill, Inc., New York.

2. Constantinou, M.C. and Symans, M.D., (1992), "Experimental and Analytical Investigation of Seismic Response of Structures with Supplemental Fluid Viscous Dampers," Report No. NCEER-92-0032, National Center for Earthquake Engineering Research, Buffalo, New York.

3. Constantinou, M.C., Soong, T.T and Dargush G.F., (1996), *Passive Energy Dissipation Systems for Structural Design and Retrofit*, Monograph of the National Center for Earthquake Engineering Research, Buffalo, New York.

4. Federal Emergency Management Agency (1995), " 1994 NEHRP Recommended Provisions for Seismic Regulations for New Buildings," Report FEMA 222A, Washington, D.C.

5. Federal Emergency Management Agency (1966), "NEHRP Guidelines for the Seismic Rehabilitation of Buildings," Reports FEMA 273 (Guidelines) and 274 (Commentary), ballot version, Washington, D.C., September.

6. Hibino, H., Kawamura, S., Hisano, M., Yamada, M., Kawamura, H., and Morita, H. (1989), "A Study on Response Control System on Structures Utilizing Damping Amplifier," Taisei Technical Research Journal, Vol. 22 (Nov.), 155-162 (in Japanese).

7. Osteraas, J. and Krawinkler, H. (1990), "Strength and Ductility Considerations in Seismic Design," Report No. 90, John Blume Earthquake Engineering Center, Stanford University, Stanford, CA.

8. Reinhorn, A.M., Li, C., and Constantinou, M.C. (1995), "Experimental and Analytical Investigation of Seismic Retrofit of Structures with Supplemental Damping Part I: Fluid Viscous Damping Devices", Technical Report NCEER-95-0001, National Center for Earthquake Engineering Research, Buffalo, New York.

9. Seleemah, A.A., and Constantinou, M.C. (1997), "Investigation of Seismic Response of Buildings with Linear and Nonlinear Fluid Viscous Dampers," Report No. NCEER-97-0004, National Center for Earthquake Engineering Research, Buffalo, New York.

10. Soong, T.T and Dargush G.F., (1996), *Passive Energy Dissipation Systems in Structural Engineering*, Wiley and Sons, London.

11. Swanson Analysis Systems IP, (1996), "ANSYS , Finite Element Program and User's Manual", Version 5.3.

12. Tsopelas, P., Constantinou, M.C., Kircher, C.A., and Whittaker, A.S., (1997), "Evaluation of Simplified Methods of Analysis for Yielding Structures", Report No. NCEER-97-00xx, National Center for Earthquake Engineering Research, Buffalo, New York.

APPENDIX A

DRAWINGS OF TESTED STRUCTURE

Note: Drawings are as provided to fabricator
(1 foot = 304.8 mm, 1 in. = 25.4 mm).

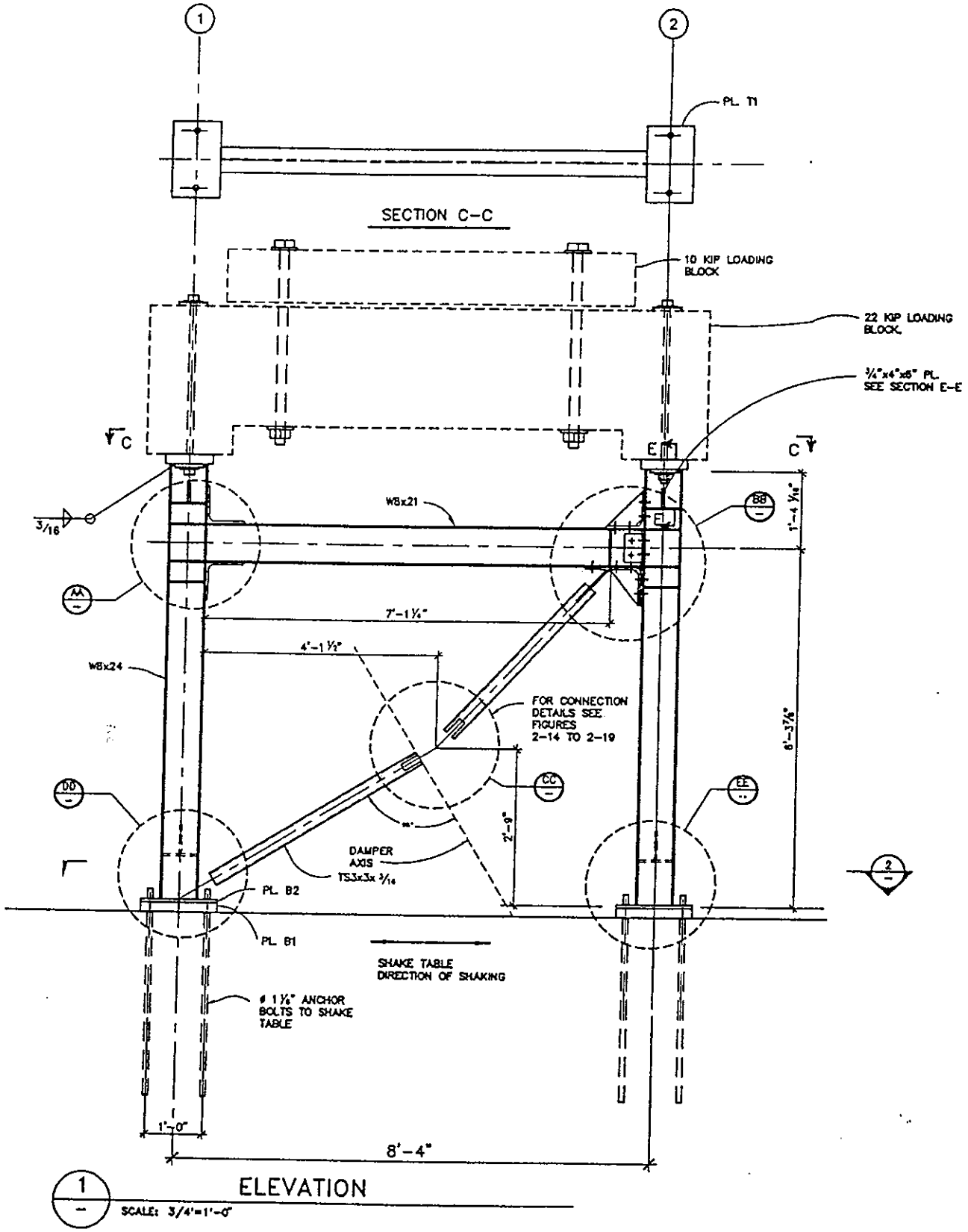
1
2
PL. T1
SECTION C-C
10 KIP LOADING BLOCK
22 KIP LOADING BLOCK
¾"x4"x6" PL. SEE SECTION E-E
C
C
E
E
W8x21
W8x24
3/16
AA
BB
CC
DD
EE
7'-1¼"
4'-1½"
FOR CONNECTION DETAILS SEE FIGURES 2-14 TO 2-19
DAMPER AXIS
TS3x3x ¾6
PL. B2
PL. B1
SHAKE TABLE DIRECTION OF SHAKING
1⅛" ANCHOR BOLTS TO SHAKE TABLE
1'-4 ⅛"
8'-3⅞"
2'-9"
1'-0"
8'-4"
2
1
ELEVATION
SCALE: 3/4"=1'-0"

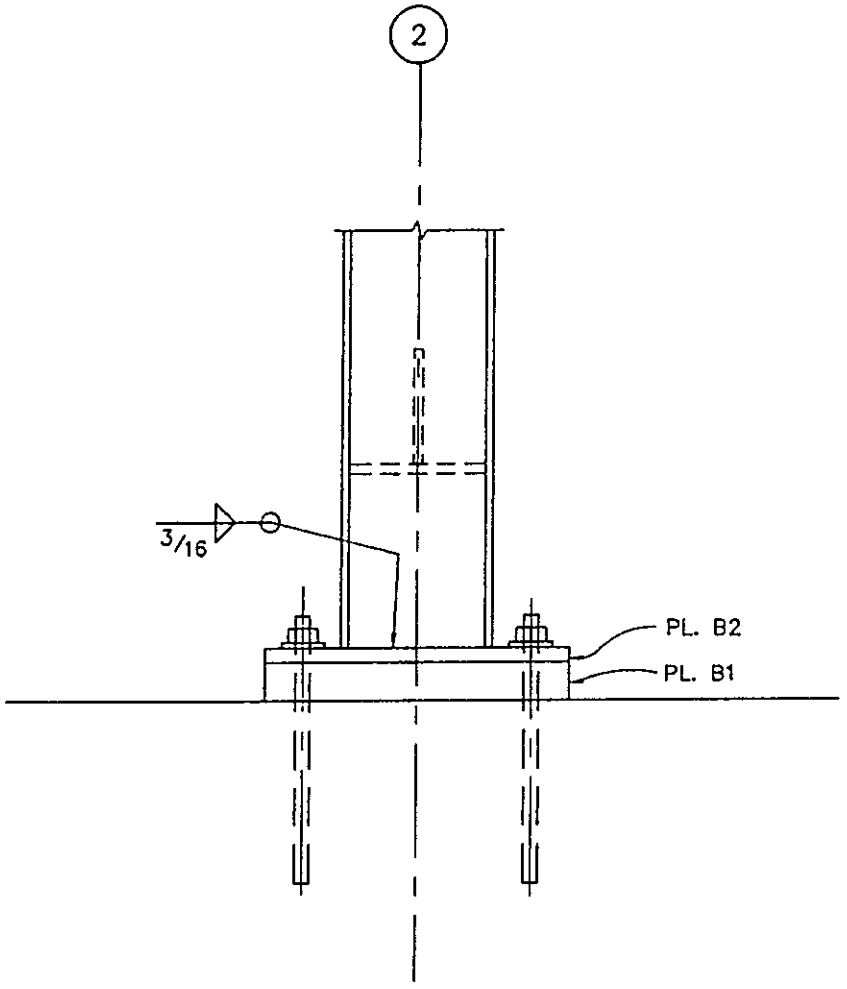

EE
—

DETAIL

SCALE: 1 1/2"=1'-0"

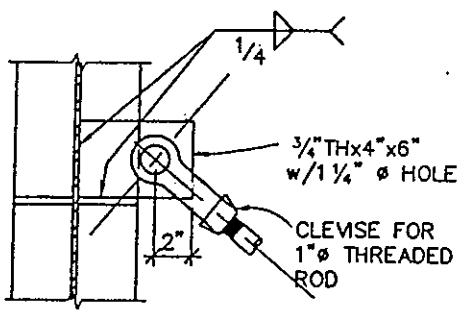

SECTION E–E

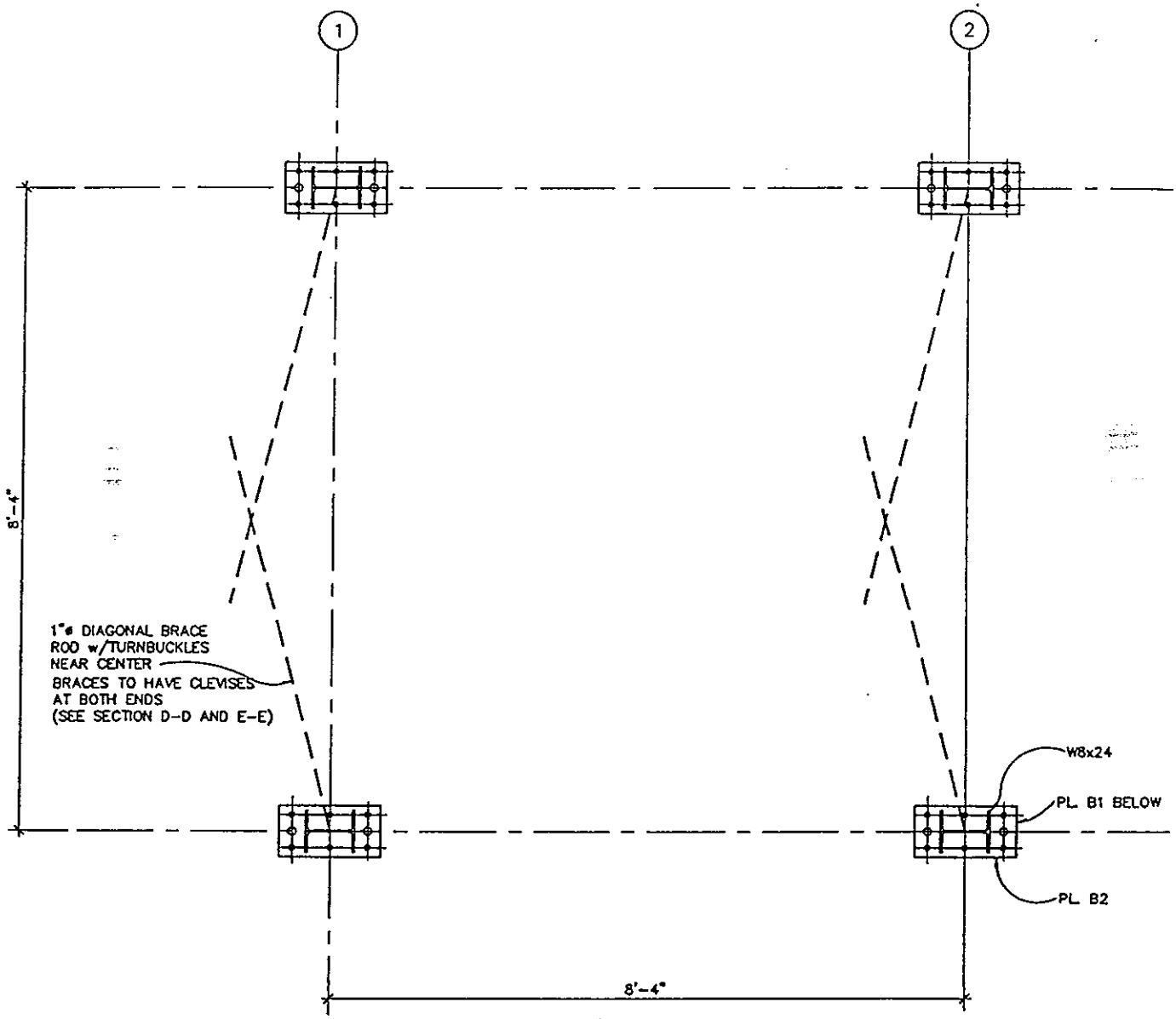

2 / – PLAN

SCALE: 3/4"=1'-0"

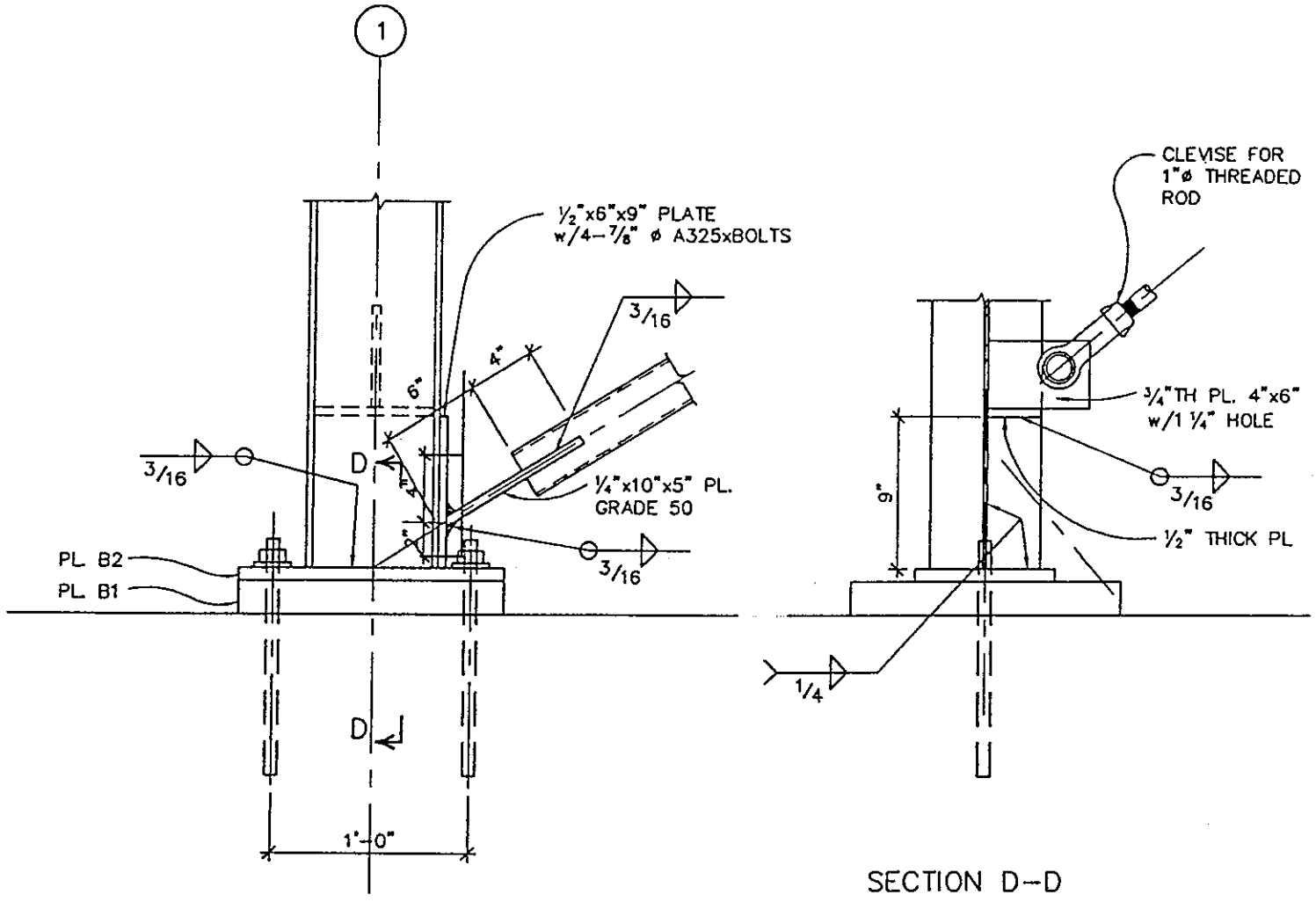

SECTION D–D

DD

DETAIL

SCALE: 1 1/2"=1'-0"

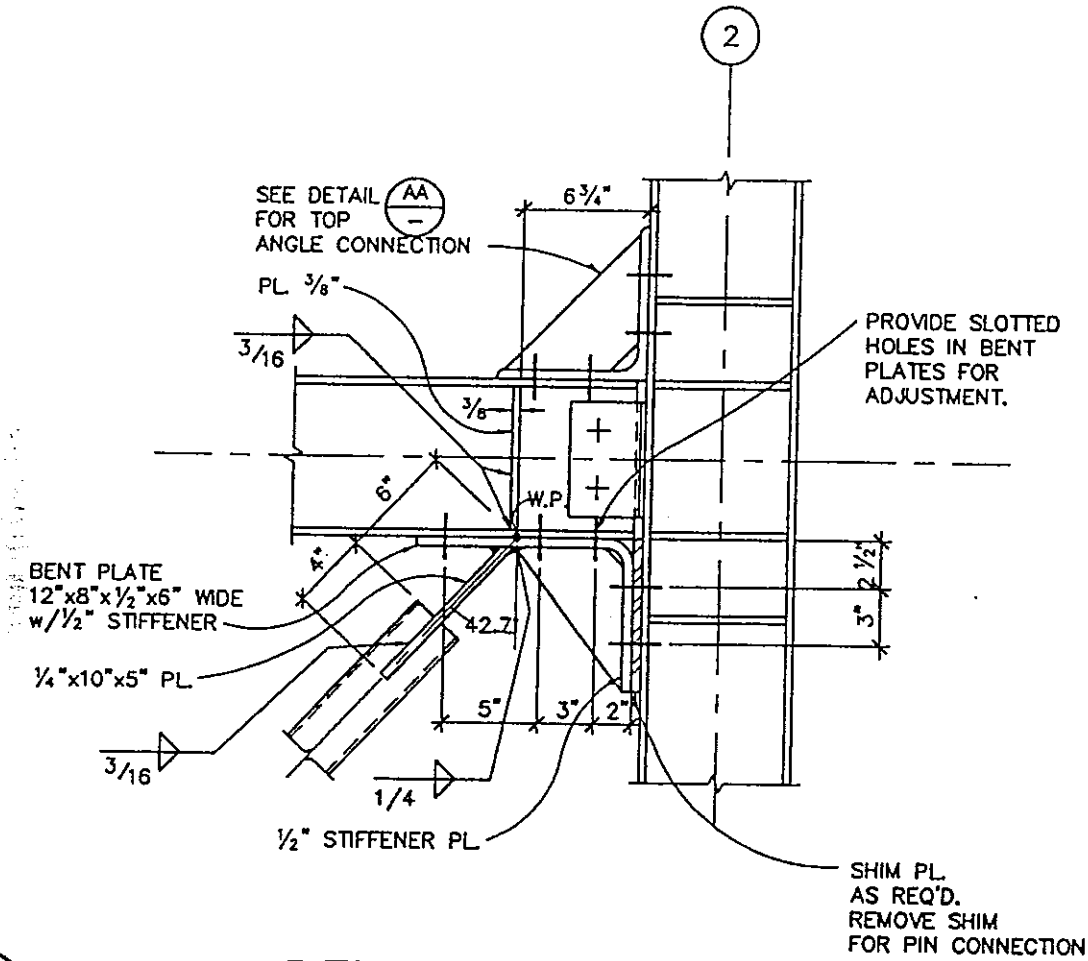

BB – DETAIL

SCALE: 1 1/2"=1'-0"

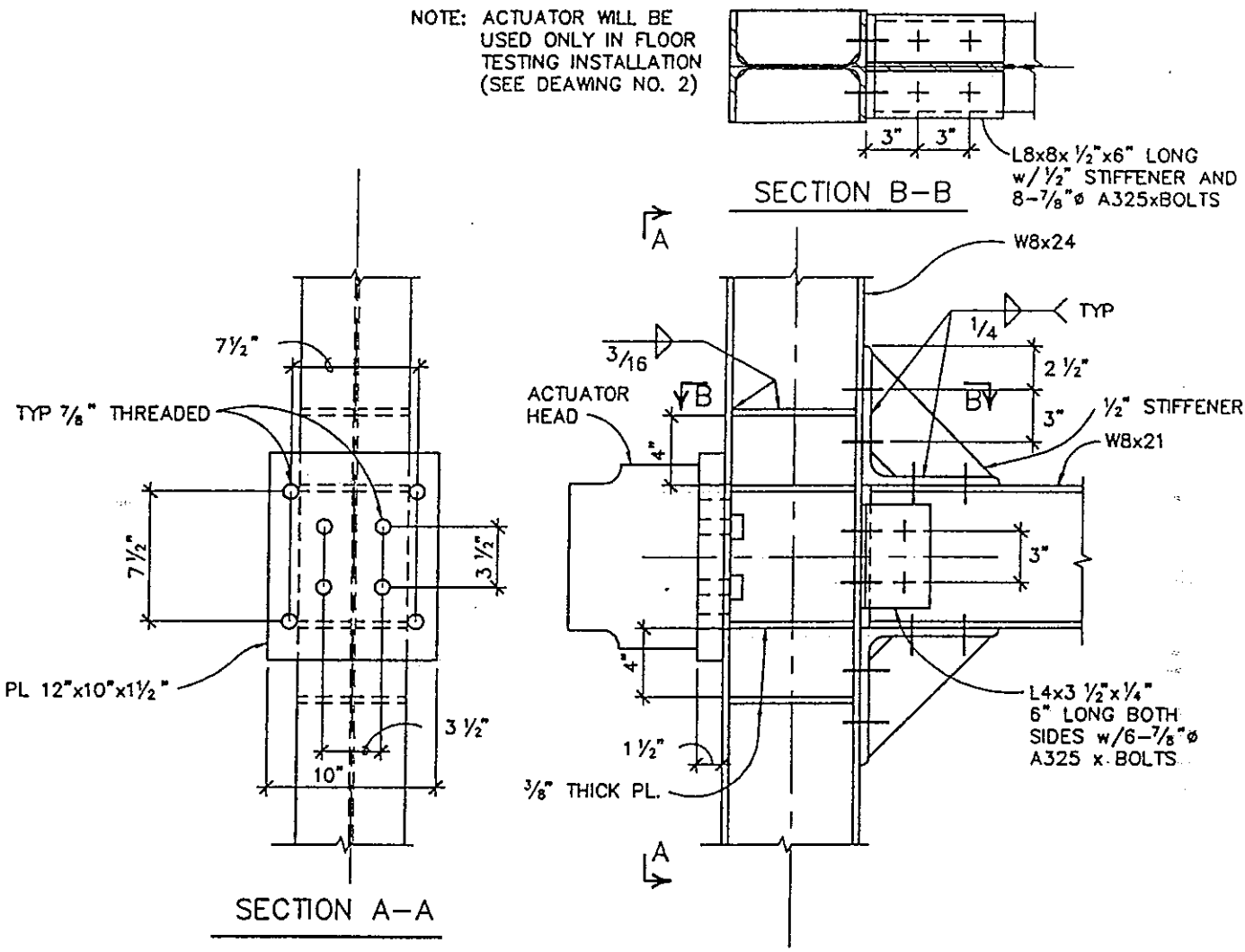

AA / —

DETAIL

SCALE: 1 1/2"=1'-0"

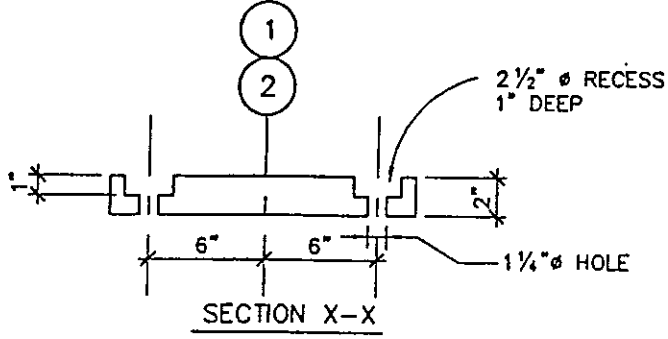

SECTION X–X

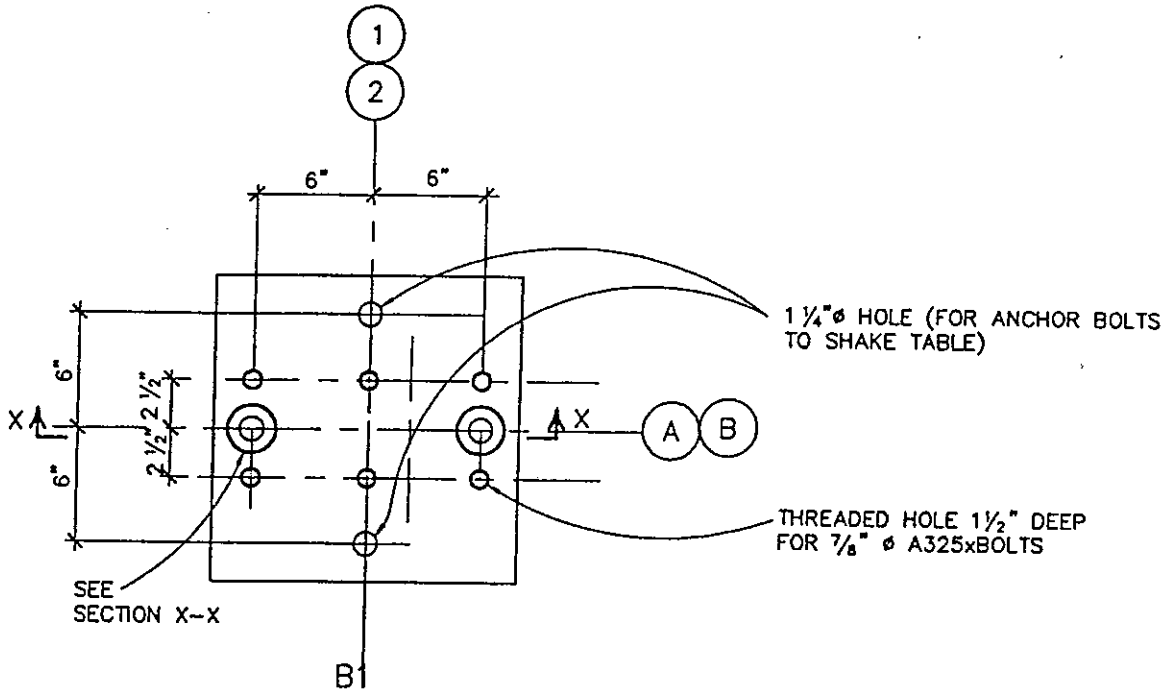

B1

16"x16"x2"

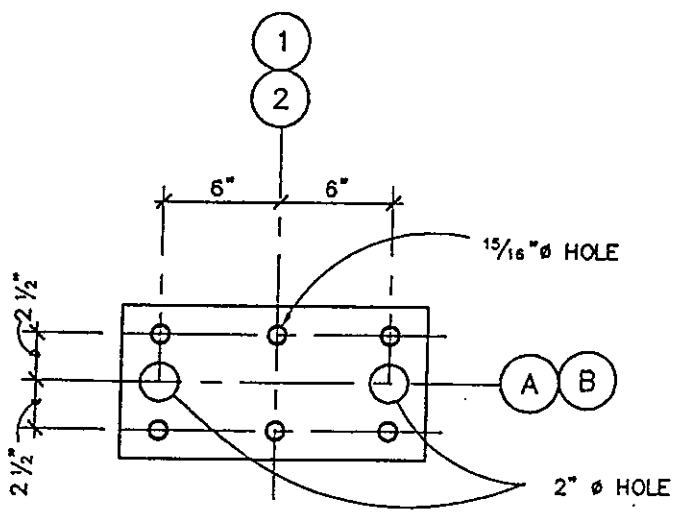

PL. B2

16"x8"x3/4"

GG / –

DETAIL FOR PL. B1

SCALE: 1 1/2"=1'–0"

APPENDIX B

RESULTS OF TESTING OF FRAME WITH SPRING LEAF CONNECTION DETAIL FOR THE TOGGLE BRACES

(1 in. = 25.4 mm, 1 kip = 4.45 kN).

ASTL01 : SIMPLE CONNECTIONS, SPRING LEAF CONFIGURATION

LOWER DAMPER, f=2 Hz, U_o= 0.25 in (04/28/97, 13:08:50)

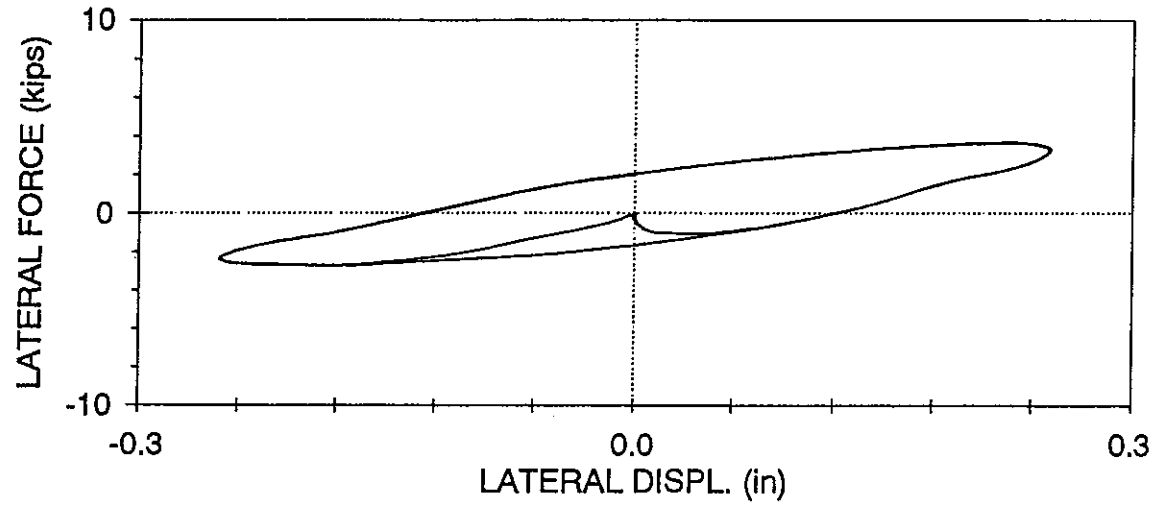

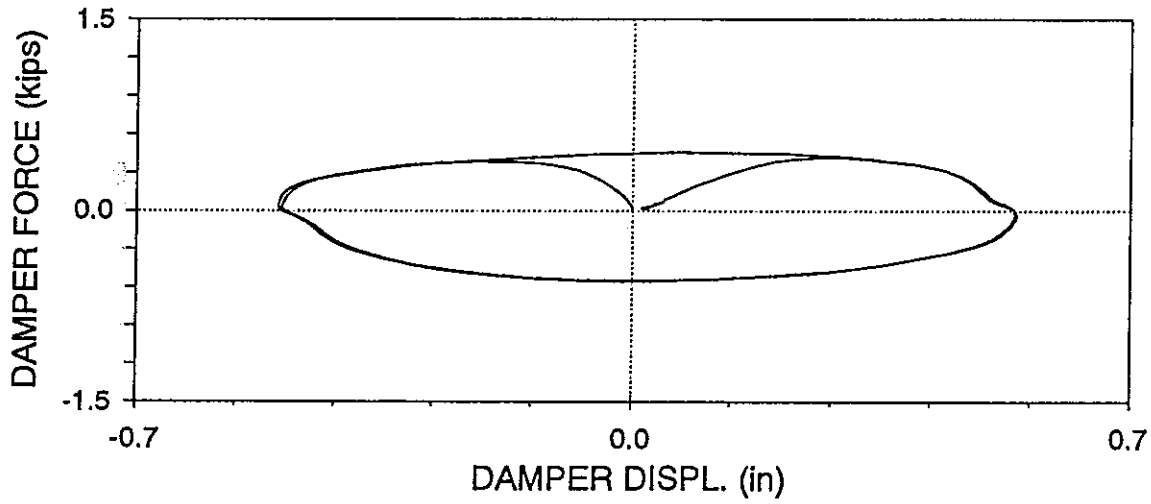

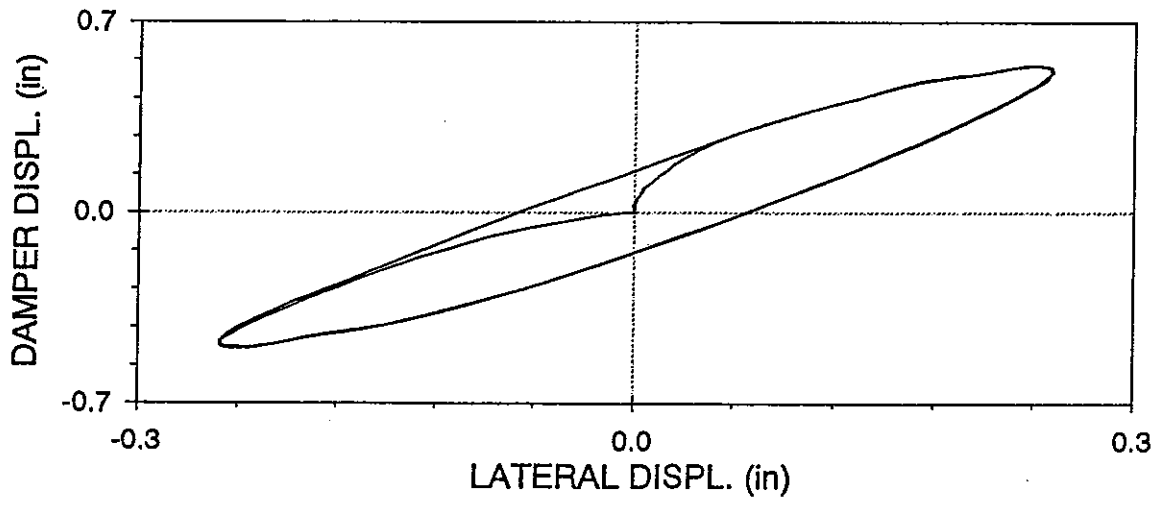

ASTL02 : SIMPLE CONNECTIONS, SPRING LEAF CONFIGURATION

LOWER DAMPER, f=0.05 Hz, U_o= 0.5 in (04/28/97, 13:13:08)

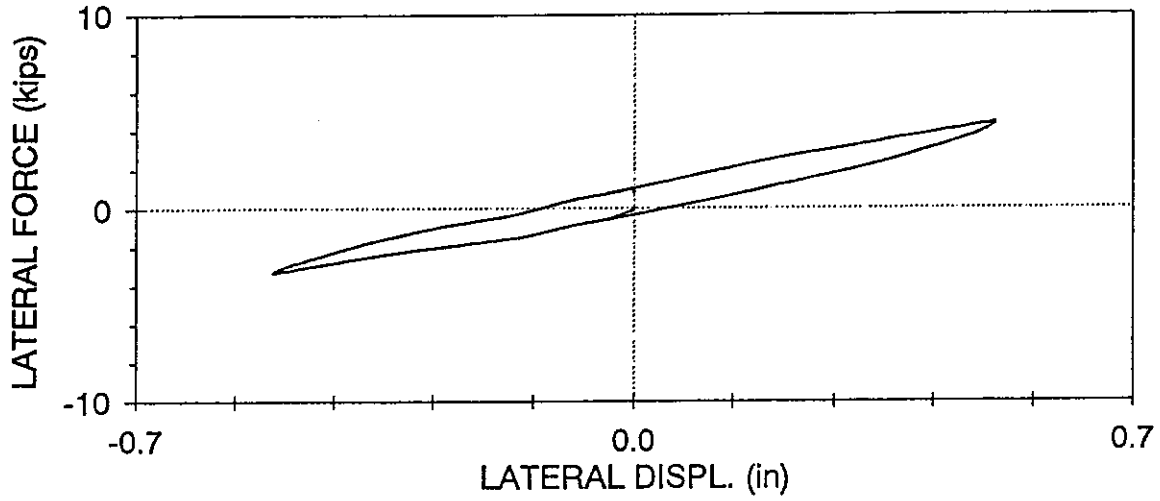

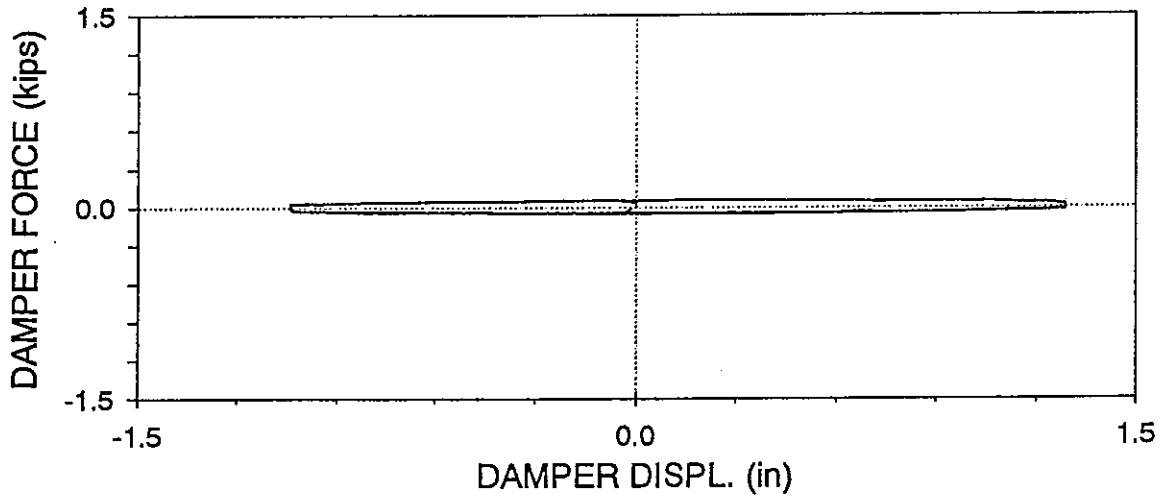

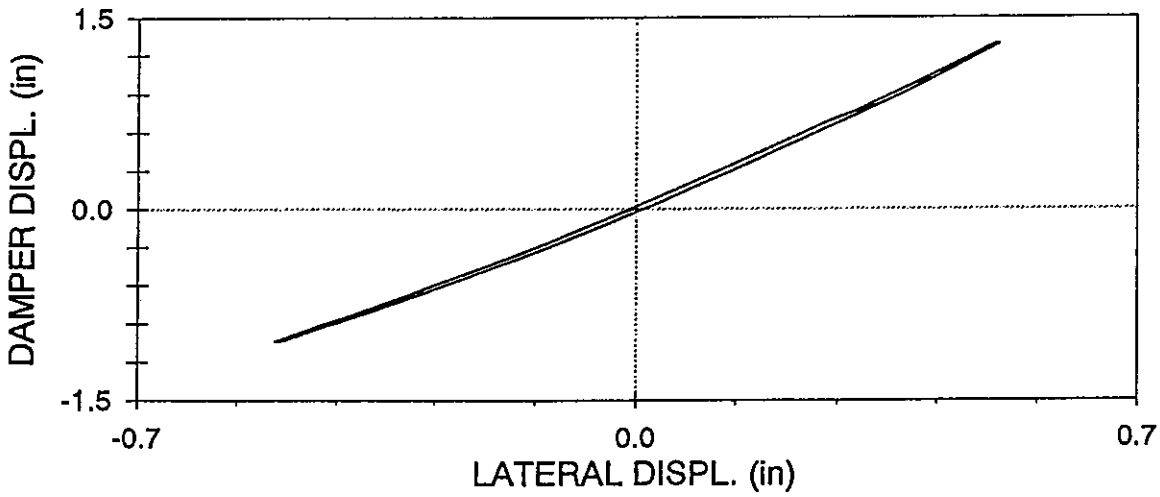

ASTL03 : SIMPLE CONNECTIONS, SPRING LEAF CONFIGURATION

LOWER DAMPER, f=2 Hz, U_o= 0.5 in (04/30/97, 13:18:07)

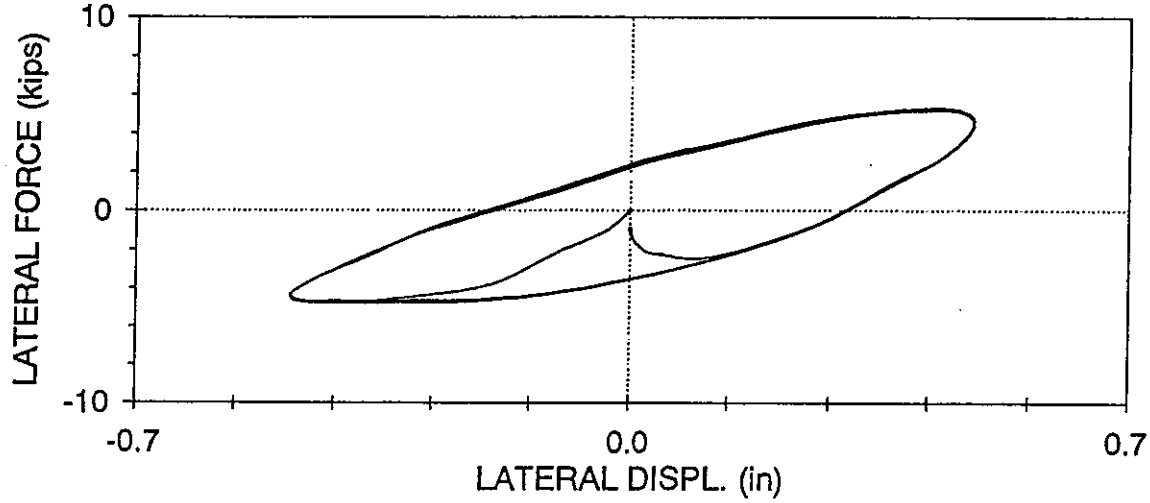

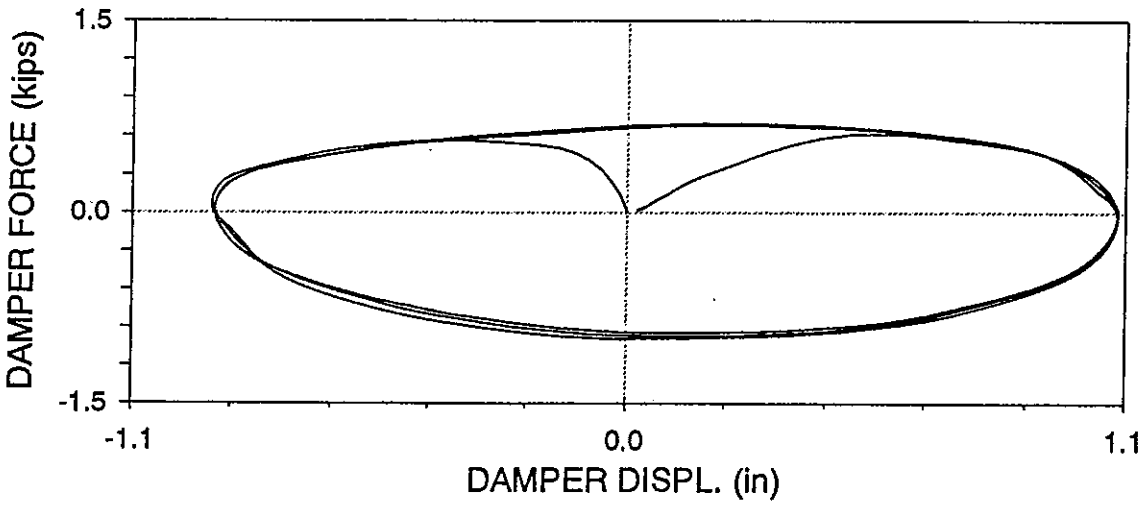

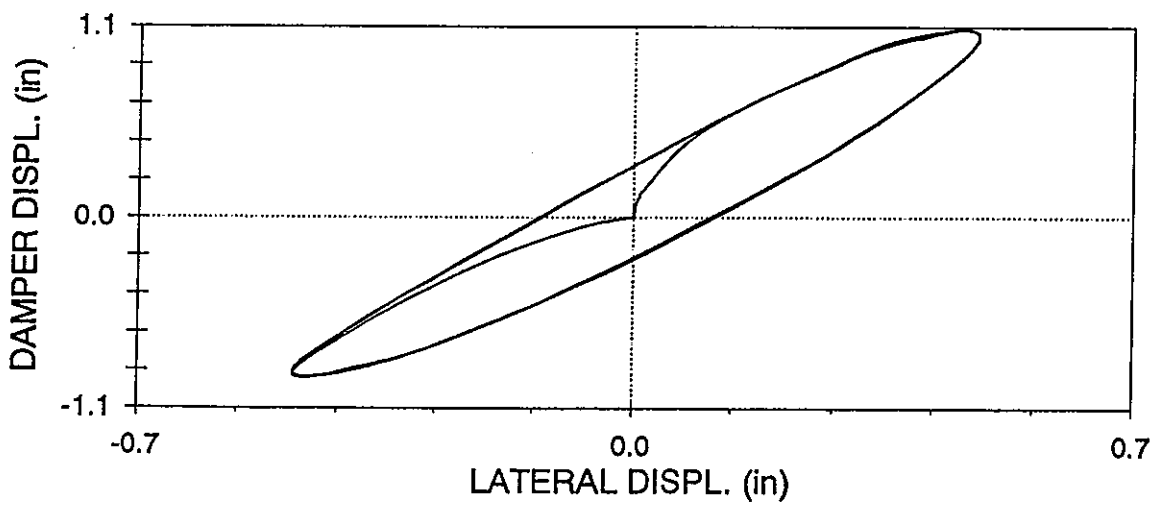

ASTL04 : SIMPLE CONNECTIONS, SPRING LEAF CONFIGURATION

LOWER DAMPER, f=3 Hz, U_o= 0.3 in (04/28/97, 13:22:36)

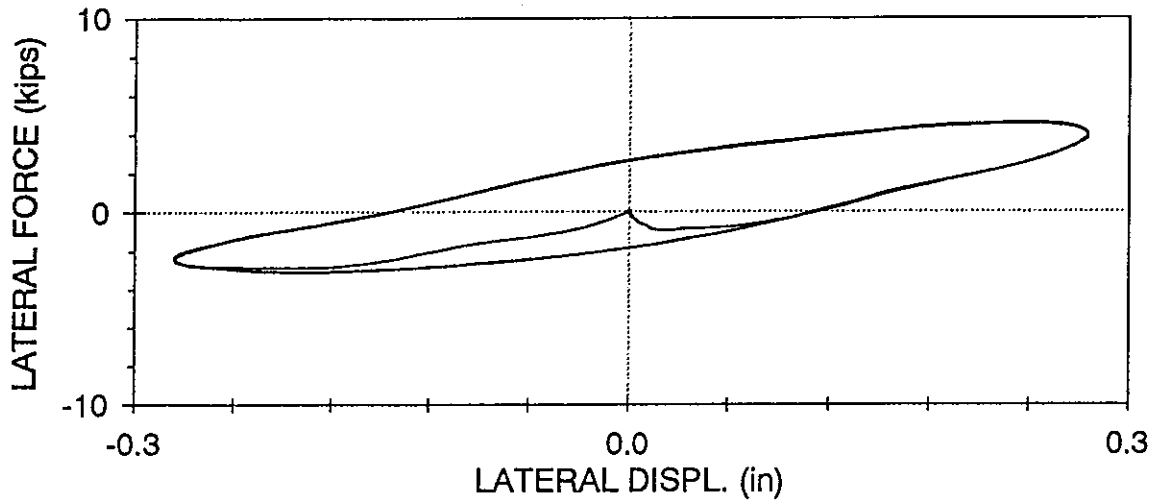

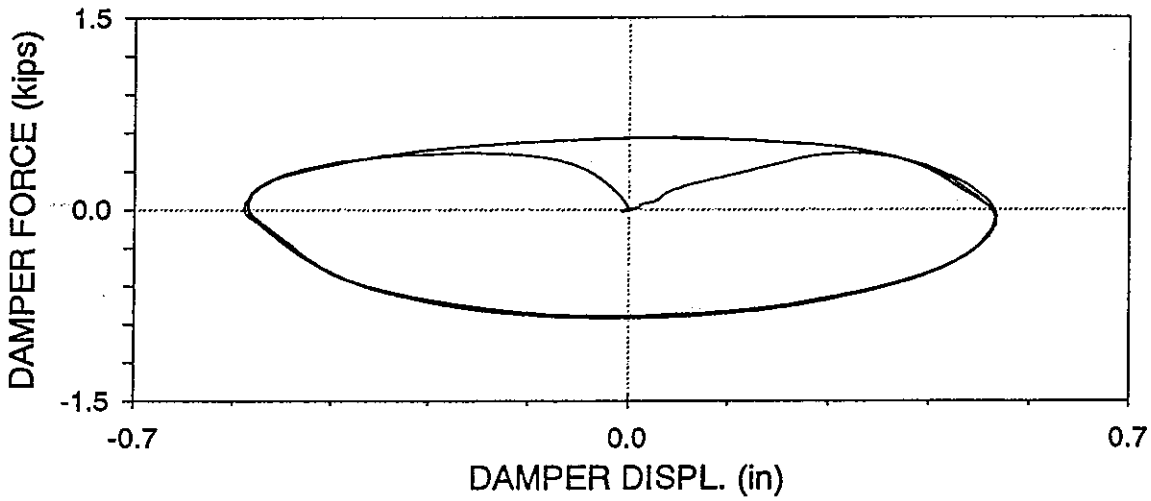

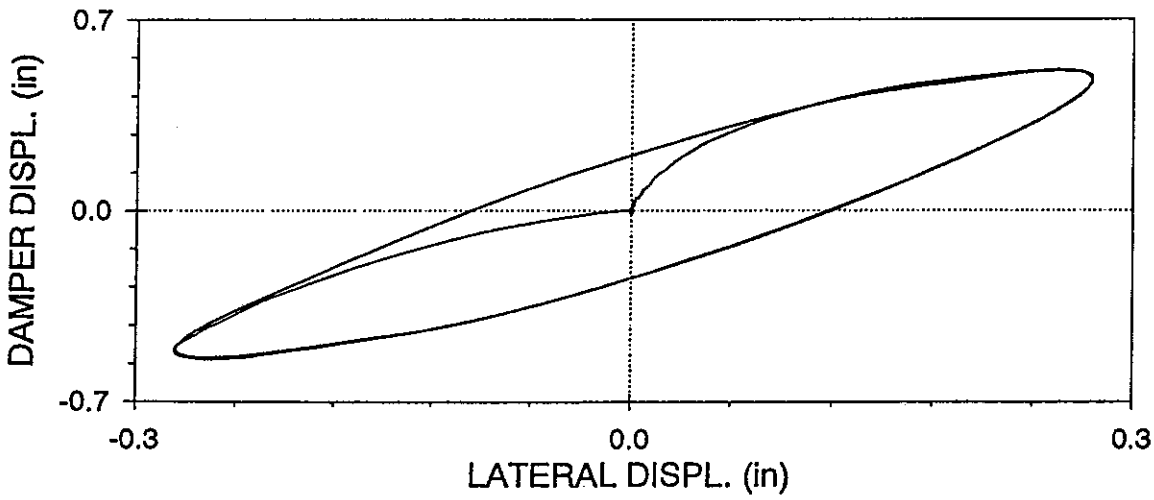

ASTL05 : SIMPLE CONNECTIONS, SPRING LEAF CONFIGURATION

LOWER DAMPER, f=2 Hz, U_o= 0.5 in (04/30/97, 12:13:02)

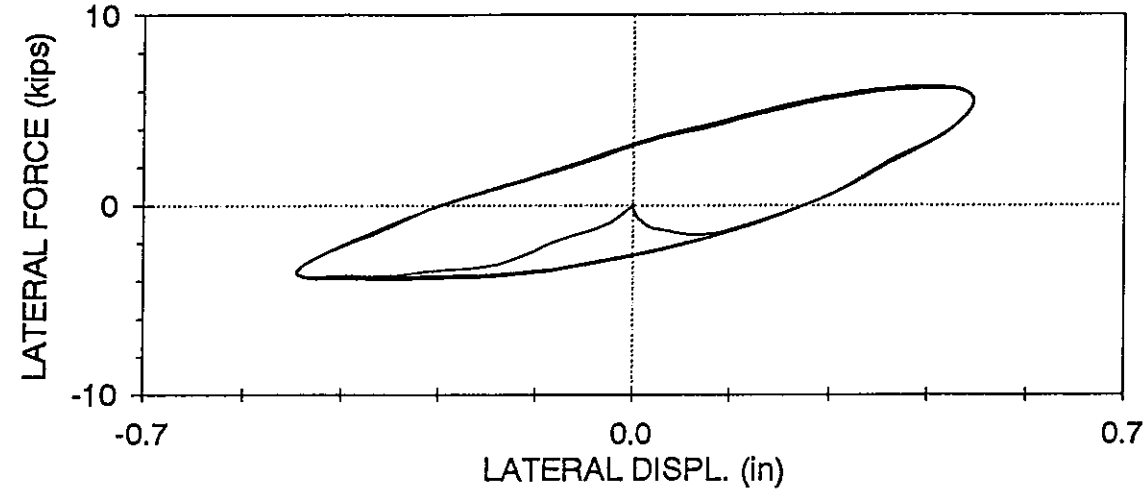

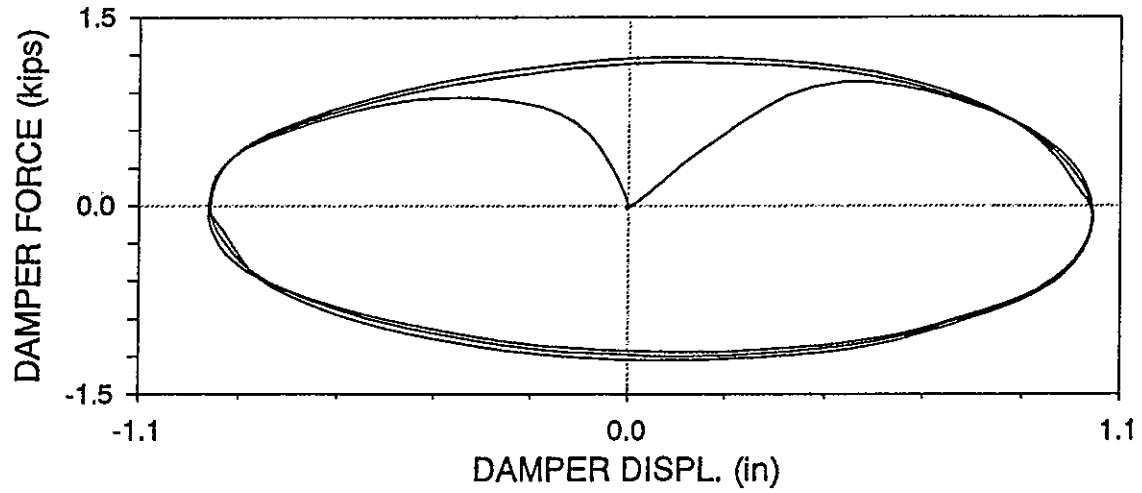

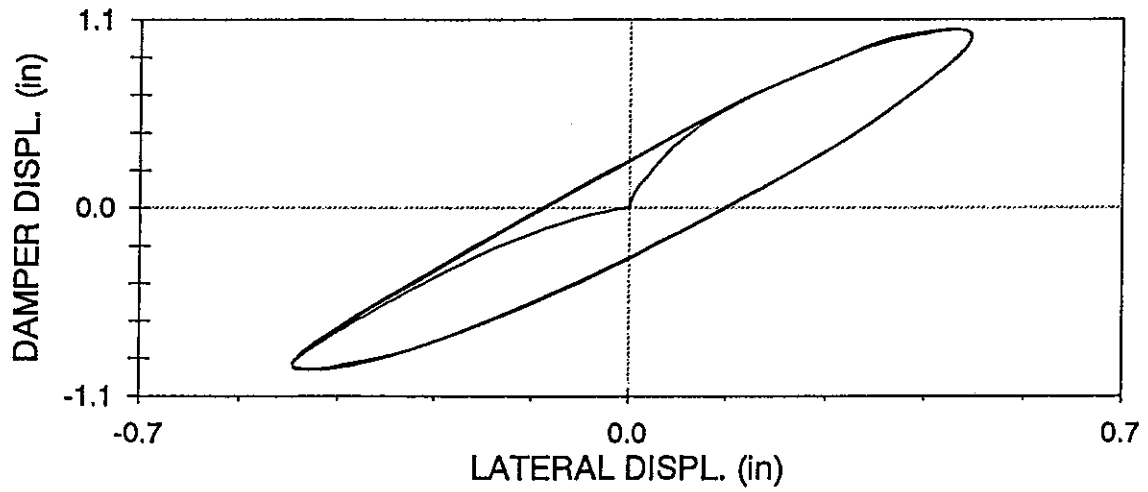

ASTL06 : SIMPLE CONNECTIONS, SPRING LEAF CONFIGURATION

LOWER DAMPER, f=0.05 Hz, U_o= 0.5 in (04/30/97, 13:28:36)

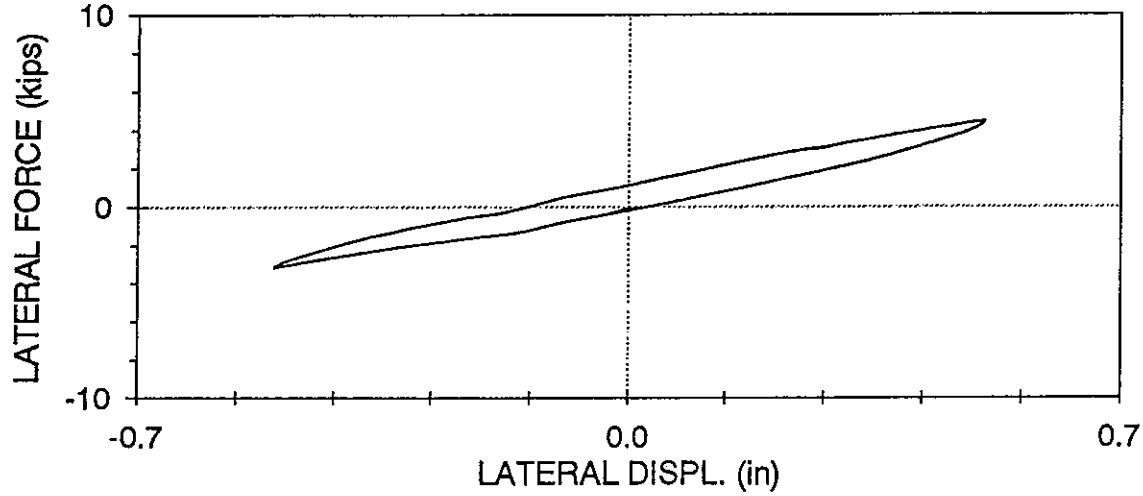

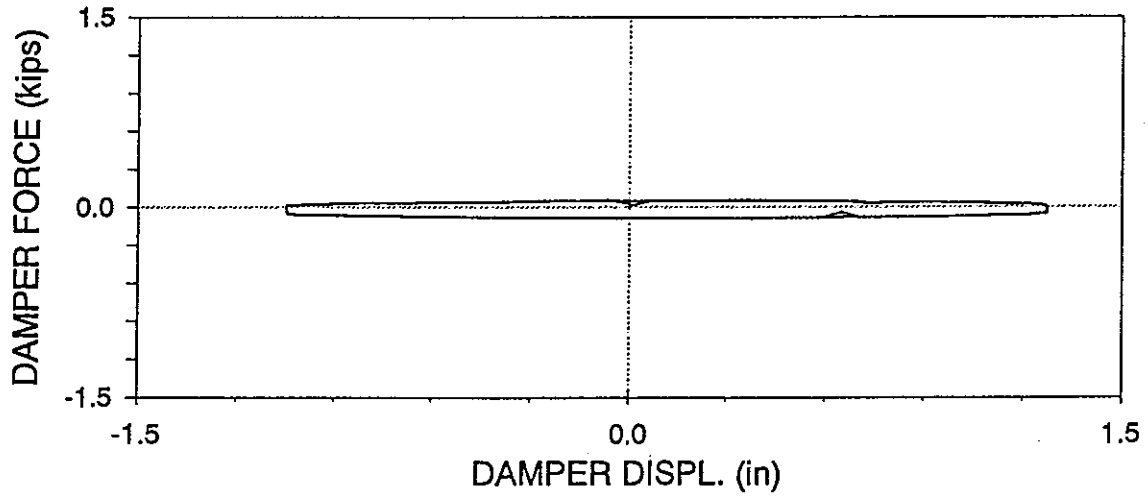

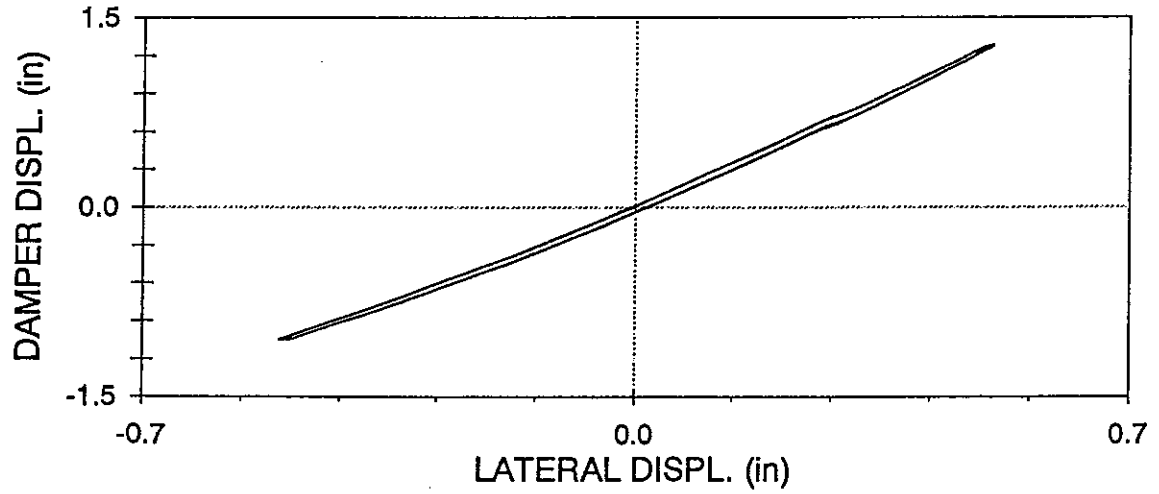

ASTL07 : SIMPLE CONNECTIONS, SPRING LEAF CONFIGURATION

LOWER DAMPER, f=2 Hz, U_o= 0.25 in (04/30/97, 13:32:32)

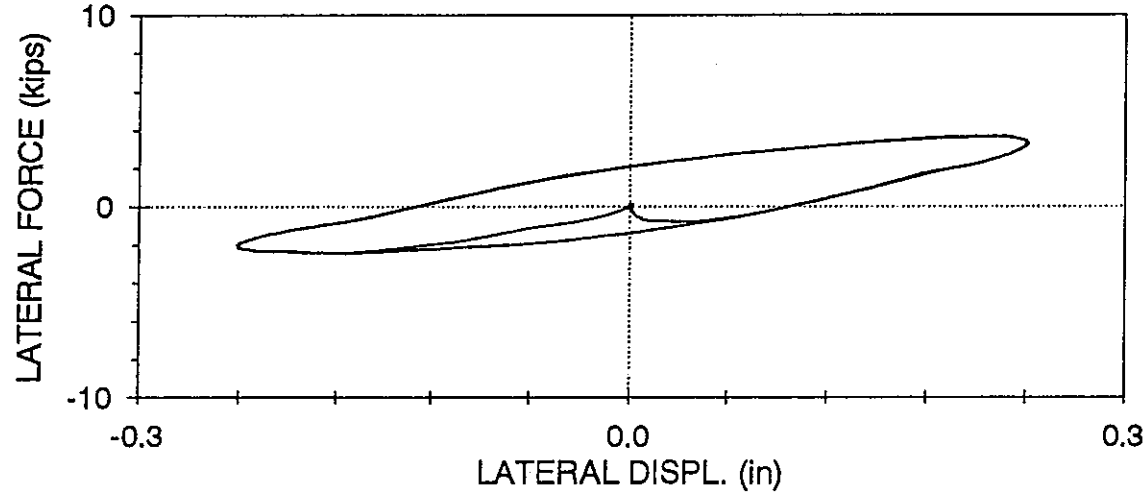

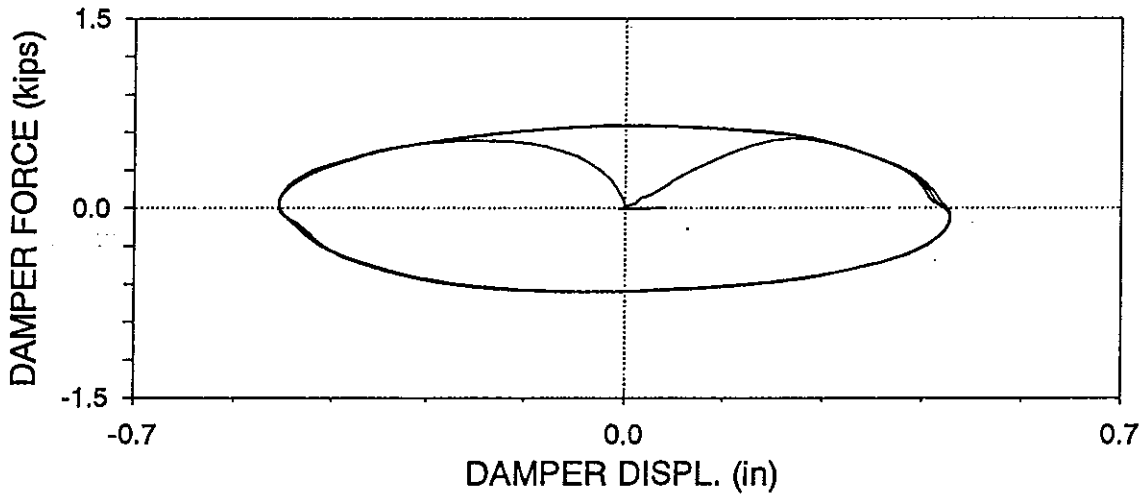

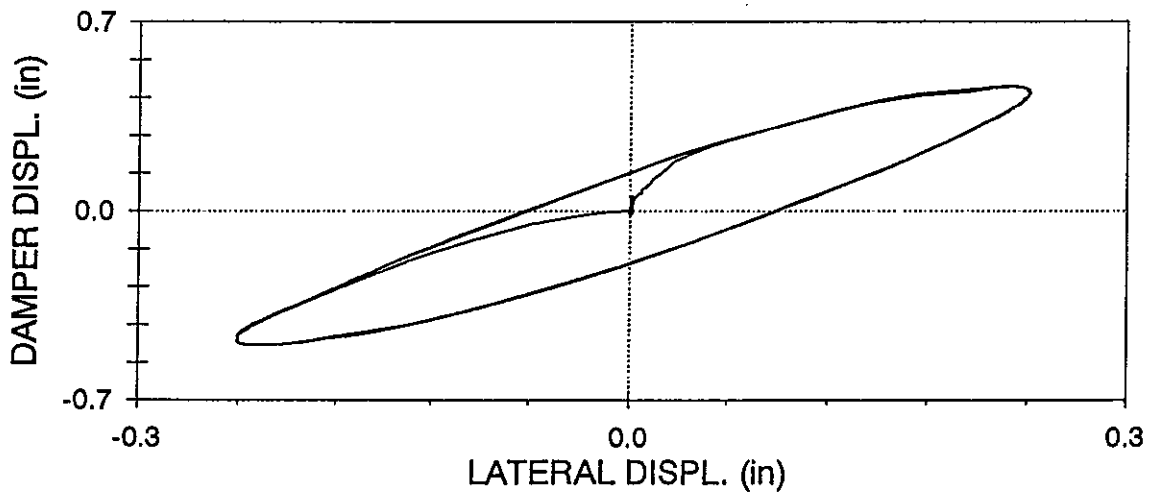

ASTL08 : SIMPLE CONNECTIONS, SPRING LEAF CONFIGURATION

LOWER DAMPER, f=3 Hz, U_o= 0.3 in (04/30/97, 13:35:53)

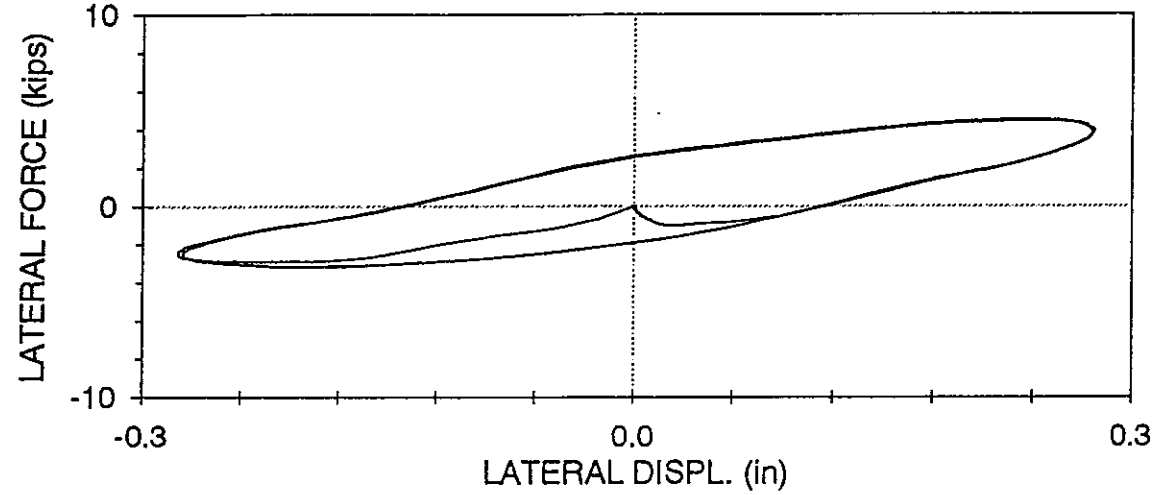

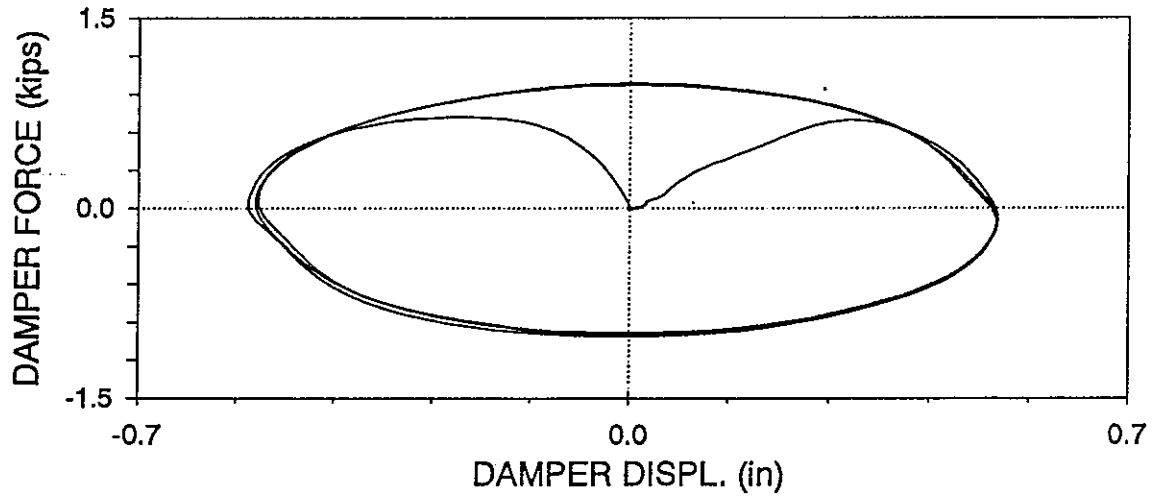

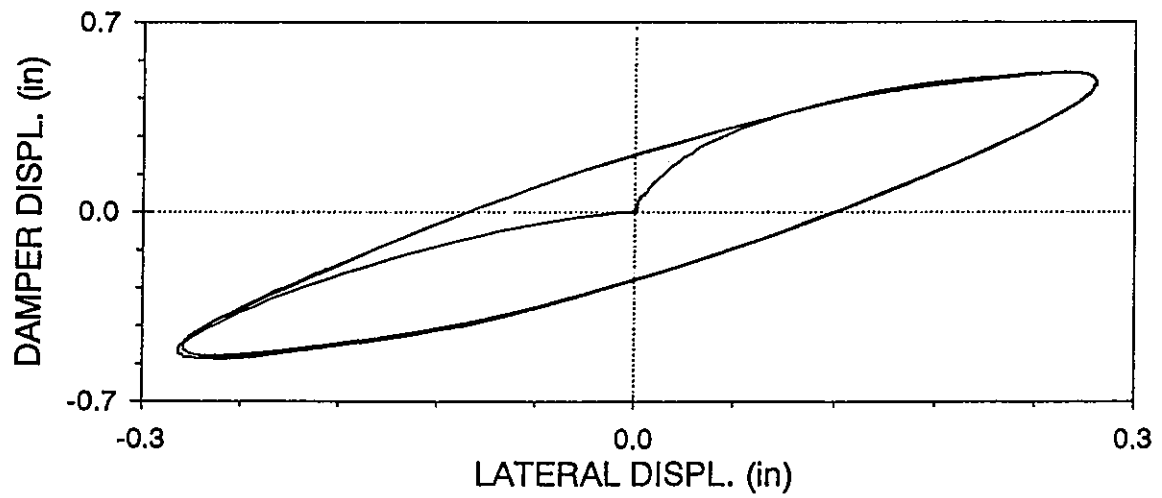

ARTL01 : RIGID CONNECTIONS, SPRING LEAF CONFIGURATION

LOWER DAMPER, f=0.05 Hz, U_o= 0.25 in (05/06/97, 14:29:41)

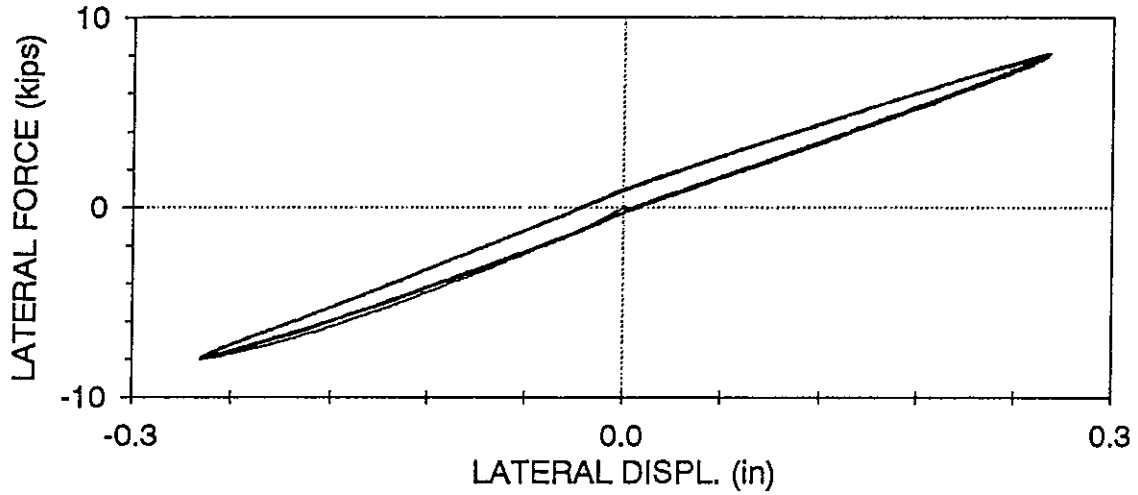

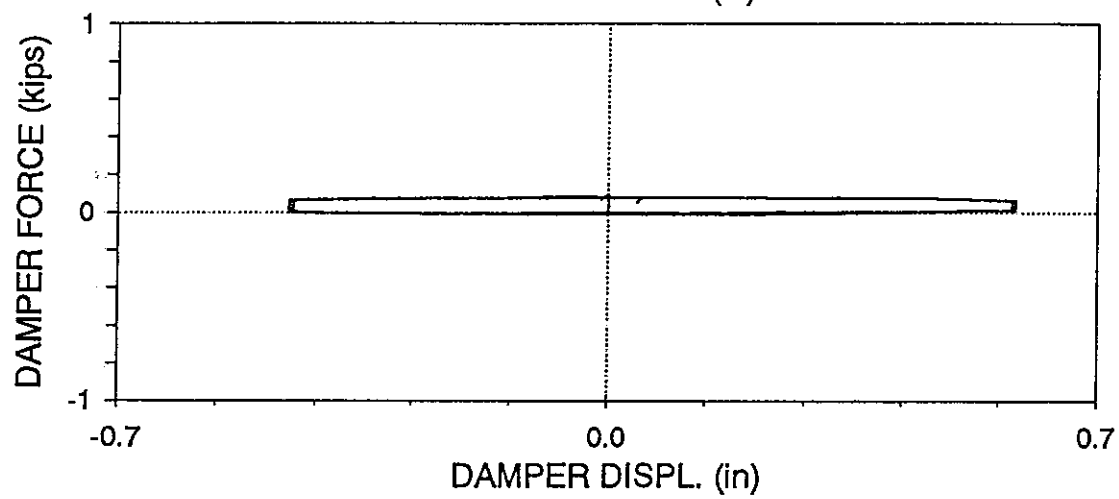

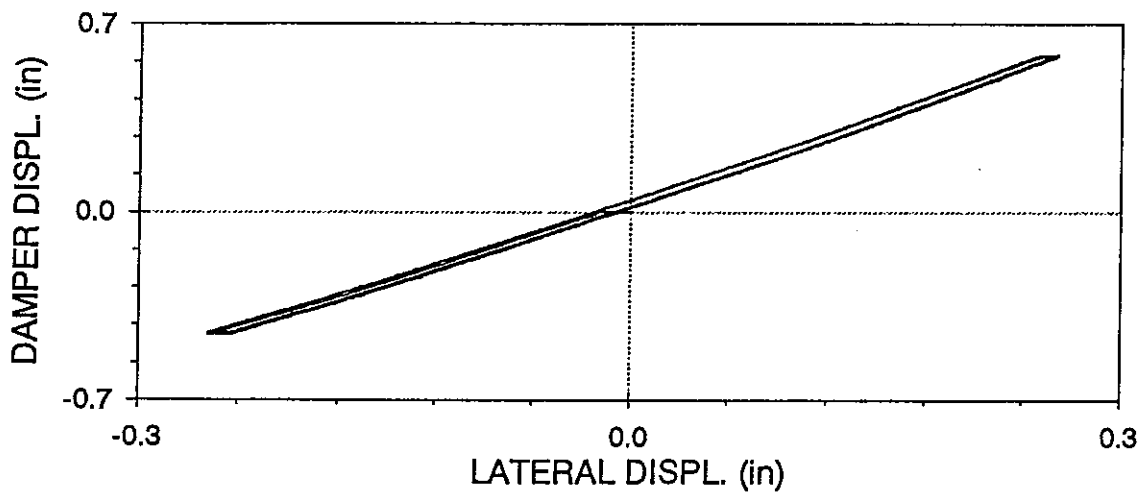

ARTL02 : RIGID CONNECTIONS, SPRING LEAF CONFIGURATION

LOWER DAMPER, f=2 Hz, U_o= 0.25 in (05/06/97, 14:36:36)

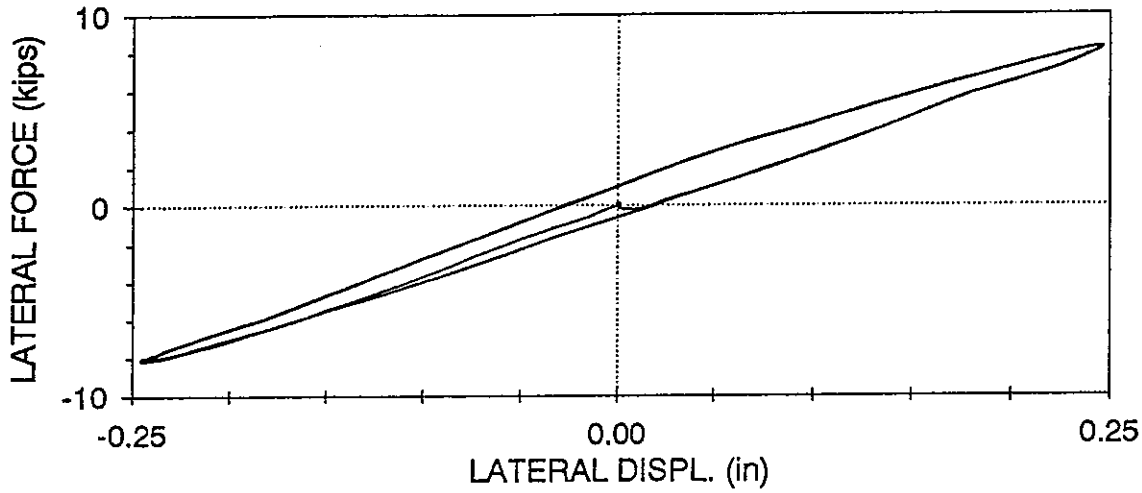

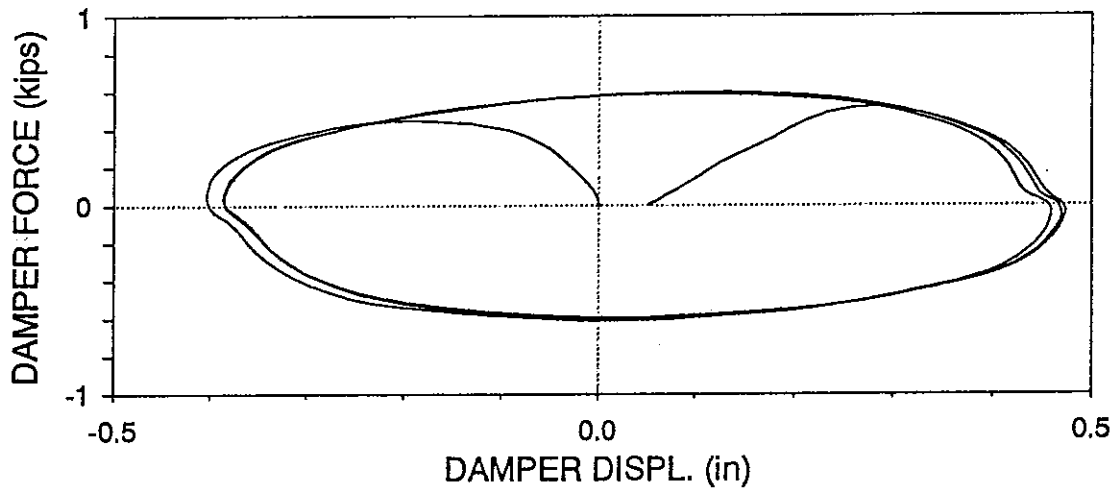

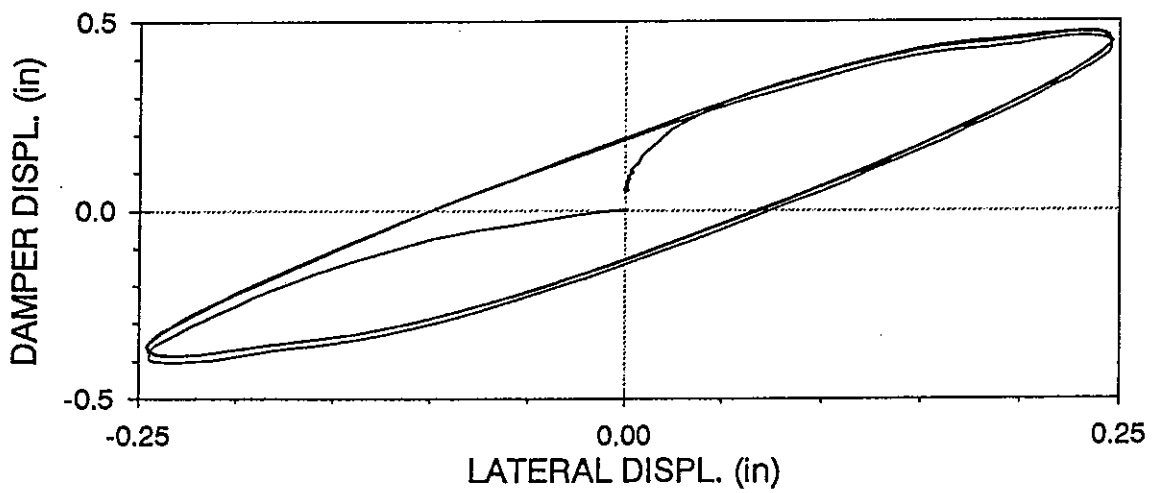

ARTL03 : RIGID CONNECTIONS, SPRING LEAF CONFIGURATION

LOWER DAMPER, f=2 Hz, U_o= 0.25 in (05/06/97, 14:38:32)

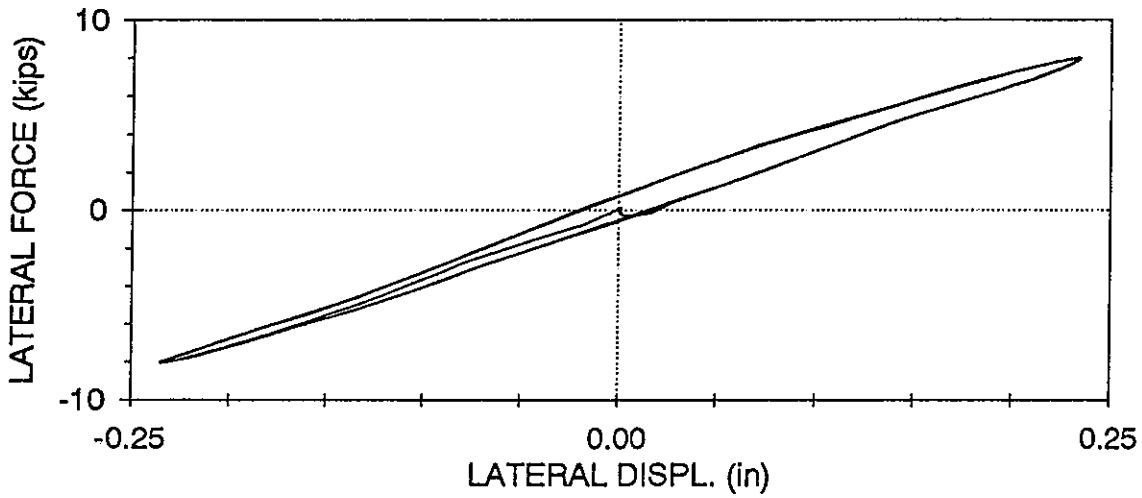

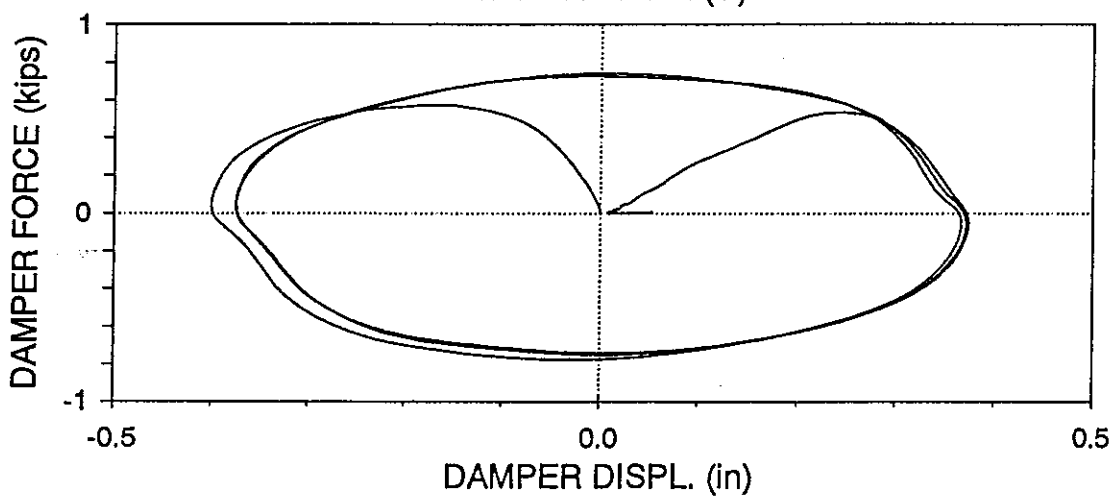

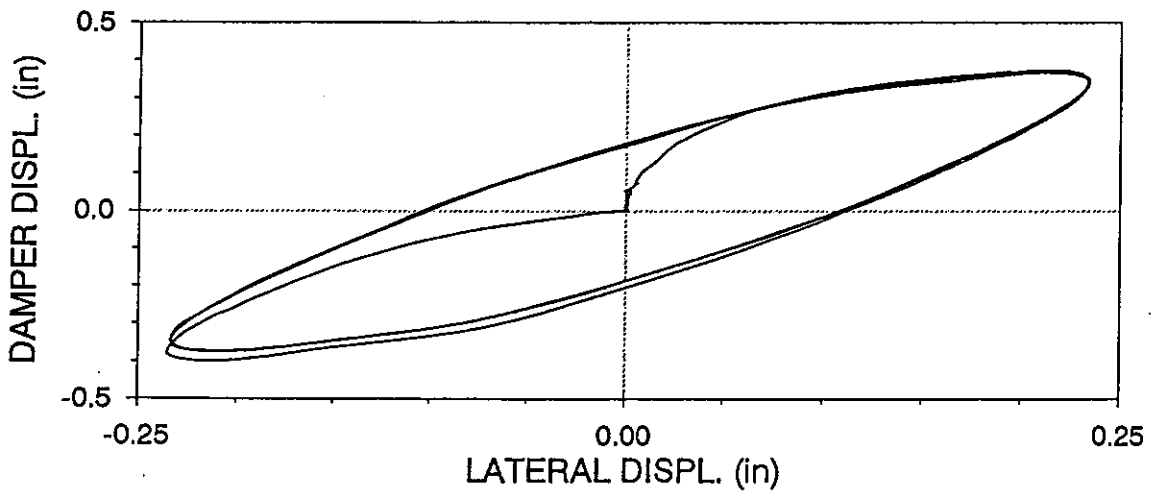

ARTL05 : RIGID CONNECTIONS, SPRING LEAF CONFIGURATION

LOWER DAMPER, f=4 Hz, U_o= 0.25 in (05/06/97, 14:44:47)

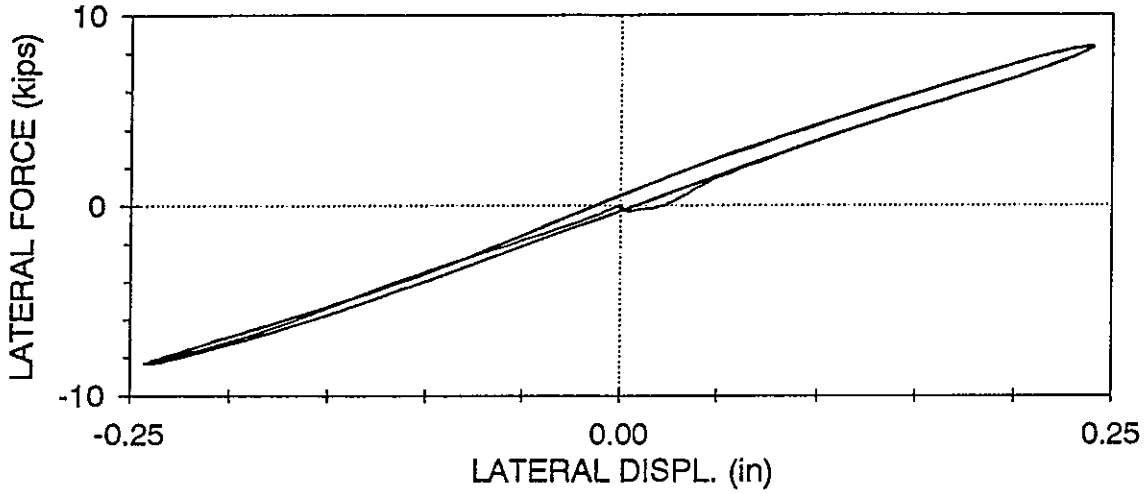

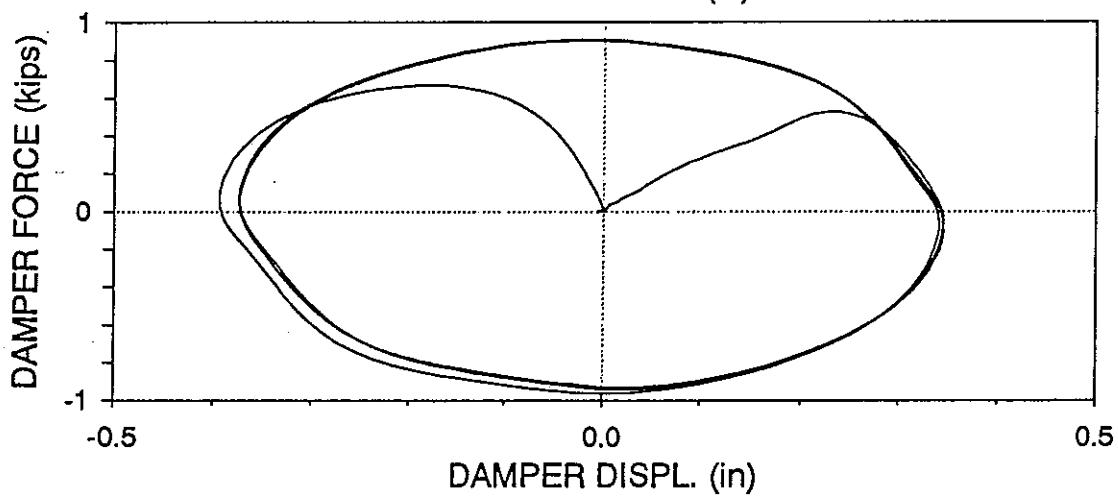

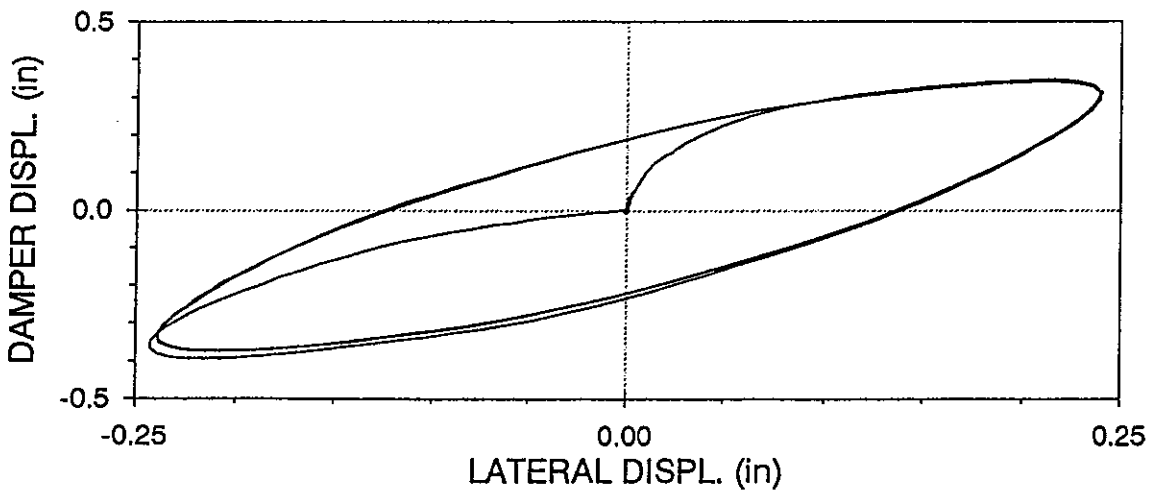

ARTL06 : RIGID CONNECTIONS, SPRING LEAF CONFIGURATION

LOWER DAMPER, f=5 Hz, U_o= 0.25 in (05/06/97, 14:49:14)

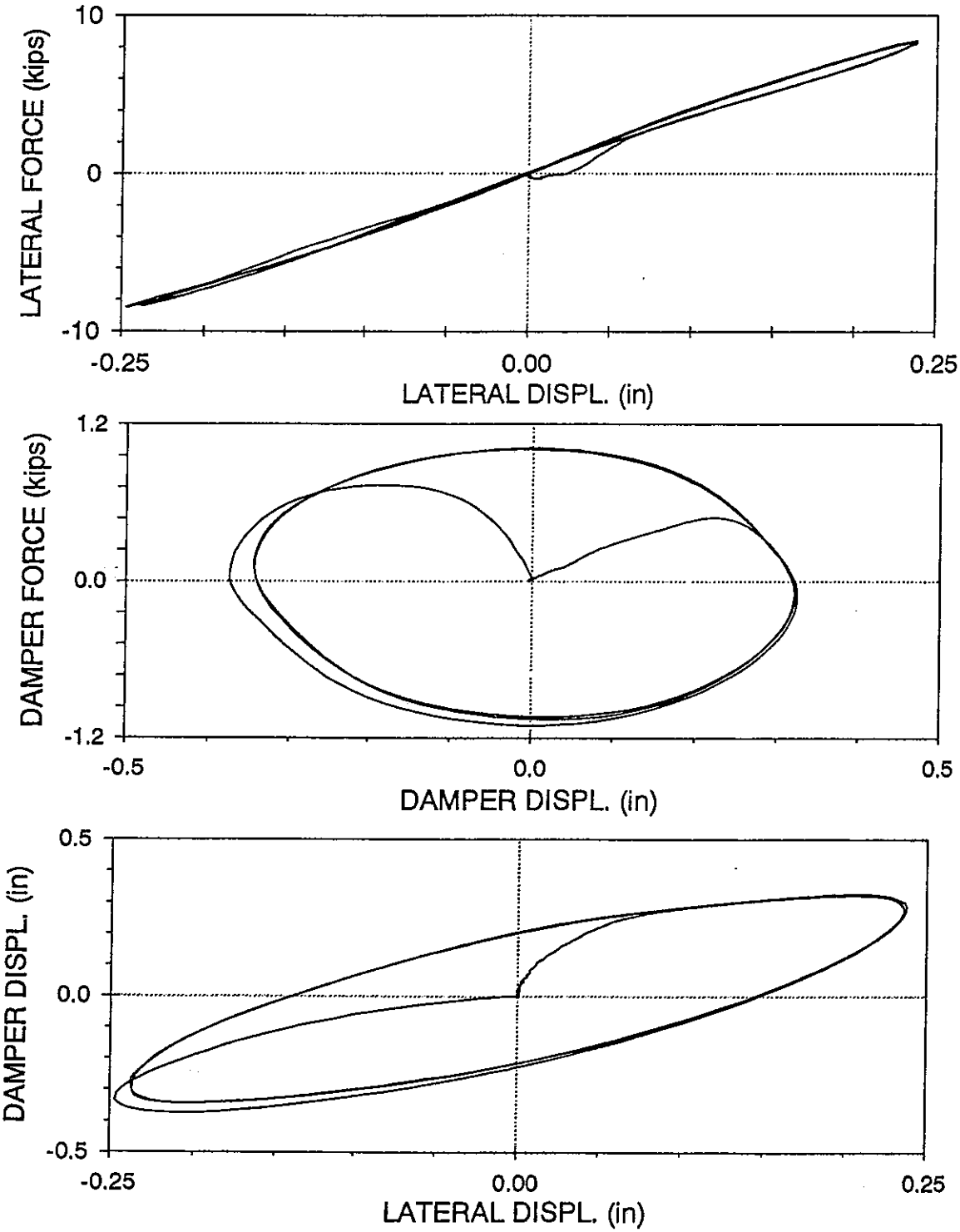

ARTU01 : RIGID CONNECTIONS, SPRING LEAF CONFIGURATION

UPPER DAMPER, f=0.05 Hz, U_o= 0.25 in (05/06/97, 15:14:02)

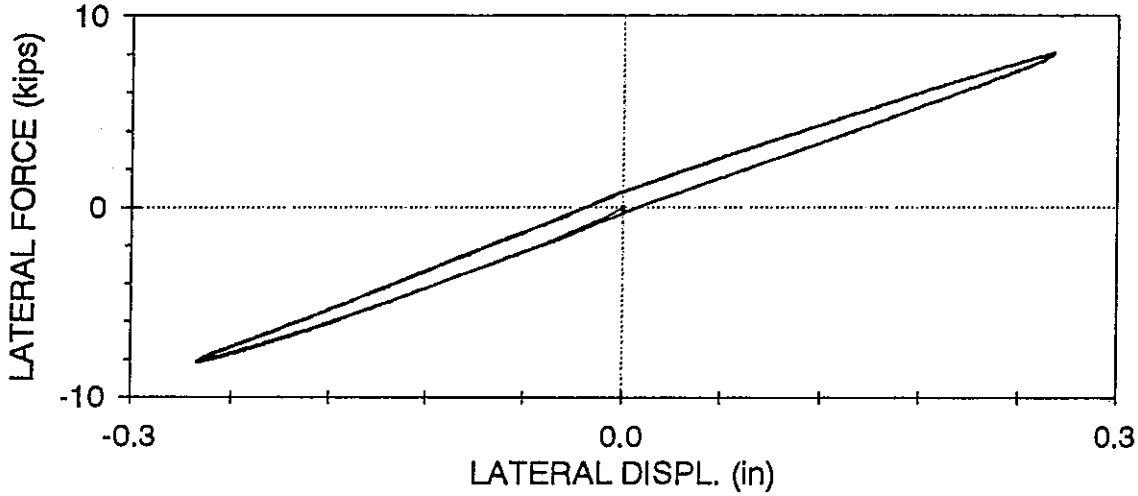

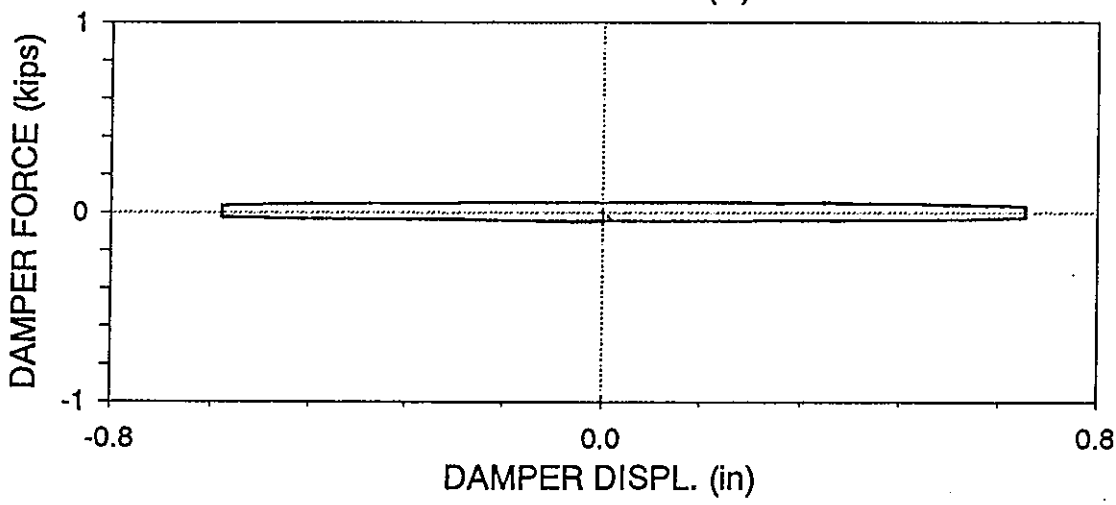

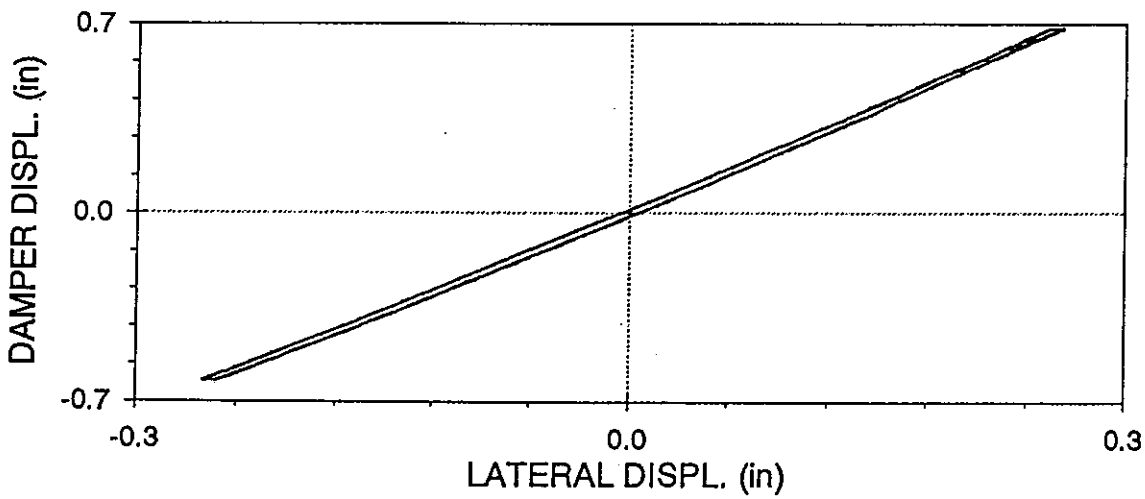

ARTU02 : RIGID CONNECTIONS, SPRING LEAF CONFIGURATION

UPPER DAMPER, f=2 Hz, U_o= 0.25 in (05/06/97, 14:44:47)

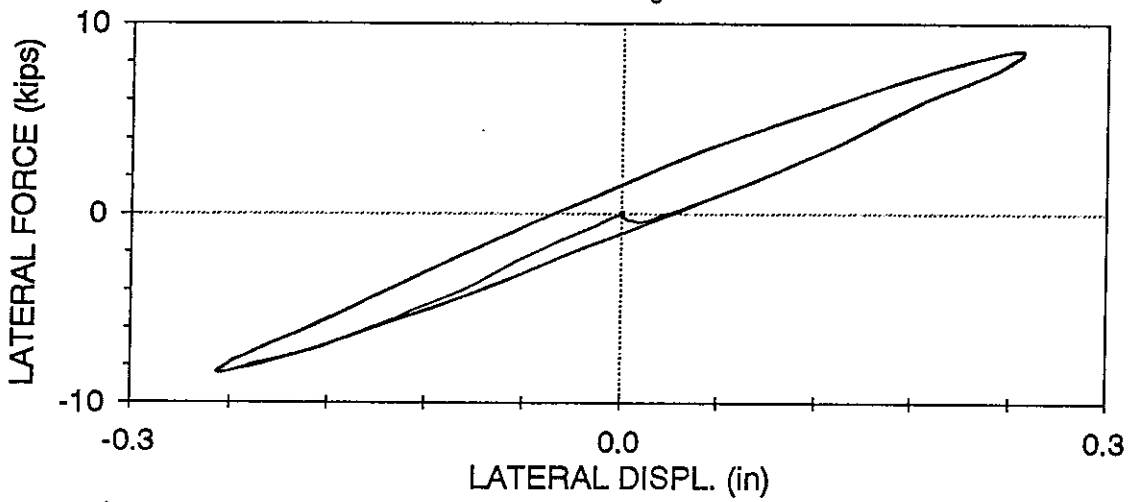

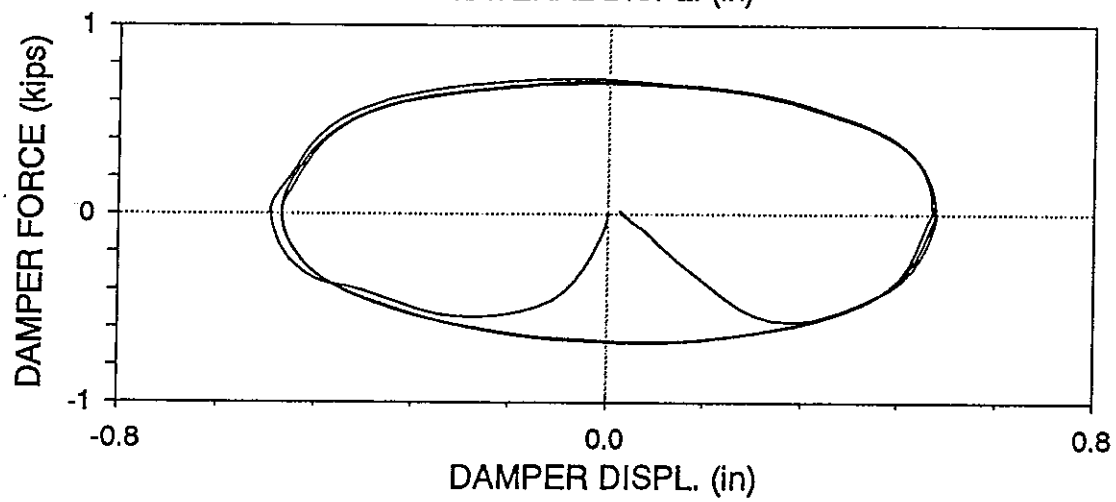

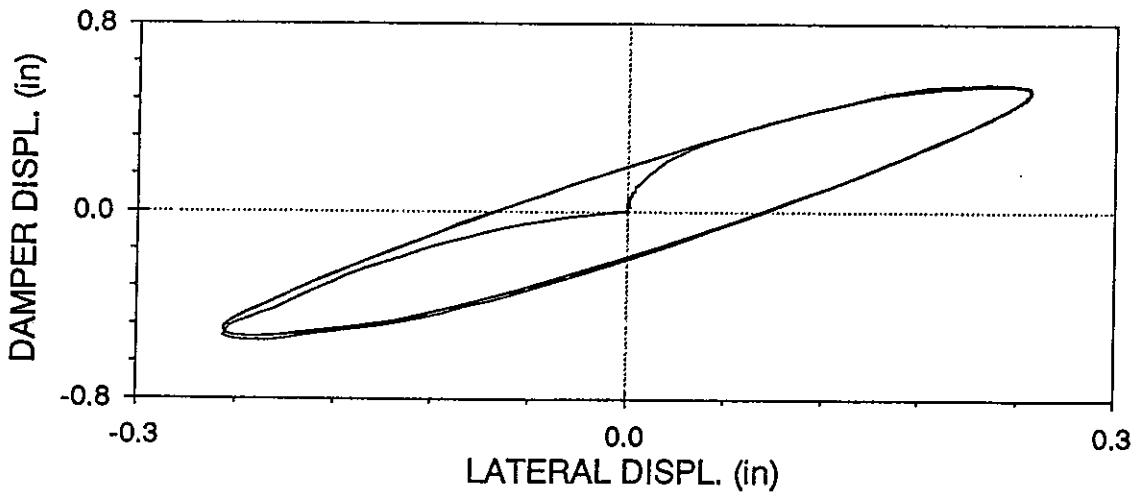

ARTU03 : RIGID CONNECTIONS, SPRING LEAF CONFIGURATION

UPPER DAMPER, f=3 Hz, U_o= 0.25 in (05/06/97, 15:18:26)

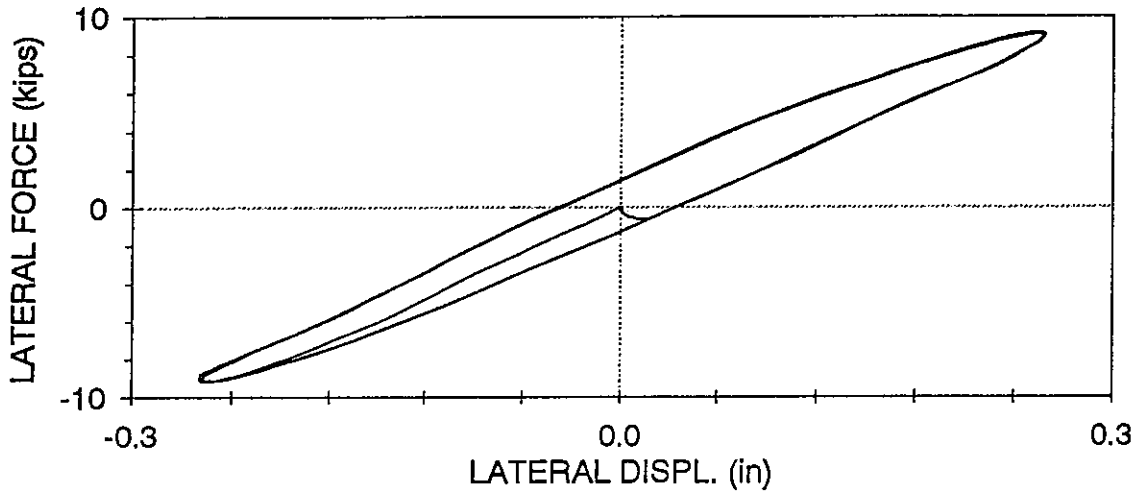

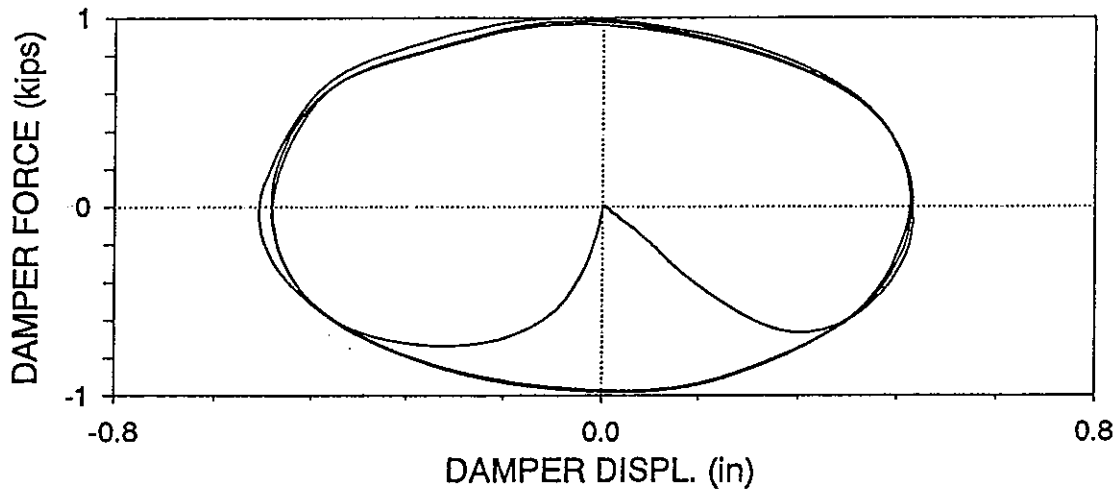

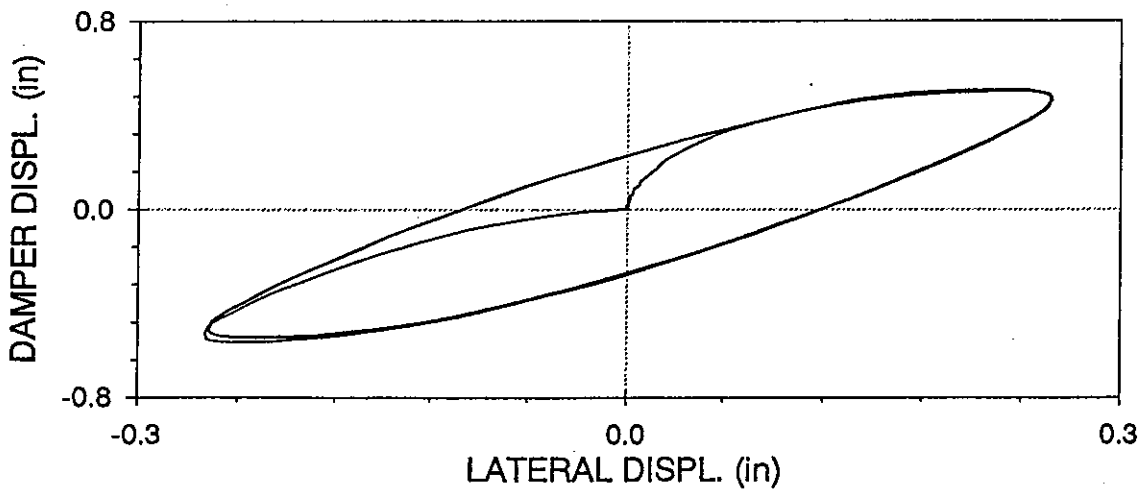

ARTU04 : RIGID CONNECTIONS, SPRING LEAF CONFIGURATION

UPPER DAMPER, f=4 Hz, U_o= 0.25 in (05/06/97, 15:20:07)

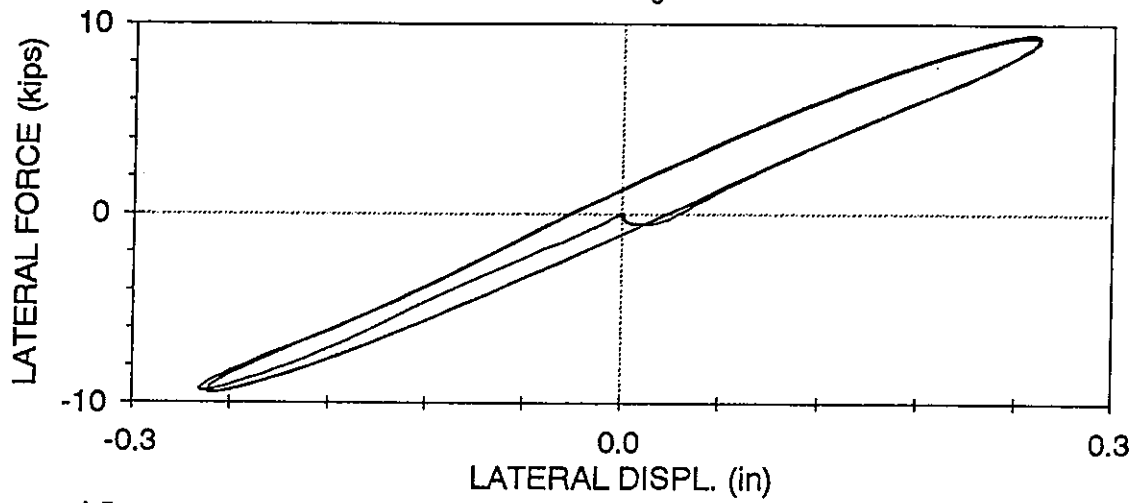

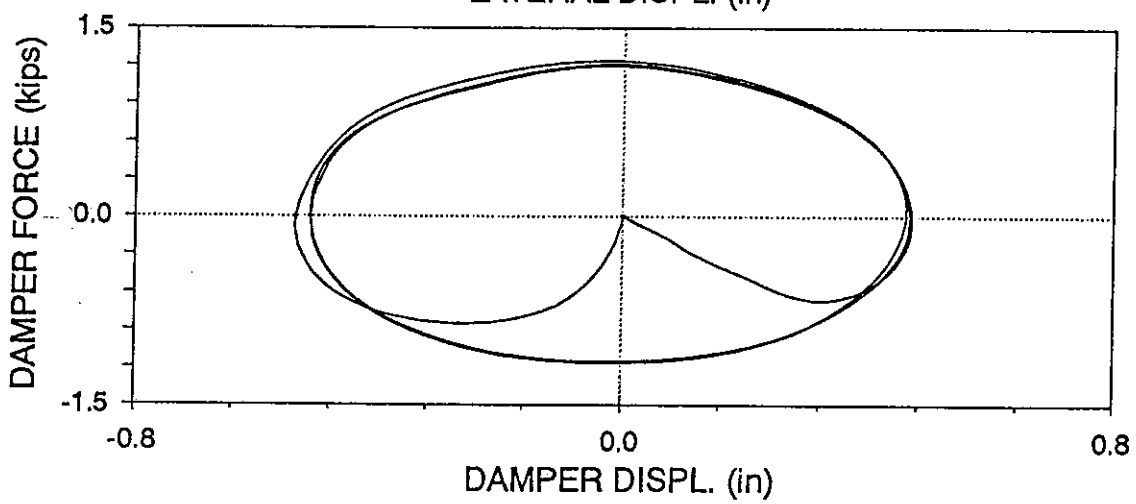

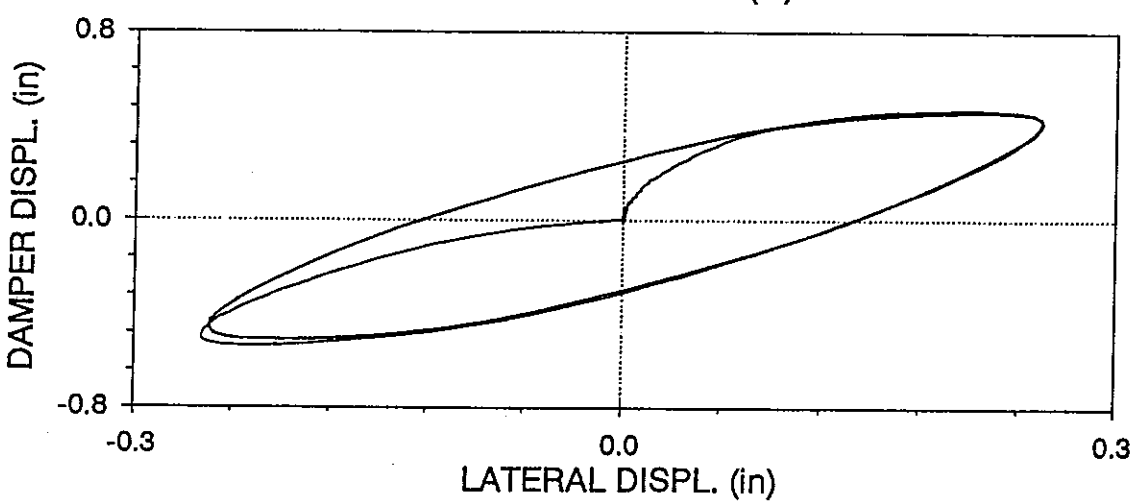

ARTU05 : RIGID CONNECTIONS, SPRING LEAF CONFIGURATION

UPPER DAMPER, f=5 Hz, U_o= 0.25 in (05/06/97, 15:21:43)

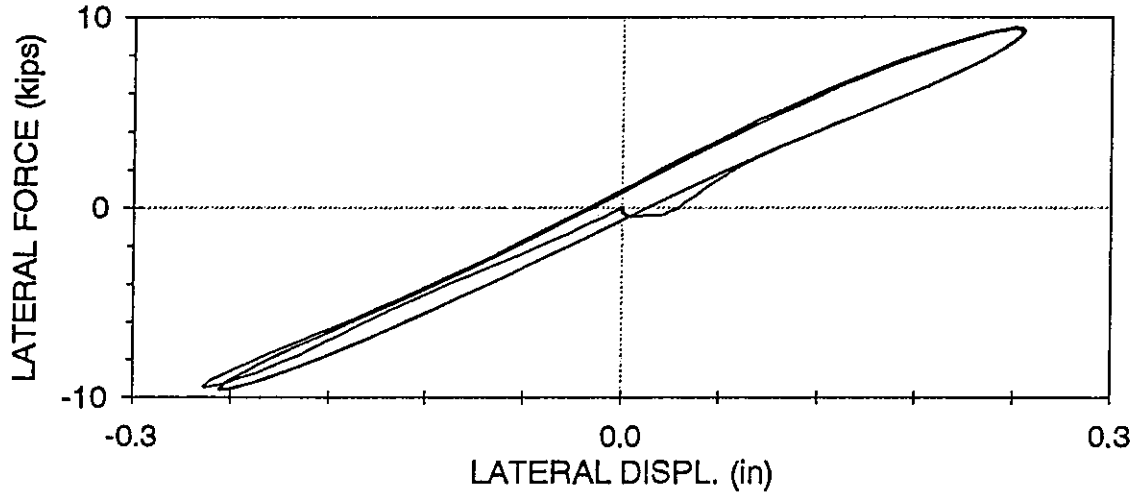

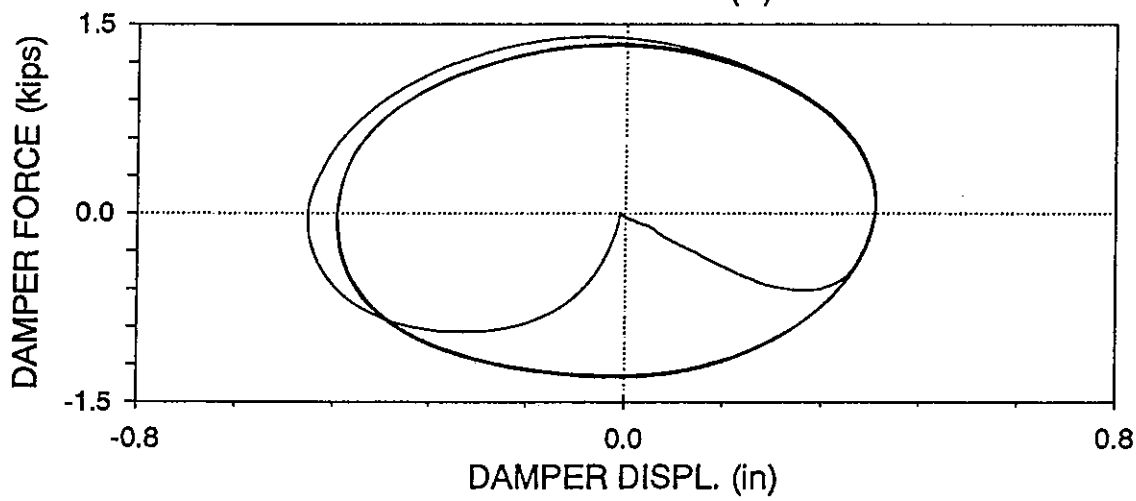

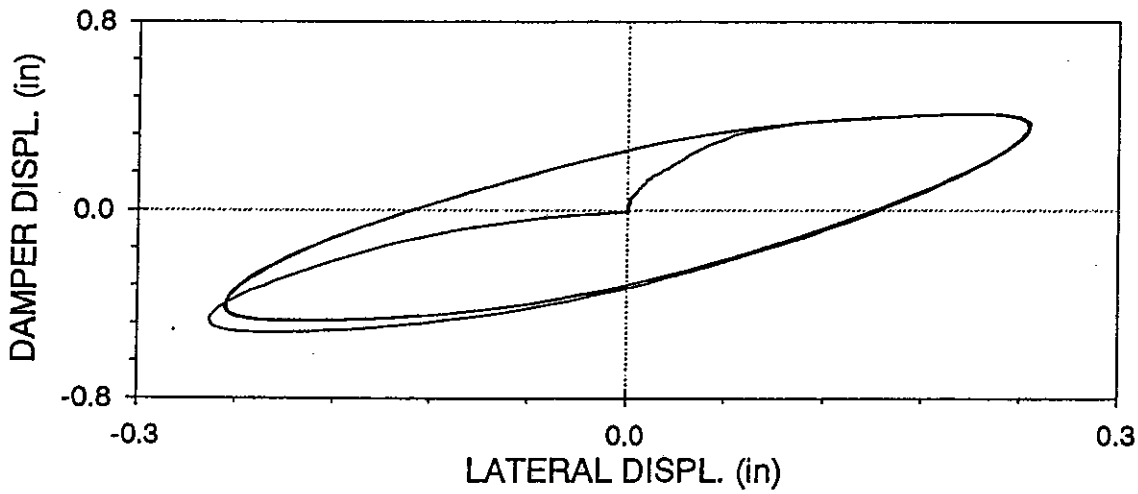

ARSTU01 : RIGID-SIMPLE CONNECTIONS, SPRING LEAF CONFIGURATION

UPPER DAMPER, f=0.05 Hz, U_o= 0.25 in (05/07/97, 10:35:37)

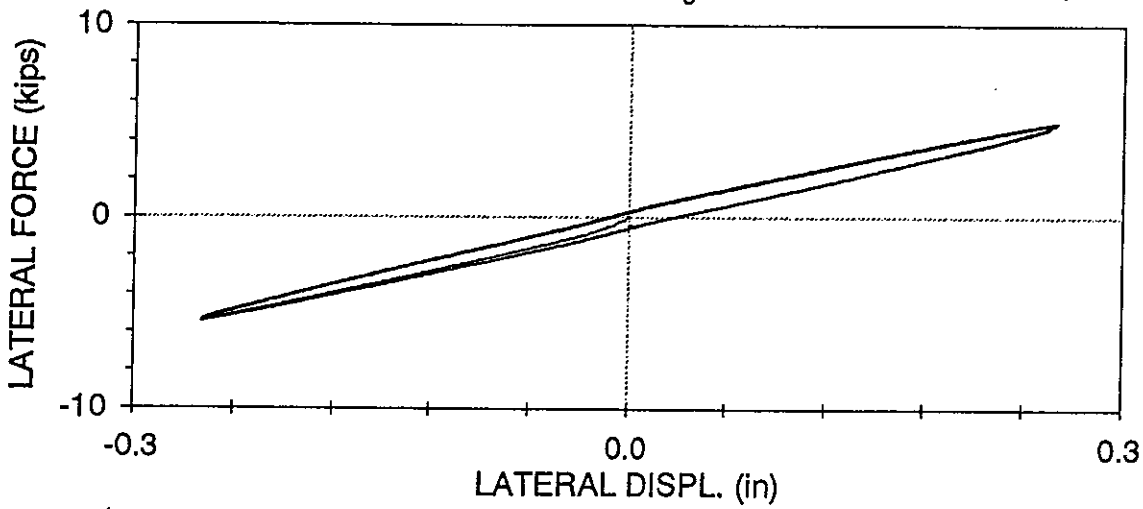

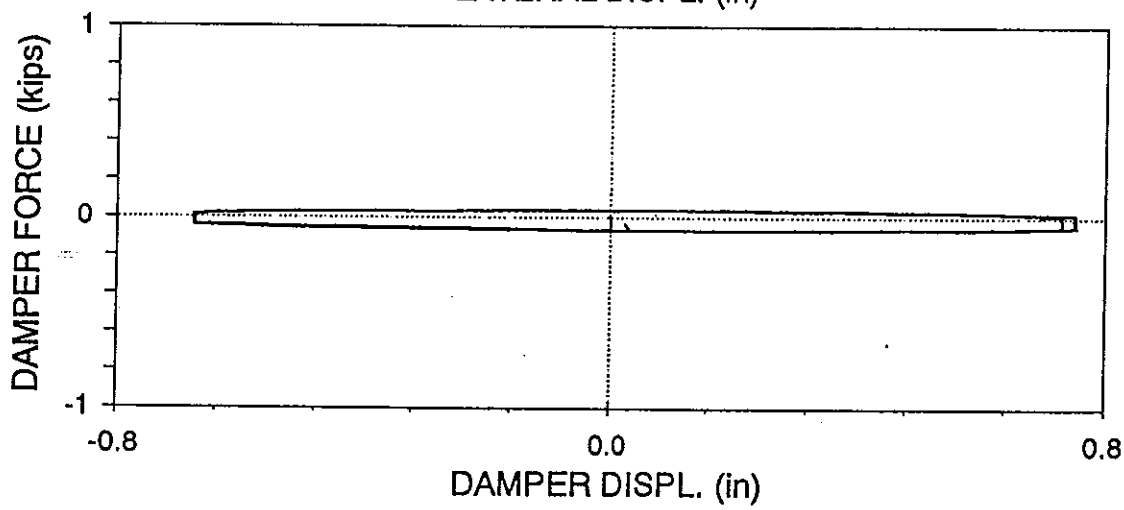

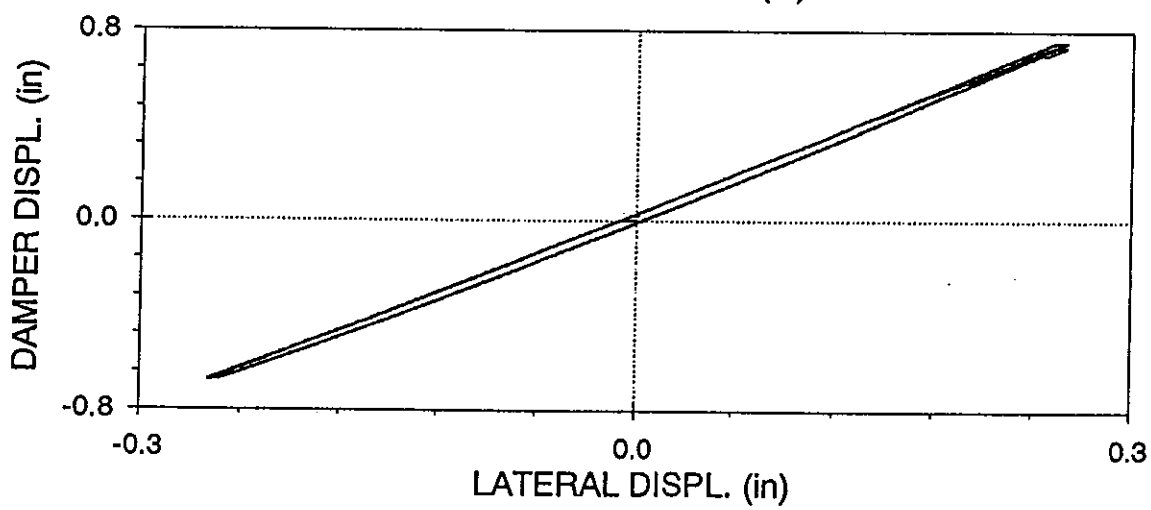

ARSTU02 : RIGID-SIMPLE CONNECTIONS, SPRING LEAF CONFIGURATION

UPPER DAMPER, f=2 Hz, U_o= 0.25 in (05/07/97, 10:39:01)

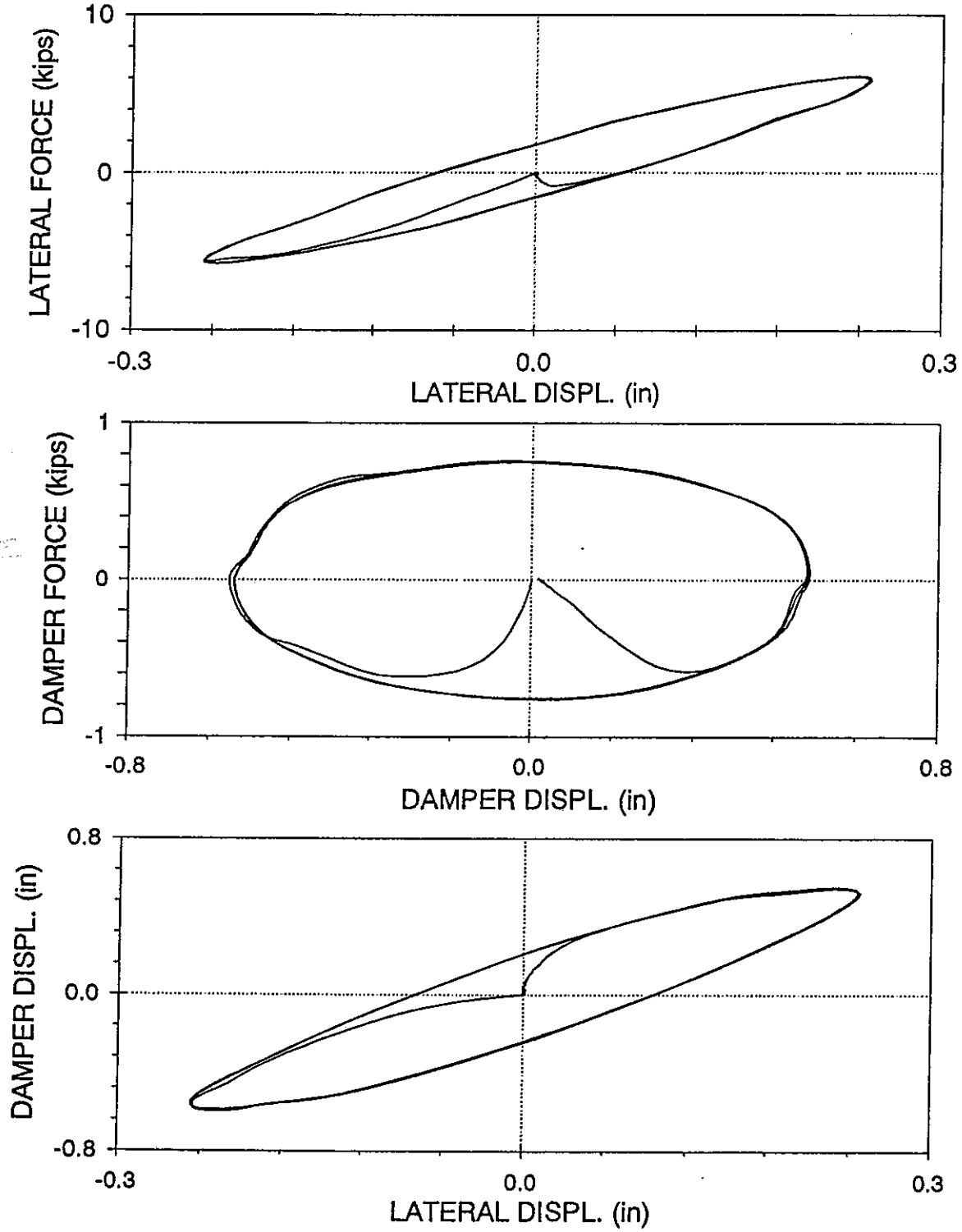

ARSTU03 : RIGID-SIMPLE CONNECTIONS, SPRING LEAF CONFIGURATION

UPPER DAMPER, f=3 Hz, U_o= 0.25 in (05/07/97, 12:32:54)

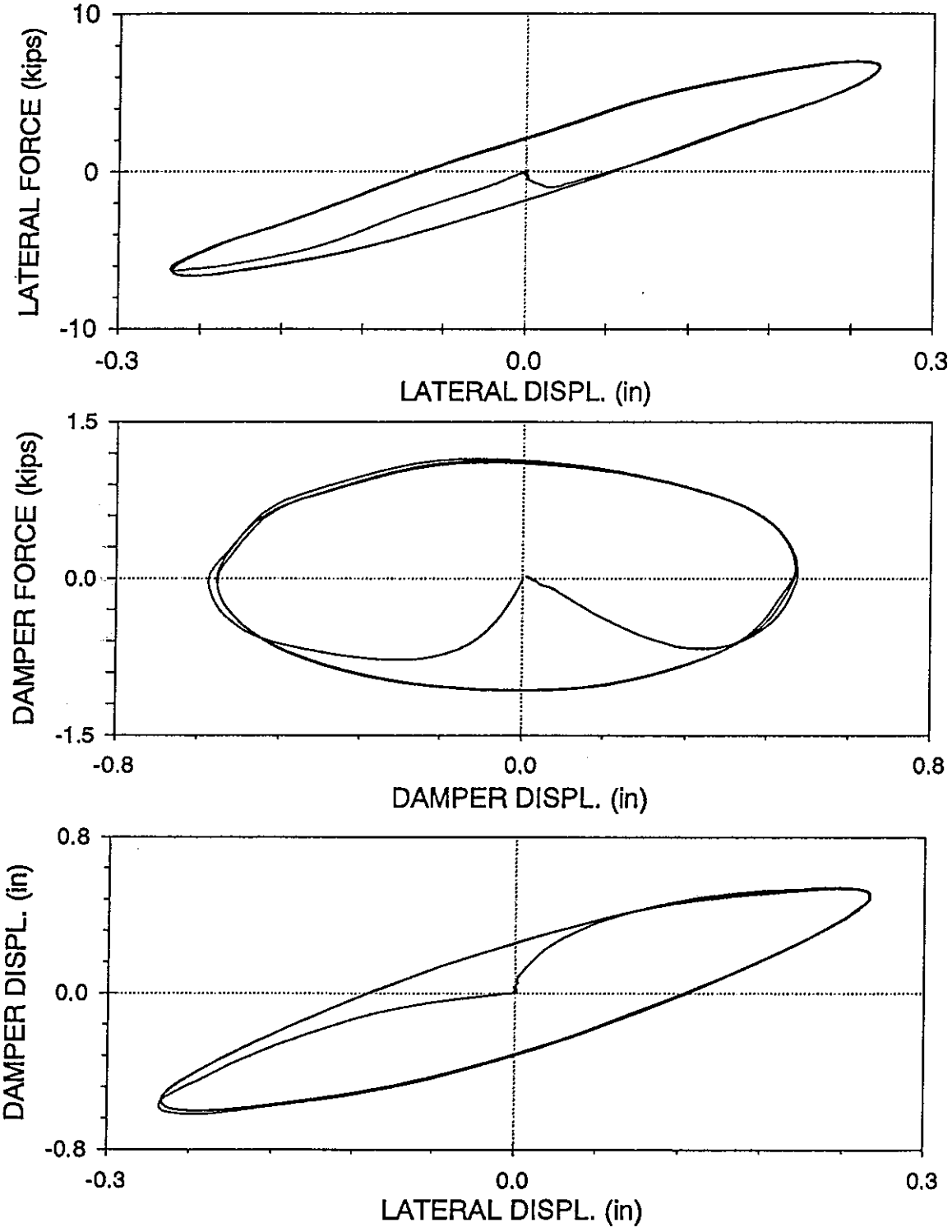

ARSTU04 : RIGID-SIMPLE CONNECTIONS, SPRING LEAF CONFIGURATION

(right column fixed) UPPER DAMPER, f=2 Hz, U_o= 0.25 in (05/07/97, 12:41:28)

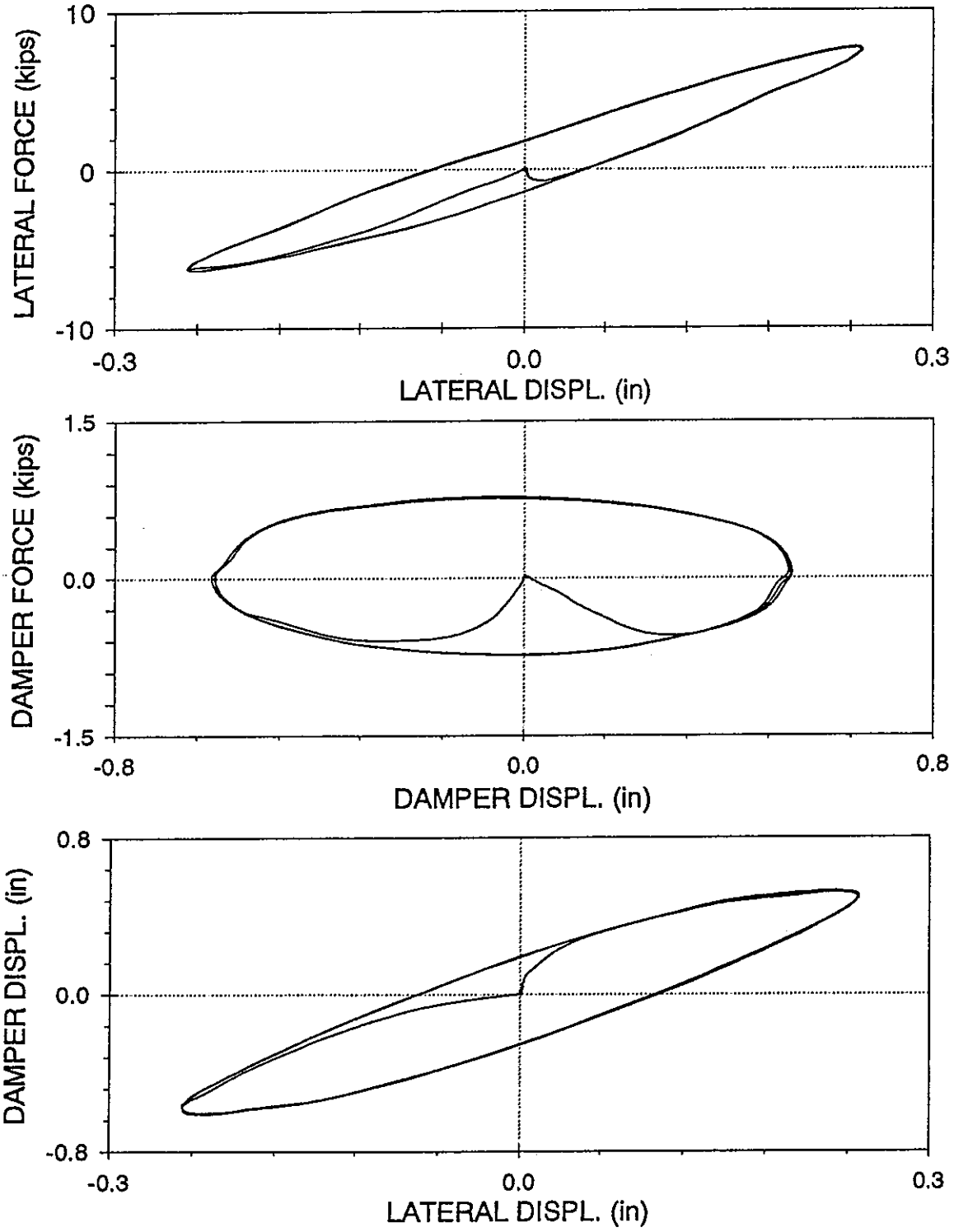

ARSTU05 : RIGID-SIMPLE CONNECTIONS, SPRING LEAF CONFIGURATION

(right column fixed) UPPER DAMPER, f=3 Hz, U_o= 0.25 in (05/07/97, 12:43:30)

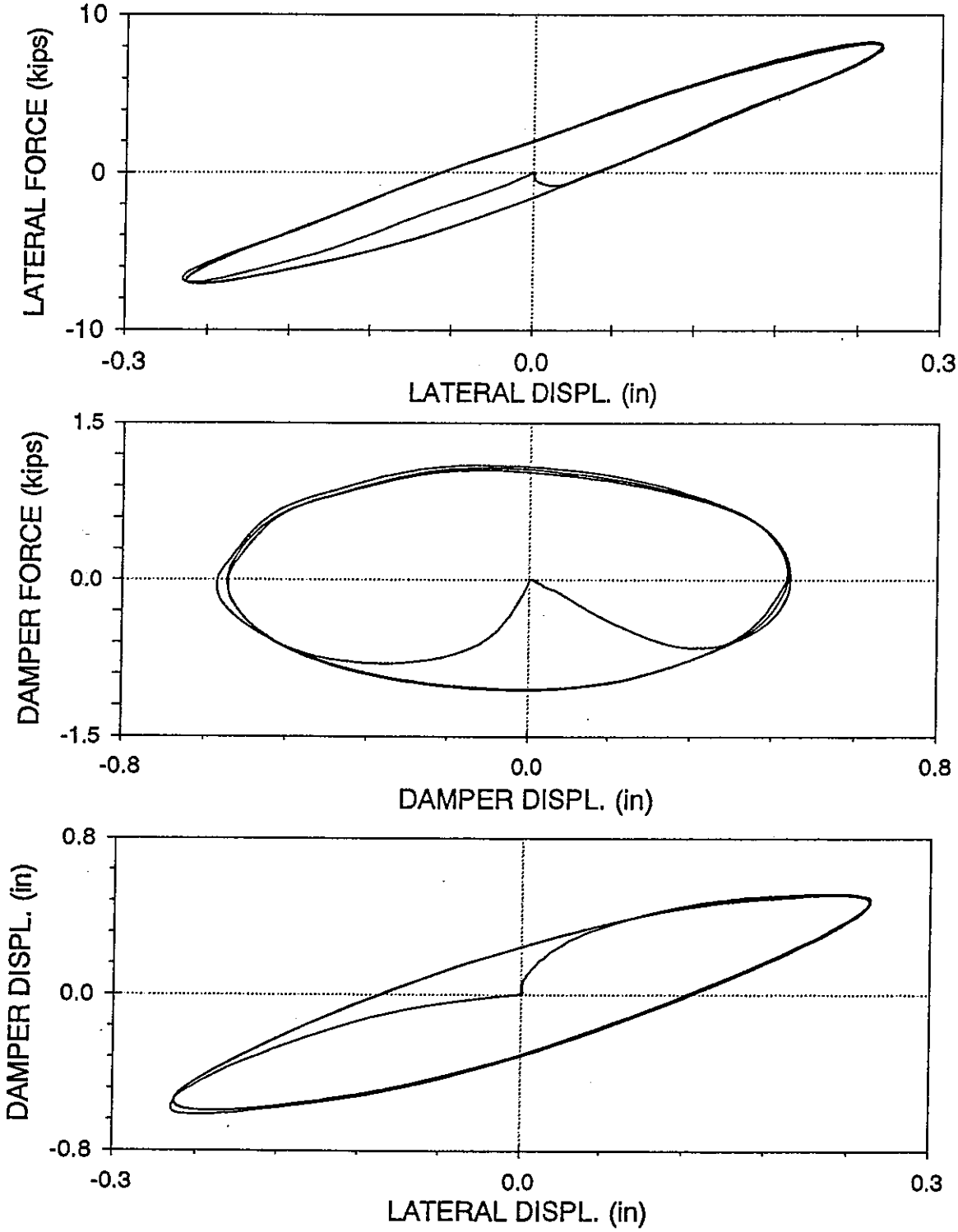

ARSTL06 : RIGID-SIMPLE CONNECTIONS, SPRING LEAF CONFIGURATION

LOWER DAMPER, f=3 Hz, U_o= 0.25 in (05/07/97, 13:24:00)

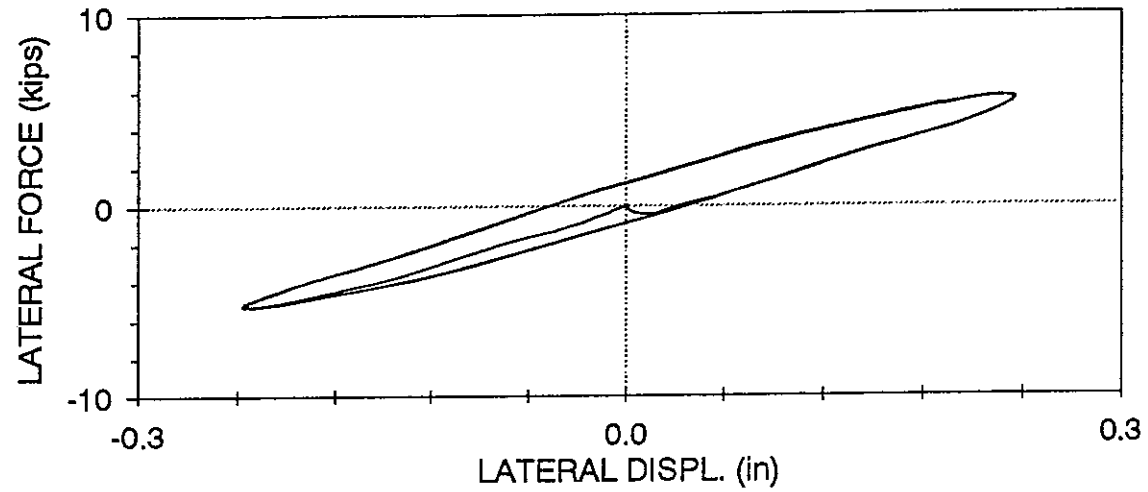

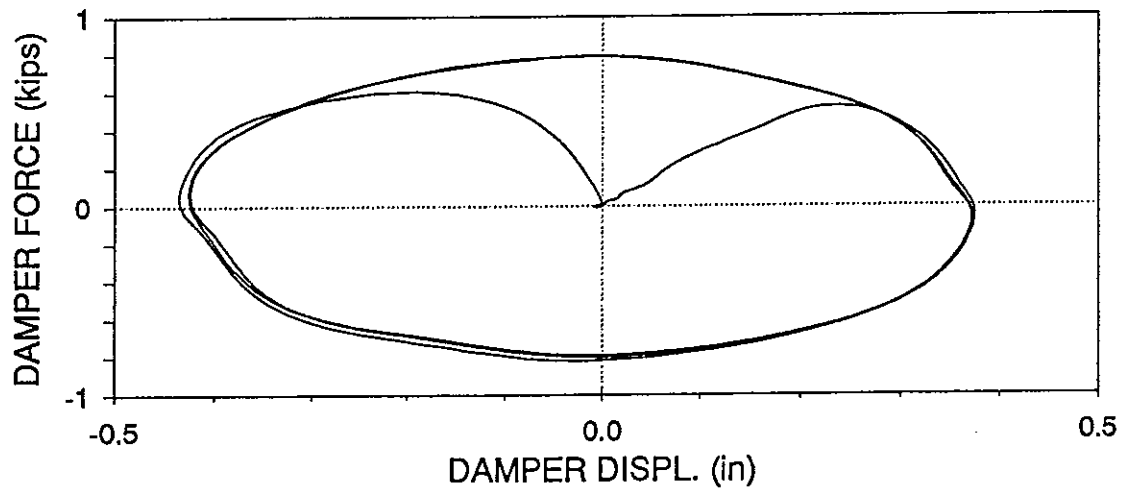

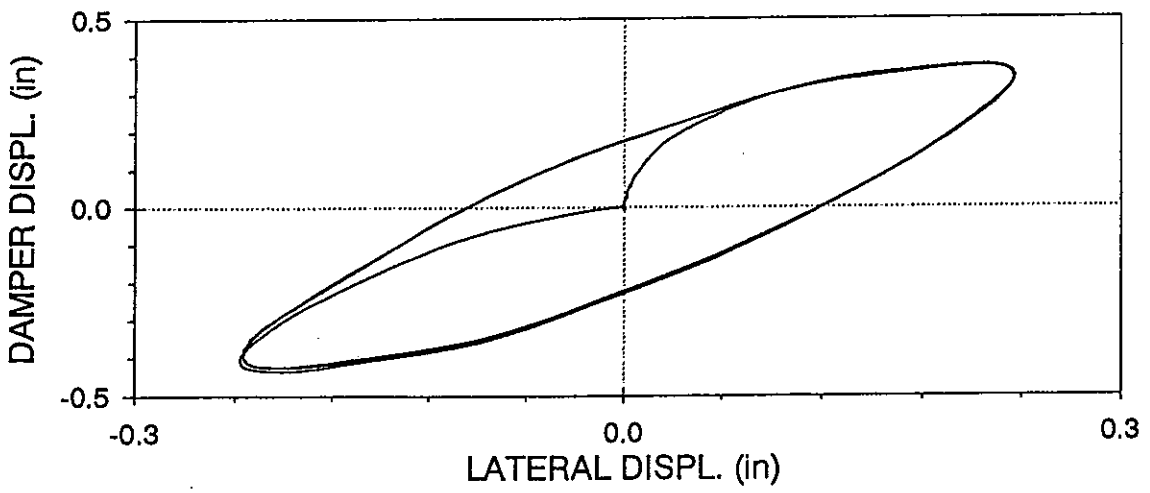

APPENDIX C

RESULTS OF TESTING OF FRAME WITH BENT PLATE CONNECTION DETAIL FOR THE TOGGLE BRACES

(1 in. = 25.4 mm, 1 kip = 4.45 kN).

Tests ASTBL05, ASTBL11 and ASTBL12 conducted with 10 cycles.

Tests ASTBL07, ASTBL08 and ASTBL09 where conducted with rigid connections except that the shim plate (see Appendix A, detail BB) of the toggle brace to beam and column connection was removed.

ASTBL01 : SIMPLE CONNECTIONS, BENT PLATE CONFIGURATION

LOWER DAMPER, f=0.05 Hz, U_o= 0.25 in (05/08/97, 09:37:43)

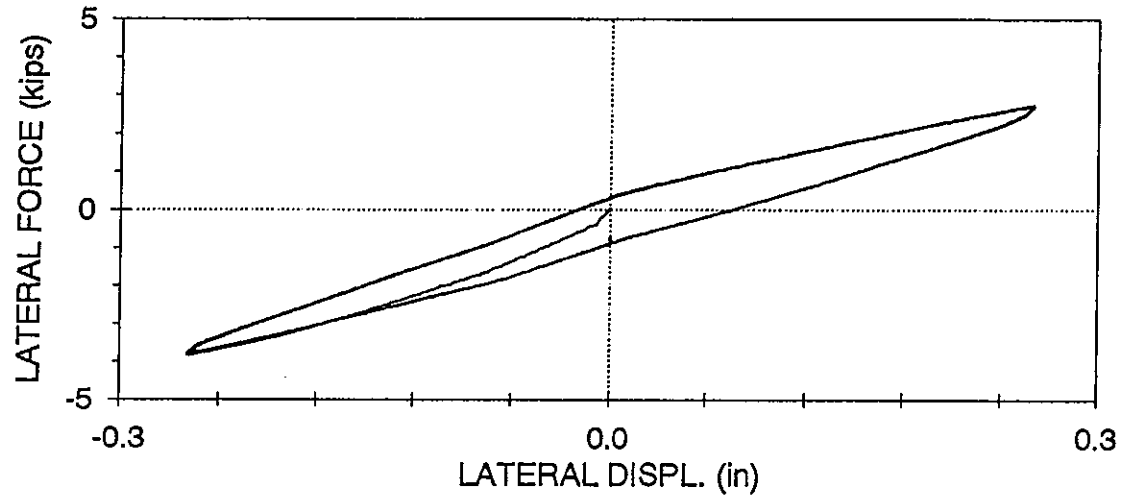

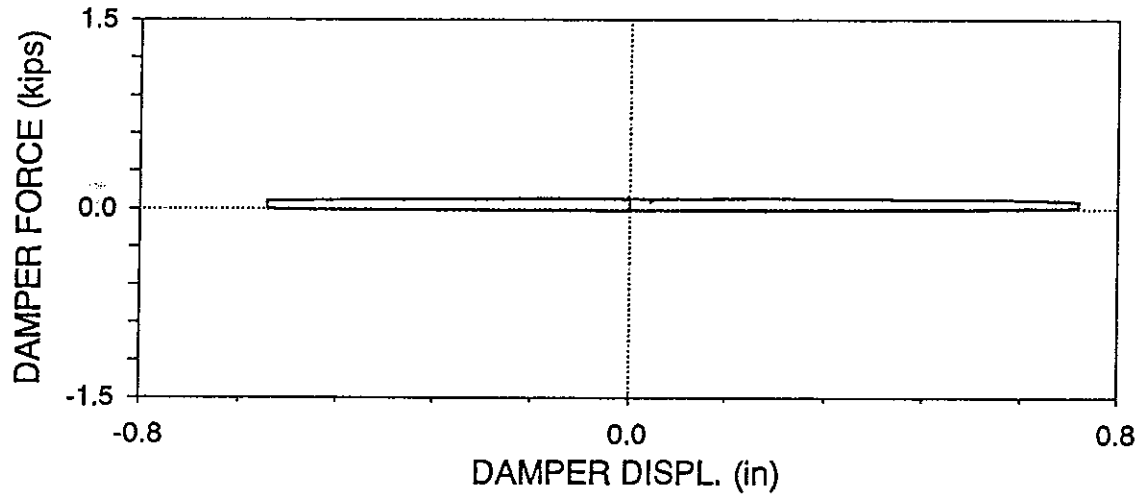

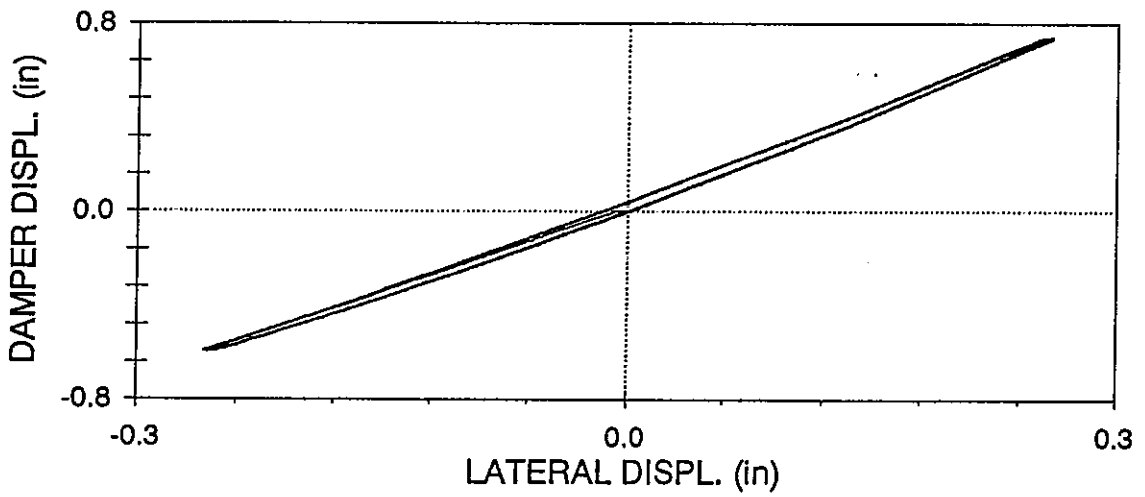

ASTBL02 : SIMPLE CONNECTIONS, BENT PLATE CONFIGURATION

LOWER DAMPER, f=0.05 Hz, U_o= 0.5 in (05/08/97, 09:40:49)

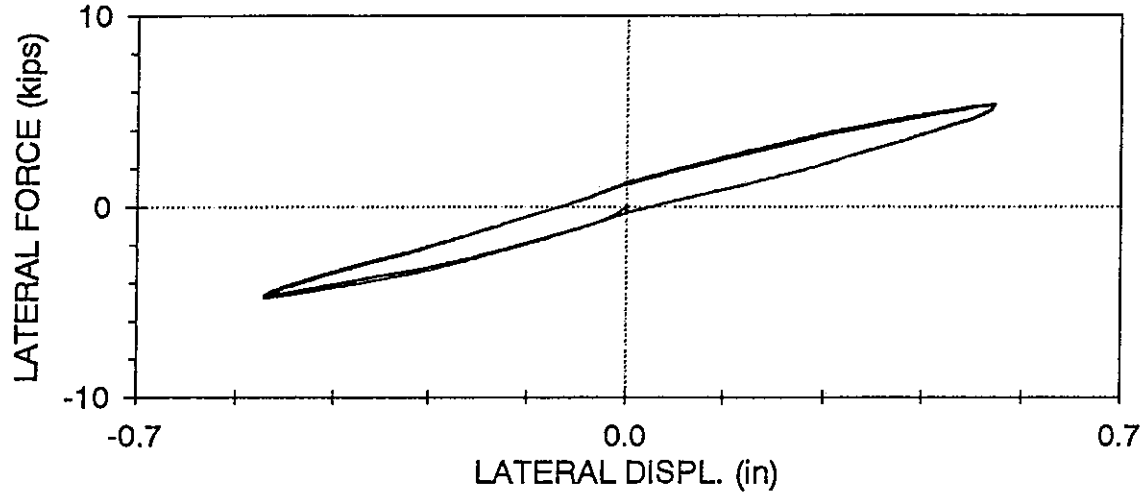

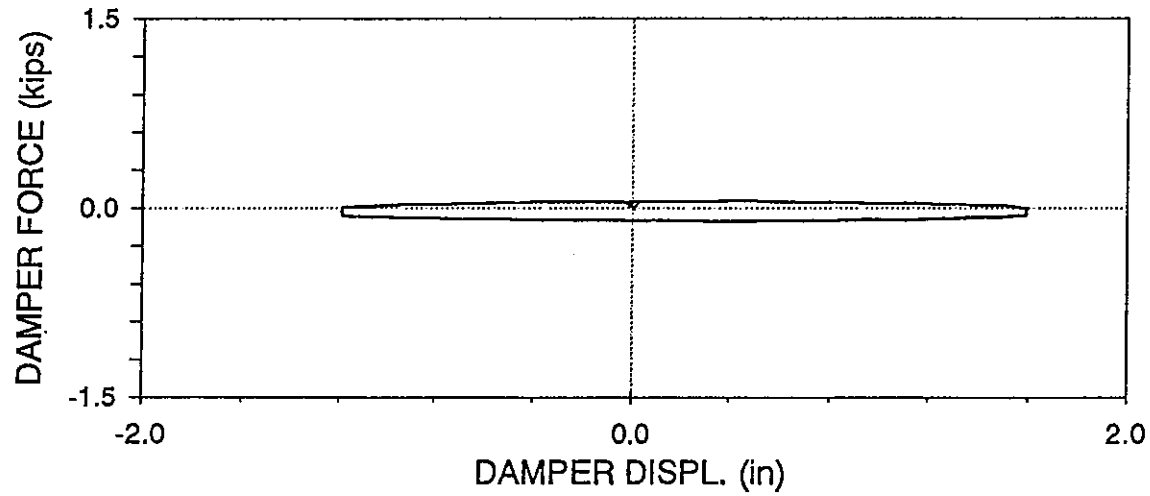

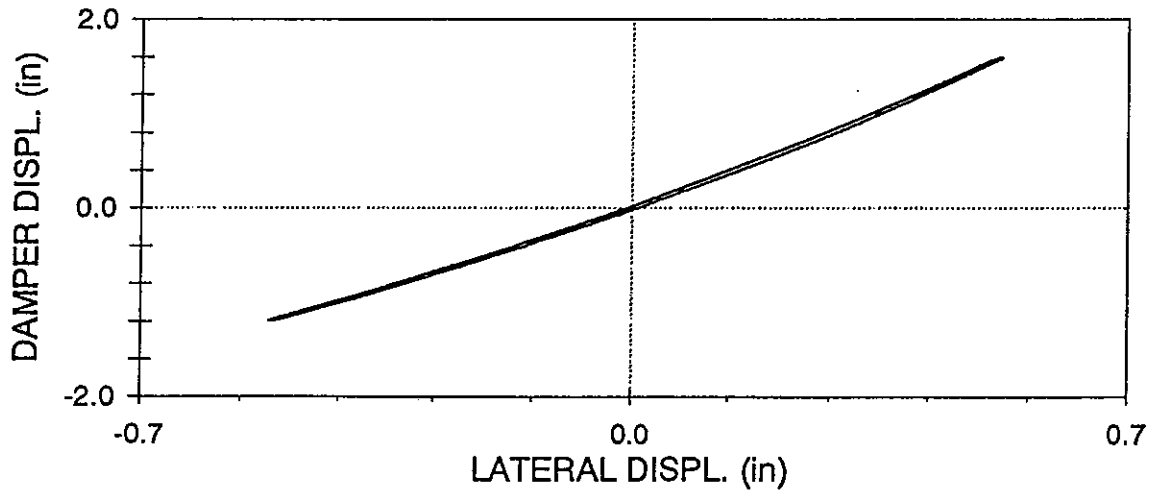

ASTBL03 : SIMPLE CONNECTIONS, BENT PLATE CONFIGURATION

LOWER DAMPER, f=2 Hz, U_o= 0.25 in (05/08/97, 09:44:52)

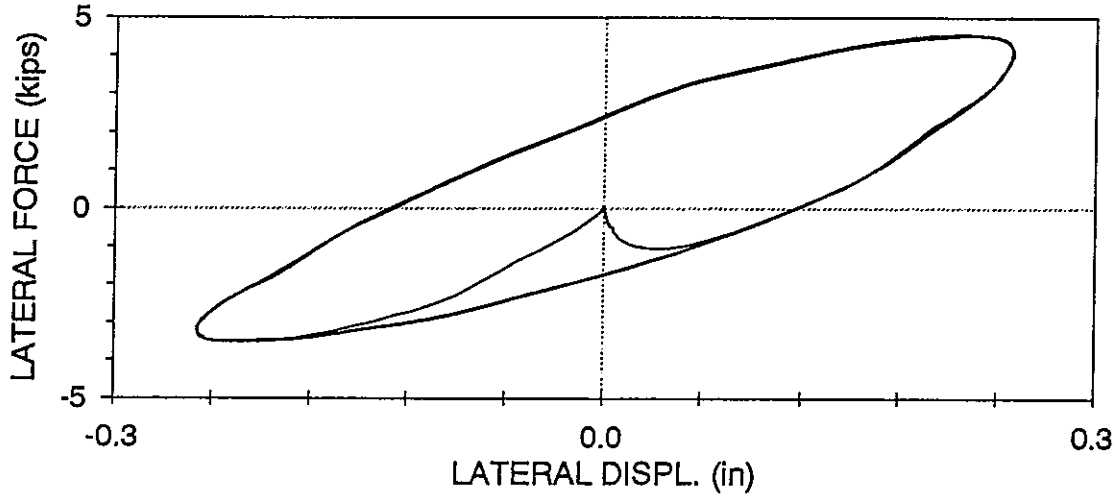

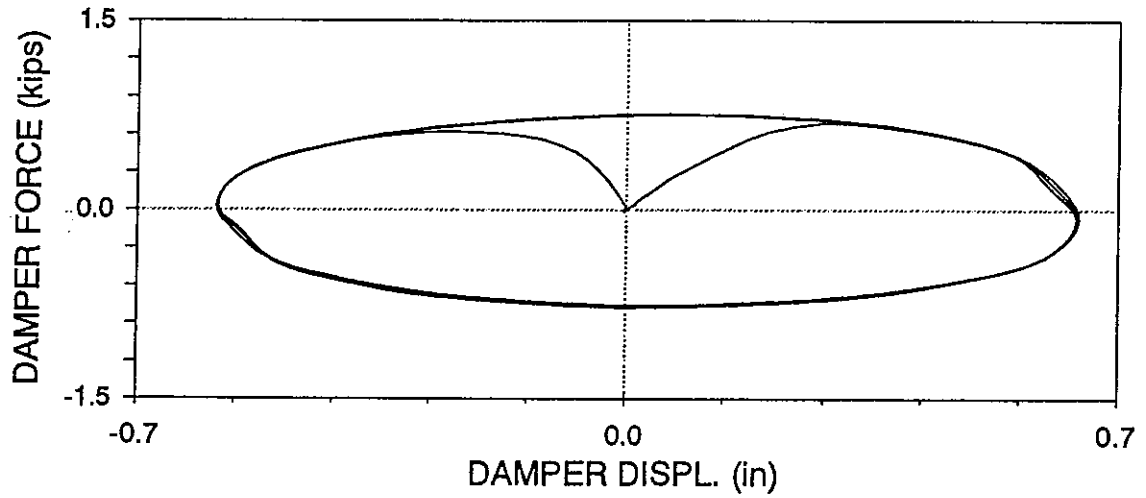

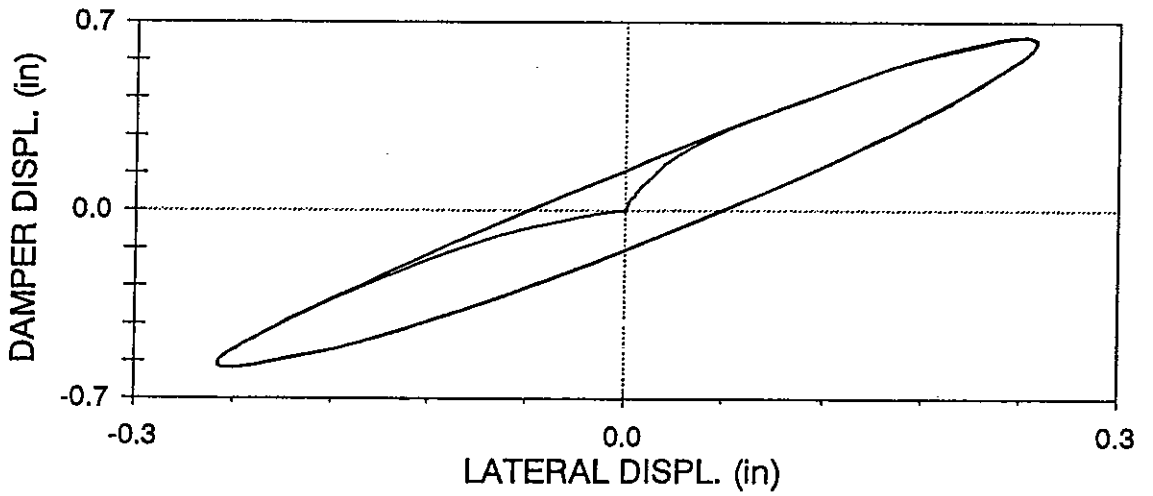

ASTBL04 : SIMPLE CONNECTIONS, BENT PLATE CONFIGURATION

LOWER DAMPER, f=2.0 Hz, U_o= 0.5 in (05/08/97, 09:46:48)

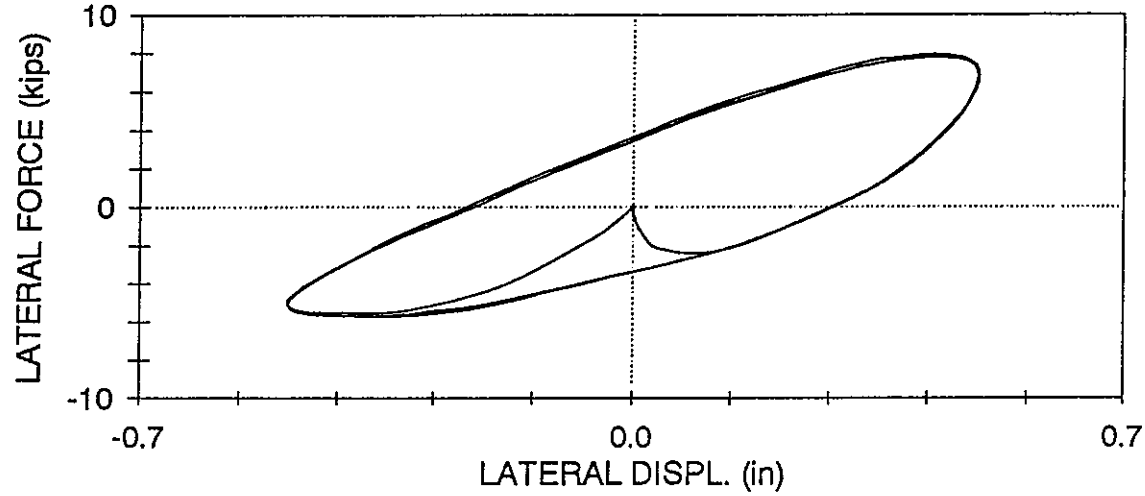

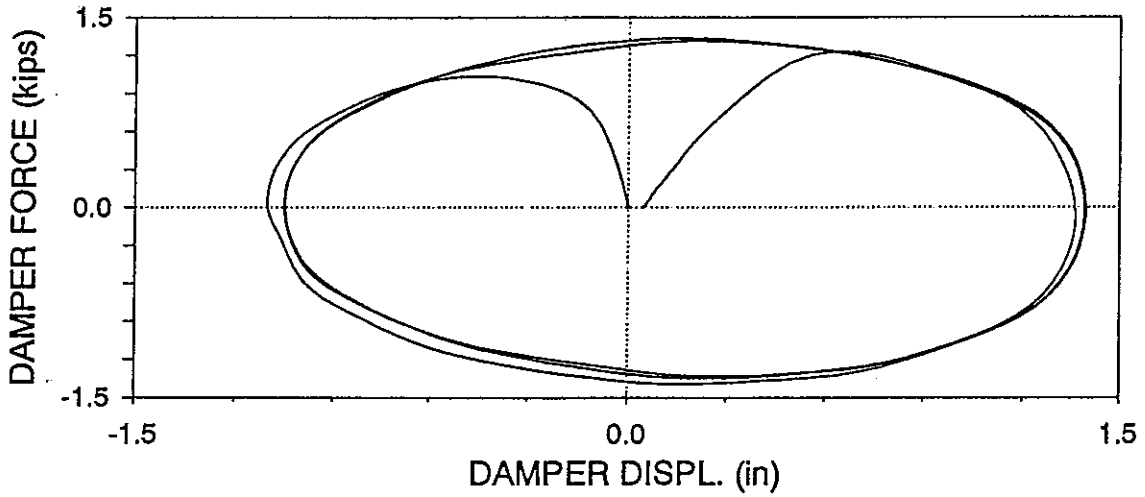

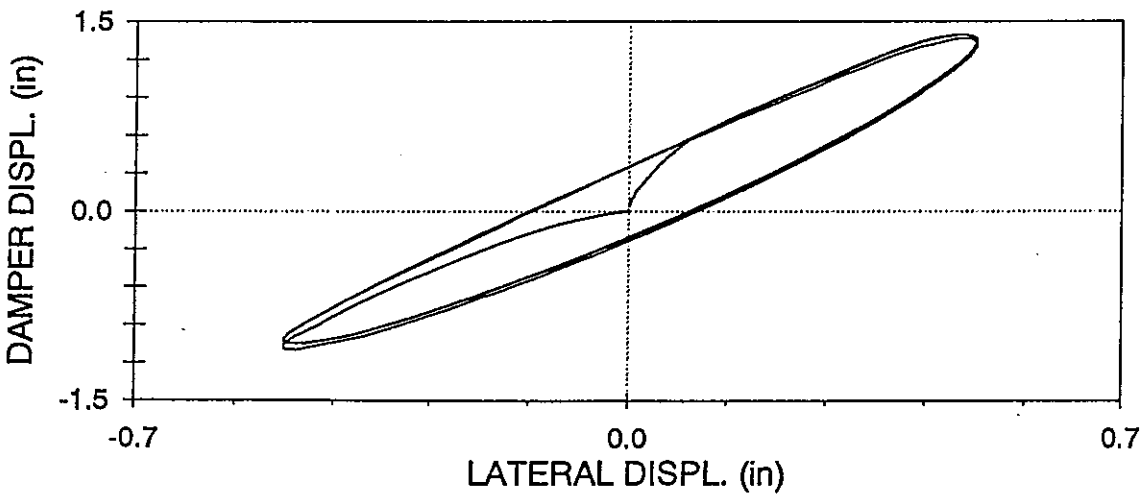

ASTBL05 : SIMPLE CONNECTIONS, BENT PLATE CONFIGURATION

LOWER DAMPER, f=2.0 Hz, U_o= 0.5 in (05/08/97, 09:49:06)

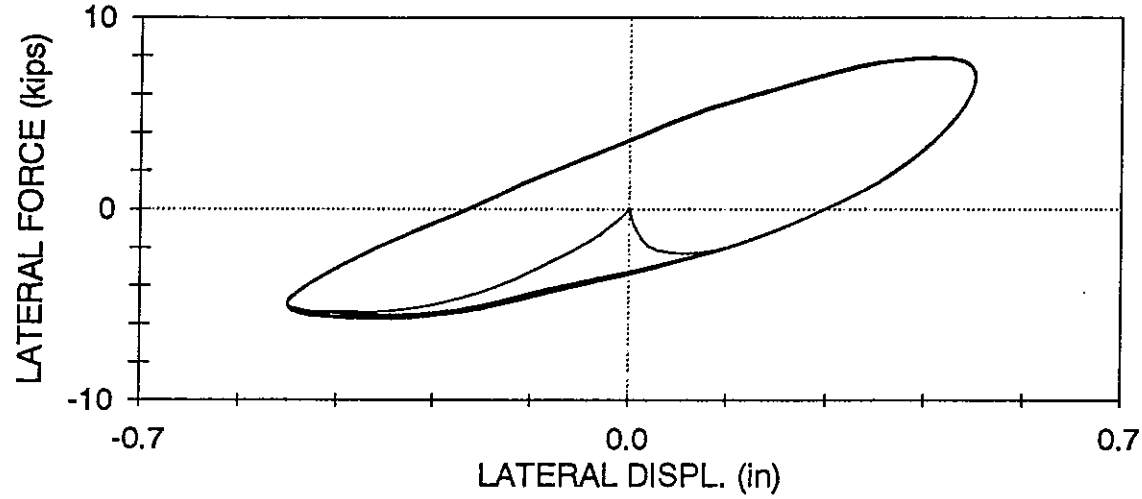

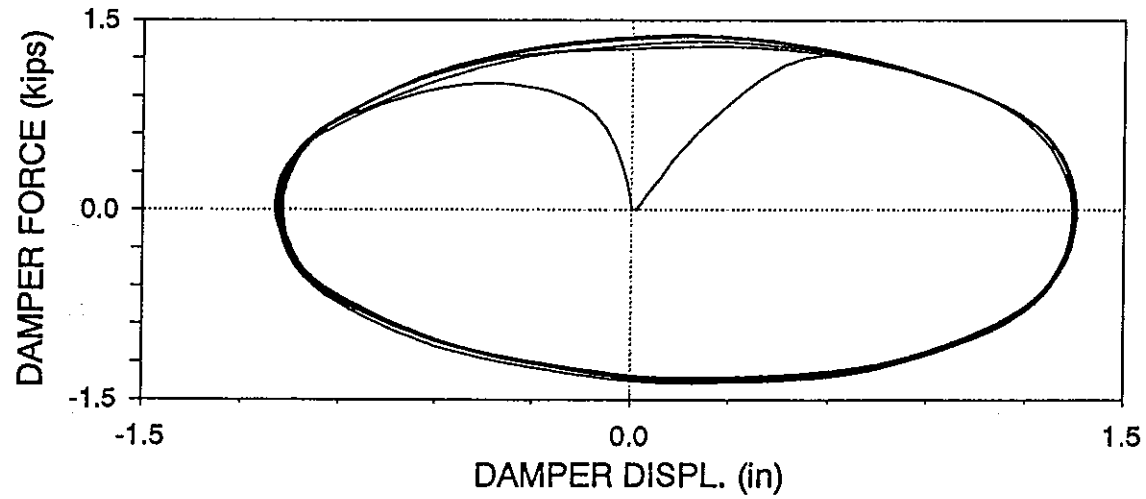

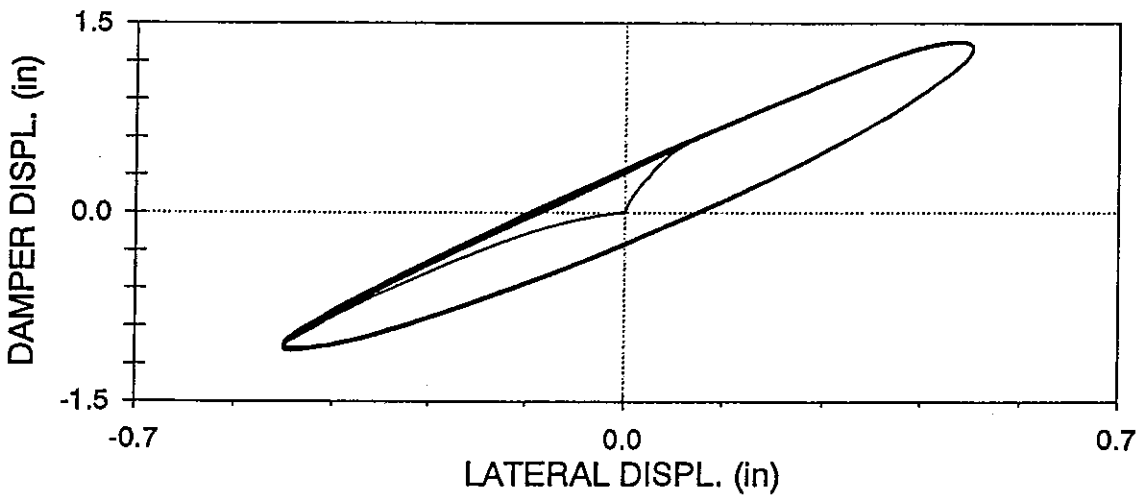

ASTBL07 : RIGID AT TOP OF BEAM, BENT PLATE CONFIGURATION

LOWER DAMPER, f=2.0 Hz, U_o= 0.25 in (05/08/97, 10:13:48)

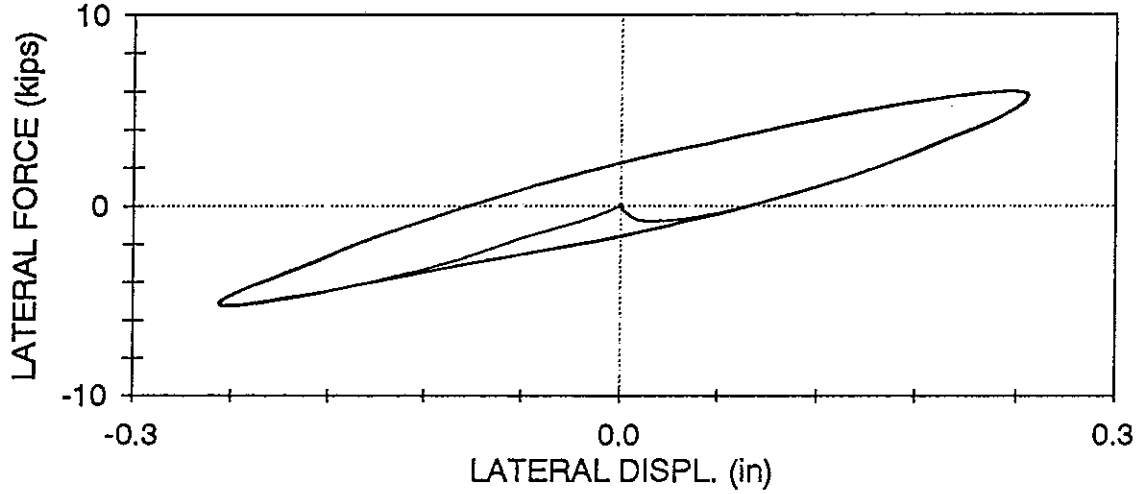

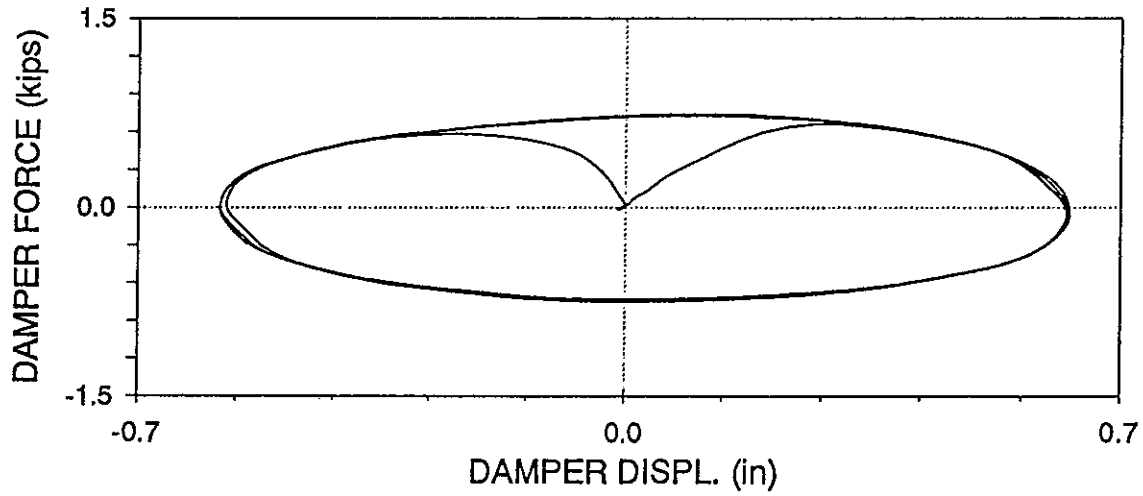

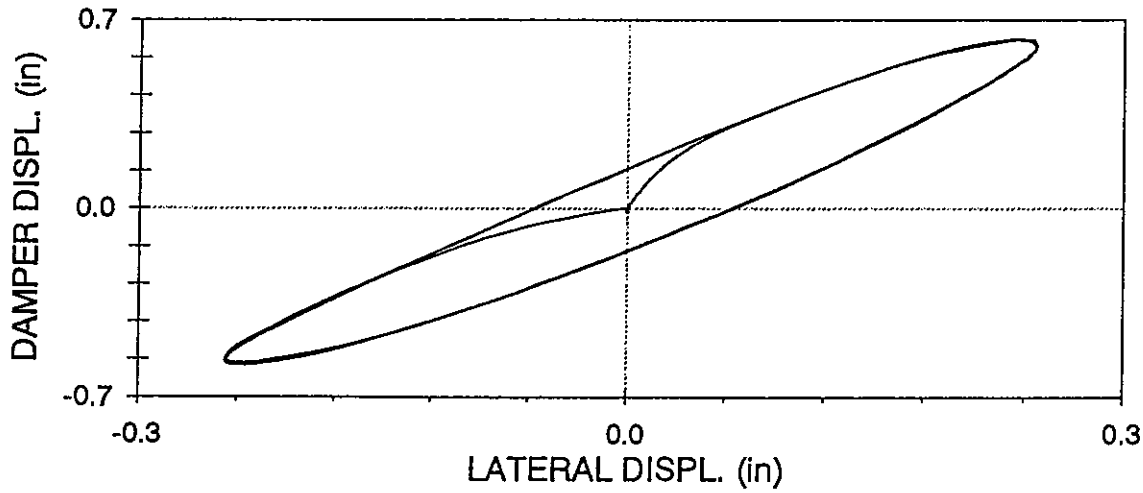

ASTBL08 : RIGID AT TOP OF BEAM, BENT PLATE CONFIGURATION

LOWER DAMPER, f=3.0 Hz, U_o= 0.25 in (05/08/97, 10:15:23)

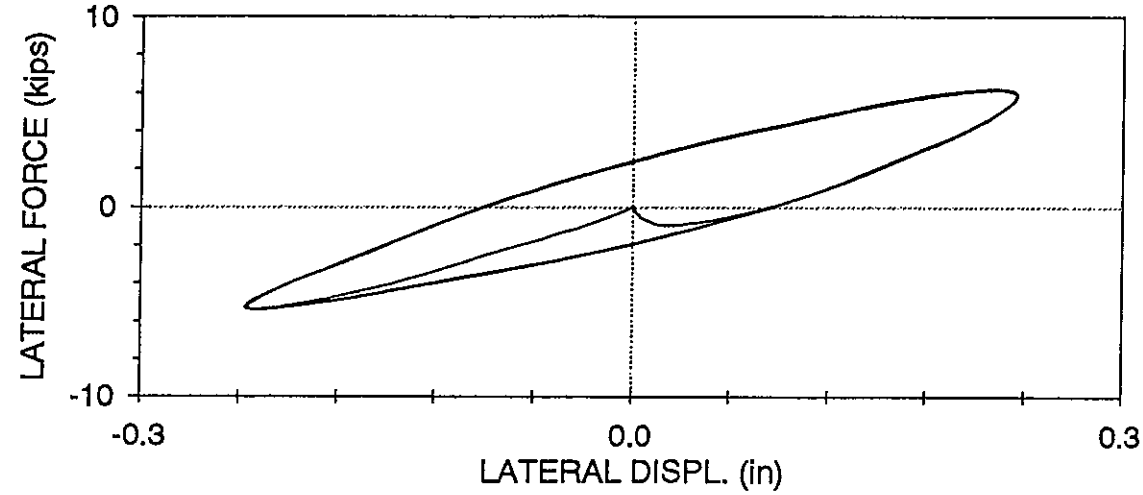

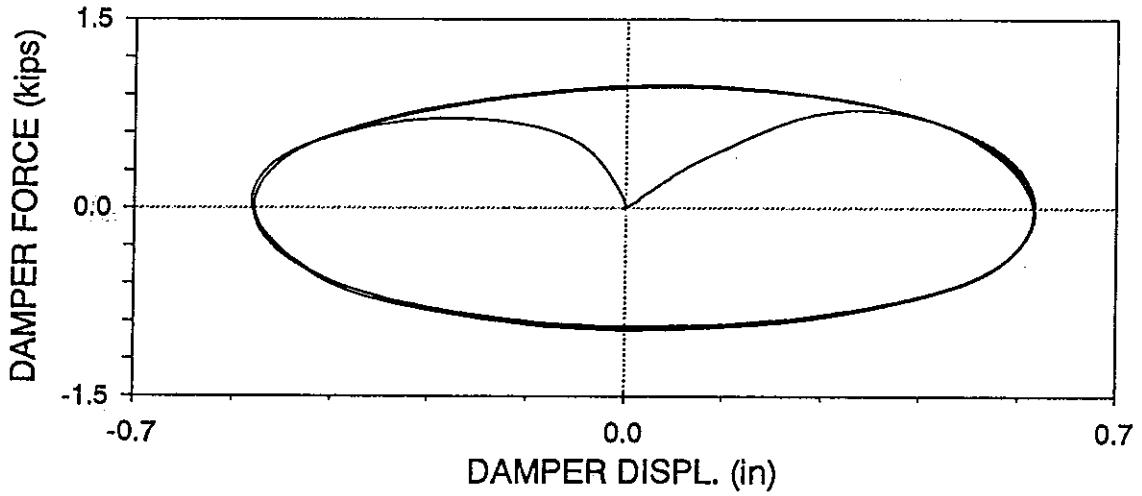

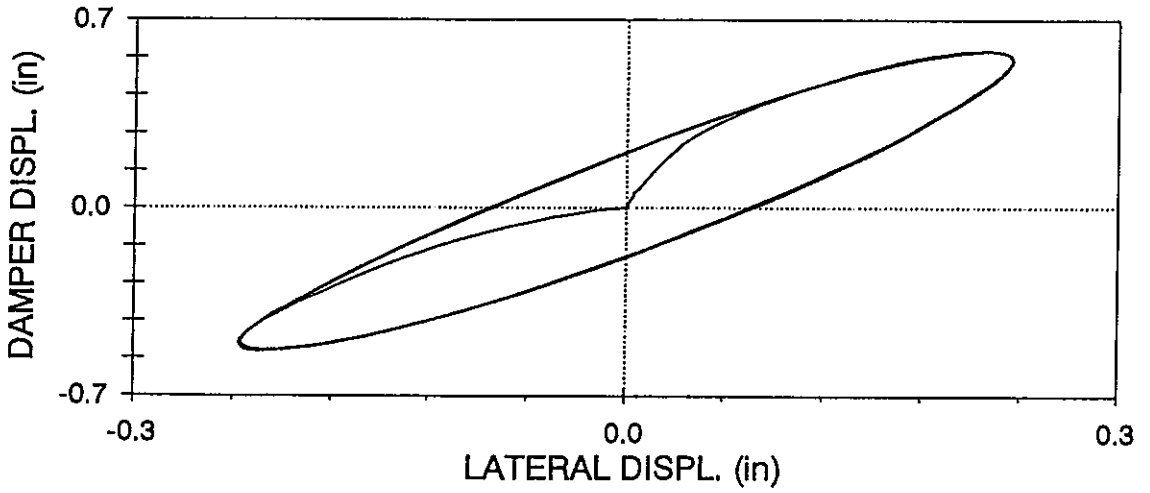

ARTBL02 : RIGID CONNECTIONS, BENT PLATE CONFIGURATION

LOWER DAMPER, f=3 Hz, U_o= 0.25 in (05/08/97, 10:49:06)

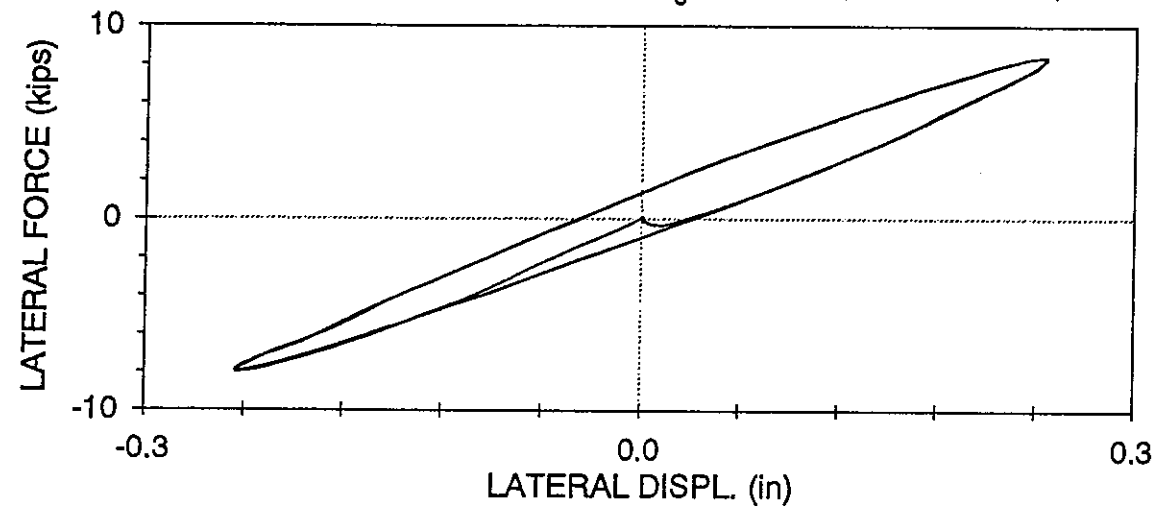

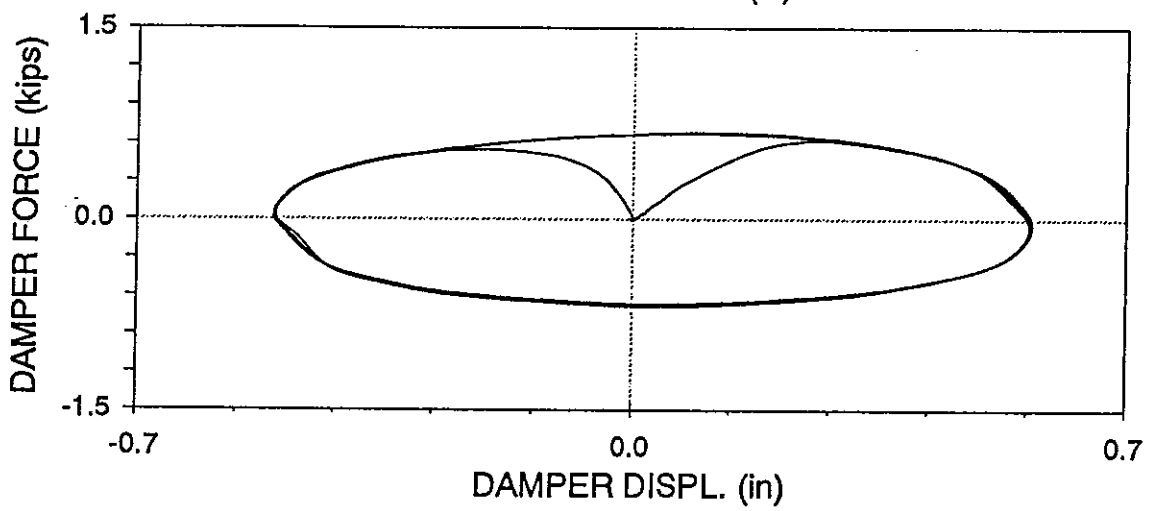

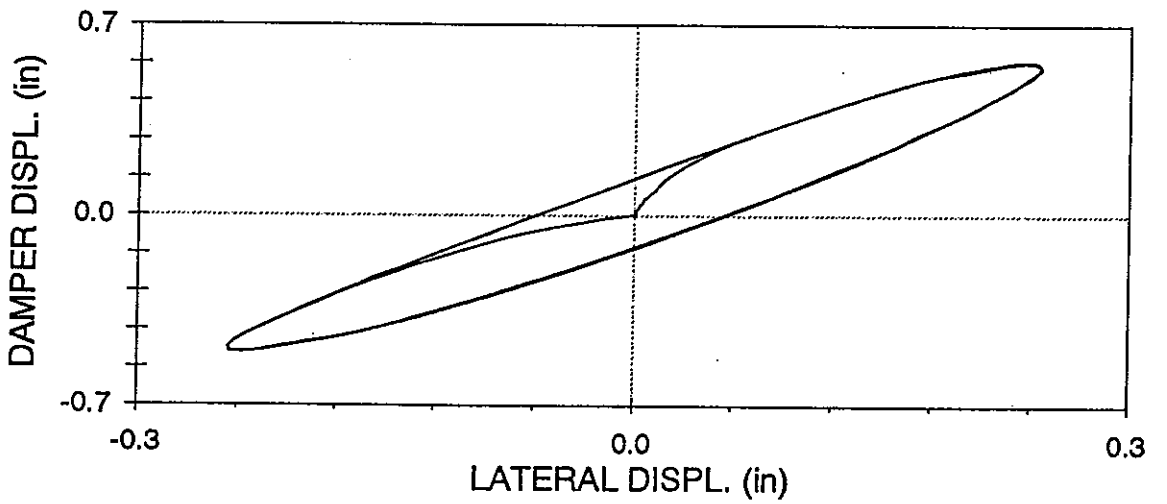

ARTBL01 : RIGID CONNECTIONS, BENT PLATE CONFIGURATION

LOWER DAMPER, f=0.05 Hz, U_o= 0.25 in (05/08/97, 10:45:42)

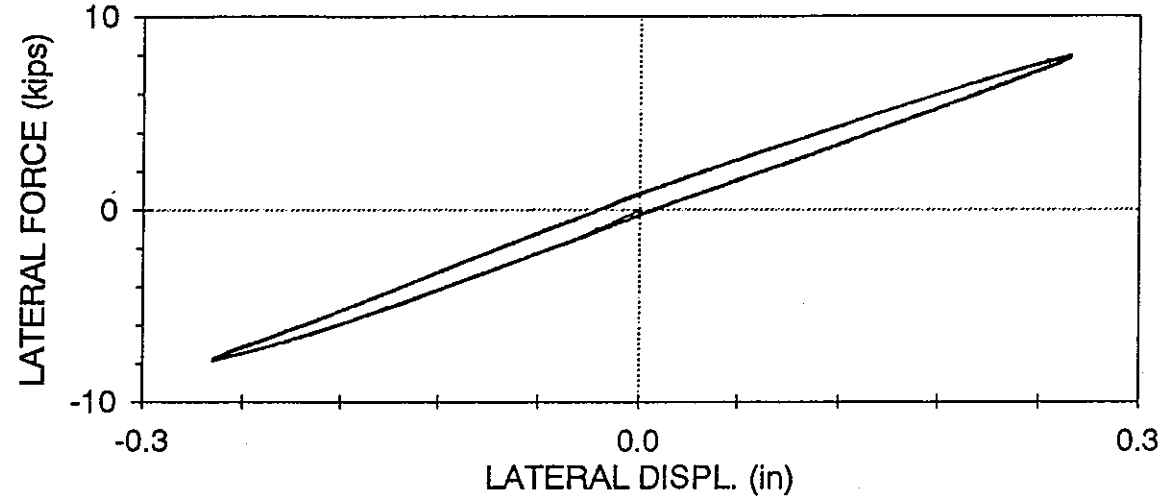

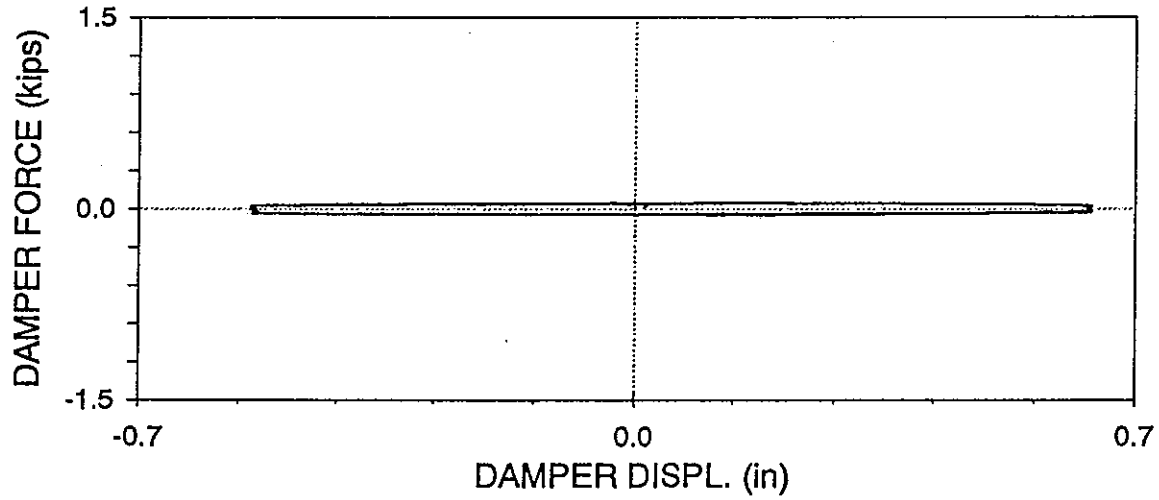

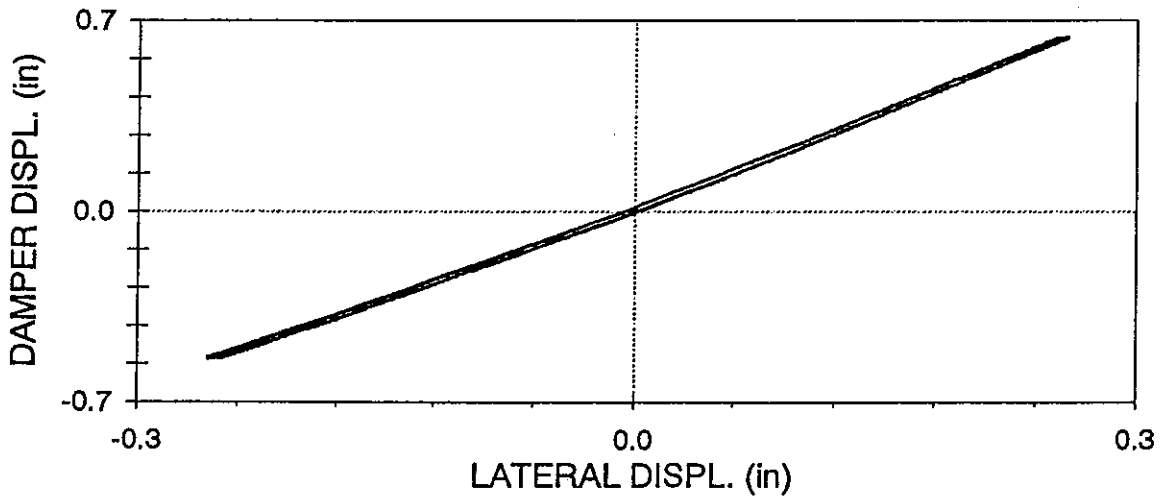

ASTBL12 : SIMPLE CONNECTIONS, BENT PLATE CONFIGURATION

LOWER DAMPER, f=2.0 Hz, U_o= 0.5 in (05/08/97, 12:17:02)

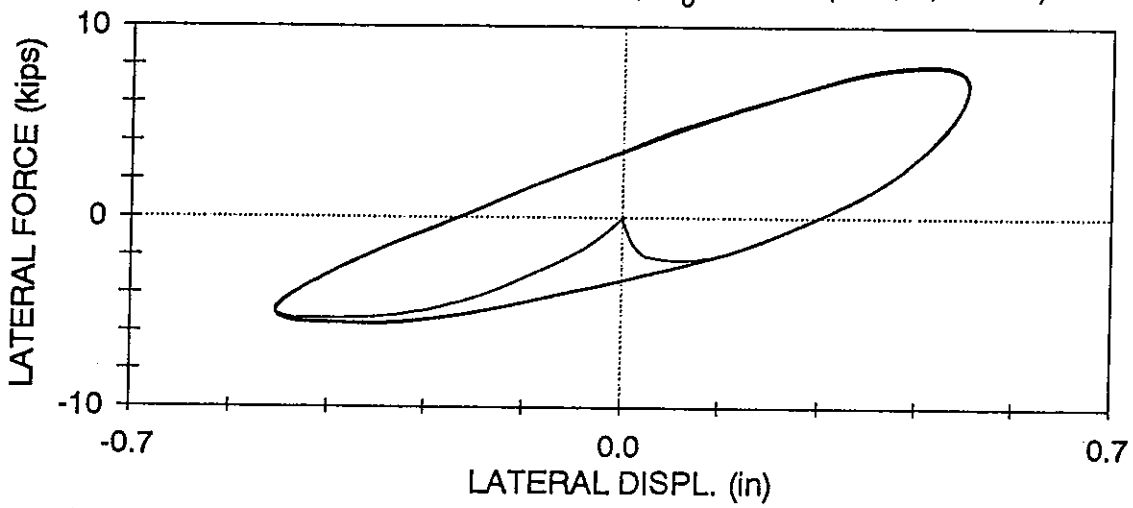

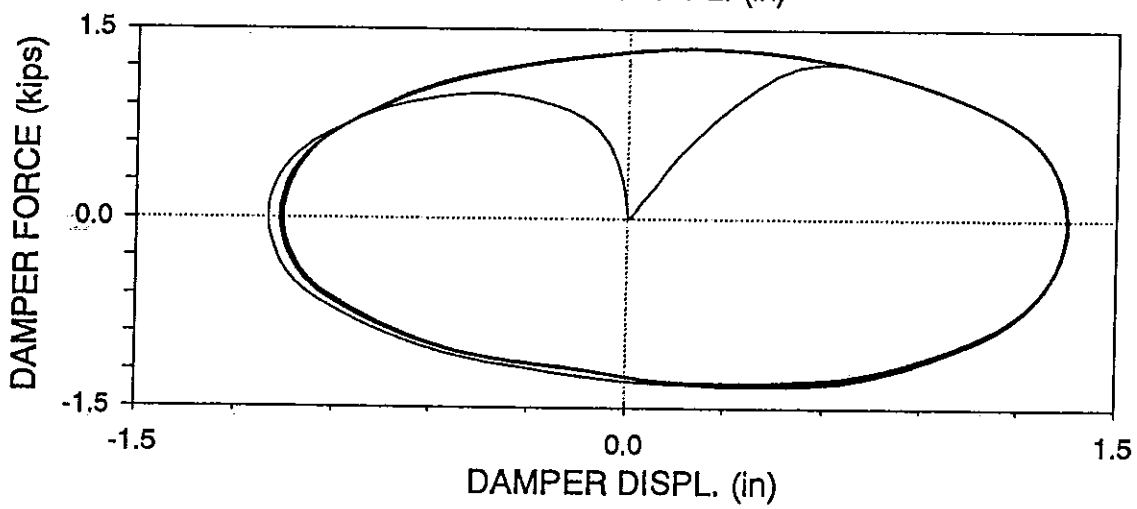

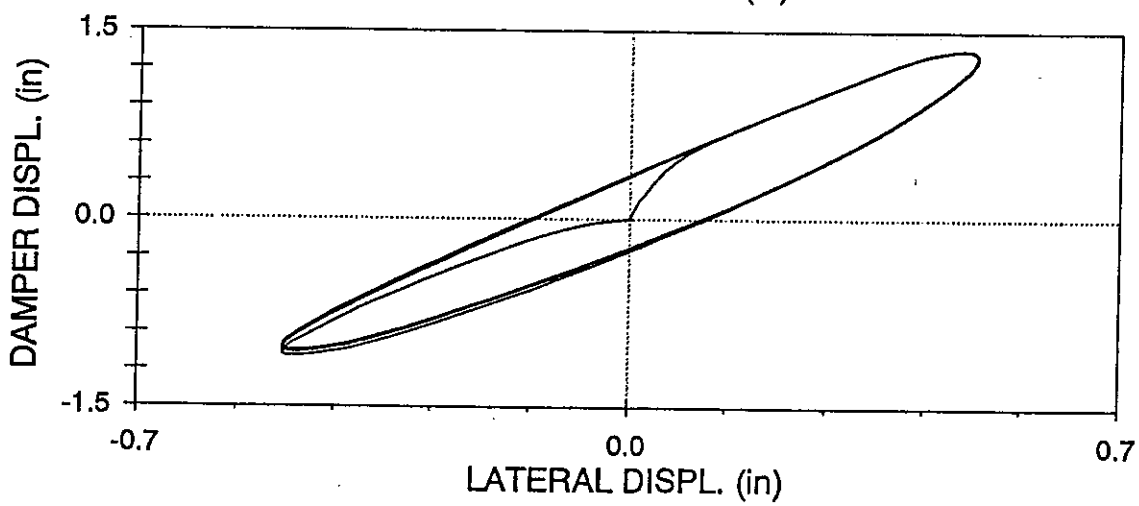

ASTBL11 : SIMPLE CONNECTIONS, BENT PLATE CONFIGURATION

LOWER DAMPER, f=2.0 Hz, U_o= 0.5 in (05/08/97, 12:13:25)

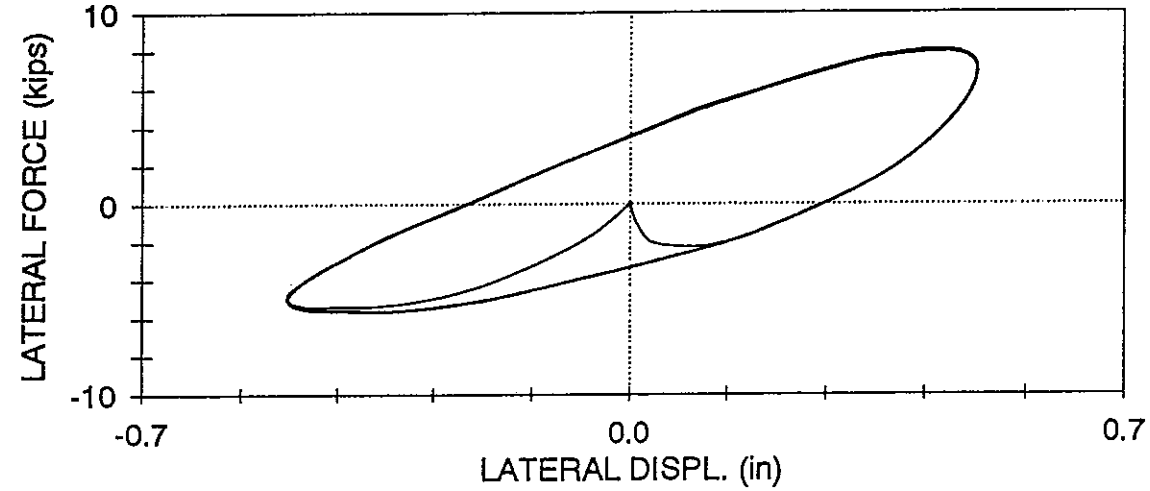

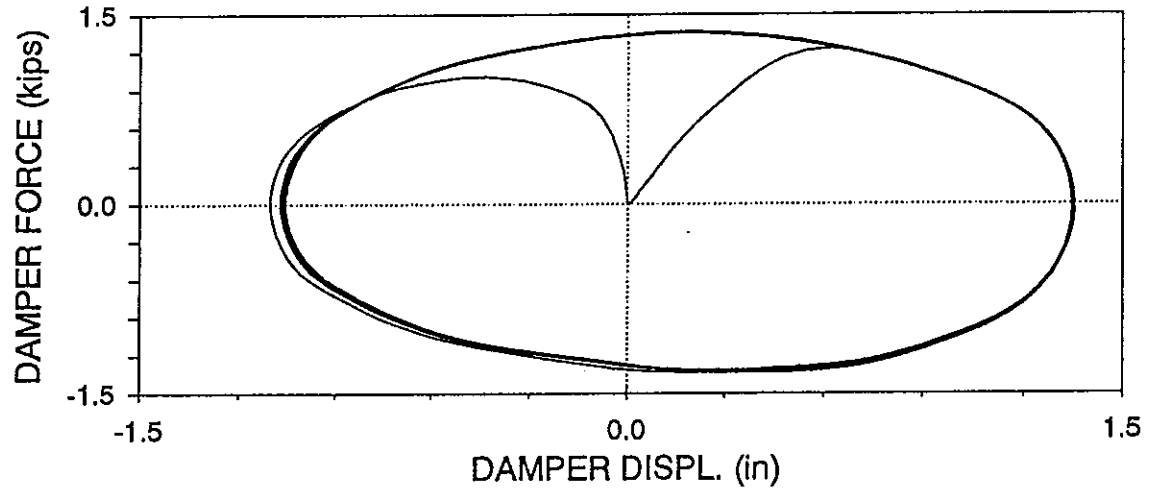

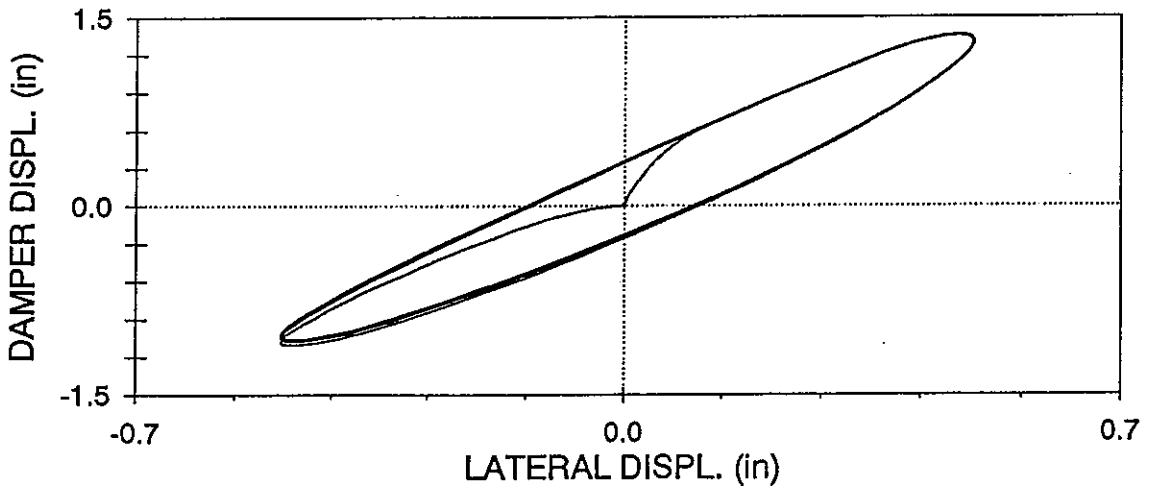

ASTBL09 : RIGID AT TOP OF BEAM, BENT PLATE CONFIGURATION

LOWER DAMPER, f=5.0 Hz, U_o= 0.25 in (05/08/97, 10:17:14)

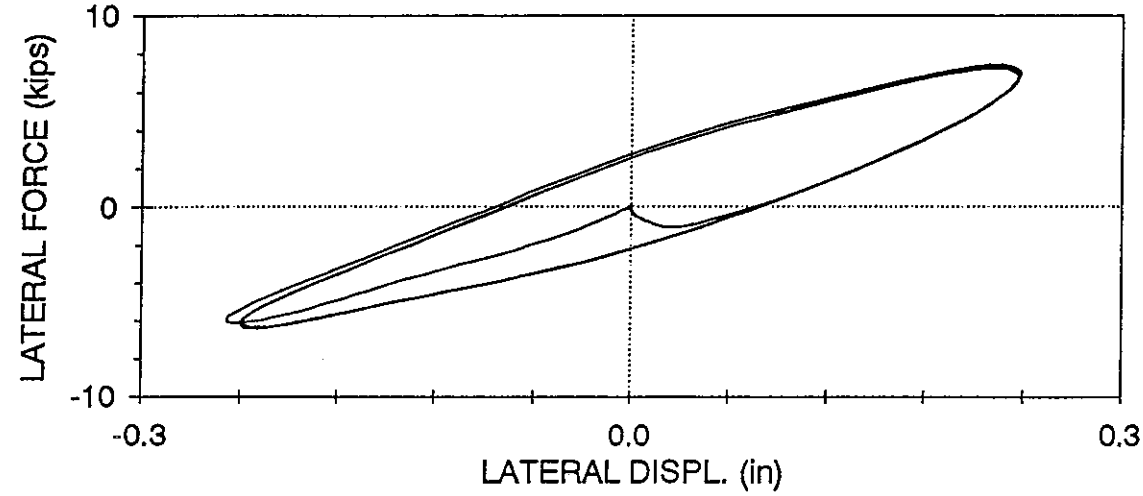

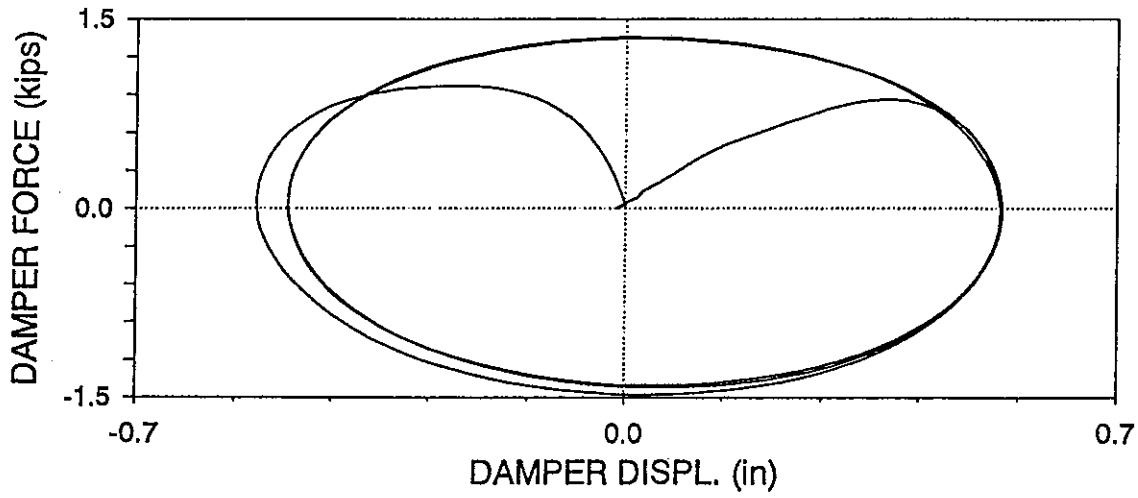

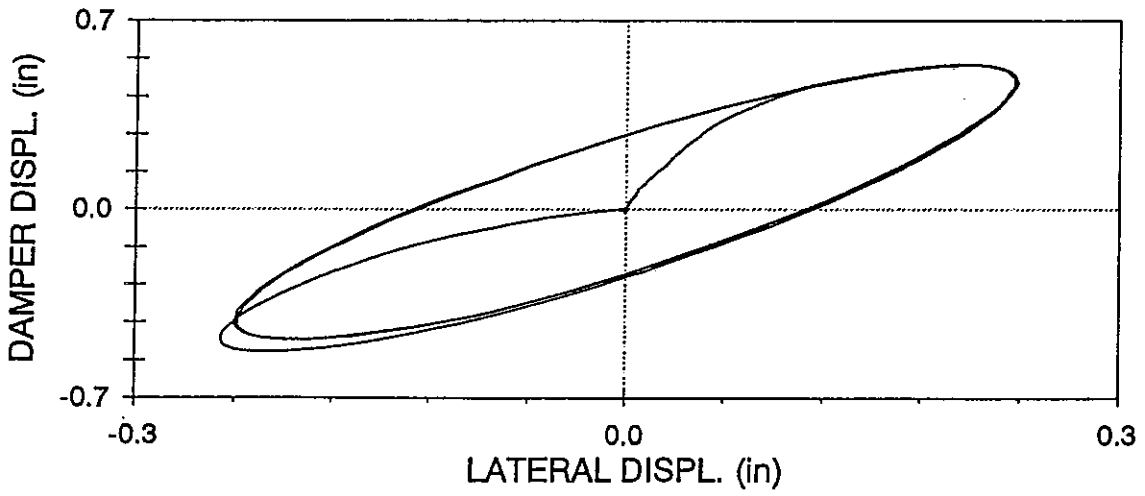

ASTBL10 : SIMPLE CONNECTIONS, BENT PLATE CONFIGURATION

LOWER DAMPER, f=2 Hz, U_o= 0.5 in (05/08/97, 12:11:40)

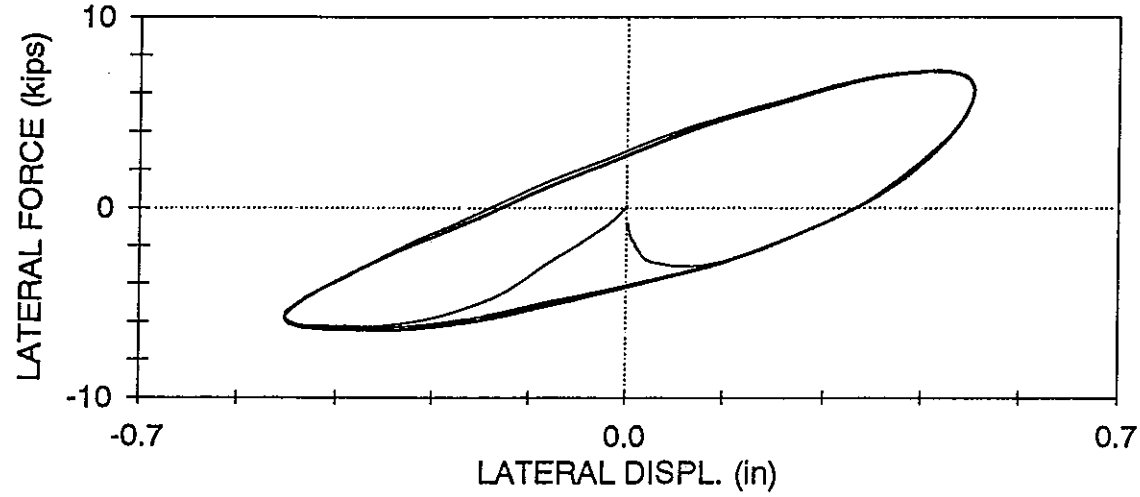

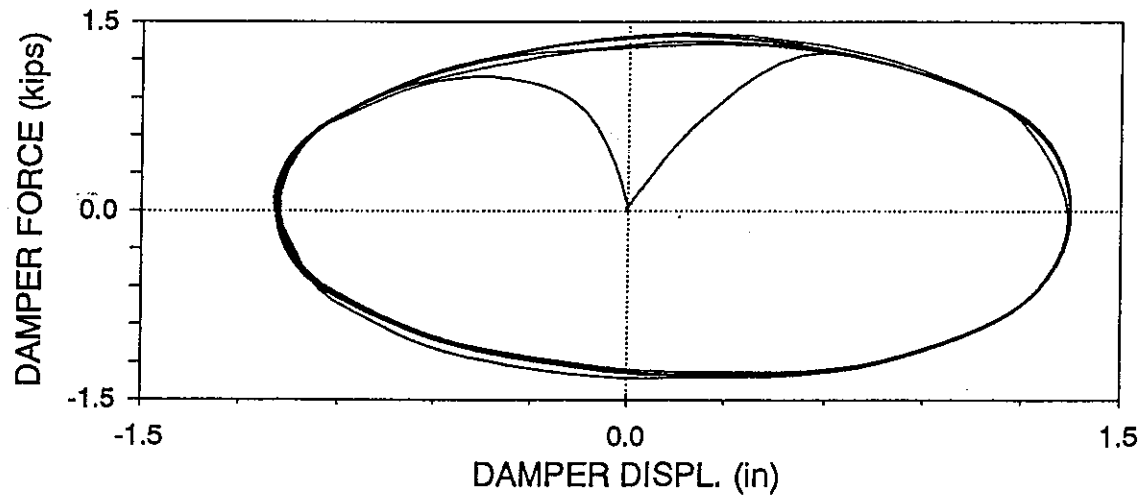

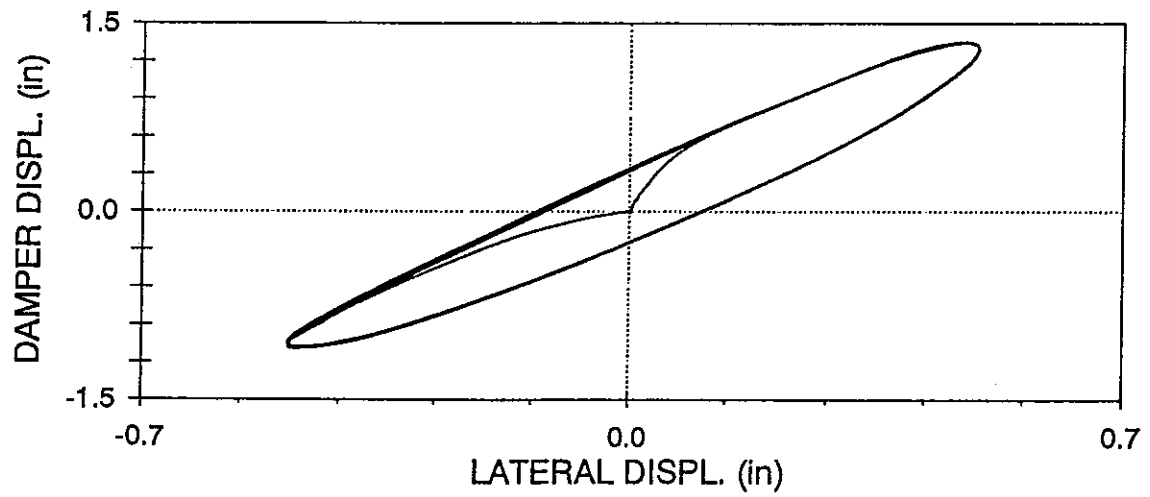

ARTBL05 : RIGID CONNECTIONS, BENT PLATE CONFIGURATION

LOWER DAMPER, f=5.0 Hz, U_o= 0.25 in (05/08/97, 10:50:52)

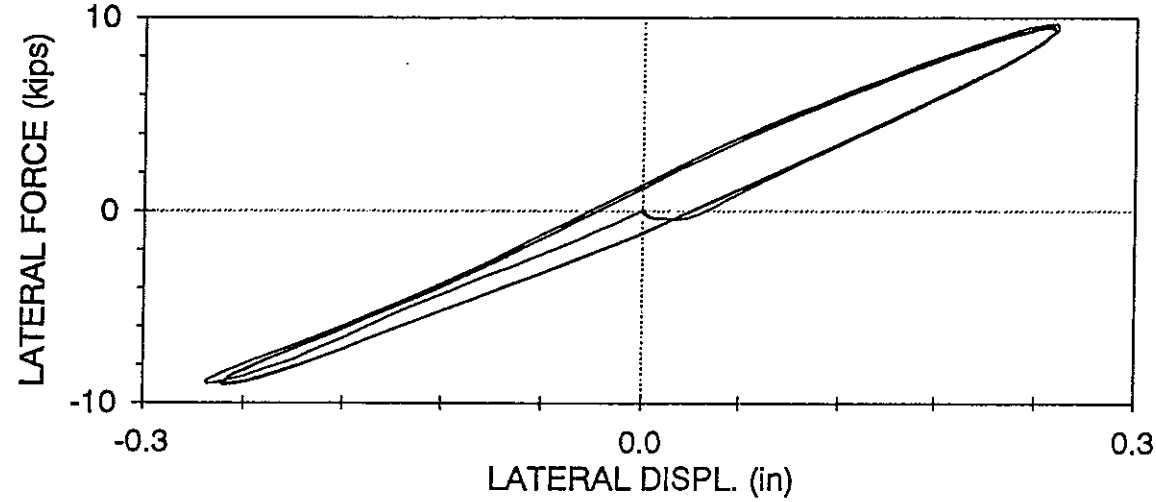

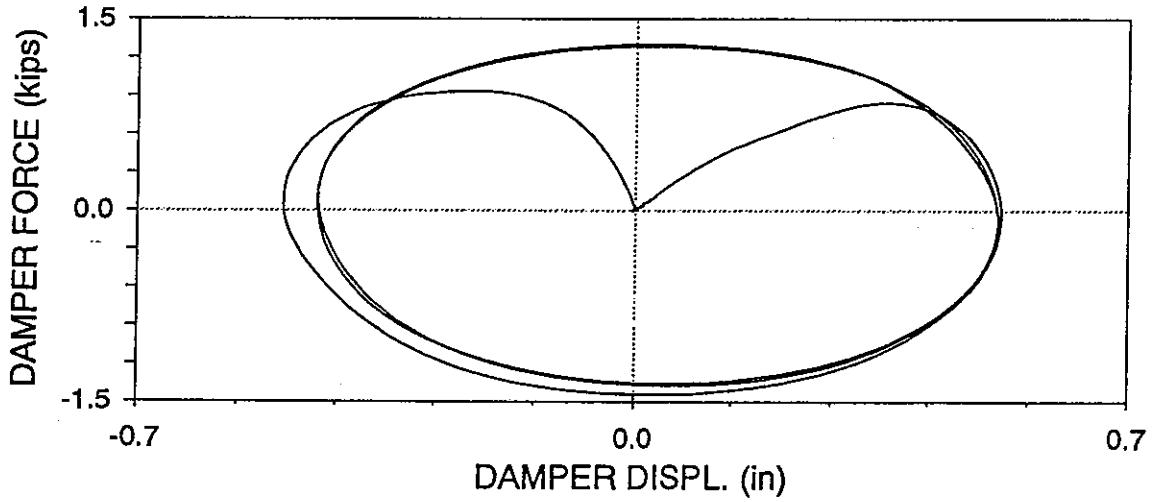

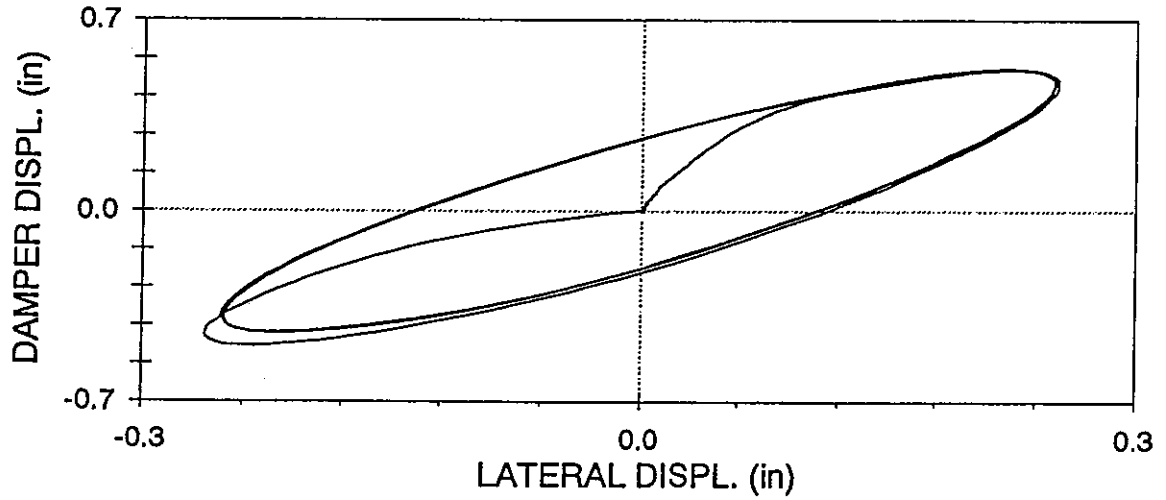

APPENDIX D

RESULTS OF TESTING OF FRAME WITH PINNED CONNECTION DETAIL FOR THE TOGGLE BRACES

(1 in. = 25.4 mm, 1 kip = 4.45 kN).

ASTPL01 : SIMPLE CONNECTIONS, PINNED TOGGLE CONFIGURATION

LOWER DAMPER, f=0.05 Hz, U_o= 0.5 in (05/14/97, 12:32:14)

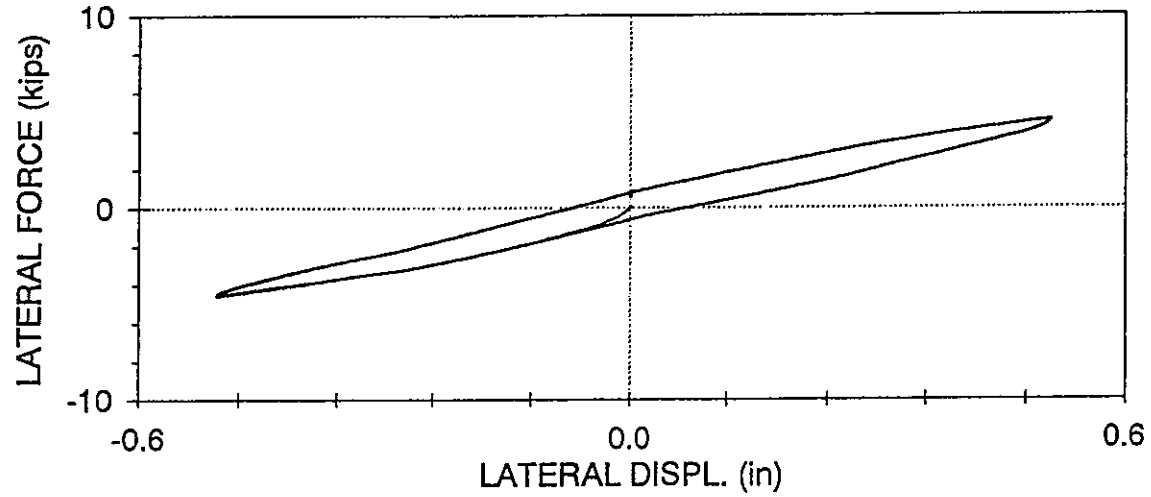

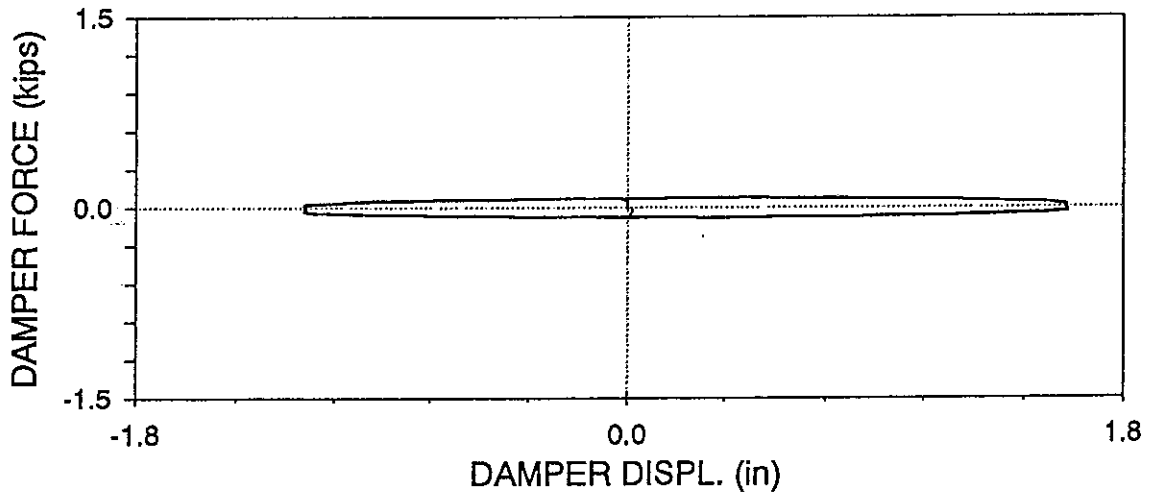

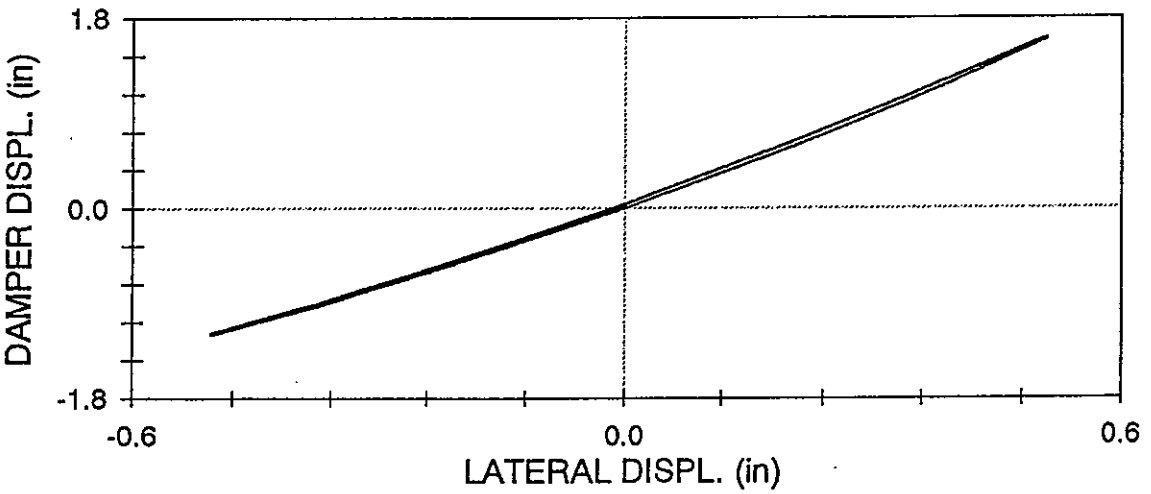

ASTPL02 : SIMPLE CONNECTIONS, PINNED TOGGLE CONFIGURATION

LOWER DAMPER, f=2.0 Hz, U_o= 0.5 in (05/14/97, 12:37:17)

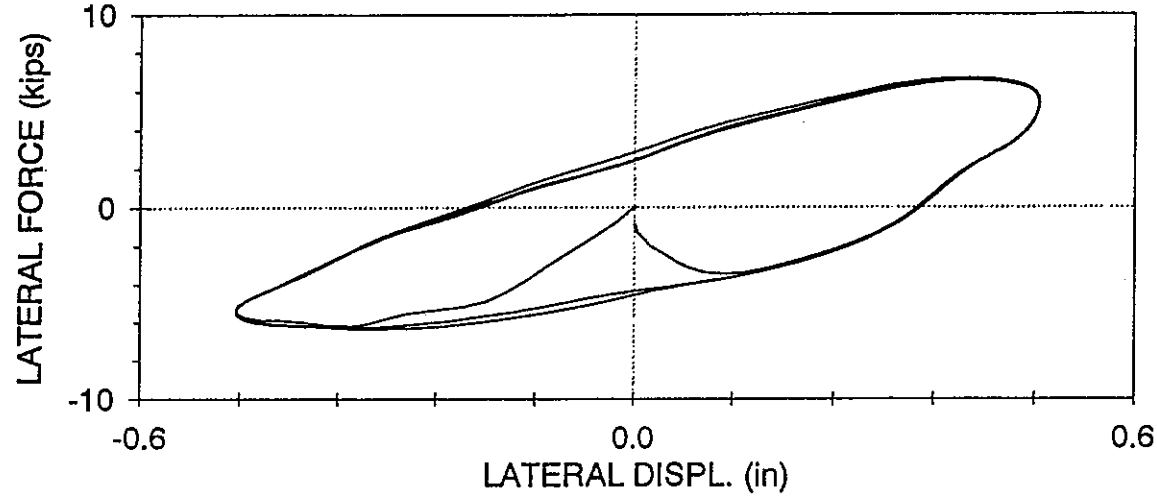

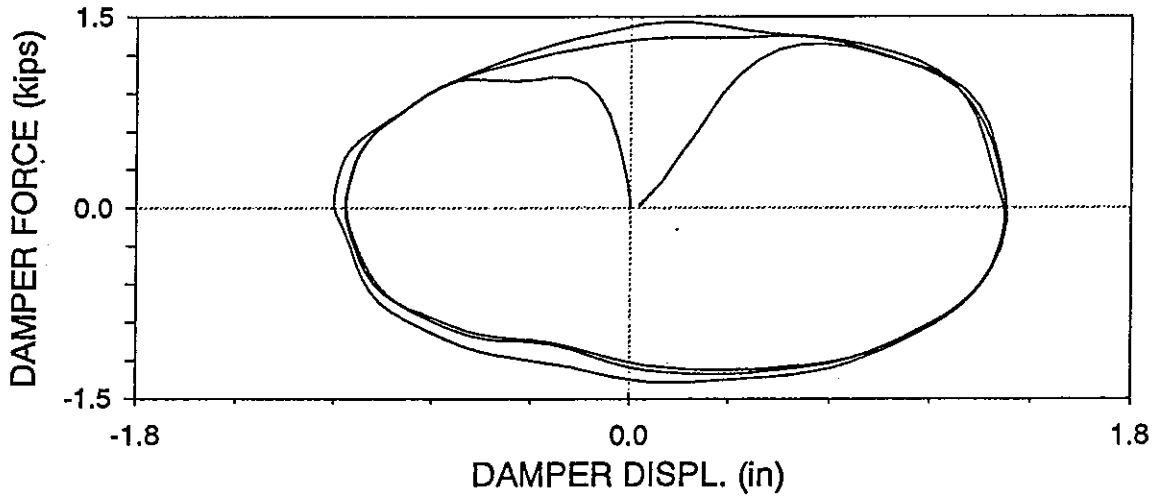

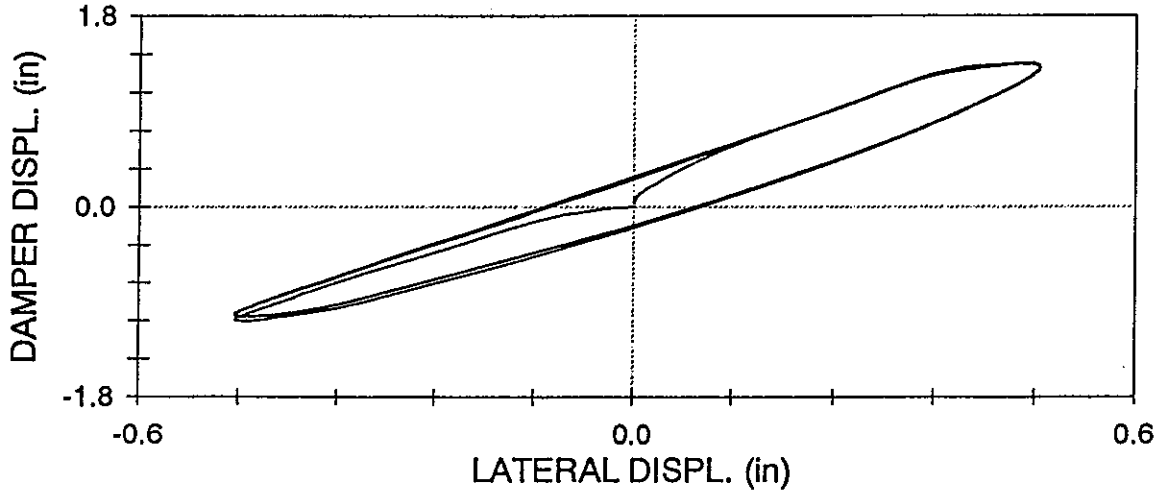

ASTPL03 : SIMPLE CONNECTIONS, PINNED TOGGLE CONFIGURATION

LOWER DAMPER, f=2.0 Hz, U_o= 0.25 in (05/14/97, 12:39:54)

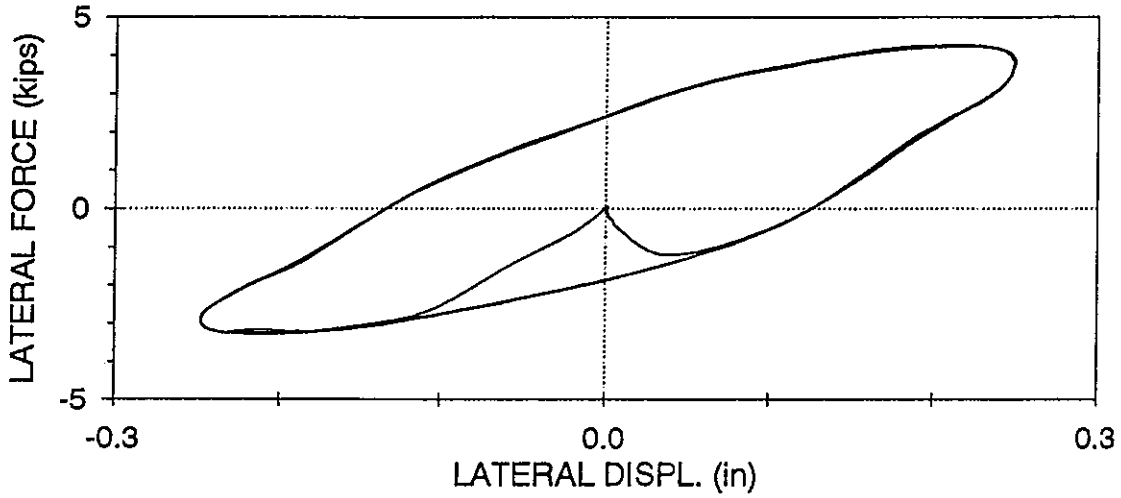

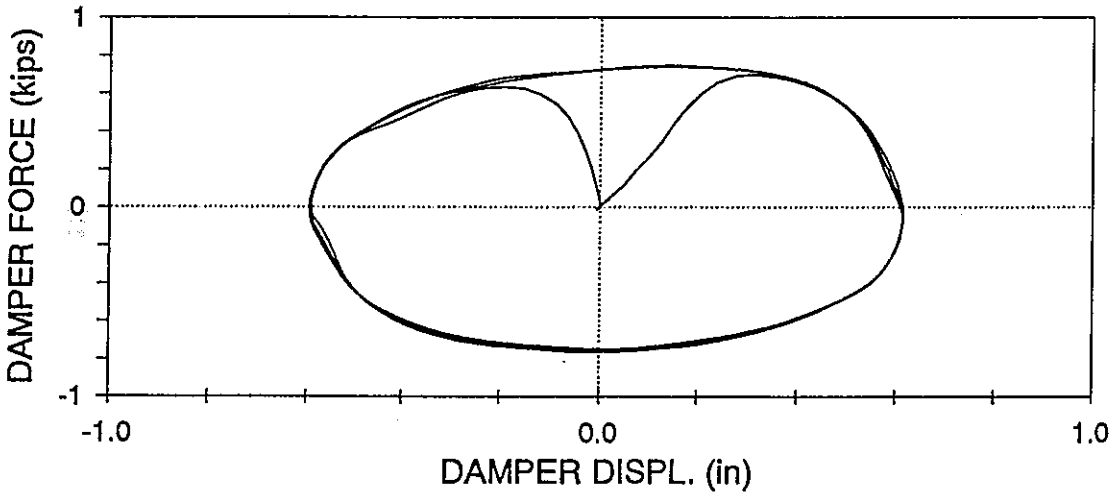

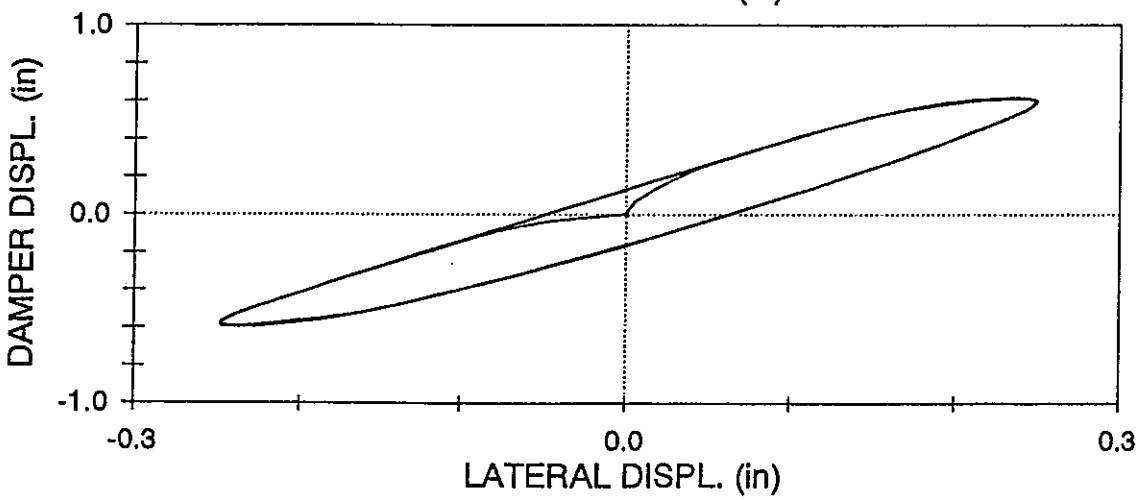

ASTPL04 : SIMPLE CONNECTIONS, PINNED TOGGLE CONFIGURATION

LOWER DAMPER, f=0.05 Hz, U_o= 0.25 in (05/14/97, 12:43:30)

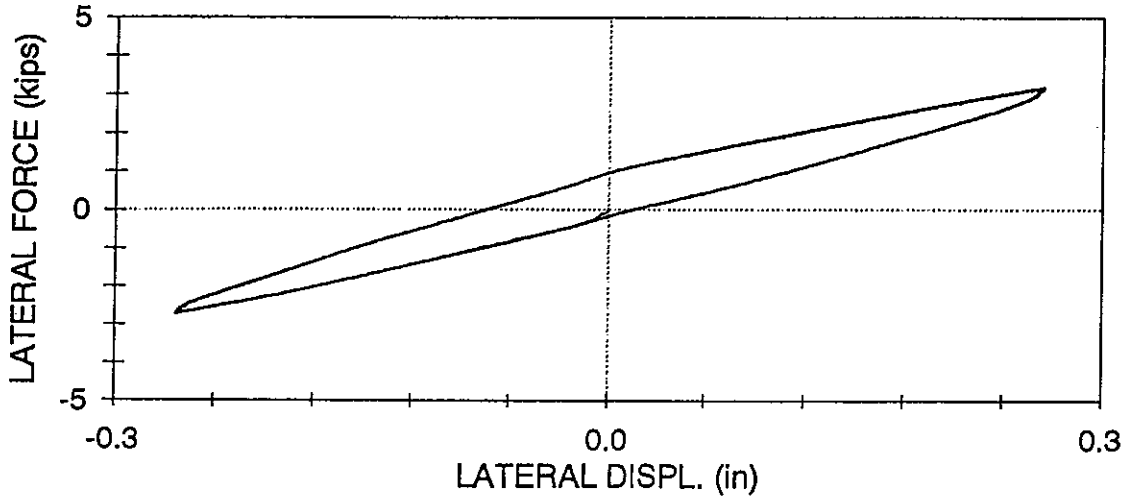

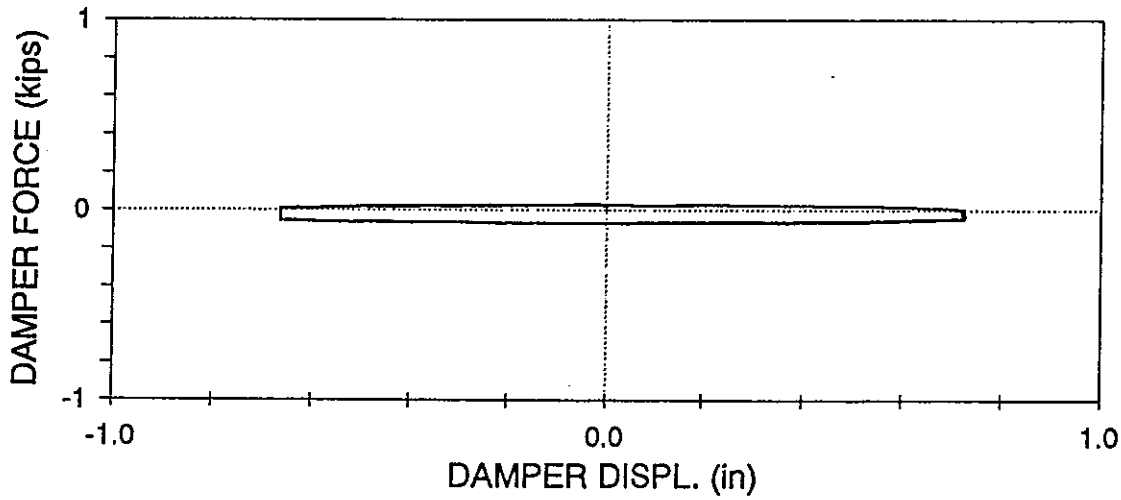

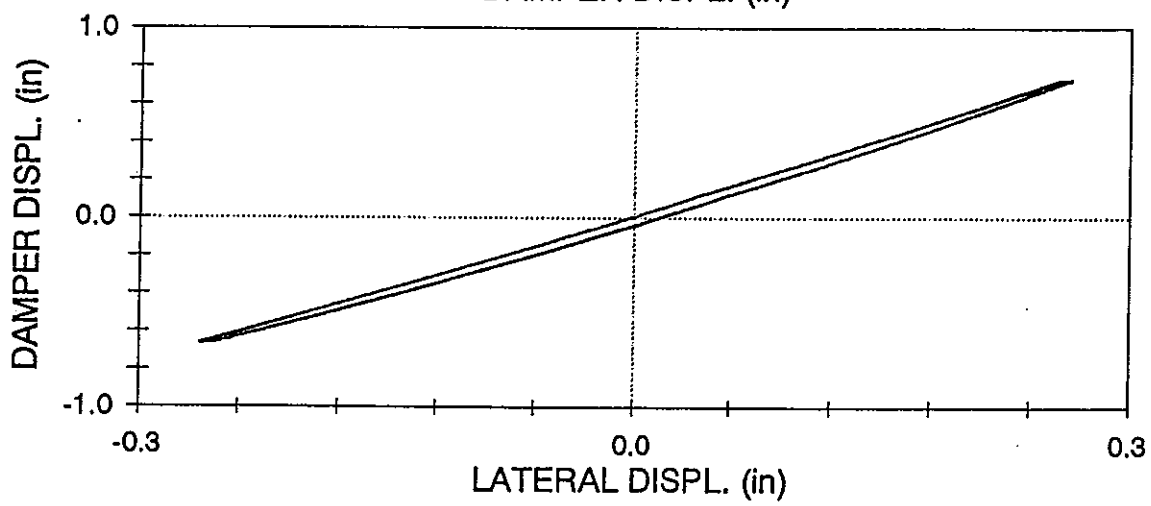

ASTPU01 : SIMPLE CONNECTIONS, PINNED TOGGLE

UPPER DAMPER, f=0.05 Hz, U_o= 0.25 in (05/16/97, 14:56:46)

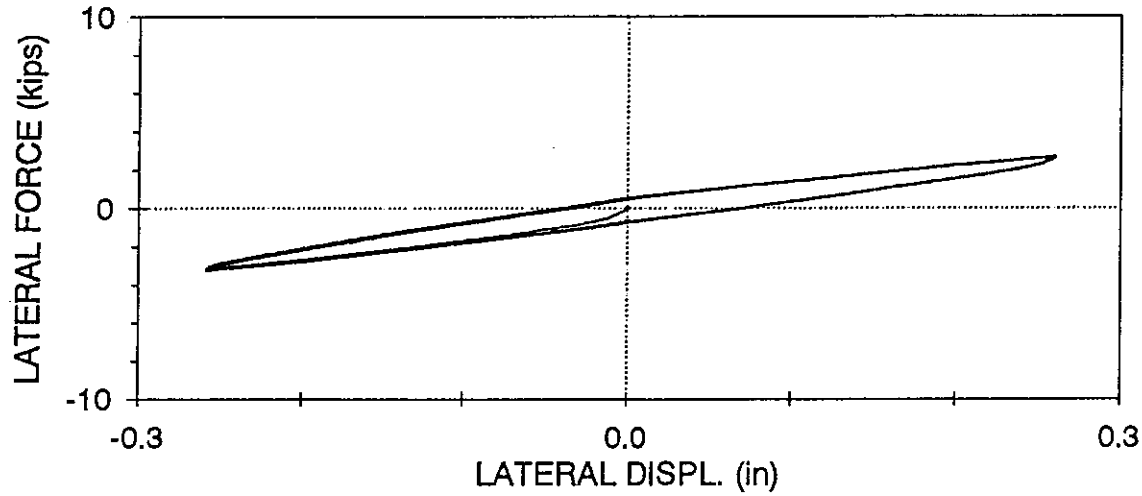

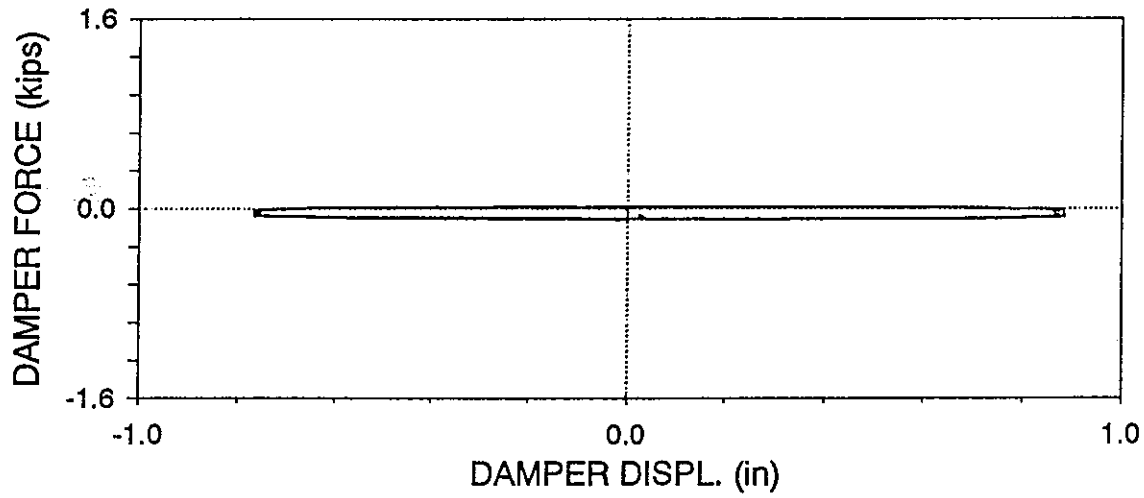

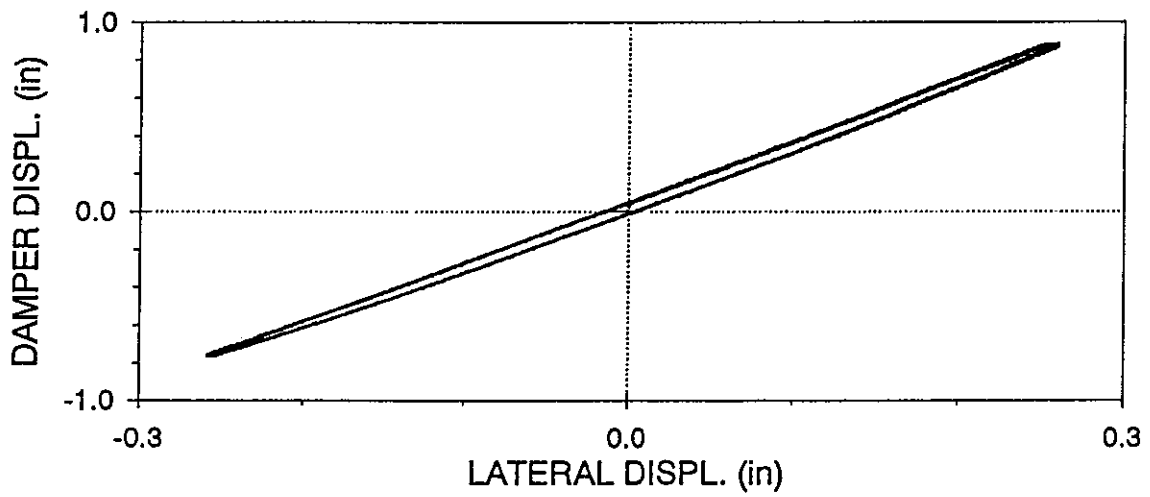

ASTPU02 : SIMPLE CONNECTIONS, PINNED TOGGLE

UPPER DAMPER, f=0.05 Hz, U_o= 0.5 in (05/16/97, 14:59:09)

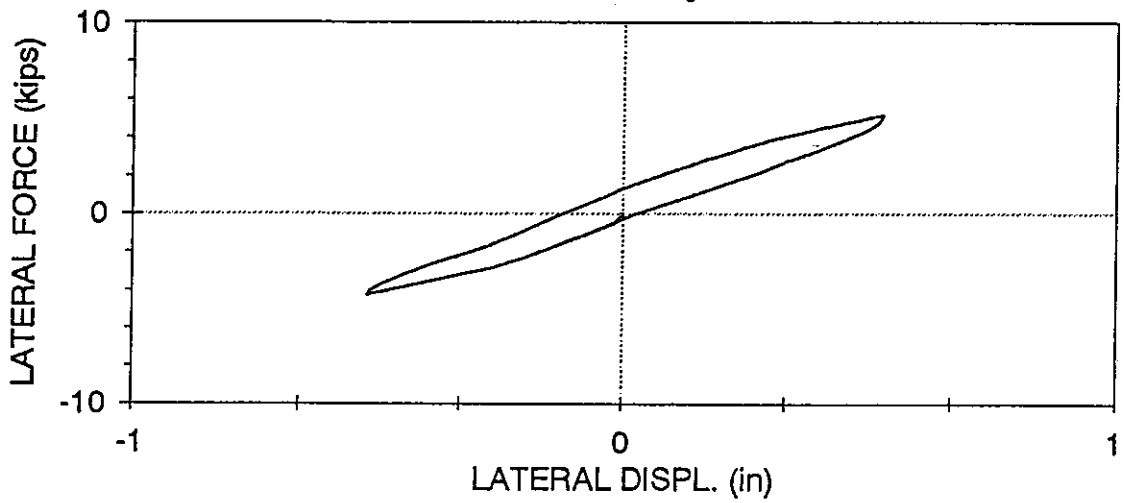

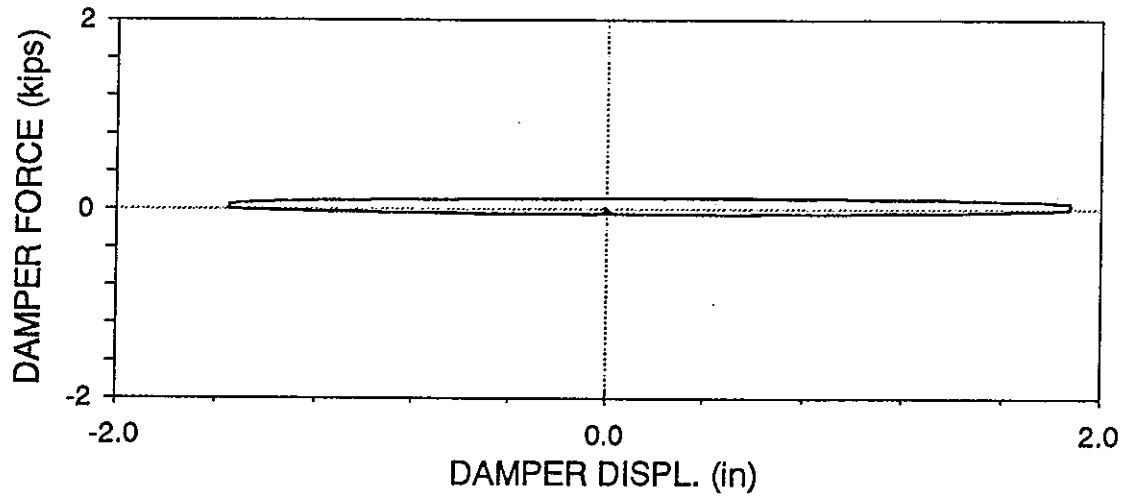

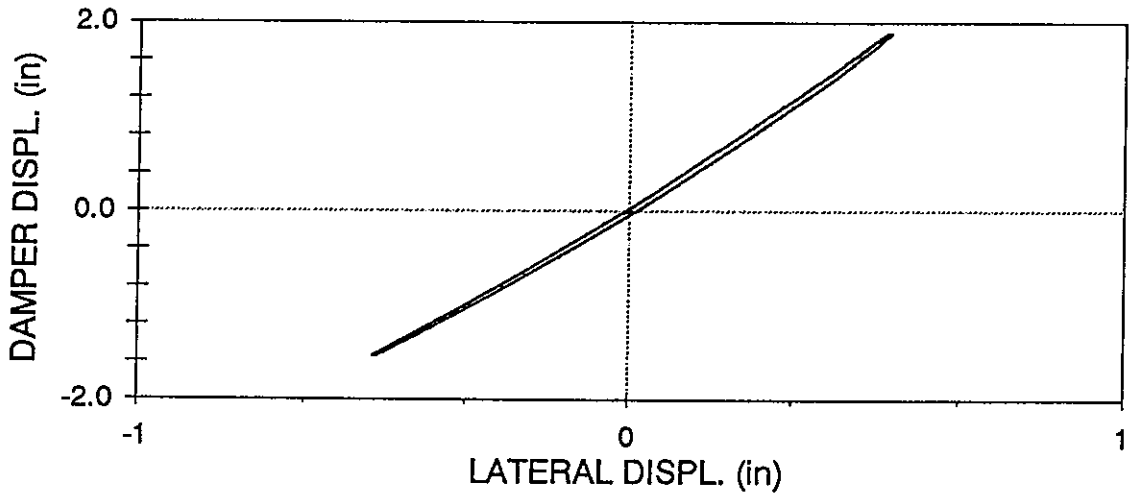

ASTPU03 : SIMPLE CONNECTIONS, PINNED TOGGLE

UPPER DAMPER, f=2.0 Hz, U_o= 0.25 in (05/16/97, 15:02:32)

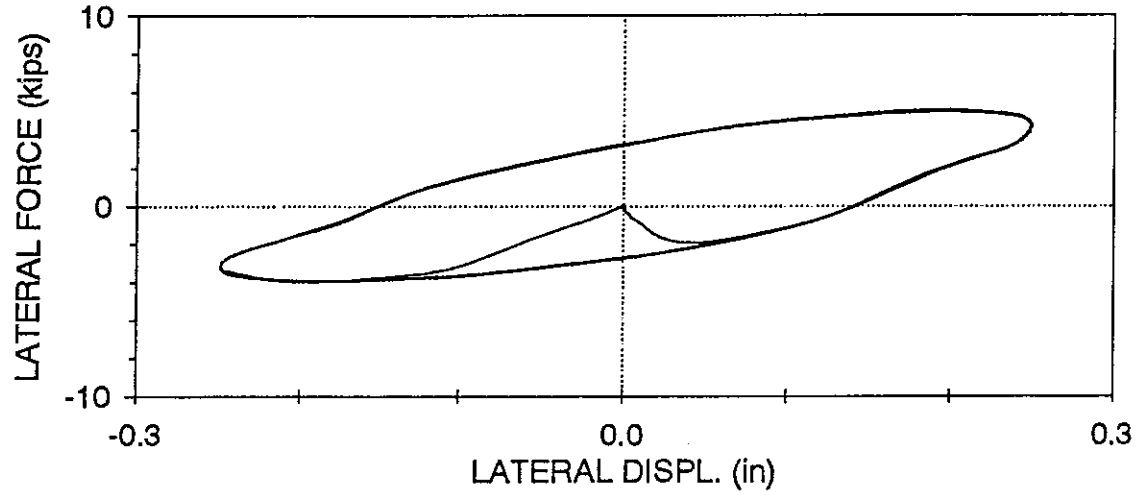

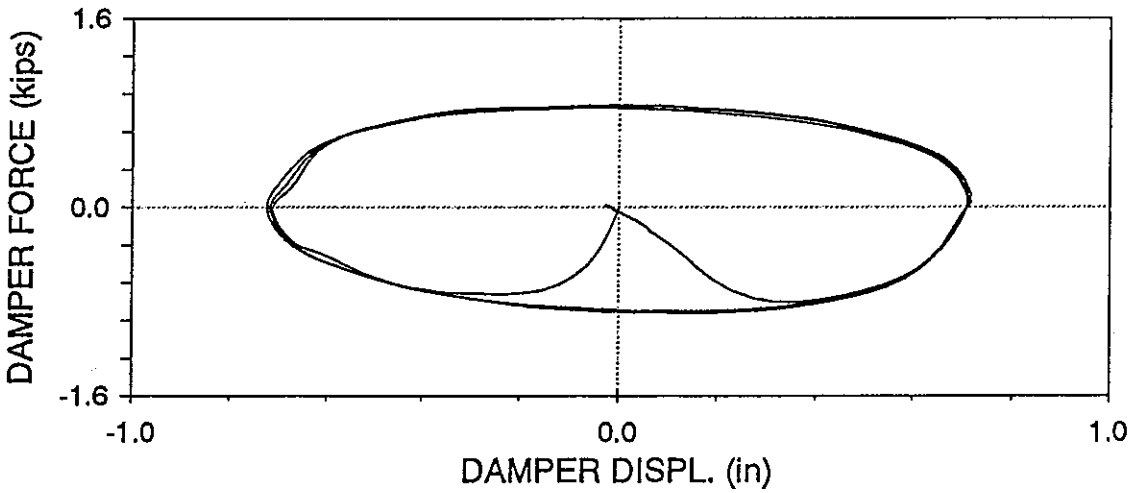

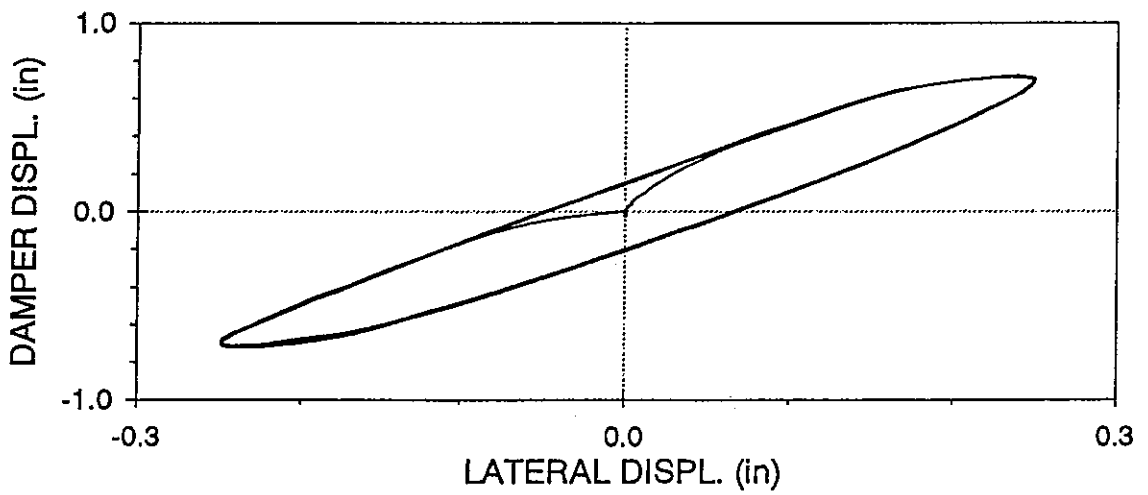

ASTPU04 : SIMPLE CONNECTIONS, PINNED TOGGLE

UPPER DAMPER, f=2.0 Hz, U_o= 0.5 in (05/16/97, 15:03:46)

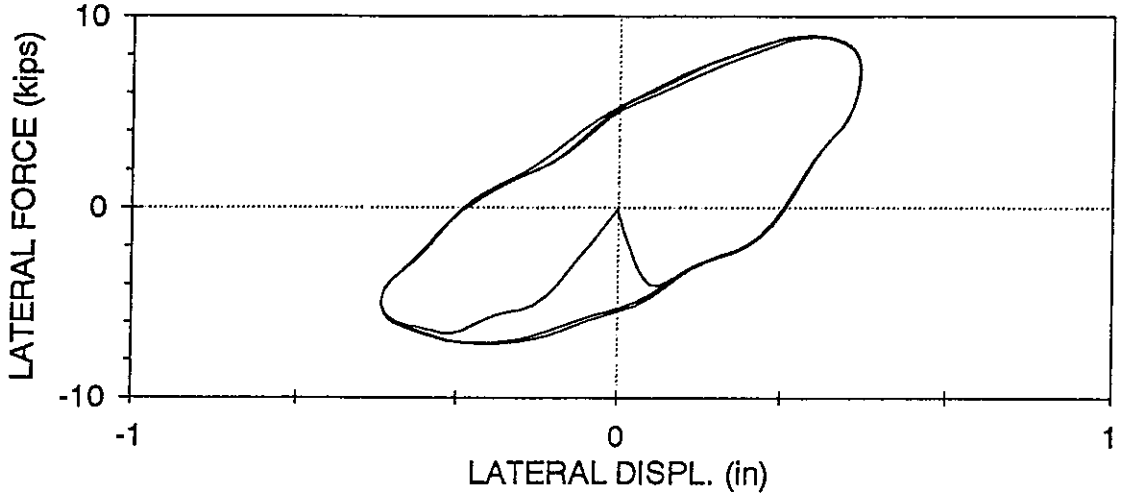

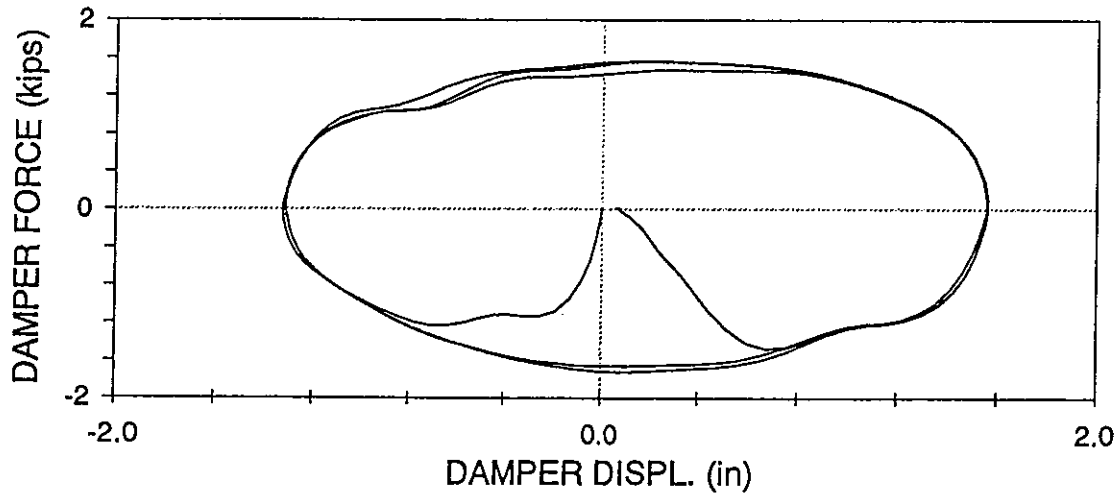

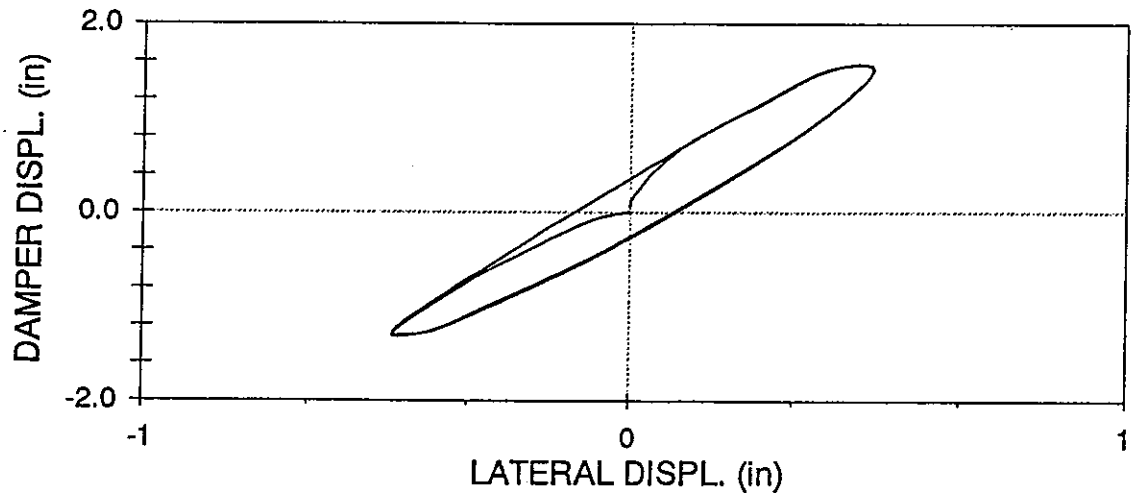

ASTPU05 : SIMPLE CONNECTIONS, PINNED TOGGLE

UPPER DAMPER, f=3.0 Hz, U_o= 0.3 in (05/16/97, 15:05:22)

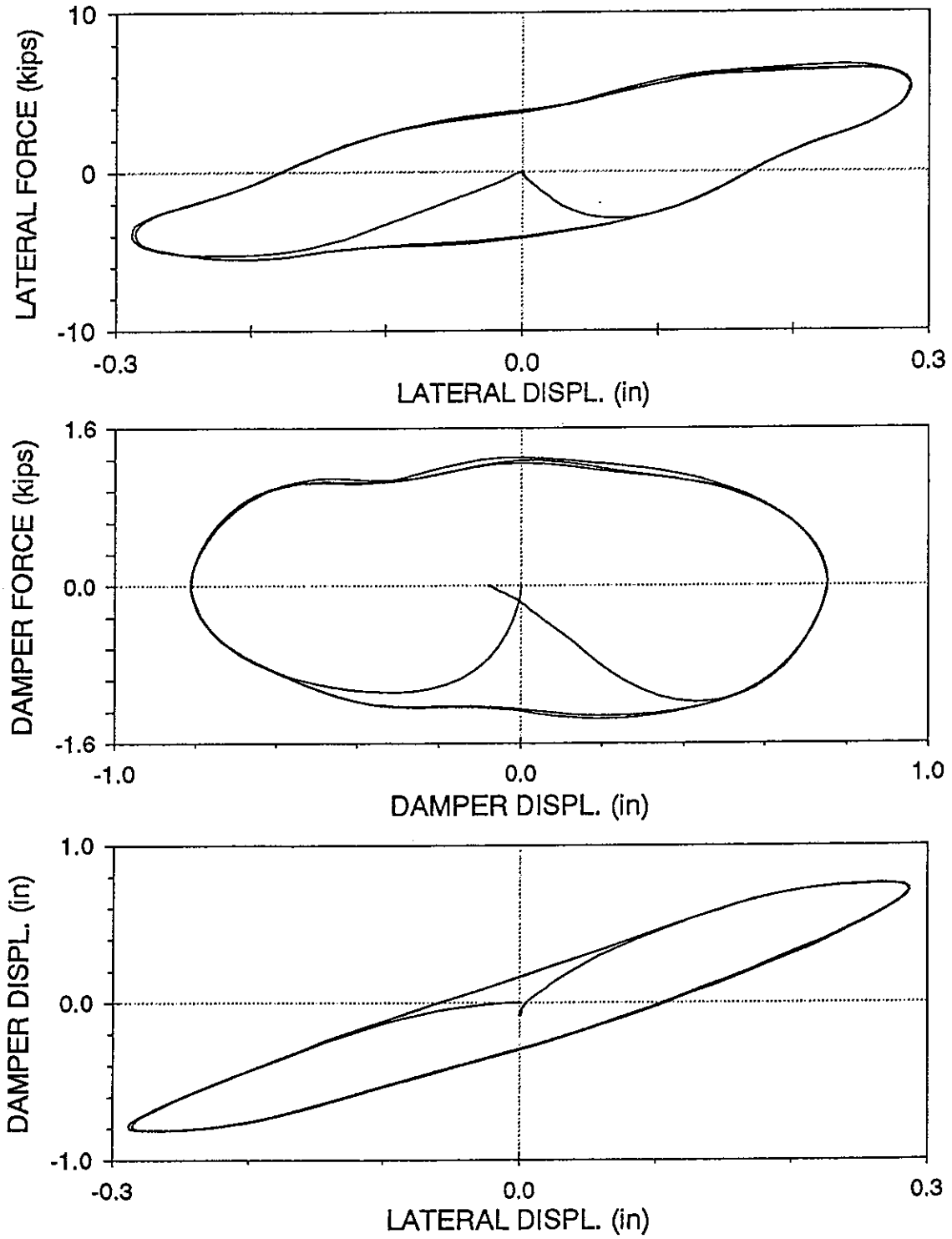

ARSTPL01 : LEFT RIGID, RIGHT SIMPLE CONNECTION, PINNED TOGGLE

LOWER DAMPER, f=0.05 Hz, U_o= 0.25 in (05/15/97, 14:54:13)

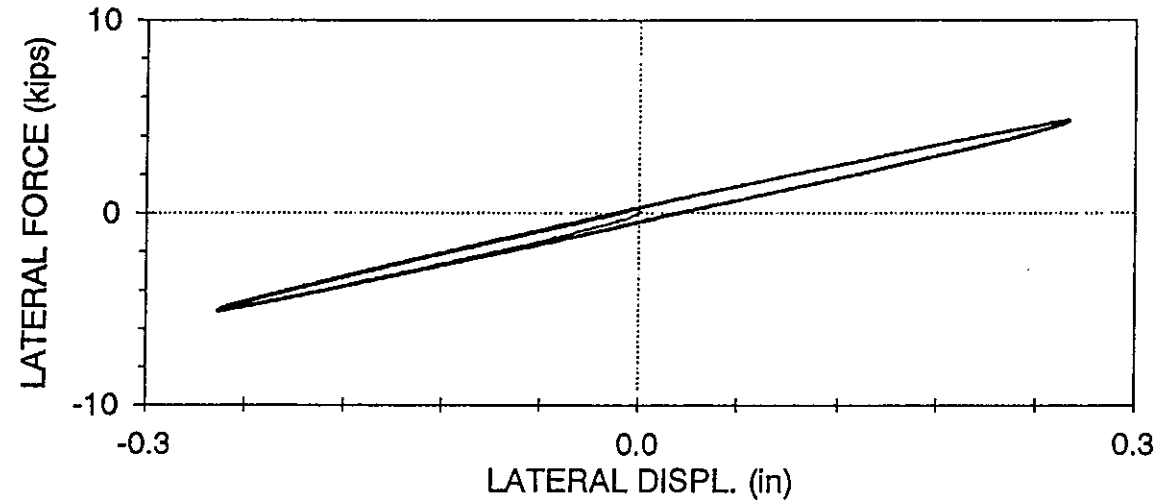

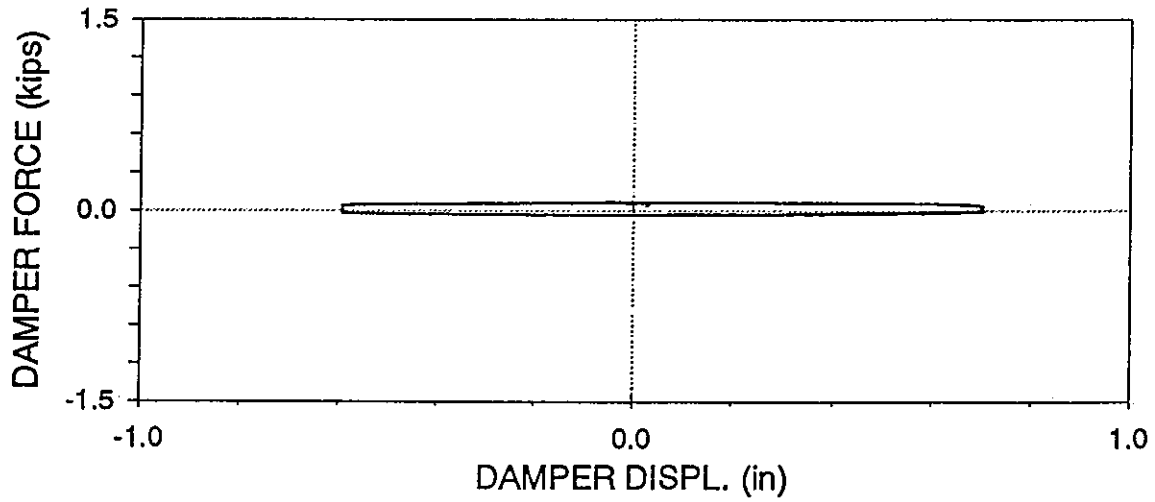

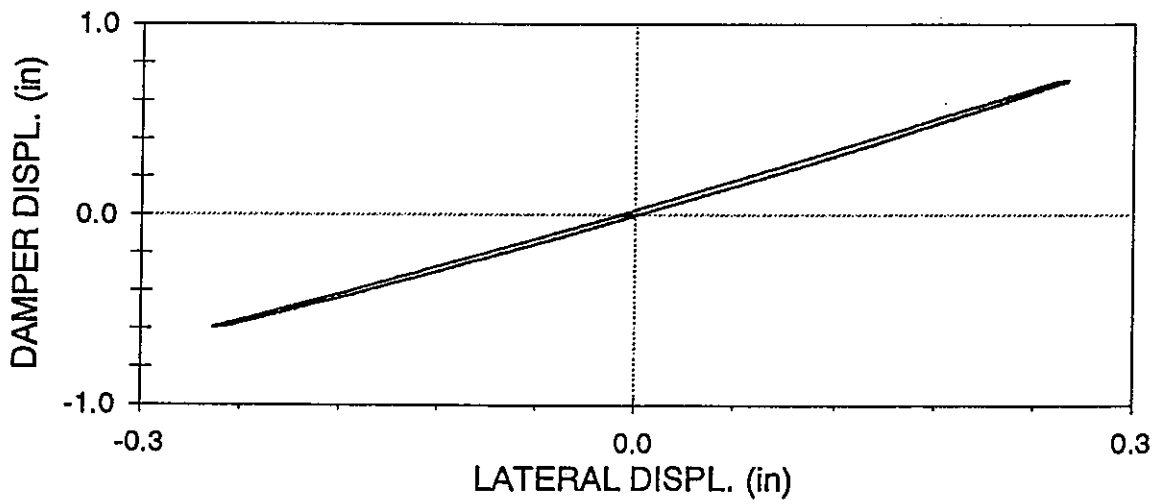

ARSTPL02 : LEFT RIGID, RIGHT SIMPLE CONNECTION, PINNED TOGGLE

LOWER DAMPER, f=2.0 Hz, U_o= 0.25 in (05/15/97, 15:00:08)

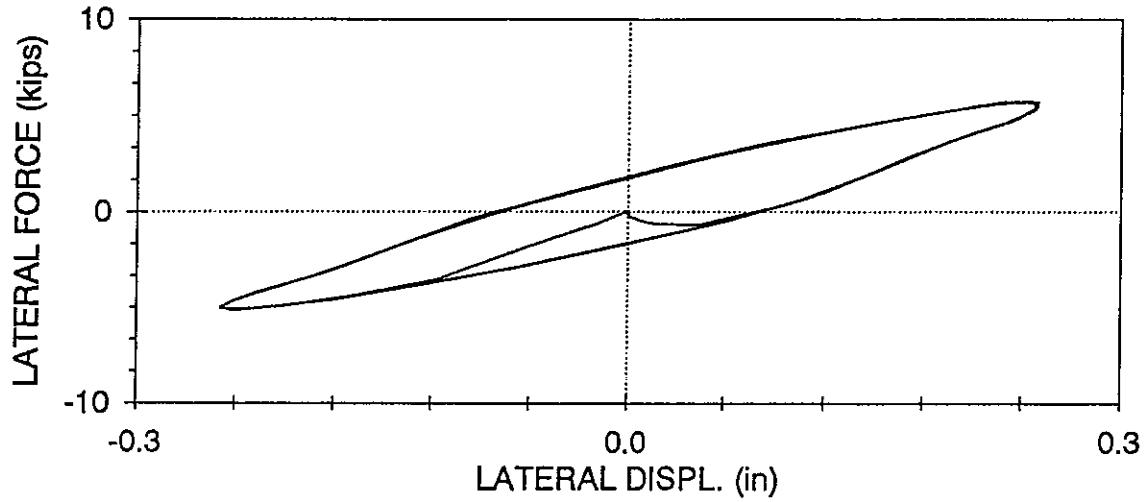

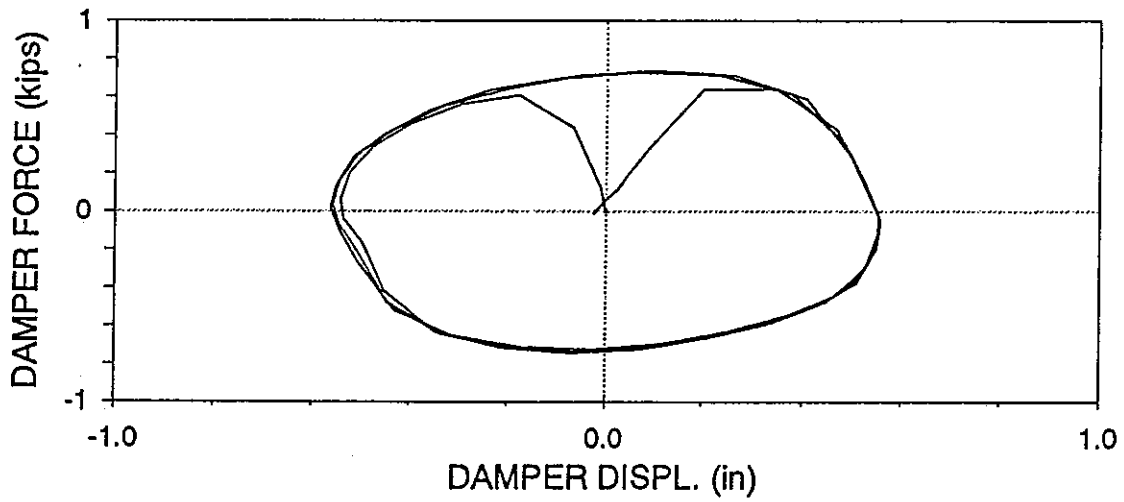

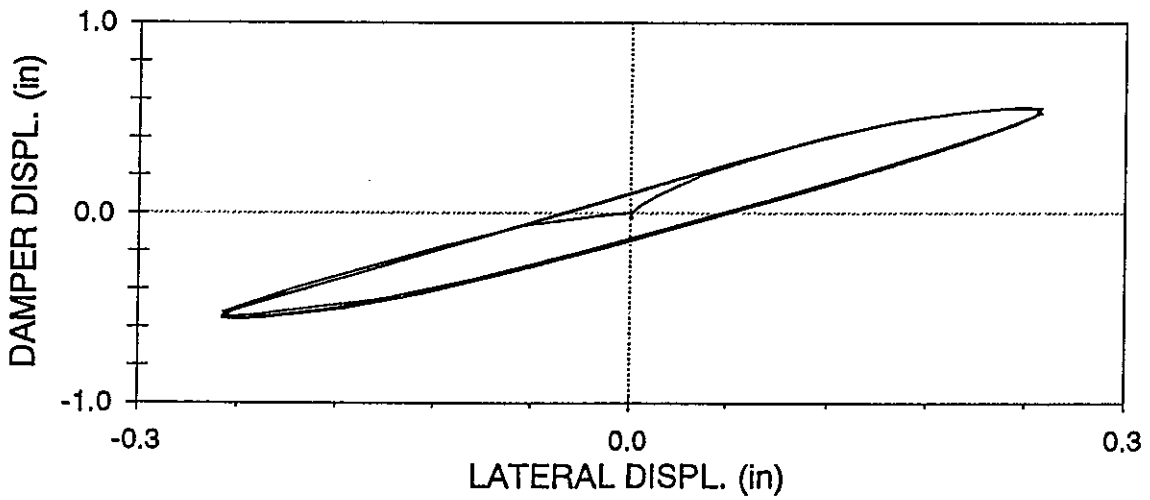

ARSTPL05 : LEFT RIGID, RIGHT SIMPLE CONNECTION, PINNED TOGGLE

LOWER DAMPER, f=4.0 Hz, U_o= 0.25 in (05/15/97, 15:15:15)

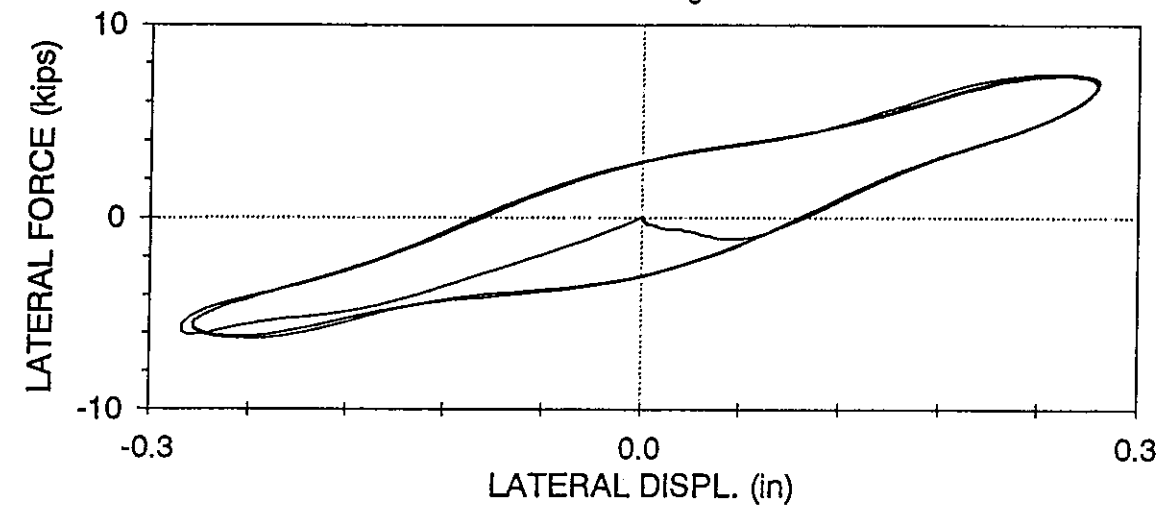

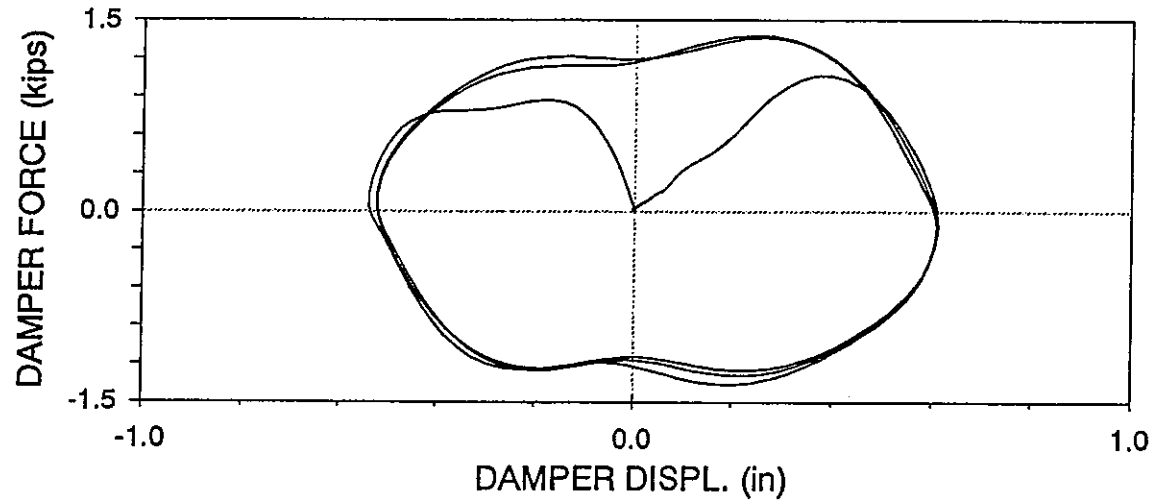

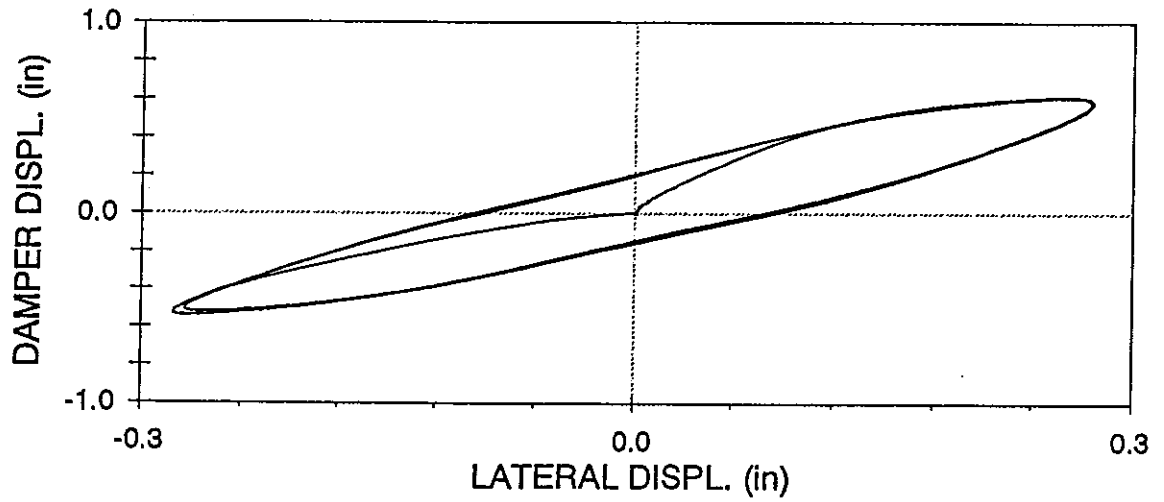

ARSTPU01 : LEFT RIGID, RIGHT SIMPLE, PINNED TOGGLE

UPPER DAMPER, f=0.05 Hz, U_o= 0.25 in (05/16/97, 10:55:03)

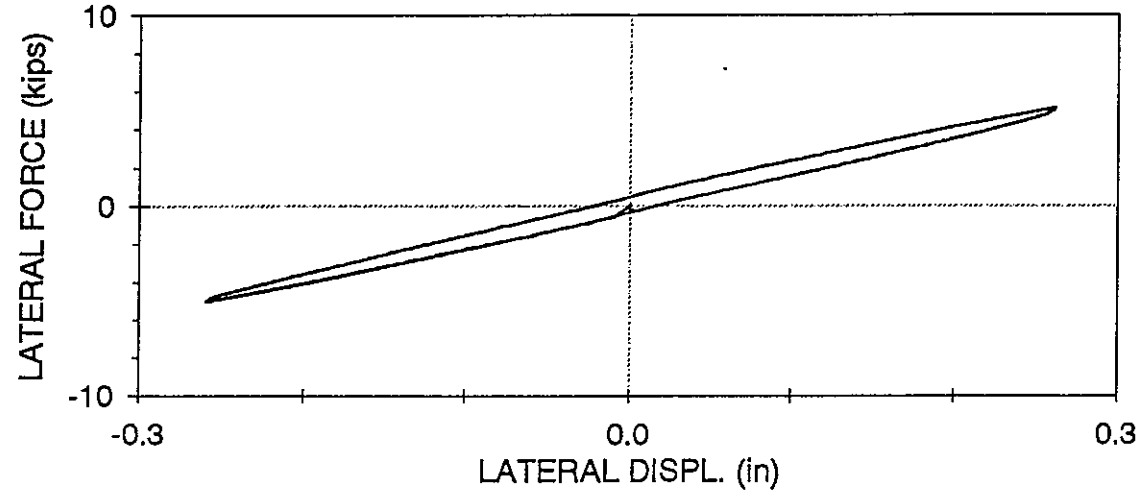

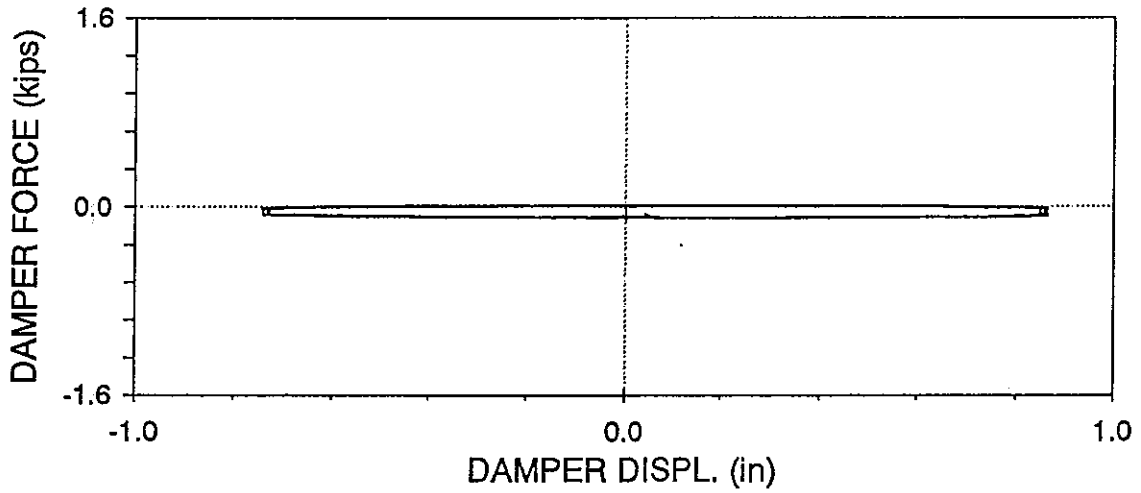

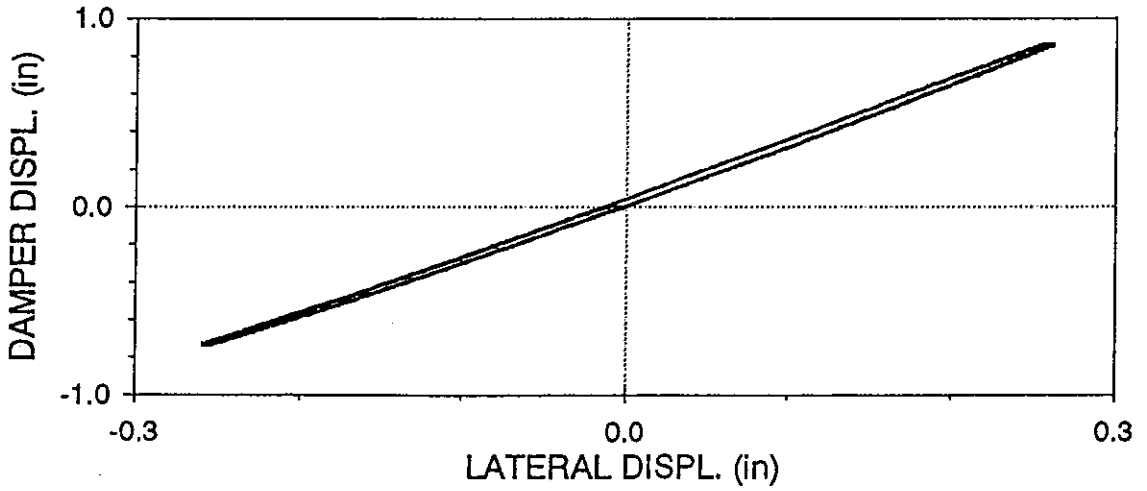

ARSTPU02 : LEFT RIGID, RIGHT SIMPLE, PINNED TOGGLE

UPPER DAMPER, f=2.0 Hz, U_o= 0.25 in (05/16/97, 10:55:03)

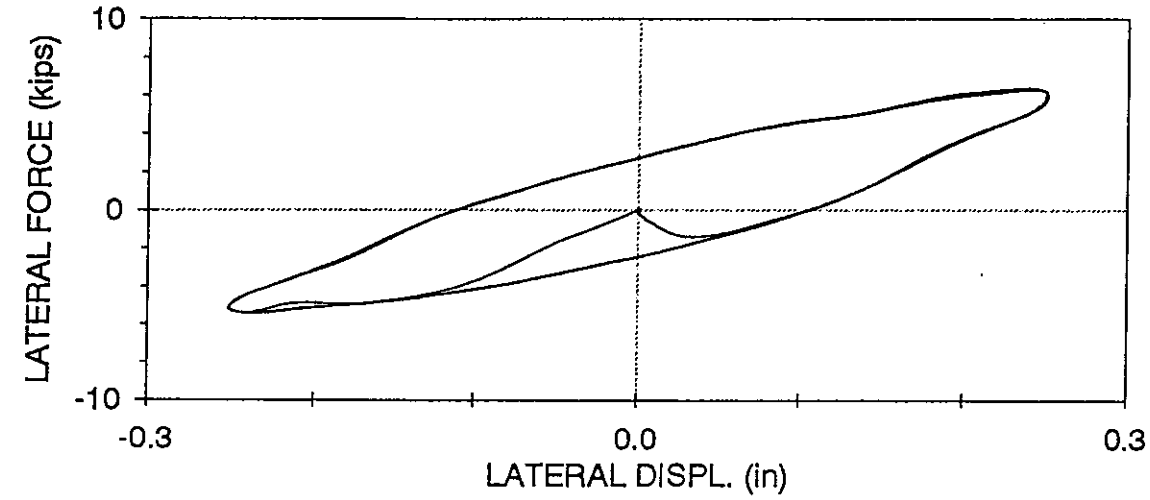

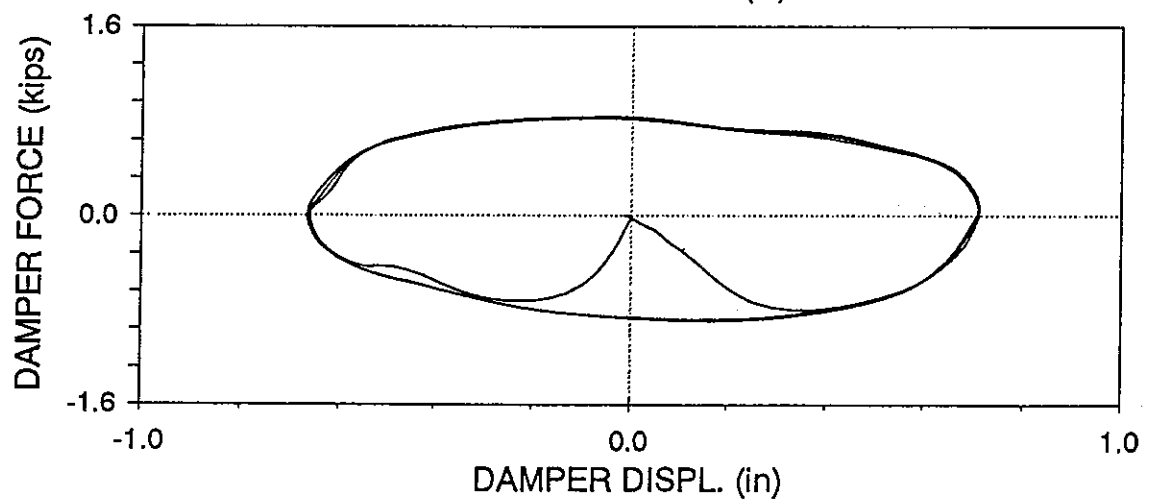

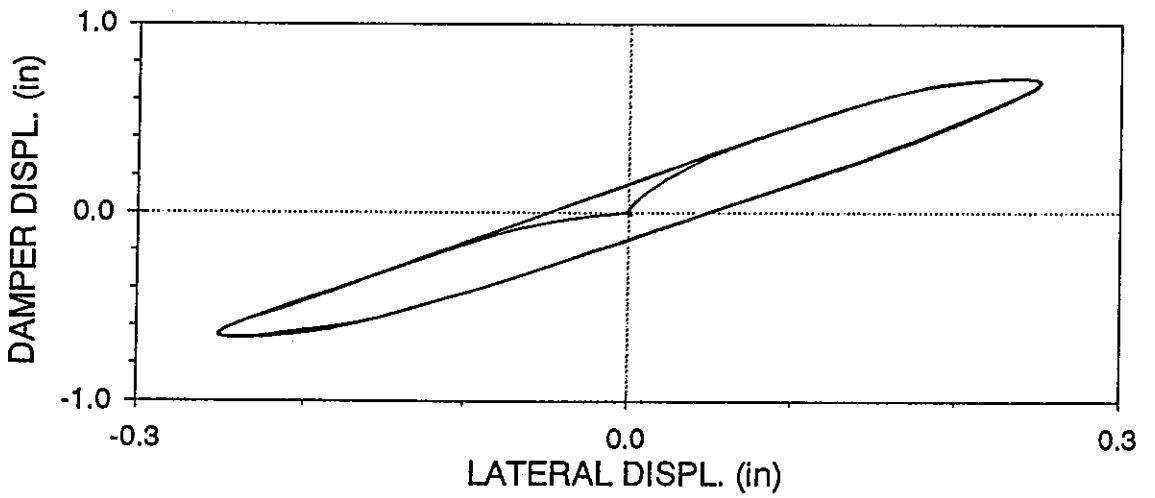

ARSTPU03 : LEFT RIGID, RIGHT SIMPLE, PINNED TOGGLE

UPPER DAMPER, f=3.0 Hz, U_o= 0.25 in (05/16/97, 11:00:25)

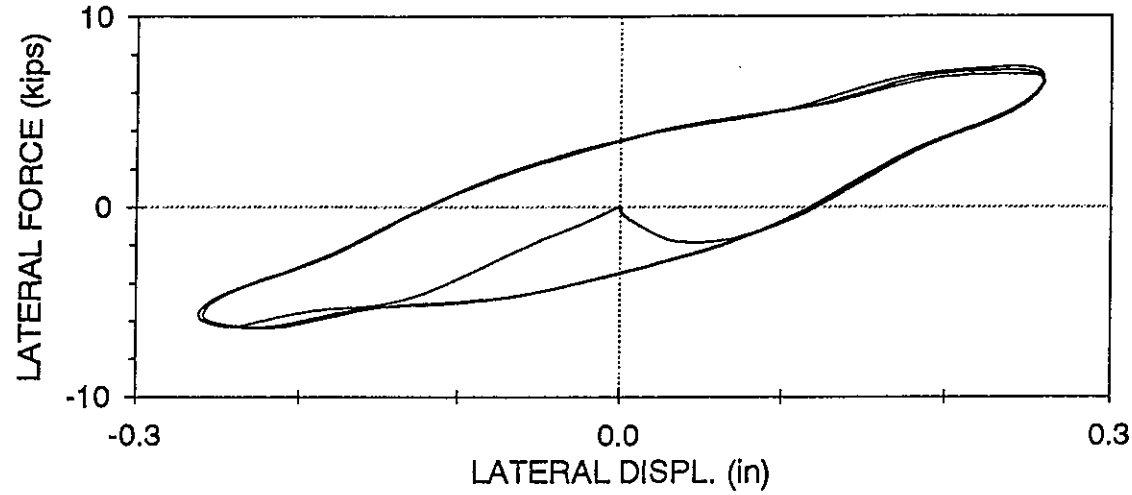

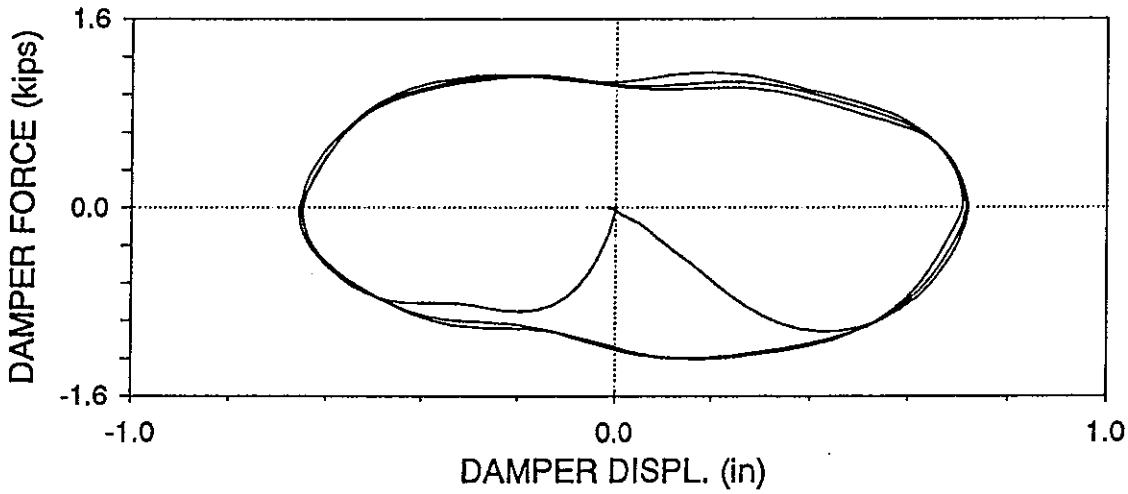

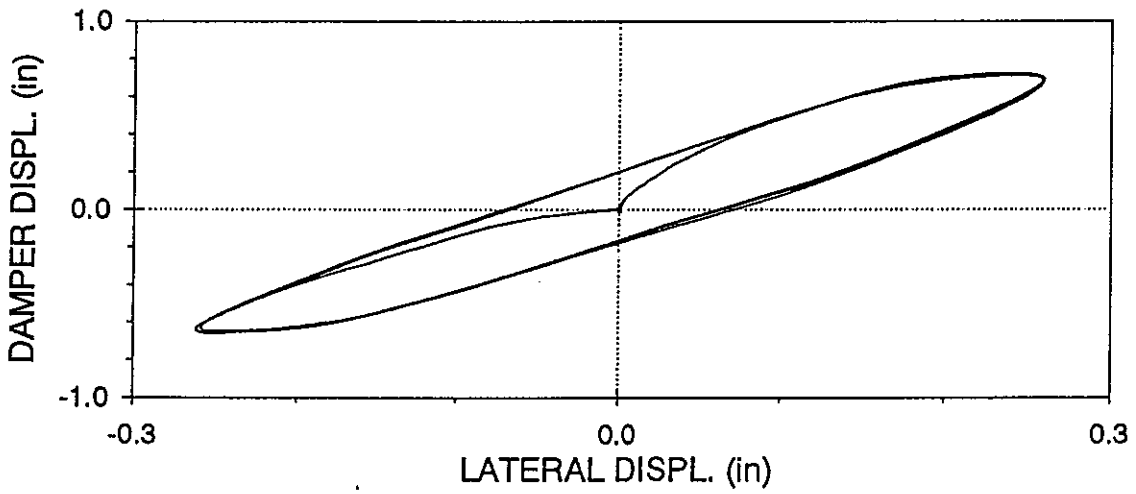

ARSTPU04 : LEFT RIGID, RIGHT SIMPLE, PINNED TOGGLE

UPPER DAMPER, f=4.0 Hz, U_o= 0.25 in (05/16/97, 11:02:29)

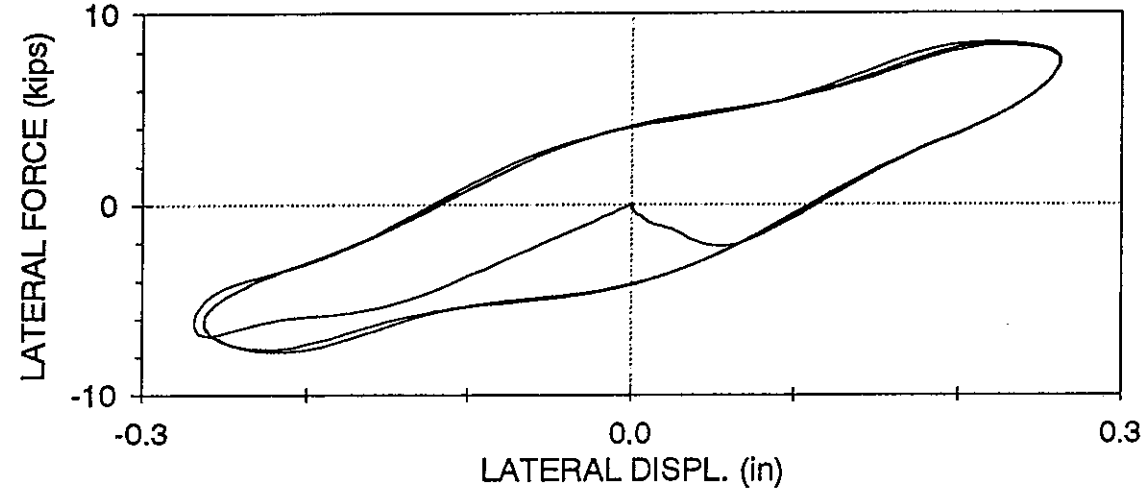

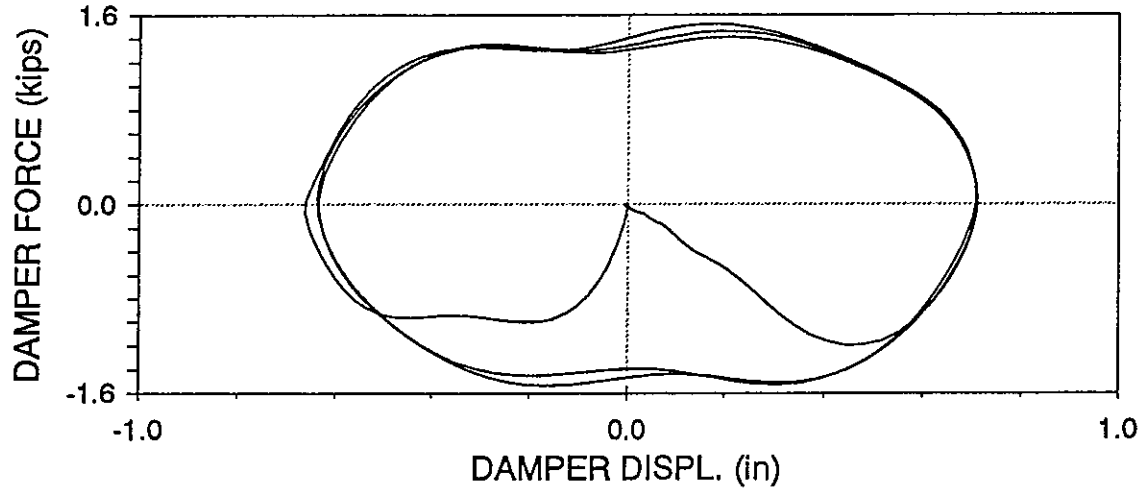

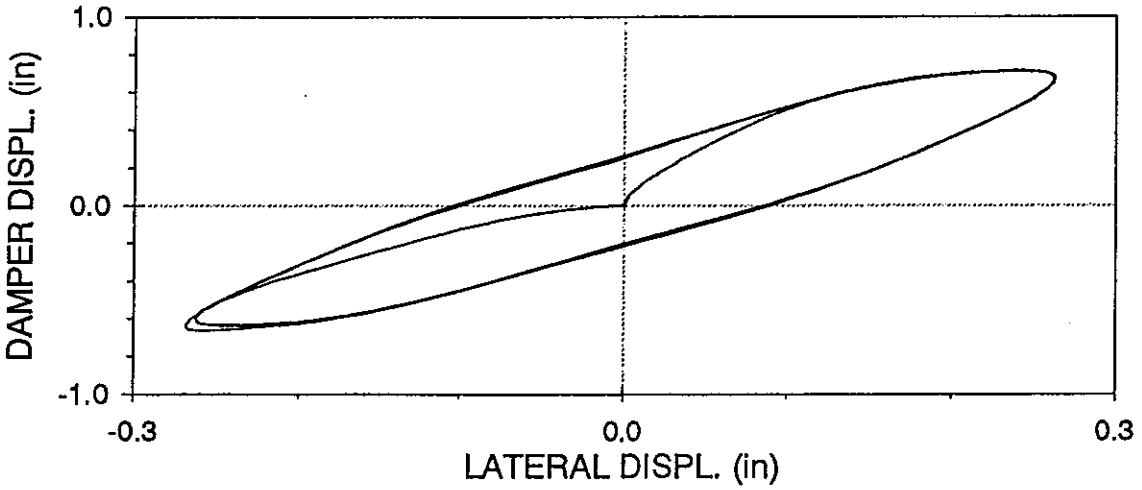

ARSTPU05 : LEFT RIGID, RIGHT SIMPLE, PINNED TOGGLE

UPPER DAMPER, f=4.0 Hz, U_o= 0.25 in (05/16/97, 11:05:07)

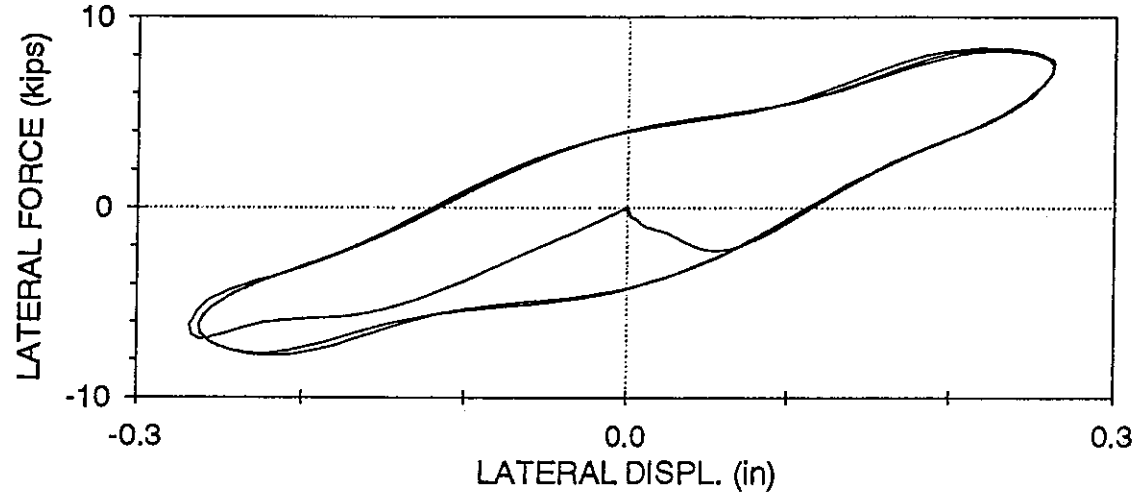

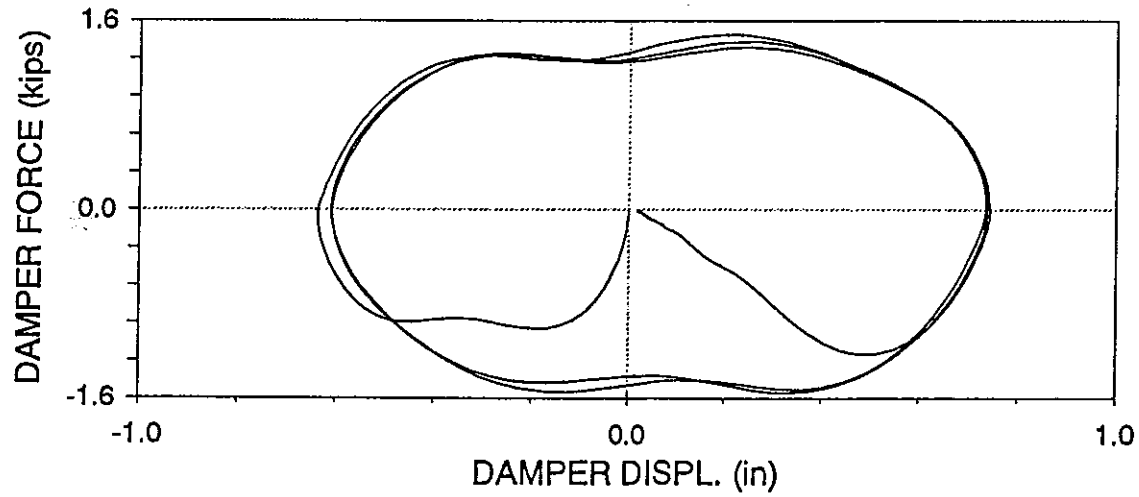

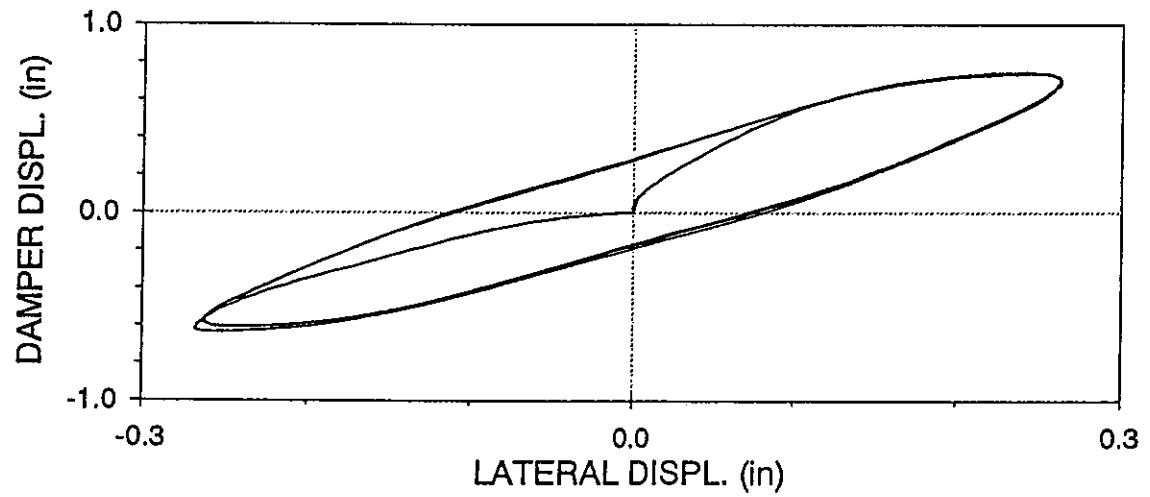

ARTPL01 : RIGID CONNECTIONS, PINNED TOGGLE CONFIGURATION

LOWER DAMPER, f=0.05 Hz, U_o= 0.25 in (05/14/97, 14:26:34)

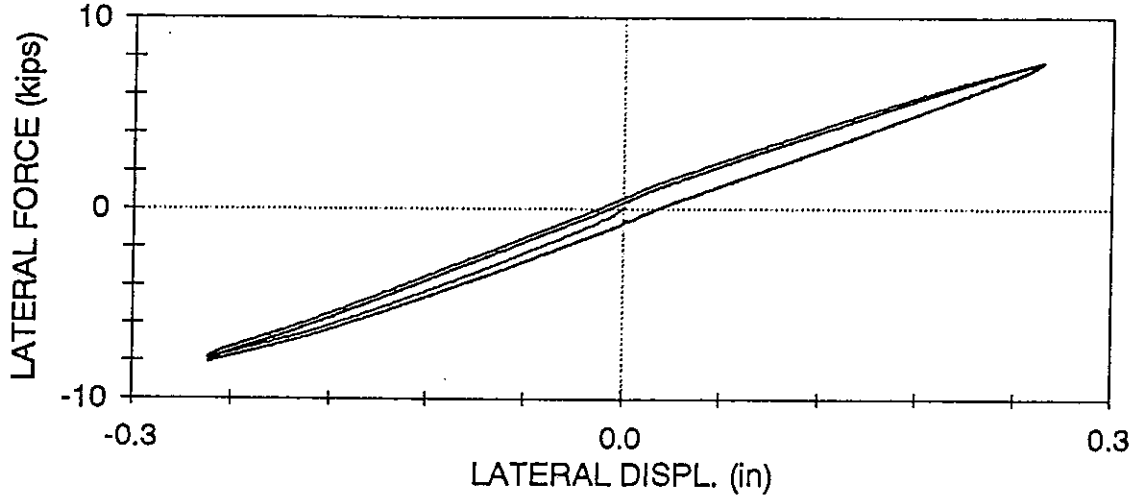

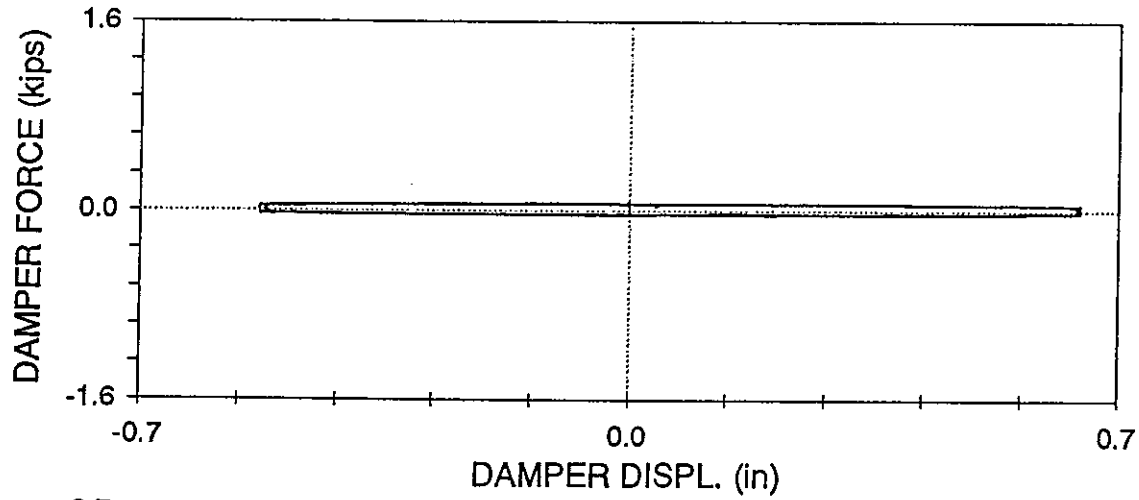

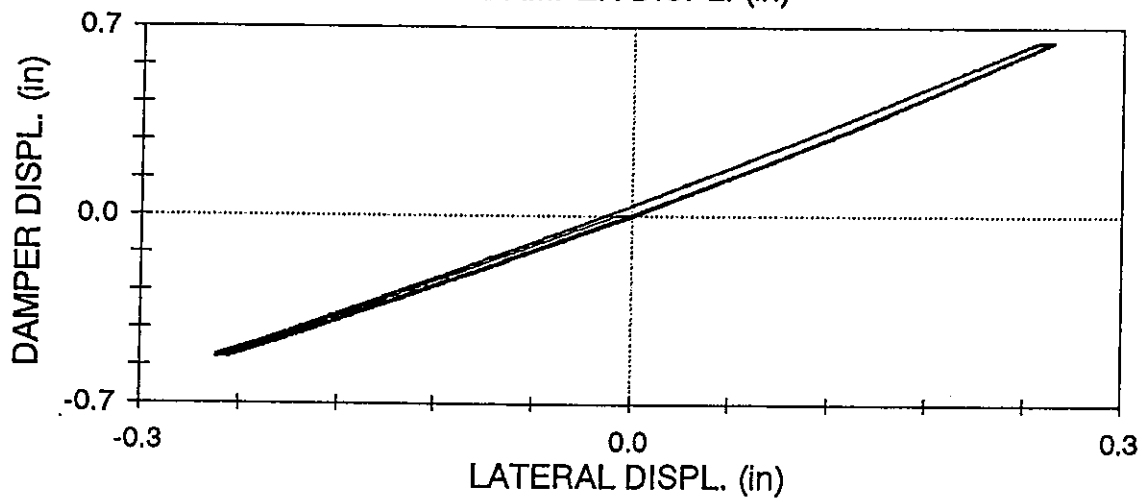

ARTPL02 : RIGID CONNECTIONS, PINNED TOGGLE CONFIGURATION

LOWER DAMPER, f=2.0 Hz, U_o= 0.25 in (05/14/97, 14:29:03)

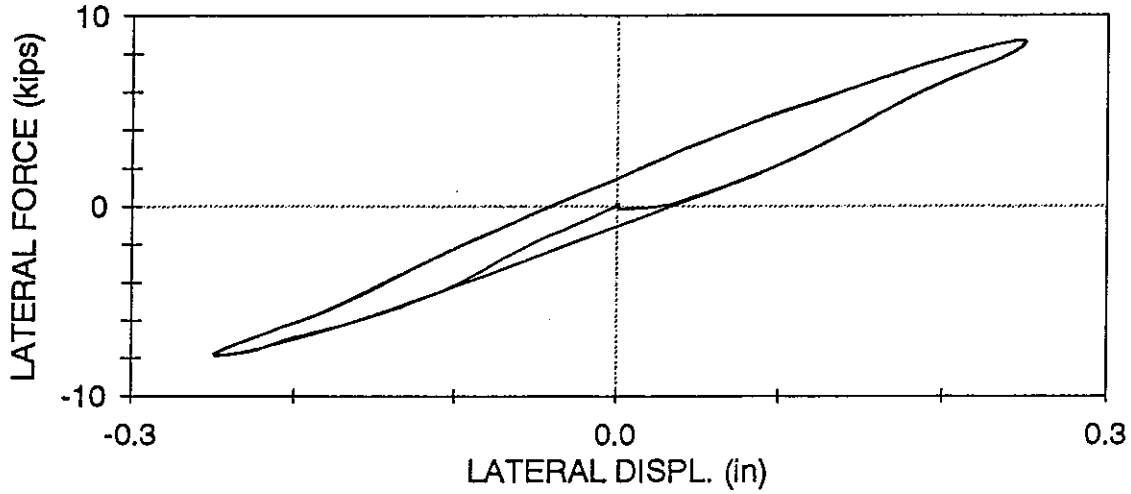

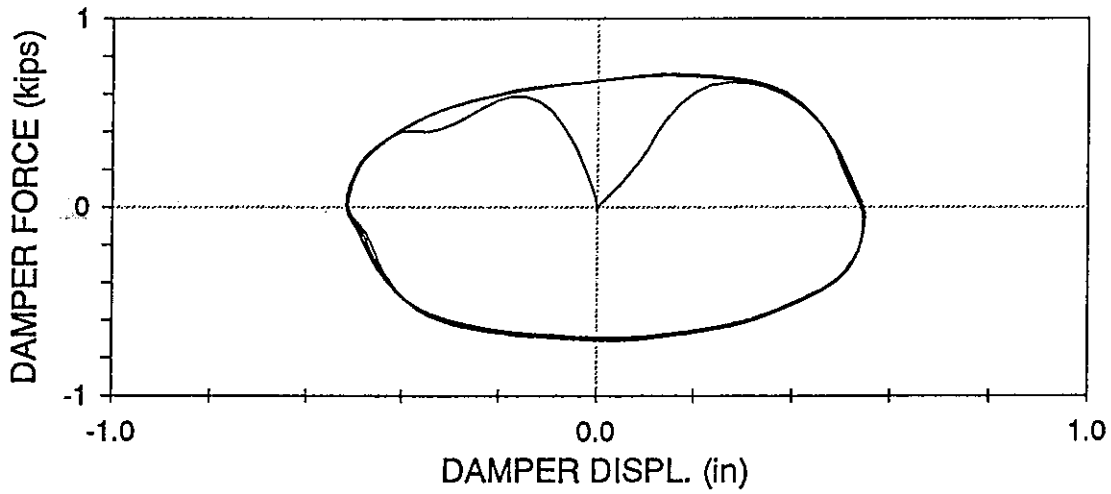

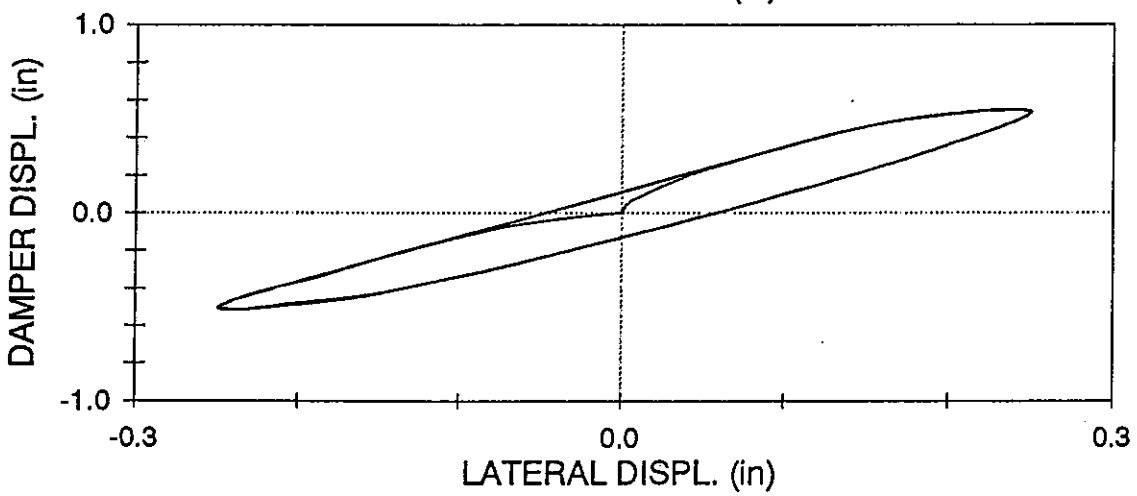

ARTPL03 : RIGID CONNECTIONS, PINNED TOGGLE CONFIGURATION

LOWER DAMPER, f=3.0 Hz, U_o= 0.25 in (05/14/97, 14:31:34)

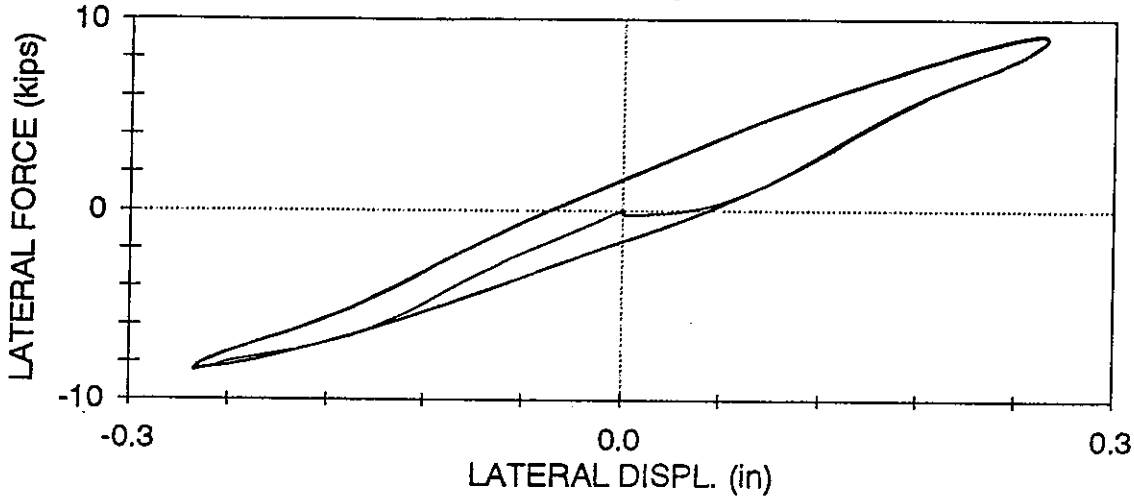

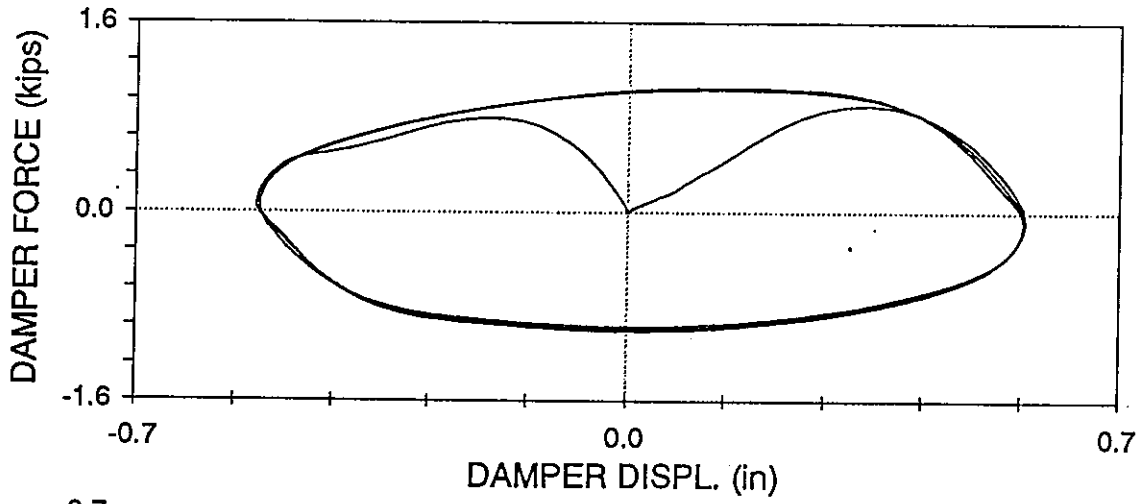

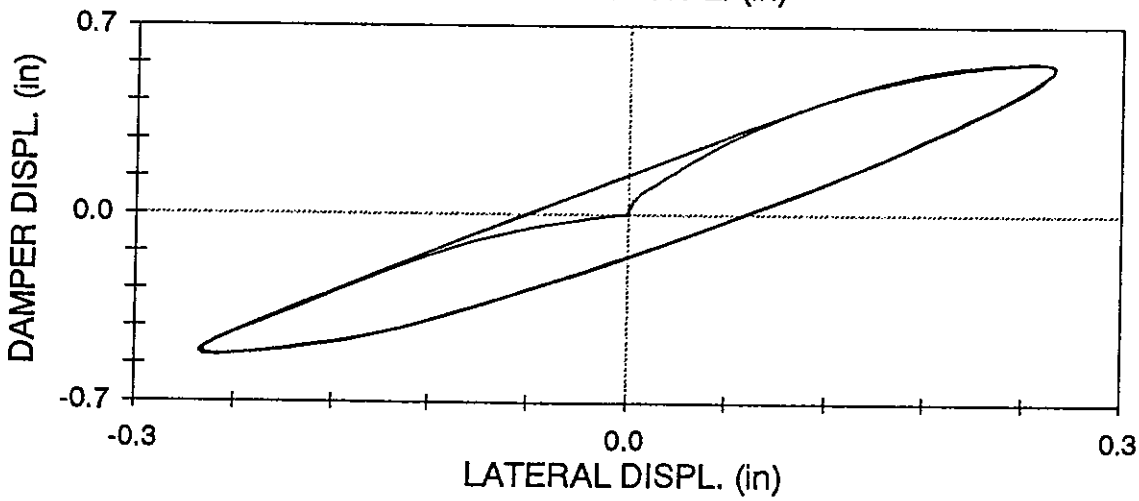

ARTPL04 : RIGID CONNECTIONS, PINNED TOGGLE CONFIGURATION

LOWER DAMPER, f=4.0 Hz, U_o= 0.25 in (05/14/97, 14:33:29)

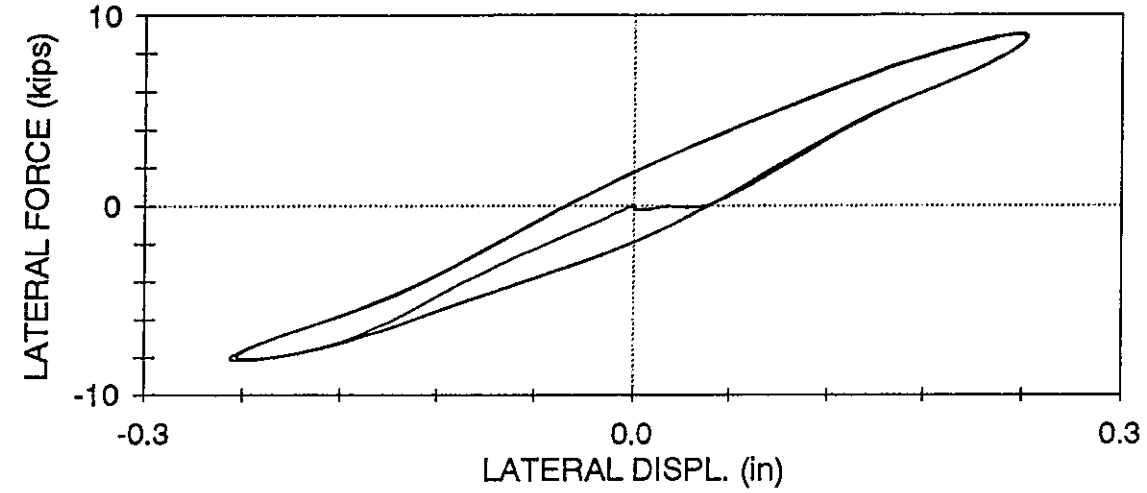

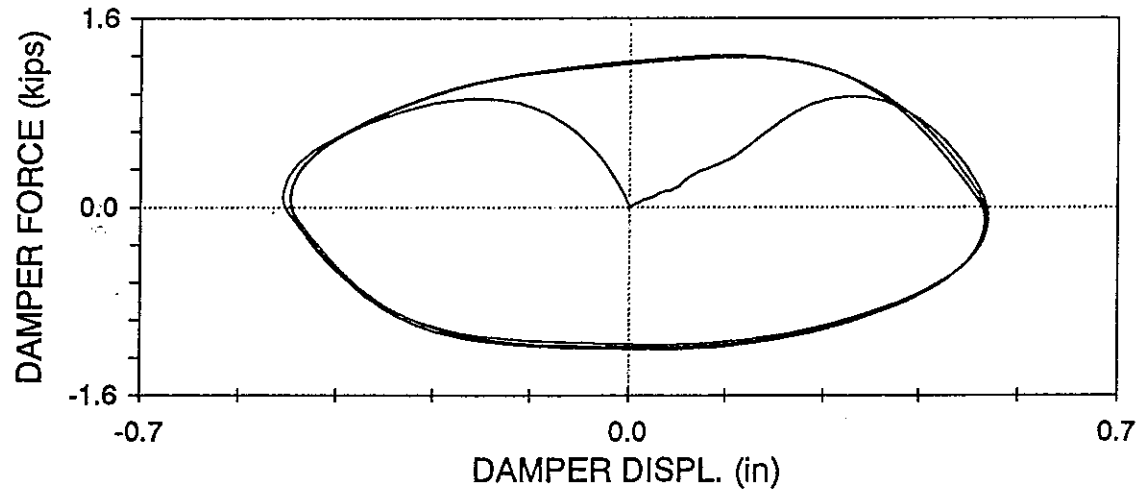

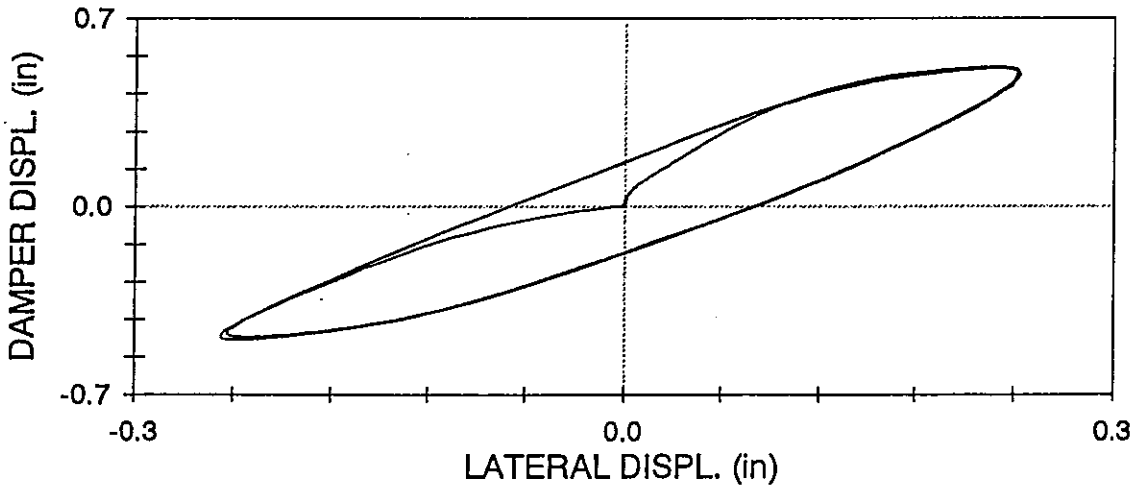

ARTPL05 : RIGID CONNECTIONS, PINNED TOGGLE CONFIGURATION

LOWER DAMPER, f=5.0 Hz, U_o= 0.25 in (05/14/97, 14:37:10)

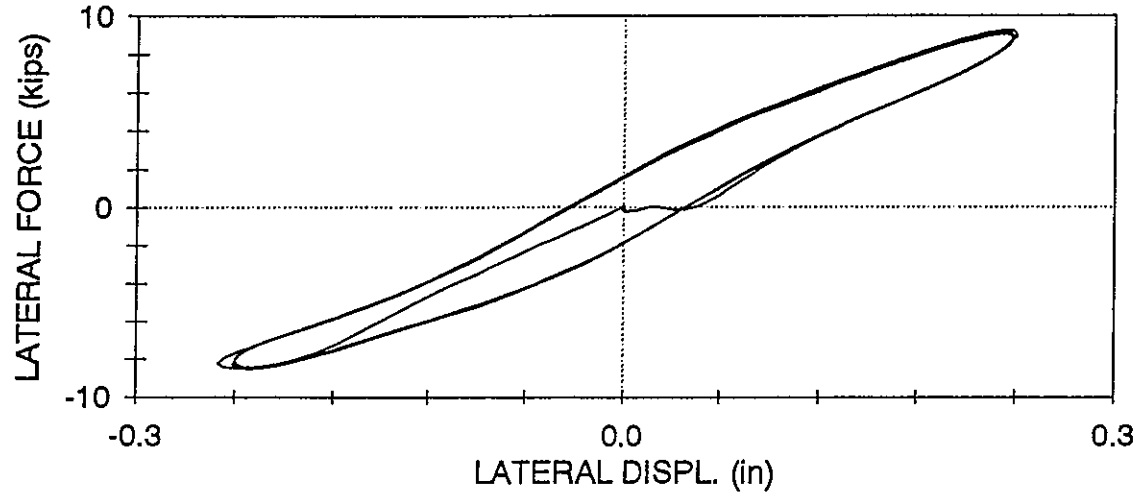

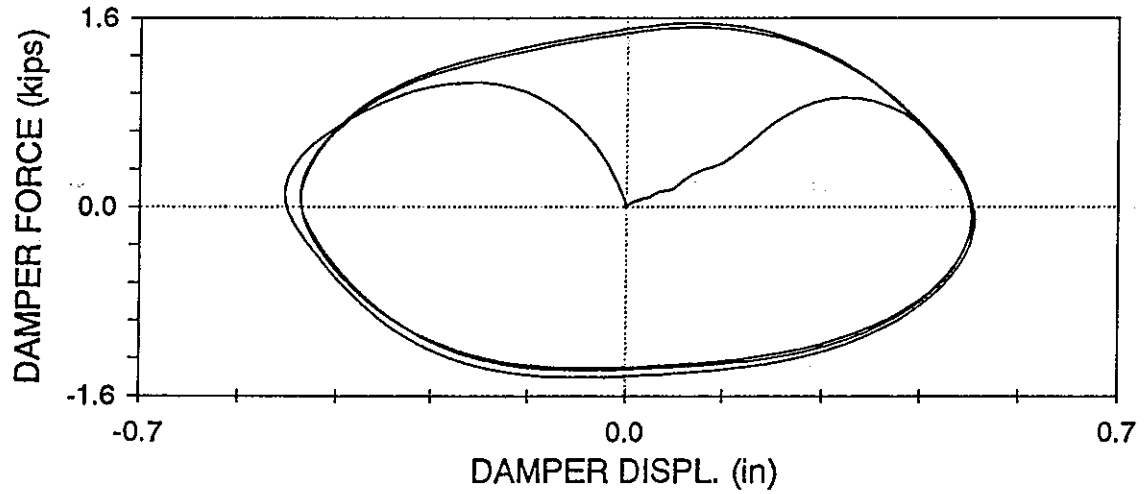

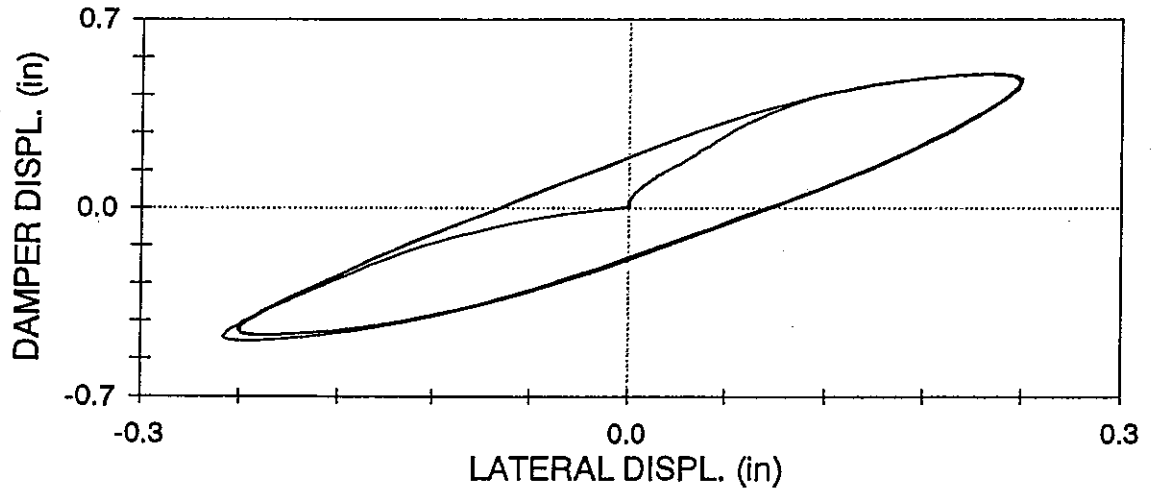

ARTPU01 : RIGID CONNECTIONS, PINNED TOGGLE

UPPER DAMPER, f=0.05 Hz, U_o= 0.25 in (05/16/97, 14:25:04)

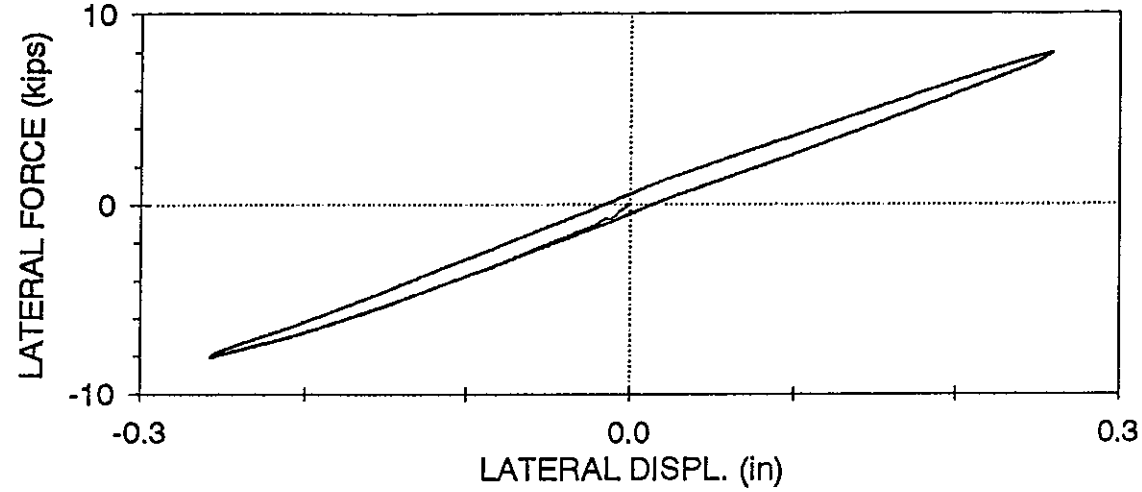

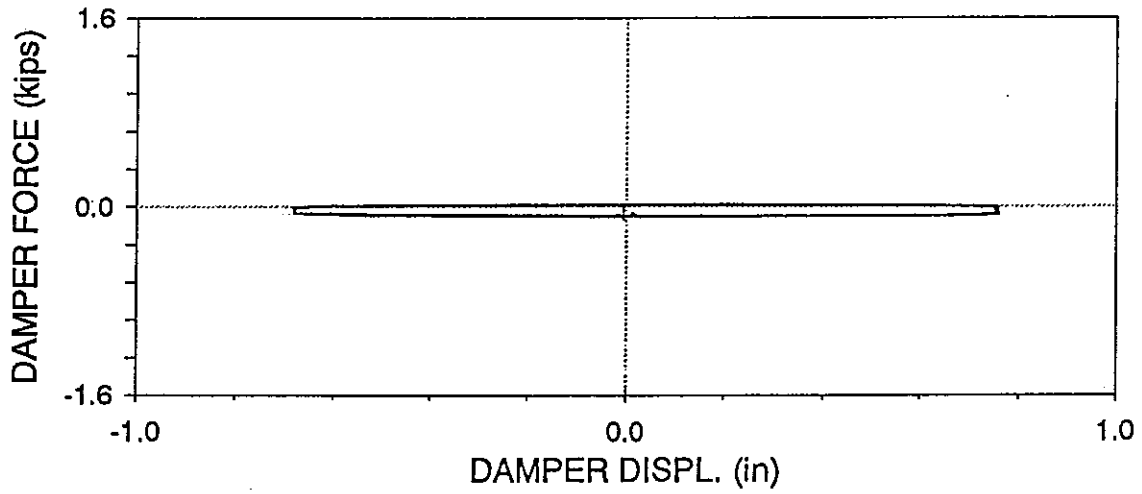

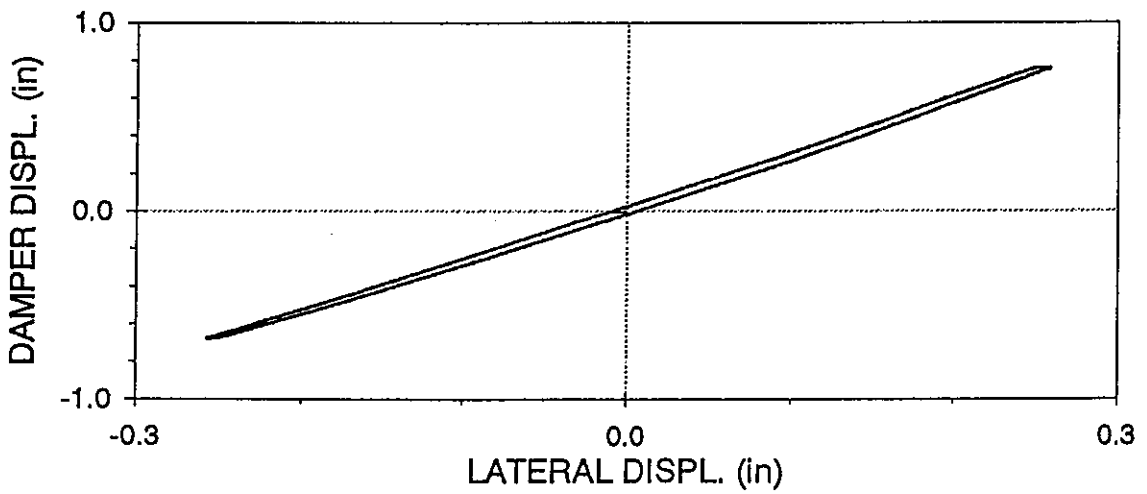

ARTPU02 : RIGID CONNECTIONS, PINNED TOGGLE

UPPER DAMPER, f=2.0 Hz, U_o= 0.25 in (05/16/97, 14:28:29)

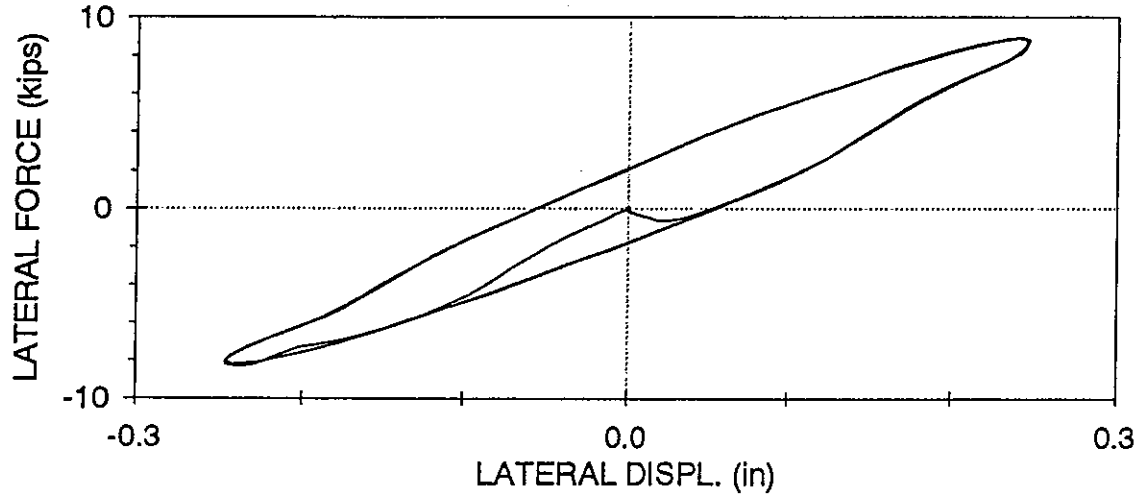

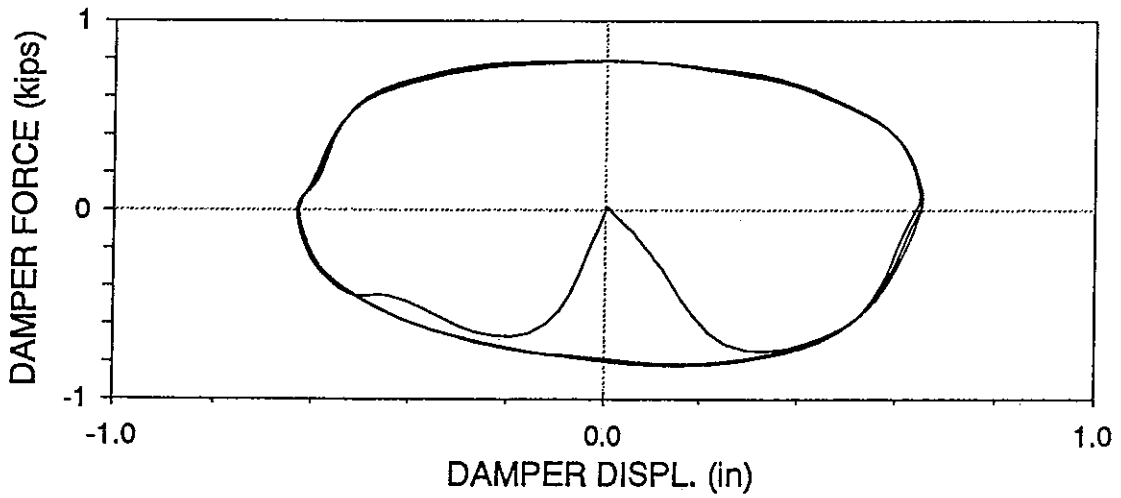

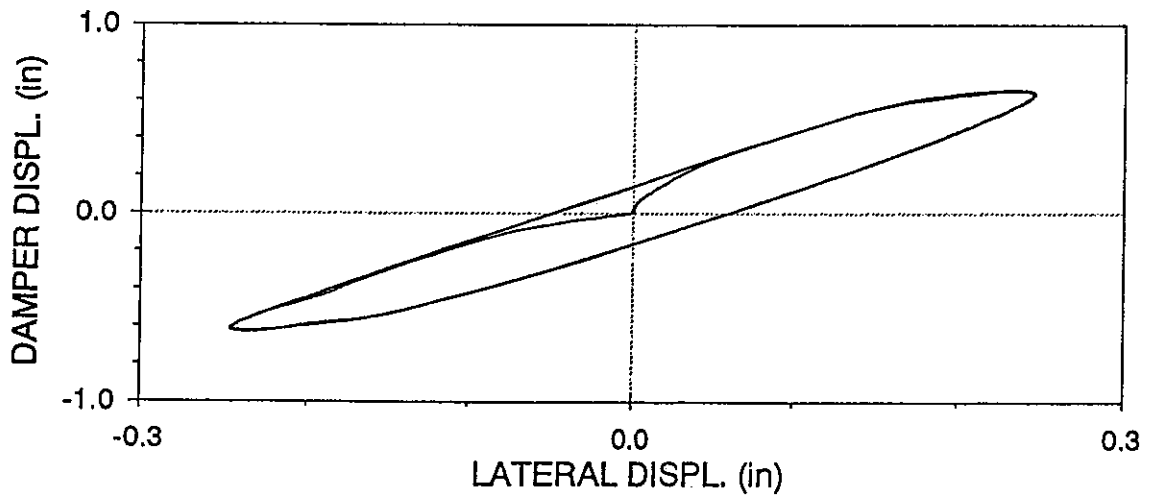

ARTPU03 : RIGID CONNECTIONS, PINNED TOGGLE

UPPER DAMPER, f=3.0 Hz, U_o= 0.25 in (05/16/97, 14:30:06)

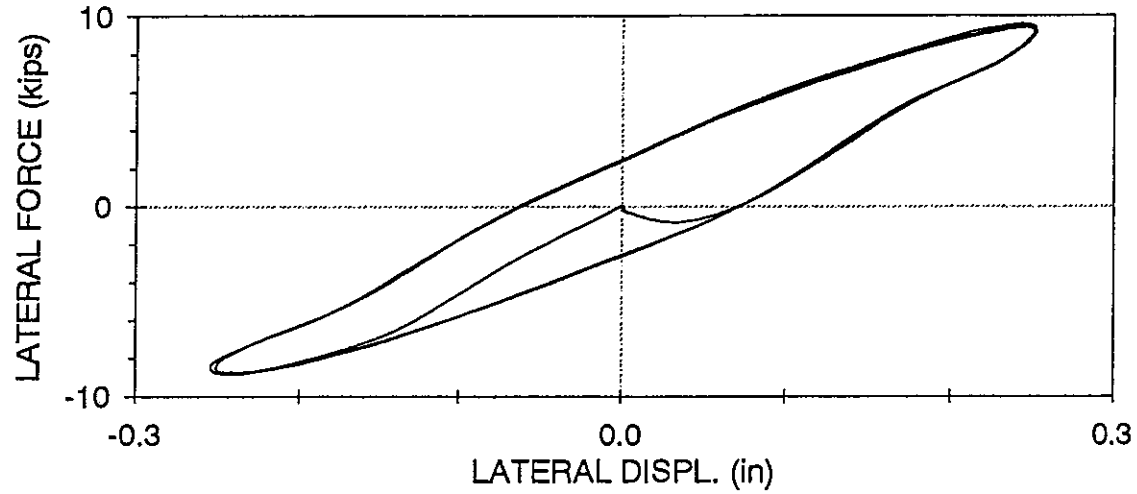

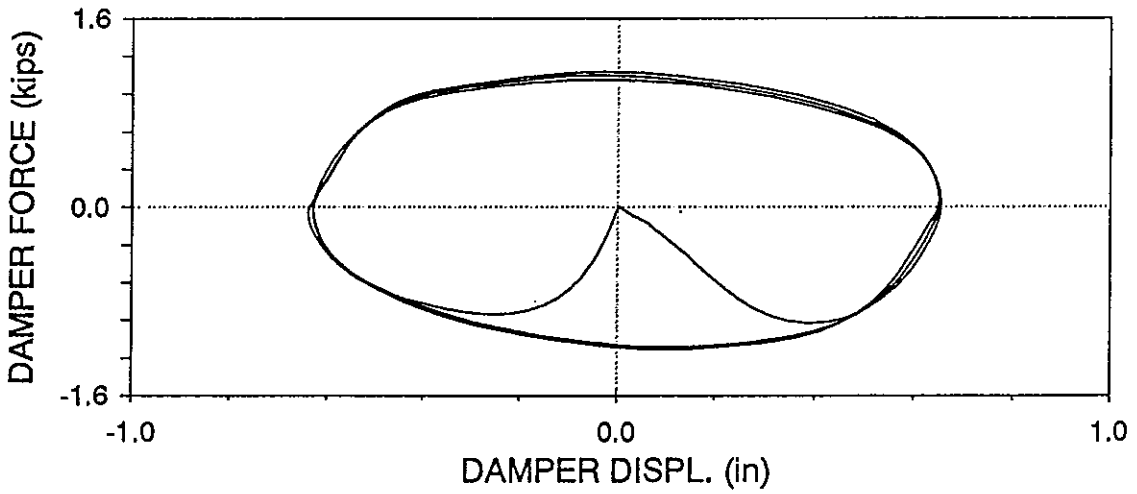

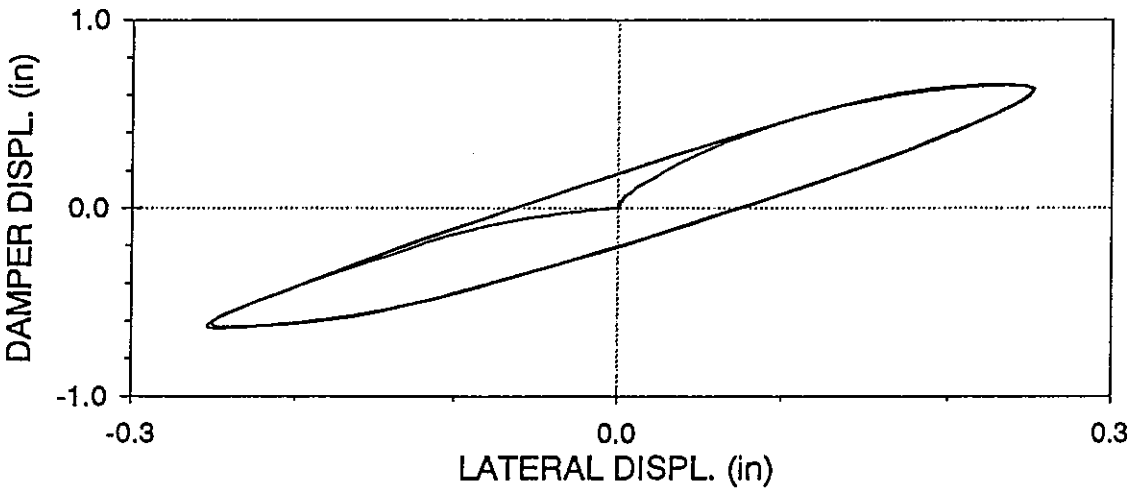

ARTPU04 : RIGID CONNECTIONS, PINNED TOGGLE

UPPER DAMPER, f=4.0 Hz, U_o= 0.25 in (05/16/97, 14:31:53)

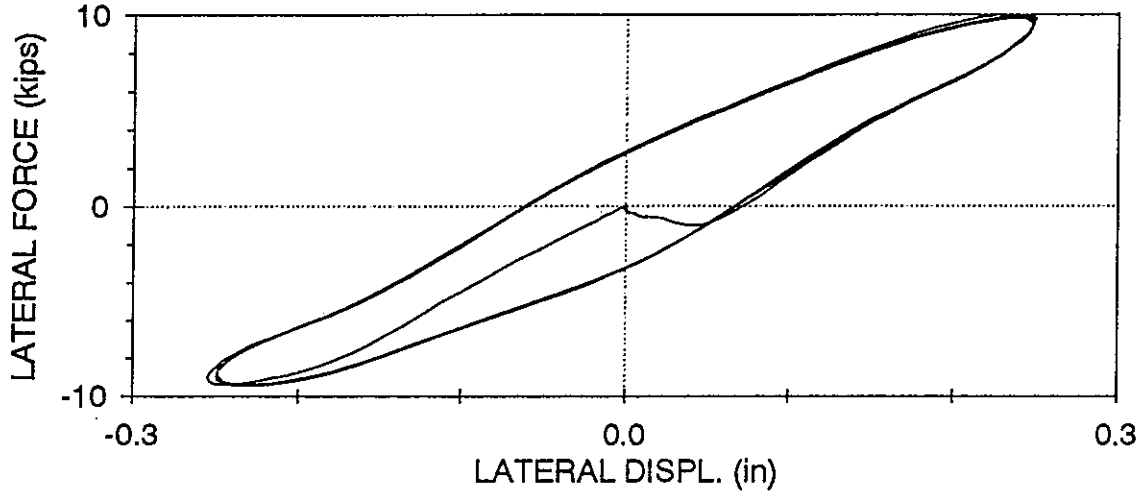

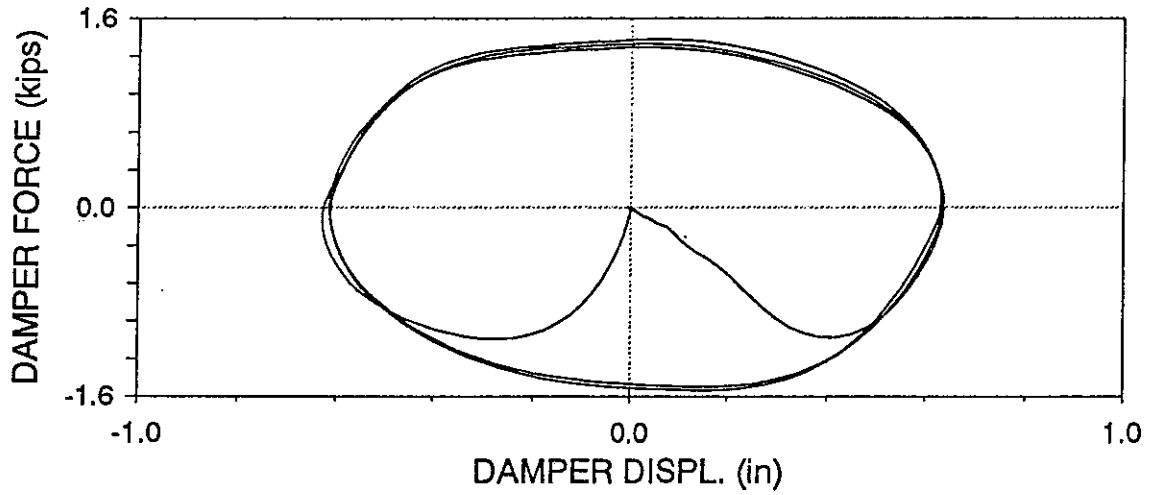

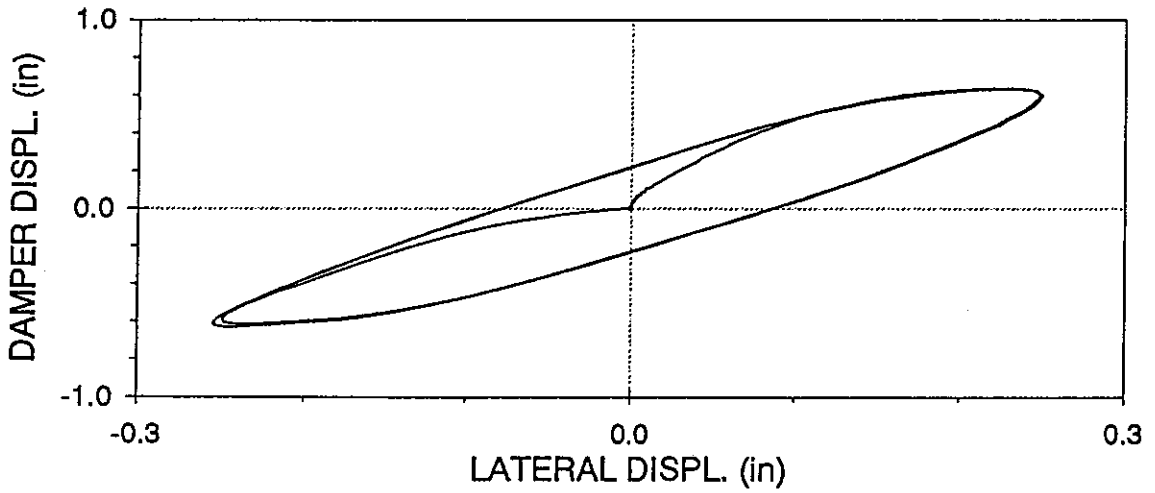

APPENDIX E

RESULTS OF SHAKE TABLE TESTING

(ALL TESTS PERFORMED WITH THE PINNED TOGGLE BRACE CONNECTION DETAIL)

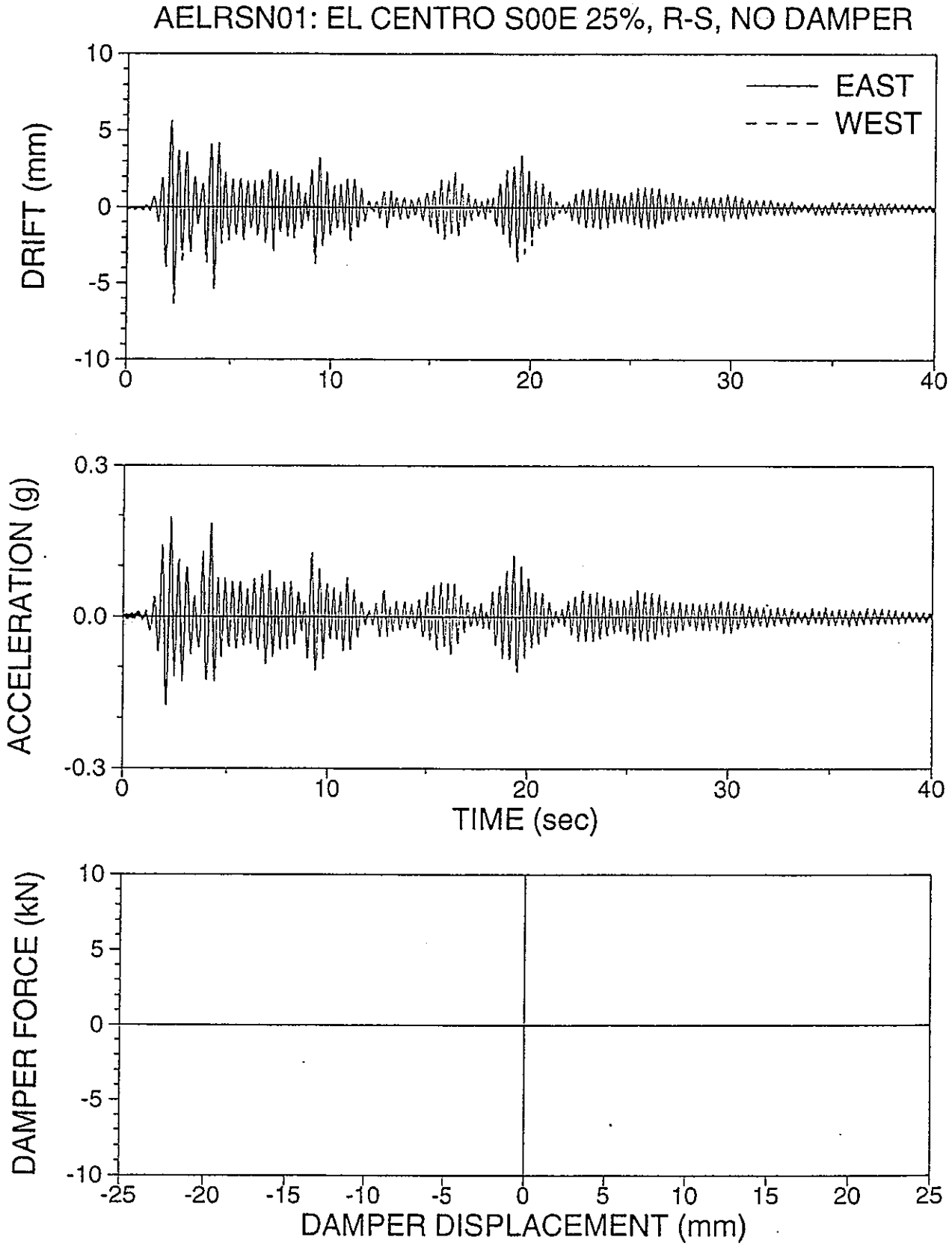
AELRSN01: EL CENTRO S00E 25%, R-S, NO DAMPER
EAST
WEST
DRIFT (mm)
10
5
0
-5
-10
0
10
20
30
40
ACCELERATION (g)
0.3
0.0
-0.3
TIME (sec)
DAMPER FORCE (kN)
-25
-20
-15
-10
-5
0
5
10
15
20
25
DAMPER DISPLACEMENT (mm)

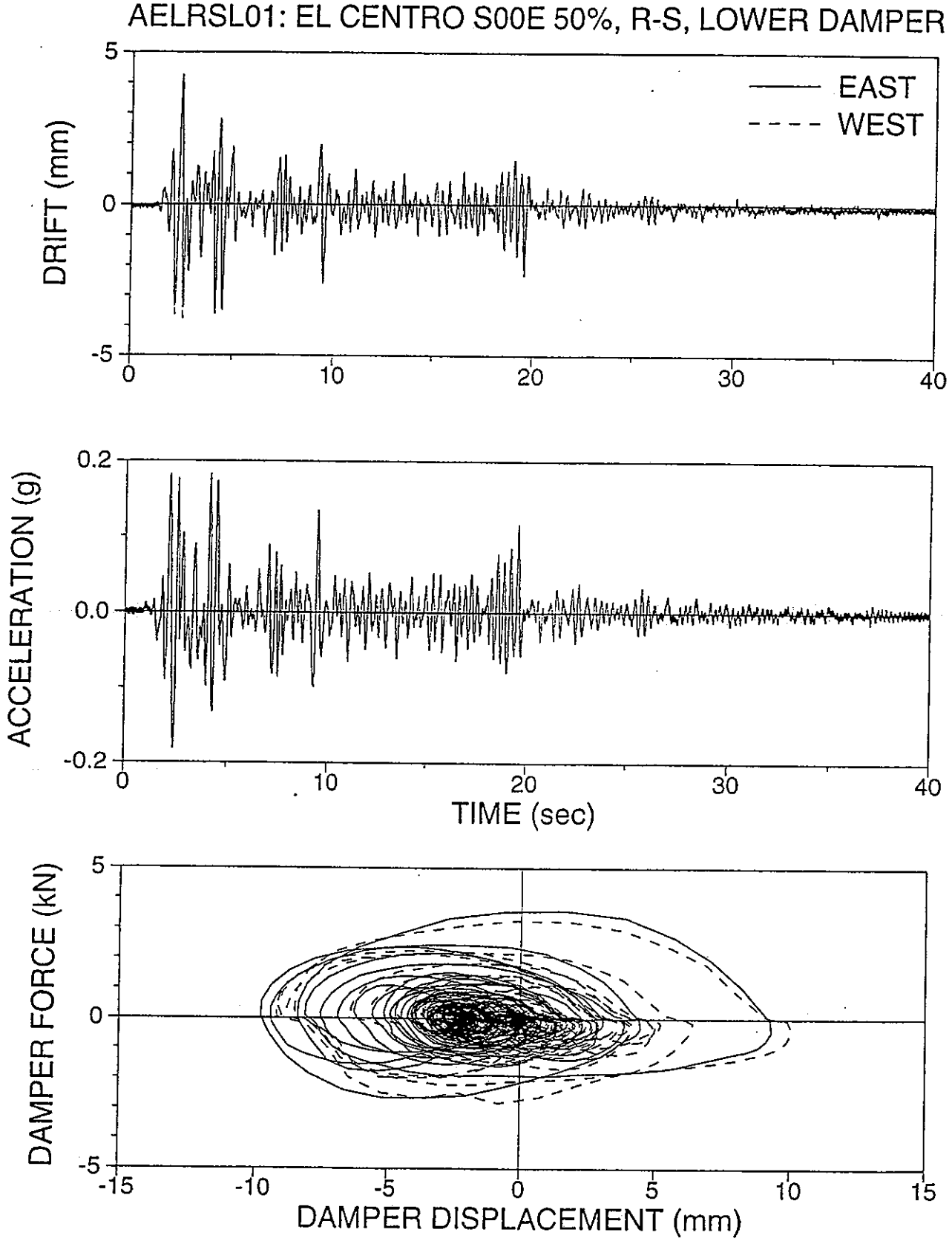
AELRSL01: EL CENTRO S00E 50%, R-S, LOWER DAMPER
EAST
WEST
DRIFT (mm)
5
0
-5
0
10
20
30
40
ACCELERATION (g)
0.2
0.0
-0.2
TIME (sec)
DAMPER FORCE (kN)
-15
-10
-5
5
10
15
DAMPER DISPLACEMENT (mm)

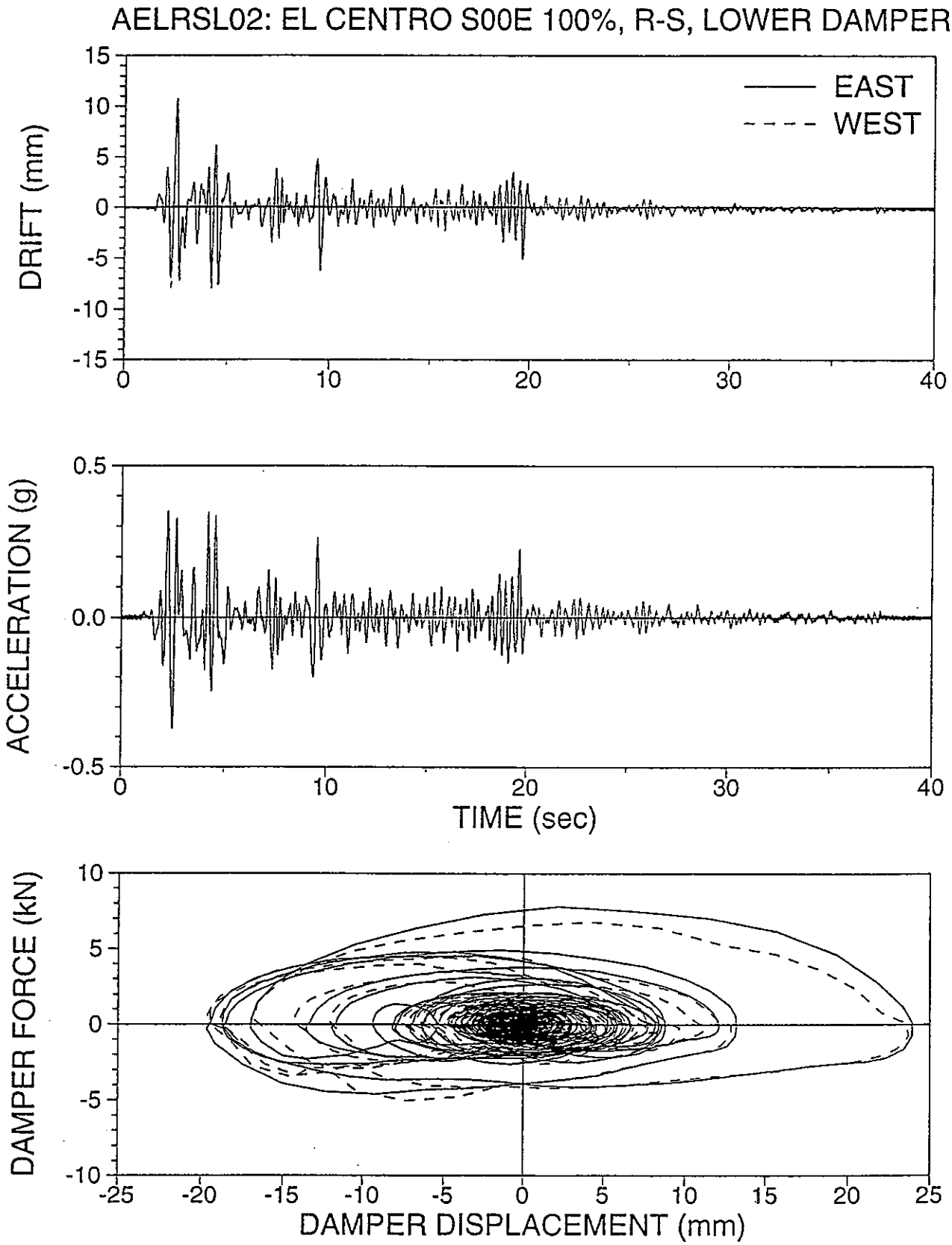
AELRSL02: EL CENTRO S00E 100%, R-S, LOWER DAMPER
EAST
WEST
DRIFT (mm)
15
10
5
0
-5
-10
-15
0
10
20
30
40
ACCELERATION (g)
0.5
0.0
-0.5
TIME (sec)
DAMPER FORCE (kN)
10
5
0
-5
-10
-25
-20
-15
-10
-5
0
5
10
15
20
25
DAMPER DISPLACEMENT (mm)

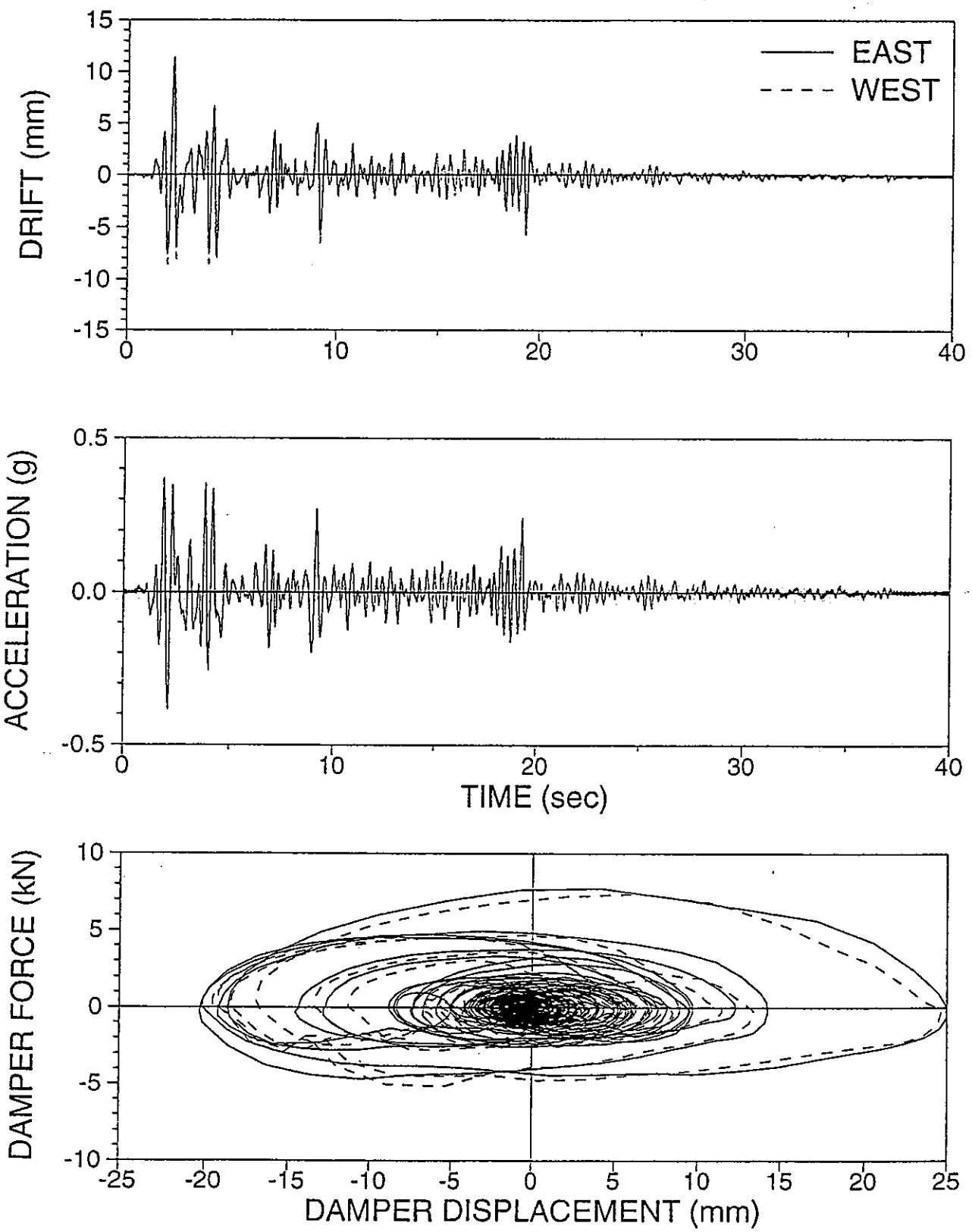
AELRSL03: EL CENTRO S00E 100%, R-S, LOWER DAMPER
DRIFT (mm)
EAST
WEST
ACCELERATION (g)
TIME (sec)
DAMPER FORCE (kN)
DAMPER DISPLACEMENT (mm)

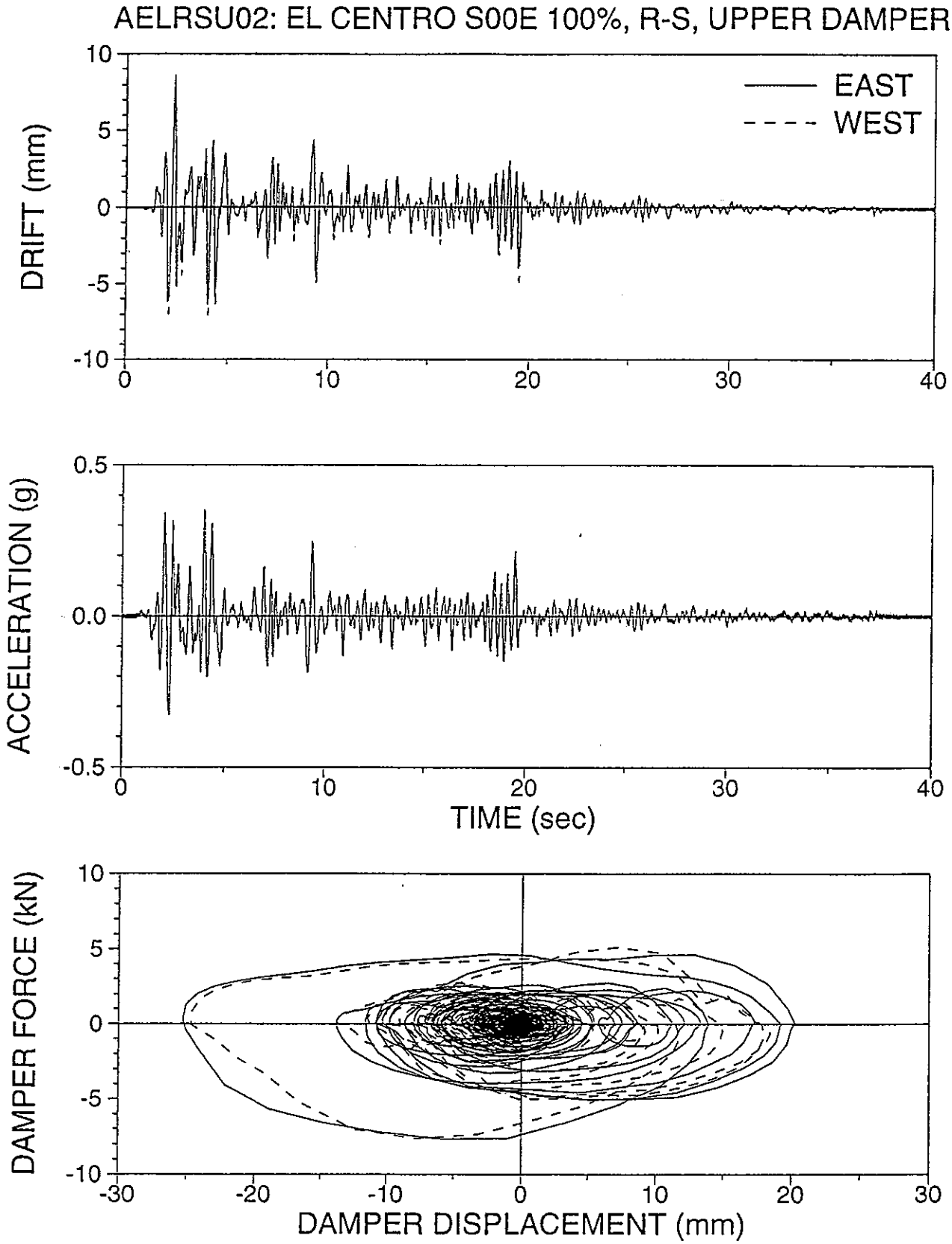
AELRSU02: EL CENTRO S00E 100%, R-S, UPPER DAMPER
EAST
WEST
DRIFT (mm)
10
5
0
-5
-10
0
10
20
30
40
ACCELERATION (g)
0.5
0.0
-0.5
TIME (sec)
DAMPER FORCE (kN)
-30
-20
DAMPER DISPLACEMENT (mm)

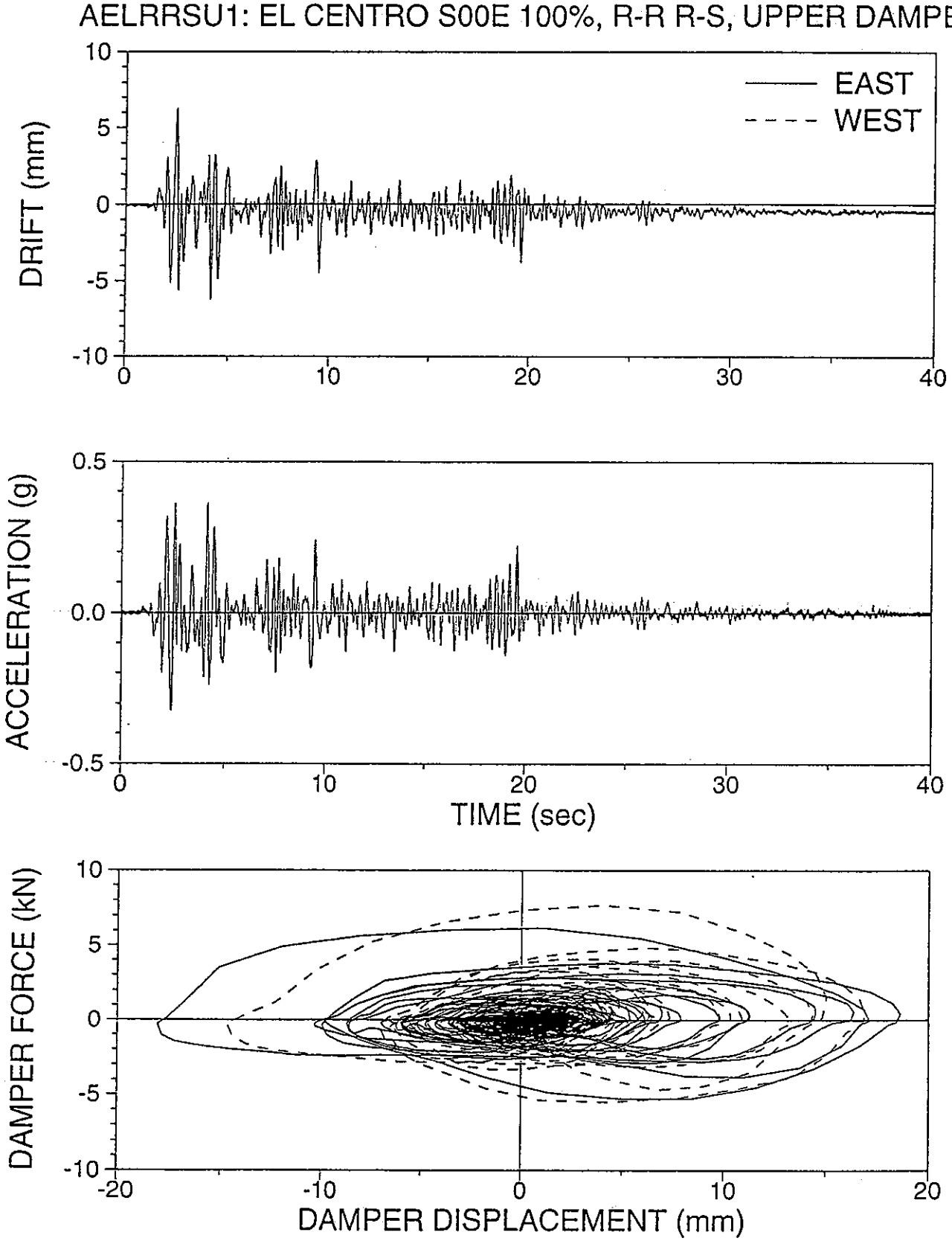
AELRRSU1: EL CENTRO S00E 100%, R-R R-S, UPPER DAMPER
EAST
WEST
DRIFT (mm)
10
5
0
-5
-10
0
10
20
30
40
ACCELERATION (g)
0.5
0.0
-0.5
TIME (sec)
DAMPER FORCE (kN)
-20
-10
DAMPER DISPLACEMENT (mm)

AEVRRSU1: EL CENTRO S00E H&V 50%,R-R R-S, UPPER DAMPER

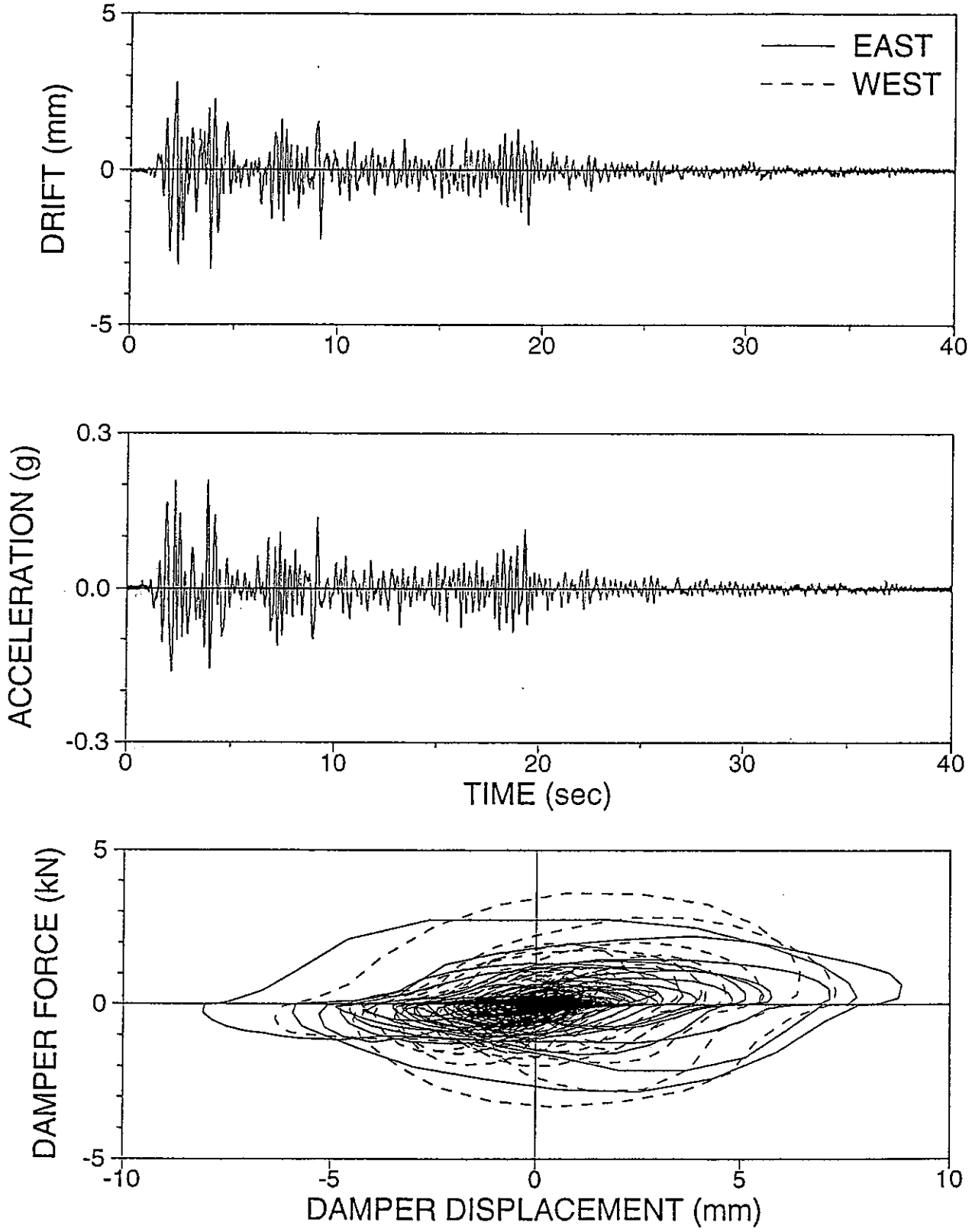

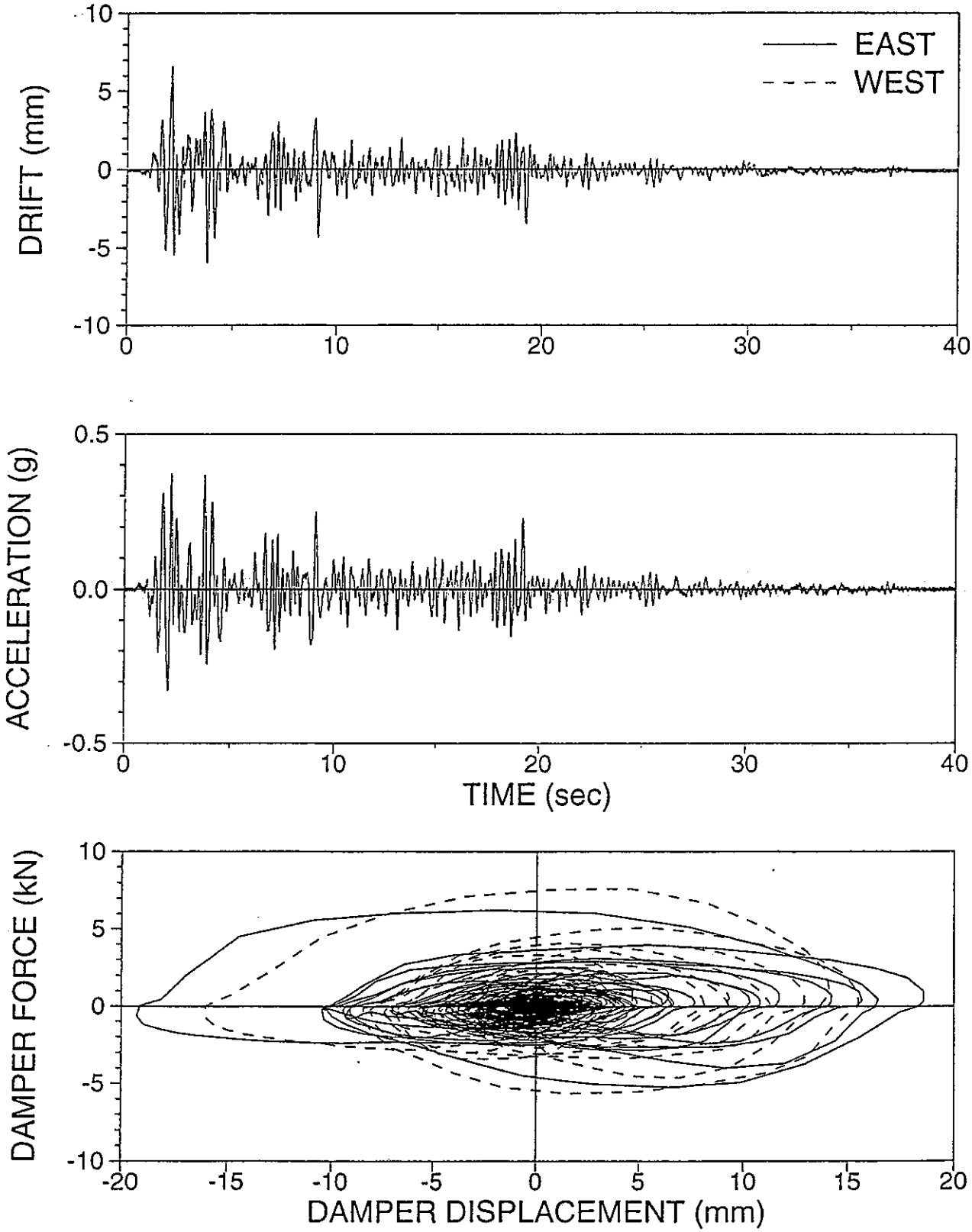
AEVRRSU2: EL CENTRO S00E H&V 100%,R-R R-S, UPPER DAMPER
EAST
WEST
DRIFT (mm)
10
5
0
-5
-10
0
10
20
30
40
ACCELERATION (g)
0.5
0.0
-0.5
TIME (sec)
DAMPER FORCE (kN)
-20
-15
-10
-5
0
5
10
15
20
DAMPER DISPLACEMENT (mm)

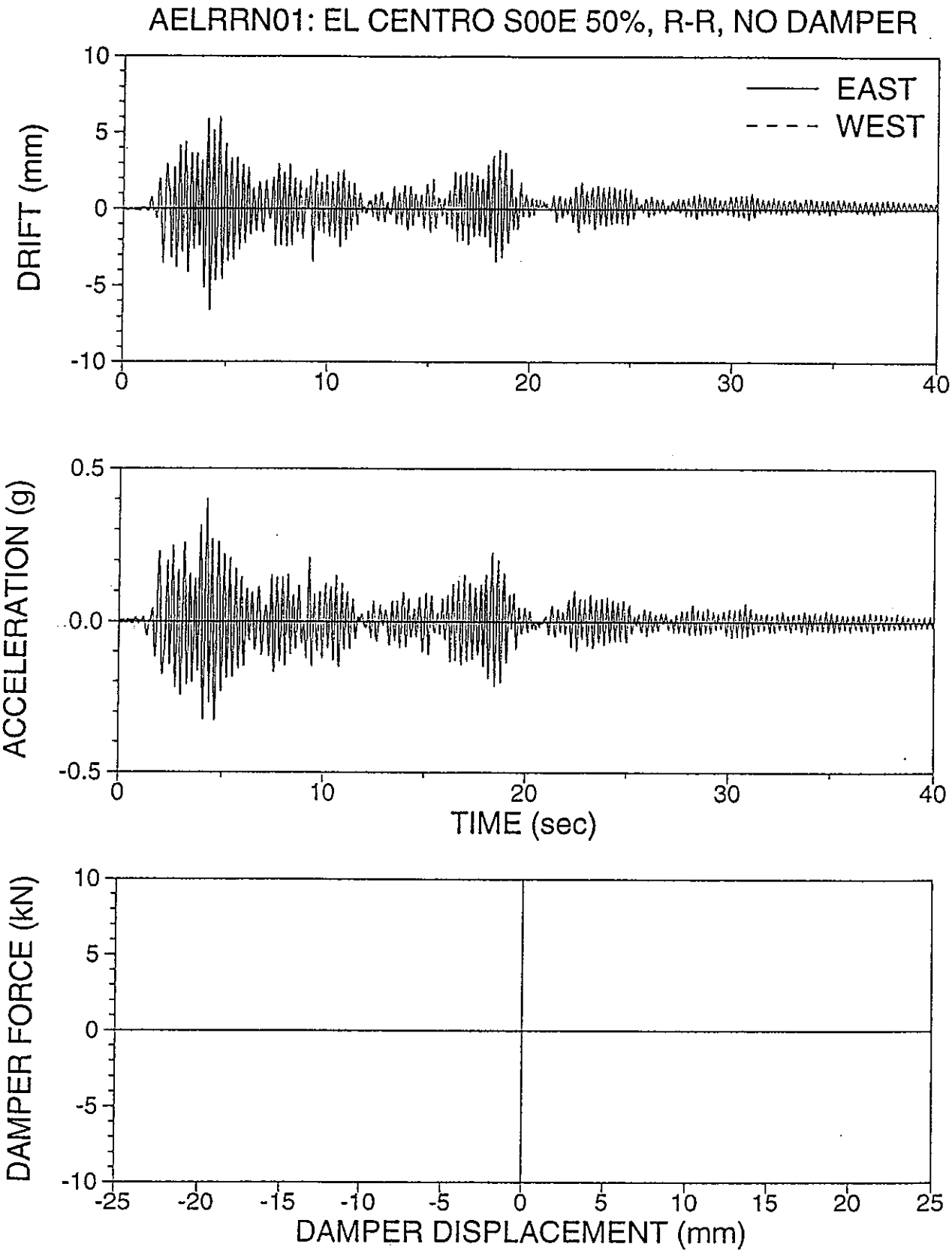
AELRRN01: EL CENTRO S00E 50%, R-R, NO DAMPER
EAST
WEST
DRIFT (mm)
10
5
0
-5
-10
0
10
20
30
40
ACCELERATION (g)
0.5
0.0
-0.5
TIME (sec)
DAMPER FORCE (kN)
-25
-20
-15
-10
-5
0
5
10
15
20
25
DAMPER DISPLACEMENT (mm)

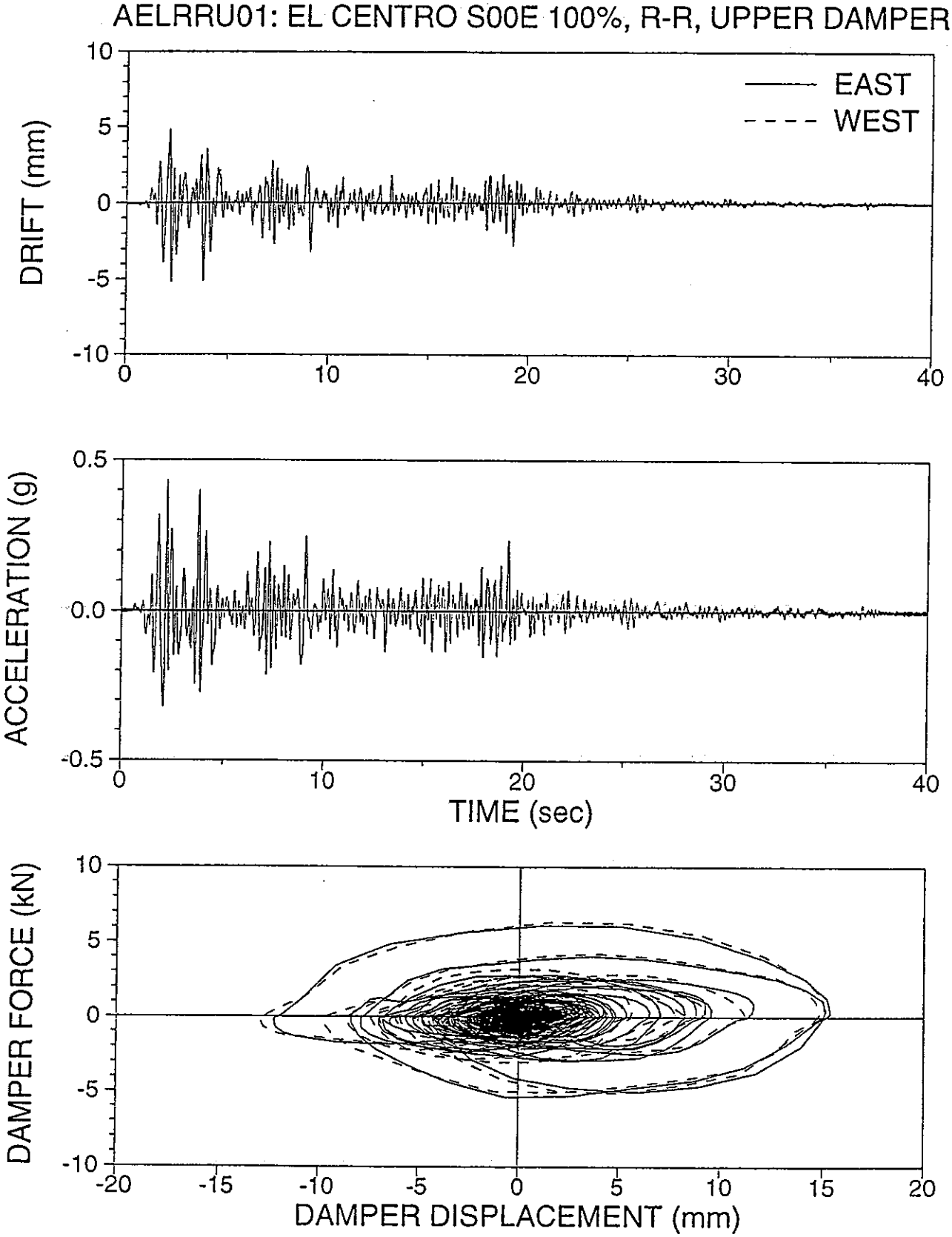
AELRRU01: EL CENTRO S00E 100%, R-R, UPPER DAMPER
EAST
WEST
DRIFT (mm)
10
5
0
-5
-10
0
10
20
30
40
ACCELERATION (g)
0.5
0.0
-0.5
TIME (sec)
DAMPER FORCE (kN)
-20
-15
-10
-5
0
5
10
15
20
DAMPER DISPLACEMENT (mm)

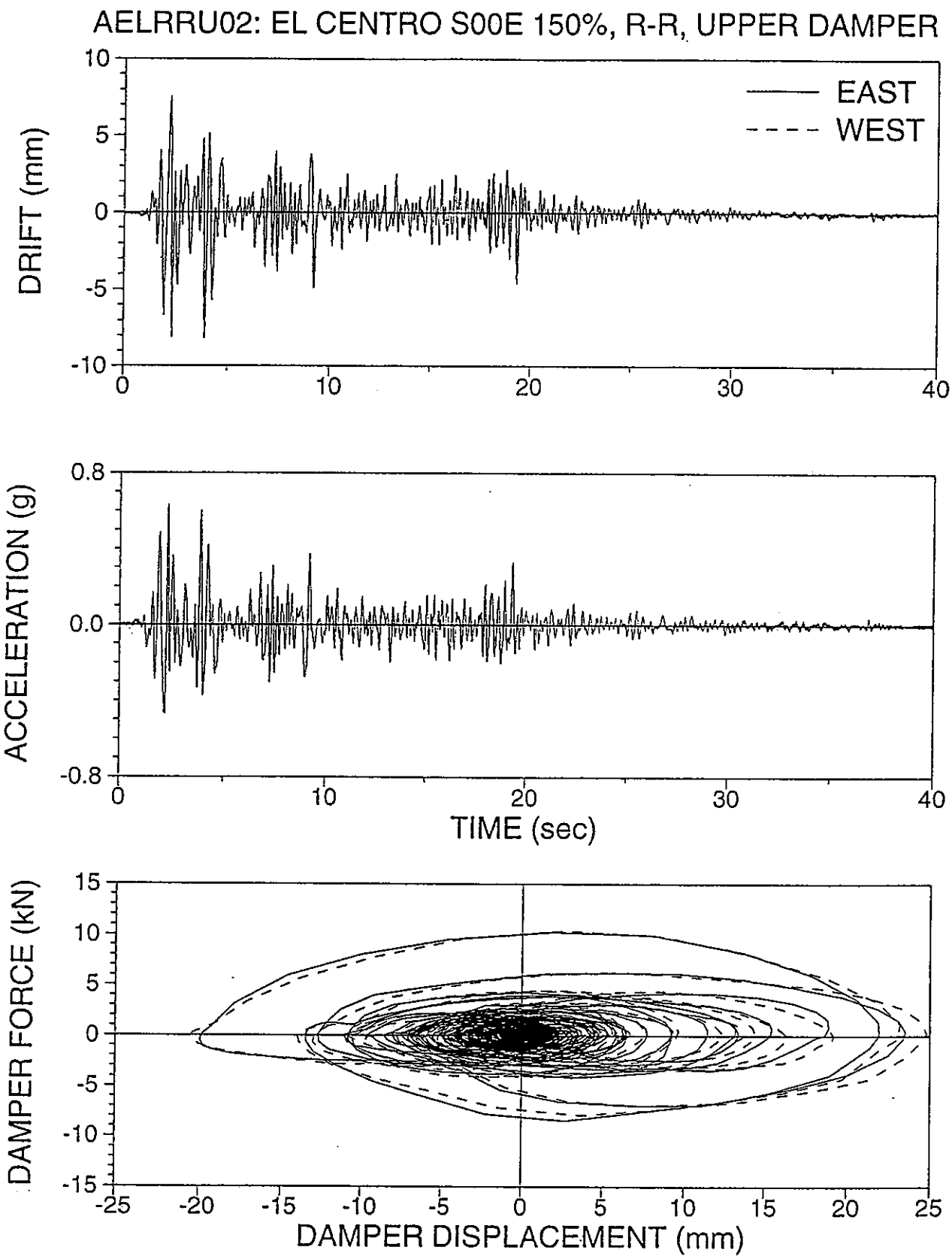
AELRRU02: EL CENTRO S00E 150%, R-R, UPPER DAMPER
EAST
WEST
DRIFT (mm)
10
5
0
-5
-10
0
10
20
30
40
ACCELERATION (g)
0.8
0.0
-0.8
TIME (sec)
DAMPER FORCE (kN)
15
10
5
0
-5
-10
-15
-25
-20
-15
-10
-5
0
5
10
15
20
25
DAMPER DISPLACEMENT (mm)

AEVRRU01: EL CENTRO S00E H&V 100%, R-R, UPPER DAMPER

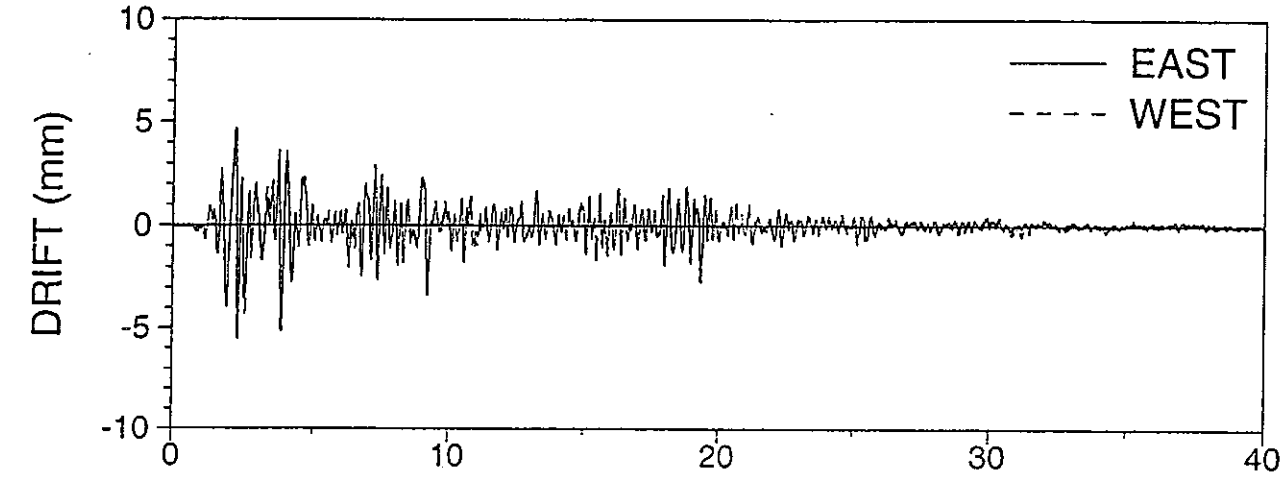

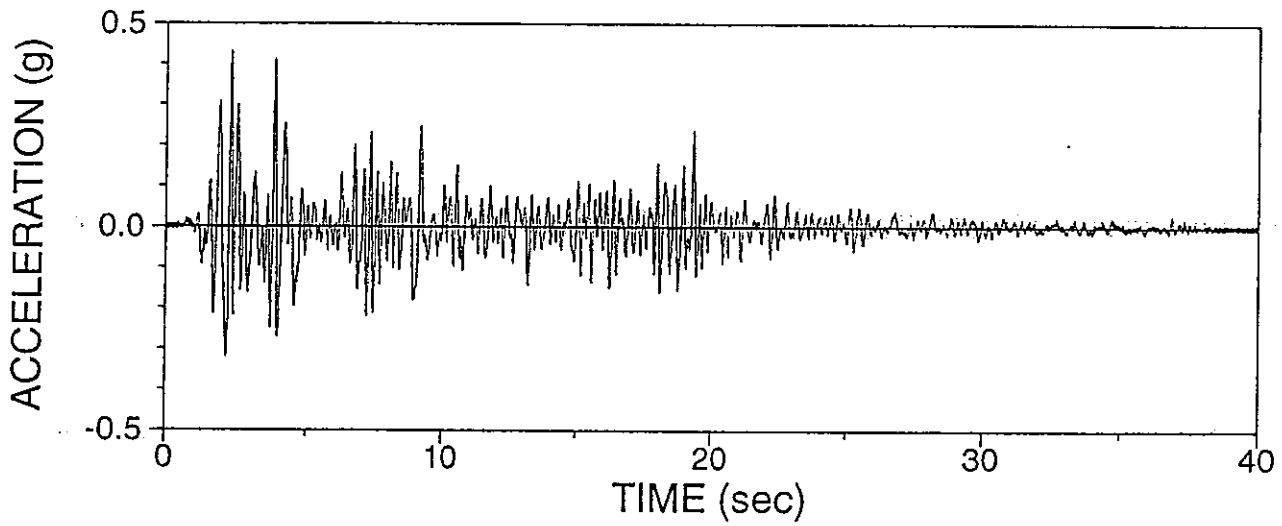

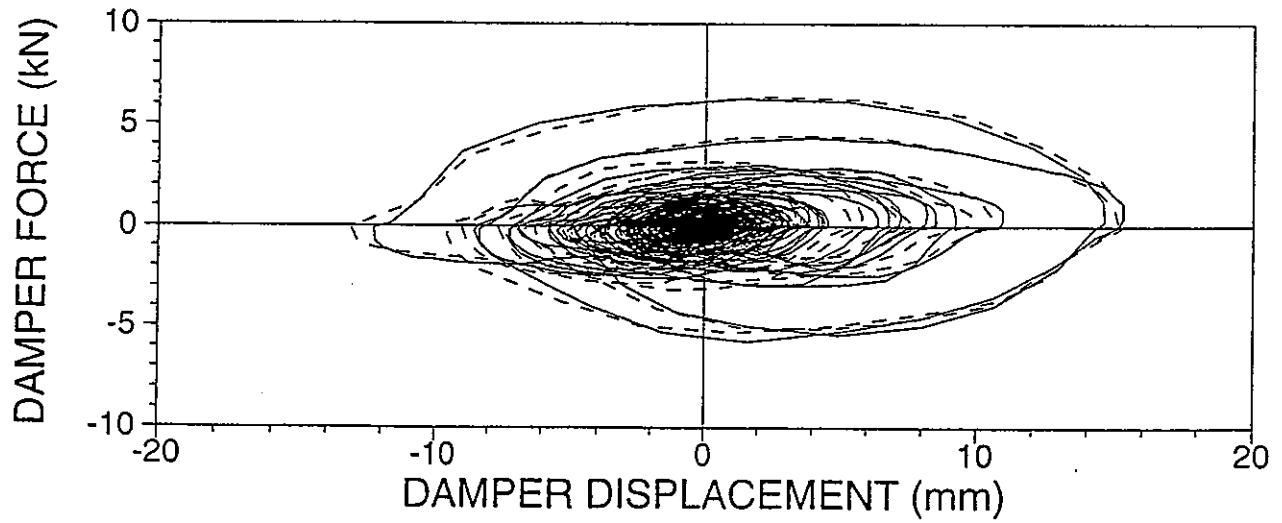

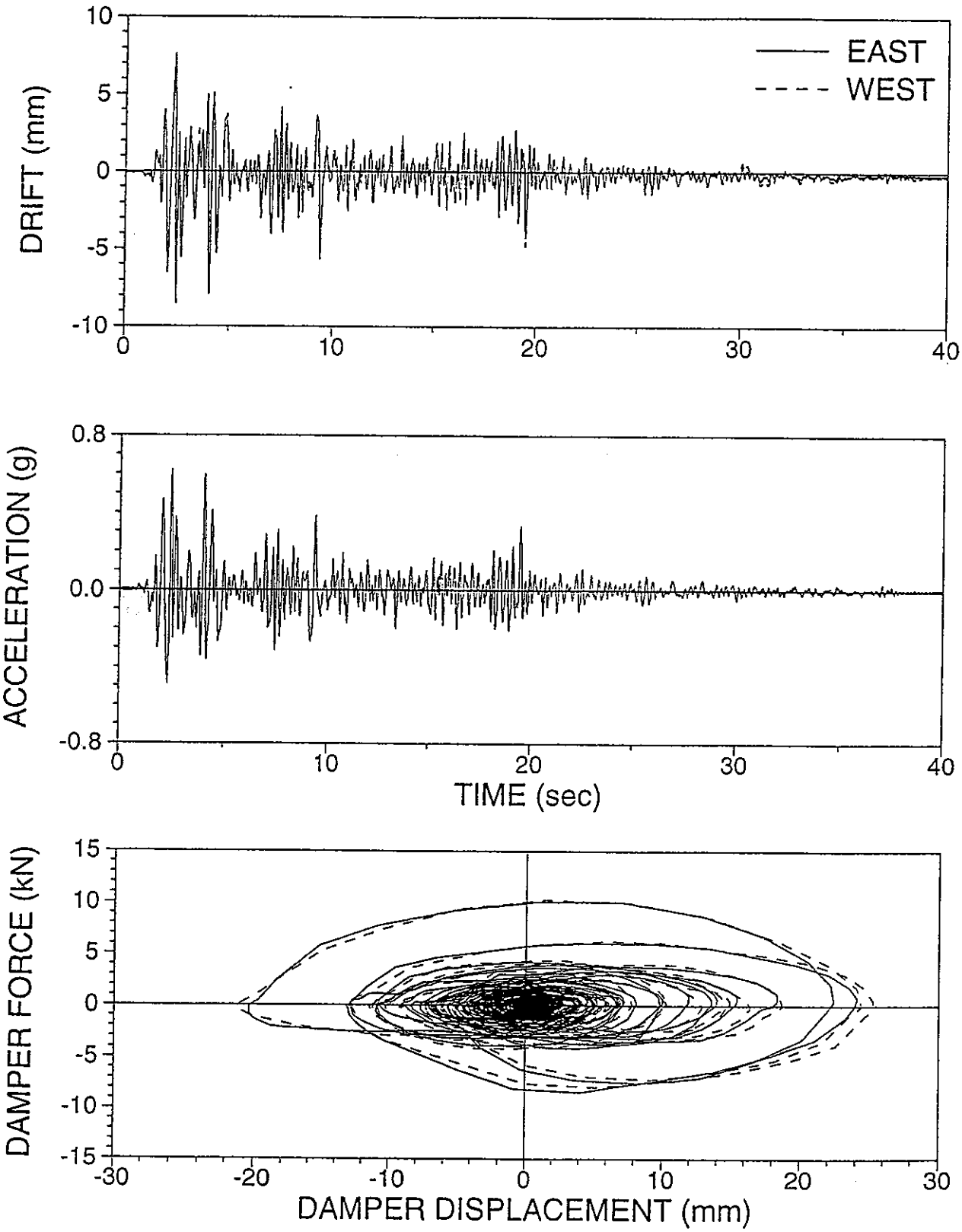
AEVRRU02: EL CENTRO S00E H%V 150%, R-R, UPPER DAMPER
EAST
WEST
DRIFT (mm)
ACCELERATION (g)
TIME (sec)
DAMPER FORCE (kN)
DAMPER DISPLACEMENT (mm)

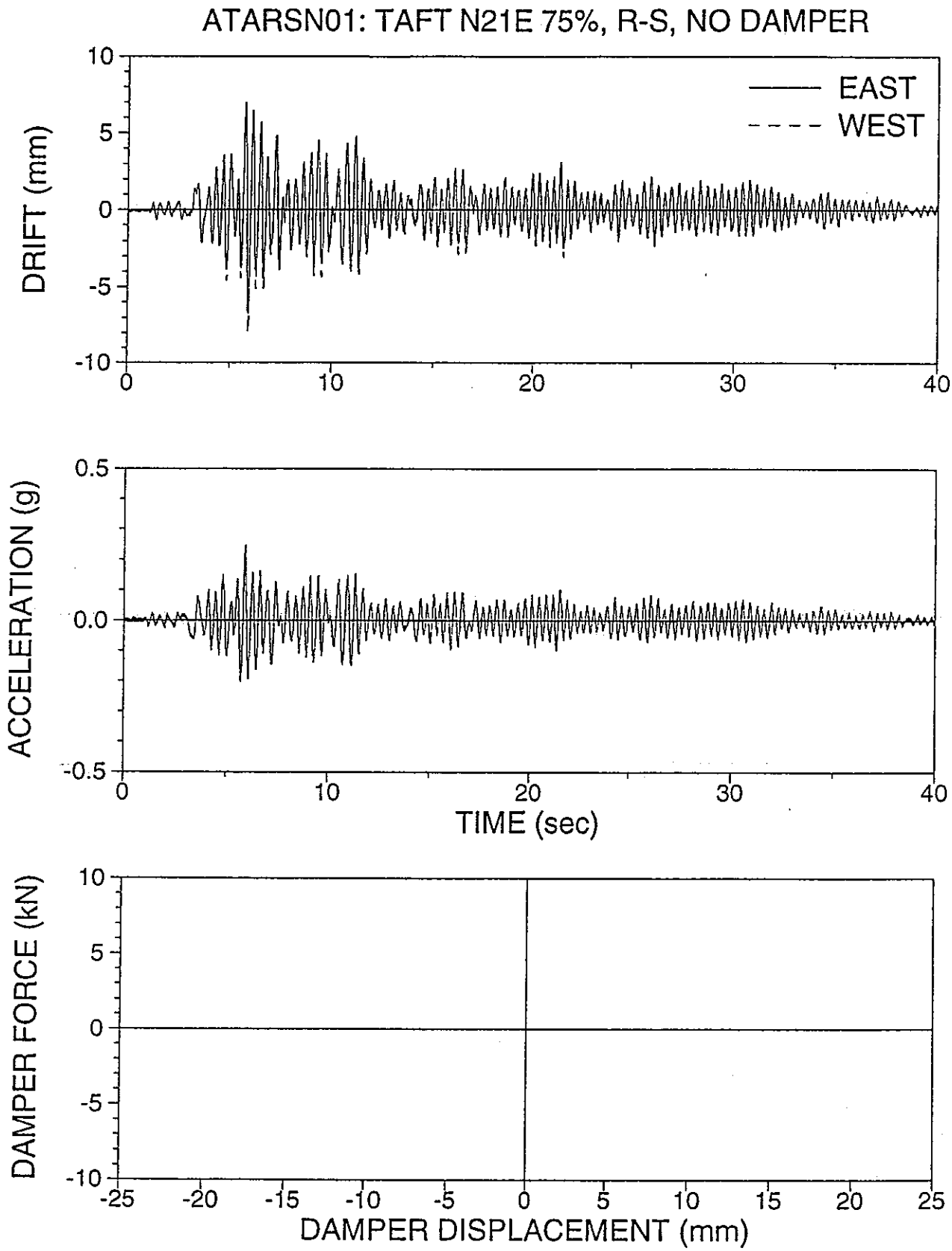
ATARSN01: TAFT N21E 75%, R-S, NO DAMPER
EAST
WEST
DRIFT (mm)
10
5
0
-5
-10
0
10
20
30
40
ACCELERATION (g)
0.5
0.0
-0.5
TIME (sec)
DAMPER FORCE (kN)
-25
-20
-15
-10
-5
5
15
DAMPER DISPLACEMENT (mm)

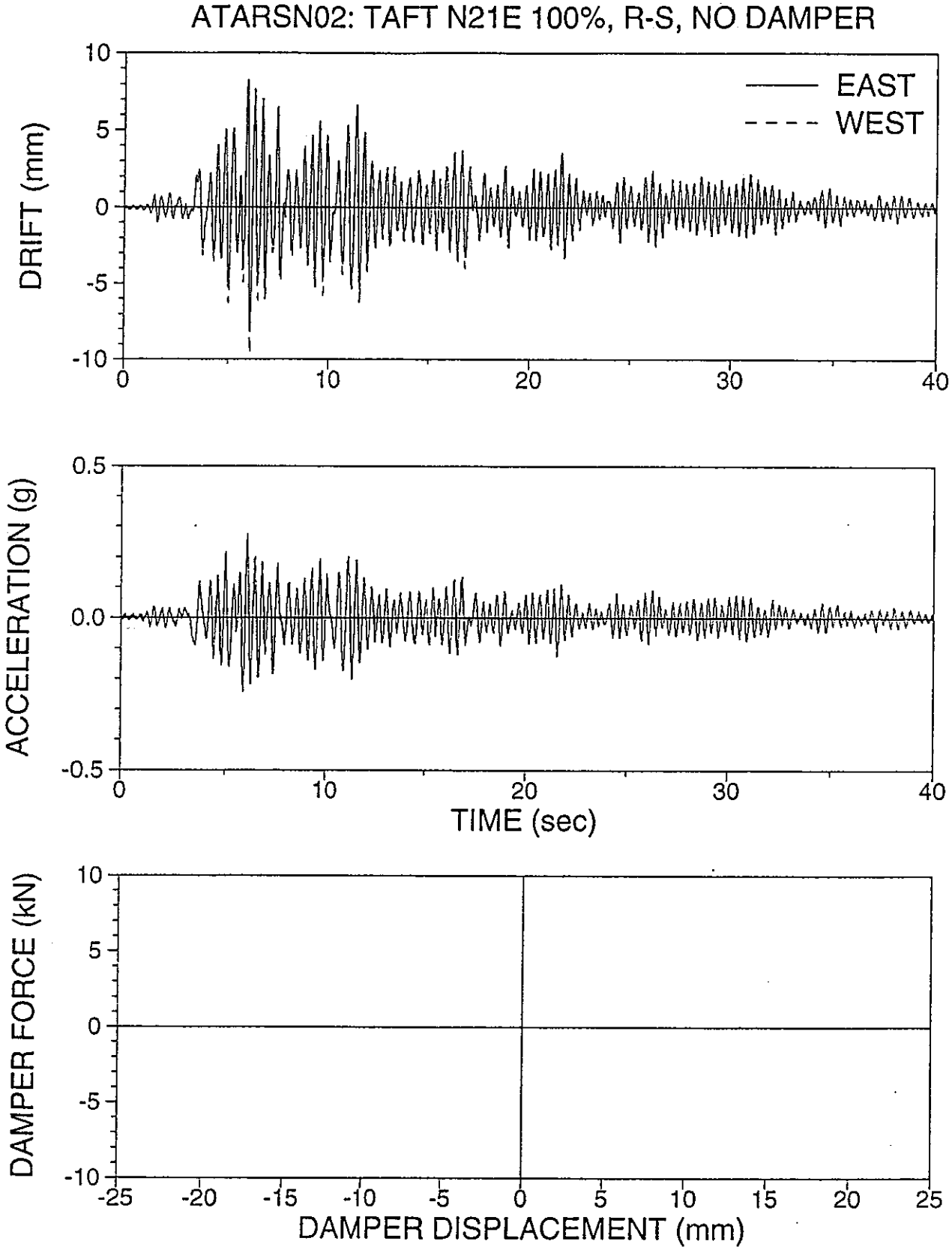
ATARSN02: TAFT N21E 100%, R-S, NO DAMPER
EAST
WEST
DRIFT (mm)
10
5
0
-5
-10
0
10
20
30
40
ACCELERATION (g)
0.5
0.0
-0.5
TIME (sec)
DAMPER FORCE (kN)
-25
-20
-15
-10
-5
0
5
10
15
20
25
DAMPER DISPLACEMENT (mm)

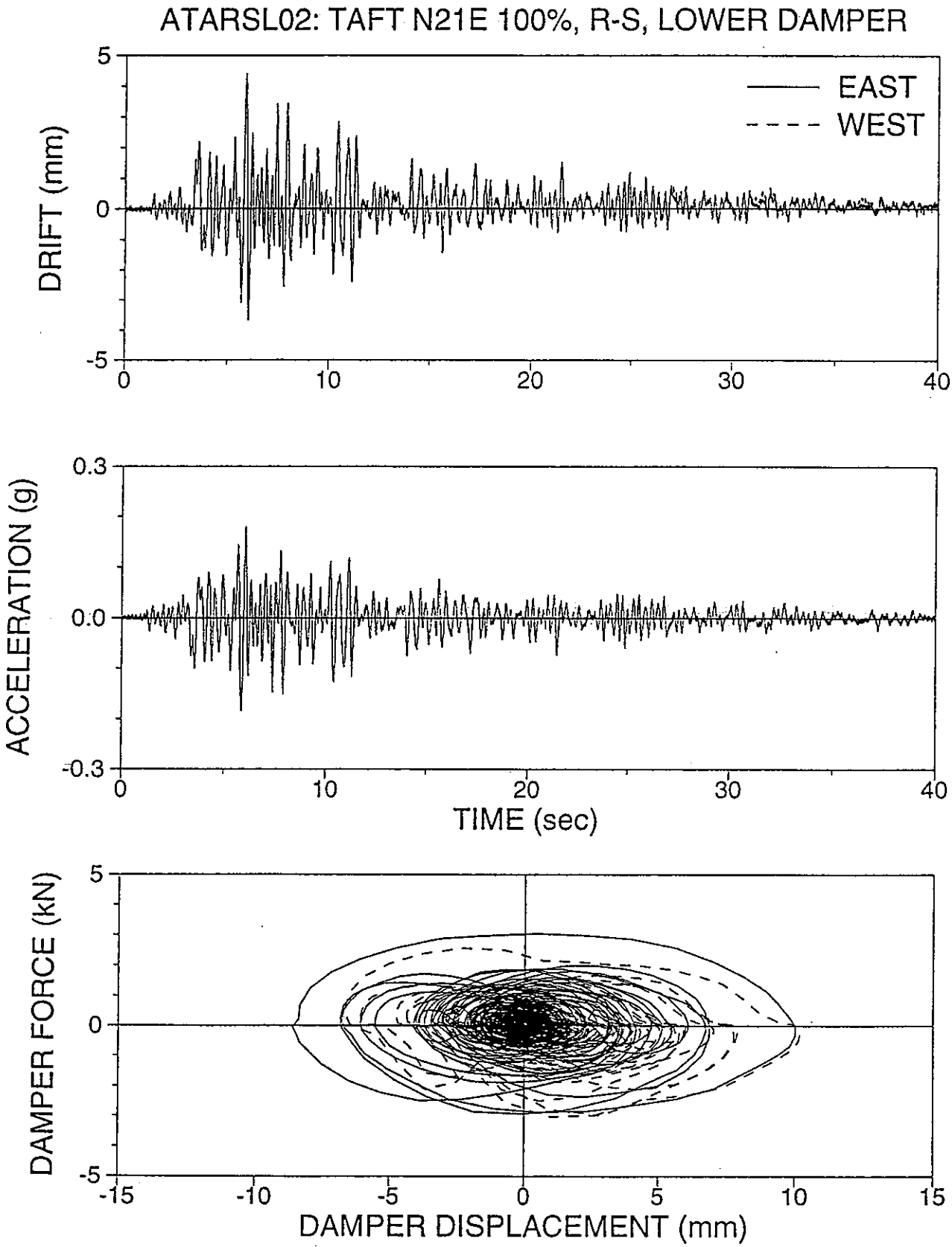
ATARSL02: TAFT N21E 100%, R-S, LOWER DAMPER
EAST
WEST
DRIFT (mm)
5
0
-5
0
10
20
30
40
ACCELERATION (g)
0.3
0.0
-0.3
TIME (sec)
DAMPER FORCE (kN)
5
0
-5
-15
-10
-5
0
5
10
15
DAMPER DISPLACEMENT (mm)

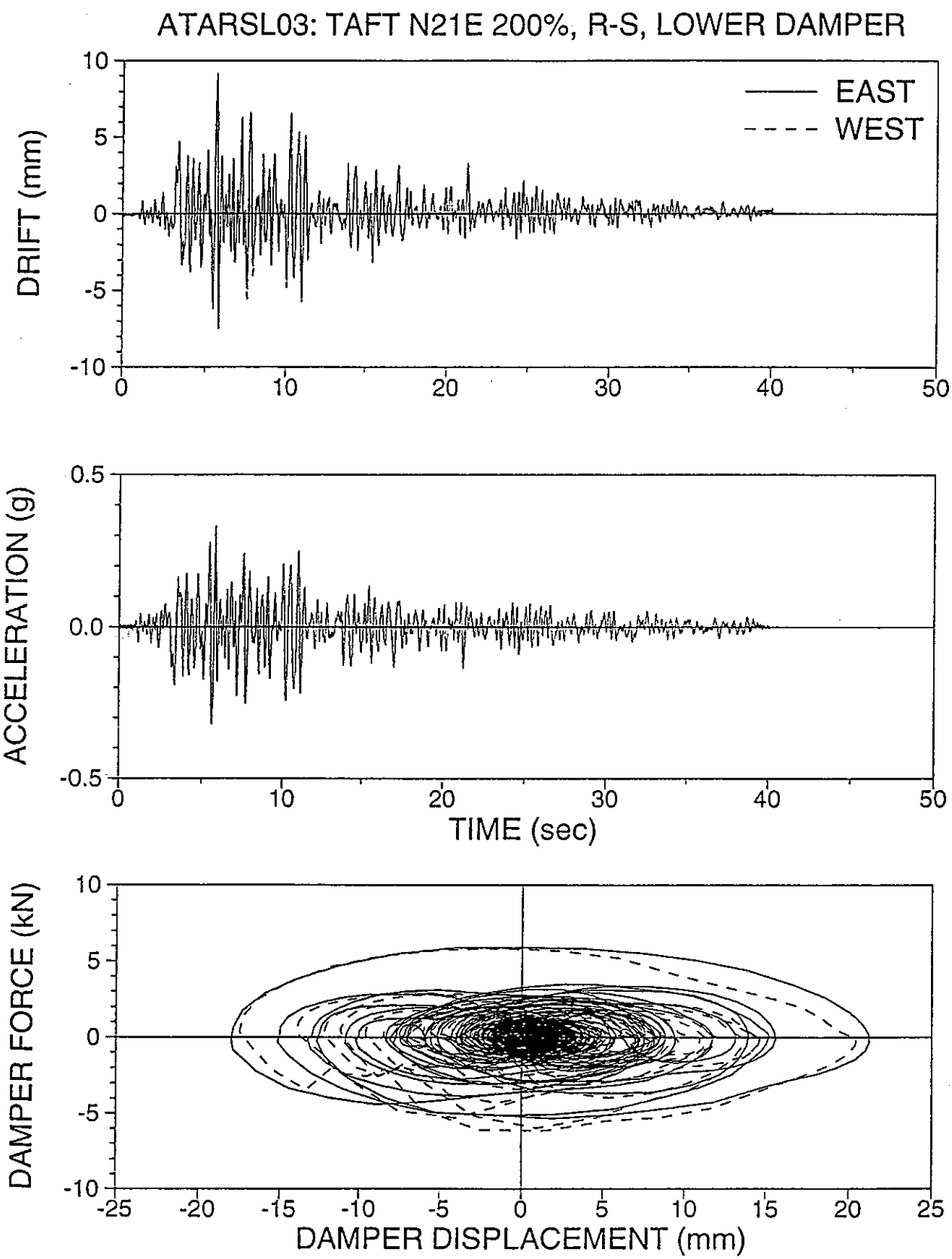
ATARSL03: TAFT N21E 200%, R-S, LOWER DAMPER
EAST
WEST
DRIFT (mm)
ACCELERATION (g)
TIME (sec)
DAMPER FORCE (kN)
DAMPER DISPLACEMENT (mm)

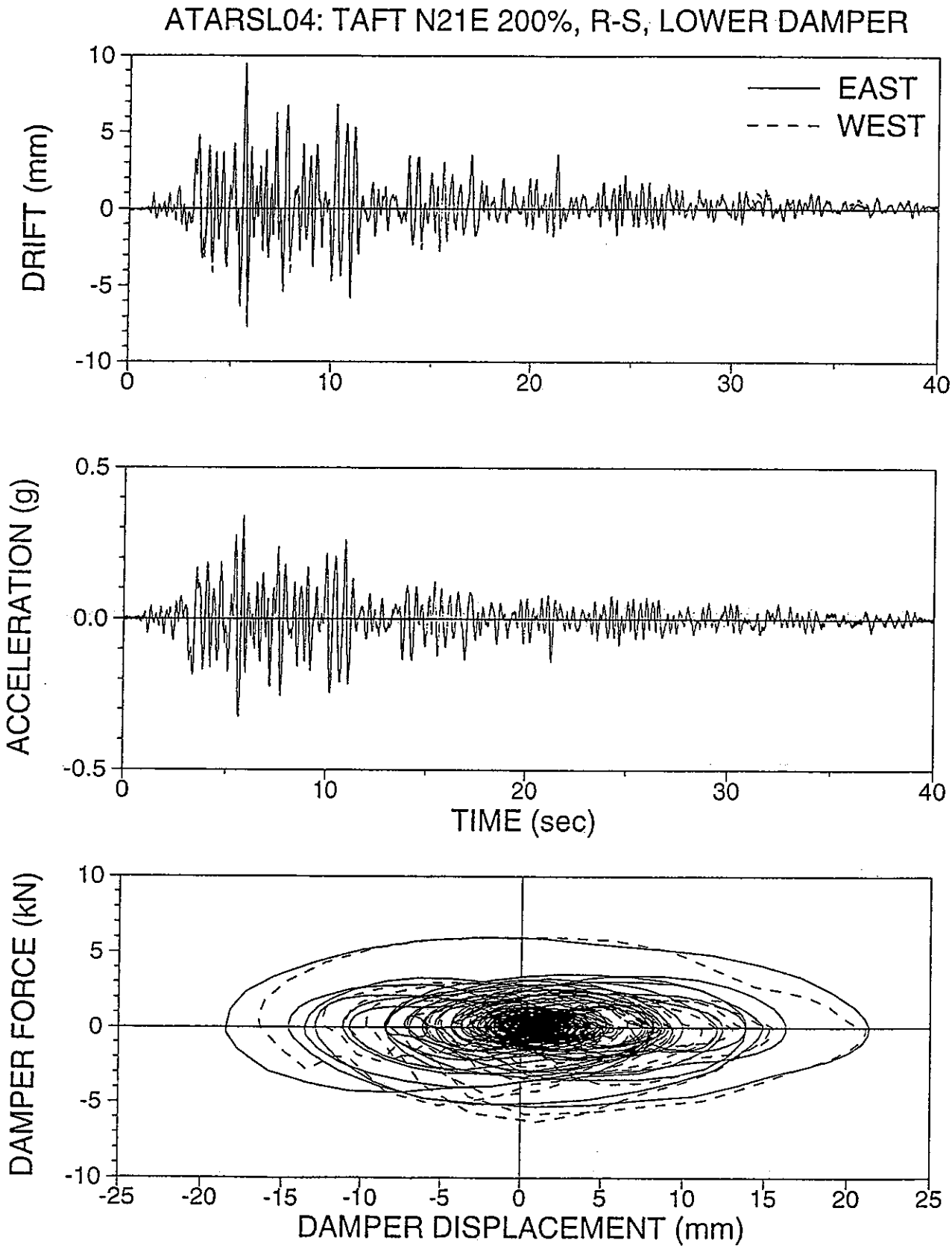
ATARSL04: TAFT N21E 200%, R-S, LOWER DAMPER
EAST
WEST
DRIFT (mm)
10
5
0
-5
-10
0
10
20
30
40
ACCELERATION (g)
0.5
0.0
-0.5
TIME (sec)
DAMPER FORCE (kN)
-25
-20
-15
-10
-5
0
5
10
15
20
25
DAMPER DISPLACEMENT (mm)

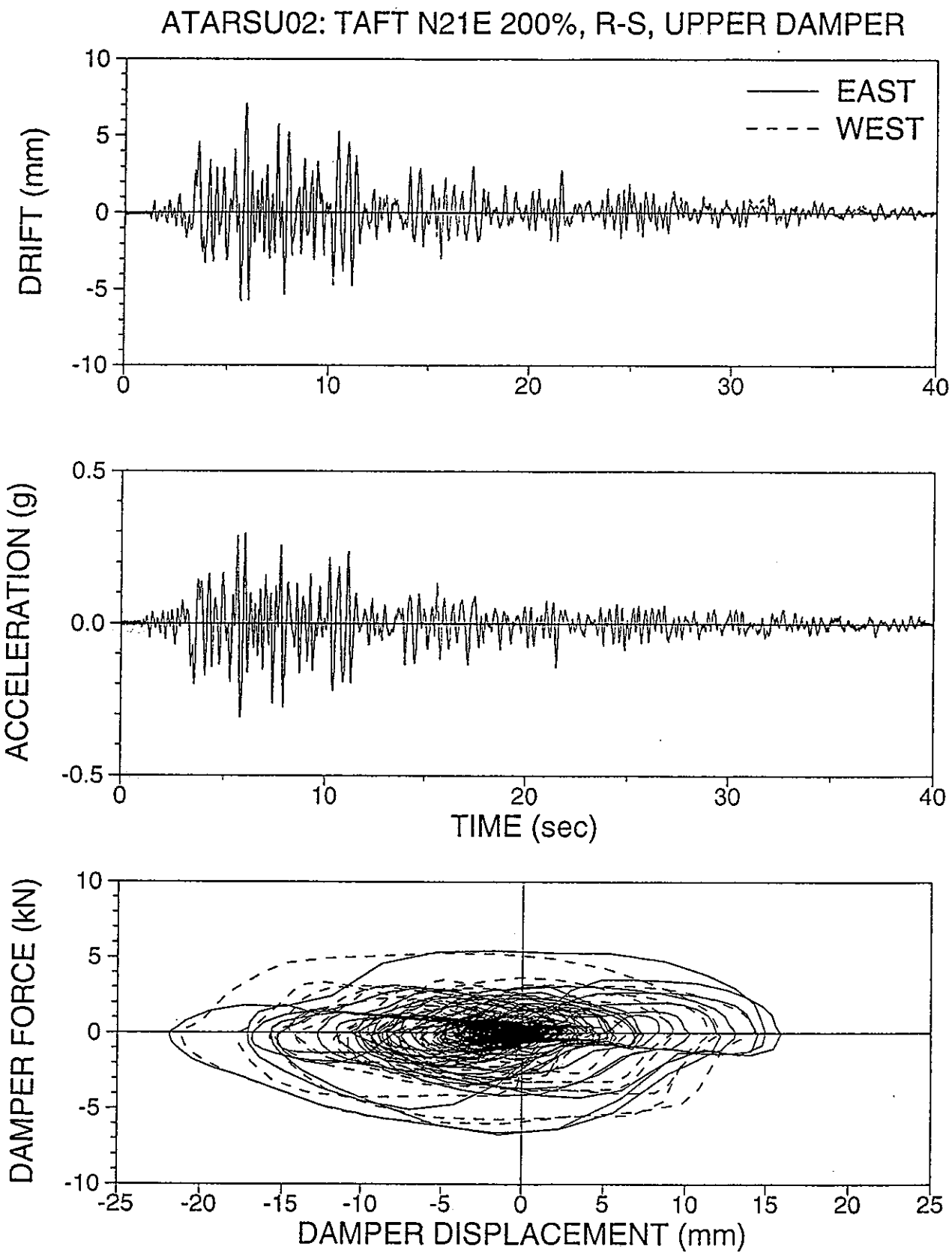
ATARSU02: TAFT N21E 200%, R-S, UPPER DAMPER
EAST
WEST
DRIFT (mm)
10
5
0
-5
-10
0
10
20
30
40
ACCELERATION (g)
0.5
0.0
-0.5
TIME (sec)
DAMPER FORCE (kN)
-25
-20
-15
-10
-5
15
20
25
DAMPER DISPLACEMENT (mm)

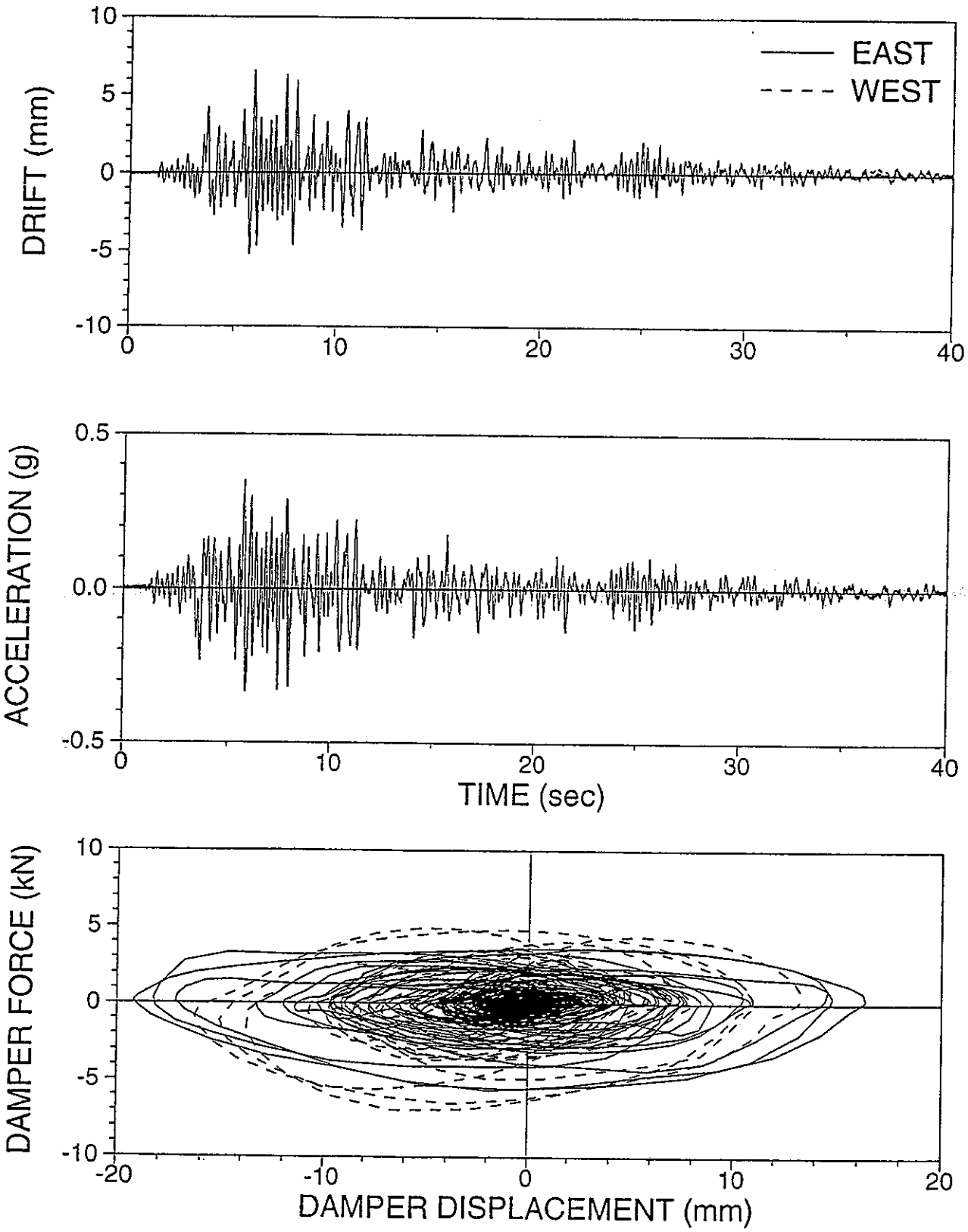
ATARRSU1: TAFT N21E 200%, R-R R-S, UPPER DAMPER
EAST
WEST
DRIFT (mm)
10
5
0
-5
-10
0
10
20
30
40
ACCELERATION (g)
0.5
0.0
-0.5
TIME (sec)
DAMPER FORCE (kN)
-20
-10
DAMPER DISPLACEMENT (mm)

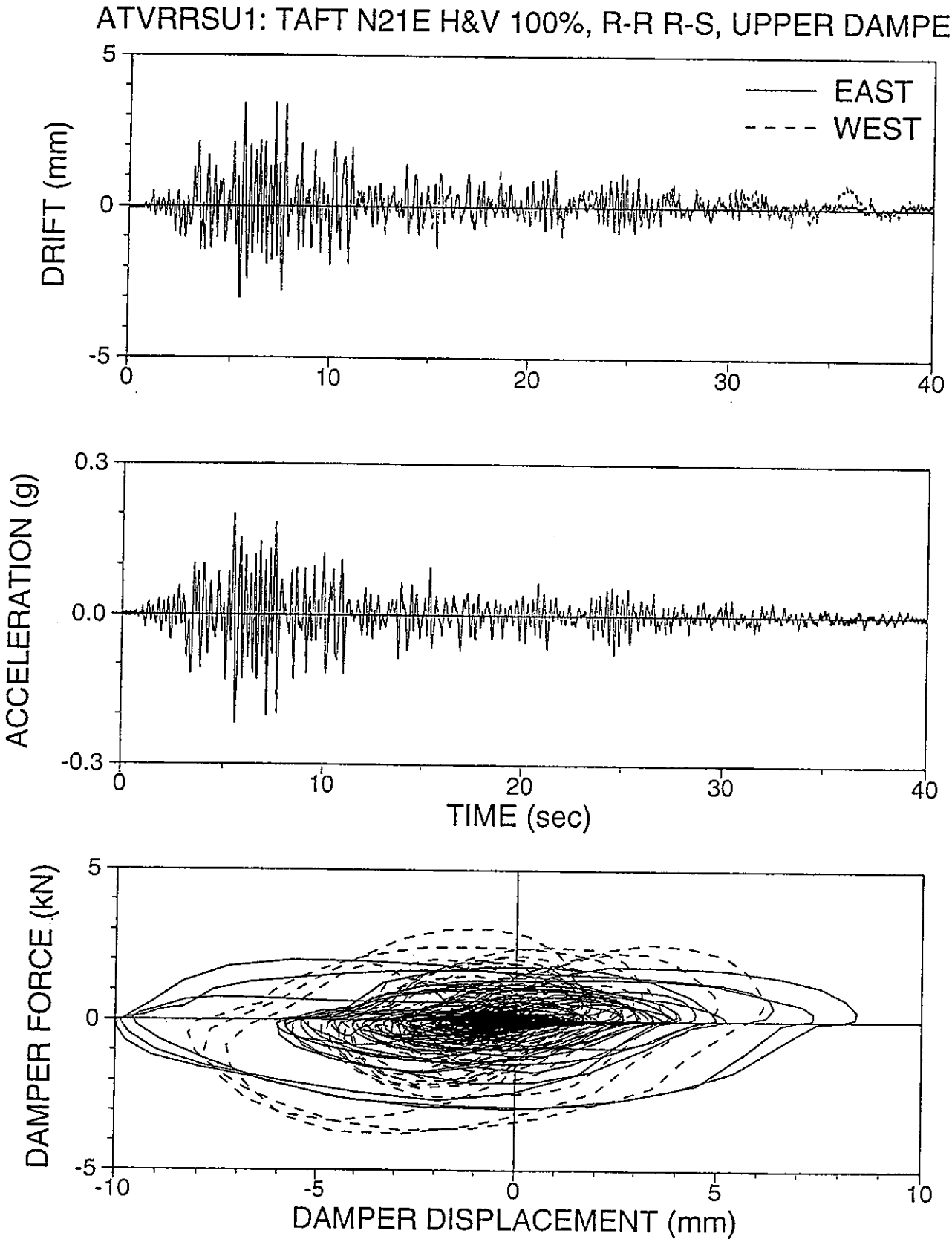
ATVRRSU1: TAFT N21E H&V 100%, R-R R-S, UPPER DAMPER
EAST
WEST
DRIFT (mm)
5
0
-5
0
10
20
30
40
ACCELERATION (g)
0.3
0.0
-0.3
TIME (sec)
DAMPER FORCE (kN)
-10
-5
5
10
DAMPER DISPLACEMENT (mm)

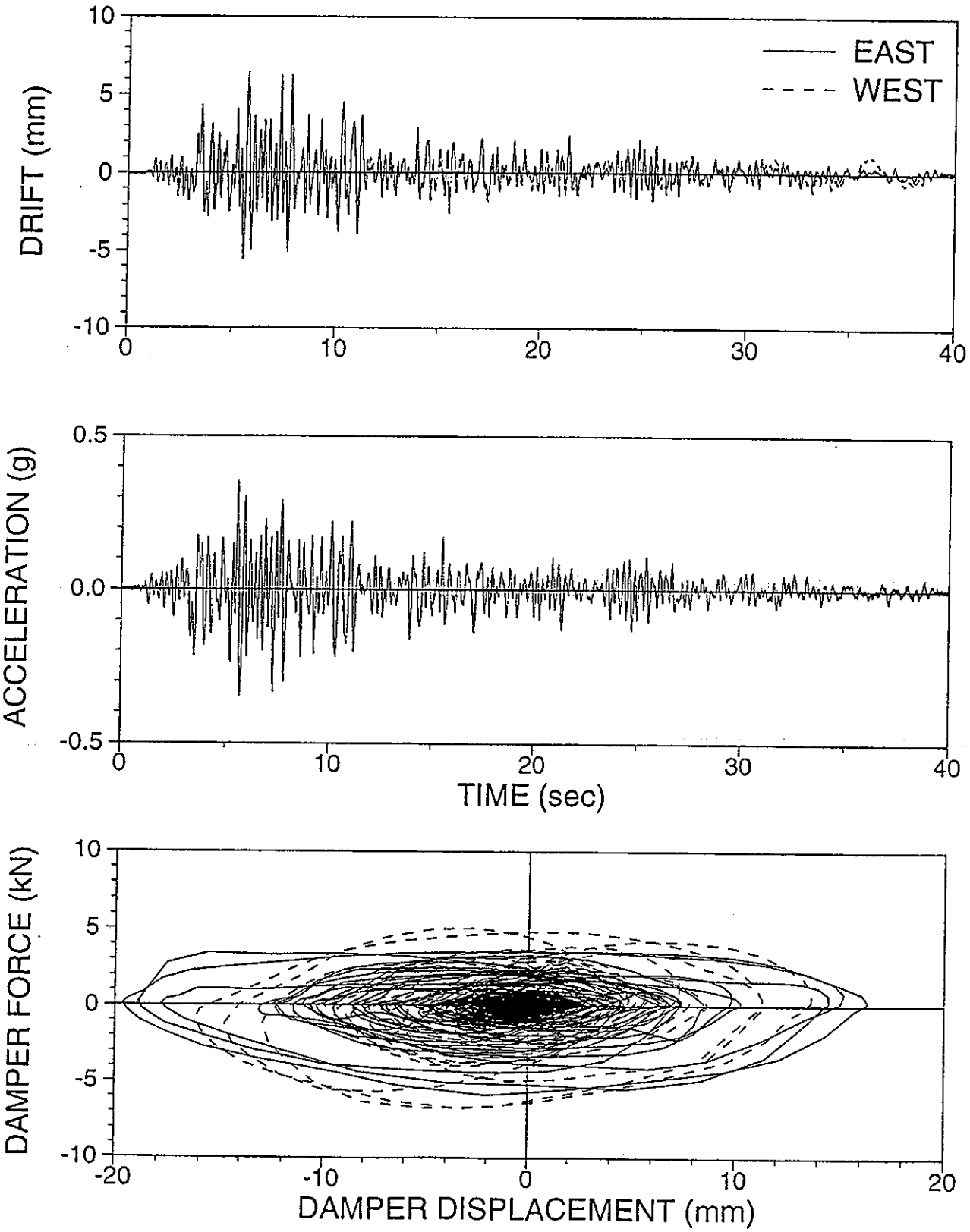
ATVRRSU2: TAFT N21E H&V 200%, R-R R-S, UPPER DAMPER
EAST
WEST
DRIFT (mm)
10
5
0
-5
-10
0
10
20
30
40
ACCELERATION (g)
0.5
0.0
-0.5
TIME (sec)
DAMPER FORCE (kN)
-20
-10
DAMPER DISPLACEMENT (mm)

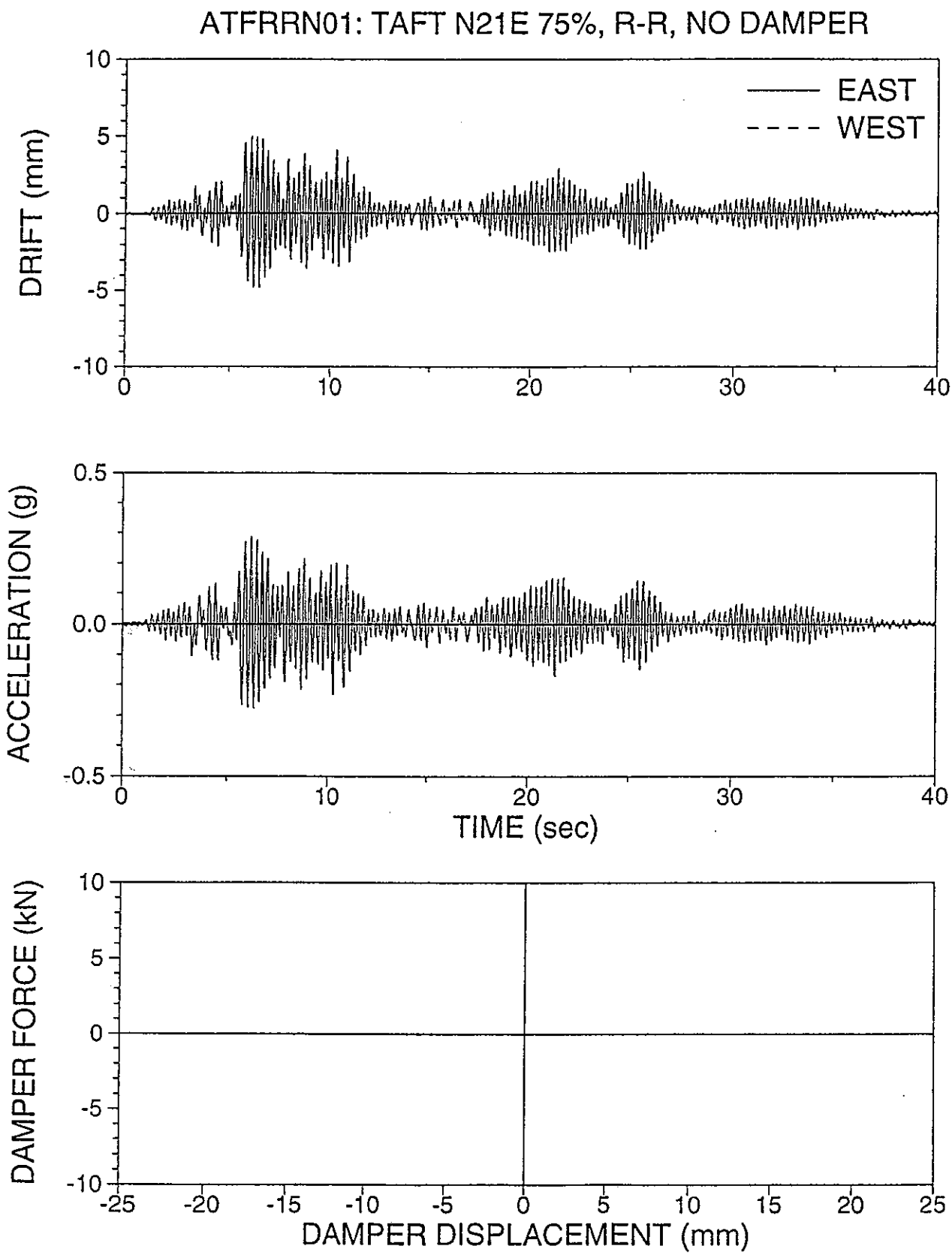
ATFRRN01: TAFT N21E 75%, R-R, NO DAMPER
EAST
WEST
DRIFT (mm)
10
5
0
-5
-10
0
10
20
30
40
ACCELERATION (g)
0.5
0.0
-0.5
TIME (sec)
DAMPER FORCE (kN)
-25
-20
-15
-10
-5
0
5
10
15
20
25
DAMPER DISPLACEMENT (mm)

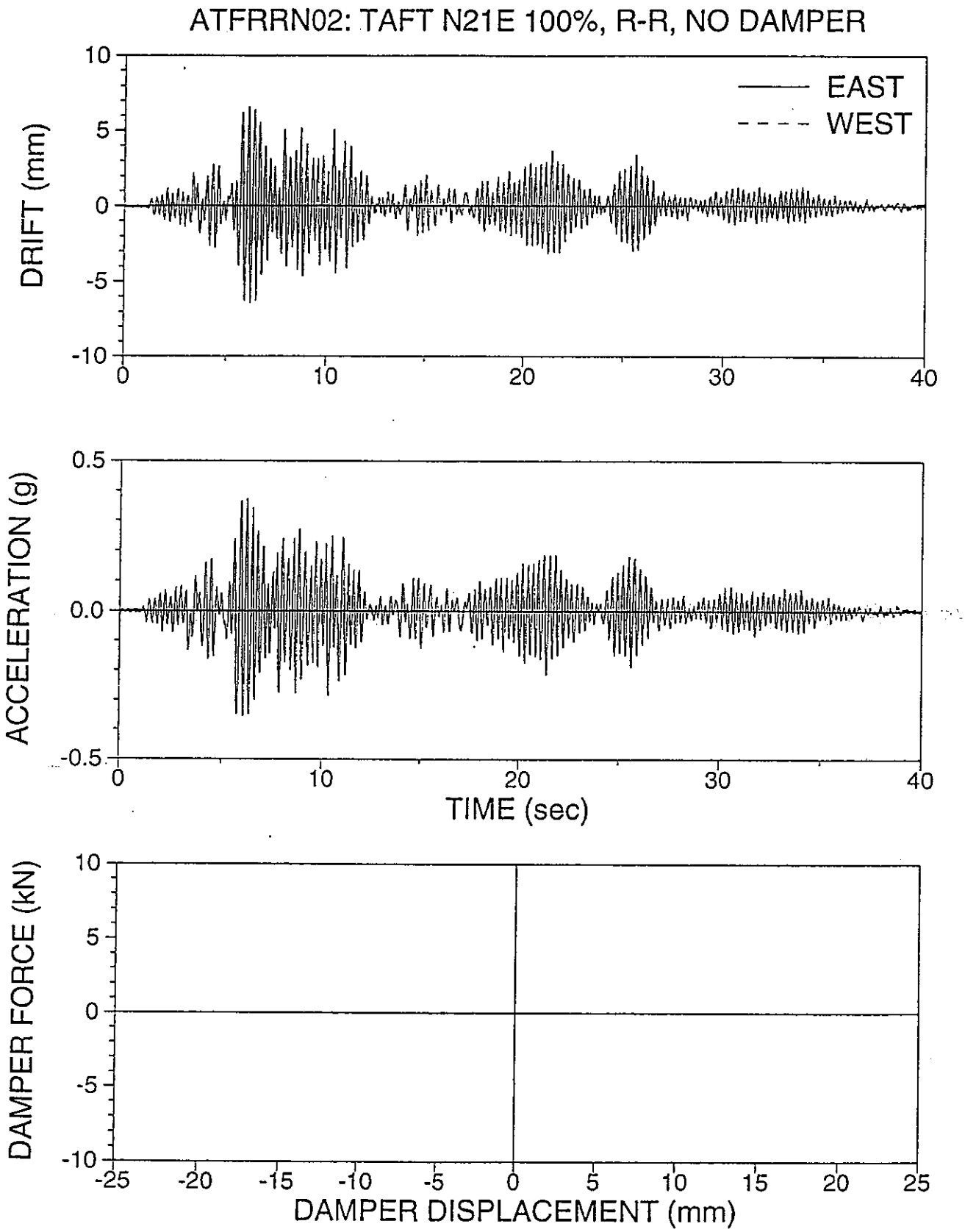
ATFRRN02: TAFT N21E 100%, R-R, NO DAMPER
EAST
WEST
DRIFT (mm)
10
5
0
-5
-10
0
10
20
30
40
ACCELERATION (g)
0.5
0.0
-0.5
TIME (sec)
DAMPER FORCE (kN)
-25
-20
-15
-10
-5
5
15
25
DAMPER DISPLACEMENT (mm)

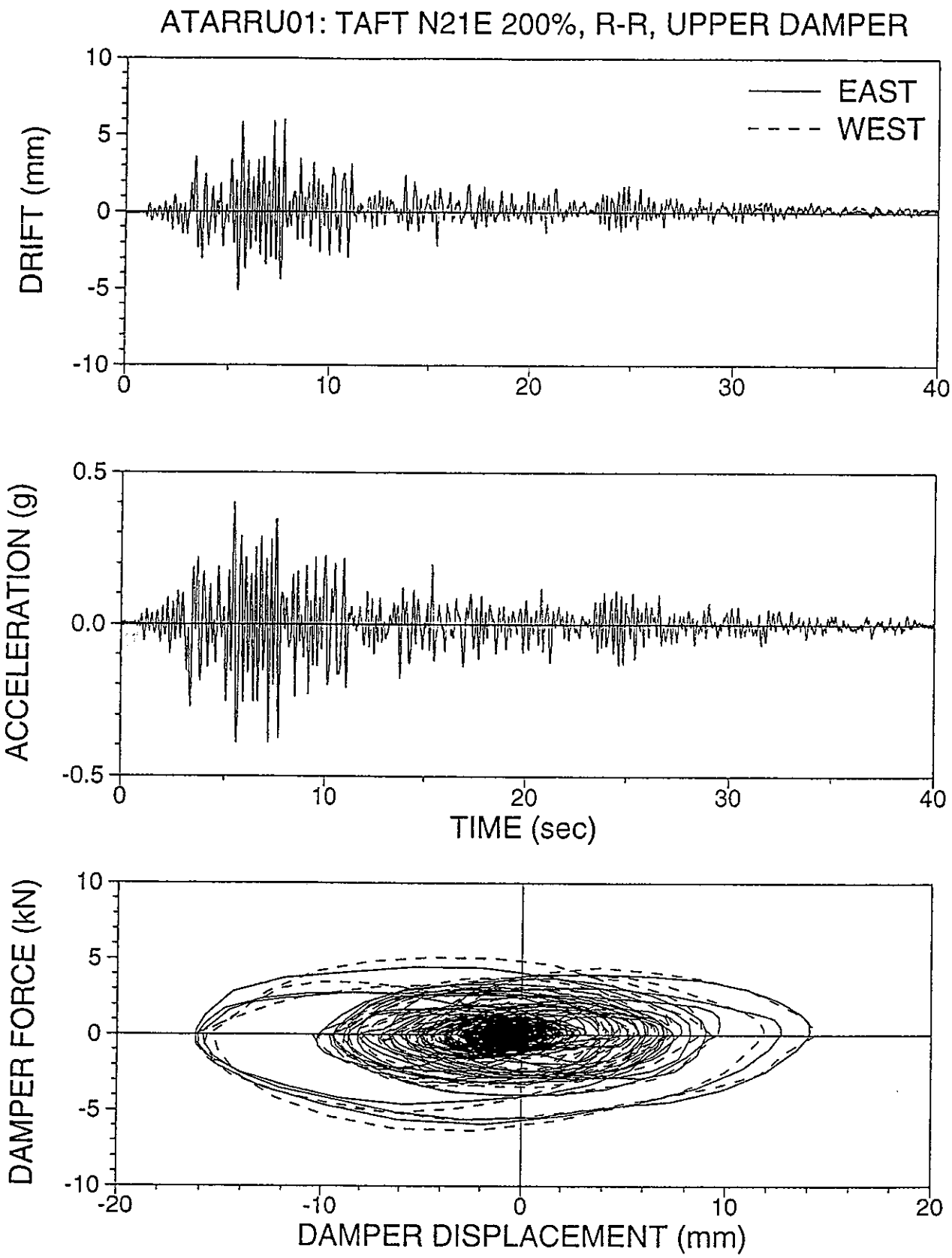
ATARRU01: TAFT N21E 200%, R-R, UPPER DAMPER
EAST
WEST
DRIFT (mm)
10
5
0
-5
-10
0
10
20
30
40
ACCELERATION (g)
0.5
0.0
-0.5
TIME (sec)
DAMPER FORCE (kN)
-20
-10
DAMPER DISPLACEMENT (mm)

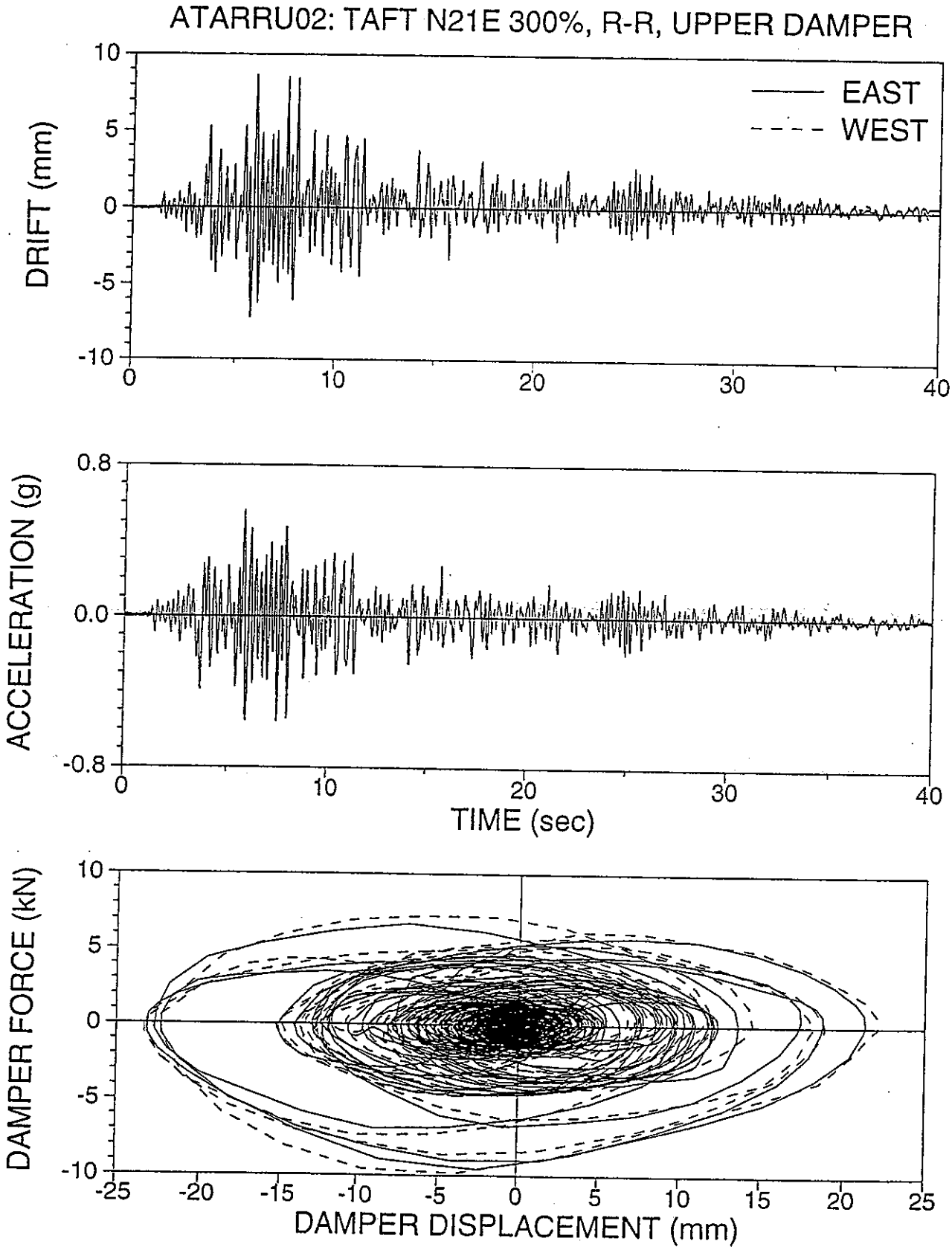
ATARRU02: TAFT N21E 300%, R-R, UPPER DAMPER
EAST
WEST
DRIFT (mm)
10
5
0
-5
-10
0
10
20
30
40
ACCELERATION (g)
0.8
0.0
-0.8
TIME (sec)
DAMPER FORCE (kN)
DAMPER DISPLACEMENT (mm)
-25
-20
-15
-10
-5
5
15
25

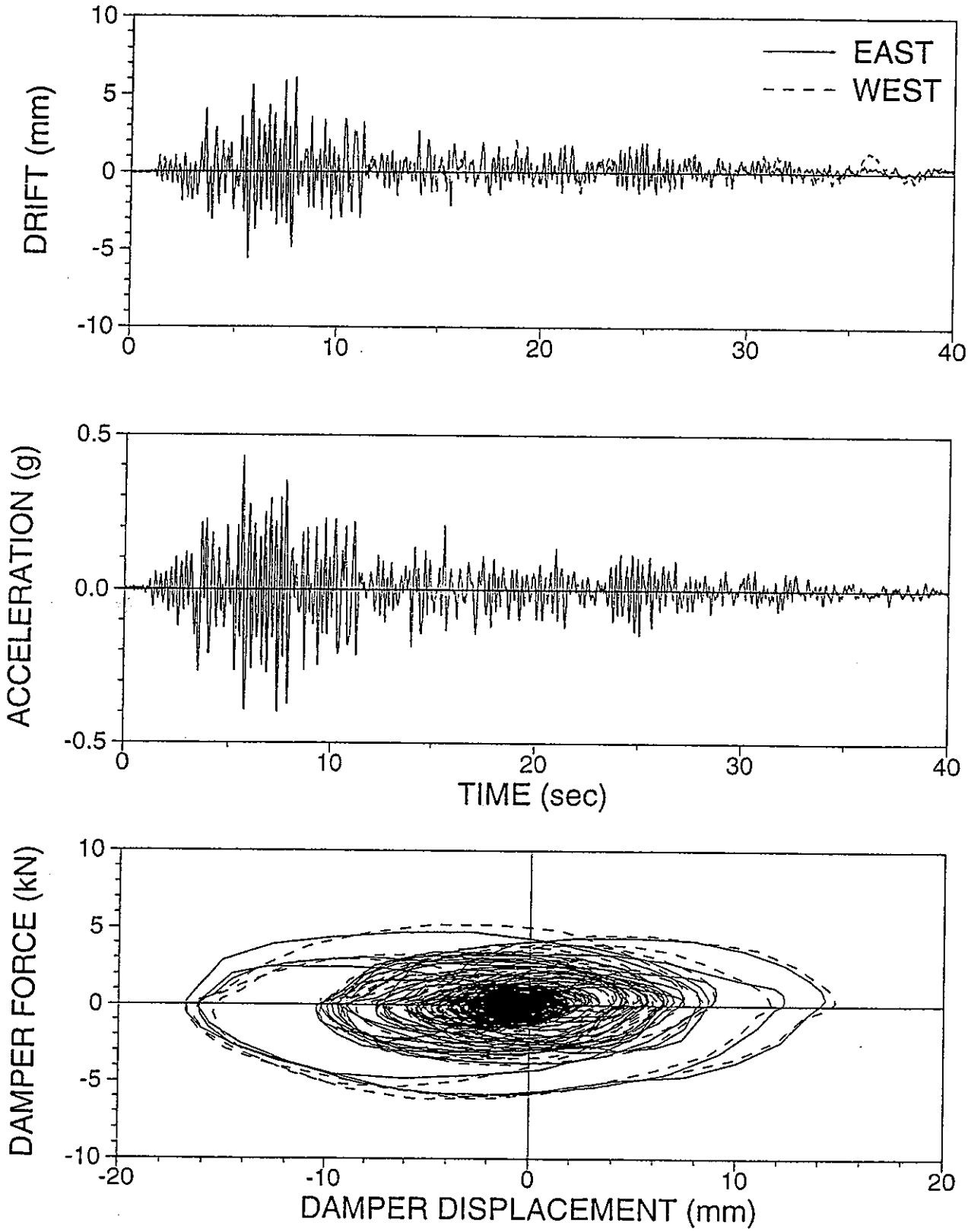
ATVRRU01: TAFT N21E H&V 200%, R-R, UPPER DAMPER
EAST
WEST
DRIFT (mm)
10
5
0
-5
-10
0
10
20
30
40
ACCELERATION (g)
0.5
0.0
-0.5
TIME (sec)
DAMPER FORCE (kN)
-20
-10
DAMPER DISPLACEMENT (mm)

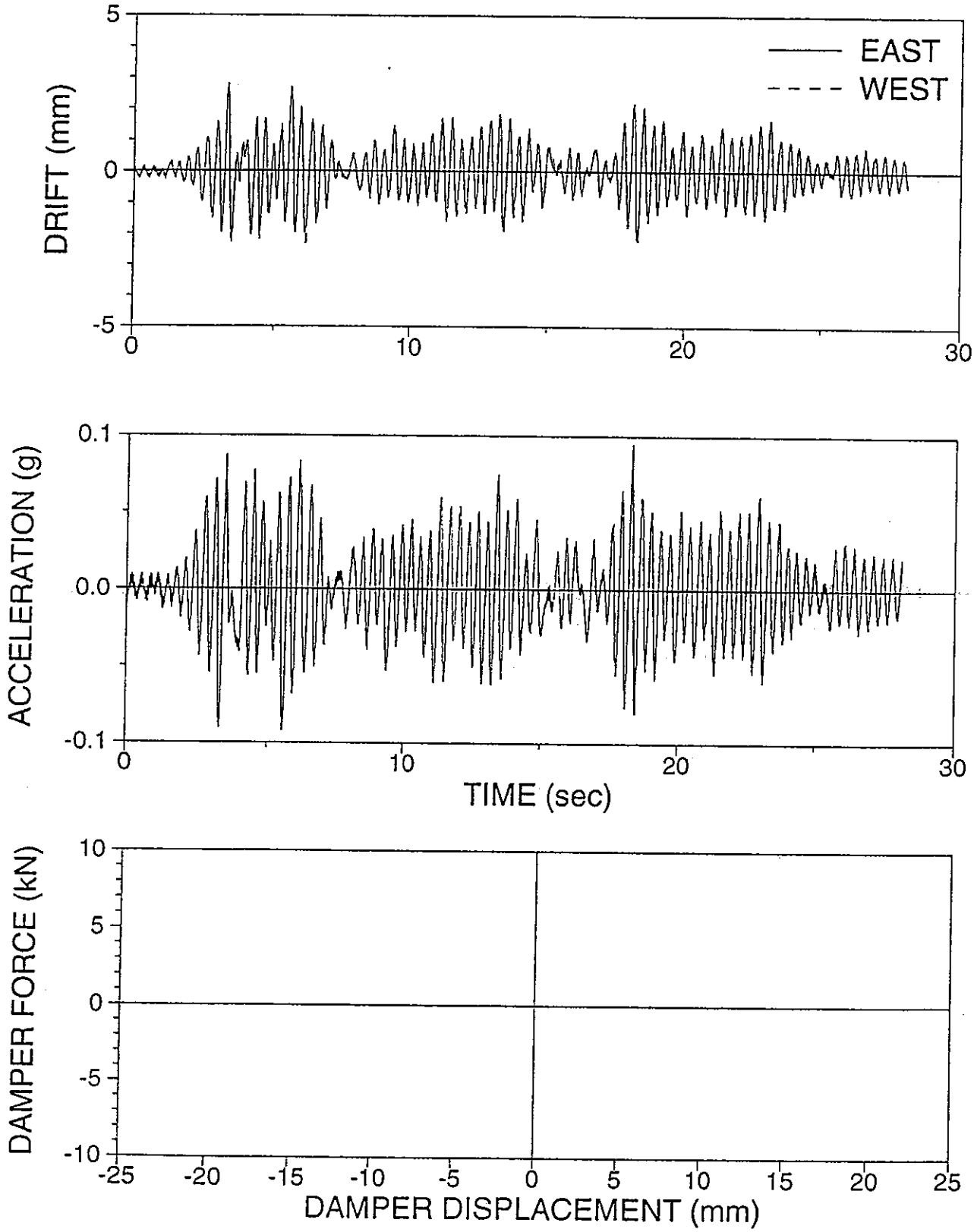
AHARSN01: HACHINOHE NS 25%, R-S, NO DAMPER
EAST
WEST
DRIFT (mm)
5
0
-5
0
10
20
30
ACCELERATION (g)
0.1
0.0
-0.1
TIME (sec)
DAMPER FORCE (kN)
10
5
0
-5
-10
-25
-20
-15
-10
-5
0
5
10
15
20
25
DAMPER DISPLACEMENT (mm)

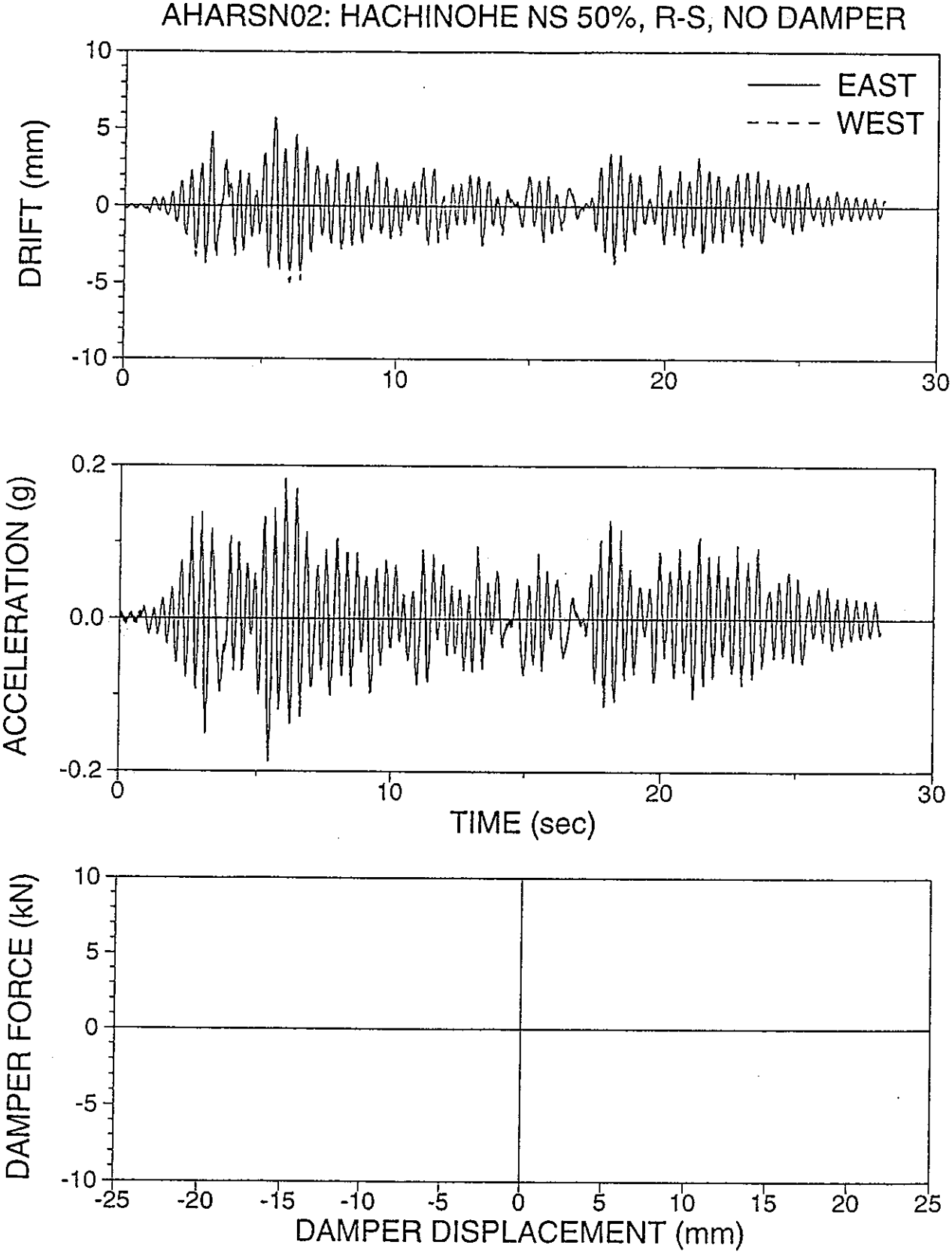
AHARSN02: HACHINOHE NS 50%, R-S, NO DAMPER
EAST
WEST
DRIFT (mm)
10
5
0
-5
-10
0
10
20
30
ACCELERATION (g)
0.2
0.0
-0.2
TIME (sec)
DAMPER FORCE (kN)
-25
-20
-15
-10
-5
0
5
10
15
20
25
DAMPER DISPLACEMENT (mm)

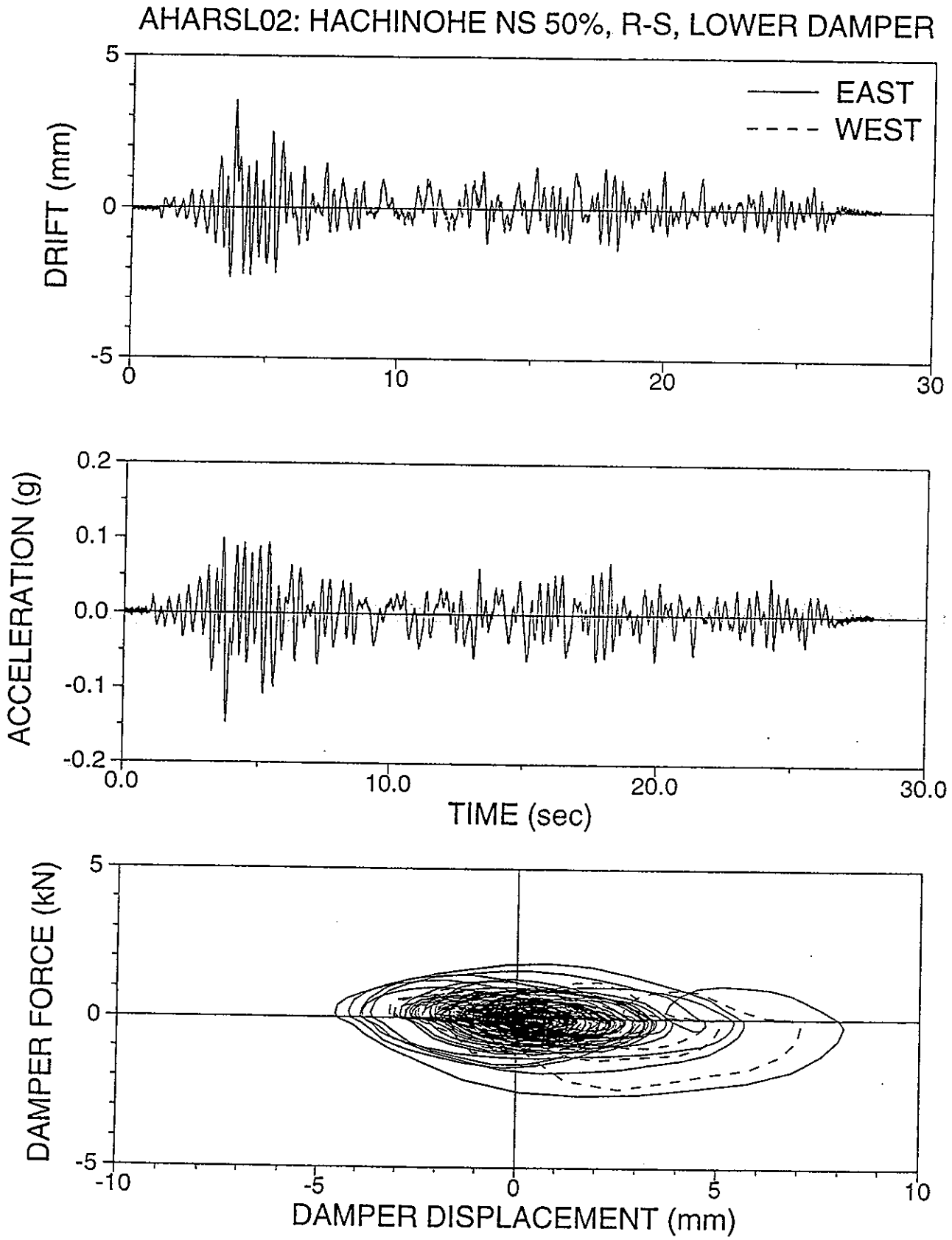
AHARSL02: HACHINOHE NS 50%, R-S, LOWER DAMPER
EAST
WEST
DRIFT (mm)
5
0
-5
0
10
20
30
ACCELERATION (g)
0.2
0.1
0.0
-0.1
-0.2
0.0
10.0
20.0
30.0
TIME (sec)
DAMPER FORCE (kN)
5
0
-5
-10
-5
0
5
10
DAMPER DISPLACEMENT (mm)

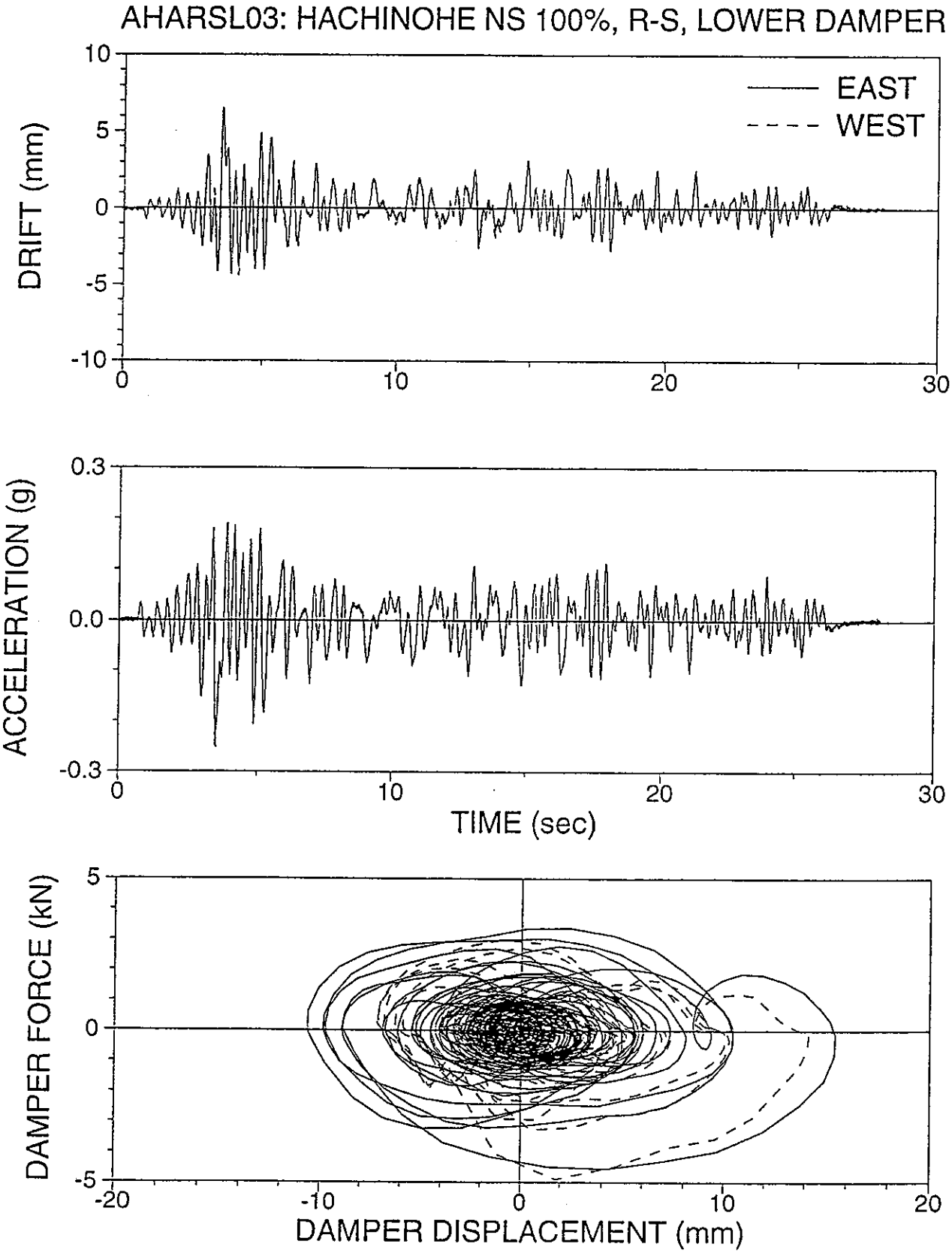
AHARSL03: HACHINOHE NS 100%, R-S, LOWER DAMPER
EAST
WEST
DRIFT (mm)
10
5
0
-5
-10
0
10
20
30
ACCELERATION (g)
0.3
0.0
-0.3
0
10
20
30
TIME (sec)
DAMPER FORCE (kN)
5
0
-5
-20
-10
0
10
20
DAMPER DISPLACEMENT (mm)

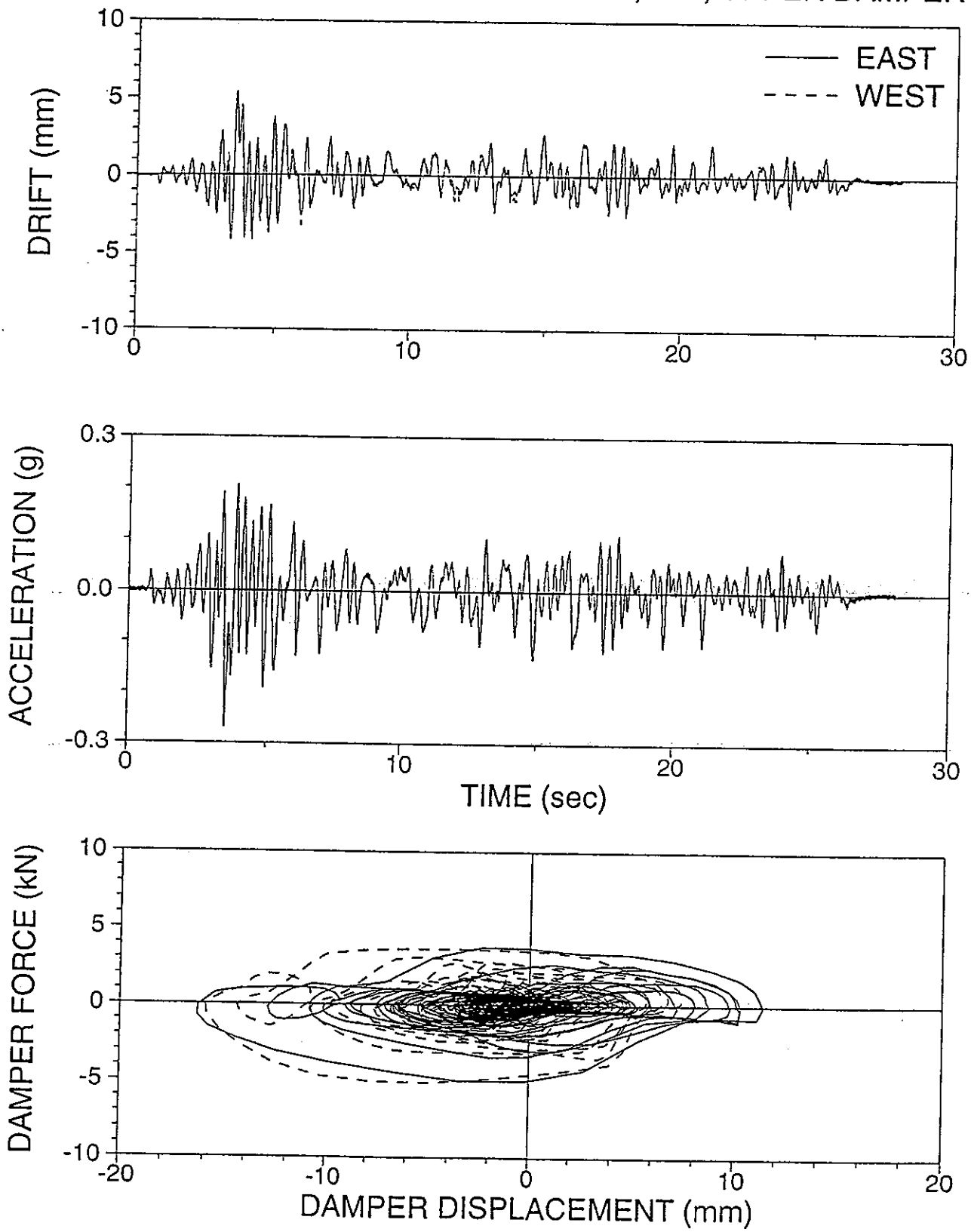
AHARSU01: HACHINOHE NS 100%, R-S, UPPER DAMPER
EAST
WEST
DRIFT (mm)
10
5
0
-5
-10
0
10
20
30
ACCELERATION (g)
0.3
0.0
-0.3
TIME (sec)
DAMPER FORCE (kN)
-20
-10
DAMPER DISPLACEMENT (mm)

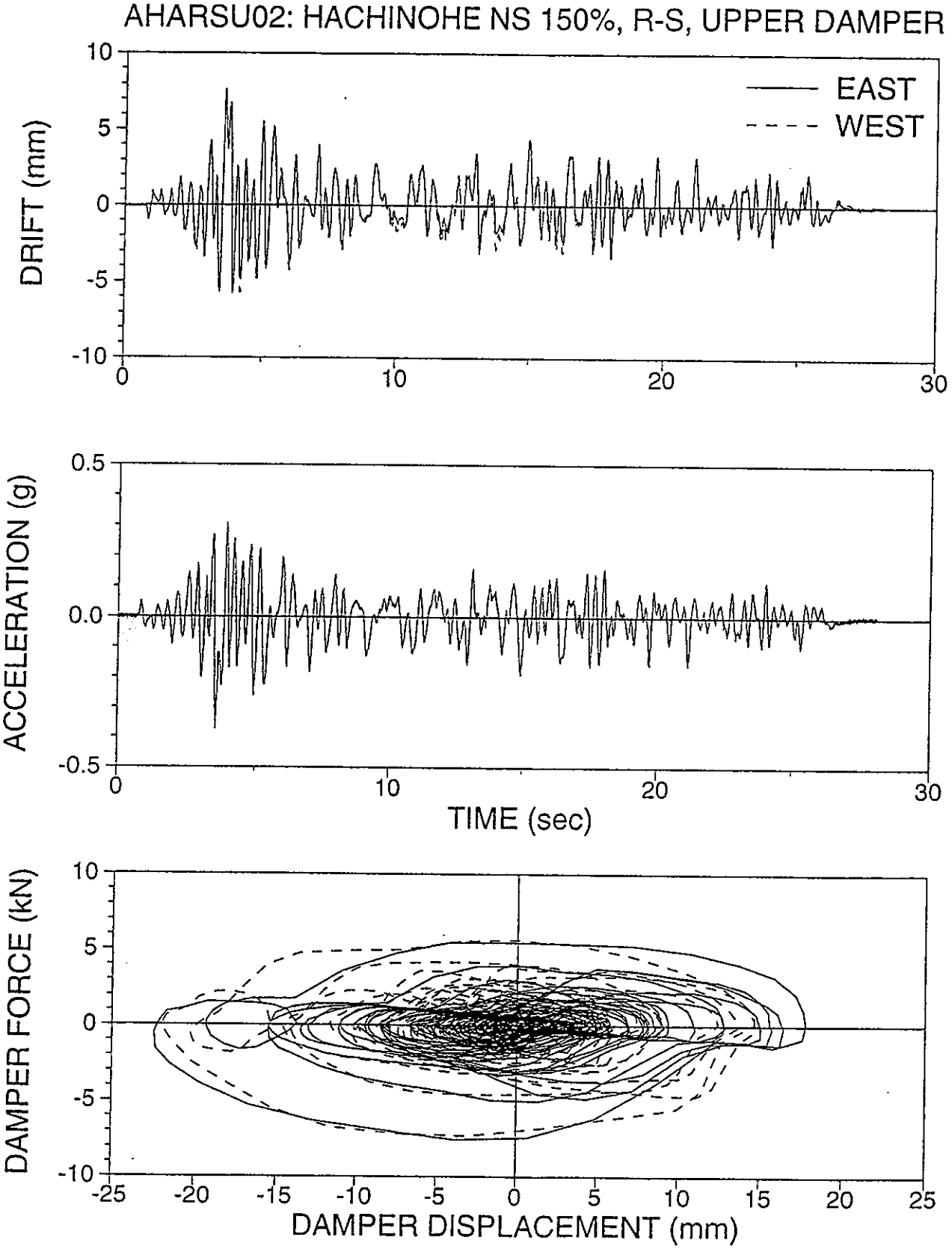
AHARSU02: HACHINOHE NS 150%, R-S, UPPER DAMPER
EAST
WEST
DRIFT (mm)
10
5
0
-5
-10
0
10
20
30
ACCELERATION (g)
0.5
0.0
-0.5
TIME (sec)
DAMPER FORCE (kN)
-25
-20
-15
-10
-5
0
5
10
15
20
25
DAMPER DISPLACEMENT (mm)

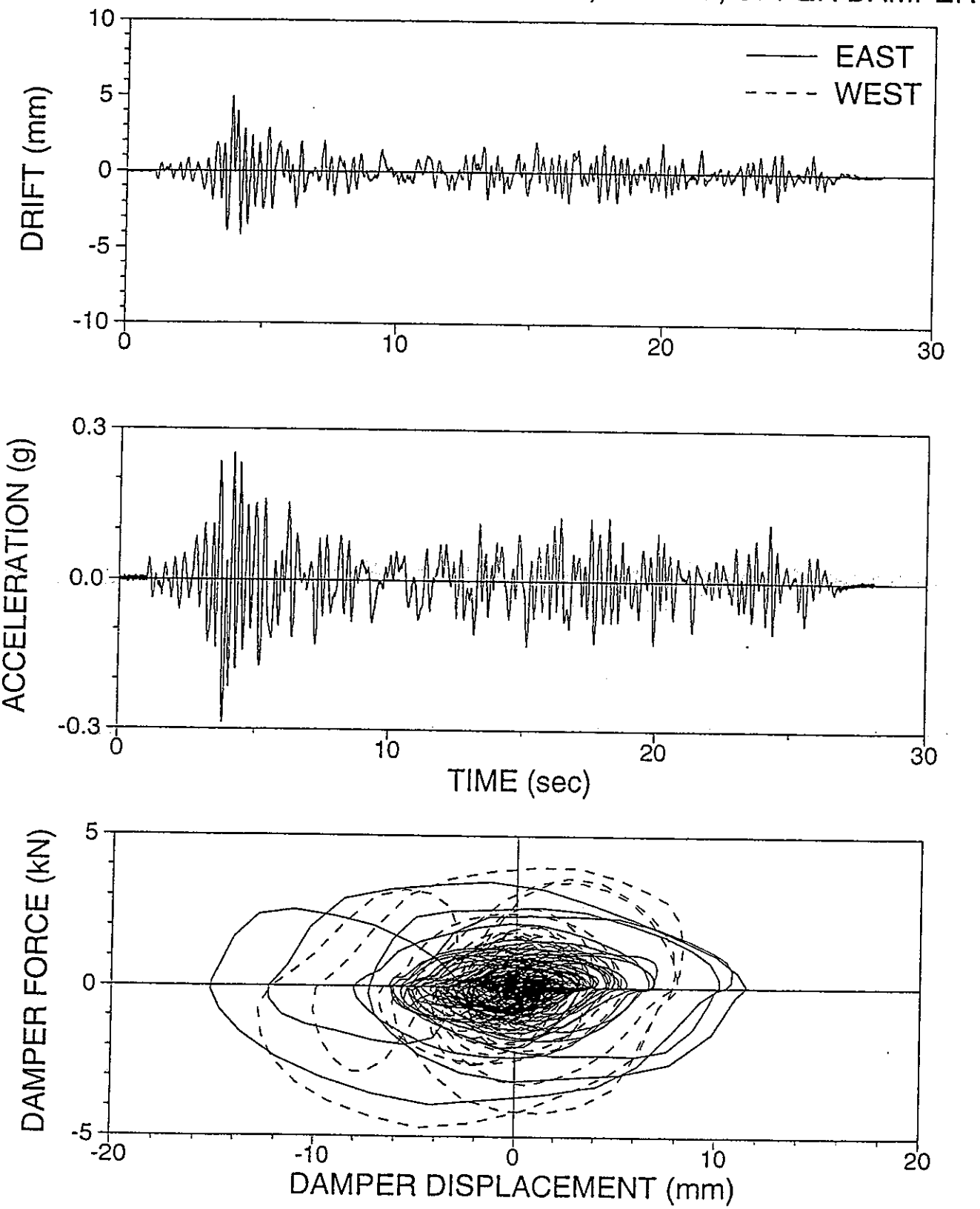
AHARRSU1: HACHINOHE NS 100%, R-R R-S, UPPER DAMPER
DRIFT (mm)
EAST
WEST
ACCELERATION (g)
TIME (sec)
DAMPER FORCE (kN)
DAMPER DISPLACEMENT (mm)

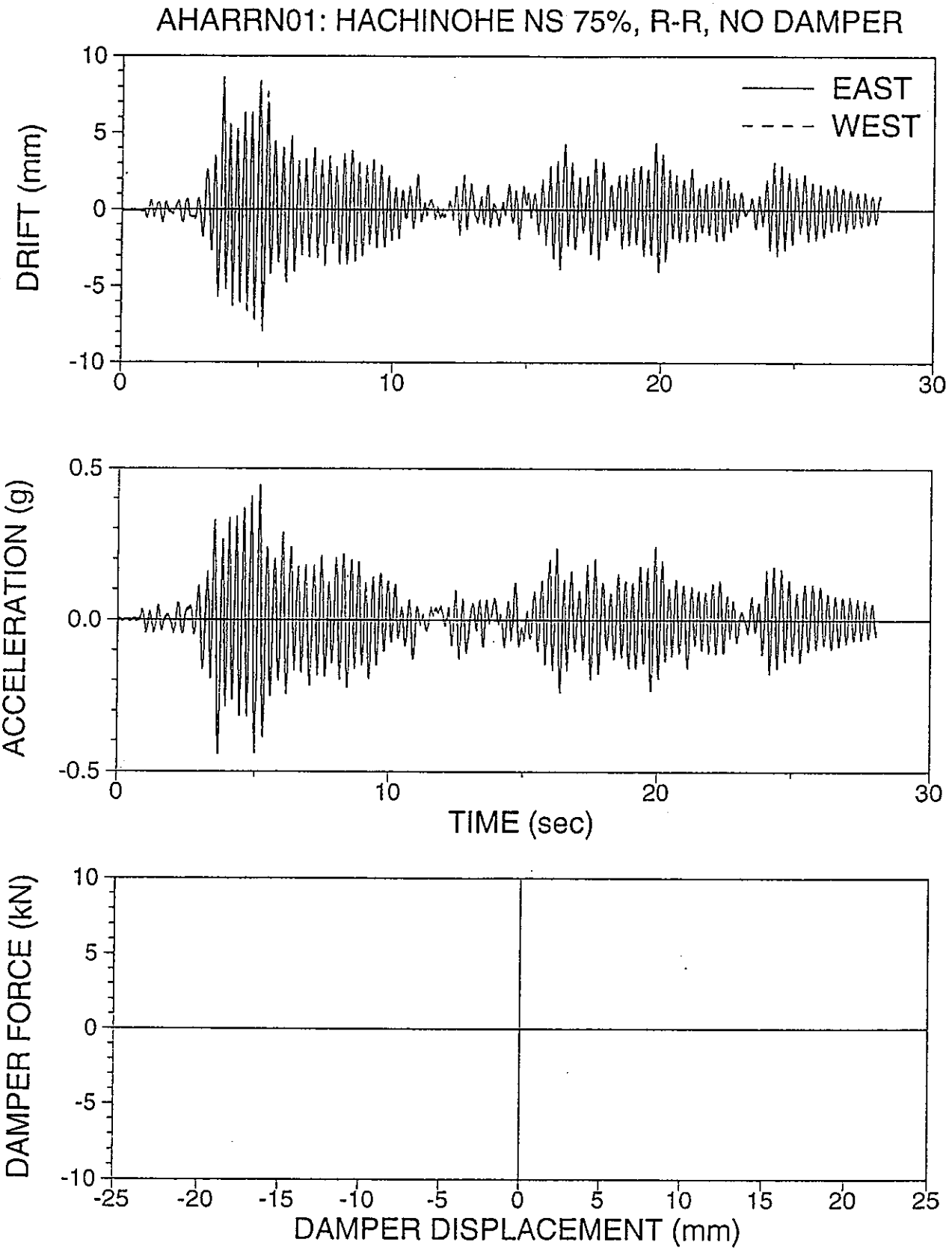
AHARRN01: HACHINOHE NS 75%, R-R, NO DAMPER
EAST
WEST
DRIFT (mm)
10
5
0
-5
-10
0
10
20
30
ACCELERATION (g)
0.5
0.0
-0.5
TIME (sec)
DAMPER FORCE (kN)
-25
-20
-15
-10
-5
0
5
10
15
20
25
DAMPER DISPLACEMENT (mm)

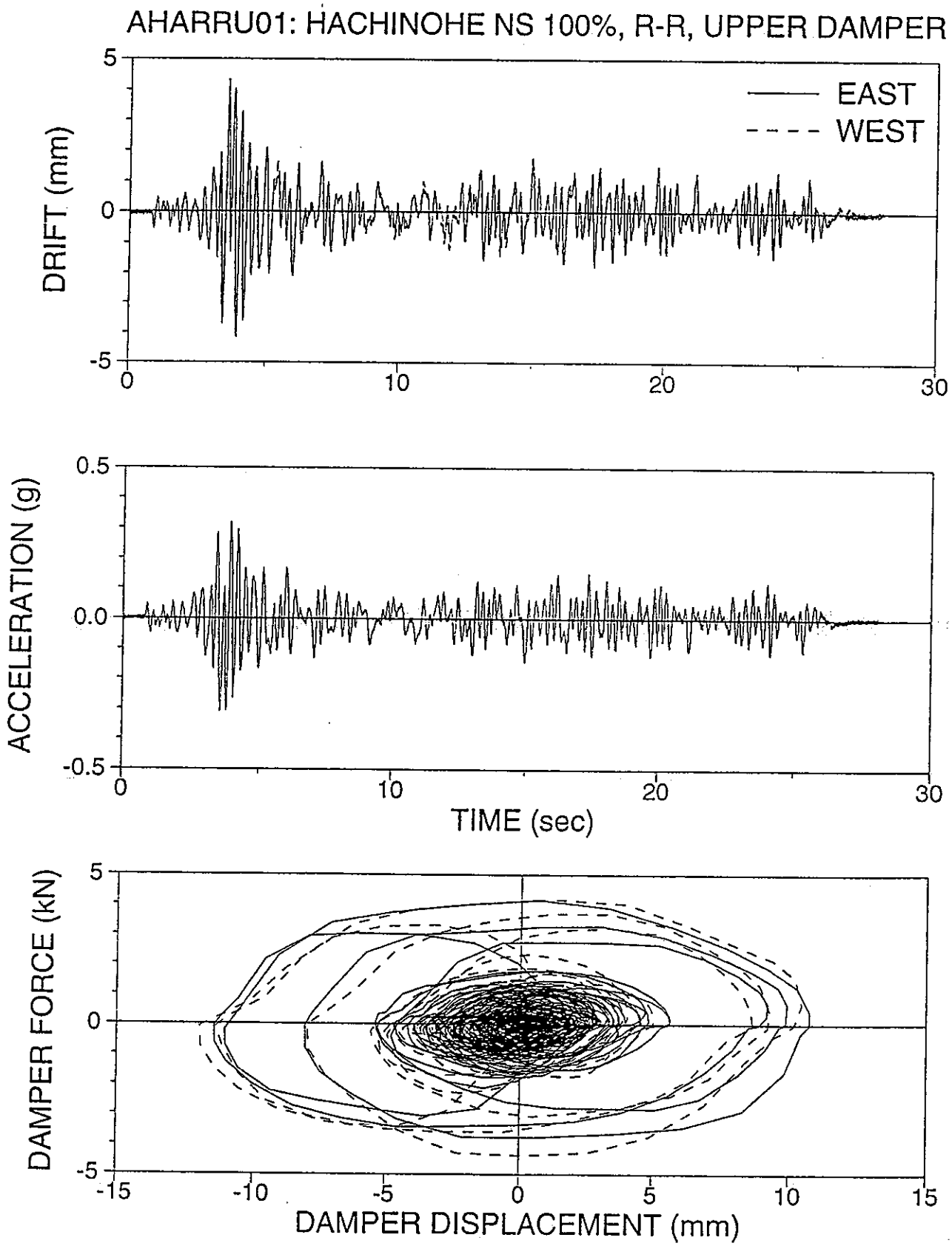
AHARRU01: HACHINOHE NS 100%, R-R, UPPER DAMPER
EAST
WEST
DRIFT (mm)
5
0
-5
0
10
20
30
ACCELERATION (g)
0.5
0.0
-0.5
TIME (sec)
DAMPER FORCE (kN)
-15
-10
-5
5
10
15
DAMPER DISPLACEMENT (mm)

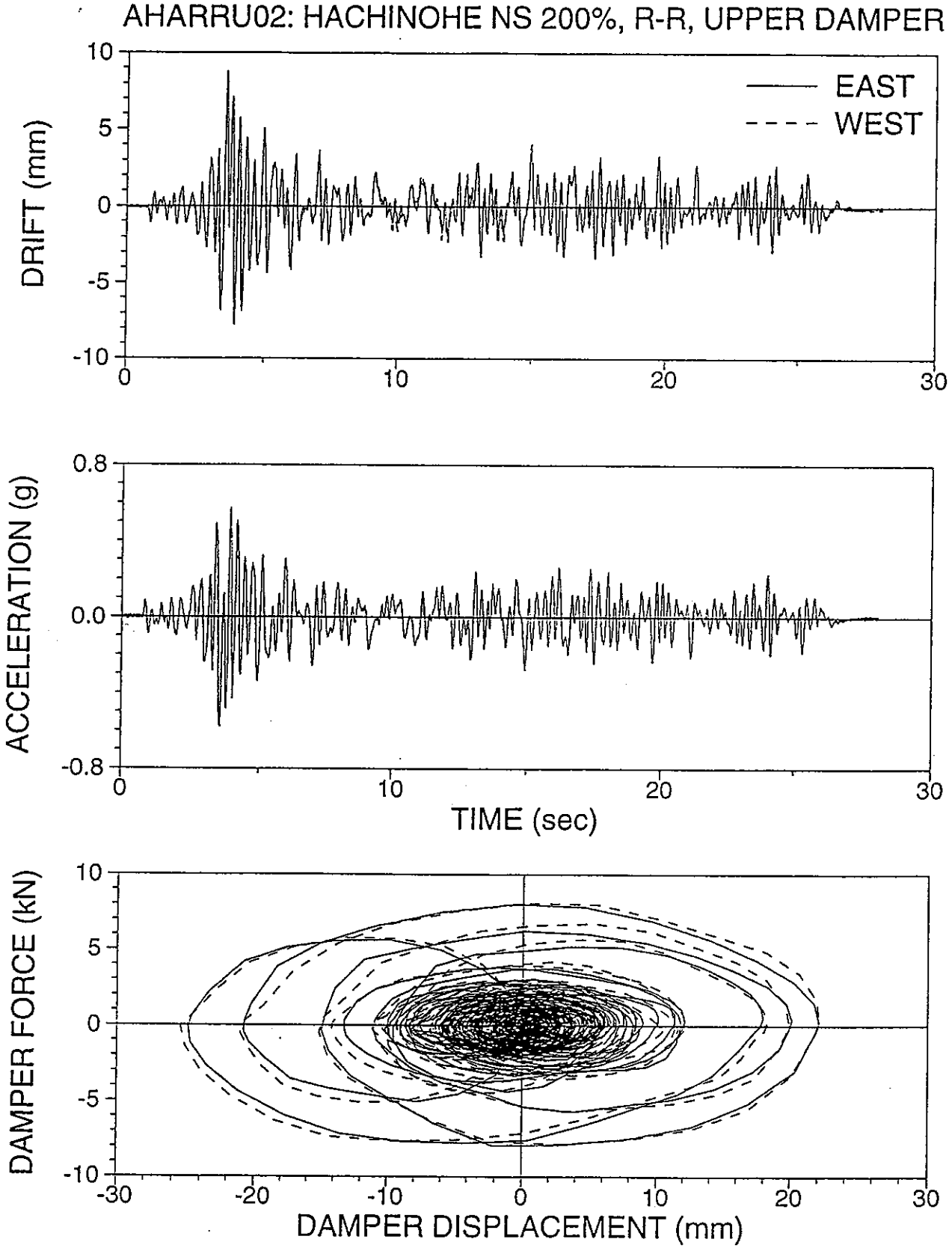
AHARRU02: HACHINOHE NS 200%, R-R, UPPER DAMPER
EAST
WEST
DRIFT (mm)
10
5
0
-5
-10
0
10
20
30
ACCELERATION (g)
0.8
0.0
-0.8
TIME (sec)
DAMPER FORCE (kN)
-30
-20
-10
DAMPER DISPLACEMENT (mm)

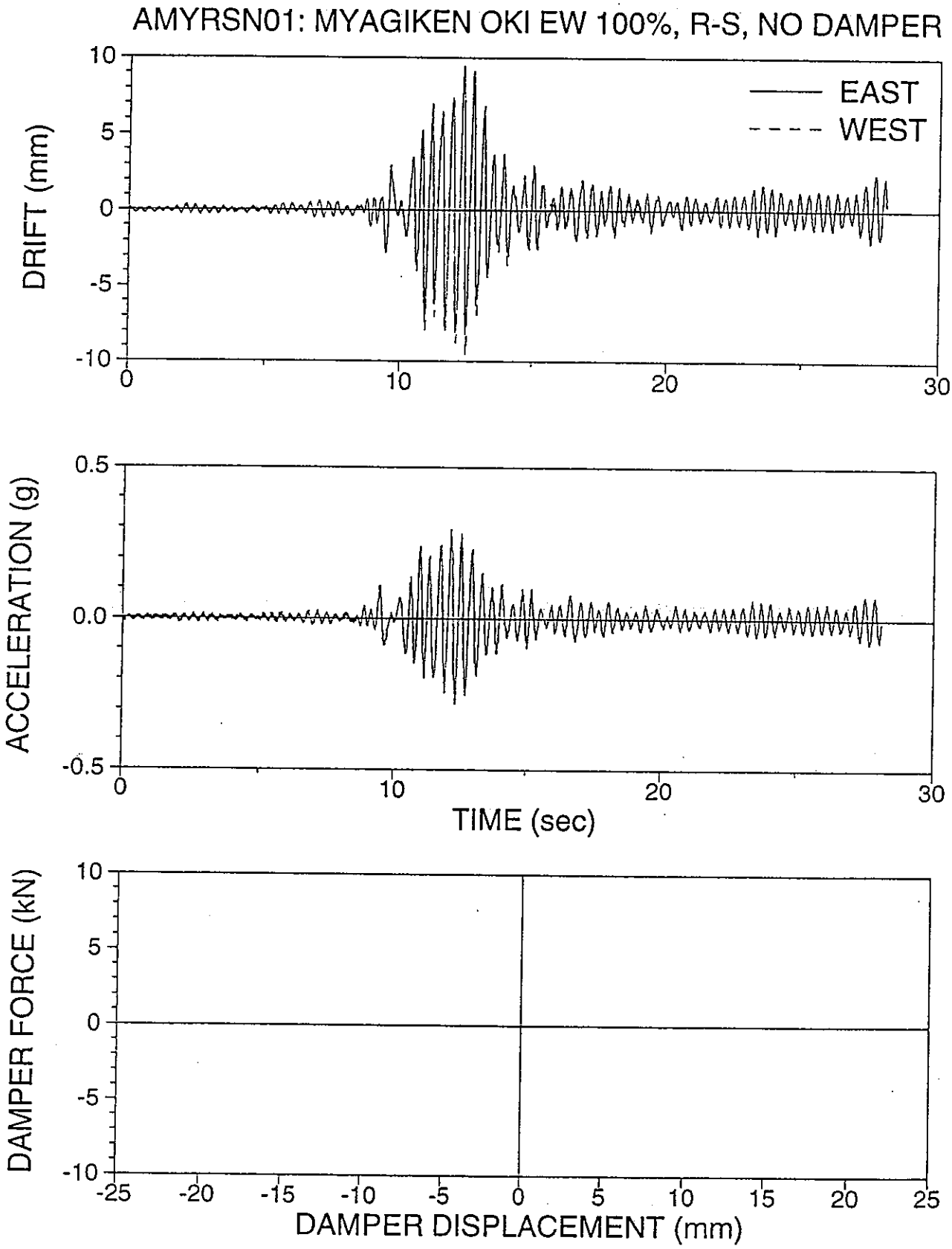
AMYRSN01: MYAGIKEN OKI EW 100%, R-S, NO DAMPER
DRIFT (mm)
EAST
WEST
ACCELERATION (g)
TIME (sec)
DAMPER FORCE (kN)
DAMPER DISPLACEMENT (mm)

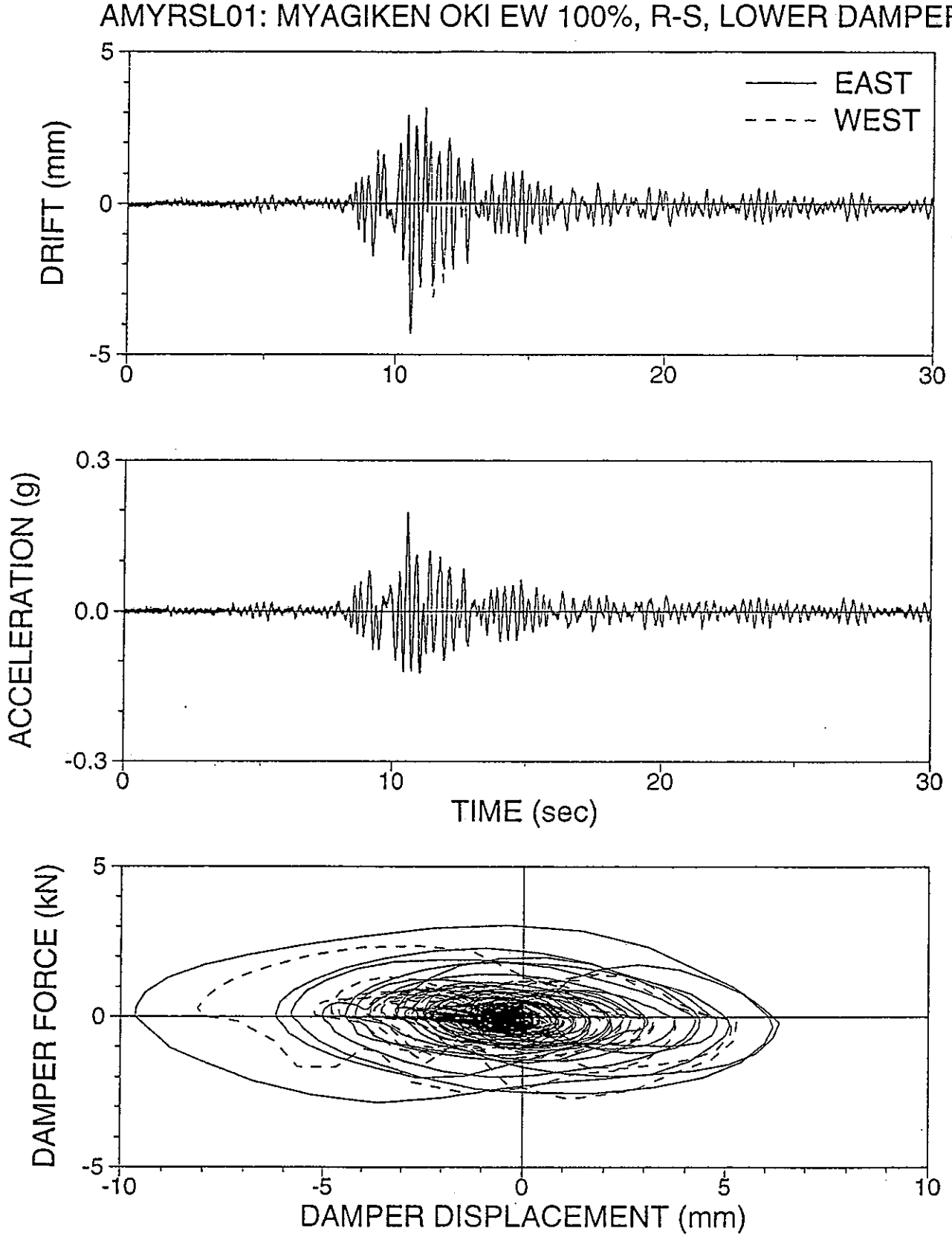
AMYRSL01: MYAGIKEN OKI EW 100%, R-S, LOWER DAMPER
EAST
WEST
DRIFT (mm)
5
0
-5
0
10
20
30
ACCELERATION (g)
0.3
0.0
-0.3
TIME (sec)
DAMPER FORCE (kN)
-10
-5
5
10
DAMPER DISPLACEMENT (mm)

AMYRSL02: MYAGIKEN OKI EW 200%, R-S, LOWER DAMPER

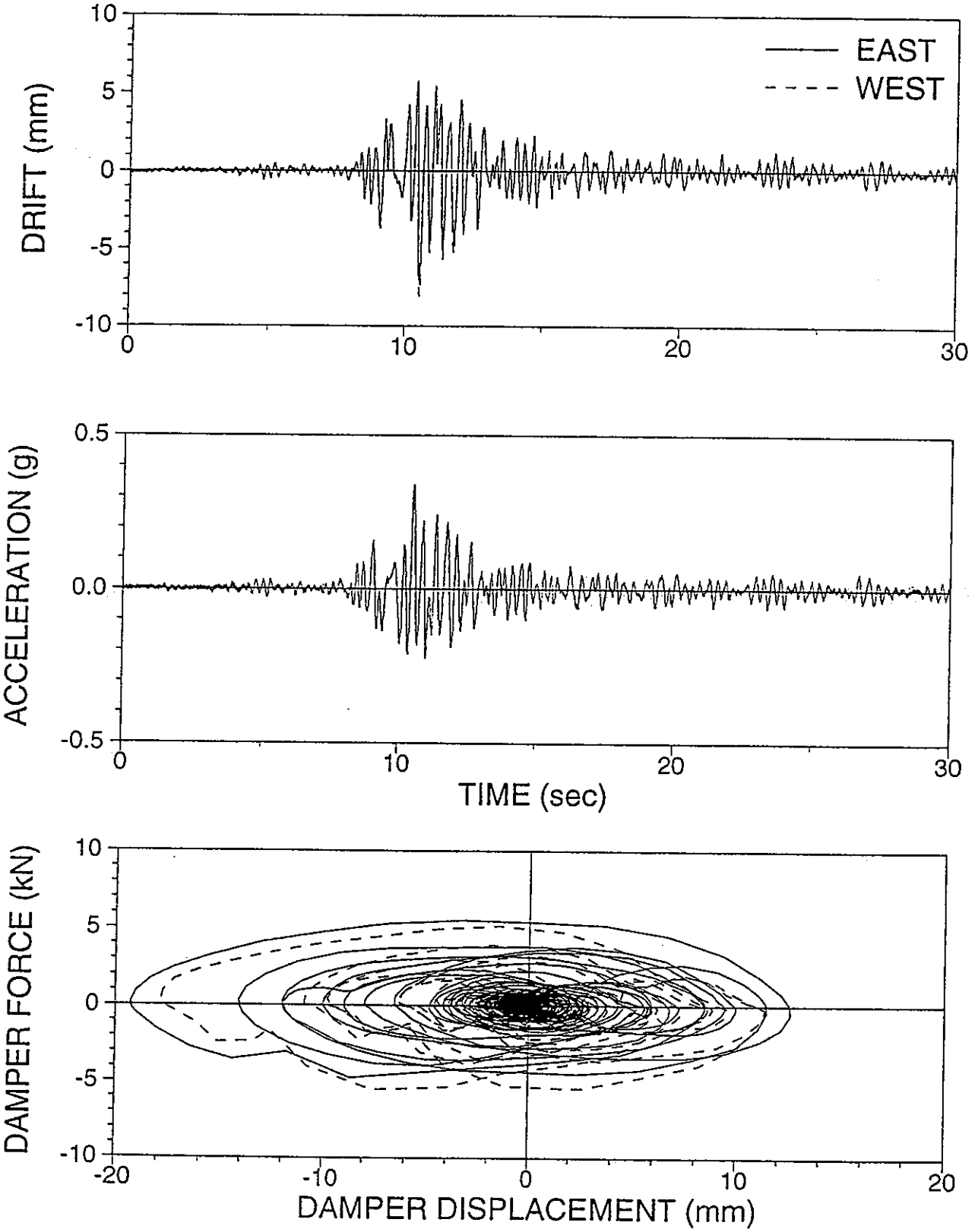

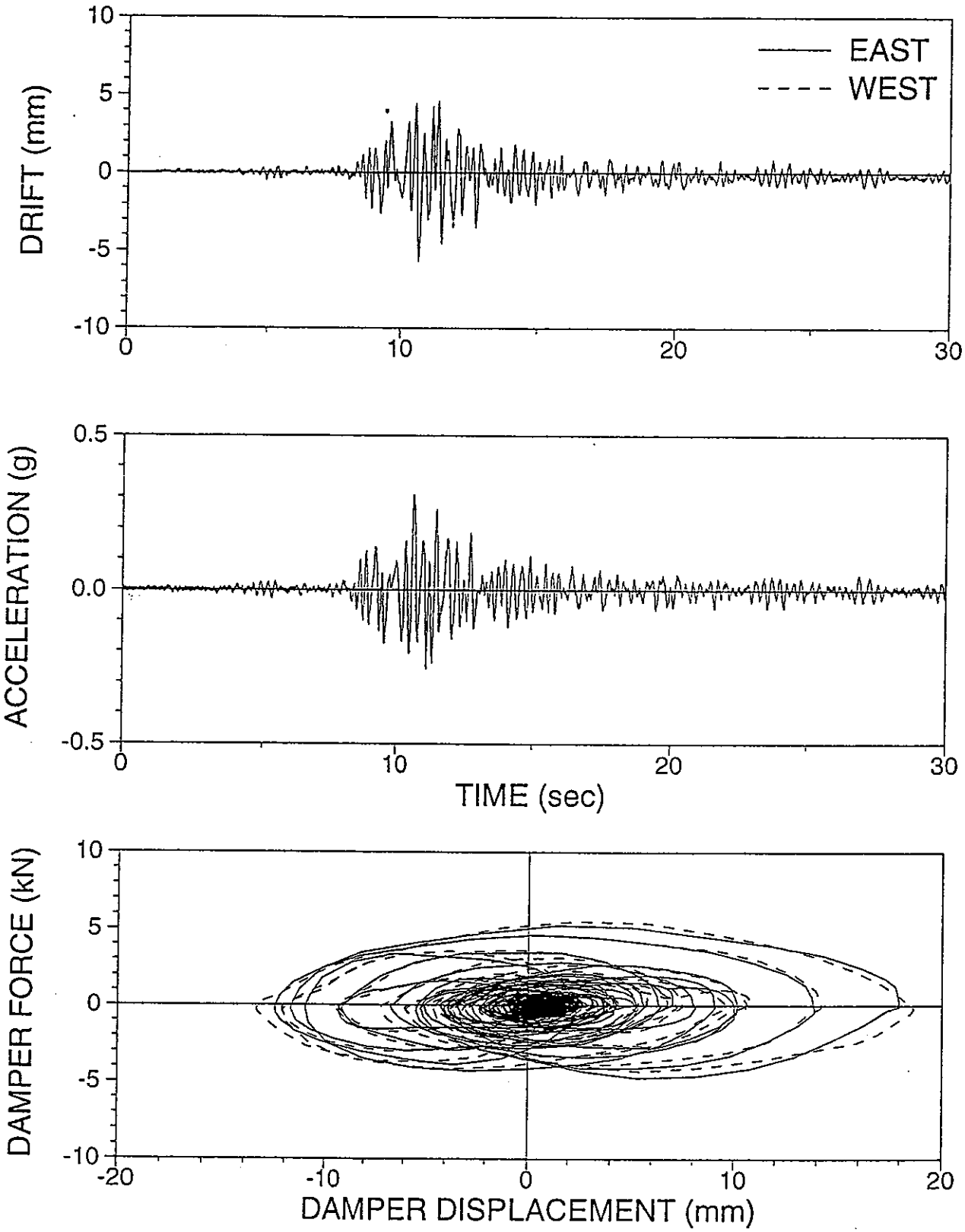
AMYRSU01: MYAGIKEN OKI EW 200%, R-S, UPPER DAMPER
EAST
WEST
DRIFT (mm)
10
5
0
-5
-10
0
10
20
30
ACCELERATION (g)
0.5
0.0
-0.5
TIME (sec)
DAMPER FORCE (kN)
-20
-10
DAMPER DISPLACEMENT (mm)

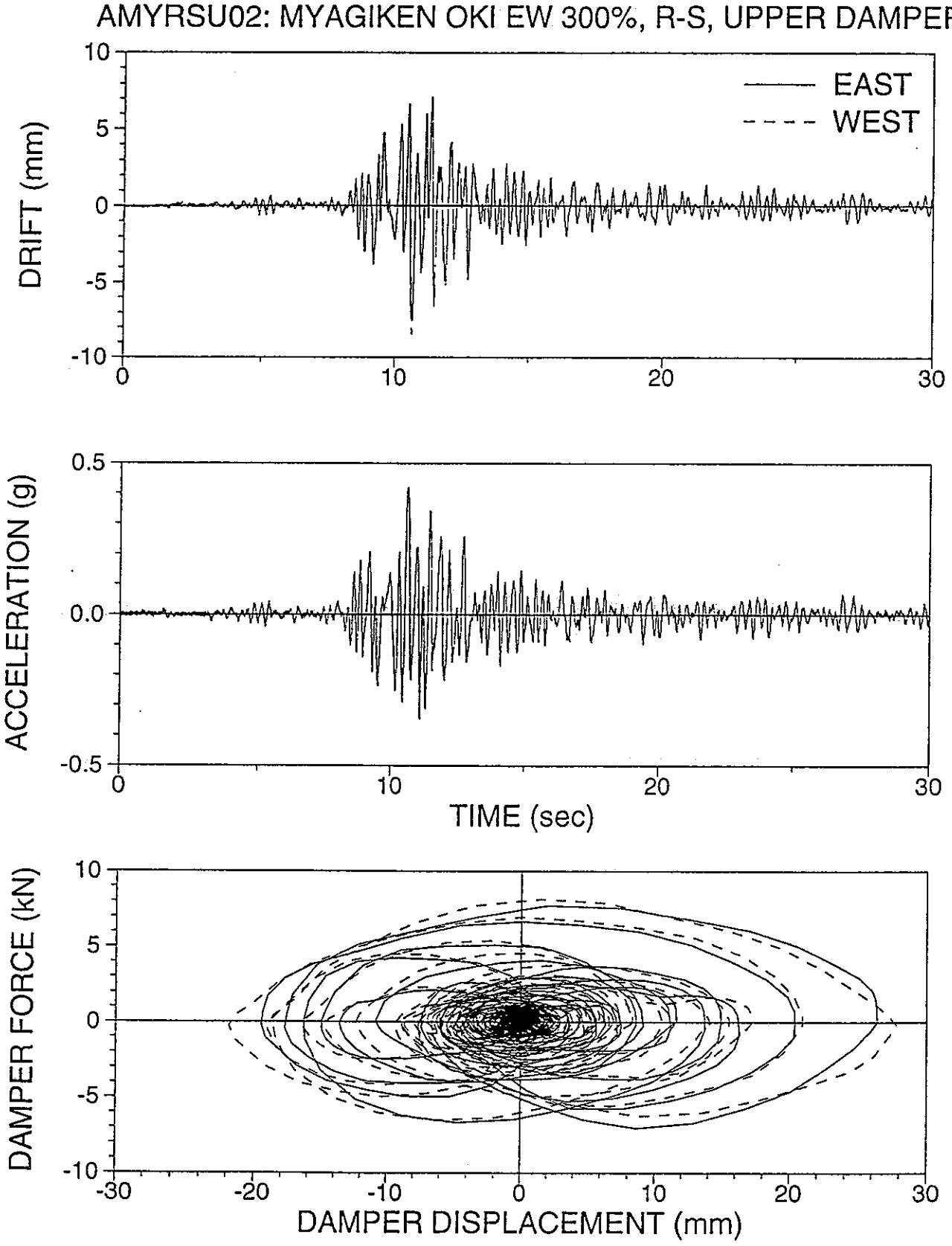
AMYRSU02: MYAGIKEN OKI EW 300%, R-S, UPPER DAMPER
EAST
WEST
DRIFT (mm)
10
5
0
-5
-10
0
10
20
30
ACCELERATION (g)
0.5
0.0
-0.5
TIME (sec)
DAMPER FORCE (kN)
-30
-20
DAMPER DISPLACEMENT (mm)

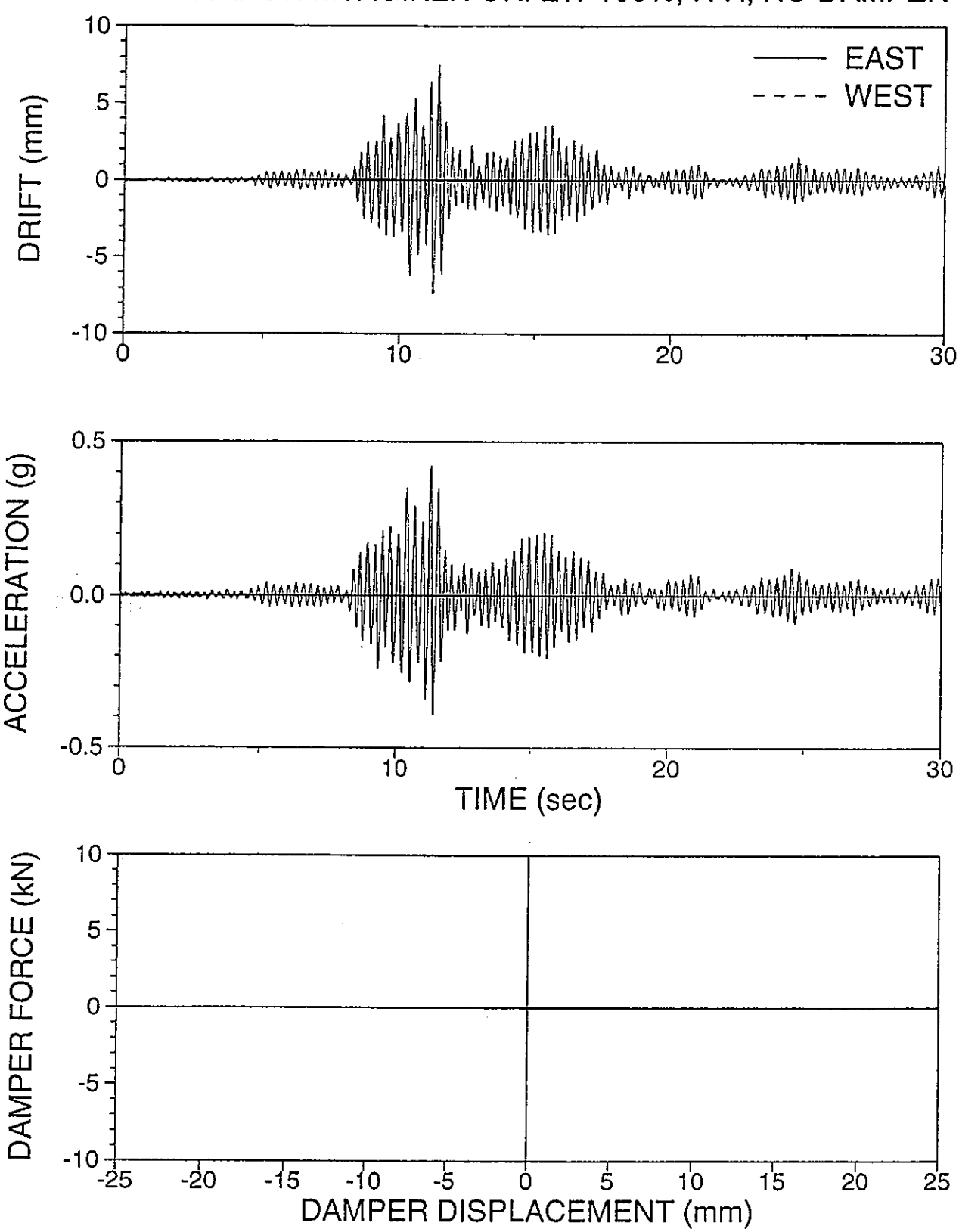
AMYRRN01: MYAGIKEN OKI EW 100%, R-R, NO DAMPER
EAST
WEST
DRIFT (mm)
10
5
0
-5
-10
0
10
20
30
ACCELERATION (g)
0.5
0.0
-0.5
TIME (sec)
DAMPER FORCE (kN)
-25
-20
-15
-10
-5
0
5
10
15
20
25
DAMPER DISPLACEMENT (mm)

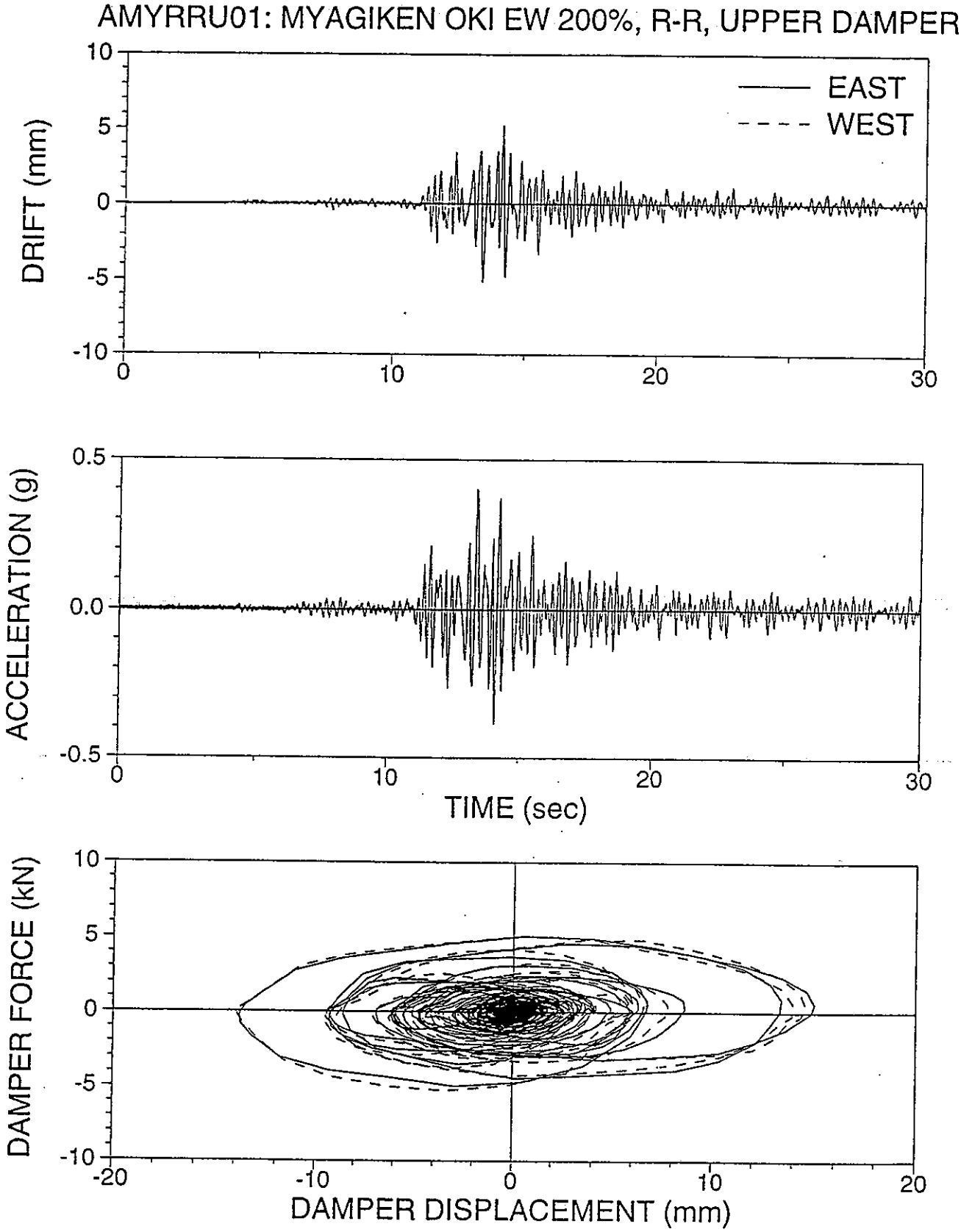
AMYRRU01: MYAGIKEN OKI EW 200%, R-R, UPPER DAMPER
EAST
WEST
DRIFT (mm)
10
5
0
-5
-10
0
10
20
30
ACCELERATION (g)
0.5
0.0
-0.5
TIME (sec)
DAMPER FORCE (kN)
-20
DAMPER DISPLACEMENT (mm)

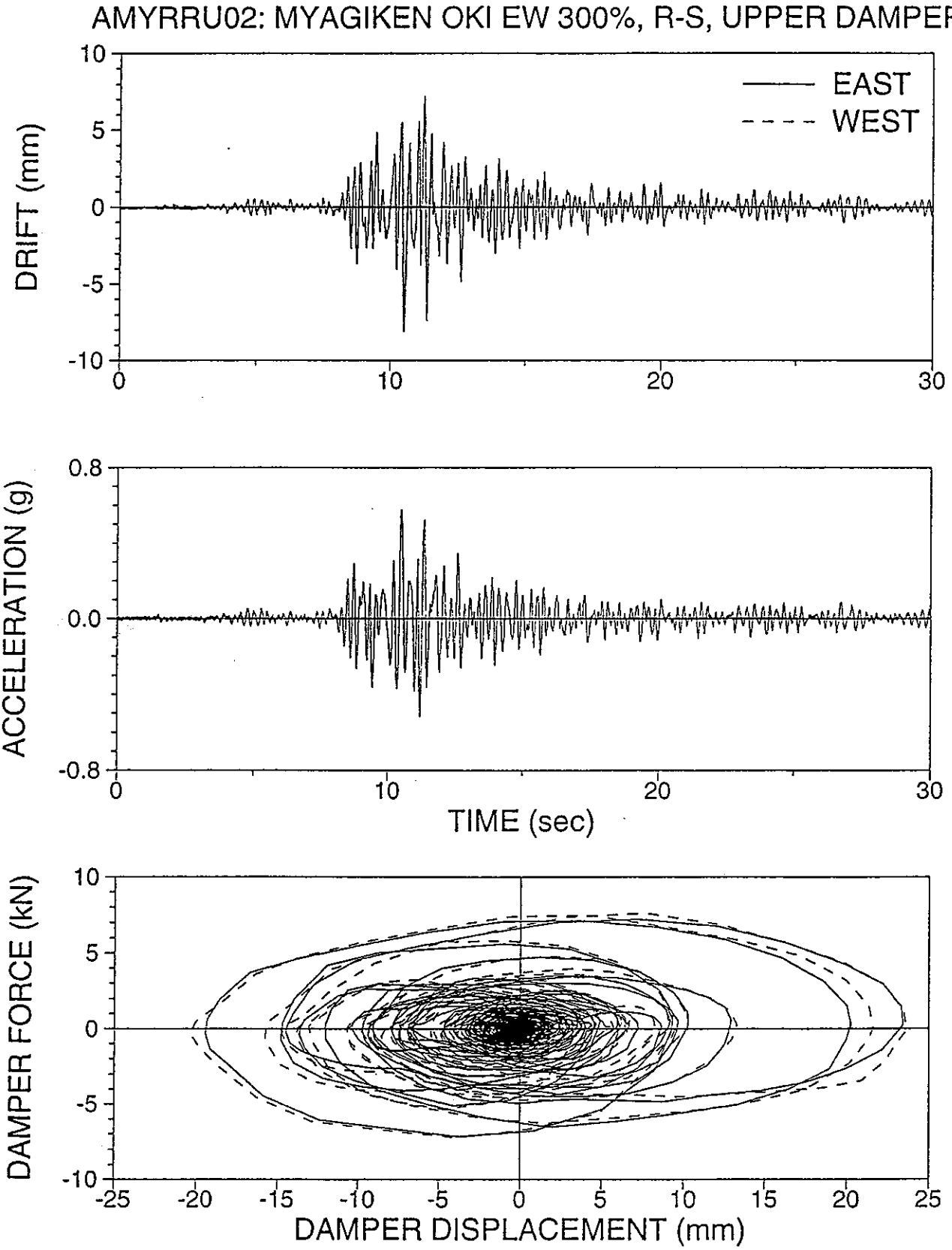
AMYRRU02: MYAGIKEN OKI EW 300%, R-S, UPPER DAMPER
EAST
WEST
DRIFT (mm)
10
5
0
-5
-10
0
10
20
30
ACCELERATION (g)
0.8
0.0
-0.8
TIME (sec)
DAMPER FORCE (kN)
DAMPER DISPLACEMENT (mm)
-25
-20
-15
-10
-5
15
25

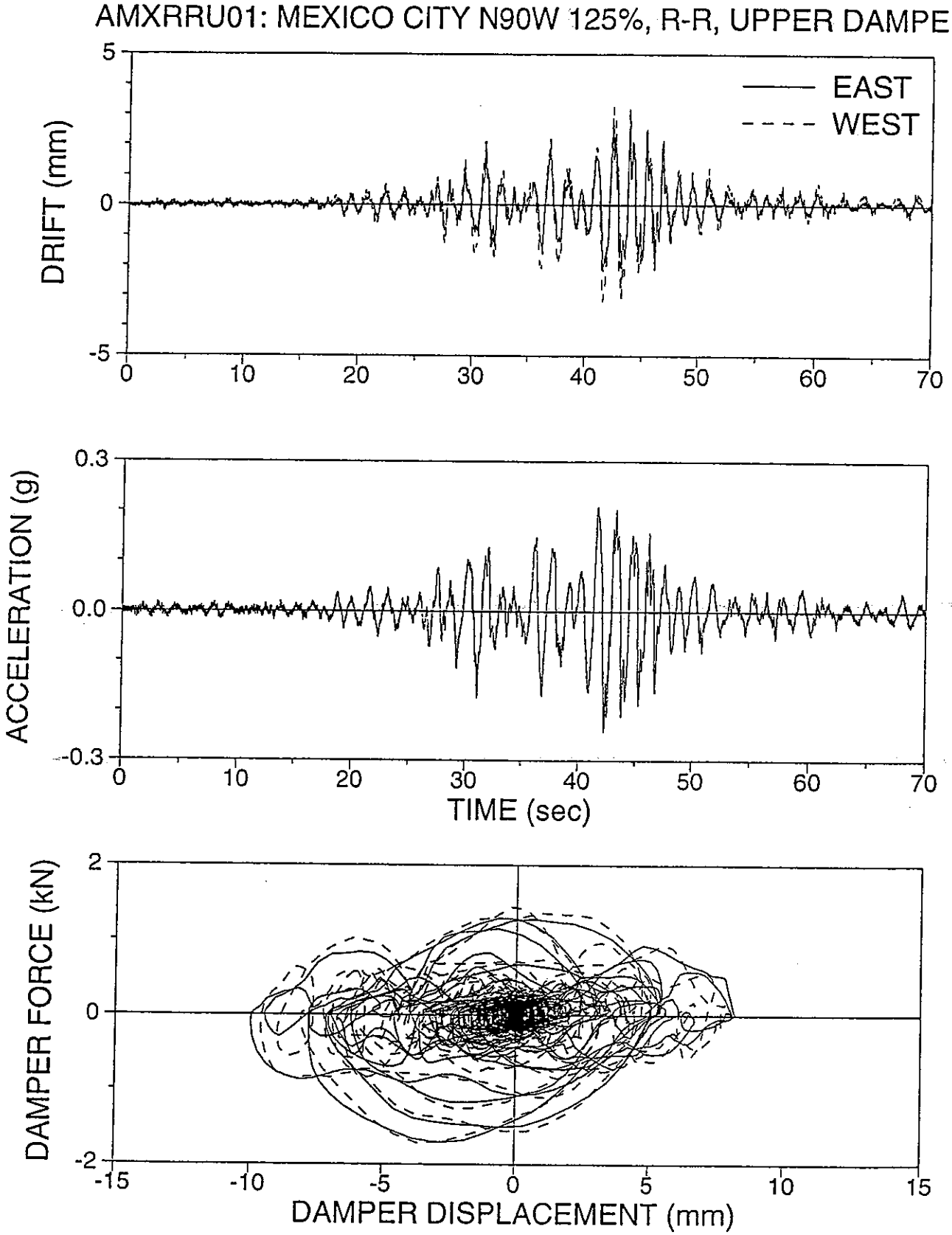
AMXRRU01: MEXICO CITY N90W 125%, R-R, UPPER DAMPER
EAST
WEST
DRIFT (mm)
5
0
-5
0
10
20
30
40
50
60
70
ACCELERATION (g)
0.3
0.0
-0.3
TIME (sec)
DAMPER FORCE (kN)
2
0
-2
-15
-10
-5
0
5
10
15
DAMPER DISPLACEMENT (mm)

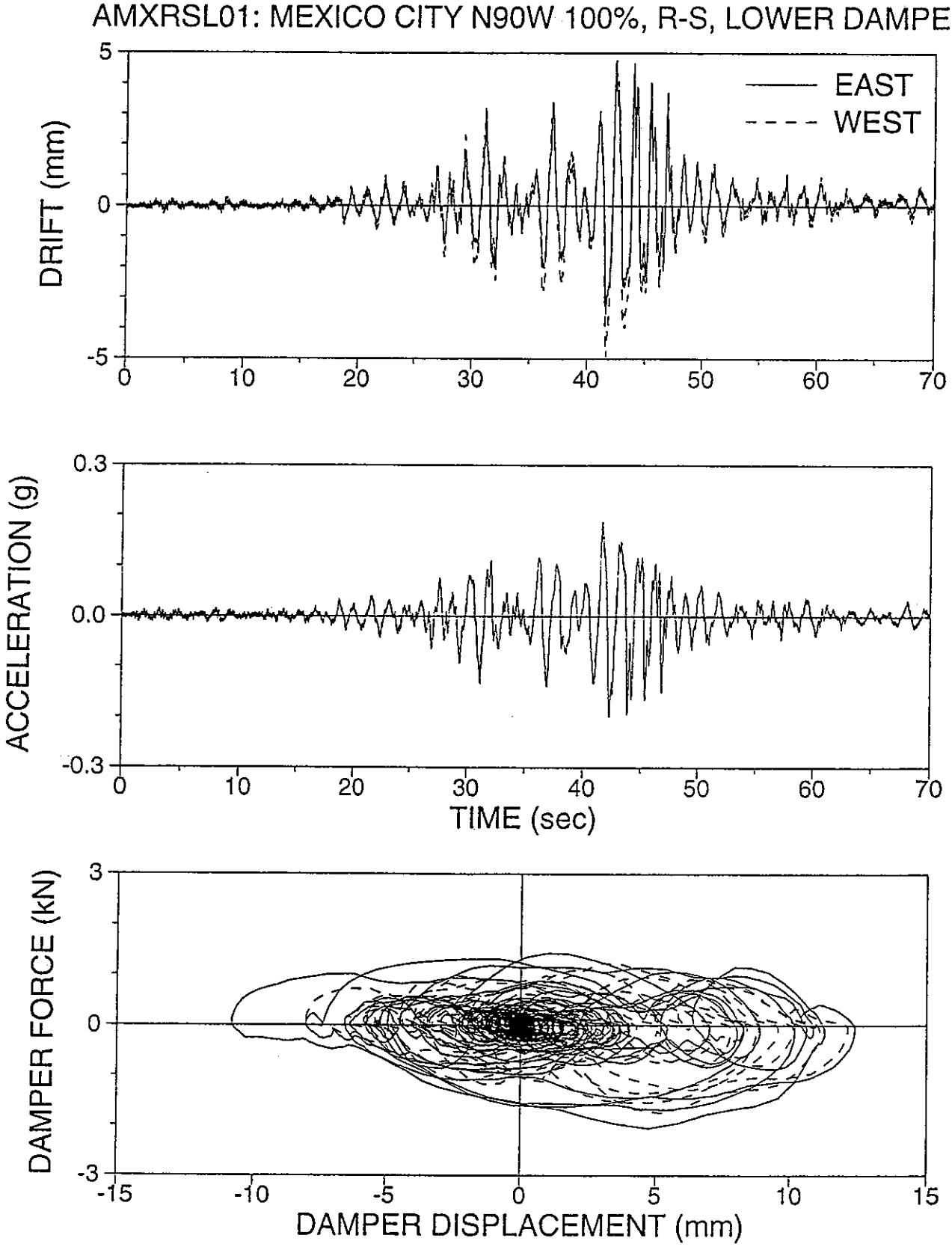
AMXRSL01: MEXICO CITY N90W 100%, R-S, LOWER DAMPER
EAST
WEST
DRIFT (mm)
5
0
-5
0
10
20
30
40
50
60
70
ACCELERATION (g)
0.3
0.0
-0.3
TIME (sec)
DAMPER FORCE (kN)
3
0
-3
-15
-10
-5
0
5
10
15
DAMPER DISPLACEMENT (mm)

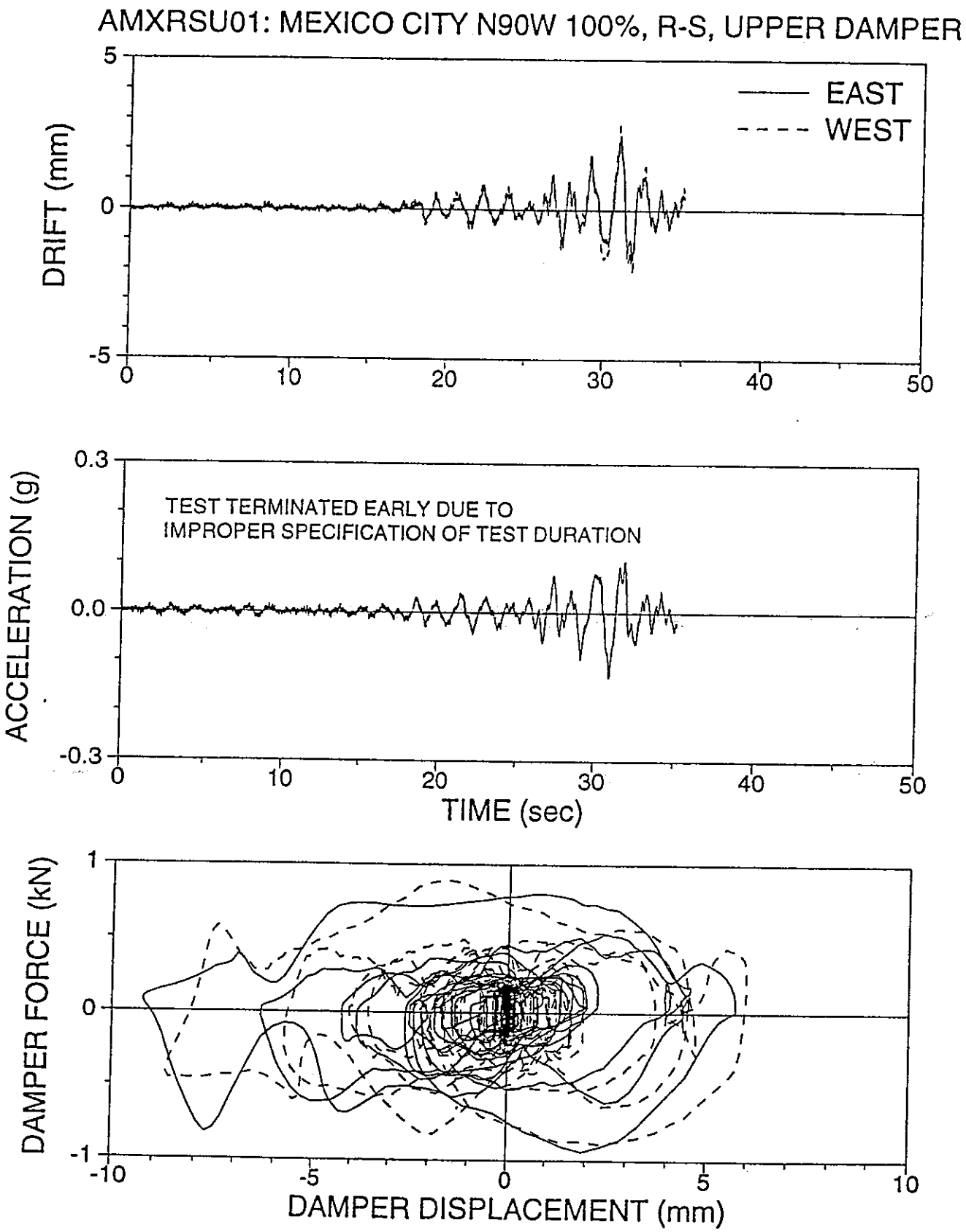
AMXRSU01: MEXICO CITY N90W 100%, R-S, UPPER DAMPER
EAST
WEST
DRIFT (mm)
5
0
-5
0
10
20
30
40
50
TEST TERMINATED EARLY DUE TO
IMPROPER SPECIFICATION OF TEST DURATION
ACCELERATION (g)
0.3
0.0
-0.3
TIME (sec)
DAMPER FORCE (kN)
1
0
-1
-10
-5
0
5
10
DAMPER DISPLACEMENT (mm)

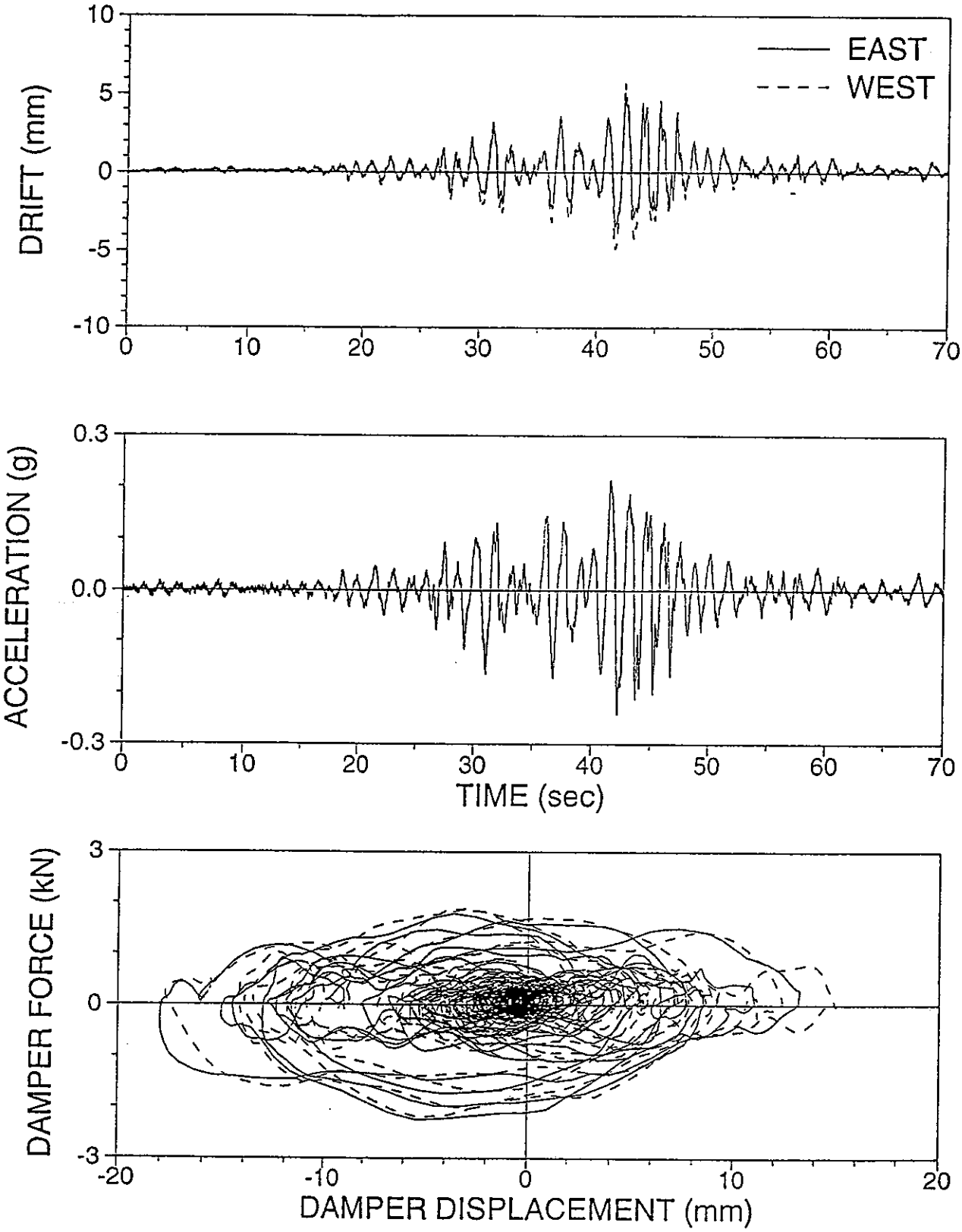
AMXRSU02: MEXICO CITY N90W 125%, R-S, UPPER DAMPER
EAST
WEST
DRIFT (mm)
10
5
0
-5
-10
0
10
20
30
40
50
60
70
ACCELERATION (g)
0.3
0.0
-0.3
TIME (sec)
DAMPER FORCE (kN)
3
0
-3
-20
-10
0
10
20
DAMPER DISPLACEMENT (mm)

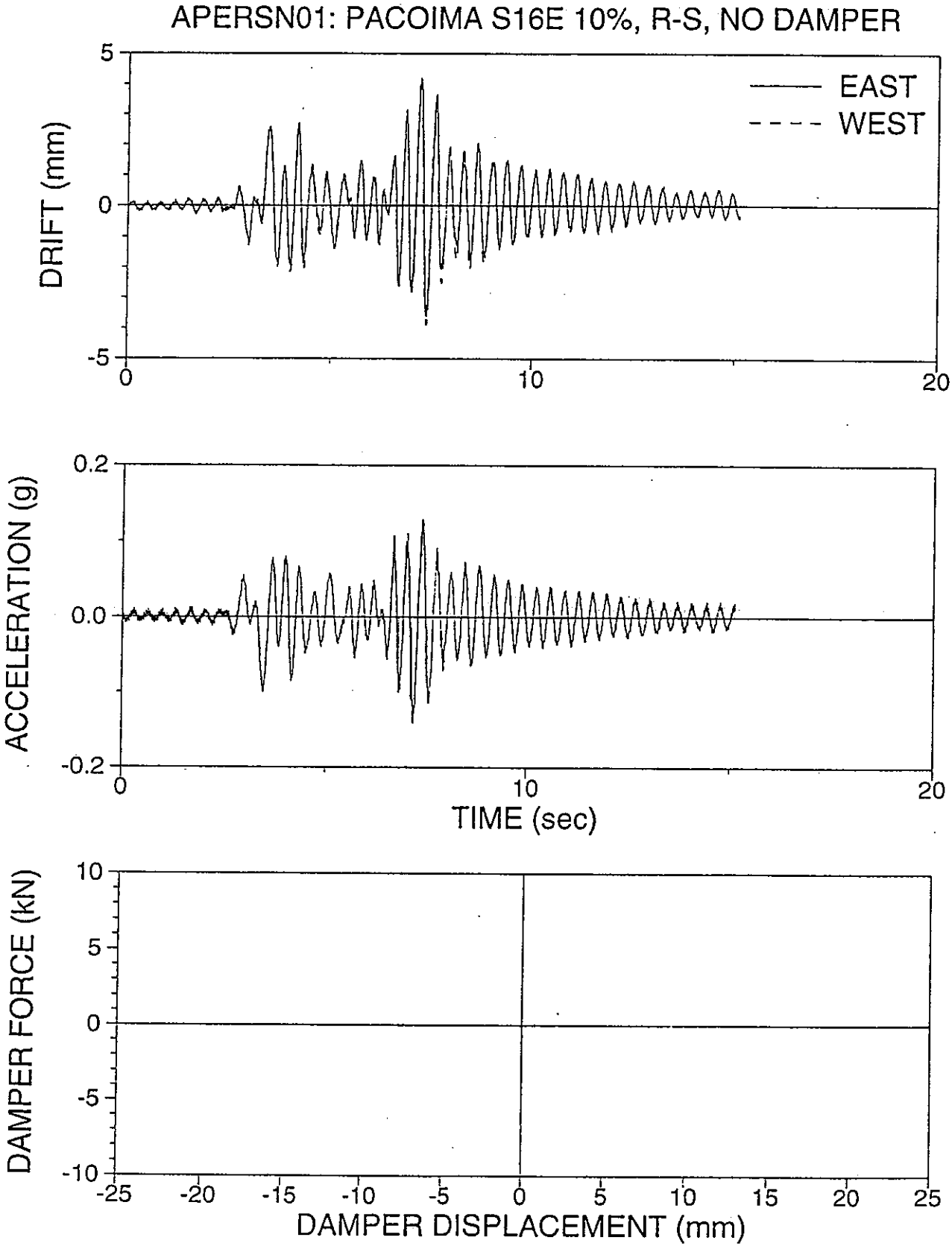
APERSN01: PACOIMA S16E 10%, R-S, NO DAMPER
EAST
WEST
DRIFT (mm)
5
0
-5
0
10
20
ACCELERATION (g)
0.2
0.0
-0.2
0
10
20
TIME (sec)
DAMPER FORCE (kN)
10
5
0
-5
-10
-25
-20
-15
-10
-5
0
5
10
15
20
25
DAMPER DISPLACEMENT (mm)

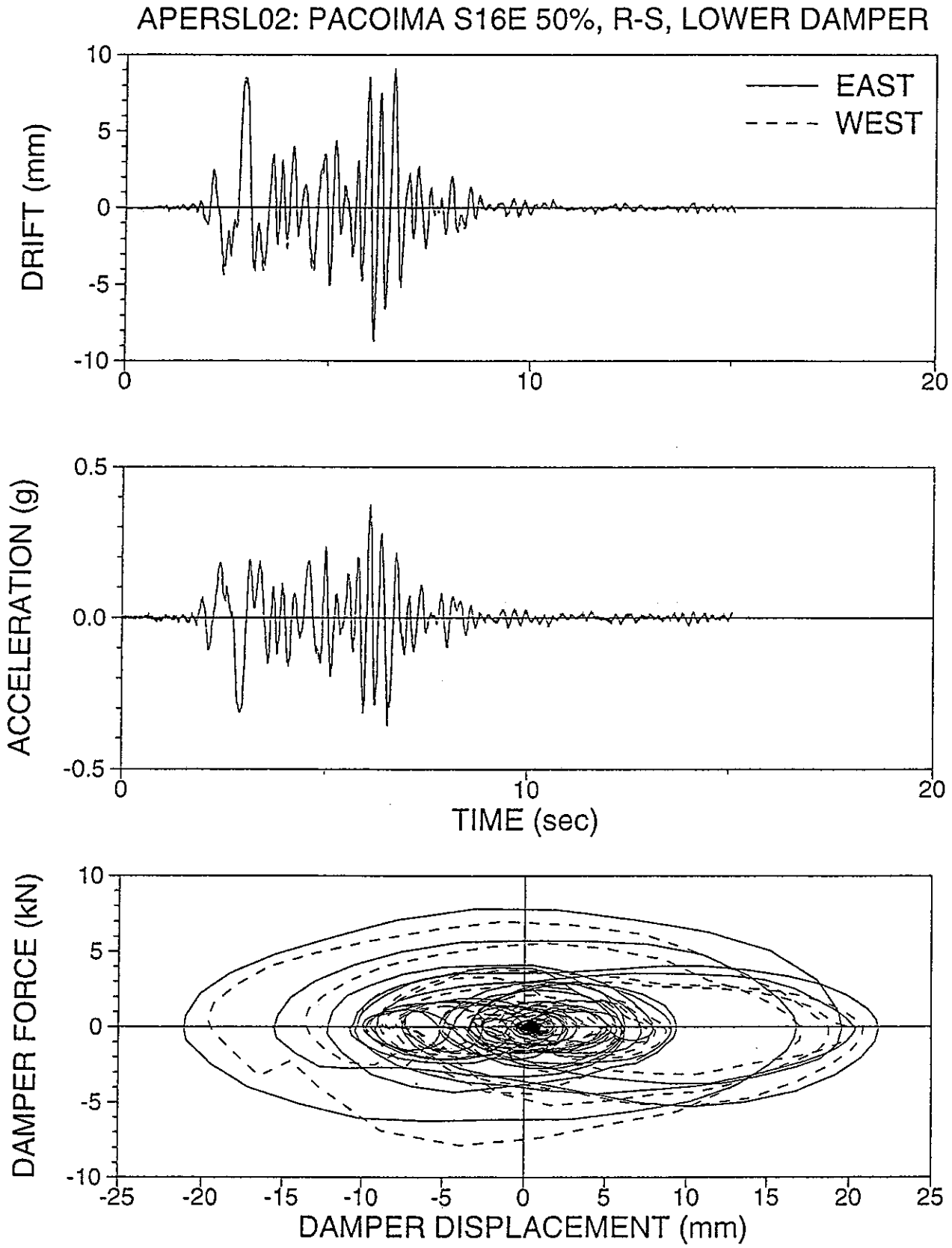
APERSL02: PACOIMA S16E 50%, R-S, LOWER DAMPER
EAST
WEST
DRIFT (mm)
10
5
0
-5
-10
0
10
20
ACCELERATION (g)
0.5
0.0
-0.5
0
10
20
TIME (sec)
DAMPER FORCE (kN)
10
5
0
-5
-10
-25
-20
-15
-10
-5
0
5
10
15
20
25
DAMPER DISPLACEMENT (mm)

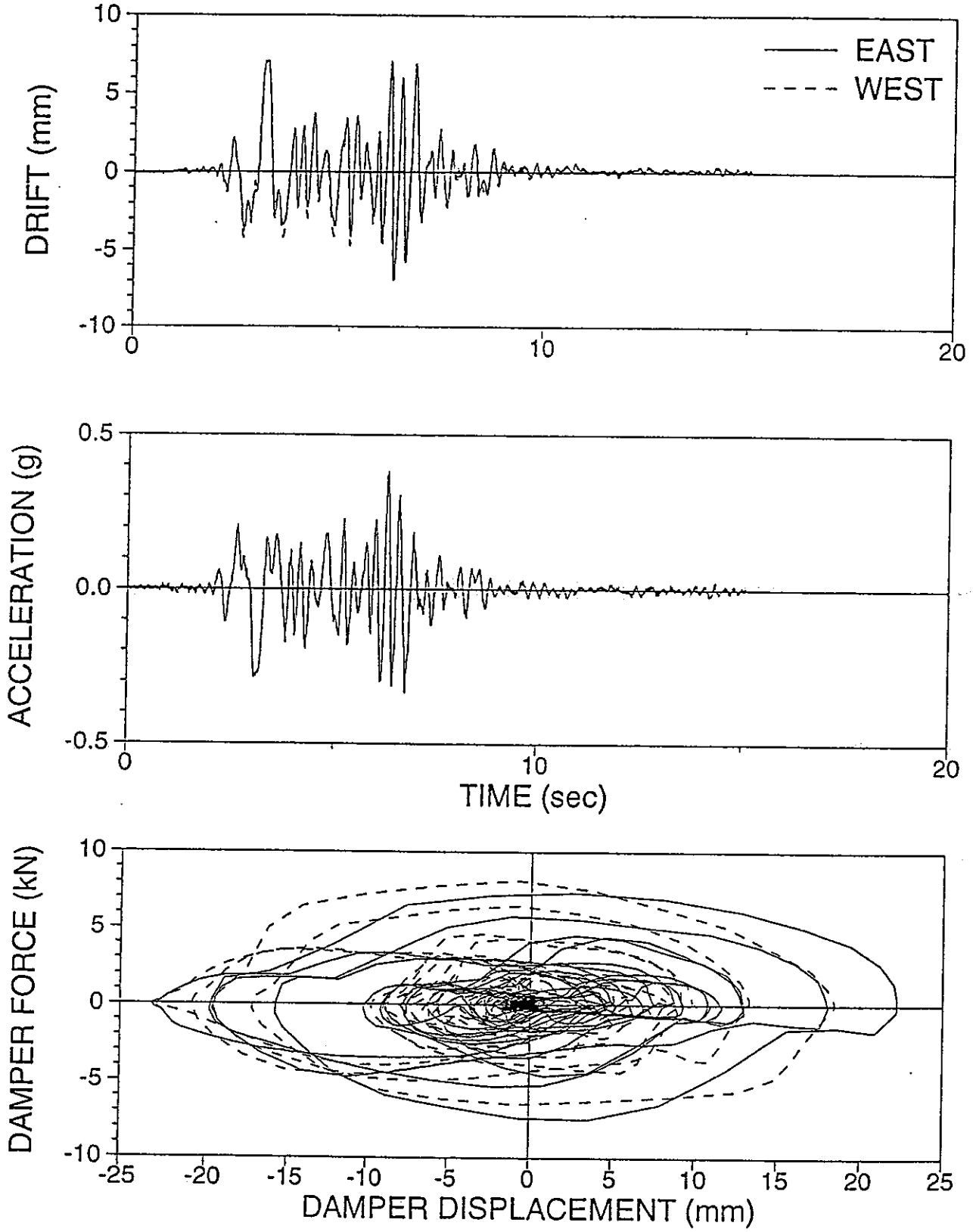
APARSU01: PACOIMA S16E 50%, R-S, UPPER DAMPER
DRIFT (mm)
EAST
WEST
ACCELERATION (g)
TIME (sec)
DAMPER FORCE (kN)
DAMPER DISPLACEMENT (mm)

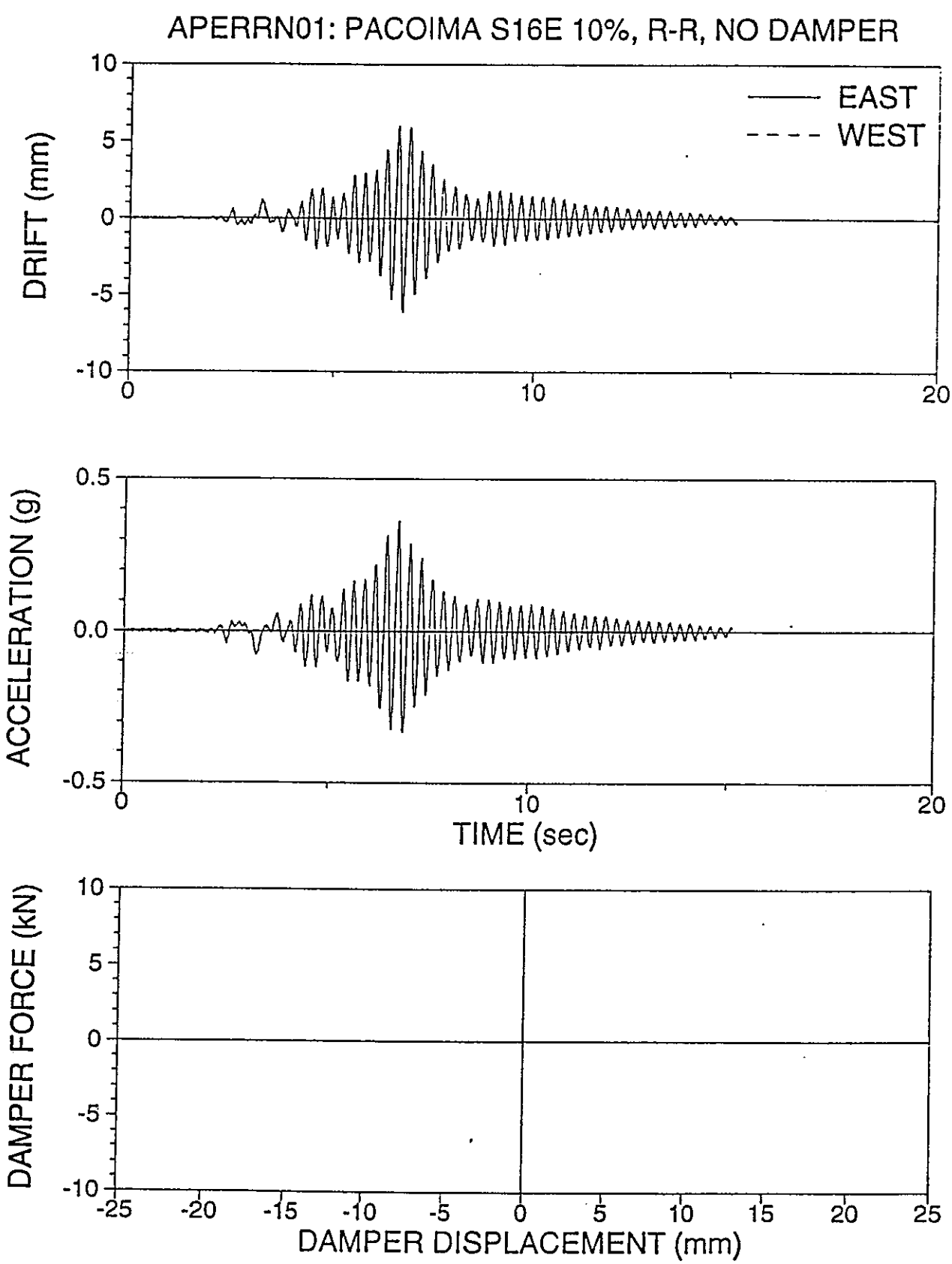
APERRN01: PACOIMA S16E 10%, R-R, NO DAMPER
EAST
WEST
DRIFT (mm)
10
5
0
-5
-10
0
10
20
ACCELERATION (g)
0.5
0.0
-0.5
0
10
20
TIME (sec)
DAMPER FORCE (kN)
10
5
0
-5
-10
-25
-20
-15
-10
-5
0
5
10
15
20
25
DAMPER DISPLACEMENT (mm)

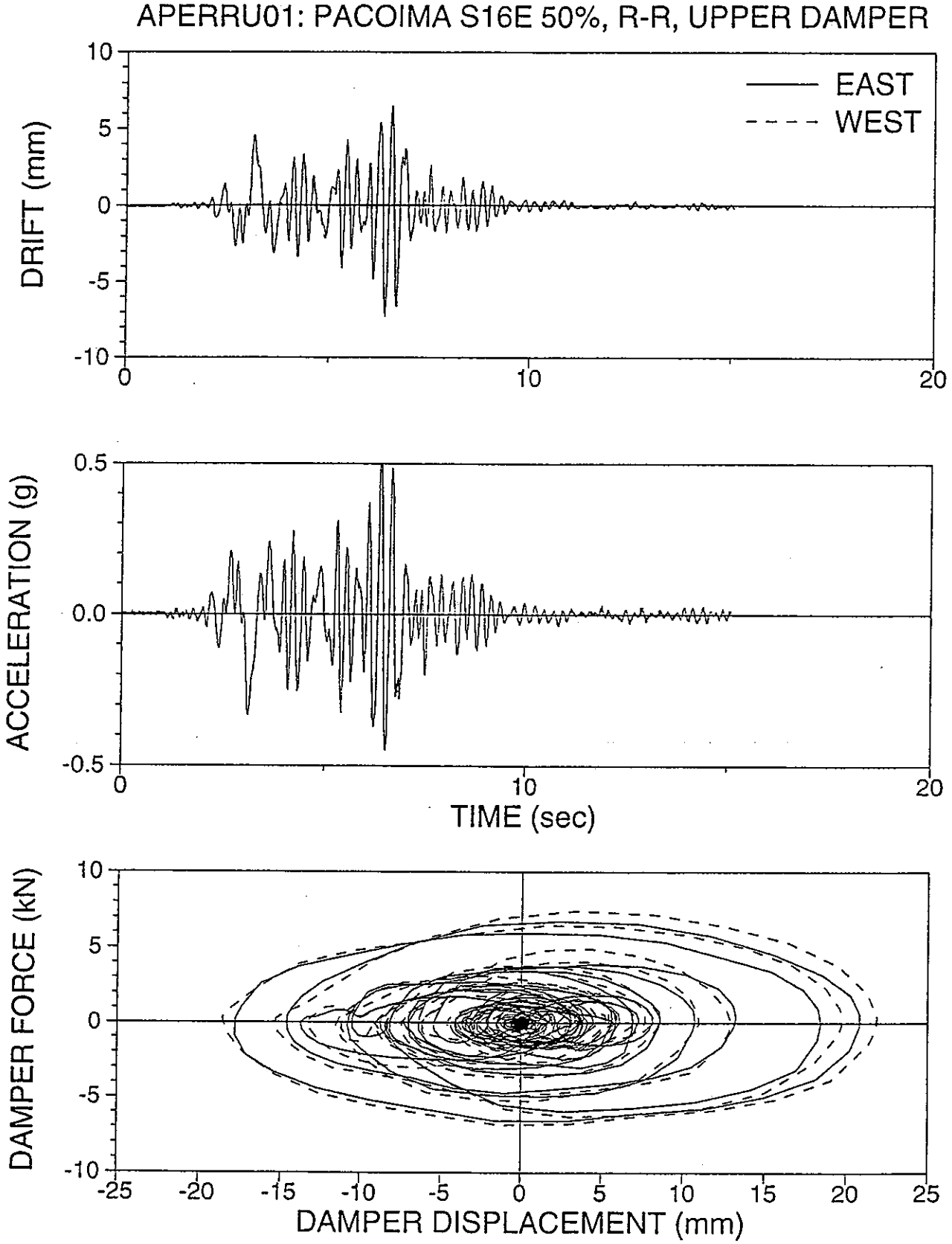
APERRU01: PACOIMA S16E 50%, R-R, UPPER DAMPER
EAST
WEST
DRIFT (mm)
10
5
0
-5
-10
0
10
20
ACCELERATION (g)
0.5
0.0
-0.5
0
10
20
TIME (sec)
DAMPER FORCE (kN)
10
5
0
-5
-10
-25
-20
-15
-10
-5
0
5
10
15
20
25
DAMPER DISPLACEMENT (mm)

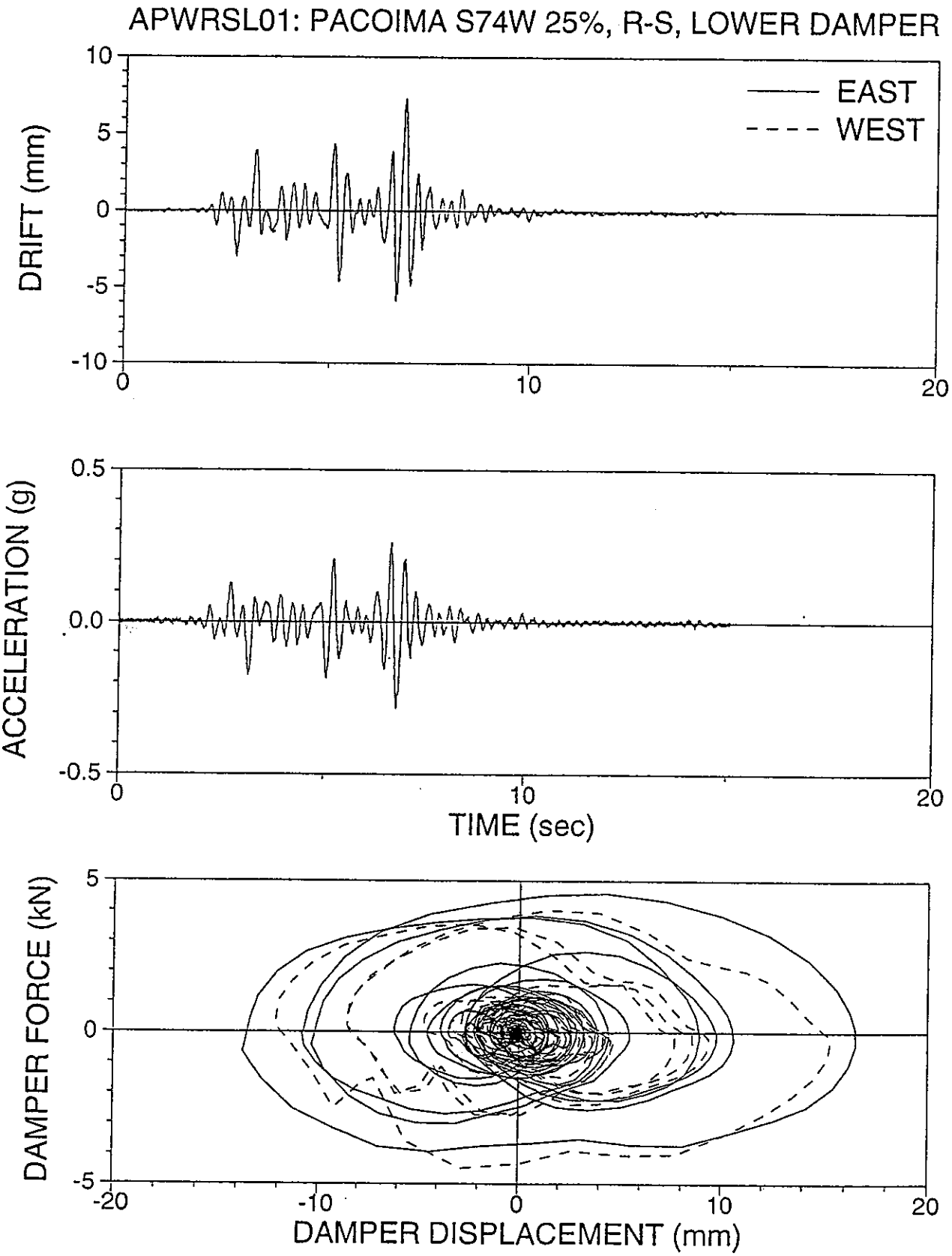
APWRSL01: PACOIMA S74W 25%, R-S, LOWER DAMPER
EAST
WEST
DRIFT (mm)
10
5
0
-5
-10
0
10
20
ACCELERATION (g)
0.5
0.0
-0.5
0
10
20
TIME (sec)
DAMPER FORCE (kN)
5
0
-5
-20
-10
0
10
20
DAMPER DISPLACEMENT (mm)

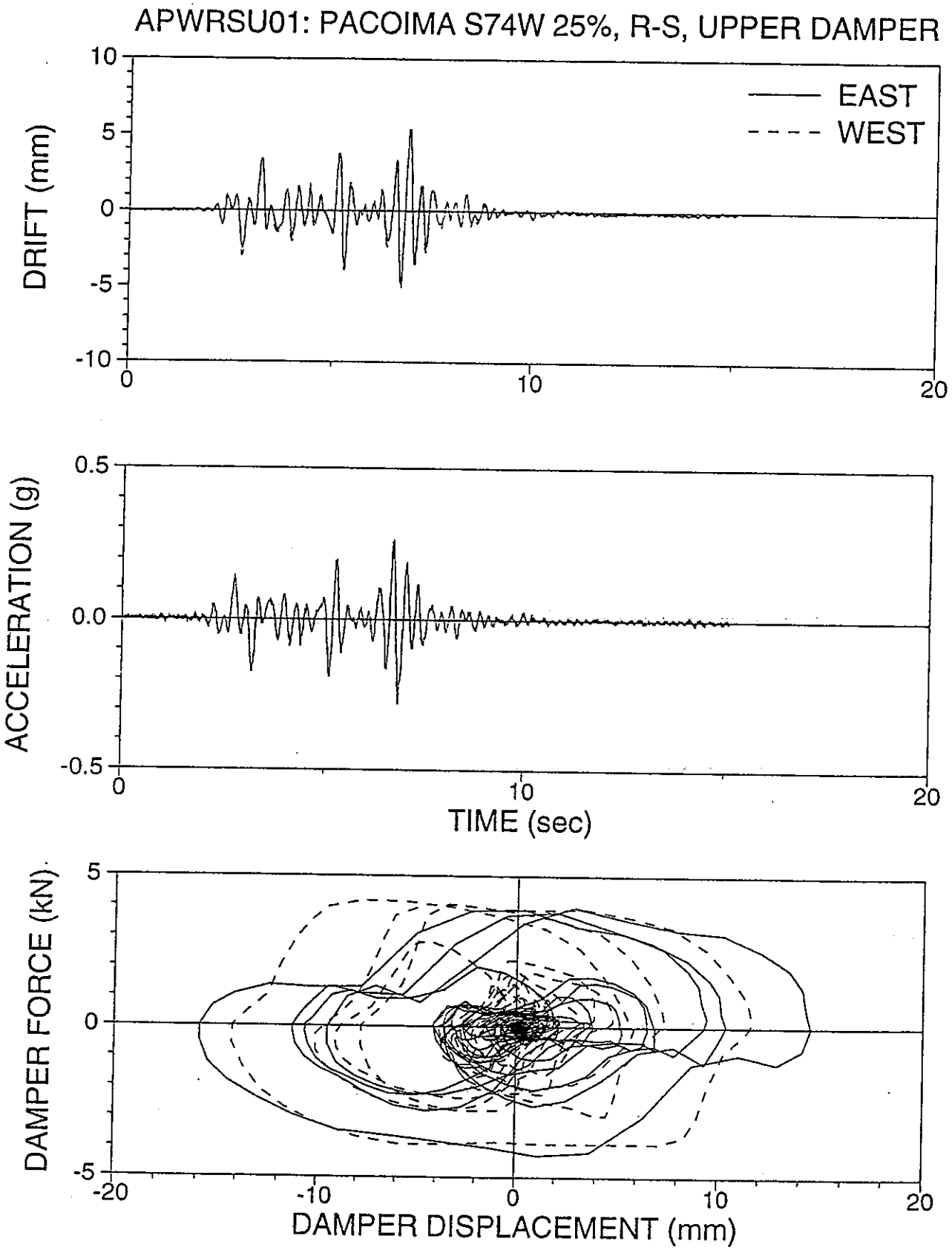
APWRSU01: PACOIMA S74W 25%, R-S, UPPER DAMPER
EAST
WEST
DRIFT (mm)
10
5
0
-5
-10
0
10
20
ACCELERATION (g)
0.5
0.0
-0.5
0
10
20
TIME (sec)
DAMPER FORCE (kN)
5
0
-5
-20
-10
0
10
20
DAMPER DISPLACEMENT (mm)

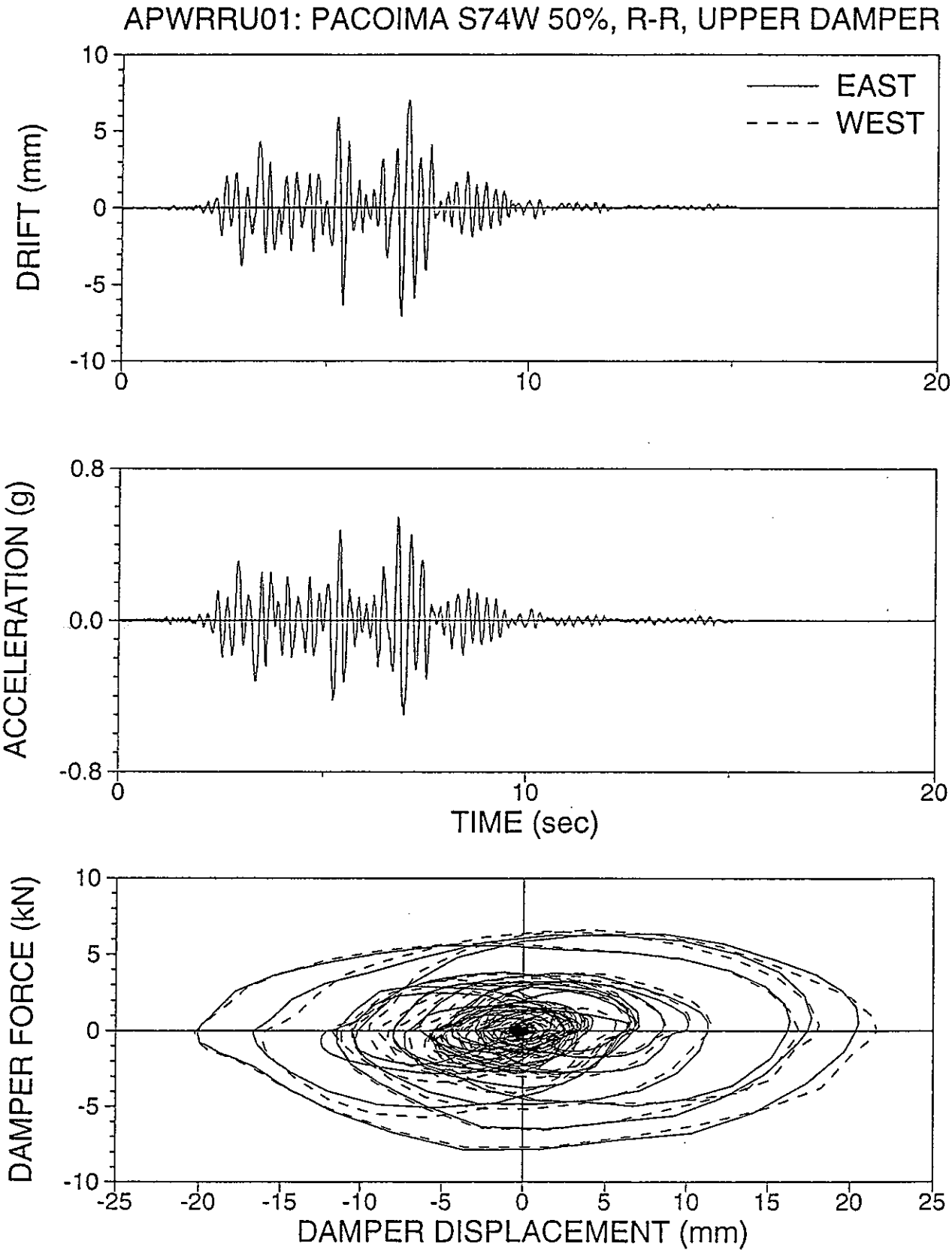
APWRRU01: PACOIMA S74W 50%, R-R, UPPER DAMPER
EAST
WEST
DRIFT (mm)
10
5
0
-5
-10
0
10
20
ACCELERATION (g)
0.8
0.0
-0.8
0
10
20
TIME (sec)
DAMPER FORCE (kN)
10
5
0
-5
-10
-25
-20
-15
-10
-5
0
5
10
15
20
25
DAMPER DISPLACEMENT (mm)

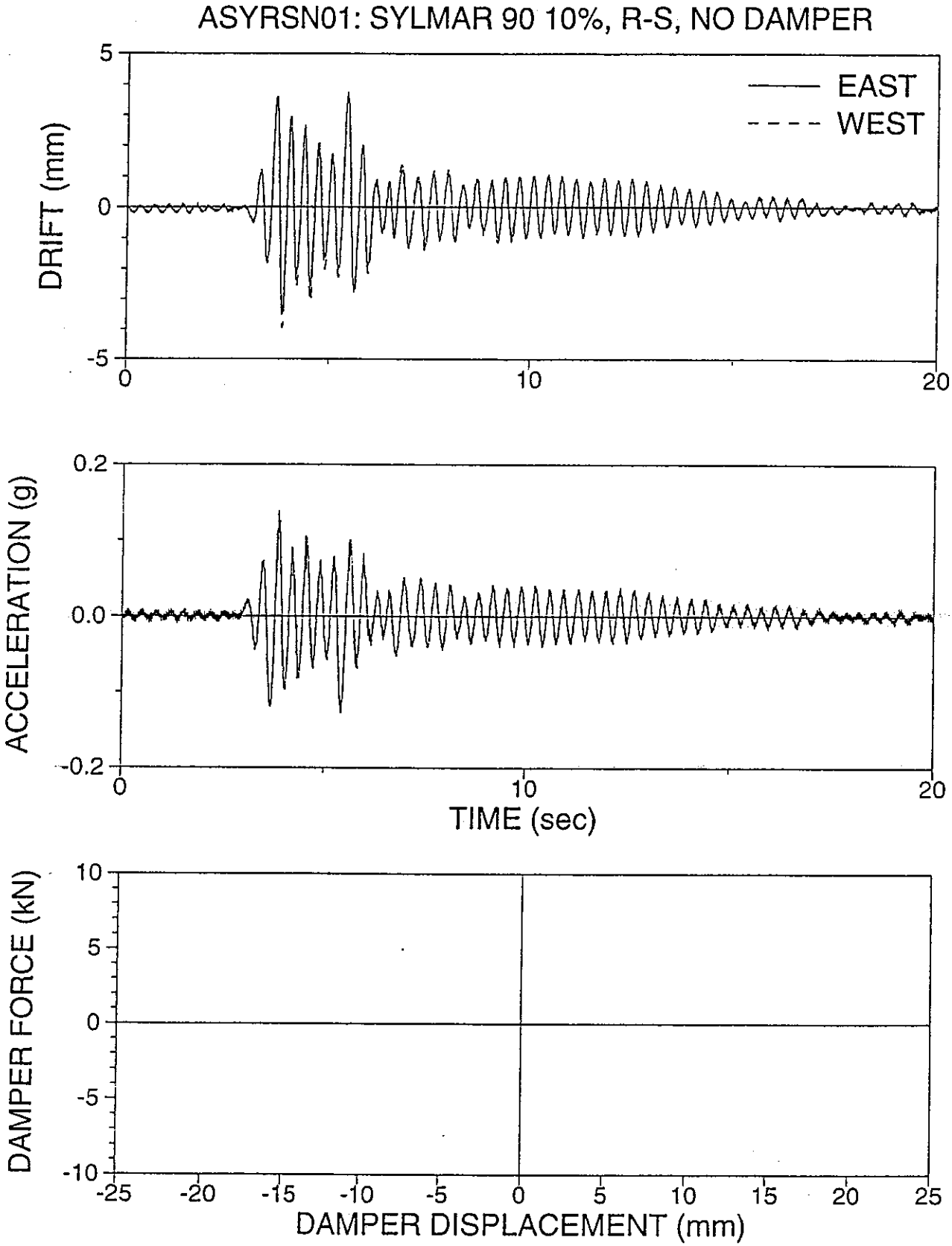
ASYRSN01: SYLMAR 90 10%, R-S, NO DAMPER
EAST
WEST
DRIFT (mm)
5
0
-5
0
10
20
ACCELERATION (g)
0.2
0.0
-0.2
0
10
20
TIME (sec)
DAMPER FORCE (kN)
10
5
0
-5
-10
-25
-20
-15
-10
-5
0
5
10
15
20
25
DAMPER DISPLACEMENT (mm)

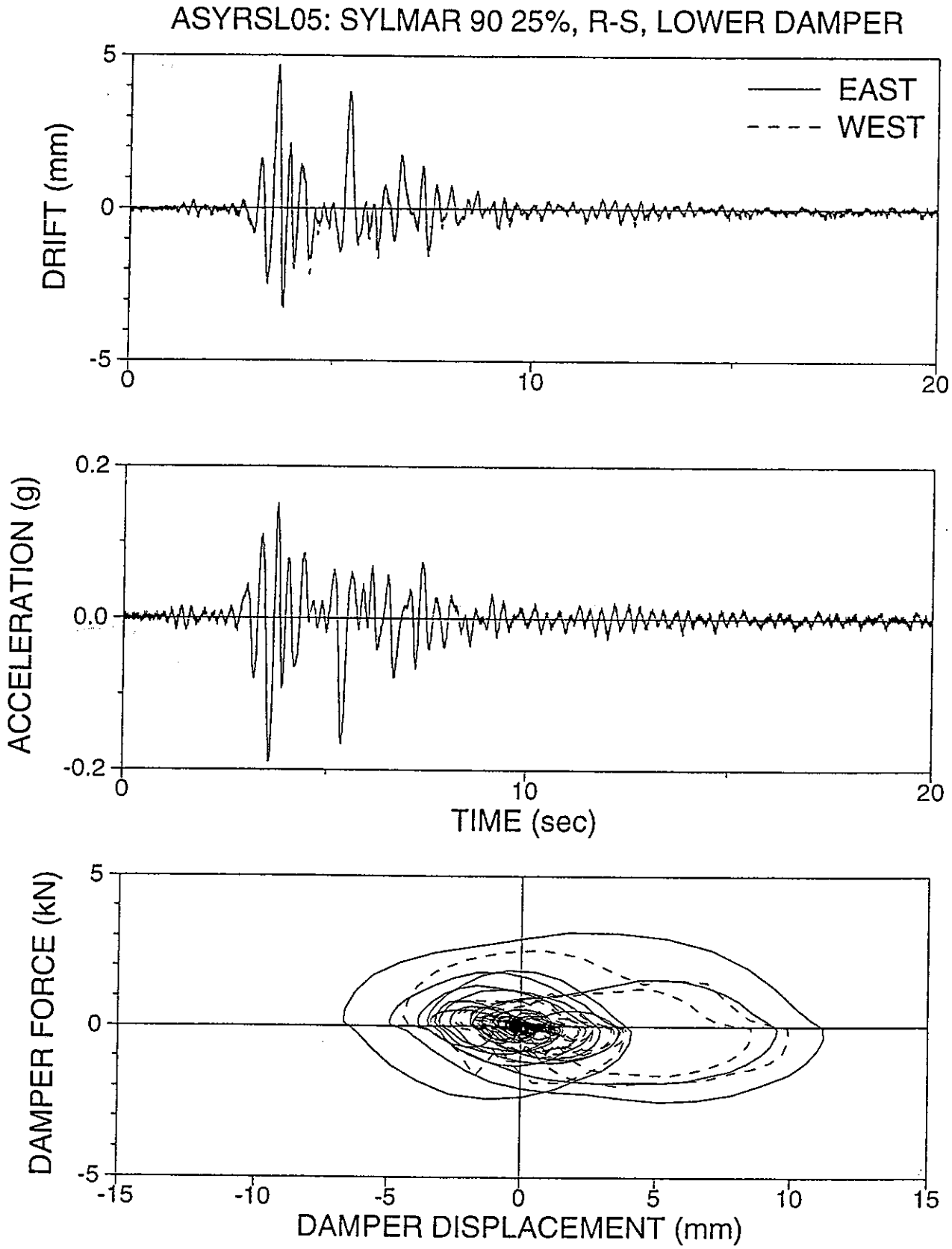
ASYRSL05: SYLMAR 90 25%, R-S, LOWER DAMPER
EAST
WEST
DRIFT (mm)
5
0
-5
0
10
20
ACCELERATION (g)
0.2
0.0
-0.2
0
10
20
TIME (sec)
DAMPER FORCE (kN)
5
0
-5
-15
-10
-5
0
5
10
15
DAMPER DISPLACEMENT (mm)

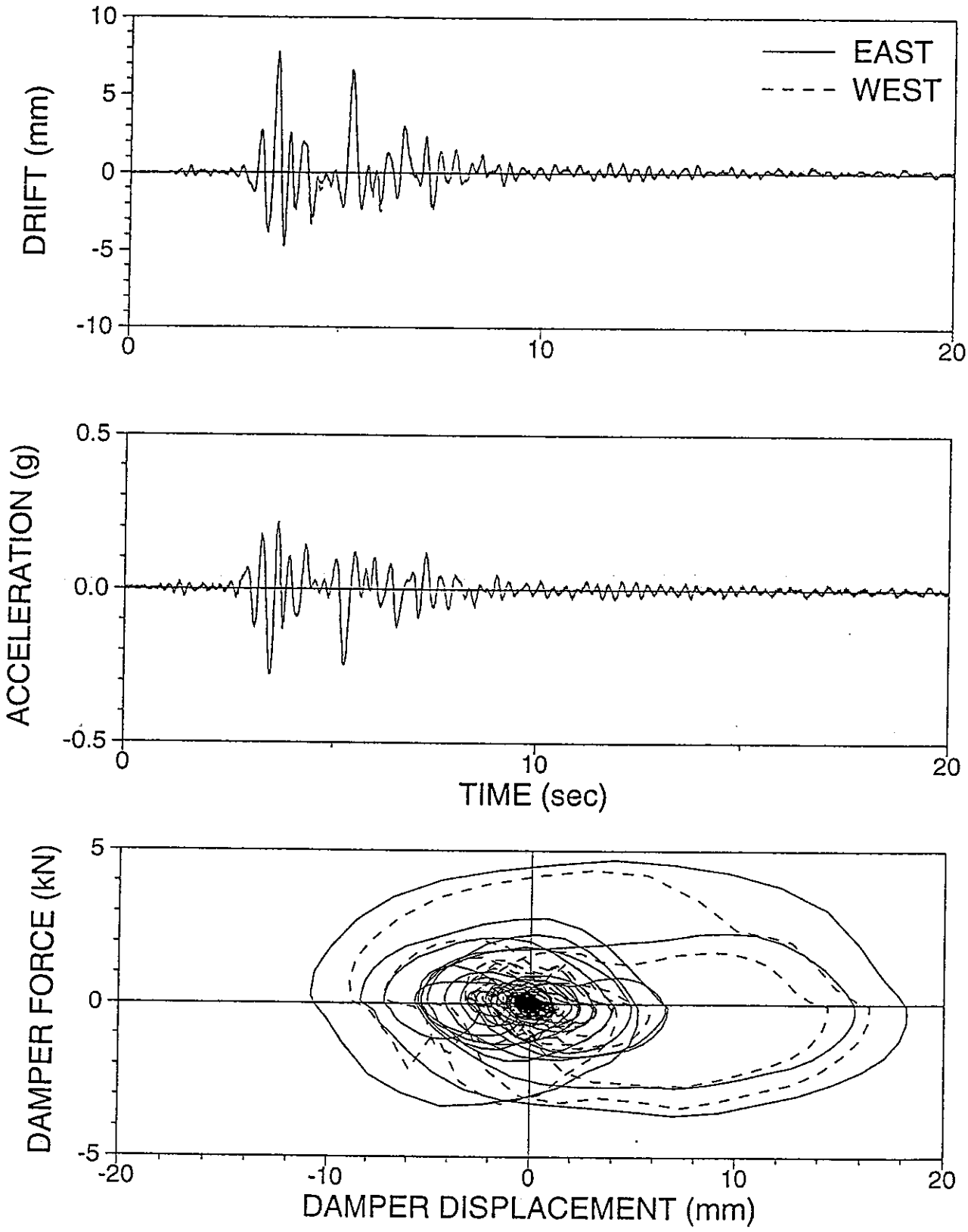
ASYRSL06: SYLMAR 90 40%, R-S, LOWER DAMPER
DRIFT (mm)
10
5
0
-5
-10
0
10
20
EAST
WEST
ACCELERATION (g)
0.5
0.0
-0.5
0
10
20
TIME (sec)
DAMPER FORCE (kN)
5
0
-5
-20
-10
0
10
20
DAMPER DISPLACEMENT (mm)

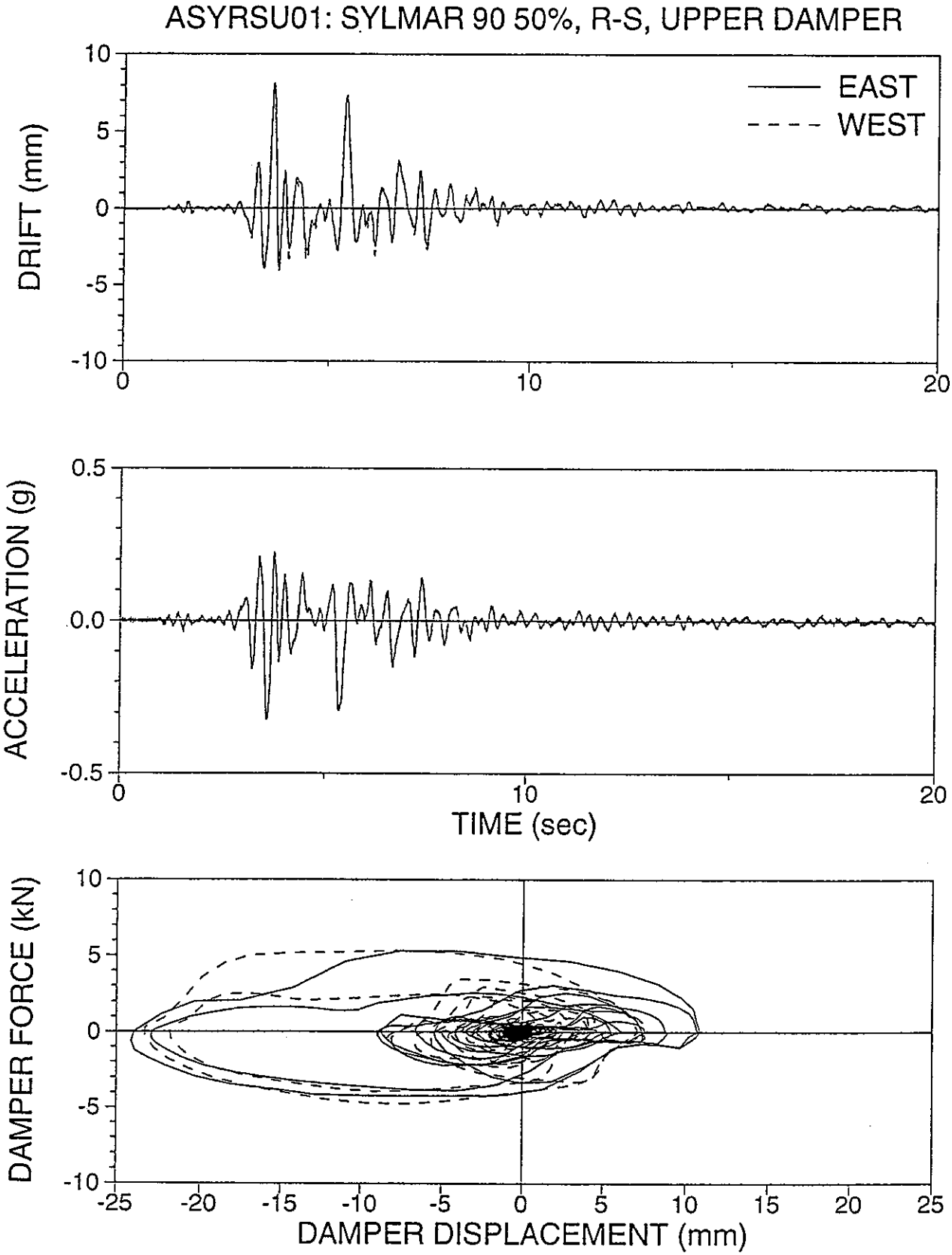
ASYRSU01: SYLMAR 90 50%, R-S, UPPER DAMPER
EAST
WEST
DRIFT (mm)
10
5
0
-5
-10
0
10
20
ACCELERATION (g)
0.5
0.0
-0.5
0
10
20
TIME (sec)
DAMPER FORCE (kN)
10
5
0
-5
-10
-25
-20
-15
-10
-5
0
5
10
15
20
25
DAMPER DISPLACEMENT (mm)

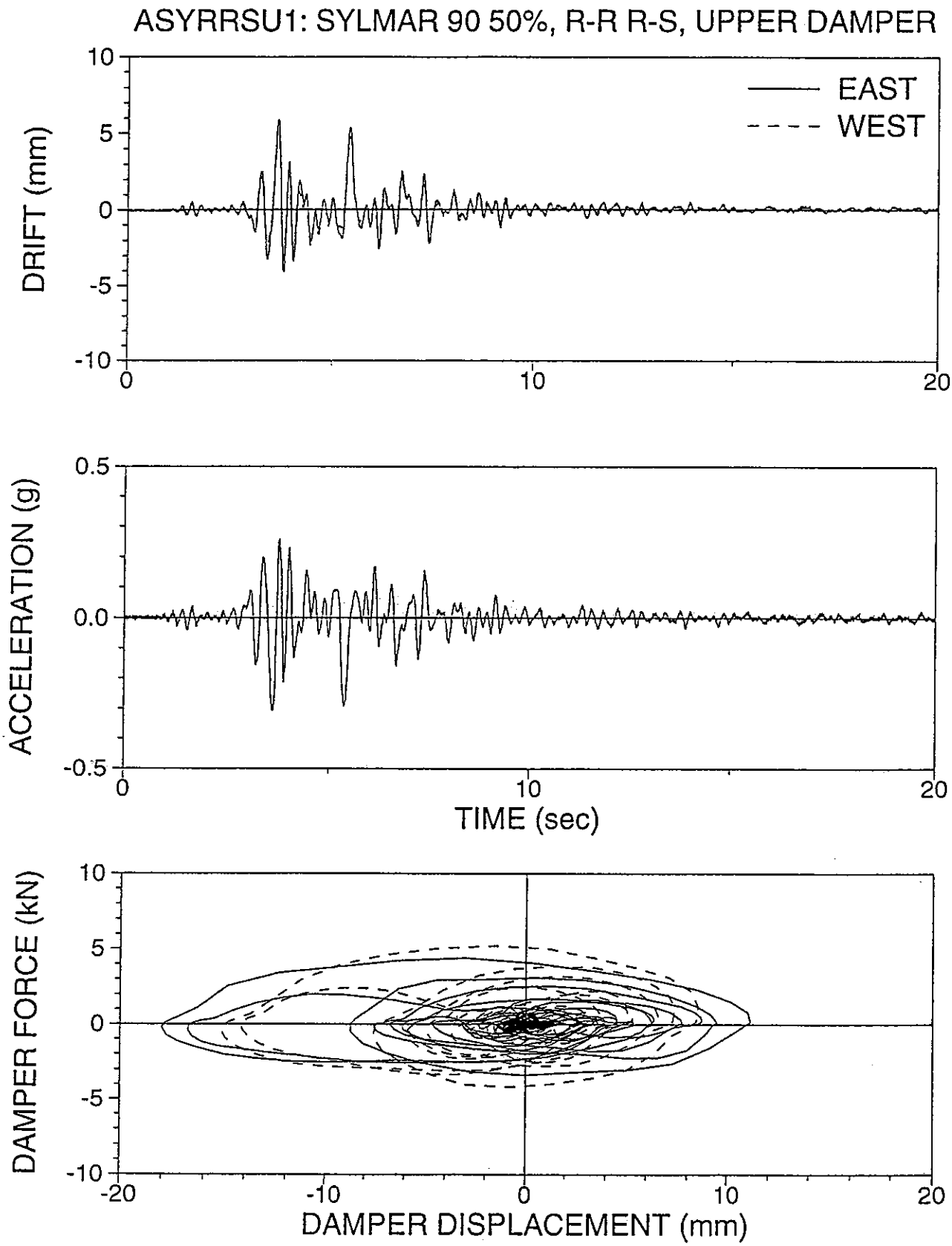
ASYRRSU1: SYLMAR 90 50%, R-R R-S, UPPER DAMPER
EAST
WEST
DRIFT (mm)
10
5
0
-5
-10
0
10
20
ACCELERATION (g)
0.5
0.0
-0.5
0
10
20
TIME (sec)
DAMPER FORCE (kN)
10
5
0
-5
-10
-20
-10
0
10
20
DAMPER DISPLACEMENT (mm)

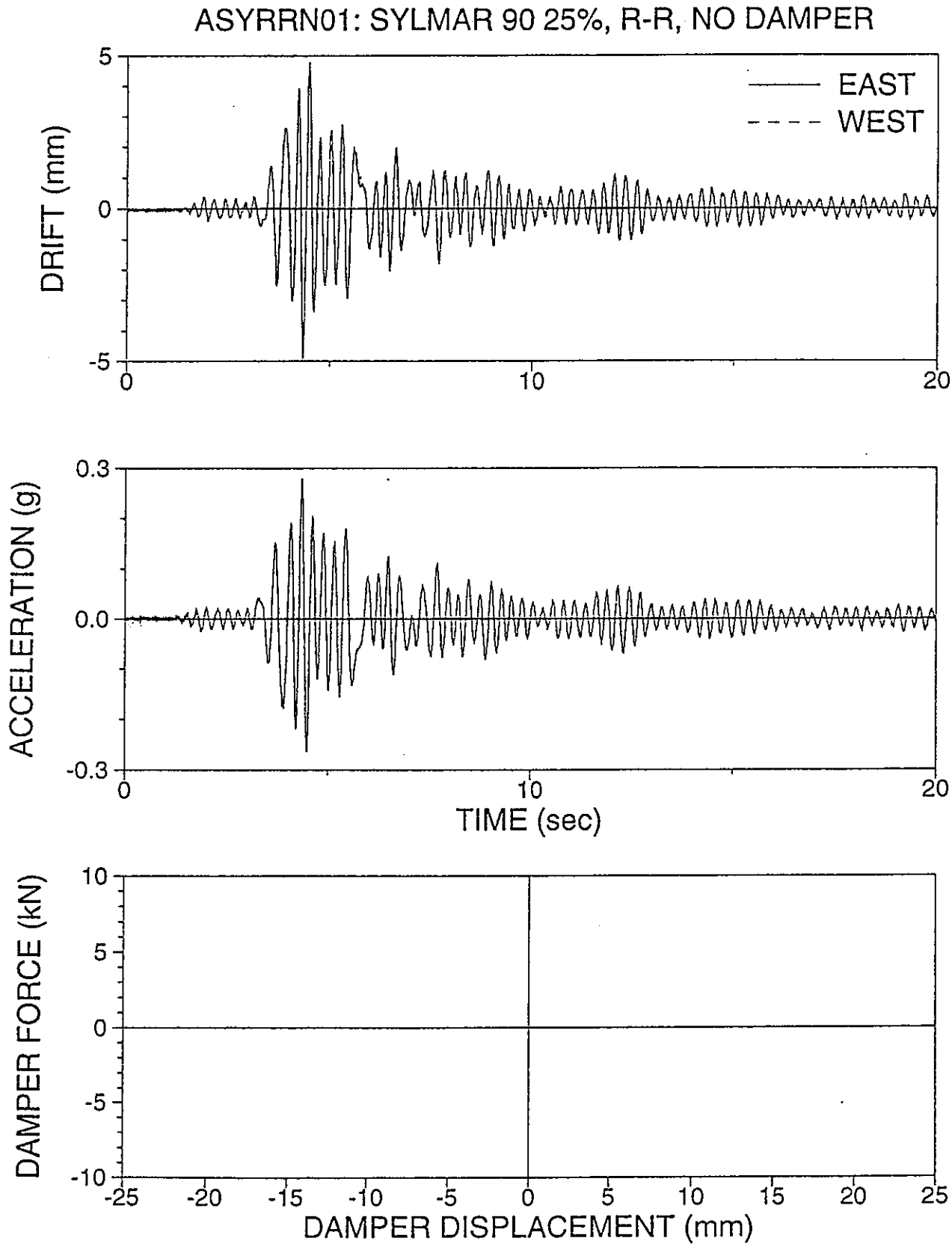
ASYRRN01: SYLMAR 90 25%, R-R, NO DAMPER
EAST
WEST
DRIFT (mm)
5
0
-5
0
10
20
ACCELERATION (g)
0.3
0.0
-0.3
0
10
20
TIME (sec)
DAMPER FORCE (kN)
10
5
0
-5
-10
-25
-20
-15
-10
-5
0
5
10
15
20
25
DAMPER DISPLACEMENT (mm)

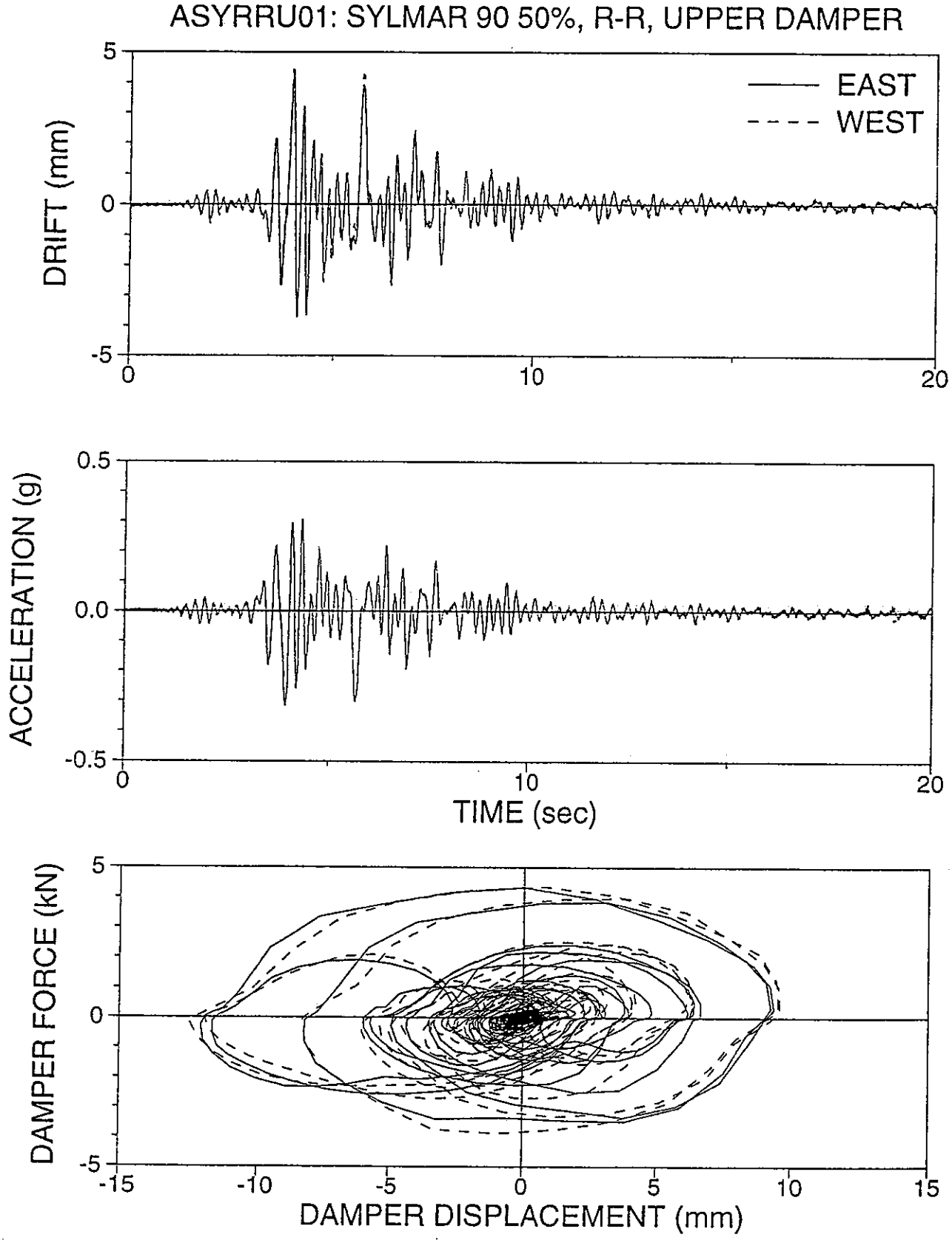
ASYRRU01: SYLMAR 90 50%, R-R, UPPER DAMPER
EAST
WEST
DRIFT (mm)
5
0
-5
0
10
20
ACCELERATION (g)
0.5
0.0
-0.5
0
10
20
TIME (sec)
DAMPER FORCE (kN)
5
0
-5
-15
-10
-5
0
5
10
15
DAMPER DISPLACEMENT (mm)

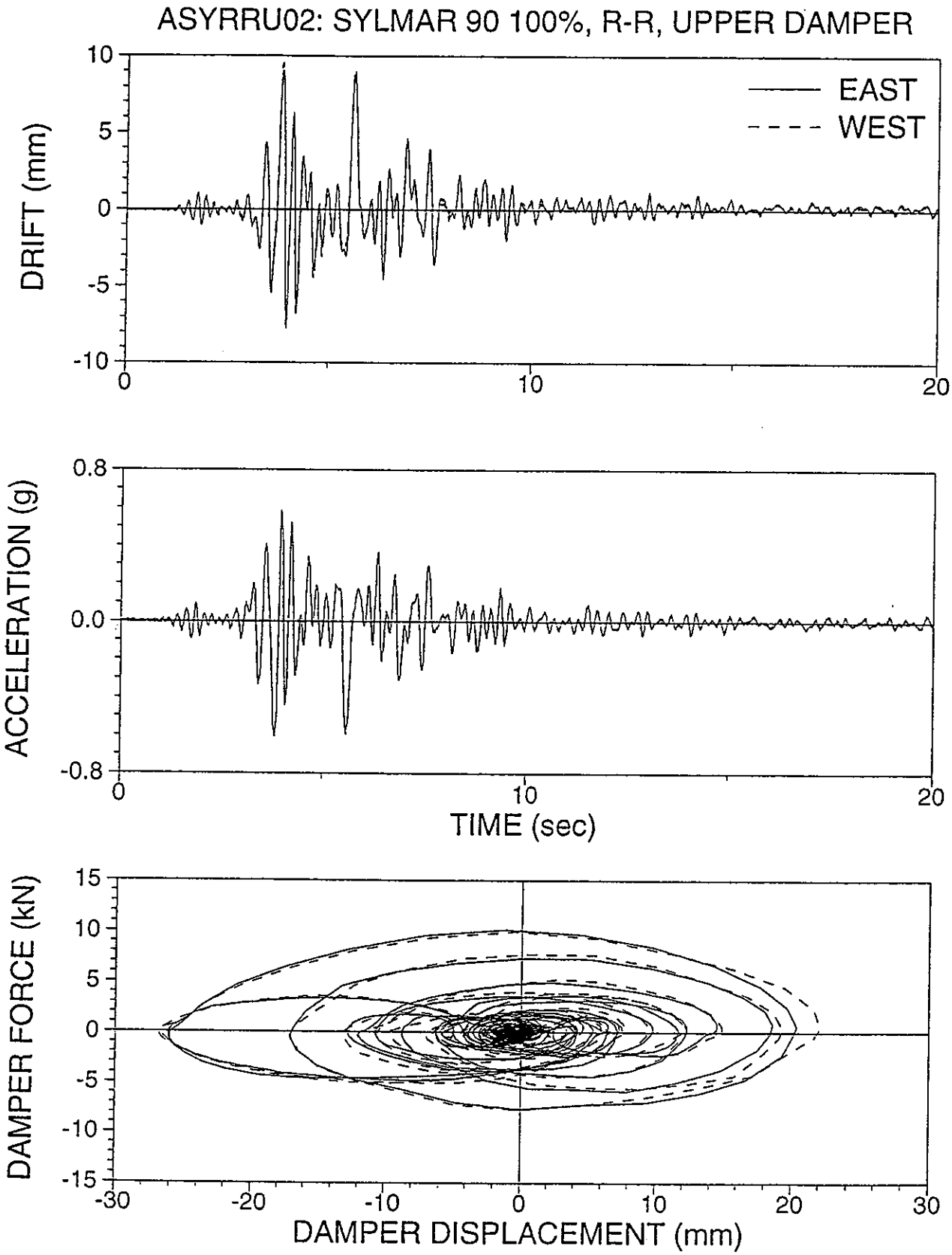
ASYRRU02: SYLMAR 90 100%, R-R, UPPER DAMPER
DRIFT (mm)
EAST
WEST
ACCELERATION (g)
TIME (sec)
DAMPER FORCE (kN)
DAMPER DISPLACEMENT (mm)

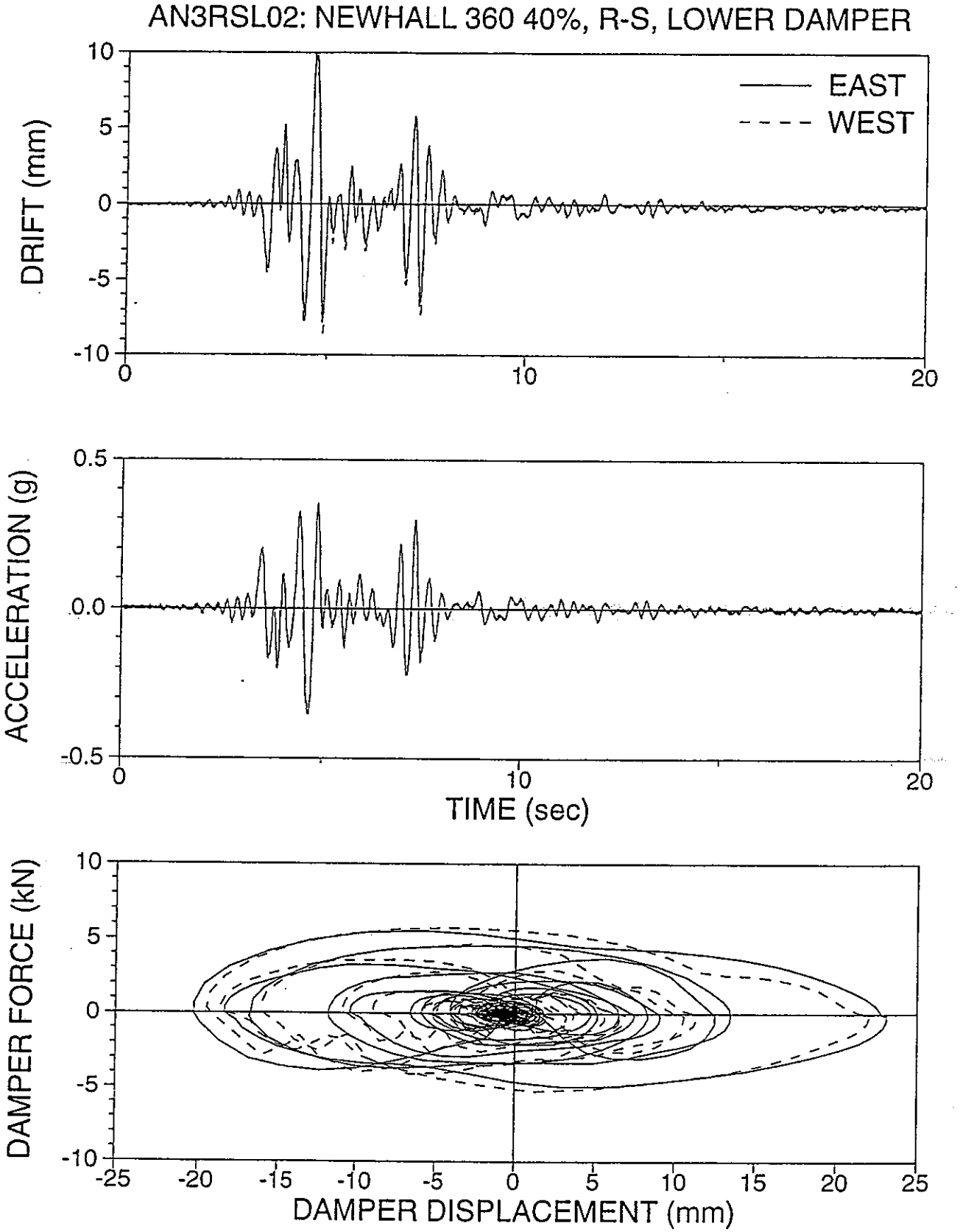
AN3RSL02: NEWHALL 360 40%, R-S, LOWER DAMPER
EAST
WEST
DRIFT (mm)
10
5
0
-5
-10
0
10
20
ACCELERATION (g)
0.5
0.0
-0.5
0
10
20
TIME (sec)
DAMPER FORCE (kN)
10
5
0
-5
-10
-25
-20
-15
-10
-5
0
5
10
15
20
25
DAMPER DISPLACEMENT (mm)

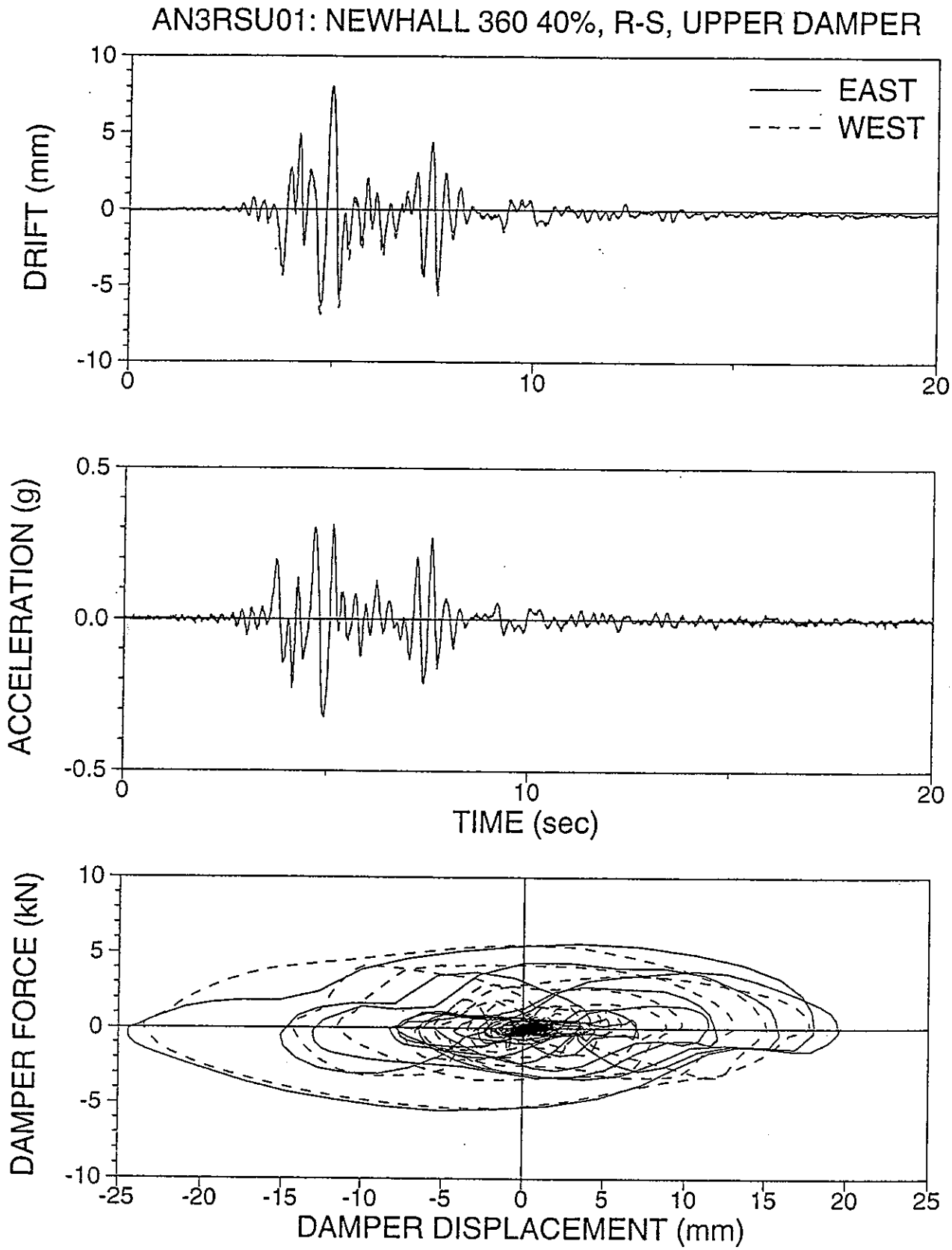
AN3RSU01: NEWHALL 360 40%, R-S, UPPER DAMPER
EAST
WEST
DRIFT (mm)
10
5
0
-5
-10
0
10
20
ACCELERATION (g)
0.5
0.0
-0.5
0
10
20
TIME (sec)
DAMPER FORCE (kN)
10
5
0
-5
-10
-25
-20
-15
-10
-5
0
5
10
15
20
25
DAMPER DISPLACEMENT (mm)

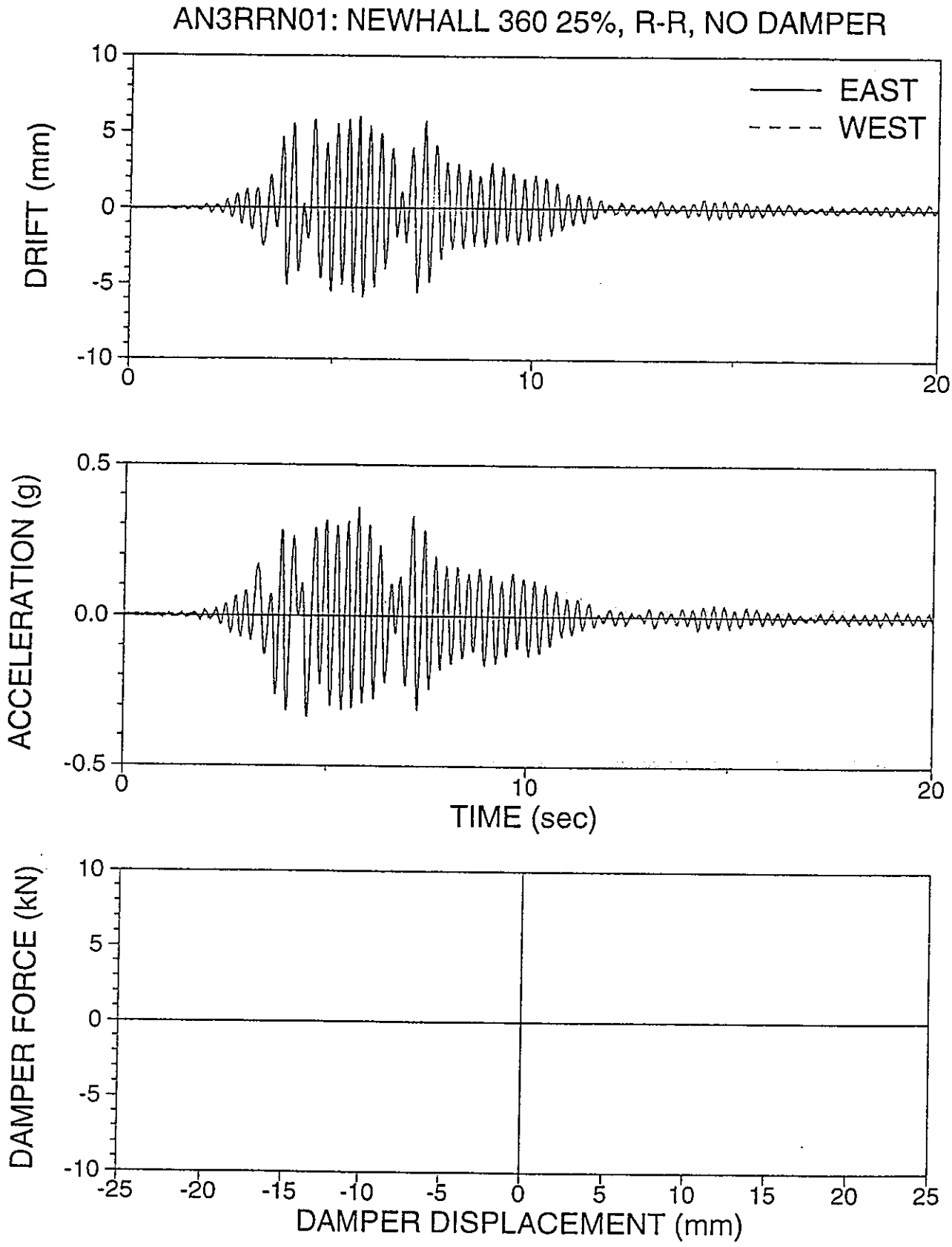
AN3RRN01: NEWHALL 360 25%, R-R, NO DAMPER
EAST
WEST
DRIFT (mm)
10
5
0
-5
-10
0
10
20
ACCELERATION (g)
0.5
0.0
-0.5
0
10
20
TIME (sec)
DAMPER FORCE (kN)
10
5
0
-5
-10
-25
-20
-15
-10
-5
0
5
10
15
20
25
DAMPER DISPLACEMENT (mm)

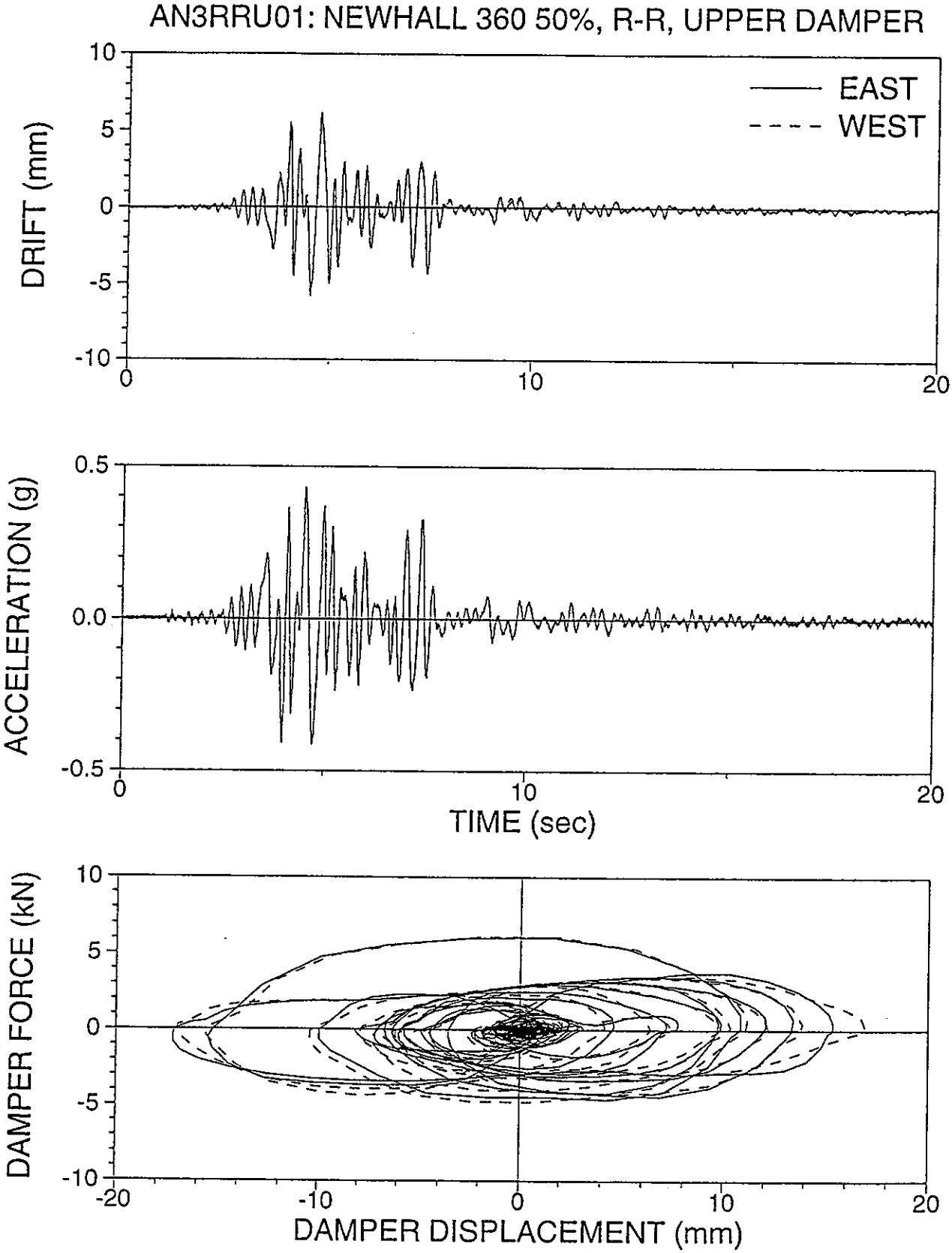
AN3RRU01: NEWHALL 360 50%, R-R, UPPER DAMPER
EAST
WEST
DRIFT (mm)
10
5
0
-5
-10
0
10
20
ACCELERATION (g)
0.5
0.0
-0.5
0
10
20
TIME (sec)
DAMPER FORCE (kN)
10
5
0
-5
-10
-20
-10
0
10
20
DAMPER DISPLACEMENT (mm)

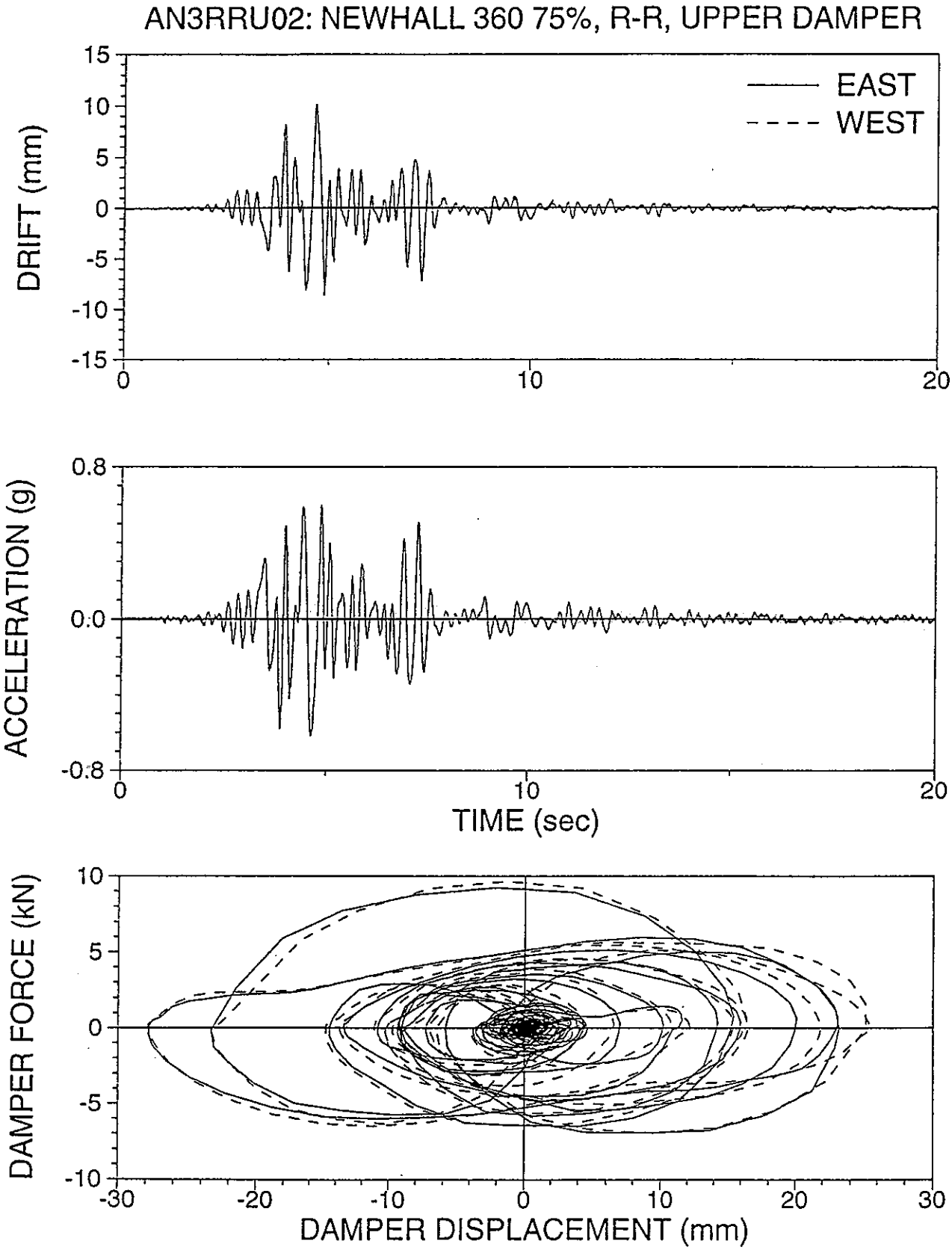
AN3RRU02: NEWHALL 360 75%, R-R, UPPER DAMPER
EAST
WEST
DRIFT (mm)
15
10
5
0
-5
-10
-15
0
10
20
ACCELERATION (g)
0.8
0.0
-0.8
0
10
20
TIME (sec)
DAMPER FORCE (kN)
10
5
0
-5
-10
-30
-20
-10
0
10
20
30
DAMPER DISPLACEMENT (mm)

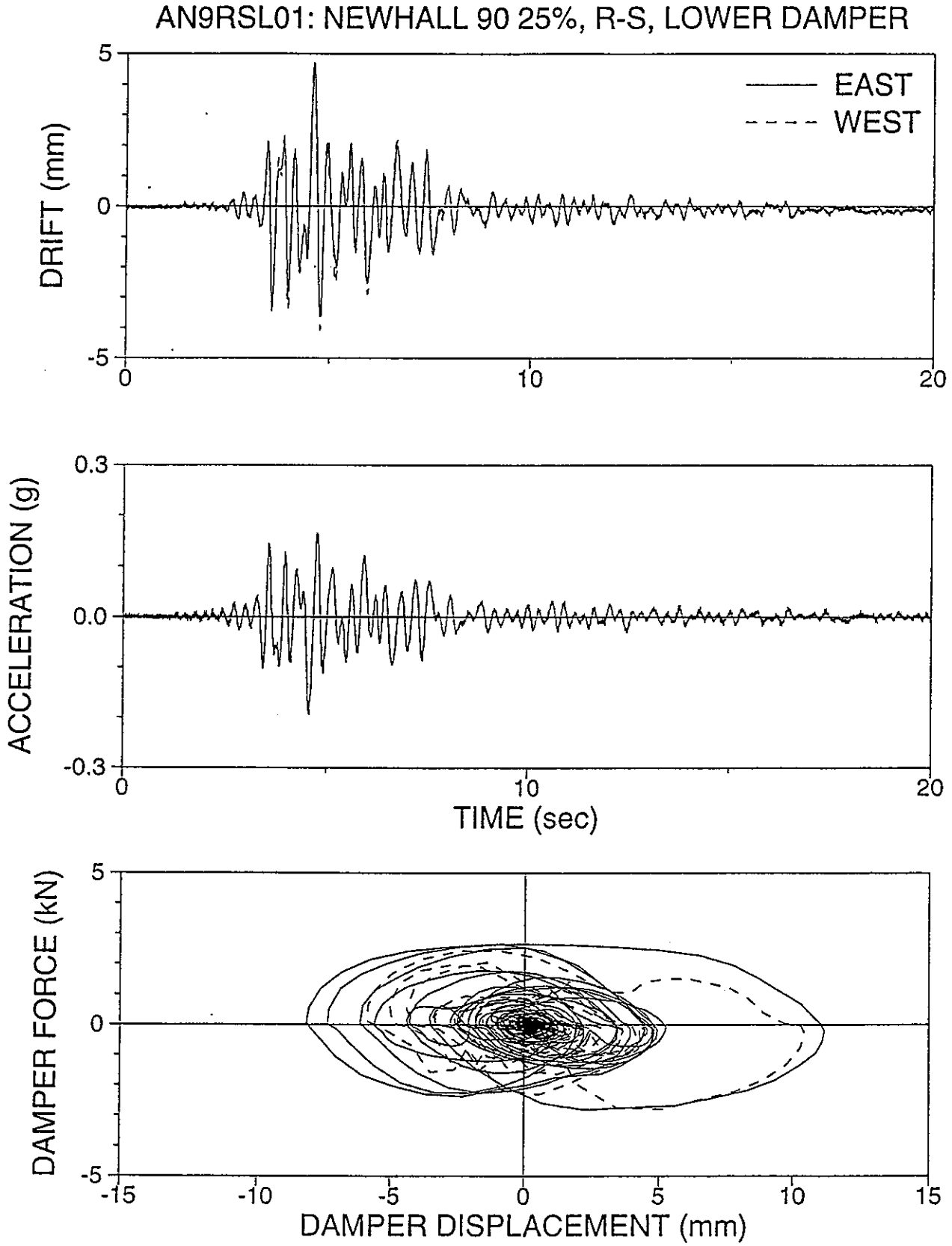
AN9RSL01: NEWHALL 90 25%, R-S, LOWER DAMPER
EAST
WEST
DRIFT (mm)
5
0
-5
0
10
20
ACCELERATION (g)
0.3
0.0
-0.3
0
10
20
TIME (sec)
DAMPER FORCE (kN)
5
0
-5
-15
-10
-5
0
5
10
15
DAMPER DISPLACEMENT (mm)

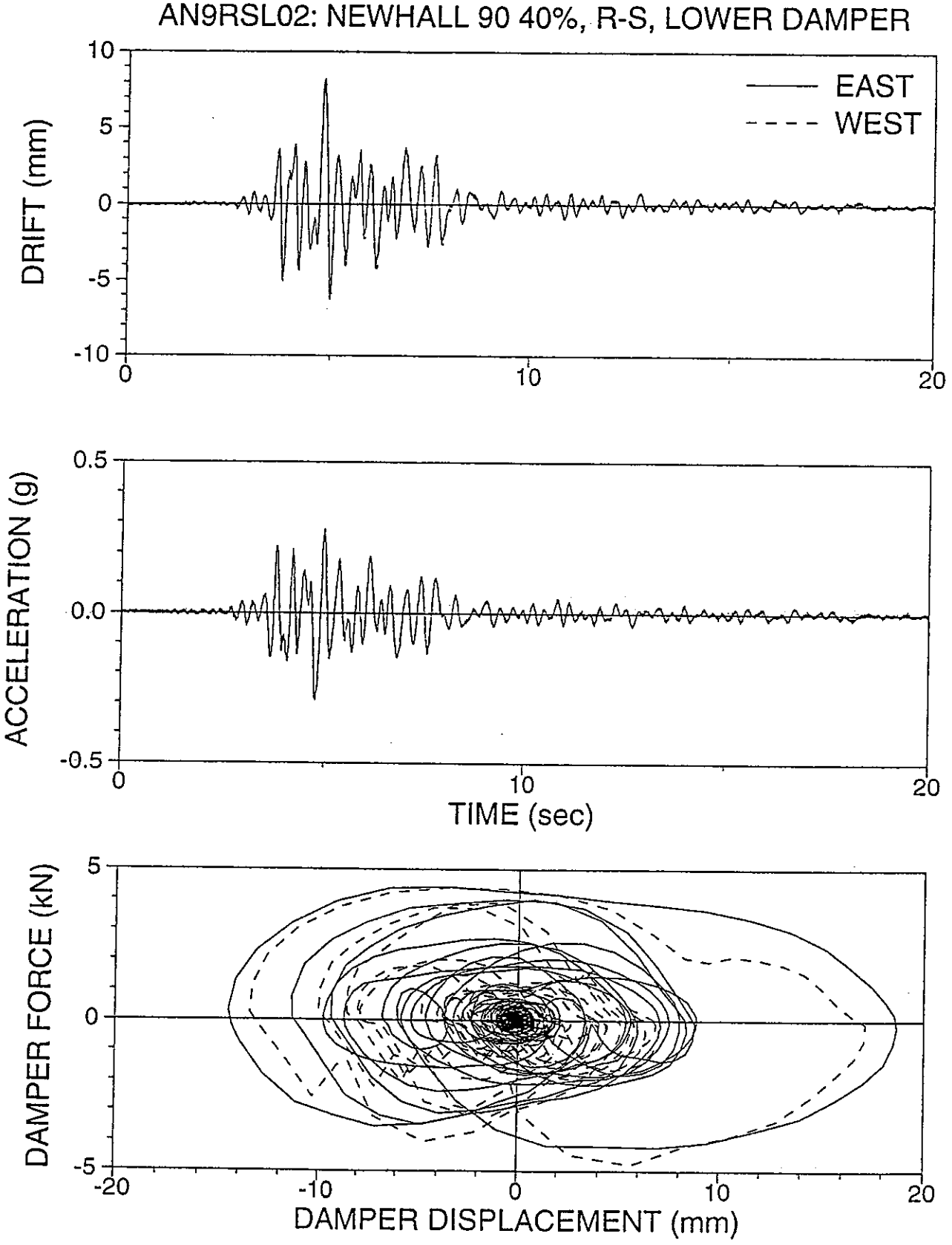
AN9RSL02: NEWHALL 90 40%, R-S, LOWER DAMPER
EAST
WEST
DRIFT (mm)
10
5
0
-5
-10
0
10
20
ACCELERATION (g)
0.5
0.0
-0.5
0
10
20
TIME (sec)
DAMPER FORCE (kN)
5
0
-5
-20
-10
0
10
20
DAMPER DISPLACEMENT (mm)

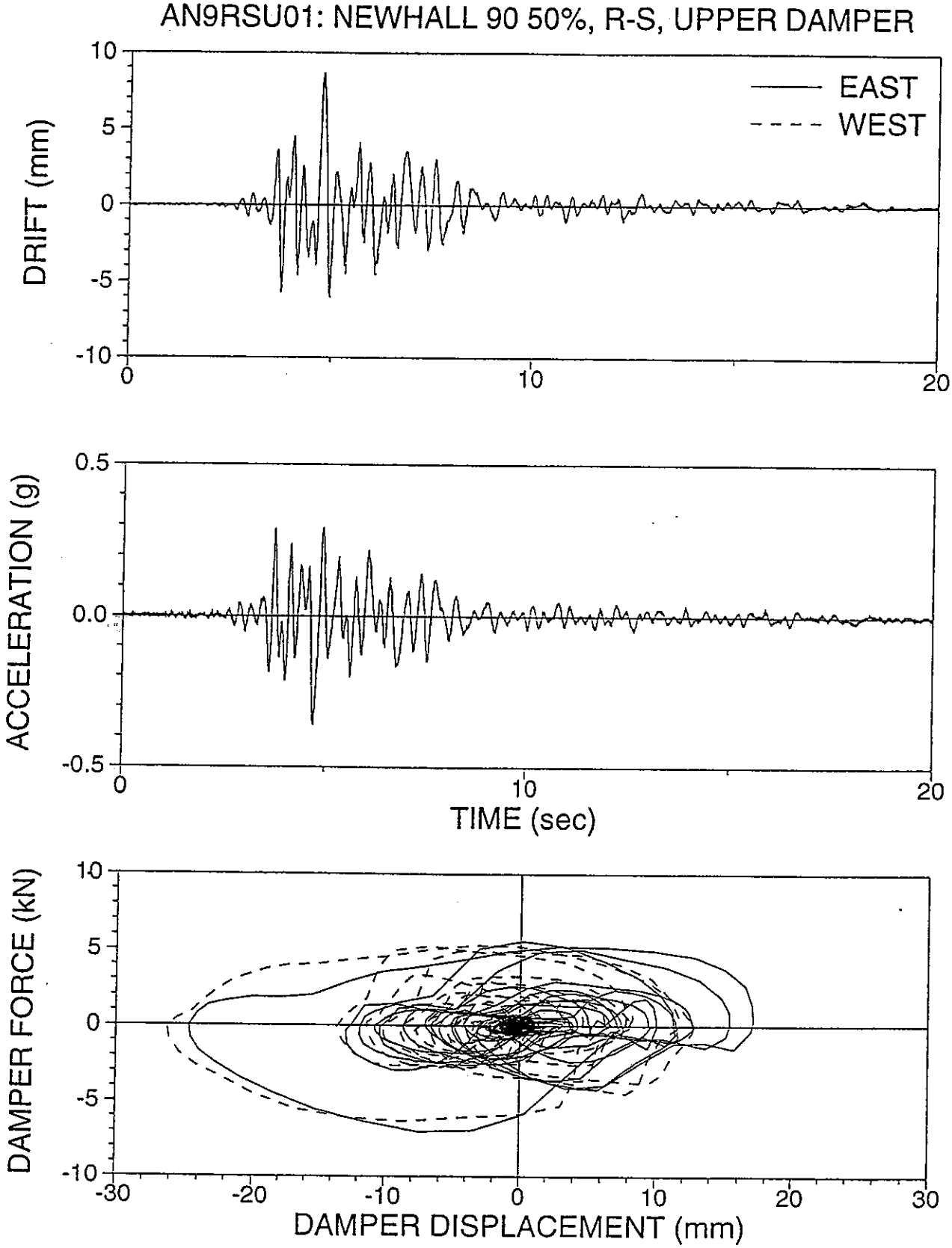
AN9RSU01: NEWHALL 90 50%, R-S, UPPER DAMPER
EAST
WEST
DRIFT (mm)
10
5
0
-5
-10
0
10
20
ACCELERATION (g)
0.5
0.0
-0.5
0
10
20
TIME (sec)
DAMPER FORCE (kN)
10
5
0
-5
-10
-30
-20
-10
0
10
20
30
DAMPER DISPLACEMENT (mm)

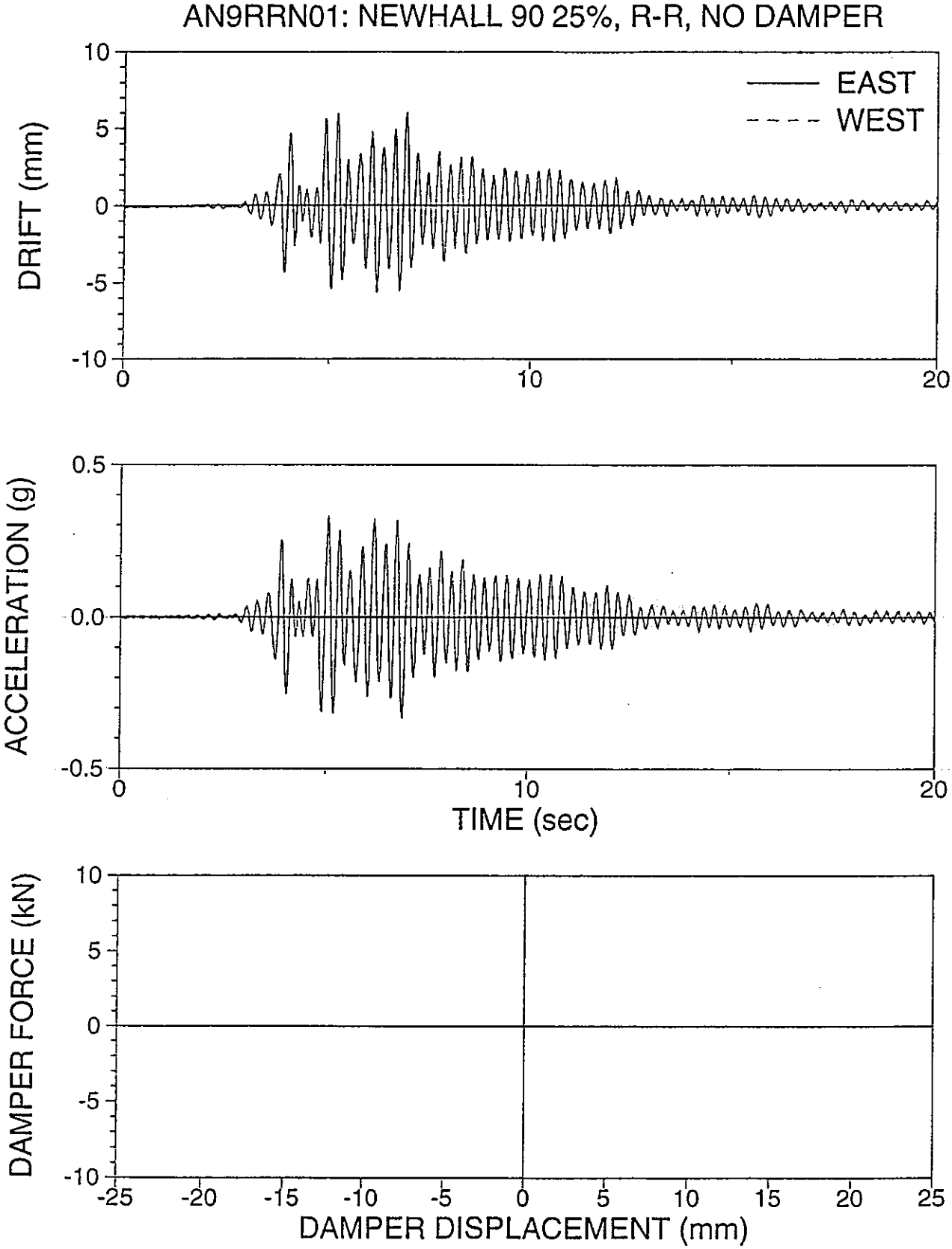
AN9RRN01: NEWHALL 90 25%, R-R, NO DAMPER
EAST
WEST
DRIFT (mm)
10
5
0
-5
-10
0
10
20
ACCELERATION (g)
0.5
0.0
-0.5
0
10
20
TIME (sec)
DAMPER FORCE (kN)
10
5
0
-5
-10
-25
-20
-15
-10
-5
0
5
10
15
20
25
DAMPER DISPLACEMENT (mm)

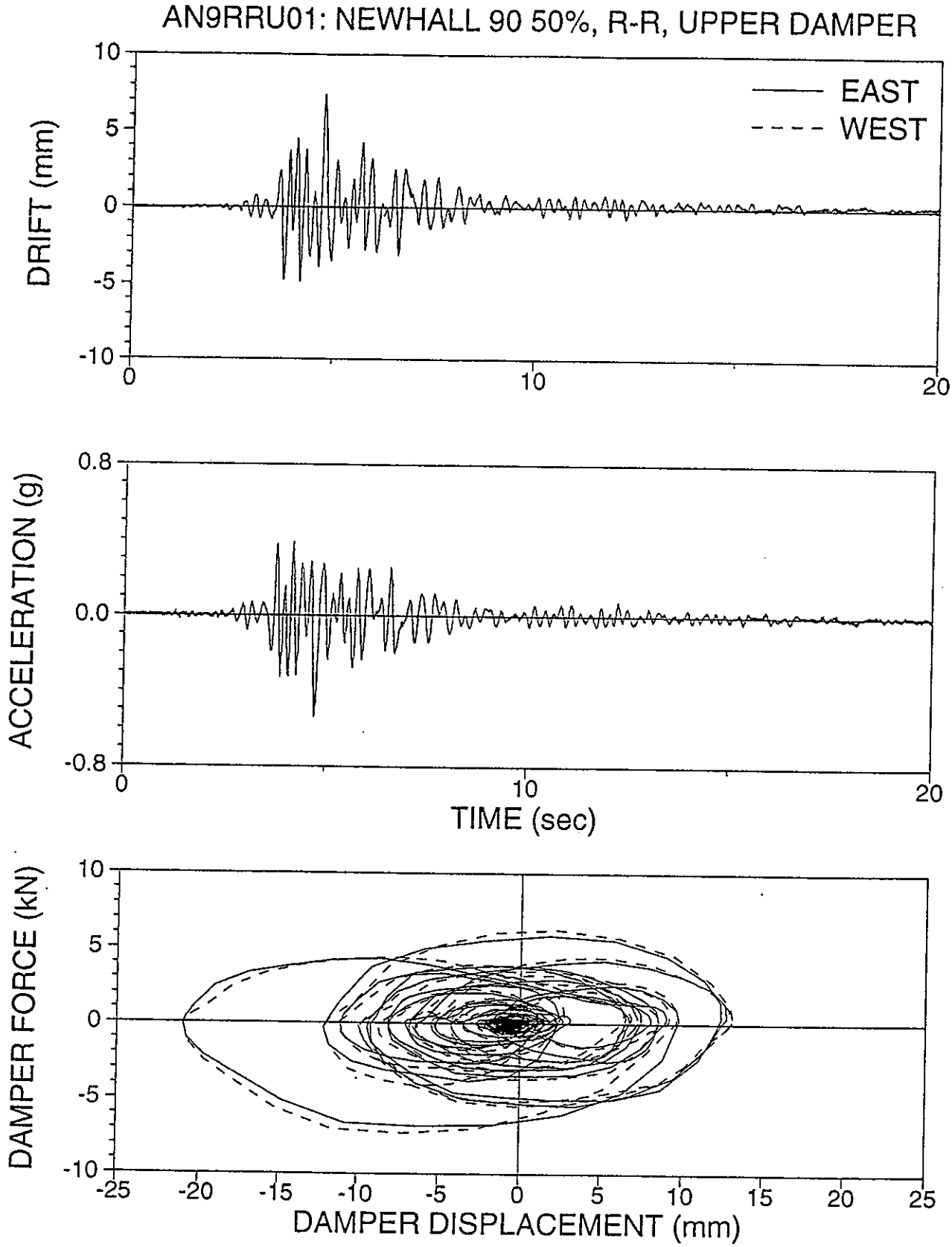
AN9RRU01: NEWHALL 90 50%, R-R, UPPER DAMPER
EAST
WEST
DRIFT (mm)
10
5
0
-5
-10
0
10
20
ACCELERATION (g)
0.8
0.0
-0.8
0
10
20
TIME (sec)
DAMPER FORCE (kN)
10
5
0
-5
-10
-25
-20
-15
-10
-5
0
5
10
15
20
25
DAMPER DISPLACEMENT (mm)

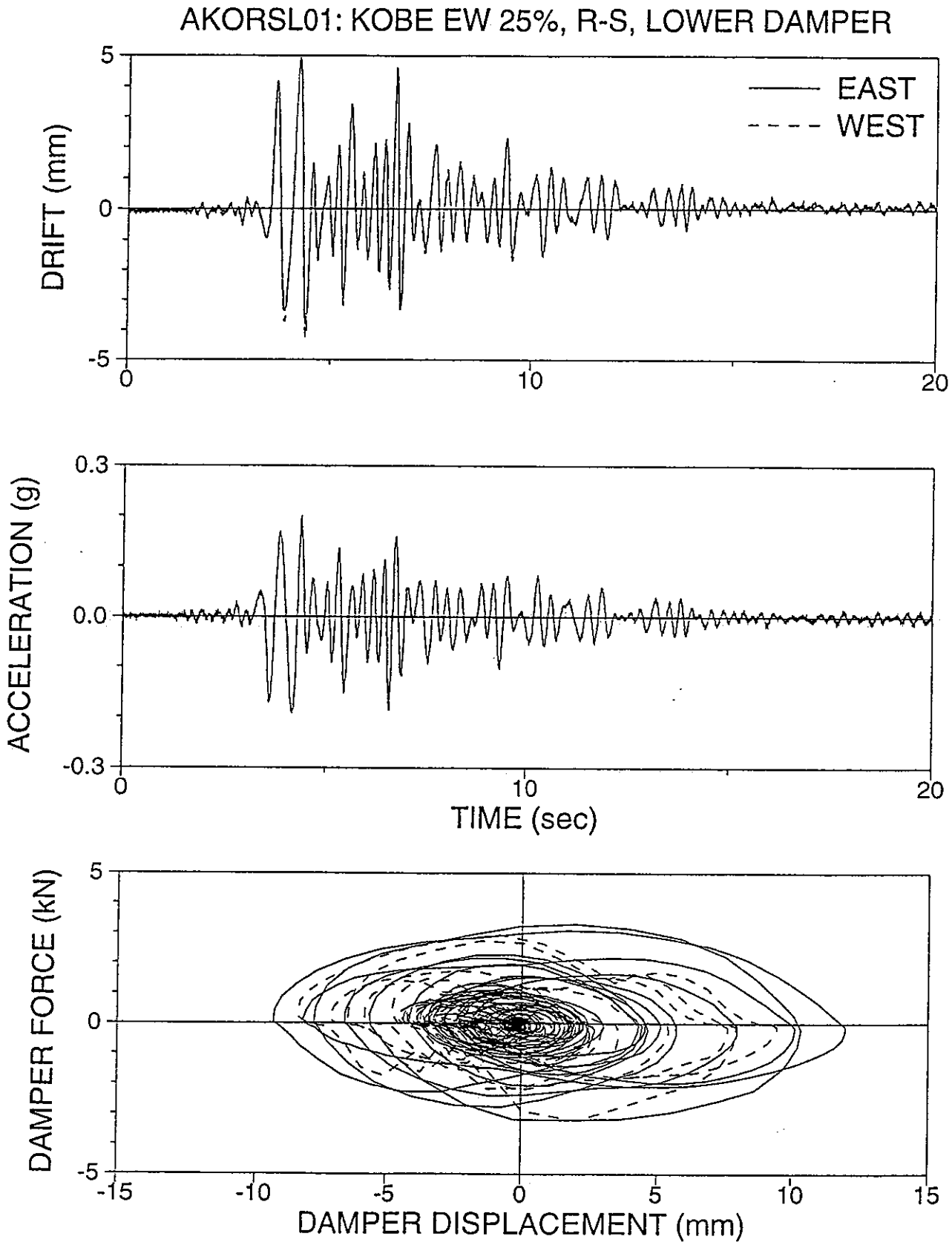
AKORSL01: KOBE EW 25%, R-S, LOWER DAMPER
EAST
WEST
DRIFT (mm)
5
0
-5
0
10
20
ACCELERATION (g)
0.3
0.0
-0.3
0
10
20
TIME (sec)
DAMPER FORCE (kN)
5
0
-5
-15
-10
-5
0
5
10
15
DAMPER DISPLACEMENT (mm)

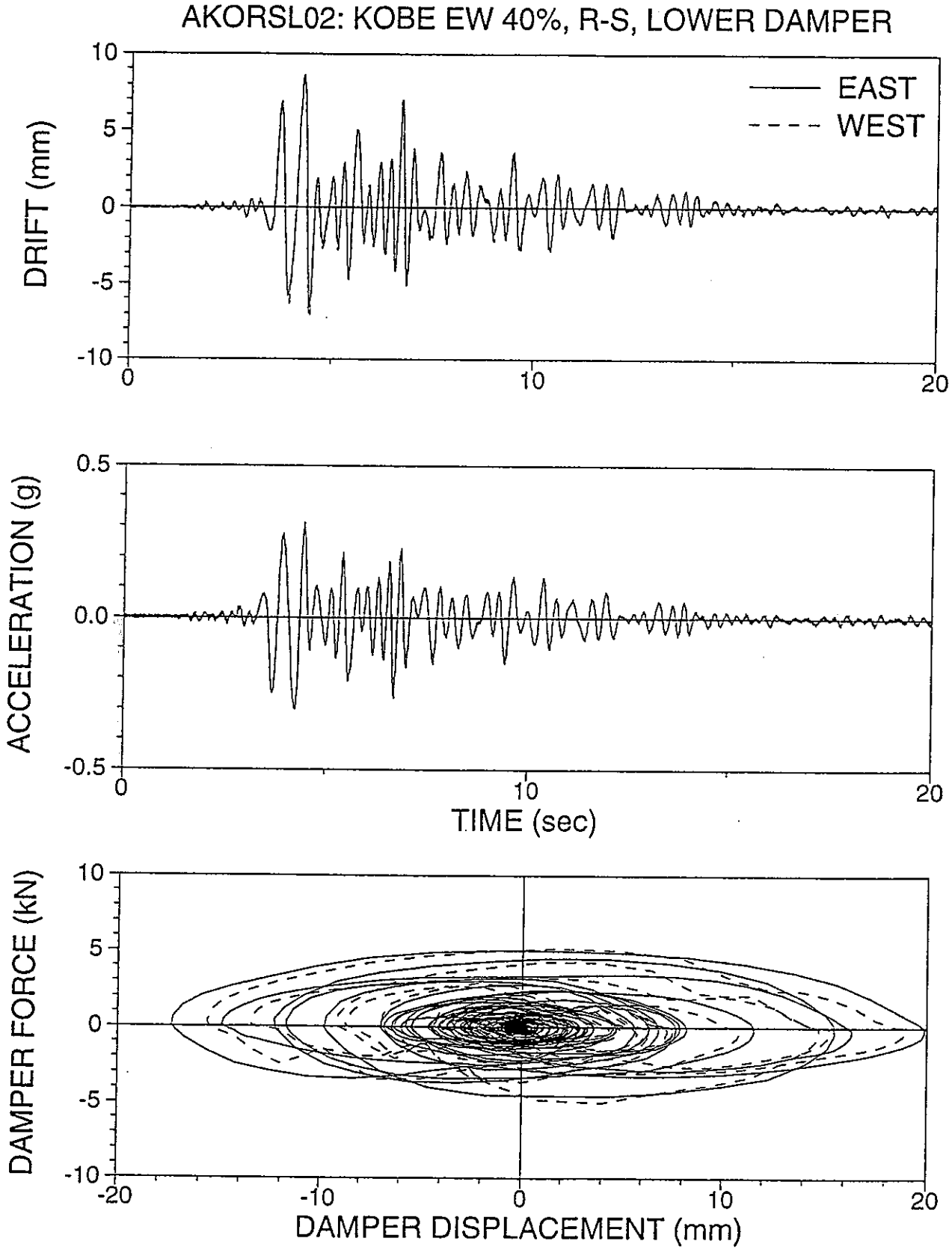
AKORSL02: KOBE EW 40%, R-S, LOWER DAMPER
DRIFT (mm)
EAST
WEST
ACCELERATION (g)
TIME (sec)
DAMPER FORCE (kN)
DAMPER DISPLACEMENT (mm)

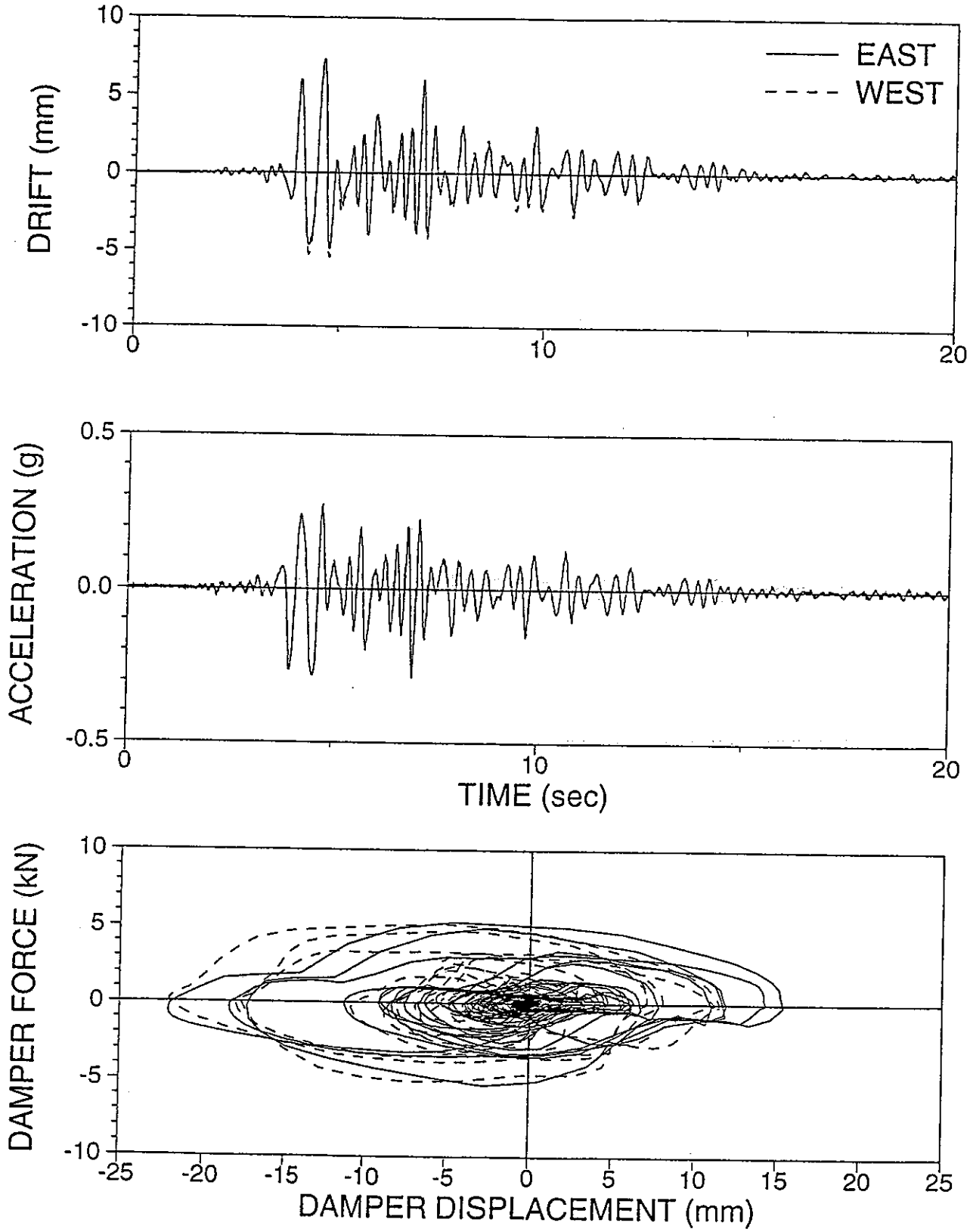
AKORSU01: KOBE EW 40%, R-S, UPPER DAMPER
DRIFT (mm)
EAST
WEST
ACCELERATION (g)
TIME (sec)
DAMPER FORCE (kN)
DAMPER DISPLACEMENT (mm)

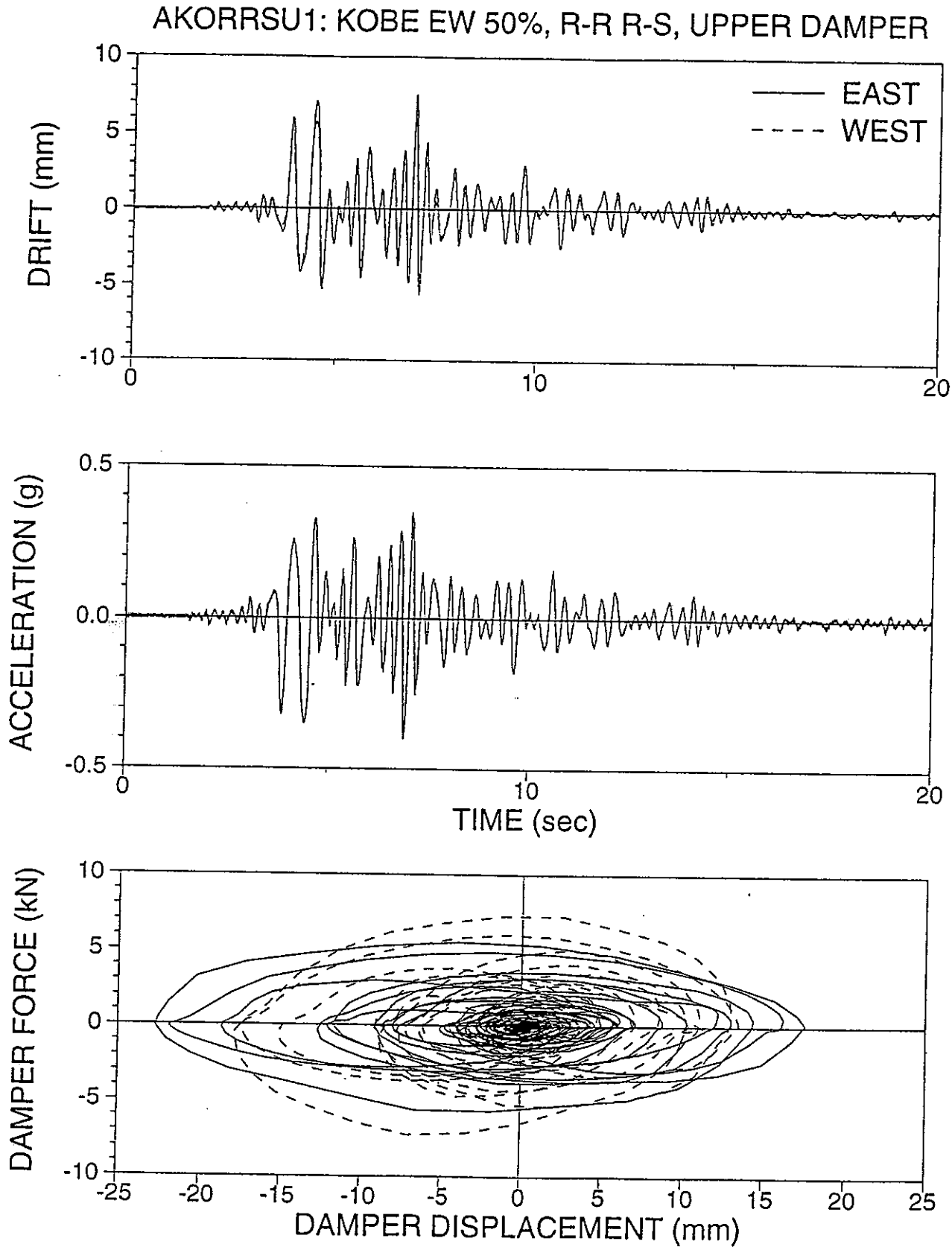
AKORRSU1: KOBE EW 50%, R-R R-S, UPPER DAMPER
DRIFT (mm)
EAST
WEST
ACCELERATION (g)
TIME (sec)
DAMPER FORCE (kN)
DAMPER DISPLACEMENT (mm)

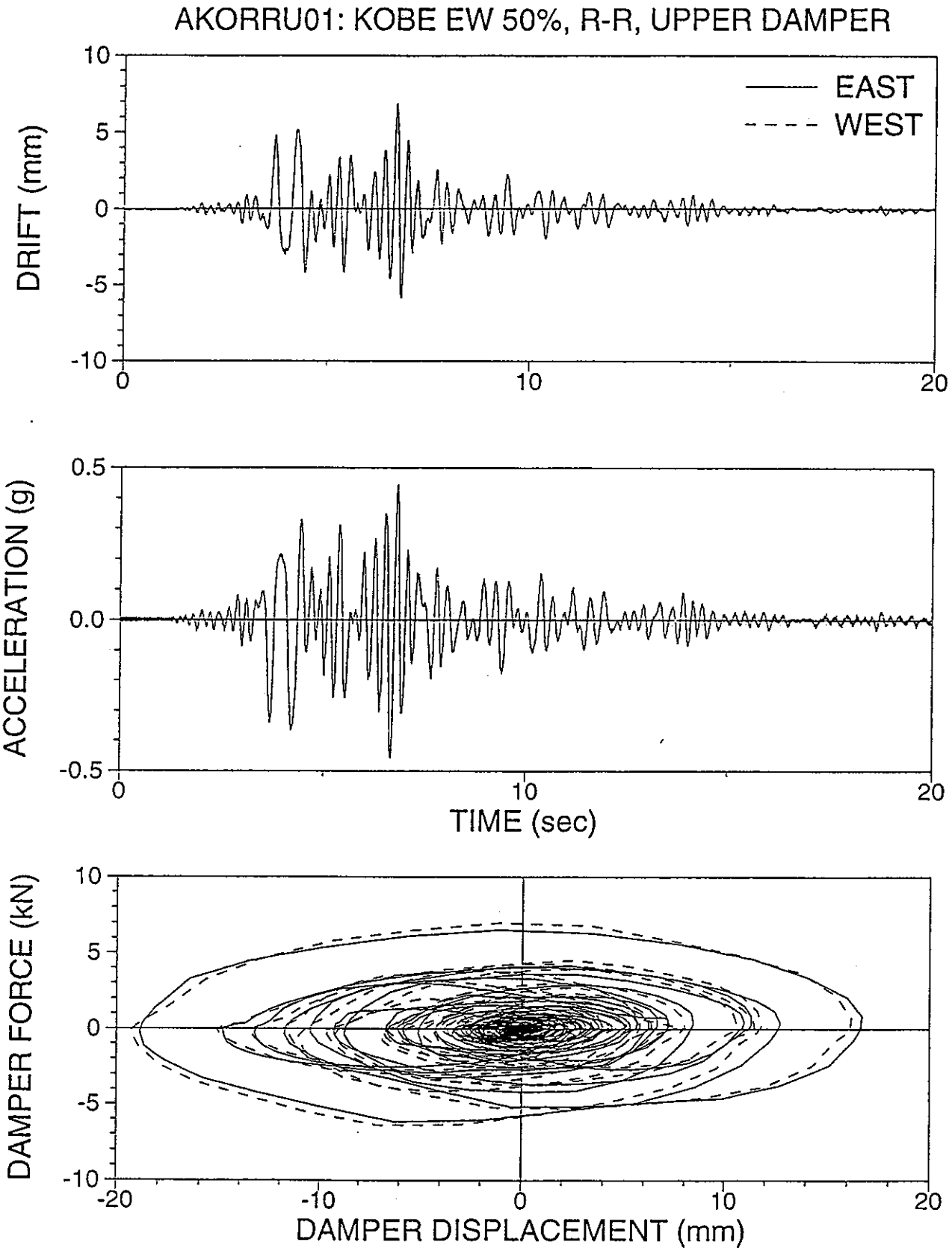
AKORRU01: KOBE EW 50%, R-R, UPPER DAMPER
EAST
WEST
DRIFT (mm)
10
5
0
-5
-10
0
10
20
ACCELERATION (g)
0.5
0.0
-0.5
0
10
20
TIME (sec)
DAMPER FORCE (kN)
10
5
0
-5
-10
-20
-10
0
10
20
DAMPER DISPLACEMENT (mm)

APPENDIX F

INPUT FILES FOR DYNAMIC ANALYSIS OF FRAME WITH ANSYS PROGRAM

ANSYS Input File for Shake Table Simulation of Frame with Rigid-Simple Connections and Lower Damper

```
/batch
/config,nres,1500
/prep7
/title, Dynamic Analysis of a Steel Frame
C*** Units are inches, radian, kips, seconds.
GRAVITY=386.22

ET,1,BEAM3
ET,2,COMBIN14,,,2
ET,3,MASS21,,,4
ET,4,COMBIN14,,6,

R,1,7.08,82.8,7.93,3.63,,
R,2,6.16,75.3,8.28,2.976,,
R,3,2.02,2.6,3.0,1.8,,
R,4,1,0.005,0.25,1,,
R,5,100,1000,1,100,,
R,6,0,0.088,
C*** R,6,0,0,
R,7,1.9419E-2
R,8,9.71E-3
R,9,1.2946E-3
R,10,5.1784E-5
R,11,2.2E-4
R,12,1.683E-4
R,13,9.0622E-5
R,14,10000,,
R,15,15000,,

MP,EX,1,29000
MP,GXY,1,11200

N,1,0,0
N,2,0,62
N,3,0,74
N,4,0,92
N,5,0,117.8
N,6,12,74
N,7,26.13,74
N,8,87.45,74
N,9,95,74
N,10,87.45,69.85
N,11,83.34,65.476
N,12,52.605,32.744
N,13,8.49,5.284
N,14,3.396,2.11
N,15,71.08,0
N,16,99,0
N,17,99,62
N,18,99,74
N,19,99,92
N,20,99,117.8
N,21,49.5,117.8
N,22,0,92
N,23,99,92
N,24,95,74
N,25,52.605,32.744
N,26,0,0
N,27,99,0

TYPE,1
REAL,1
EN,1,1,2
EN,10,17,16

REAL,2
EN,12,6,7
EN,13,7,8

REAL,3
EN,18,11,12
EN,19,13,25

REAL,4
EN,17,10,11
EN,20,14,13

REAL,5
EN,2,2,3
EN,3,3,4
EN,4,22,5
EN,5,5,21
EN,6,21,20
EN,7,20,19
EN,8,23,18
EN,9,18,17
EN,11,3,6
EN,14,8,9
EN,15,24,18
EN,16,8,10
EN,21,1,14


TYPE,2
REAL,6
EN,22,15,25

TYPE,3
REAL,7
EN,23,21

REAL,8
EN,24,5
EN,25,20
```

```
REAL,9
EN,26,19
EN,27,4

REAL,10
EN,28,18
EN,29,3

REAL,11
EN,30,6
EN,31,8

REAL,12
EN,32,17
EN,33,2

REAL,13
EN,34,12

TYPE,4
REAL,14
EN,35,26,1
EN,36,27,16

REAL,15
EN,37,24,9

CP,1,UX,4,22
CP,2,UY,4,22
CP,3,UX,19,23
CP,4,UY,19,23
CP,7,UX,9,24
CP,8,UY,9,24
CP,9,UX,12,25
CP,10,UY,12,25

D,1,UX,0,,,,UY
D,15,UX,0,,,,UY
D,16,UX,0,,,,UY
D,26,ALL
D,27,ALL

FINISH

/SOLU
ANTYPE,TRANSIENT
OUTRES,ALL,LAST
C*** NLGEOM,ON
BETAD,0.0042

*ASK,JUNK,HIT RETURN,0

*DIM,ACCEL,ARRAY,1001,1
*DIM,TIM,ARRAY,1001,1
*VLEN,1001
*VREAD,ACCEL(1),ersl2acc
(E18.12)
*VREAD,TIM(1),ersl2tim
(E18.12)
ESEL,ALL
*DO,TSTEP,1,1001
TIME,TIM(TSTEP)
ACEL,ACCEL(TSTEP)*GRAVITY,,
SOLVE
*ENDDO
SAVE
FINISH

/POST26
NUMVAR,10
NSOL,2,3,U,X,JOINTDSP
ESOL,3,22,,NMISC,1,DMPDISP
ESOL,4,22,,NMISC,2,DMPVEL
ESOL,5,22,,NMISC,3,DMPFORCE
DERIV,6,2,1,,JOINTVEL
DERIV,7,6,1,,JOINTACC
PROD,7,7,,,JOINTACC,,,(1/GRAVITY),,
/OUTPUT,OUTPUT,DAT
PRVAR,2,3,5,7
/OUTPUT,,,,
PLVAR,7
FINISH
```

ANSYS Input File for Shake Table Simulation of Frame with Rigid-Rigid Connections and Upper Damper

```
/batch
/config,nres,1500
/prep7
/title, Dynamic Analysis of a Steel Frame
C*** Units are inches, radian, kips, seconds.
GRAVITY=386.22

ET,1,BEAM3
ET,2,COMBIN14,,,2
ET,3,MASS21,,,4
ET,4,COMBIN14,,6,

R,1,7.08,82.8,7.93,3.63,,
R,2,6.16,75.3,8.28,2.976,,
R,3,2.02,2.6,3.0,1.8,,
R,4,1,0.005,0.25,1,,
R,5,100,1000,1,100,,
R,6,0,0.088,
C*** R,6,0,0,
R,7,1.9419E-2
R,8,9.71E-3
R,9,1.2946E-3
R,10,5.1784E-5
R,11,2.2E-4
R,12,1.683E-4
R,13,9.0622E-5
R,14,1000,,
R,15,0.0,,

MP,EX,1,29000
MP,GXY,1,11200

N,1,0,0
N,2,0,62
N,3,0,74
N,4,0,92
N,5,0,117.8
N,6,12,74
N,7,26.13,74
N,8,87.45,74
N,9,95,74
N,10,87.45,69.85
N,11,83.34,65.476
N,12,52.605,32.744
N,13,8.49,5.284
N,14,3.396,2.11
N,15,71.08,0
N,16,99,0
N,17,99,62
N,18,99,74
N,19,99,92
N,20,99,117.8
N,21,49.5,117.8
N,22,0,92
N,23,99,92
N,24,95,74
N,25,52.605,32.744
N,26,0,0
N,27,99,0

TYPE,1
REAL,1
EN,1,1,2
EN,10,17,16

REAL,2
EN,12,6,7
EN,13,7,8

REAL,3
EN,18,11,12
EN,19,13,25

REAL,4
EN,17,10,11
EN,20,14,13

REAL,5
EN,2,2,3
EN,3,3,4
EN,4,22,5
EN,5,5,21
EN,6,21,20
EN,7,20,19
EN,8,23,18
EN,9,18,17
EN,11,3,6
EN,14,8,9
EN,15,9,18
EN,16,8,10
EN,21,1,14


TYPE,2
REAL,6
EN,22,7,25

TYPE,3
REAL,7
EN,23,21

REAL,8
```

```
EN,24,5
EN,25,20

REAL,9
EN,26,19
EN,27,4

REAL,10
EN,28,18
EN,29,3

REAL,11
EN,30,6
EN,31,8

REAL,12
EN,32,17
EN,33,2

REAL,13
EN,34,12

TYPE,4
REAL,14
EN,35,26,1
EN,36,27,16

REAL,15
EN,37,24,9

CP,1,UX,4,22
CP,2,UY,4,22
CP,3,UX,19,23
CP,4,UY,19,23
CP,5,UX,12,25
CP,6,UY,12,25

D,1,UX,0,,,,UY
D,16,UX,0,,,,UY
D,26,ALL
D,27,ALL

FINISH

/SOLU
ANTYPE,TRANSIENT
OUTRES,ALL,LAST
C*** NLGEOM,ON
BETAD,0.0032

*ASK,JUNK,HIT RETURN,0

*DIM,ACCEL,ARRAY,1001,1
*DIM,TIM,ARRAY,1001,1
*VLEN,1001
*VREAD,ACCEL(1),elrru1,acc
(E18.12)
*VREAD,TIM(1),ersl2tim
(E18.12)
ESEL,ALL
*DO,TSTEP,1,1001
TIME,TIM(TSTEP)
ACEL,ACCEL(TSTEP)*GRAVITY,,
SOLVE
*ENDDO
SAVE
FINISH

/POST26
NUMVAR,10
NSOL,2,3,U,X,JOINTDSP
ESOL,3,22,,NMISC,1,DMPDISP
ESOL,4,22,,NMISC,2,DMPVEL
ESOL,5,22,,NMISC,3,DMPFORCE
DERIV,6,2,1,,JOINTVEL
DERIV,7,6,1,,JOINTACC
PROD,7,7,,,JOINTACC,,,(1/GRAVITY),,
/OUTPUT,OUTPUT,DAT
PRVAR,2,3,5,7
/OUTPUT,,,,
PLVAR,7
FINISH
```

ANSYS Input File for Cyclic Loading Simulation of Frame with Rigid-Simple Connections and Lower Damper

```
/batch
/config,nres,1500
/prep7
/title, Dynamic Analysis of a Steel Frame
C*** Units are inches, radian, kips, seconds.
GRAVITY=386.22

ET,1,BEAM3
ET,2,COMBIN14,,,2
ET,3,MASS21,,,4
ET,4,COMBIN14,,6,

R,1,7.08,82.8,7.93,3.63,,
R,2,6.16,75.3,8.28,2.976,,
R,3,2.02,2.6,3.0,1.8,,
R,4,1,0.005,0.25,1,,
R,5,100,1000,1,100,,
R,6,0,0.088,
C*** R,6,0,0,
R,7,0
R,8,0
R,9,0
R,10,5.1784e-4
R,11,0
R,12,0
R,13,9.0622E-5

R,14,10000,,
R,15,15000,,

MP,EX,1,29000
MP,GXY,1,11200

N,1,0,0
N,2,0,62
N,3,0,74
N,4,0,92
N,5,0,117.8
N,6,12,74
N,7,26.13,74
N,8,87.45,74
N,9,95,74
N,10,87.45,69.85
N,11,83.34,65.476
N,12,52.605,32.744
N,13,8.49,5.284
N,14,3.396,2.11
N,15,71.08,0
N,16,99,0
N,17,99,62
N,18,99,74
N,19,99,92
N,20,99,117.8
N,21,49.5,117.8
N,22,0,92
N,23,99,92
N,24,95,74
N,25,52.605,32.744
N,26,0,0
N,27,99,0

TYPE,1
REAL,1
EN,1,1,2
EN,10,17,16

REAL,2
EN,12,6,7
EN,13,7,8

REAL,3
EN,18,11,12
EN,19,13,25

REAL,4
EN,17,10,11
EN,20,14,13

REAL,5
EN,2,2,3
EN,3,3,4
EN,4,22,5
EN,5,5,21
EN,6,21,20
EN,7,20,19
EN,8,23,18
EN,9,18,17
EN,11,3,6
EN,14,8,9
EN,15,24,18
EN,16,8,10
EN,21,1,14


TYPE,2
REAL,6
EN,22,15,25

TYPE,3
REAL,7
EN,23,21

REAL,8
EN,24,5
```

```
EN,25,20

REAL,9
EN,26,19
EN,27,4

REAL,10
EN,28,18
EN,29,3

REAL,11
EN,30,6
EN,31,8

REAL,12
EN,32,17
EN,33,2

REAL,13
EN,34,12

TYPE,4
REAL,14
EN,35,26,1
EN,36,27,16

REAL,15
EN,37,24,9

CP,1,UX,4,22
CP,2,UY,4,22
CP,3,UX,19,23
CP,4,UY,19,23
CP,7,UX,9,24
CP,8,UY,9,24
CP,9,UX,12,25
CP,10,UY,12,25

D,1,UX,0,,,,UY
D,15,UX,0,,,,UY
D,16,UX,0,,,,UY
D,26,ALL
D,27,ALL

FINISH

/SOLU
ANTYPE,TRANSIENT
OUTRES,ALL,LAST
C*** NLGEOM,ON
BETAD,0.0042
NSUBST,10,,,

*DIM,DISPL,ARRAY,301,1
*DIM,TIM,ARRAY,301,1
*VLEN,301
*VREAD,DISPL(1),harm005hz.dsp
(e18.11)
*VREAD,TIM(1),harm005hz.tim
(e18.11)
ESEL,ALL
*DO,TSTEP,1,301
TIME,TIM(TSTEP)
D,3,UX,DISPL(TSTEP),,,,
SOLVE
*ENDDO
SAVE
FINISH

/POST26
NUMVAR,20
NSOL,2,3,U,X,JNTDISPL
ESOL,3,22,,NMISC,1,DMPDISPL
ESOL,4,22,,NMISC,3,DMPFORCE
ESOL,5,2,,SMISC,8,COMP2
ESOL,6,3,,SMISC,2,COMP3
ESOL,7,11,,SMISC,1,COMP11
ADD,8,5,6,7,DF,,,-1.0,-1.0,1.0
RFORCE,9,1,F,X,SUPORT1
RFORCE,10,16,F,X,SUPORT2
RFORCE,11,15,F,X,SUPORT3
ADD,12,9,10,11,TOTFORCE
/OUTPUT,OUTPUT,DAT
PRVAR,2,3,4,12
/OUTPUT,,,,
PLVAR,8,12
FINISH
```

ANSYS Input File for Cyclic Loading Simulation of Frame with Rigid-Rigid Connections and Upper Damper

```
/batch
/config,nres,1500
/prep7
/title, Dynamic Analysis of a Steel Frame
C*** Units are inches, radian, kips, seconds.
GRAVITY=386.22

ET,1,BEAM3,,,,,,1
ET,2,COMBIN14,,,2
ET,3,MASS21,,,4
ET,4,COMBIN14,,6,

R,1,7.08,82.8,7.93,3.63,,
R,2,6.16,75.3,8.28,2.976,,
R,3,2.02,2.6,3.0,1.8,,
R,4,1,0.005,0.25,1,,
R,5,100,1000,1,100,,
R,6,0,0.088,
C*** R,6,0,0,
R,7,0
R,8,0
R,9,0
R,10,5.1784e-4
R,11,0
R,12,0
R,13,9.0622E-5

R,14,5000,,
R,15,0.0,,

MP,EX,1,29000
MP,GXY,1,11200

N,1,0,0
N,2,0,62
N,3,0,74
N,4,0,92
N,5,0,117.8
N,6,12,74
N,7,26.13,74
N,8,87.45,74
N,9,95,74
N,10,87.45,69.85
N,11,83.34,65.476
N,12,52.605,32.744
N,13,8.49,5.284
N,14,3.396,2.11
N,15,71.08,0
N,16,99,0
N,17,99,62
N,18,99,74
N,19,99,92
N,20,99,117.8
N,21,49.5,117.8
N,22,0,92
N,23,99,92
N,24,95,74
N,25,52.605,32.744
N,26,0,0
N,27,99,0


TYPE,1
REAL,1
EN,1,1,2
EN,10,17,16

REAL,2
EN,12,6,7
EN,13,7,8

REAL,3
EN,18,11,12
EN,19,13,25

REAL,4
EN,17,10,11
EN,20,14,13

REAL,5
EN,2,2,3
EN,3,3,4
EN,4,22,5
EN,5,5,21
EN,6,21,20
EN,7,20,19
EN,8,23,18
EN,9,18,17
EN,11,3,6
EN,14,8,9
EN,15,9,18
EN,16,8,10
EN,21,1,14


TYPE,2
REAL,6
EN,22,7,25

TYPE,3
REAL,7
EN,23,21

REAL,8
```

```
EN,24,5
EN,25,20

REAL,9
EN,26,19
EN,27,4

REAL,10
EN,28,18
EN,29,3

REAL,11
EN,30,6
EN,31,8

REAL,12
EN,32,17
EN,33,2

REAL,13
EN,34,12

TYPE,4
REAL,14
EN,35,26,1
EN,36,27,16

REAL,15
EN,37,24,9

CP,1,UX,4,22
CP,2,UY,4,22
CP,3,UX,19,23
CP,4,UY,19,23
CP,5,UX,12,25
CP,6,UY,12,25

D,1,UX,0,,,,UY
D,16,UX,0,,,,UY
D,26,ALL
D,27,ALL

FINISH
```

```
/SOLU
ANTYPE,TRANSIENT
OUTRES,ALL,LAST
C*** NLGEOM,ON
BETAD,0.0032
NSUBST,10,,,

*ASK,JUNK,HIT RETURN,0

*DIM,DISPL,ARRAY,301,1
*DIM,TIM,ARRAY,301,1
*VLEN,301
*VREAD,DISPL(1),harm2hz,dsp
(e18.11)
*VREAD,TIM(1),harm2hz,tim
(e18.11)
ESEL,ALL
*DO,TSTEP,1,301
TIME,TIM(TSTEP)
D,3,UX,DISPL(TSTEP),,,,
SOLVE
*ENDDO
SAVE
FINISH

/POST26
NUMVAR,20
NSOL,2,3,U,X,JNTDISPL
ESOL,3,22,,NMISC,1,DMPDISPL
ESOL,4,22,,NMISC,3,DMPFORCE
ESOL,5,2,,SMISC,8,COMP2
ESOL,6,3,,SMISC,2,COMP3
ESOL,7,11,,SMISC,1,COMP11
ADD,8,5,6,7,DF,,,-1.0,-1.0,1.0
RFORCE,9,1,F,X,SUPORT1
RFORCE,10,16,F,X,SUPORT2
C*** RFORCE,11,15,F,X,SUPORT3
ADD,11,9,10,,TOTFORCE
/OUTPUT,OUTPUT,DAT
PRVAR,2,3,4,11
/OUTPUT,,,,
PLVAR,8,11
FINISH
```